

073 Evaluation of Wave
Forecasting Models and
Forecast Wind Fields in
the Canadian Context

The Environmental Studies Research Funds are financed from special levies on the oil and gas industry and administered by the Canada Oil and Gas Lands Administration for the Minister of Energy, Mines and Resources, and by the Northern Affairs Program for the Minister of Indian Affairs and Northern Development.

The Environmental Studies Research Funds and any person acting on their behalf assume no liability arising from the use of the information contained in this document. The opinions expressed are those of the authors and do not necessarily reflect those of the Environmental Studies Research Funds agencies. The use of trade names or identification of specific products does not constitute an endorsement or recommendation for use.

ENVIRONMENTAL STUDIES RESEARCH FUNDS

REPORT NO. 073

June 1988

EVALUATION OF WAVE FORECASTING MODELS

AND

FORECAST WIND FIELDS

IN THE CANADIAN CONTEXT

Sandra L.M. Hodgins
Donald O. Hodgins

Seaconsult Marine Research Ltd.
820-1200 West 73rd Avenue
Vancouver, British Columbia

Scientific Adviser: V.R. Swail

The correct citation for this report is:

Hodgins, S.L.M., and D.O. Hodgins. 1988. Evaluation of wave forecasting models and forecast wind fields in the Canadian context. Environmental Studies Research Funds Report No. 073. Ottawa. 356 p.

Published under the auspices of
the Environmental Studies Research Funds
ISBN 0-920783-72-4
©1988 - Seaconsult Marine Research Ltd.

TABLE OF CONTENTS

	<u>Page</u>
Acknowledgements	xiv
Summary	xv
Résumé	xviii
Acronyms, Abbreviations and Non-SI Symbols	xxii
1.0 INTRODUCTION	1
2.0 SEA STATE DESCRIPTION: THE BASIS FOR MODELLING	3
2.1 The Spatial-Temporal Character of Ocean Waves	3
2.1.1 Spatial Measurements	3
2.1.2 Temporal Measurements	5
2.2 Wave Properties at a Point	7
2.2.1 Wave Parameterization	7
2.2.2 Spectral Parameterizations	11
2.3 Parametric Spectra	18
2.3.1 The PM Spectrum	21
2.3.2 The JONSWAP Spectrum	21
2.4 The Energy Balance Equation	24
2.5 Wave Model Output Products	25
3.0 USER REQUIREMENTS	31
3.1 The Perspective of This Review	31
3.2 Marine Weather and Wave Forecast Services	34
3.2.1 Government of Canada Services	34
3.2.2 Private Forecasting Services	42
3.3 End-user Wave Forecast Requirements	45
3.3.1 Offshore Oil and Gas Operators	45
3.3.2 Commercial Fishing and Tow Operators	54
3.3.3 Private Forecasting Firms	57
3.3.4 Canadian Naval and Other Government Requirements	57
3.3.5 Recreational Boaters	61
3.4 Summary	62

TABLE OF CONTENTS
(Continued)

	<u>Page</u>
4.0 WAVE MODELS	67
4.1 Parametric Wave Height Models	67
4.2 Parametric Spectral Wave Models	72
4.2.1 Hasselmann's Model	72
4.2.2 NORSWAM: A Hybrid Model for Wind-Sea and Swell	85
4.2.3 GONO: The Dutch Operational Forecast Model	89
4.2.4 Donelan's Model	98
4.2.5 The Ross Hurricane Model	104
4.2.6 The Norwegian Model	108
4.3 Discrete Spectral Models	111
4.3.1 General Descriptions	111
4.3.2 The Gelci Model: DSA-5	116
4.3.3 The PTB Model: Pierson's Contribution	120
4.3.4 SOWM and GSOWM: The FNOC Models	128
4.3.5 Cardone's Influence: The ODGP and Subsequent Models	135
4.3.6 The Resio Model	144
4.3.7 The DHI System 20 Model	158
4.3.8 The British Meteorological Office (BMO) Model	160
4.3.9 Japanese Models" Isozaki and Uji	172
4.3.10 Two Decoupled Propagation Models--VENICE and SPECREF	174
4.4 Wave Model Specifications	191
4.4.1 Model Domain	193
4.4.2 Shallow Water Regions	193
4.4.3 Grid and Spectral Resolution	194
4.4.4 Time-Step of Integration	198
4.4.5 Possible Models	198
5.0 WIND FIELD SPECIFICATION FOR WAVE FORECASTING	205
5.1 Wind Requirements for Wave Modelling	205
5.2 CMC's Spectral Hemispheric Forecast Model	207
5.2.1 The Governing Equations	208
5.2.2 The Spectral Solution Method	210
5.2.3 Boundary Conditions and Initialization	211
5.2.4 Model Output	212
5.3 Implications for Wave Modelling	212
5.3.1 Horizontal Resolution	212
5.3.2 Vertical Resolution	213

TABLE OF CONTENTS
(Continued)

	<u>Page</u>
6.0 EVALUATION OF CMC FORECAST WINDS	215
6.1 Measured Wind Data Resources	215
6.1.1 Offshore Oil Rig Data	215
6.1.2 AES Sable Island Data	217
6.2 CMC Forecasts Compared With Rig Winds	221
6.2.1 Data Presentation Formats	221
6.2.2 Reduction of Rig Winds to Near-Surface	226
6.2.3 Discussion of Comparisons	228
6.3 CMC Forecasts Compared With Sable Island Winds	231
6.3.1 CMC Versus Sable Island for Rig Period	231
6.3.2 Calibration of Sable Island Winds	234
6.3.3 CMC Versus Adjusted Sable Island Winds	237
6.4 Assessment of CMC Wind Fields for Wave Forecasting	241
6.4.1 Access	241
6.4.2 Timeliness	244
6.4.3 Reliability	245
6.4.4 Implications of Wind Field Errors	247
6.5 Wind and Wave Modelling Strategy	250
7.0 CONCLUSIONS	255
8.0 RECOMMENDATIONS	259
References	263
Appendices	277
4.1 Non-Dimensional Parameters	279
4.2 List of Contacts for Wave Model Information	281
6.1 Comparison of Rowan Gorilla 10-m Reduced Winds with CMC Forecasts	283
6.2 Comparison of Unmodified Sable Island 10-m Winds with CMC Forecasts for Rig Period	305
6.3 Comparison of Adjusted Sable Island Winds with CMC Forecasts	327

LIST OF TABLES

<u>Table</u>	<u>Page</u>
3.1 Partial List of Environmental Thresholds for Drilling Operations	47
3.2 Summary of Wave Forecast Requirements Offshore Oil and Gas Drilling Operations	50
4.1 Matrix Elements for Donelan's Model	100
4.2 Comparison of DSA-5 Significant Wave Height Predictions with SEASAT Altimeter Wave Data	121
4.3 Comparison of DSA-5 Significant Wave Height Predictions With Visual Wave Observations at 45°W 16°N	121
4.4 Comparison of Predicted and Observed Wave Heights as a Function of Modelled Energy Source Terms in Resio's WAVAD	157
4.5 Principal Dates in the Development of the BMO Model	170
4.6 Recent Canadian Hindcast Studies Using Discrete Spectral Wave Models	192
4.7 Three Frequency Resolution Definitions	199
4.8 Summary of Key Wave Model Characteristics	201
4.9 Short List of Models for Canadian Wave Forecasting	202

LIST OF FIGURES

<u>Figure</u>		<u>Page</u>
2.1	Levelled contour analysis of the ocean surface.	4
2.2	A typical surface displacement record lasting about 18 min.	8
2.3	Definition sketch on zero-crossing wave height and period.	9
2.4	Variance spectral density $E(f)$ of $\eta(t)$ recorded at 06:59 GMT, February 15, 1982 on the Grand Banks.	13
2.5	Two-dimensional wave energy spectrum from SWOP. The units of energy (contoured) are ft^2s .	15
2.6	Approximate directional spectrum for wave record 12 β .	17
2.7	The directional spreading function $G(\theta)$ for various powers, s .	19
2.8	Variation of the spreading function, s , with non-dimensional frequency, f/f_p .	20
2.9	A series of fetch limited wave spectra for offshore winds at JONSWAP stations 5, 7, 9, 10 and 11.	23
2.10	Schematic diagram of the spectral wave energy balance.	26
3.1	Marine forecast areas in British Columbia coastal waters.	36
3.2	Well-developed sea states for strong winds, gale and storm force winds.	38
3.3	Typical small radiofax receiver (Alden MARINEFAX IV) suitable for installation on smaller vessels.	41
3.4	Typical weather forecast issued for the Grand Banks by a private meteorological forecasting firm.	43
3.5	Significant wave height field (produced by Seaconsult's SEAWAV [®] forecast system based on Resio's discrete spectral wave model WAVAD).	59
3.6	Illustration of the daily forecasting schedule and prediction lead times used by METOC for the Canadian Department of National Defence.	60
4.1	Map showing locations of the hindcast site, the wind measuring station, and the Waverider buoys.	69

LIST OF FIGURES
(Continued)

<u>Figure</u>		<u>Page</u>
4.2	Time-series of predicted significant wave height and period, together with measured characteristic wave height and peak period.	70
4.3	Comparison of hindcast and recorded wave heights in Lake Superior in October 1965.	71
4.4	Comparison of the α to v relationship with wave data from many sources.	75
4.5	Time-series plots of (a) mean zero-upcrossing period $T_{m0,2}$, (b) significant wave height H_s for the Fulmar and K-13 locations during the hindcast period November 20-26, 1981.	77
4.6a	Comparison of exact computations of the two-dimensional functions S_{n1} with the parameterized form.	80
4.6b	Comparison of the exact one-dimensional distribution S_{n1} with the discrete interaction approximation for a JONSWAP spectrum.	81
4.7	Comparison of the growth of fetch-limited one-dimensional spectra computed using (a) the discrete interaction approximation and (b) the exact form of S_{n1} .	83
4.8	Comparison of the response of a two-dimensional wave spectrum to a sudden 90° change in wind direction.	84
4.9	Grid used in the numerical wave model.	86
4.10	Characteristic rays used in NORSWAM.	87
4.11	Example of the wind field input to NORSWAM.	88
4.12	Spectral comparisons between observed data and NORSWAM for NW winds.	90
4.13	Spectral comparisons between observed data and NORSWAM for SE winds.	92
4.14	Correlation of wave heights and periods at Stevenson for eight similar storms.	93

LIST OF FIGURES
(Continued)

<u>Figure</u>		<u>Page</u>
4.15	The GONO grid and the position of the verification points.	96
4.16	Typical wave chart as produced by GONO.	97
4.17	Comparison of measured and hindcast wave heights and periods during a storm in Lake Ontario (Donelan's model).	102
4.18	Comparison of hindcast with observed wave heights and periods from Donelan's model.	103
4.	19 Comparison of modelled and measured wind speed (a) and modelled significant wave height and peak spectral period with observed values (b).	106
4.20	Comparison of modelled with measured parameters during hurricane BELLE: (a) significant wave height at EB15, (b) maximum predicted spectra superimposed on maximum measured spectrum at EB15, and (c) maximum predicted spectra at EB41.	107
4.21	The Neumann spectrum and co-cumulative spectrum.	109
4.22	Computed and observed significant wave heights for the period 31/10 to 03/11, 1966.	110
4.23	Schematic diagram comparing the Neumann, JONSWAP and Sanders' spectra.	112
4.24	Norwegian model grid showing land contours.	113
4.25	Comparison of observed and computed wave heights (upper panel). Intercomparison of spectral moments (lower panel).	114
4.26	Comparison of the DSA-5 spreading function with the cosine-squared law.	118
4.27	DSA-5 model grid for the North Atlantic Ocean.	119
4.28	Variation of the difference between DSA-5 significant wave height predictions and SEASAT altimeter data (top panel) and visual wave observations (lower panel) as a function of observed wave height.	122
4.29	Comparison of $H_{1/3}$ from the DSA-5 model with visual observations at 45°N 16°W.	123
4.30	Correlation of $H_{1/3}$ SEASAT with $H_{1/3}$ DSA-5 model.	124

LIST OF FIGURES
(Continued)

<u>Figure</u>		<u>Page</u>
4.31	The locations on a Mercator Projection of the triangles that constitute the icosahedral-gnomonic projection.	126
4.32	Partitioning of the world oceans on the icosahedral-gnomonic projection.	127
4.33	Typical surface wind reports from ships at sea input to the wind field analysis for SOWM.	129
4.34	Typical surface pressure analysis from which wind fields are derived for input to SOWM.	130
4.35	Significant wave height field corresponding to the surface pressure analysis shown in Fig. 4.34.	132
4.36	Typical wind field input to SOWM.	133
4.37	Spectral comparison during a North Pacific storm in October, 1973.	134
4.38	Typical wind field used as input to GSOWM (northern hemisphere simulation).	136
4.39	Typical significant wave height field from GSOWM.	137
4.40	Grid system used in the PTB wave hindcast model in the Gulf of Mexico (ODGP).	139
4.41	Comparisons during hurricane CAMILLE: (a) predicted and measured wind at Burwood, and (b) hindcast and measured significant wave heights at ODGP stations 1, 2 and 3.	140
4.42	Hindcast and measured significant and maximum wave heights at each ODGP station (storm maxima) during hurricane CAMILLE.	141
4.43	Hindcast and measured maximum one-dimensional spectra at ODGP station 1 during hurricane CAMILLE.	142
4.44	Duration limited spectra from the SAIL model for a steady 20 m/s wind speed.	145
4.45	WINCH model grid.	146
4.46	Correlation of measured and WES predicted wave heights: (a) storm maxima and (b) full-range values.	147
4.47	WES model grid for the North Atlantic Ocean.	149

LIST OF FIGURES
(Continued)

<u>Figure</u>		<u>Page</u>
4.48	Waverider and hindcast comparison points used by Baird and Readshaw.	150
4.49	Correlation of hindcast (WES model) with storm maxima (Waverider data) off Nova Scotia and Newfoundland.	151
4.50	Energy regimes within a spectrum during active wave growth.	152
4.51	The 12-point interpolation scheme for the energy at any point P within the S20 grid.	161
4.52	Energy from the shaded area is advanced in the S20 transport scheme to the new time level.	162
4.53	Model grid for the DHI S20 application to the North Sea.	163
4.54	Time-series comparison of significant wave height measured during the November 1981 storm with the S20 prediction.	164
4.55	Correlation of measured versus predicted storm maximum significant wave heights for 18 separate events in the North Sea.	165
4.56	Grid points of the BMO fine mesh wave model.	169
4.57	Monthly mean and rms errors at (a) South Uist, (b) Isles of Scilly and (c) St. Gowan.	171
4.58	Time-series wave heights at South Uist for November 1980 (a) using all data and (b) using only 00 and 12 GMT data.	173
4.59	North Atlantic Ocean model grid used by Isozaki and Uji.	175
4.60	Comparison of modelled versus measured wind speed and significant wave height.	176
4.61	Comparison of predicted and observed one-dimensional wave spectra at the station "J" during December 1959.	177
4.62	Observed and computed significant wave heights at the tower (above) for records of February 12, 1976, and March 10, 1976.	182
4.63	Spectra of six records (see Fig. 4.62) during February 12, 1976 storm.	183

LIST OF FIGURES
(Continued)

<u>Figure</u>		<u>Page</u>
4.64	Observed and computed significant wave height in the Tyrrhenian Sea.	184
4.65	Disposition of wave and wind instrumentation providing data for the wave model intercomparisons.	188
4.66	SPECREF grid and the system of nested WAVAD grids.	189
4.67	Regressions of H_S -predicted onto H_S -measured for deep ($h > 25$ m) and shallow ($h < 25$ m) water on Sable Island Bank for the four hindcast storms for WAVAD (upper panels) and SPECREF (lower panels).	190
4.68	Wave refraction of 12.4-s period waves approaching Sable Island from the WSW.	195
4.69	Refraction of 16-s waves entering Queen Charlotte Sound and Hecate Strait from the south and impinging on the east coast of the Queen Charlotte Islands.	196
4.70	Canada's west (A) and east (B) coasts resolved by a $2^\circ \times 2^\circ$ latitude-longitude deep water wave modelling grid.	197
5.1	Schematic representation of the vertical structure of the model showing the distribution of model variables.	209
6.1	Locations of CMC wind forecast data.	216
6.2	Schematic diagram of the Rowan Gorilla jack-up drilling rig.	218
6.3	West Olympia O-51 (Rowan Gorilla) meteorological data from September 1 to end of the drilling program, November 10, 1985.	219
6.4	Location of the wind anemometer on Sable Island and the surrounding topography.	220
6.5	Time-series of meteorological parameters at Sable Island from September 1985 to February 1986.	222
6.6	Relationship of forecast times $F(00)$, $F(12)$ and $F(24)$ to observation times for calculation of error statistics.	225
6.7	Superposition of Rowan Gorilla rig winds as measured at 113 m elevation and the time-series of 10 m reduced winds.	227

LIST OF FIGURES
(Continued)

<u>Figure</u>		<u>Page</u>
6.8	Time-series comparisons of the Rowan Gorilla rig winds with CMC 00, 12 and 24 hour forecast winds.	229
6.9	Scatterplots and standard error statistics for the CMC 00 hour forecasts in relation to the Rowan Gorilla rig winds.	230
6.10	Standard error statistics for the CMC F(00), F(12) and F(24) data in relation to the Rowan Gorilla rig winds.	232
6.11	Monthly error statistics for the CMC F(00), F(12) and F(24) data in relation to the Rowan Gorilla rig winds.	233
6.12	Unmodified Sable Island data compared with CMC 00 hour forecast.	235
6.13	Unmodified Sable Island data compared with 10-m reduced rig winds.	236
6.14	Standard error statistics for the CMC F(00), F(12) and F(24) data in relation to the adjusted Sable Island winds (rig period: September to November 1985).	238
6.15	Monthly error statistics for the CMC F(00), F(12) and F(24) data in relation to the adjusted Sable Island winds.	239
6.16	Scatterplots and standard error statistics for the CMC 00 hour forecasts in relation to the adjusted Sable Island winds from September 1985 to February 1986.	242
6.17	Possible schemes for dissemination of wind and wave forecasts.	246
6.18	Illustration of the consequences of missing two successive forecast intervals.	248
6.19	Conceptual framework for wave forecasting in Canadian waters.	251

ACKNOWLEDGEMENTS

The following organizations and personnel have contributed to this study.

Seaconsult Marine Research Ltd.

Sandra L.M. Hodgins, M.A.Sc. (Project Manager)

Donald O. Hodgins, Ph.D., P.Eng.

Robert Dal-Santo, B.Sc.

Canadian Meteorological Centre

Robert Hone

Clement S. Yang, Ph.D.

We also wish to acknowledge the contributions made by Husky/Bow Valley, Mobil, Shell, Home Oil, Petro-Canada, Dome, Esso, the Atlantic Weather Centre, the Arctic Weather Centre and the Pacific Weather Centre in providing information on user requirements and other aspects of forecast meteorology, and to thank the individuals who took time out of busy schedules for the interviews.

SUMMARY

Wave forecasting requirements in Canadian waters together with current approaches to numerical wave prediction and the derivation of forecast wind fields by the Canadian Meteorological Centre (CMC) are reviewed in this report. A strategy is then given for organizing regional wave forecasts in relation to CMC's existing numerical weather prediction services, and recommendations on the steps required to achieve a high level of wave forecasting are presented.

User requirements consist generally of hourly or six-hourly forecasts of combined sea wave heights and periods for lead times of 12 to 24 hours for the commercial fishery, and out to 36 and 48 hours for the navy and offshore operators. When swell is expected its height, period, direction and duration should be specified. Exploratory drilling and offshore construction operations that are motion-sensitive may also require wave spectra. The forecast data are specified in two formats, one showing temporal variations in wave properties at one location (for offshore drilling operations), and one showing the two-dimensional fields of heights, periods, and directions at several times (for most other users). These requirements for wave data in Canadian waters are best met using numerical wave prediction models. In many areas--the B.C. coast, Beaufort Sea, Hudson Bay, Gulf of St. Lawrence and Scotian Shelf--shallow water effects must be taken into account. Model grid scales of the order of 2 to 20 km are required to resolve bathymetry, landforms and sea ice.

Numerical wave prediction models are based on one of two approaches: empirical laws relating wave height and period to wind field properties and generation area, or semi-empirical relationships between wave energy spectra and wind over the generation area. Most modern models adopt the spectral approach in order to include the most generally correct formulation of wave physics that is applicable without restriction in water of arbitrary depth and to wind fields of arbitrary geometry and rate of change. Of the spectral models, coupled discrete codes and decoupled propagation models are most applicable in Canadian waters. Recommended codes include WAVAD, DHI-S20, ODGP, and SPECREF. Of these, all but ODGP are completely generalized for shallow water processes. In regions with no swell originating in remote

storms, Donelan's model may also be considered; however, for the Beaufort Sea, Gulf of St. Lawrence and southern Hudson Bay, shallow water processes would have to be added to this code.

CMC produces twice-daily prognosis wind fields suitable for wave modelling. These fields are available about four hours after data time, and represent surface winds approximately 15 m above the sea surface ($\sigma = 0.998$). A rational strategy to numerical wave prediction on the east and west coasts, including Davis Strait, would involve running deep water coarse grid wave models over the ocean basins, and one or more nested fine grid wind and wave models in the coastal areas. In the Beaufort Sea and Hudson Bay, separate wind and wave models would be implemented.

It is concluded that to satisfy user needs for accurate, timely wave forecasts, numerical calculations must be complete within six hours of data time. Typically, shallow water coupled discrete spectral wave models would require about three hours execution time on the latest generation of 32-bit microcomputers for 48-hour forecasts. Thus, to meet a six-hour target, coarse grid wave models and local area wind models must be run in parallel with the CMC hemispheric model, which means that CMC must adopt a semi-continuous output procedure that differs, in principle, from the single access time provided in this study. The use of more powerful processors would shorten the time to prepare the local numerical wind and wave prognoses, but access to wind data from the hemispheric model would still be required at several times during the run of that model at CMC.

We have also found that much of the expertise in numerical wave prediction exists in the private sector in Canada, ranging from operational software development to research on modelling theory. Given timely wind data from CMC, there are no impediments in communications or computer technology to establishing either private or government regional wave forecasting centres in Canada. However, some specific problems will have to be addressed to improve wave forecasting skill:

- (1) Local area wind models to adjust CMC winds for orographic and subsynoptic scale effects are required for each fine grid wave model; at present, suitable procedures are not in place in all areas.

- (2) Objective data assimilation algorithms for wind, wave and sea ice information are required to take advantage of existing resources (e.g., offshore buoys) and expected developments in remote sensing.
- (3) Models currently do not treat wave growth, decay and transmission in the marginal ice zone; a study to synthesize present knowledge leading to a rational set of experiments or theoretical investigations to overcome this deficiency is required.
- (4) Marginal ice zone parameterization and resolution by the Atmospheric Environment Service (AES) Ice Branch is inadequate for wave modelling near sea ice (Beaufort Sea, Gulf of St. Lawrence, Hudson Bay)--a study should be undertaken to define ice parameters required for wave modelling in and near the marginal zone, linking these to data that can be obtained from AES now and in the future.
- (5) Detailed deep-water spectral verifications are required as part of developing a wave modelling capability; the existing database is inadequate for this purpose now, and should be expanded.
- (6) CMC winds were found to contain errors quantified by long term statistical trends (e.g., average biases from 1 to 4 knots in speed) that increased with prognosis lead time; however, such error measures provide no insight into what to expect by way of wave model performance since spatial coherence and timing differences could not be quantified. A meaningful definition of wind field error should be developed and used to evaluate prognosis winds.
- (7) Documentation of CMC wind modelling procedures suitable for use by wave modellers is required.
- (8) A comprehensive survey of user requirements for wave forecast products, focused on other than the offshore oil industry and comparable to the recent government-sponsored study on the west coast, should be undertaken in other regions to define the minimum national needs.

RESUME

Dans le présent rapport on examine les exigences de la prévision des vagues dans les eaux canadiennes ainsi que les approches courantes de la prévision numérique des vagues et la dérivation des champs de vent prévus par le Centre météorologique canadien (CMC). On présente ensuite une stratégie de structuration des prévisions régionales des vagues en rapport avec les services existants de prévision météorologique numériques au CMC ainsi que des recommandations quant aux étapes qui permettront de rendre des plus fiables la prévision des vagues.

Les utilisateurs ont en général besoin, aux heures ou aux six heures, de prévisions combinées des hauteurs et des périodes des vagues en mer émises de 12 à 24 heures à l'avance dans le cas des pêches commerciales et de 36 à 48 heures à l'avance dans le cas de la marine et des exploitants au large. Lorsque de la houle est prévue, sa hauteur, sa période, sa direction et sa durée devraient être spécifiées. Les forages d'exploration et les travaux de construction au large qui sont sensibles au mouvement peuvent exiger également des spectres des vagues. Les données de prévision sont spécifiées en deux formats, l'un illustrant les variations temporelles des propriétés des vagues en un emplacement (pour les travaux de forage au large) et l'autre présentant des champs bidimensionnels de hauteurs, de périodes et de directions à plusieurs moments (pour la plupart des autres utilisateurs). Ces exigences en données sur les vagues dans les eaux canadiennes sont au mieux satisfaites au moyen des modèles numériques de prévision des vagues. Il faut également tenir compte des effets des eaux peu profondes dans un grand nombre de régions dont la côte de C.-B., la mer de Beaufort, la baie d'Hudson, le golfe du Saint-Laurent et la plate-forme Scotian. Des modèles avec grilles dont les échelles varient de 2 à 20 km sont nécessaires pour obtenir une résolution adéquate pour la bathymétrie, la morphologie et les glaces de mer.

Les modèles numériques de prévision des vagues sont basés sur l'une ou l'autre de deux approches: sur des lois empiriques mettant en relation la hauteur et la période des vagues avec les propriétés du champ de vent et la zone de génération, ou sur des relations semi-empiriques entre les spectres d'énergie des vagues et le vent dans la zone de génération. La plupart des

modèles modernes sont basés sur la méthode spectrale afin d'obtenir la meilleure représentation générale de la physique des vagues qui soit applicable sans restriction dans des eaux de profondeur arbitraire et à des champs de vent de géométrie et de taux de variations arbitraires. Parmi les modèles spectraux, les plus applicables dans les eaux canadiennes mentionnons les modèles discrets couplés et les modèles découplés de propagation. Parmi les programmes recommandés on compte le WAVAD, le DHI-S20, le ODGP et le SPECREF; de ces derniers, seul le ODGP n'est pas complètement généralisé pour les processus en eau peu profonde. Dans les régions où aucune houle n'est engendrée par des tempêtes éloignées, le modèle de Donelan peut également être pris en considération; toutefois pour la mer de Beaufort, le golfe du Saint-Laurent et la baie d'Hudson méridionale, les processus en eau peu profonde devront être ajoutés à ce programme.

Le CMC produit deux fois par jour des pronostics sur les champs de vent qui conviennent pour la modélisation des vagues. Ces champs sont disponibles environ quatre heures après l'heure d'obtention des données et représentent les vents de surface à approximativement 15 m au-dessus de la surface de la mer ($\sigma=0,998$). Une stratégie nationale de prévision numérique des vagues pour les côtes Est et Ouest, incluant le détroit de Davis, exigerait le passage de modèles à grille grossière pour les eaux profondes dans les bassins océaniques et d'un ou plusieurs modèles à grille fine emboîtée pour le vent et les vagues dans les régions côtières. Pour la mer de Beaufort et la baie d'Hudson des modèles distincts pour le vent et les vagues devraient être mis en oeuvre.

On conclut, que pour satisfaire aux besoins des utilisateurs en prévisions précises et opportunes pour les vagues, les calculs devraient être complétés moins de six heures après l'obtention des données. De manière caractéristique, les modèles spectraux discrets couplés pour les vagues en eau peu profonde exigent un délai d'exécution d'environ trois heures sur les micro-ordinateurs de 32 bits de dernière génération pour les prévisions de 48 heures. Ainsi, pour atteindre la cible des six heures, les modèles de vagues à grille grossière et les modèles de vent appliqués à l'échelle locale doivent être passés simultanément au modèle hémisphérique du CMC, ce qui signifie que le CMC doit adopter une procédure de sortie en semi-continu

qui différera, en principe, du temps d'accès unique prévu dans le cadre de la présente étude. L'utilisation d'organes de traitement plus puissants permettrait de préparer en moins de temps les pronostics locaux pour le vent et les vagues, mais l'accès aux données sur les vents du modèle hémisphériques serait encore nécessaire à plusieurs moments pendant le passage de ce modèle au CMC.

Nous avons également constaté qu'une bonne part de l'expérience en prévision numérique des vagues existe dans le secteur privé au Canada, depuis la mise au point de logiciels opérationnels aux recherches sur la théorie de la modélisation. Si des données opportunes sur les vents sont disponibles du CMC, la technologie des communications et l'informatique ne posent aucun obstacle à l'établissement de centres régionaux privés ou gouvernementaux de prévision des vagues au Canada. Toutefois, certains problèmes spécifiques devront être étudiés afin d'améliorer l'aptitude à formuler des prévisions des vagues:

- (1) Des modèles locaux pour les vents sont nécessaires afin de corriger les données sur les vents du CMC de manière à tenir compte des effets orographiques et des effets à l'échelle subsynoptique pour chacun des modèles à grille fine; les procédures convenables ne sont actuellement pas au point dans toutes les régions.
- (2) Des algorithmes objectifs d'assimilation des données sur les vents, les vagues et les glaces de mer sont nécessaires afin de tirer avantage des ressources existantes (bouées au large) et des progrès prévus en télédétection.
- (3) Les modèles ne traitent actuellement pas la croissance, l'atténuation et la transmission des vagues dans la zone glacielle marginale; une étude visant à synthétiser les connaissances actuelles et qui mènerait à un ensemble rationnel d'expériences ou de recherches théoriques est nécessaire pour remédier à cette lacune.
- (4) Le paramétrage et la résolution pour la zone glacielle marginale par la Direction des glaces du Service de l'environnement atmosphérique (SEA) sont actuellement inadéquates pour la modélisation des vagues près des glaces de mer (mer de Beaufort, golfe du Saint-Laurent, baie d'Hudson); une étude devrait être entreprise afin de déterminer les paramètres des

glaces nécessaires pour la modélisation des vagues dans la zone marginale et à proximité de celle-ci, ainsi que pour relier ces paramètres à des données qui peuvent, ou pourront à l'avenir, être obtenues du SEA.

- (5) Des vérifications spectrales détaillées en eaux profondes sont nécessaires à titre de partie intégrante du développement de l'aptitude à modéliser les vagues; la base de données existante est actuellement inadéquate à cette fin et devrait être augmentée.
- (6) Il a été constaté que les données sur les vents du CMC renfermaient des erreurs quantifiées à l'aide de tendances statistiques à long terme (p. ex. des biais de 1 à 4 noeuds pour les vitesses) qui augmentent en fonction des périodes de validité des pronostics; toutefois de telles erreurs de mesure ne fournissent aucunement un aperçu du rendement du modèle des vagues auquel il faut s'attendre puisque la cohérence spatiale et les différences de synchronisation ne pouvaient être quantifiées. Une définition rationnelle de l'erreur pour le champ de vent devrait être élaborée et utilisée pour évaluer les pronostics des vents.
- (7) Une documentation des procédures de modélisation des vents appliquées par le CMC et pouvant être utilisée par les spécialistes de la modélisation des vagues est nécessaire.
- (8) Un relevé exhaustif des besoins des utilisateurs en produits de prévision des vagues, centré sur d'autres utilisateurs que ceux de l'industrie pétrolière au large et comparable à l'étude récemment parrainée par le gouvernement sur la côte Ouest, devrait être entrepris afin de définir les besoins minimums au niveau national.

LIST OF ACRONYMS, ABBREVIATIONS AND NON-SI SYMBOLS

AES	Atmospheric Environment Service
BMO	British Meteorological Office
CASP	Canadian Atlantic Storm Project
CCIW	Canada Centre for Inland Waters
CD	coupled discrete (model class; see also DS)
CH	coupled hybrid (model class)
CMC	Canadian Meteorological Centre, Dorval, P.Q.
DFO	Fisheries & Oceans Canada
DFO(IOS)	Fisheries & Oceans Canada, Institute of Ocean Sciences, Patricia Bay, B.C.
DHI	Danish Hydraulics Institute
DND	Department of National Defence
DP	decoupled propagation (model class)
DS	discrete spectral (model class; see also CD)
FNOC	Fleet Numerical Oceanographic Center, Monterey
GAPS	Gulf of Alaska Pilot Study
GLERL	Great Lakes Environmental Research Laboratory
GMT	Greenwich Mean Time (see also Z)
GSOWM	Global Spectral Ocean Wave Model (FNOC model)
HRS	Hydraulic Research Station, Wallingford, U.K.
IOS	Institute of Oceanographic Sciences, U.K.
JONSWAP	Joint North Sea Wave Program
MANMAR	manual marine (met. recording convention used at sea)
METOC	Meteorological and Oceanographic Centre
MPI	Max Plank Institute, Hamburg
MSL	mean sea level
NWP	numerical weather prediction
ODGP	Ocean Data Gathering Program
PM	Pierson-Moskowitz (an empirical spectrum)
PST	Pacific Standard Time
PTB	Pierson-Tick-Baer
RAO	response amplitude operator
SMB	Sverdrup-Munk-Bretschneider
SOWM	Spectral Ocean Wave Model (FNOC model)
SPECREF	Spectral Refraction model
SWAMP	Sea Wave Modelling Project
SWIM	Shallow Water Intercomparison of Three Numerical Wave Prediction Models
SWOP	Stereo Wave Observation Program
TC	Transport Canada
TMA	Texel-Marsen-Arsloe (an empirical spectrum)
WAM	Wave Model (international group for 3rd-generation models)
WAVAD	Waves (Advanced) model (an earlier version was called ADWAVE)
WES	U.S. Army Waterways Experiment Station, Vicksburg
WIS	Wave Information Study
WRIPS	Waverider Information Processing System
Z	zulu, meaning Greenwich Mean Time (see GMT)
°T	degrees true (i.e., relative to true north)
mb	millibar (a meteorological unit of pressure 1000 mb = 100 kPa)
nmi	nautical miles (1 nmi = 1.852 km = 1.15 statute miles)
rms	root mean square

1.0 INTRODUCTION

The purpose of this report is to present recommendations on how to provide wave forecasts in Canadian waters that satisfy user needs in the marine community. The recommendations follow from an understanding of how sea-states are parameterized, and hence how they are modelled using wind forecasts generated with numerical weather prediction models. The recommendations also follow from a review of end-user requirements for sea-state parameters, the lead times necessary in forecasts and the accuracies expected. Attention here is focused on the needs of offshore exploratory drilling operators, but includes other groups such as commercial fishermen, tow boat operators, consultants, navy and recreational boaters.

This review, being technical nature, discusses the approach taken to numerical wave prediction, what models have been developed in the past, which ones are current and under development, and which of these appear suitable for meeting Canadian needs. A strategy for wave forecasting is presented that deals with how one can organize regional wave forecasting in relation to the Canadian Meteorological Centre's (CMC's) existing numerical weather prediction services. This strategy considers the demands of wave prediction models for computer capacity and the feasibility of running these models fast enough to meet operational constraints.

This report recommends that wave forecasting services will best serve the user community if they are regional in scope and expertise rather than nationally centralized to produce a purely objective product. However, it does not argue who should provide those wave forecasting services. Parallel developments in wave models, microcomputer technology and data communications mean that such services could be organized by government or private sector firms, or the two working together. In fact, much of the wave modelling expertise in Canada resides in the private sector now, and several firms already provide numerical wave prediction services.

The report is organized into eight sections. Sea-state parameterization is considered first (Section 2) followed by a review of user requirements in Section 3. This review begins with a summary of what sea-state forecasts are presently available from government and private firms. Wave models are

discussed in Section 4, and CMC's numerical weather prediction model is described briefly in Section 5 in relation to wave forecasting requirements. An evaluation of CMC forecast winds is then discussed in Section 6 and concludes with a recommended wave forecasting strategy, linking the wave model specifications with the CMC operational weather model. Section 7 gives a summary of the conclusions, organized by report section, followed by the final recommendations in Section 8.

2.0 SEA-STATE DESCRIPTION: THE BASIS FOR MODELLING

To understand the statistical and numerical wave modelling procedures that have evolved, it is necessary to appreciate both the actual character of a wind-generated wave field and the conceptual simplifications that are employed to render the physical reality mathematically tractable.

2.1 The Spatial-Temporal Character of Ocean Waves

2.1.1 Spatial Measurements

To gain an impression of how waves usually appear in the ocean a contour plot of one stereo pair of aerial images is shown in Fig. 2.1. This plot, in which the white areas are wave crests and the dark areas troughs, was drawn from a regular 90 x 60 point grid of spot wave heights derived from the stereo images. The waves shown here were in the generation area with, at the time of the photographs, a mean overwater wind of 18 knots from 330°T. There is a discernible alignment of the crests implying a mean direction of propagation at about 30° to the right of the wind vector. Superimposed on this average pattern is a great deal of fine structure (down to about 20 m in length) which can be interpreted as the superposition of a large number of wave patterns of different wave lengths travelling at different angles to the wind.

If the range of angles associated with the individual wave patterns is wide, then the overall wave pattern appears disordered (as in Fig. 2.1), and the wind-waves are short-crested with the length along a crest only a few times the dominant wave length. Only after waves have propagated away from the active generation area do they become sorted out into long-crested swell waves.

The spatial, or directional character of wind-waves is now recognized to be important to engineering design. Recent papers by Huntington and Gilbert (1979), Huntington (1981), and Battjes (1981) discuss the analysis of wave loading on various structures in short-crested seas. Demonstrations seen in the wave tank at the Hydraulic Research Station (HRS), Wallingford, U.K., on the behaviour of ship hulls in short- and long-crested seas were also convincing as to the importance of the proper spatial description of sea-states for structural analysis (S.W. Huntington, HRS, pers. comm., 1981).

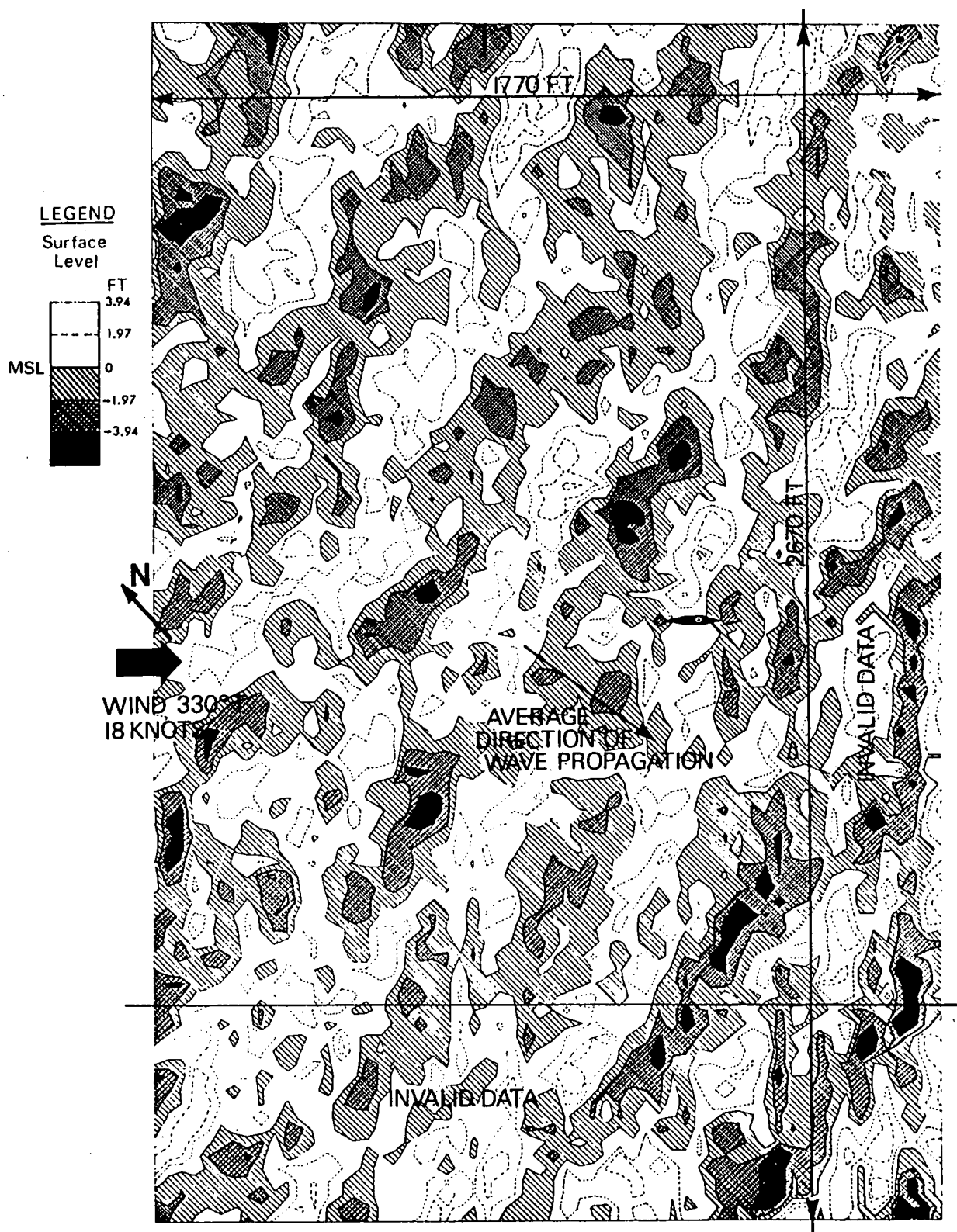


Fig. 2.1 Levelled contour analysis of the ocean surface. Contour interval 0.2 mm, where 0.1016 mm = 1 foot. Shaded areas are below mean sea level and clear areas are above mean sea level. (From Coté et al., 1960).

Measurement of the spatial properties of waves, by stereo image processing as used in the Stereo Wave Observation Program (SWOP) (Coté et al., 1960) and by Holthuijsen (1981), or by contour radar techniques (Walsh et al., 1978; 1981) is not yet practical as a means of routinely collecting ocean wave data. This is largely due to the complexity and expense of remote sensing and the subsequent data processing. Practical wave measurements are, therefore, made with relatively simple devices at fixed locations over some time interval. The wave properties that can be derived from a point-source time-series provide only a rough parametric description of the heights of waves and the angular spread of the energy about the mean wave direction. Nothing can be derived on the crest lengths and other three-dimensional details of the surface wave field. Most of the effort of wave modelling is thus directed to predicting simple wave parameters, equivalent to those derived from measurements, as a function of time. However, any model requires many point measurements to calibrate and verify its performance, often under a variety of environmental forcing conditions.

2.1.2 Temporal Measurements

Wave measurements at a point have been made with a wide variety of instruments which can be placed in three general classes: surface-piercing instruments, pressure-measuring devices and inertial measurements of wave accelerations (Stewart, 1980). In most cases, instruments in the first two classes have been made for special purpose applications or they have water depth limitations. Inertial instruments, which follow the sea surface, provide wave height measurements by twice integrating in time the acceleration signal of a vertically stabilized platform, and some instrument models also measure buoy tilt in two orthogonal directions.

One commercial instrument, the Datawell Waverider, has been used almost exclusively to collect offshore wave data in Canadian waters. These data are non-directional and any indication of wave direction must be inferred from the local wind. This procedure is unreliable for large unconfined water bodies and inadequate for directional wave model verification. A recent improvement (circa 1982) to these instruments has been effected by addition of a satellite transmission package. The modified Waveriders (called WRIPS buoys) can provide nearly real-time wave sensing to a shore

location from a mooring anywhere on the continental shelf.

Buoys that measure tilt in addition to the heave signal, called heave-pitch-roll buoys, provide estimates of the directional wave energy spectrum. Because the buoys measure wave slope, estimates of the directional distribution of all waves, regardless of their wavelength, can be obtained with a resolution of $\pm 50^\circ$ (Stewart, 1980). Although various buoy designs have some limitations--for example, the smaller, disk-shaped buoys do not accurately measure wave slopes near the tops of large breaking waves, the monster discus buoys tend to damp out the high frequency wave response but survive better in heavy seas, and the intermediate-sized toroidal buoys tend to capsize in heavy seas--the information they provide adds another dimension to our knowledge of the wave field. Because most wind-wave models are capable of providing directional information, measurements made with directional buoys are immediately useful for verifying the modelling process.

Heave-pitch-roll buoys are now available commercially, and in the case of the Datawell WAVEC, provide generally accepted measurements of wave height, and mean wave direction and angular spreading as functions of frequency. The spreading exponent, discussed in more detail later, is based on assumed models for the shape of distribution functions that have only one mode. In shallow water, where refraction may produce energy peaks in two or more distinct modes, these assumed forms for the angular distribution of energy are no longer valid. Multiple modes may also arise in nature when locally generated wind sea and swell cross, a situation that may arise in eastern Canadian waters when rapidly moving low pressure systems stall over the Labrador Sea. Then large waves generated by the system further south propagate across locally generated seas in the area where the storm is nearly stationary. One of the major problems with heave-pitch-roll measurements is the lack of a critical test of the goodness-of-fit of these assumed directional distributions. It is not yet possible to be sure that the derived results actually represent the sea-state well, although in most cases intuition suggests that they do.

The data recovered from any of these instruments is the time-series heave signal, η , with sufficient resolution to measure 2-s wave periods. The directional buoys provide two orthogonal slope signals referred for convenience to east and north. The acceleration signal $d^2\eta/dt^2$ is not usually available since it is integrated in the frequency rather than in the time domain.

Traditionally, wave buoys have been set to sample for a few (18 to 35) minutes once in every three hours. When the sea-state is fairly stationary, this sampling procedure provides adequate resolution. During storms, the offshore regulatory guidelines now specify that waves are continuously recorded when either wind speed or wave height exceeds a predetermined threshold. Such data are invaluable in assessing wave model performance during severe sea-states.

2.2 Wave Properties at a Point

Although the following discussion is based on measured data, the parameter definitions apply equally to wave modelling.

2.2.1 Wave Parameterization

A typical "20-minute" wave trace, $\eta(t)$, is shown in Fig. 2.2, composed of about 4000 data points containing approximately 90 twelve-second waves. It is clear that the wave amplitudes are highly variable, although the wave periods appear to be somewhat less so. Also apparent in this record is a wave group comprised of three consecutive large amplitude waves centred about the 250-second point of the time-series.

Individual wave heights are usually defined as the vertical distance from one wave trough (maximum negative excursion) to the next wave crest (maximum positive measurement). The corresponding wave period is the elapsed time between the zero-downcrossing preceding the trough and the zero-downcrossing following the crest. An enlarged illustration of these individual H and T definitions is shown in Fig. 2.3.

In most circumstances, the volume of information contained in a wave trace (e.g., Fig. 2.2) is too great to either comprehend or store. Instead, the η time-series is characterized by a few parameters (often just one

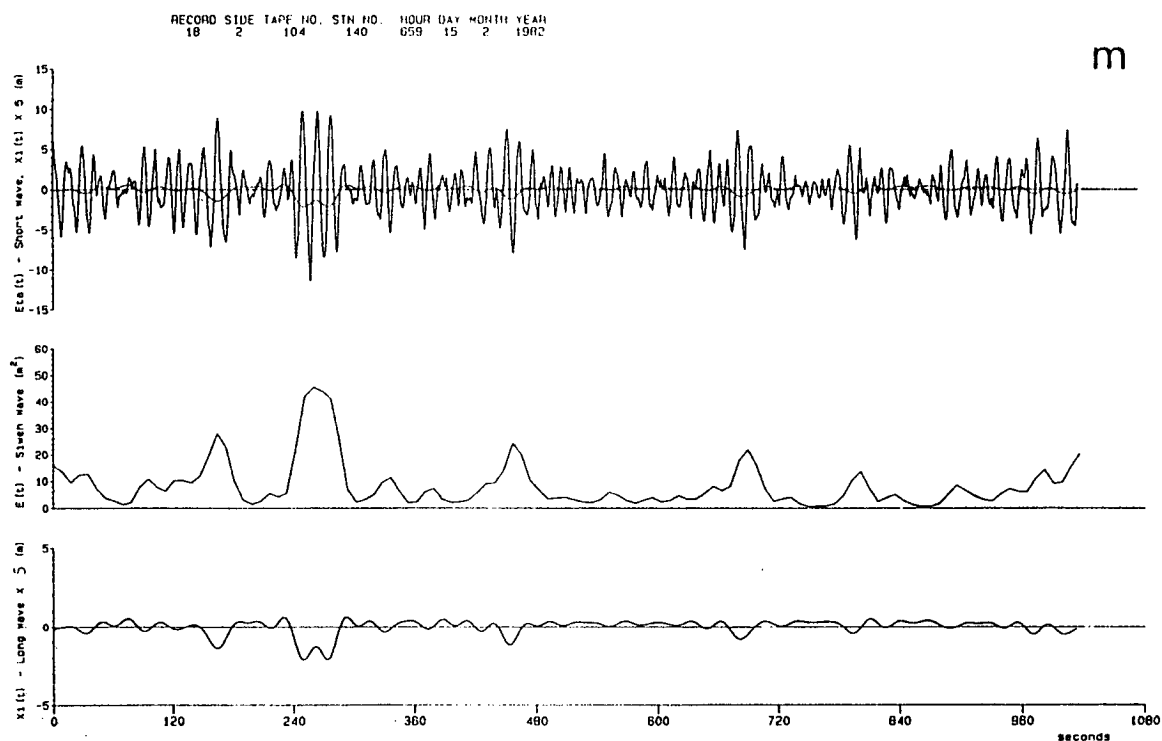


Fig. 2.2 A typical surface displacement record lasting about 18 min. This time-series was recorded at Station 140 on the Grand Banks at 06:59 GMT on February 15, 1982.

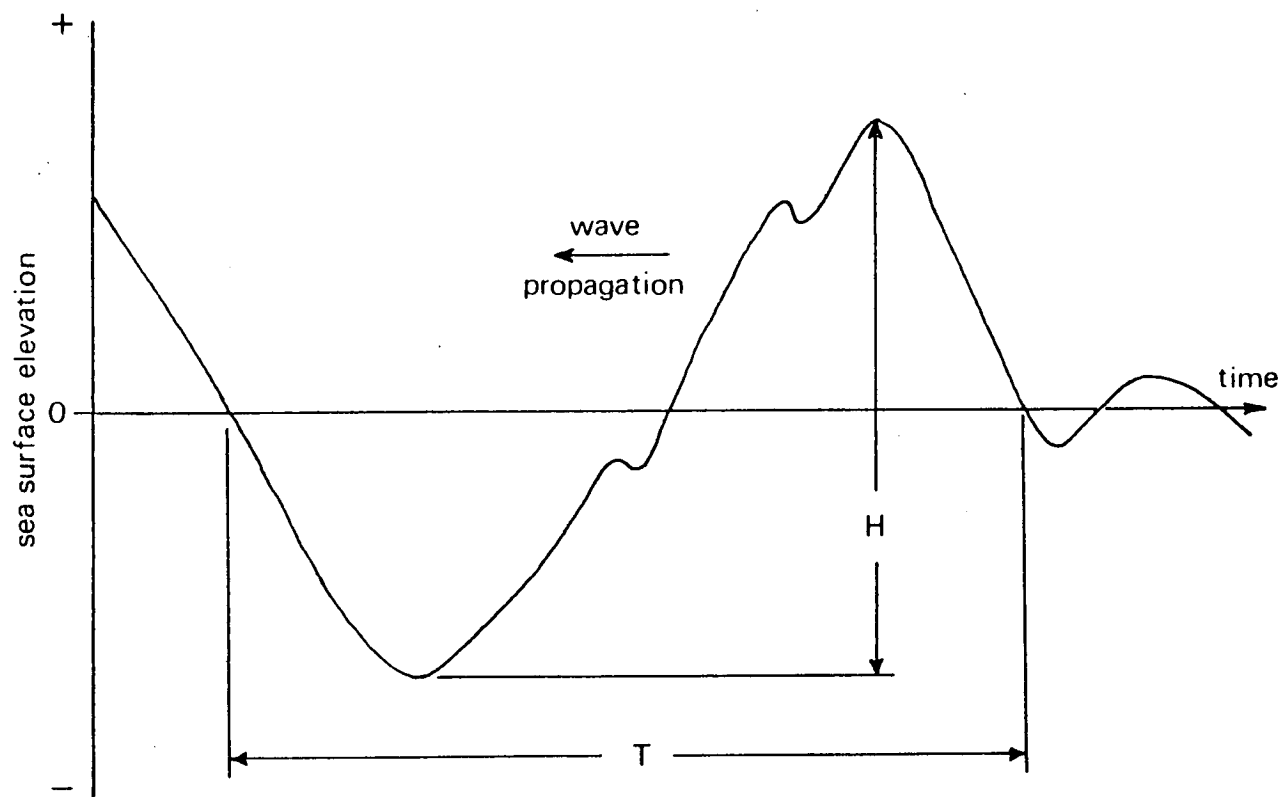


Fig. 2.3 Definition sketch on zero-crossing wave height and period.

representative wave height and one period), and a set of statistical arguments is employed to describe the probable size distribution of the individual heights and periods in the original sample. As yet, however, there is no theory to predict the likely ordering of those waves in time (or space).

The statistical theory of waves is based on the generally valid assumption that the sea surface displacement η is a random, normally-distributed function and that the envelope of that signal has a Rayleigh distribution (Longuet-Higgins, 1952). The probability density function of wave heights is written in general as

$$p(H) = \lim_{\Delta H \rightarrow 0} \frac{\text{Prob. } [H < H(t) \leq H + \Delta H]}{\Delta H} \quad (2.1)$$

which is the probability that at any time, t , the wave height $H(t)$ lies between values H and $H + \Delta H$. For the Rayleigh distribution, (2.1) becomes in the limit

$$p(H) = \frac{H}{4\sigma_\eta} \exp \left[-\frac{1}{8} \left(\frac{H}{\sigma_\eta} \right)^2 \right] \quad (2.2)$$

where σ_η is the standard deviation of the sea surface displacement $\eta(t)$.

The probability distribution function, expressing the probability that a wave height H exceeds a certain wave height H_0 , is defined as

$$P(H > H_0) = \int_{H_0}^{\infty} p(H) dH \quad (2.3)$$

Integrating (2.2) gives the Rayleigh distribution function as

$$P(H) = \exp \left[-\frac{1}{8} \left(\frac{H}{\sigma_\eta} \right)^2 \right] \quad (2.4)$$

Thus knowing only σ_η , the probable distribution of the individual wave heights is described by (2.2) and the probability of exceeding any particular value of H is specified by (2.4).

One of the most useful wave height parameterizations is the significant wave height defined as the average of the one-third highest waves in a sample and

denoted as $H_{1/3}$. An approximation of $H_{1/3}$ can be obtained for Rayleigh distributed wave heights (see for example Sarpkaya and Isaacson, 1981) which we will symbolize as H_s to distinguish the estimate from the exact average:

$$H_s = 4\sigma_\eta \quad (2.5)$$

The probability concept can be extended to give estimates of the most probable maximum wave height in a sequence of N consecutive waves. This value corresponds to the maximum in the probability density function, i.e., where $dp/dH = 0$. Forristall (1978) gives this expression as

$$H_{\max} = \sigma_\eta (8 \ln N)^{1/2} [1 + \gamma/2 \ln N] \quad (2.6)$$

where γ is 0.5722, a constant.

H_{\max} is not to be confused with the largest wave possible, but is the maximum wave with the greatest chance of occurring in N waves. For example, in a hindcast with wind fields that change every three hours, it is often assumed that sea-state conditions are stationary in 3-hour bands, and that the value $H_{\max}(3\text{-hours})$ can be estimated. If, for example, the average zero-crossing period of the waves is 12 s, then $N=900$ and

$$H_{\max}/\sigma_\eta = 7.68 \quad (2.7)$$

Since $H_s/\sigma_\eta = 4$, $H_{\max}/H_s = 1.92$; that is the maximum wave height is 1.92 times the significant wave height.

It is generally recognized that the Rayleigh distribution becomes progressively less accurate with increasing wave height, but if heights good to within 10% are adequate, it is acceptable. Improvements have been published by Forristall (1978), Longuet-Higgins (1980), Tayfun (1981) and summarized by Forristall (1984).

2.2.2 Spectral Parameterizations

The time-series shown in Fig. 2.2 is clearly oscillatory in time with a dominant periodicity. This periodic character of ocean waves is as important as the amplitudes of the signal. Time-series of this form are most conveniently analyzed in the frequency domain by Fourier transforming the time domain signal to provide a distribution of wave energy E as a

function of frequency f which is called a variance (or energy or power) spectrum. The analysis of ocean wave data by this method using the Fast Fourier Transforms provides a succinct description of the sea-state during each sampling period. The method was described by Pierson and Marks in 1952, and is now the standard spectral analysis technique for sea surface displacement records.

A distinct drawback to the spectral representation is that, in practice, E is a discrete function defined at evenly spaced frequencies. Thus, the resolution of the longer period (10 to 20 s) storm wave energy is quite poor since there are only half as many spectral energy estimates between 10 and 20 s (0.1 to 0.05 Hz) as there are between 5 and 10 s (0.2 to 0.1 Hz). Thus the greatest uncertainty in measured spectra (i.e. spectra calculated from measured η -series) is in the period range of most importance for wave modelling.

Non-Directional Spectra

Usually the data collected in 20-minute samples by a Waverider, for example, are analyzed to give one spectrum; one such spectrum is shown in Fig. 2.4, calculated from the data in Fig. 2.2. This spectrum is sharply peaked, produced by wind-waves with a dominant period of about 12 s.

The most important property of the variance spectrum is that

$$\sigma_{\eta}^2 = \int_0^{\infty} E(f) df = m_0 \quad (2.8)$$

linking the standard deviation of the sea level displacement with the integral of the wave energy spectrum. Thus the significant wave height can be approximated by

$$H_{m_0} = 4\sqrt{m_0} \quad (2.9)$$

denoted here as H_{m_0} to indicate that it has been calculated from the variance spectrum and not from a wave-by-wave analysis of the time domain data ($H_{1/3}$) or directly from the standard deviation of the sea surface (H_g).

Another important parameter that is derived from the spectrum is the peak spectral period defined as the inverse of the frequency band containing the

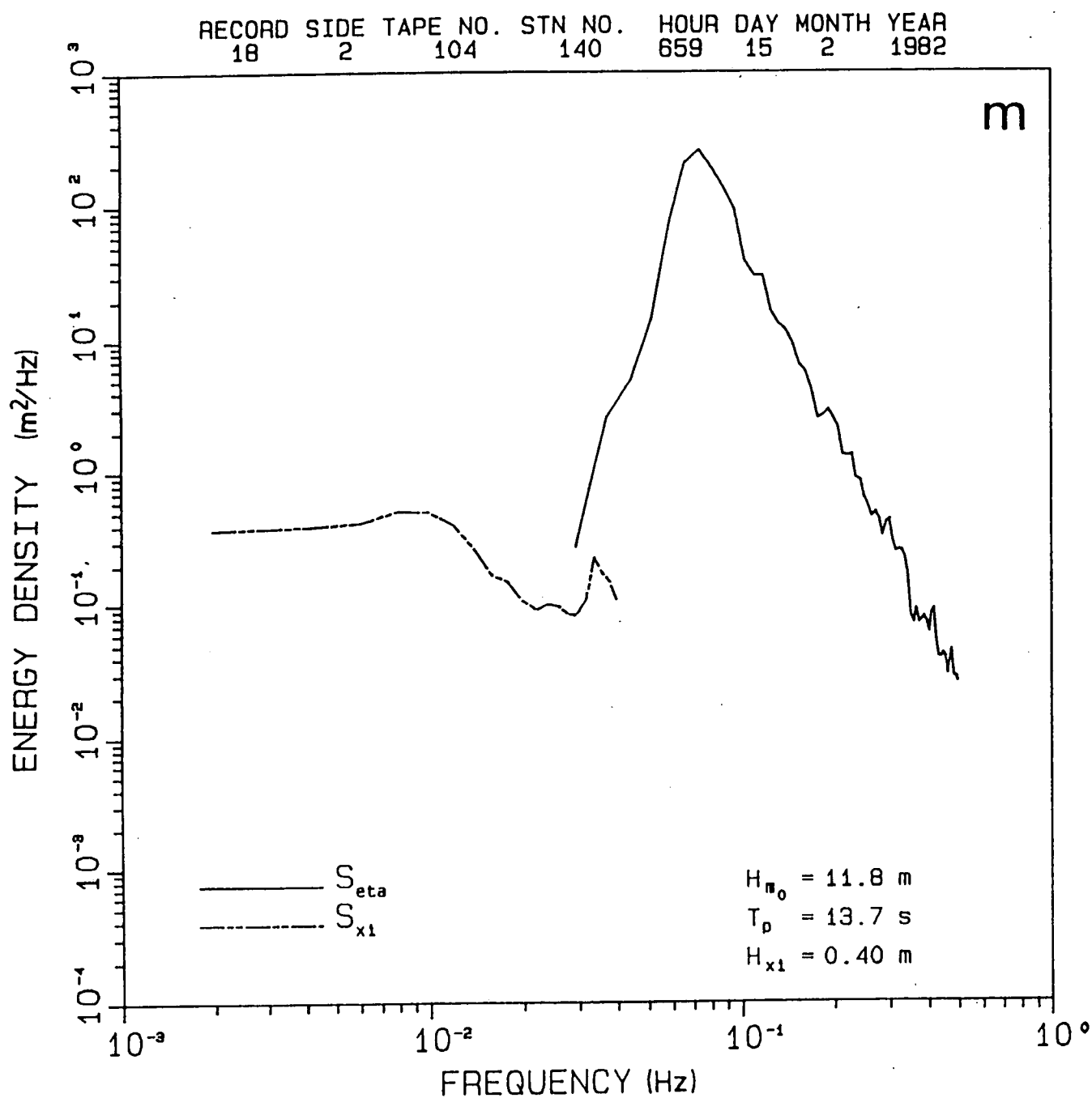


Fig. 2.4 Variance spectral density $E(f)$ of $\eta(t)$ recorded at 06:59 GMT, February 15, 1982 on the Grand Banks.

largest energy content, f_p :

$$T_p = 1/f_p \quad (2.10)$$

The power spectral approach to analyzing wave data provides a suitable parameterization of the sea-state: the dominant periodicities are identified, together with a measure of the average wave amplitude variance in the sample, and from that the significant wave height. From these parameters and a known distribution function for heights, maximum wave heights with specified probabilities of occurrence can then be calculated.

A number of studies (e.g. Wilson and Baird, 1972) have shown that for well-developed sea-states, the peak spectral periods and significant wave heights calculated from the spectrum correlate well with those values obtained in wave-by-wave analyses.

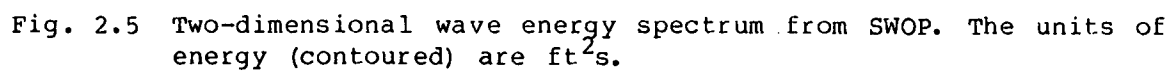
It must be emphasized that a spectrum is a statistical representation and that the estimate for each frequency has a corresponding range of confidence limits. Furthermore, phase information about the individual sinusoidal waves making up the spectrum is not retained in the analysis process, and consequently, information on the structure of amplitude or phase modulations, such as wave groups, is lost.

Directional Spectra

In deriving spectra the sea-state is considered to be a random process which may be represented by an infinite number of sinusoidal components travelling with different wave lengths, frequencies, and directions (referred to, say, the direction of the wind vector). Two-dimensional spectra can be represented in two ways:

- 1) in terms of wave length, λ , or wave number ($k=2\pi/\lambda$) and direction; and
- 2) in terms of frequency and direction.

A two-dimensional wave number spectrum is shown in Fig. 2.5 for the SWOP data in Fig. 2.1: it shows the variation of energy density $F(k, \theta)$ about the wind direction. The plot is made easier to interpret with the wave length scale (in feet). The predominant energy is contained in waves approximately 280 feet long travelling toward $180^\circ T$. There is some energy, determined



above the signal noise, down to wave lengths of about 60 feet. The secondary peak at $270^\circ T$ represents swell propagating toward the west: its energy content is obviously much lower than the wind-sea energy.

The polar representation of $F(f, \theta)$ shown in Fig. 2.6, which was calculated from data measured with a ship-borne recorder in October, 1959 (Cartwright, 1963) is the conventional method of specifying the energy density as a function of frequency and direction. The synoptic weather chart in Fig. 2.6 shows the storm pattern with respect to the observation point (station K): the winds were westerly and the predominant wave direction was $120^\circ T$; that is, waves were moving from the storm centre, toward the ESE.

Both directional spectra for F show smoothly varying functions for wave energy about the wind direction (or perhaps more appropriately, about the mean direction of wave propagation, θ_0) with a dominant energy peak. The Cartwright spectrum is slightly more symmetric about the mean wave direction than the SWOP spectrum; both spectra suggest, however, that a fairly simple parameterization of the spectrum should be possible.

The usual approach is to consider the two-dimensional spectrum to be equivalent to a one-dimensional spectrum multiplied by a spreading function $G(f, \theta)$, such that

$$F(f, \theta) = E(f) \cdot G(f, \theta) \quad (2.11)$$

where G must satisfy

$$\int_{-\pi}^{\pi} G(f, \theta) d\theta = 1 \quad (2.12)$$

Much of the effort following the work of SWOP (Coté et al., 1960), by Mitsuyasu et al. (1975), Mitsuyasu (1981), and Hasselmann et al. (1973) has been directed toward establishing the best functional form for G . The most widely used forms are:

cosine-squared (St. Denis and Pierson, 1953)

$$G(\theta) = \begin{cases} \frac{2}{\pi} \cos^2 \theta, & |\theta| \leq \pi/2 \\ 0 & \text{otherwise} \end{cases} \quad (2.13)$$

where G is independent of wave frequency;

cosine-power (Longuet-Higgins et al., 1961)

$$G(\theta) = C(s) \cos^{2s} \left(\frac{\theta - \theta_0}{2} \right) \quad (2.14)$$

where $C(s)$ is the normalizing factor needed to ensure that (2.12) is satisfied, and s is a function of frequency. This spreading function is shown for values of s in Fig. 2.7. The normalizing factor is given by expansions in terms of Gamma functions (see e.g. Sarpkaya and Isaacson, 1981, p. 517; Borgman, 1969). Mitsuyasu et al. (1975) and Mitsuyasu and Mizuno (1971) have demonstrated the appropriateness of (2.14) for all frequencies and have given the variation of s with frequency (Fig. 2.8). This figure shows that the largest values, of about 10, occur at the peak frequency; that is, the wave energy is well focussed along the mean wave direction. At higher and lower frequencies the energy is more spread out around the mean direction of wave propagation.

The spectral wave parameters determined from directional wave measurements are the spectral energy $E(f)$, the spreading function $s(f)$ and the mean wave direction, also as a function of frequency. Because the cosine function is symmetric, the resulting two-dimensional spectrum is also symmetric (in direction) at each frequency. Two-dimensional spectra provide information on the directional properties of the sea-state only to within the resolving power of the instrumentation and data analysis methods.

The spread of energy about the mean direction of wave travel also indicates, qualitatively, how confused the sea is. It provides a link to a picture like that in Fig. 2.1 that, in a very subjective way, allows one to speculate on the composition of the wave field. The one-dimensional spectra frequently are bimodal--one mode corresponding to swell and another to a locally-generated wind sea, and these are often well resolved. Although the wind-sea directionality might be inferred in one-dimensional spectra from the wind, there is no basis on which to estimate the swell direction.

2.3 Parametric Spectra

Over the past few decades, there have been numerous attempts to formulate a

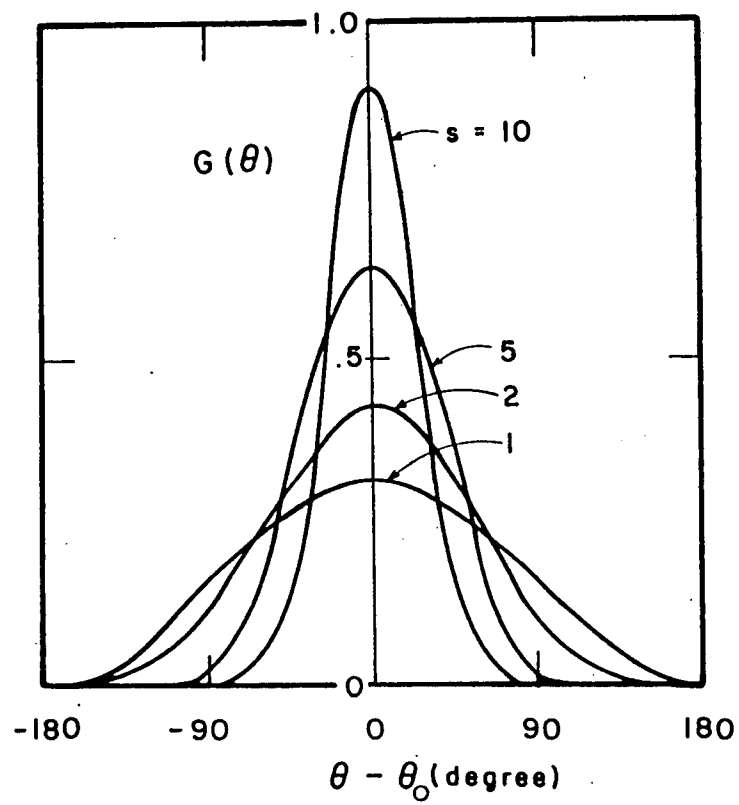


Fig. 2.7 The directional spreading function $G(\theta)$ for various powers, s .

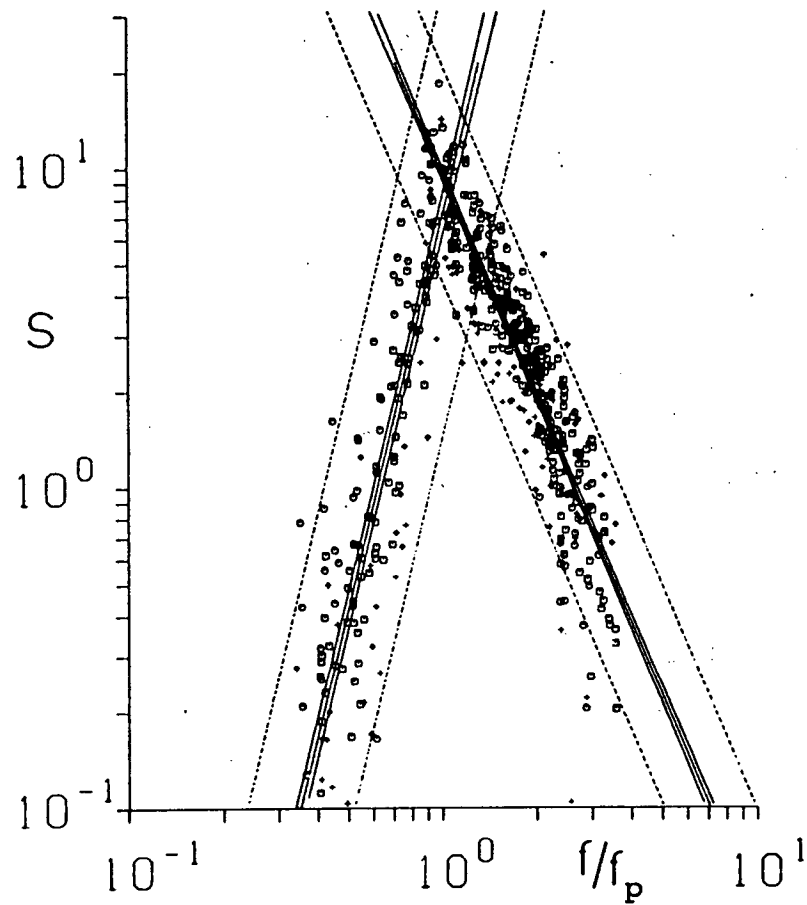


Fig. 2.8 Variation of the spreading function, s , with non-dimensional frequency, f/f_p . (From Hasselmann et al., 1980).

"universal" spectral equation, defined in terms of only a few physical parameters (e.g., wind speed, fetch, significant wave height, and characteristic wave period). Of these formulations (called parametric spectra), the two most commonly encountered ones are the Pierson-Moskowitz (PM) spectrum and the Joint North Sea Wave Program (JONSWAP) spectrum.

Such parametric spectra are important in two respects for wave modelling. First, if they represent the spectrum that is in equilibrium between growth and dissipation processes for a given steady wind under specified fetch conditions, they can be used as an upper bound on wave growth. In this role they function as "saturation" spectra; in older models the PM spectrum was often used this way. The disadvantage in doing this is that it forces the predicted spectrum to conform to the predetermined saturated spectral form, at least over some range of frequencies, and the model result is then only as good as the bounding form. Naturally, these equilibrium spectra have been carefully derived from oceanic measurements, and are expected to be representative of fully-developed sea states.

Second, because these spectral forms contain only a few defining parameters (from 2 to 5) they can be used as the basis for predictive models provided that the variation of each parameter with wind speed, fetch, and duration can be established. This approach evolved out of the JONSWAP experiment (Hasselmann et al., 1973) and paved the way for a whole new class of models.

2.3.1 The PM Spectrum

Pierson and Moskowitz (1964) proposed the following spectral form for fully-developed wind seas based on the similarity theory of Kitaigorodskii (1962).

$$\hat{E}(f) = \alpha g^2 (2\pi)^{-4} f^{-5} \exp[0.74 \left(\frac{g}{2\pi U} \right)^4 / f^4] \quad (2.15)$$

in which

α is Phillips' constant (=0.0081) and

U is wind speed.

Many models use the PM spectrum as the energy saturation limit for growth.

2.3.2 The JONSWAP Spectrum

The Joint North Sea Wave Program was carried out in 1968 and 1969 to obtain

wave spectral data of sufficient quality and density to determine empirically the structure of the source function, by which energy is transferred from the wind into the wave field (Hasselmann et al., 1973). The experiment was a natural extension of the work of Snyder and Cox (1966) and Barnett and Wilkerson (1967) who investigated the growth of wave components and spectra in space and time.

Analysis of the data showed that fetch-limited growing wind-sea spectra exhibited a sharp spectral peak that shifted toward lower frequencies as the spectrum revolved. The one-dimensional frequency spectrum $E(f)$, was parameterized with a function of the form:

$$\hat{E}(f) = \alpha g^2 (2\pi)^{-4} f^{-5} \exp\left(\frac{-5}{4} \left(\frac{f}{f_p}\right)^{-4}\right) \gamma \exp\left(\frac{-(f-f_p)^2}{2\sigma^2 f_p^2}\right) \quad (2.16)$$

where

$$\sigma = \begin{cases} \sigma_a & \text{if } f < f_p \\ \sigma_b & \text{if } f > f_p \end{cases}$$

α = the Phillips' constant

f_p = frequency at the point of maximum energy
(peak frequency)

σ_a, σ_b = shape factors

$\gamma \exp \frac{-(f-f_p)^2}{2\sigma^2 f_p^2}$ = peak enhancement factor which multiplies the PM spectrum function.

The peak enhancement factor heightens the spectrum in fetch-limited seas to model the overshoot effect measured in JONSWAP, and revealed earlier by Barnett and Wilkerson (1967). The overshoot effect describes the observation that under steady wind conditions, the energy in higher frequencies can exceed the eventual equilibrium energy level attained at those frequencies. Five spectra are shown in Fig. 2.9, at different fetches in the JONSWAP program: both measured and fitted spectra (Equation 2.16) are shown. The increasing energy content toward longer fetches (10 and 11), as well as the shift of the peak frequency f_p toward lower frequencies is evident.

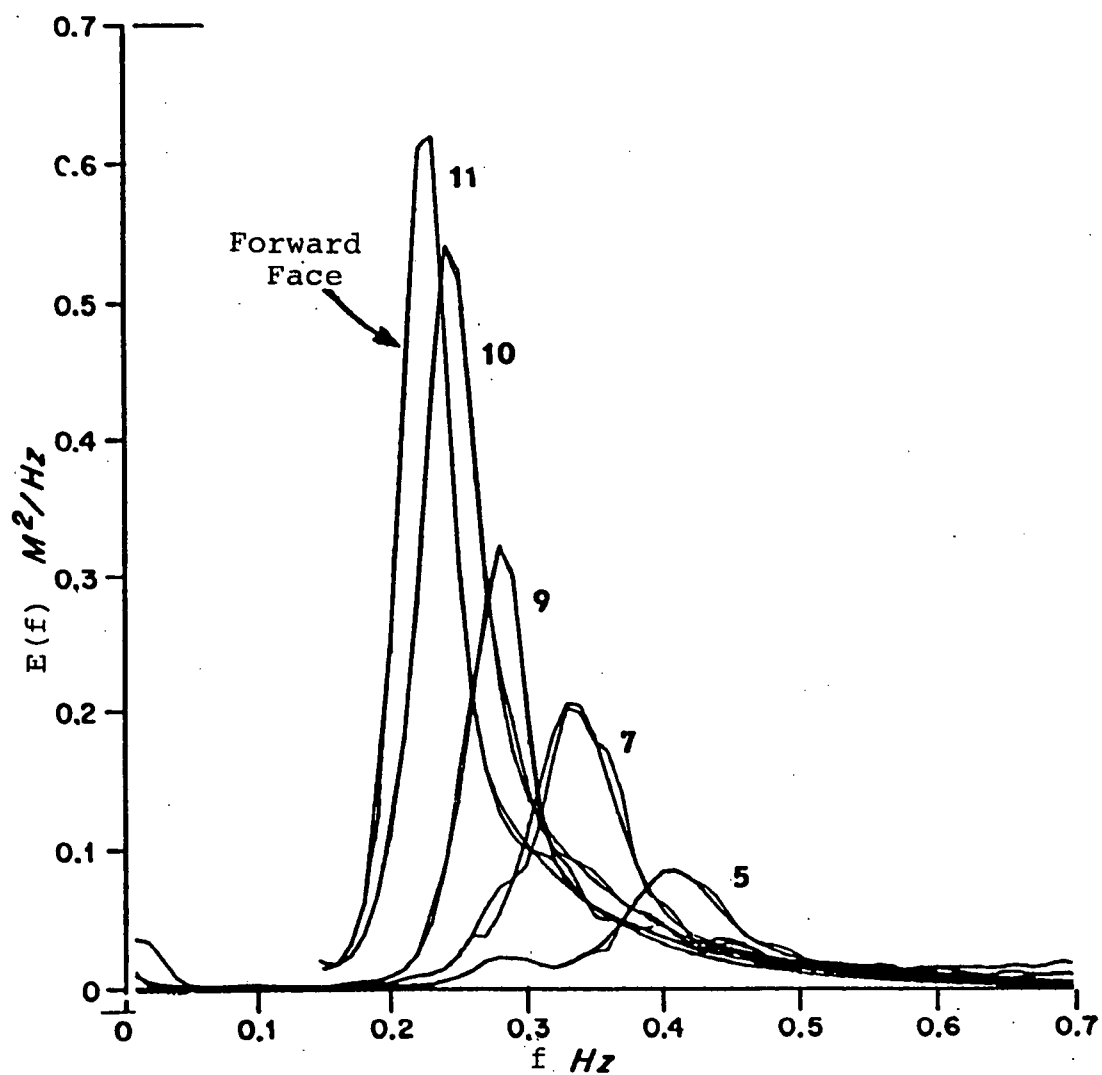


Fig. 2.9 A series of fetch limited wave spectra for offshore winds at JONSWAP stations 5, 7, 9, 10 and 11. (From Hasselmann et al., 1973).

Hasselmann et al. (1973) interpreted the evolution of sharply peaked spectra in terms of a nonlinear transfer of energy, due to resonant wave-wave interactions, which move energy going into central frequencies from the wind toward both higher and lower frequencies in the spectrum. This process is found to be self-stabilizing so that the same functional form for the spectrum is always applicable. The nonlinear energy transfer also accounts for the continual shift of the peak energy toward lower frequencies and explains the large growth rates of waves on the so-called forward face of the spectrum.

2.4 The Energy Balance Equation

Virtually all wave prediction models are based on equations describing the conservation of wave energy at specified locations. The processes that must be considered are: propagation of wave energy toward and away from the point, growth due to local winds, nonlinear transfer processes that redistribute energy between frequency components, and dissipation due to whitecapping and bottom friction. The energy balance describing these processes is written as

$$\frac{\partial}{\partial t} F(f, \theta) - c_g \cdot \nabla F(f, \theta) = S(f, \theta) \quad (2.17)$$

where c_g is the wave group velocity as a function of f and S is the net energy source function.

In some models this equation is integrated with respect to θ to yield the energy equation, written here in one spatial dimension (Hasselmann et al., 1976).

$$\frac{\partial}{\partial t} E(f) + c_g(f) \cdot \frac{\partial E(f)}{\partial x} = S(f) \quad (2.18)$$

In modelling applications, $F(f, \theta)$ can be obtained by applying a spreading function to the solution of (2.18) as described by (2.11).

The net energy source function S which governs the input of energy to the wave field was described by Hasselmann et al. (1973) in terms of three processes:

$$S = S_{in} + S_{nl} + S_{ds} \quad (2.19)$$

with the following meaning:

- S_{in} = the input of energy from the wind
- S_{nl} = the nonlinear energy transfer process
- S_{ds} = the energy dissipation process (whitecapping).

These processes are shown schematically in Fig. 2.10, together with the resultant net transfer curve as a function of frequency.

The nonlinear transfer mechanism plays a crucial role. The magnitude of S_{nl} can be computed by integrating the Boltzmann equations (Hasselmann, 1962; 1963a; 1963b; Sell and Hasselmann, 1972) or by the method of Longuet-Higgins (1975) as reported by Fox (1976). Because these computations are complex and computer-time consuming, they are not done routinely within the wave modelling context. Methods of including the nonlinear transfer mechanism are discussed with the individual models that incorporate it later in this report.

In JONSWAP, the term S_{nl} was evaluated for individual test cases and combined with the data for S to examine the remaining two terms in (2.19), i.e., $S_{in} + S_{ds} = S - S_{nl}$. S_{ds} was assumed to account for all dissipation mechanisms, primarily whitecapping, but also for energy transfers between spectral components such as the attenuation of long waves by damped short waves (Hasselmann et al., 1973). Assuming that S_{in} has a similar distribution to the spectrum itself, in accordance with linear wave growth theories, the process model shown in Fig. 2.10 can be inferred. The partition of energy between S_{in} and S_{ds} could not, however, be derived directly from the JONSWAP data.

2.5 Wave Model Output Products

Wave models may be grouped in three classes:

- (1) parametric wave height models in which simple empirical rules relate significant wave height and period to wind speed and fetch or duration of that wind;
- (2) parametric spectral models in which an invariant spectral form as

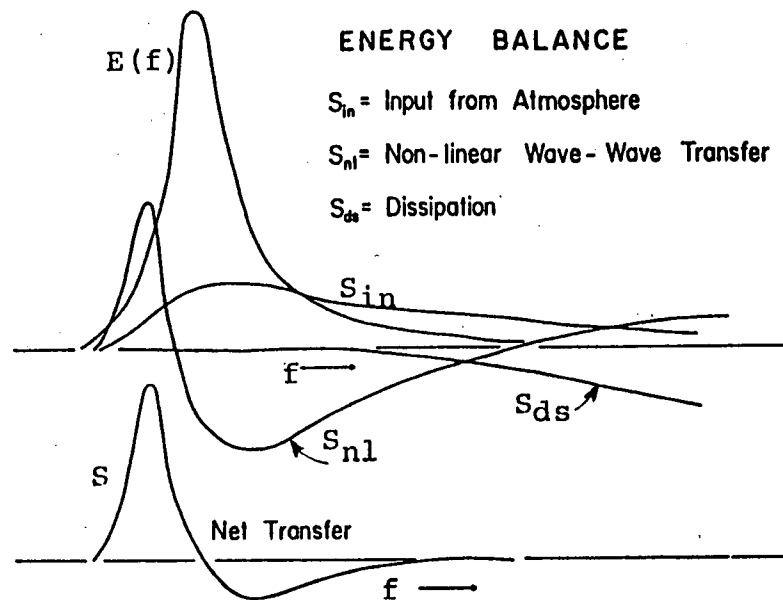


Fig. 2.10 Schematic diagram of the spectral wave energy balance. (From Hasselmann et al., 1973).

a continuous function of frequency is assumed, the details of which are defined by a few parameters (peak frequency, spectral peakedness, the Phillips parameter, and so on): by modelling the sources and sinks of wave energy, the conservation of energy equation can be solved for the spectral parameters and, hence, the wave spectrum itself; and.

- (3) discrete spectral models in which energy in discrete frequency bins is propagated with the appropriate group velocity, and wave growth and decay are modelled with empirical relationships to obtain a directional wave spectrum defined in space and time at pre-selected sets of discrete frequencies and directions.

As a result, the wave forecast data products that can be obtained from each are somewhat different. There are also a number of hybrid models in which wind sea is modelled by the parametric spectral method and swell is defined by the discrete spectral approach or ray tracing techniques.

The spectral models have evolved with improvements in understanding of the physics of wave generation. The "first-generation" models were discrete spectral formulations that considered the frequency bins to be independent of each other. Hasselmann et al. (1973) have shown not only that interactions between the frequencies (wave-wave interactions) are important, but also that during the growth stage of wind seas, they are the principal source of energy on the low frequency forward face of the spectrum. The "second-generation" of discrete spectral models mimicked these interactions by redistribution of the energy over the frequency bins after each modelling time step. It was the difficulty of generalizing this energy redistribution mechanism for arbitrary spectra that gave impetus to the parametric spectral modelling method. These models too are "second generation," however, in that they have had to include a priori restrictions on spectral shape because an accurate representation of the nonlinear wave-wave interaction process that can be evaluated economically is not available.

The "third-generation" model proposed by the WAM Group (Komen, 1984) will be based on a complete representation of all source terms in the energy conservation equation that will remove all a priori restrictions on spectral

shape. Some preliminary results of this third-generation model have been presented (Komen, 1984), but full implementation is still a few years away.

Output Forms

Parametric wave height models are site-specific formulations which take a time-series of wind speed and direction at the forecast site and a definition of open-water fetch in a set of directional sectors to produce a time-series of significant wave height, significant wave period, and predominant wave direction. For more than one forecast site, the model is simply re-run with the appropriate wind forcing and fetch. Since there is no explicit modelling of wave propagation, swell cannot be included.

Parametric spectral wave models are usually applied on a two-dimensional grid, and provide predictions of the one-dimensional spectrum $E(f)$ at each grid point and at each time step. From these data, the fields of H_{m0} and T_p are readily derived. Swell is usually included in the spectrum. Wind sea and swell directions can also be obtained from the local wind and the direction of rays containing dominant swell energy respectively.

Discrete spectral models differ by describing the two-dimensional spectrum in terms of a finite number of frequencies and directions; for example, this description is often written

$$F(f, \theta, \vec{x}, t) = F(f_m, \theta_n, \vec{x}, t),$$

$$f_m = 0.040 + 0.015m \text{ Hz, } m = 0, 1, \dots, 16$$

$$\theta_n = 15n \text{ degrees, } n = 1, \dots, 24$$

where the continuum spectrum $F(f, \theta, \vec{x}, t)$ is resolved with 17 frequency bands (periods of 3.6 to 25 s) and 24 directional bands (15° each) at each point \vec{x} and time t . The models, also applied on a two-dimensional grid, give spectral predictions consisting of about 400 degrees of freedom. Wind-sea and swell energies are resolved for direction to the extent of the chosen discretization. Two-dimensional (f, θ) spectra, showing multi-modal forms where these occur, are readily plotted, and as above, fields of H_{m0} and T_p can be obtained by integrating the spectra at each grid point. In principle these models provide more information than can be derived from heave-pitch-

roll measurements; thus, they are not totally verifiable with present methods of recording directional data.

Limitations of the Spectral Description

All modern wave modelling developments admit the impossibility of simulating the deterministic structure of individual waves and are based on reproducing the variance spectrum.

It is worth reviewing, then, the major limitations associated with wave spectra before discussing in detail the modelling approaches, which are so dominated by the "spectral convention." The chief difficulty is the loss of phase information and the aggregation of wave-by-wave properties into one statistical picture. As a result, the spectra provide quantitative data about average or probabilistic parameters of the wave field in terms of a sample of a few hundred waves.

An examination of virtually any time-series of water surface displacement shows, however, modulations in height or period associated with groups of large waves. The problem in analyzing these wave groups is that they are an intermittent phenomenon, at least in terms of the length of present data samples, and if they have a periodicity it is not clearly evident. Work on wave groups has been reported by Goda (1970), Nagai (1973), Nolte and Hsu (1973), Rye (1974), Ewing (1973), Goda (1976), Funke and Mansard (1979) and Donelan (1979). The important point here is that the spectral representation provides no insight into the magnitude of large waves in a group, or the probability of wave group occurrence at a particular location. Thus a model which seeks to relate changes in spectral energy to changes in wind cannot provide data on wave grouping and, extending this notion, on the formation of episodic waves or other individual-wave properties.

The fundamental concept behind the spectral approach is that the sea waves represent a stationary, random process in which the total variation can be represented as an infinite set of sinusoidal waves, each of which propagates energy at its own group velocity. Non-linear processes are known to take place within the wave field (Hasselmann, 1962; 1963a; 1963b) but these are assumed to be weak processes that slowly exchange energy between waves of

different frequency. The models described in this report view the air-sea interface this way.

The recent work of Toba (1978), Lake et al. (1977) and Lake and Yuen (1978) challenges this theory. Preliminary observations show that the group velocity of waves with frequencies higher than the spectral peak frequency deviates significantly from linear theory, and that instead, these short wave group velocities are coupled to the dominant waves in the spectrum. Toba (1978) and Lake and Yuen (1978) argue that the wave spectrum is governed not by weakly, but by strongly nonlinear processes. The spectrum in this sense represents a coherent system of bound waves, not a system of randomly propagating free waves.

Data collected to date supporting this proposition come from laboratory flume experiments, and their applicability to open ocean conditions has not been demonstrated. Models based on the theory of strong interactions (Schroedinger Equation), or weak interactions (many of the currently available spectral models) both produce growing spectra with an f^{-5} high-frequency dependence, and source functions linked to the spectral peak location. For this reason, the use of either theoretical base with empirical coupling to the wind must lead to similar results (Resio, 1981). The question of which physics to model the spectral evolution with in the ocean is as yet unresolved. The purpose of introducing these arguments here is to present a counter-view of the processes governing the wave spectra from that described by Hasselmann, upon which so much subsequent modelling has been based.

3.0 USER REQUIREMENTS

The users of wave forecast information compose a very diverse group: offshore oil and gas operators, commercial shipping, commercial fisheries, government (military, Coast Guard, certain regulatory and research departments), and recreational boaters. For all of them, the common and overriding requirement is for marine forecasts that allow them to judge correctly for themselves the safety and efficiency of their proposed endeavours.

Economic constraints sharpen the focus of requirements for especially the first three user groups--offshore oil and gas operators, commercial shipping and fisheries--in terms of greater precision and accuracy in the prognoses. Because of the diversity of operations in day-to-day hydrocarbon exploration and the restricted geographical extent of a given wellsite, the needs of this group are the most varied although not necessarily the most demanding.

3.1 The Perspective of This Review

The objective of this portion of the study was to enumerate the wave forecast requirements of each user group as they perceive and relay them, taking geographical variations into consideration. Interviews were conducted with many east coast and Beaufort Sea oil operators (Petro-Canada, Mobil, Home, Shell, Husky/Bow Valley, Esso and Dome); with several branches of the Atmospheric Environment Service (Canadian Meteorological Centre, Montreal; Arctic Weather Centre personnel in Edmonton; Pacific Weather Centre, Vancouver; and AES, Atlantic Region, Bedford); with METOC personnel in Halifax to identify military requirements; and with west coast Canadian Coast Guard. In the case of the offshore operators, requirements were discussed with those individuals responsible for making decisions directly affected by weather: logistics managers dealing with supply vessels and helicopter services, environmental coordinators responsible for interpreting forecast information for operational and safety needs (emergency evacuation), tool pushers on rigs and the rig masters who ultimately have responsibility for vessel safety. Comments were also received from representatives of the west coast fishing industry, the east coast fishery, tug and barge operators and a few recreational boaters. User needs in the Great Lakes that are uniquely identifiable for that geographical region have not been addressed.

These communications revealed a good general understanding of sea-state and, through experience, how it affects individual operations. The typical descriptors are characteristic wave height, period, and direction, but to small vessel operators wave steepness and phenomena caused by interaction with bathymetry, topography and currents are also significant parameters that might be forecast.

In discussing users' needs, it is important to recognize the diversity of opinion that such a wide-ranging community generates. This diversity is apparent not only among user groups, but also within the groups themselves, depending upon the background, experience and responsibilities of the individual to whom one is speaking. There are short-term (say 0 to 24 h) and long-term site-specific requirements, and also short- and long-term regional needs. These may be satisfied by relatively general threshold-duration criteria for some users, but others may require fairly precise storm maxima specification. Recreational and fishing industry mariners are accustomed to descriptors like "storm" and "gale" and understand their vessels' capabilities in those terms whereas the oil and gas industry is more quantitative and can specify activity sea-state thresholds to the nearest metre or half metre. This ability is a natural consequence of experience at sea where it is instinctive to calibrate crucial activities (diving, inspection, and some down-hole functions on floating rigs) to visual and Waverider observations that are essentially always available on the rigs. Transiting vessels may have exceptional requirements for very localized warnings where orographic effects influence sea-state over short spatial scales or where opposing currents exacerbate otherwise acceptable wave conditions by steepening and breaking.

Inevitably, the comments elicited are coloured by a national awareness of the importance of sea-state generated by three recent events, all of them caused by intense storms--loss of the Ocean Ranger rig and crew in February 1982 on the Grand Banks, losses to the nearshore fishing fleets in 1984 and 1985 off the west coast of Vancouver Island, and the extensive damage to an artificial island resulting in the loss of a drilling rig and barge in September 1985 in the Beaufort Sea. Because there was no loss of life in the Beaufort event, and undoubtedly because, after nearly five years, the

impact of the Ocean Ranger sinking is fading, the perceived importance of sea-state forecasting is a stronger issue among west coast fishermen than in the Canadian oil and gas operations.

The instinct of the offshore industry to these "disasters" is to add more "armour" through stronger components, better design and improved operating procedures to increase the survivability of their physical facilities and thereby to ensure the safety of their personnel. Furthermore, it is very unlikely that the outcome of either oil industry event was influenced by sea-state forecasting. This technical approach to dealing with life at sea clearly affects the perception of wave prognosis requirements in an industry with a goal to make tactical decision making as independent of environment as possible.

The fishing fleets are much more vulnerable, they recognize it and they express their concern for improving all aspects of weather reporting and forecasting, often in well-focused, pointed terms. Their problems are exacerbated on the west coast by short open seasons for some valuable species, most notably for herring which must be harvested in a brief period that is likely to contain late winter, early spring storms. These mariners have a more holistic approach to environment than those whose vessels lend them more personal safety and comfort. Those operators who are self-employed will also tend to take more risks than employees whose remuneration is not so intimately tied to occupational success. With a view to minimizing those risks, more reliance on the various forms of governmental assistance (like weather forecasting) is a natural reaction.

The remainder of this section discusses the uses of wave forecast data and the expectations of users in terms of timeliness, precision, accuracy and presentation concentrating on the opinions expressed by offshore oil and gas operators. The needs of the other user groups are also reviewed, particularly those that contrast the oil and gas industry demands. Recommendations of how these wide-ranging needs might be met are given in Section 8.

Other background information may be found in Hodgins and Harry (1984),

Hodgins (1984), and LeBlond (1984). A survey of over 700 west coast users of weather information services was conducted in 1986 jointly by AES, Vancouver and the Institute of Ocean Sciences, Sidney, B.C. (R.F. Henry, IOS, pers. comm., 1986). Use has been made of these other investigations to interpret and expand some of the comments obtained in this study.

3.2 Marine Weather and Wave Forecast Services

Marine weather forecasts are issued by regional offices of the Atmospheric Environment Service (AES) for both eastern Canadian waters and British Columbia coastal areas. These forecasts contain sea-state information in addition to meteorological parameters, and are broadcast by Canadian Coast Guard radio stations, Weatheradio Canada, and in some instances by commercial radio stations. Facilities for continuous VHF-FM weather broadcasts are also being upgraded along Canadian coasts. Arctic weather and ice forecasts are provided by AES but do not routinely contain sea-state information.

In addition to these services available from Environment Canada and the Coast Guard, site- or route-specific weather and sea-state forecasts are provided by private firms under contract to various end-users. These include services to the offshore oil and gas industry, and services to commercial shipping agencies for optimum ship routing. Navies also make use of weather and sea-state forecasts for ship routing. The relationship of the private forecast firms in Canada to the Atmospheric Environment Services has been discussed by Hodgins and Harry (1984).

In this section we review the type of information contained in marine forecasts issued by these agencies, and discuss how various end-users make use of the information in their activities. This review provides a basis for summarizing their requirements for wave data and improved services.

3.2.1 Government of Canada Services

"Marine weather forecasts" are issued four times daily by AES, and are supplemented as required by "marine warnings." The marine warnings are advisories of changes in weather that pose a hazard to mariners. The forecasts consist of a "synopsis" followed by marine area forecasts. The east and west coasts of Canada are divided into "areas" that separate

offshore waters from coastal zones, and allow for spatial variations in weather; the breakdown for western Canada is shown in Fig. 3.1 and a similar but larger system of 28 areas is used in eastern coastal waters. The area forecasts are followed by an "outlook" valid for 24 hours. A typical marine forecast for the west coast is reproduced below:

"Synopsis

Light to moderate winds are blowing across all marine areas early this morning and visibilities are good. A developing storm located near 40 north 150 west with central pressure 1000 millibars is moving northeast at 35 knots and is expected to reach a position 300 miles west of Cape Scott early Tuesday morning with a central pressure of 975 millibars. This storm will bring easterly gales to the off-shore areas this evening and to the remainder of the areas tonight and Tuesday. The associated frontal system will likely bring 4 to 5 hours of storm force southeasterly winds to some areas on Tuesday. Visibilities will become restricted in rain and fog patches on Tuesday.

•
•
•

NORTH COAST: Dixon Entrance

Gale warning issued. Variable winds of 15 knots becoming southeast 30 this evening and increasing to southeast gales 35 to 45 early Tuesday. Cloudy. Rain beginning after midnight. Visibilities 3 miles in rain. Outlook--gale to storm force southeasterlies.

OFFSHORE: Bowie

Gale warning issued. Southeast winds 20 knots increasing to easterly gales 35 to 45 knots this evening. Cloudy. Rain and fog patches tonight. Visibilities 3 miles in rain and near zero in fog. Seas 2 metres increasing to 7 to 10 metres tonight. Outlook--northwesterly gales. Seas 5 to 8 metres."

The forecast elements include wind speed with information on gusts or squalls as necessary, including descriptive terms, wind directions, sky cover, "weather," temperature, and visibility. Sea-state is given as a wave height range that represents the significant wave height of the combined seas (i.e., wind-sea plus swell). Wave periods and directions are not routinely specified.

In the synopsis or outlook, wind speeds may be given in descriptive terms which have the following meanings:

Light Winds	0-11 knots
Moderate Winds	12-19 knots
Strong Winds	20-34 knots
Gales	35-47 knots
Storm Force Winds	48 knots and higher
Hurricane Force Winds	64 knots and higher.

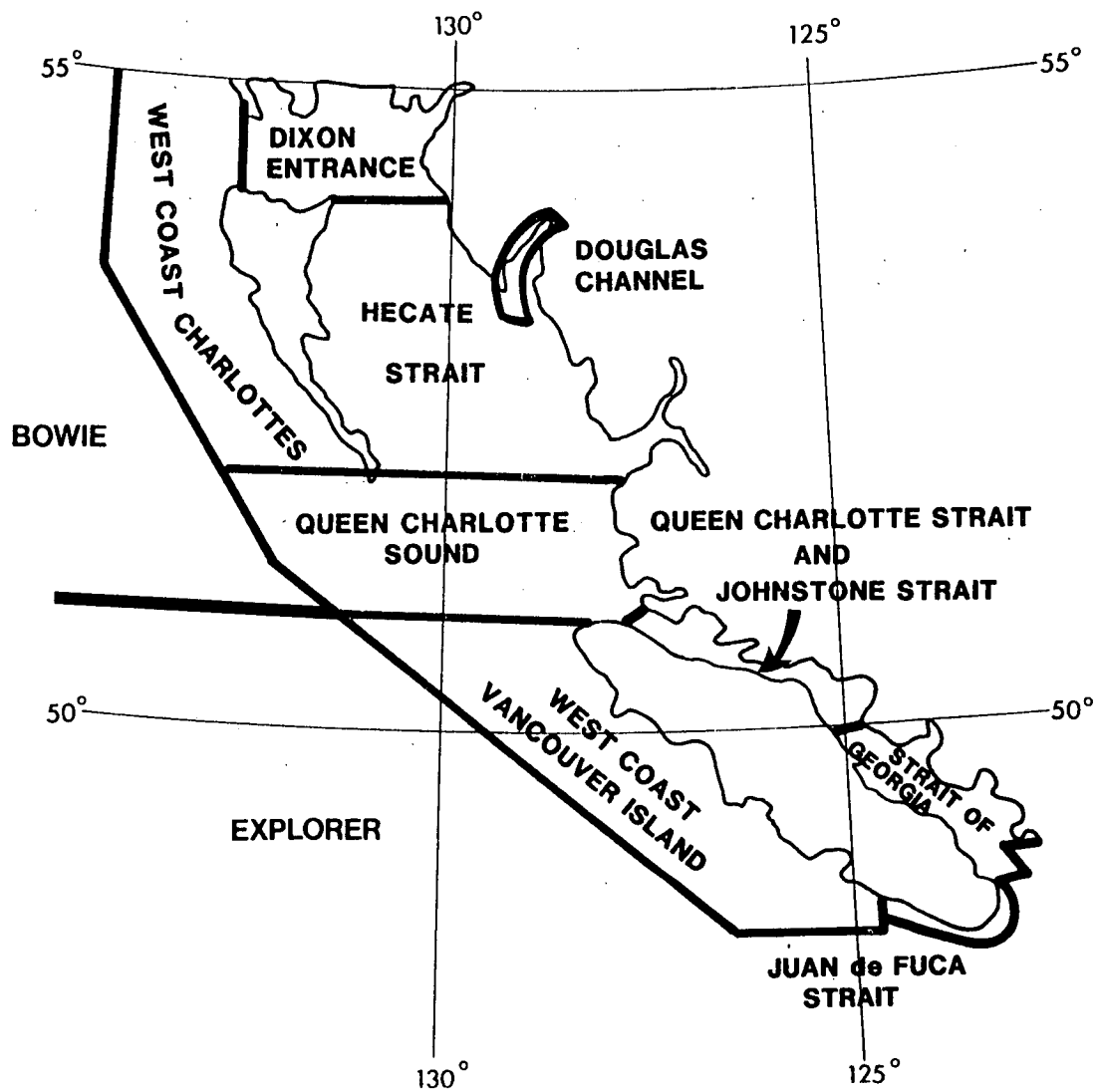


Fig. 3.1 Marine forecast areas in British Columbia coastal waters.

The term "weather" includes rain, snow, showers, snowshowers, thunderstorms, thundershowers and hail, drizzle, freezing drizzle or rain, mixed snow and rain, fog and mist. Visibility is forecast in nautical miles, but only if it is less than six nautical miles. Some restrictions to visibility are also used with the following meanings:

Fog	near zero (less than 0.5 n.m.)
Mist	1-6 n.m.
Rain or Showers	2-6 n.m.
Snow or Snowshowers	0-3 n.m.

(Source: "How to Use Marine Weather Forecasts," published by Environment Canada).

This Environment Canada publications also provides guidance for interpreting the sea-state forecast, which gives combined sea wave heights in the marine area forecasts.

"In the marine forecast, the significant wave height is used in the computation of the seas. The significant wave height is the average of one-third of the highest waves or the height of waves an observer is most likely to report. For example mariners should be aware with respect to significant wave heights, the following relationships occur:

Most frequent wave height is	.5 times the significant wave height
Average wave height is	.6 times the significant wave height
Height of the highest 10%	1.3 times the significant wave height
Height of the highest 1%	1.7 times the significant wave height
One wave in 1200	1.9 times the significant wave height

Wind waves occur where the wind is blowing. Swells are waves that have moved away from the wind generating areas and frequently give warning of an approaching storm.

With fully developed seas, winds of:

15-25 knots will likely produce waves of about	2-3 metres
25-35 knots will likely produce waves of about	3-6 metres
35-45 knots will likely produce waves of about	6-9 metres
45-55 knots will likely produce waves of about	9-12 metres
55-65 knots will likely produce waves of about	12-16 metres."

Thus mariners are given an indication of what to expect by way of the maximum wave height (about twice the forecast wave height) and by way of significant height ranges. These height ranges lead to a precision of roughly $\pm 15\%$ in the expected height, reflecting natural variability in sea-states due to differences in wind speed, storm motion, and fetch.

Most mariners also recognize the descriptive wind terms and can relate these, rather qualitatively, to a corresponding sea-state. For example, Fig. 3.2 shows three photographs of well-developed seas under near-gale



Strong winds: BEAUFORT FORCE 7

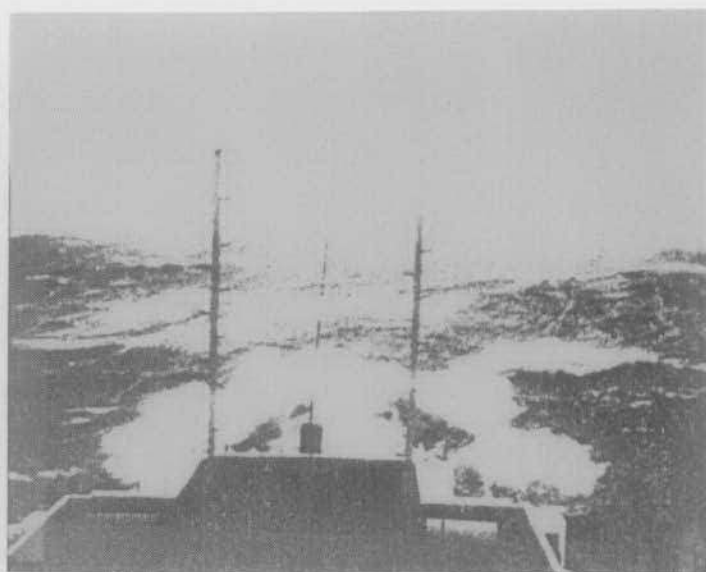
Sea criterion: sea heaps up and white foam from breaking waves begins to be blown in streaks along the direction of the wind.

Date/Time of photograph: 1961-02-28-1900 GMT

Height of camera above sea: 14 m

Wind speed: 28-33 knots, mean 30 knots

Waves at time of picture:			
	Direction (°T)	Period (s)	Height (m)
Sea waves	300	6	4
Swell	250	9	3



Gale: BEAUFORT FORCE 9

Sea criterion: high waves; dense streaks of foam along the direction of the wind; crests of waves begin to topple, tumble and roll over; spray may affect visibility.

Date/Time of photograph: 1961-01-17-2130 GMT

Height of camera above sea: 11 m

Wind speed: 41-47 knots, mean 44 knots

Waves at time of picture:			
	Direction (°T)	Period (s)	Height (m)
Sea waves	120	7	6
Swell	-	-	-



Storm: BEAUFORT FORCE 10

Sea criterion: very high waves with long overhanging crests; the resulting foam, in great patches, is blown in dense white streaks along the direction of the wind; on the whole, the surface of the sea takes on a white appearance; the tumbling of the sea becomes heavy and shocklike; visibility affected.

Date/Time of photograph: 1961-03-14-2330 GMT

Height of camera above sea: 5 m

Wind speed: 48-55 knots, mean 52 knots

Waves at time of picture:			
	Direction (°T)	Period (s)	Height (m)
Sea waves	340	9	7
Swell	-	-	-

Fig. 3.2 Well-developed sea states for strong winds, gale and storm force winds.

winds, gale force winds and storm winds. Similar photographs are published for hurricane winds (Beaufort force 11 and 12) by Kotsch (1983) amongst others. Thus the wind definitions used in the forecasts and warnings have, to some extent, an implied sea-state condition associated with them.

Marine warnings are issued at any time in response to storms impacting a region or area. Seven types of warnings are used by AES:

Small Craft Warnings

For winds of 20-34 knots
These warnings are issued
between April and November in
only some marine areas.

Gale Warnings

For winds of 35-47 knots.

Storm Warnings

For winds of 48 knots and
higher, associated with
non-tropical storms.

Tropical Storm Warnings

For winds of 48-64 knots
and associated with
tropical storms.

Hurricane Warning

For winds of 65 knots or
greater and associated
with a hurricane.

Freezing Spray Warnings

For conditions which cause
hazardous freezing spray
conditions.

Special Marine Warning

For conditions which may be
hazardous to marine interests.
Such warnings might include
severe thunderstorms or severe
freezing precipitation.

The text of the warnings contains the following points: the marine areas affected in the next 24 hours; the location of the storm centre at the present times and in 24 hours; the intensification of the storm during the 24-hour period; when and where the forecasted condition will start; expected wind speeds; how long the condition will last; severity of conditions; cause, i.e., deepening storm, frontal system, etc.; and the name of tropical storm or hurricane, if appropriate.

A sample marine warning for B.C. coastal waters would read,

"Gale warning issued by Environment Canada at 4 a.m. PST Monday
November 04 1985 for
Dixon Entrance
Hecate Strait
Queen Charlotte Sound
West Coast Charlottes
Bowie
Explorer
West Coast Charlottes

A developing storm with central pressure 1000 millibars located near 40 north 150 west early this morning, is moving northeast at 35 knots and will reach a position 300 miles west of Cape Scott early Tuesday with a central pressure of 975 millibars. Easterly gales of 35 to 45 knots will move into the Bowie and Explorer regions this evening and southeasterly gales will affect all northern areas and the West Coast of Vancouver Island later tonight."

Wave height information is not usually given in the warnings; the descriptive wind terms outlined above provide the only guidance on what to expect by way of sea-state conditions.

These forecasts and warnings are intended for voice broadcast and are widely used by fishermen, recreational boaters, commercial tow operators and coastal shipping. Few of these vessels are equipped with fax facilities; most depend on VHF radio contact.

For larger vessels that have radiofax equipment (Fig. 3.3) a series of weather charts can be received that may include:

- surface weather analyses showing the latest weather systems and patterns based on the latest synoptic surface weather observations;
- surface weather prognostic charts indicating the predicted positions of highs, lows, fronts, etc., 12 and 24 hours into the future. On some broadcasts, the predictions extend to 36 and 48 hours into the future;
- surface wind analyses showing the direction and speed of the surface wind;
- surface wind prognostic charts showing the predicted direction and speed of surface winds for the next 12-48 hours;
- wave analyses depicting the characteristics of sea and swell height and direction of movement;
- wave prognostic charts showing the predicted state of the sea conditions for the next 12-24 hours;
- sea-ice charts delineating the sea-ice areas with their known characteristics in addition to known positions of icebergs;
- significant weather depiction charts showing frontal systems with associated cloud patterns, and areas of precipitation and fog;
- satellite weather images showing cloud patterns and the positions of extra-tropical storms and disturbances, and hurricanes, typhoons, tropical storms, and the intertropical convergence zone (ITCZ); and
- oceanographic charts providing a variety of information (some still experimental). This information includes sea surface temperature (SST), colour zones, areas of divergence and convergence, mixed layer depth (MLD) data, and ocean current data.

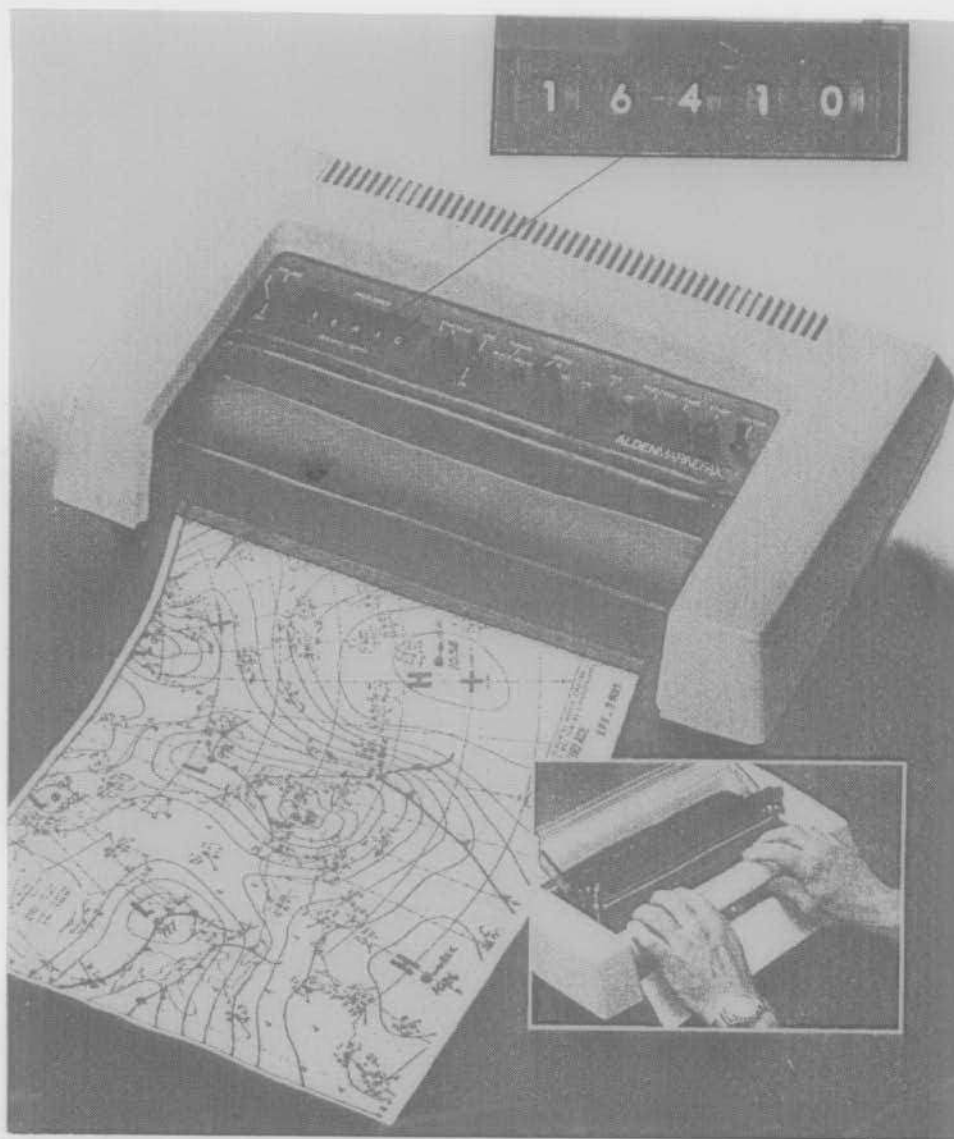


Fig. 3.3 Typical small radiofax receiver (Alden MARINEFAX IV) suitable for installation on smaller vessels. (From Kotsch, 1983).

In terms of sea-state the charts contain combined significant wave height contoured in metres. The analysis charts also contain reports on sea and swell giving an indication of heights, periods and directions. Analysis and prognosis charts are prepared twice daily in Canada by the Meteorological and Oceanographic (METOC) Centres of the Department of National Defence.

The contoured analysis and prognosis charts can be read with a precision of about ± 0.1 m at a given location. However, the accuracy is probably no better than $\pm 20\%$ of combined wave height in an average statistical sense. Little quantitative data on accuracy appears to be available, due perhaps to the fact that marine-wave observations, including buoy measurements, are used to prepare the charts. Thus independent data for verification are extremely limited. A study by Jones et al. (1980) established the equivalence of significant wave heights derived from Seasat altimeter data with those extracted from the METOC charts, and a later investigation by Hodgins and Hodgins (1983) using Scotian Shelf Waverider data omitted from the METOC analysis showed that METOC significant heights were correlated with the Waverider characteristic heights (H_{m0}). However, there were only 52 paired comparison points in this second study and the scatter about the regression line was large; thus it was not meaningful to attempt to quantify accuracy. Time-series comparisons of METOC wave heights with Waverider measurements (Hodgins and Harry, 1984; Seakem and Seaconsult, 1983) have shown that the H_s -predictions capture the major variations in the wave height field but that there is a wide scatter in predictions for different storms and different lead times (12 h, 24 h, 36 h).

3.2.2 Private Forecasting Services

In Canada, private sector marine forecasting services have been established to meet the needs of the offshore oil and gas industry. Fig. 3.4 shows a typical weather forecast prepared for one location on the Grand Banks. It contains more wave data than the AES forecasts; specifically, wind-wave heights and primary swell heights are distinguished, periods are given for both wave types, and directions are indicated for the swell component. The combined wave height and period are also predicted. These data are specified in 6-hour increments out to 37.5 hours thus forming a time-series of expected sea conditions at the site of interest. The balance of the

Weather Forecast for XXXXXXXXXX issued at 0700 NDT, 10 September 1985

Warnings: None

AES Warnings: None

Valid:	NDT	0930	1530	2130	0330	0930	1530	2130
	Date	10 Tues			11 Wed			

Wind (Anemometer at 275 ft)								
Direction	340	300	270	230	190	150	150	
Speed (Kt)	18	18	20	18	18	22	34	
Max Wind (Kt)	22	22	24	22	22	26	38	

Wind Wave								
Height (Ft)	02	02	03	02	03	05	07	
Period (Sec)	02	02	03	02	03	04	06	

Primary Swell								
Direction	350	350	350	350	350	N11	N11	
Height (Ft)	07	06	06	05	03	0	N11	
Period (Sec)	08	08	08	08	08	N11	N11	

Combined Sea								
Sig Ht (Ft)	07	06	06	05	04	05	07	
Max Ht (Ft)	11	10	10	08	06	06	11	

Sky Cover	SCT	SCT	BKN	BKN	OVC	OVC	OVC
Vis (NM)	10	10	10	06	02	01	1/2
Weather	(Nil)	(Mist)	(Rain and Fog)
Temp (Deg C)	09	09	10	10	11	10	10
Pressure (MB)	1012	1016	1020	1016	1013	1011	1008

Synopsis:

Weak high pressure area SW of Newfoundland will move eastwards today and Wednesday as a low centre over the lower Great Lakes moves eastwards deepening slowly. Winds are expected to approach gale force over the northern Grand Banks late on Wednesday as the low approaches.

Forecast for period 0800 LT to 2400 LT 10 September:

Wind : W'yly-NW'yly 16-20 kts.
 Sig Wave Ht : 5-8 ft.
 Weather : Increasing cloudiness
 Visibility : 8-12 NM
 Temperature : 9-12 deg C

Forecast for Period 0000 LT to 2400 LT 11 September:

Wind : Backing to S'yly then SE'yly and increasing by evening to 30-35 kts.
 Sig Wave Ht : Dropping to 4-6 ft then rising to 6-8 ft.
 Weather : Mist patches at first. Rain and fog later.
 Visibility : Lowering to 0-2 NM in rain and fog otherwise 6-10 NM
 Temperature : 9-12 deg C

Outlook for days 3, 4 and 5 valid until 2400 LT 14 September:

Thursday : Wind shifting to NW'yly gales 32-38 kts. A few showers. Good visibility. Sig wave ht. 6-8 ft. Temperature 9-12 deg C.
 Friday : Wind dropping to NW'yly-W'yly 18-24 kts. Fair. Good visibility. Sig wave ht. falling to 4-6 ft. Temperature 9-12 deg C.
 Saturday : Wind dropping to light. Fine. Good visibility. Sig. wave ht. 4-6 ft. Temp 9-12 deg C.

Fig. 3.4 Typical weather forecast issued for the Grand Banks by a private meteorological forecasting firm. (From Dello Stritto et al., 1985).

forecast deals with the same weather elements as the AES product including a synopsis and an extended outlook to 5 days.

The forecast firms employ a variety of wave prediction models, including spectral wave models, to assist in generating the prognoses. Guidance from these model outputs and the METOC charts are then combined with forecaster skill to produce the final forecast product. We note that wave spectra, or spectral properties other than significant wave height and some measure of wave period, are not incorporated into the forecast.

Site-specific forecasts are usually issued in hardcopy form two to four times daily for the offshore operators. Updates are issued as dictated by rapid or unexpected changes in weather. In addition, an operator usually receives a daily briefing from a forecast meteorologist at his shorebase.

Other private sector forecasting services include optimum track ship routing. According to Kotsch (1983) the service was established in the early 1950's by the U.S. Navy, but is now offered to commercial shipping interests by firms such as Oceanroutes, Inc. The objective of this service is to determine transocean routes that will provide the fastest passage with maximum safety for crew and passengers and greatest security for the cargo and hull by considering the weather and oceanography along alternate routes. However, ship routing selection factors are not restricted just to weather and sea-state; they may also include operational constraints such as schedule, fuel economies, insurance restrictions, navigational hazards, restricted zones; vessel specifications like type, speed, draft, trim, stability, deck load-ballast, seakeeping characteristics and navigational aids; and cargo type, and security needs.

According to J. Williams of Oceanroutes (pers. comm., 1987) the type of forecast data provided to end-users varies widely. For commercial ships forecasts may consist simply of dead reckoning instructions updated every 24 hours as the route is optimized for weather. Specialist users may have other requirements, however, some of which include forecasts of vessel response (heave, pitch and roll) and forecasts of ocean wave spectra (for seakeeping calculations) in addition to conventional weather elements. These end-users typically are involved in heavy lift operations, pipe laying

operations and deep-sea towage of heavy structures or barges. The format and frequency of update of these products is tailored to individual user requirements.

Firms like Oceanroutes are also end-users of some forecast products themselves. Their requirements are discussed in more detail in the following section.

3.3 End-user Wave Forecast Requirements

The purpose of this section is to review actual end-user requirements identified in our interviews and from literature. Where possible we also discuss the opinions expressed regarding possible improvements.

3.3.1 Offshore Oil and Gas Operators

Wave forecast requirements are considered here for three kinds of activities affected by weather and sea-state: drilling operations, oil spill and ice movement prediction, and dredging and caisson operations. Future requirements in a fourth category, production developments, are also discussed. Each places different demands on the content, accuracy, duration and timeliness of wave data.

Drilling Operations

For historical reasons that have to do mainly with the development of offshore exploratory drilling practice before accurate wave forecasts became available, weather forecast requirements of operators centre on wind rather than sea-state. This point was brought out clearly in the report on the adequacy of weather forecasting services for the Canadian offshore (Hodgins, 1984) prepared for the Royal Commission on the Ocean Ranger Marine Disaster, and re-emphasized by Dello Stritto et al. (1985). In this second paper, for example, the authors note that many rig foremen actually plan on the basis of winds and use real-time wave observations as feedback, rather than giving equal weight to both winds and waves, even knowing that certain activities are sea-state dependent. Except when severe storms are forecast, drilling generally continues unaffected by weather until certain operational limits are reached. These limits vary depending upon the type of platform (semi-submersible, or ship shape floating units, either anchored or dynamically

positioned, and jack-up units); typical environmental thresholds for semi-submersibles and jack-ups are summarized in Table 3.1. Additional operations thresholds not listed here include anchor tensions, heave, pitch, roll, and riser angle for floating units, together with limits based on combinations of several factors. These additional factors are primarily sea-state dependent.

Dello Stritto et al. (1985) note that only under the most severe storm conditions, or for certain well activities (testing, running casing, well logging, and maintenance totalling about 10% of the time) is there a requirement for wind forecasts accurate to within 15%. These activities are not in themselves motion sensitive: it is rig evacuation criteria (launching lifeboats and survival capsules) that govern since there is an increased potential of fires, blowouts or gas escapes. The primary requirement here is for wind data, not sea-state information.

Crane operations, transfer of personnel, offloading of supply boats, and anchor handling are motion sensitive. Planning these activities requires forecast wind and wave data. Operations thresholds for sea-state are usually expressed in terms of maximum combined wave height (Table 3.1) or significant wave height. In our surveys general satisfaction was expressed with the content, format, and timing of sea-state forecasts presented by private contractors since the information matches what is required on the rig and at the shorebase. This opinion most probably follows from the fact that reliance is given to the wind forecast, and that sea-state forecasts (as distinct from reports of actual conditions) do not limit or constrain decisions in a way that can be traced to problems in the past. It also appears that simple transfer functions for heave, roll, or other motion responses that are based on wave height/period characteristics work well enough, to the extent that they are used in planning these activities at all.

It is quite obvious, however, that since many present-day wave forecasts are derived from spectral wave models, motion response characteristics of floating rigs or vessels could be predicted using techniques commonly employed by naval architects. Specifically, response amplitude operators

Table 3.1

**Partial List of Environmental Thresholds
for Drilling Operations**

	<u>Semi-Submersibles</u>			<u>Jack-Ups</u>		
	<u>Wind Speed (knts)</u>		<u>Maximum Combined Seas(ft)</u>	<u>Wind Speed (knts)</u>		<u>Maximum Combined Seas(ft)</u>
	<u>1-Minute Mean</u>	<u>Gust</u>		<u>1-Minute Mean</u>	<u>Gust</u>	
Crane Operation	40	50	20	40	50	-
Transfer by Personnel Basket	30	40	12-15	30	40	12-15
Supply Boat Alongside	40	50	15-20	40	50	15-20
Anchor Handling	40	50	15-20	-	-	-
Drill Surface Hole	50	60	15-20	45	55	15-20
Drill(stack and rack)	50	70	35	-	-	-
Running Casing	35	45	15	35	45	15
w/Stack Installed	45	50	30	45	50	-
Tripping	50	70	35	50	70	-
Production Testing	40	50	18	40	50	-
Logging	50	60	35	50	60	-
Hang-off	50	70	35	-	-	-
Disconnect	60	-	40	-	-	-

Note: A full list of operations thresholds includes limits for anchor tensions, heave, pitch, roll and riser angle, as well as limits based of combinations of several factors.

(Source: Dello Stritto et al., 1985)

(RAO's) are used as transfer functions to convert a wave energy spectrum into response (heave, pitch or roll) spectra from which significant or maximum response can be calculated. It would be possible to derive riser angle and anchor tensions from these responses as well.

In our interviews with shore-based personnel, and especially with the captains and foremen on two Husky/Bow Valley semi-submersible rigs operating on the Grand Banks we explored "upgrading" forecasts (e.g., 42- to 48-hour prognoses) to include these response characteristics. The questions covered such aspects as whether or not motion parameters would be useful, and whether or not they would be regarded as accurate enough to assist in planning. With one exception, this idea was greeted with considerable skepticism, ranging to the emphatically negative. The concerns really centred on a lack of confidence that the predictions would be accurate enough to be useful. The point raised repeatedly was that the response characteristics are too sensitive to deck load distributions and ballasting conditions (information not available to the wave forecasters in time to incorporate into their calculations) to be accurately predicted with mathematical models. The exception noted was W. Thompson of Petro-Canada who identified wave spectra and semi-submersible heave as forecast requirements, and that these were being introduced on a trial basis with some east coast operations in 1985.

In view of these findings it is possible to consider wave forecast requirements for drilling operations in two categories: end-user needs as they are perceived now and relate to established practice, and improvements to the existing set of parameters that would enhance forecast utility. Most of the users who were interviewed recognize the uncertainties in both wind and wave prognoses, and make allowances for this uncertainty in using forecasts. Because the forecasts are viewed as guidance material that by definition cannot be very precise, we found that end-users have considerable difficulty in quantifying what precision and accuracy are good enough, or even desirable, for their needs. Consequently, in an attempt to be as quantitative as possible we have generalized typical accuracies for combined wave height reported by Nordco (1983) for a Grand Banks program (discussed by Hodgins and Harry, 1984) and applied these to the summary of user needs.

This applications seems largely valid since the end-user community has expressed general satisfaction with the forecast product available to the end of 1986.

User requirements for sea-state forecasts, as they are perceived now, are summarized in Table 3.2. These parameters are used in planning motion-sensitive activities to assess the likelihood that operations thresholds will be exceeded over the two-day forecast interval. The most important parameters are combined sea heights and periods; less reliance is placed on wind-sea and swell components except where swell dominates. In this case, swell direction may also be considered in the placement of supply boats relative to a drilling unit but this type of decision is based mainly on actual conditions rather than longer-term forecasts.

A demand for particularly high forecast accuracy occurs for jack-down operations with jack-up rigs. The operating weather window is governed by sea-state and continuous periods of 24 h or more with combined sea significant wave heights below given thresholds may be required. None of the operators identified parameters additional to those in Table 3.2 as being required, but rather that accuracies within 15% or better beyond 24 h are desirable.

No other wave properties such as steepness, sea-state grouping or spectral shape parameters were identified as forecast requirements. Spectra and shape parameters are discussed under improvements: these data have a direct connection to vessel motion prediction. On the other hand, steepness and grouping are secondary factors, useful perhaps for climatological purposes and the design of production facilities, but not easily related to operations thresholds that affect drilling activities. For this reason they are not required.

Three areas of sea-state forecast improvement were identified through these discussions. The first, with probably the highest priority, is an improvement in the accuracy of parameters now being reported for lead times from 18 to 48 hours. This improvement relates directly to the demonstrated deterioration in forecast skill beyond 24 hours found over eastern Canadian waters, and beyond 18 hours in the Beaufort Sea.

Table 3.2

**Summary of Wave Forecast Requirements for
Offshore Oil and Gas Drilling Operations**

BASIC PARAMETERS

Sea State Property	Parameter	Precision	Accuracy	Lead Time and Interval
wind sea*	sig. height	0.3 m	$\pm 10\%$	48 h @ 6 h intervals
	peak period	1 s	± 1 s	
swell	sig. height	0.3 m	$\pm 10\%$	
	period	1 s	± 1 s	
	direction	8 point compass	$\pm 20^\circ$	
combined sea	sig. height	0.3 m	$\pm 10\%$	
	period	1 s	± 1 s	
	max. height	0.3 m	-	

DESIRED ENHANCEMENTS

Sea State Property	Parameter	Precision	Accuracy	Lead Time and Interval
wind sea*	sig. height	0.3 m	$\pm 8\%$	12 h @ 1 h intervals
	sig. period	1 s	$\pm 10\%$	12-48 h @ 6 h intervals
swell	sig. height	0.3 m	$\pm 8\%$	12 h @ 1 h intervals
	period	1 s	$\pm 10\%$	12-48 h @ 6 h intervals
	direction	8 point compass	$\pm 20^\circ$	
combined sea	sig. height	0.3 m	$\pm 8\%$	12 h @ 1 h intervals
	period	1 s	$\pm 10\%$	12-48 h @ 6 h intervals
	max. height	0.3 m		
spectrum	1-D spectrum	15 frequency bands	$4\sqrt{m_0}$ within 15%	12 h @ 1 h intervals 12-48 h @ 6 h intervals

*wind sea directions are assumed to coincide with the local wind direction.

The second area of improvement concerns increased accuracy and resolution of short-term forecasts from 0 to 12 h. Users did not identify a need for additional parameters but rather for an improvement in the accuracy (within 10%) and resolution (hourly) of wave height information available now.

These improvements appear to be related mainly to optimizing existing operations procedures and not to fundamental changes in drilling or safety offshore. Dello Stritto et al. (1985) confirm this idea in their paper on wind requirements.

Finally we return to the question of improvements to the "wave" parameter set itself. The skepticism expressed about predicted motion response parameters for floating drilling units was apparently based on experience and judgement found working on the rigs; there was no indication that forecast heave and roll, for example, had ever been systematically tested for accuracy against rig measurements. Thus it seems likely, at least in Canadian theatres, that the reliability to be expected of motion parameters is untested and unknown. In principle, if the vessel response can be predicted from forecast wave spectra and operations limits related to these response parameters (for example, crane derating curves as a function of crane motion at the deck) then decisions can be made with more assurance, and operations can be optimized for efficiency and safety.

Given the level of numerical wave prediction modelling now routinely carried out (Clancy et al., 1986; Golding, 1983; Houghton, 1984) motion response forecasting is certainly feasible. It remains to validate such predictions with rig measurements to determine their reliability and to establish that the extra computations are warranted in terms of improved operations.

Oil Spill and Ice Movement Prediction

Mathematical models (e.g., Seaconsult, 1984) are used for predicting actual trajectories of oil spills, and form an important component of spill monitoring and control responses (Dello Stritto et al., 1985). Wind prognoses and residual sea currents are the main input requirements for oil spill models, since the very near-surface currents dominate the motion. However, some models contain weathering functions, one of which is the loss of oil from the slick due to downward turbulent mixing. The source of

energy for this downward mixing is taken to be breaking waves, and in models it is assumed that the volume loss rate of oil can be related to sea-state specified by a simple parameter such as significant wave height. In the early 1970's the Warren Spring Laboratories work specified sea-state only as "low, medium or high"; recently this mechanism has been quantified by relating wave height to wind speed (a simple universal correlation). This removes the necessity for separate wind and wave forecasts as a requirement for spill trajectory calculations, thus simplifying the real-time demands for data during an emergency.

In principle, however, the models can be formulated to accept sea-state data directly and the trajectory predictions could be upgraded to include volume losses resulting from wave breaking and mixing. No such need was identified by the offshore oil and gas operators but it is possible with existing forecast sea-state information. Because the relationships between oil loss and whitecapping are empirical, wave data in the form of significant wave height (Table 3.2) are sufficient. To upgrade forecasts to include wave spectra, a whitecapping model (e.g., Ochi and Tsai, 1983) or some estimate of turbulence below the wave field (e.g., Melville et al., 1985) would be logical only with a parallel improvement in the formulation for downward mixing of oil.

Sea ice and iceberg drift forecasts are major components of offshore ice management systems. In tactical ice management off the east coast, that is within 20 to 30 km of the drilling unit, wind and particularly wind direction are the prime factors in forecasting ice motion and deciding upon towing or avoidance strategies. Sea state forecasts independent of the wind are not required; actual wave conditions are sufficient for tactical decision making.

Strategic ice management requires 24- to 72-hour wind forecasts over the northern Grand Banks. These winds are used in simple ice drift models together with background currents to predict changes in position of individual bergs, or of the sea-ice edge. As Dello Stritto et al. (1985) note the accuracy of individual berg positions is often poor but the description of the iceberg ensemble is adequate for planning purposes. Sea

state data were not identified as a requirement for strategic ice management.

Tactical iceberg management often makes use, however, of drift models that are based on simple force balance equations (Mountain, 1980). Hsiung and Aboul-Azm (1982) published an extended formulation incorporating wave drift forces. In their numerical examples they show that such drift forces can be of the same order of magnitude as all other forces (wind, water drag, Coriolis and sea surface slope) combined on a 200,000 tonne tabular iceberg. As with oil spill models it is possible to incorporate sea-state data into iceberg trajectory models using formulations such as that described by Hsiung and Aboul-Azm. However, given the uncertainties in iceberg geometry and wind and wave forecasting in an operational setting, and the higher priorities given to iceberg detection and tracking, upgrading of trajectory models to incorporate sea-state (wave height, period and direction) as a prognostic variable was not identified as a requirement.

Dredging and Caisson Set-Down Operations

In the Beaufort Sea the most demanding forecast requirements are related to construction, especially the final steps of installing large caissons. These operations require a 24- to 36-hour weather window with combined sea significant heights of less than about one metre. Thus the forecast requirement is for wave height persistence below threshold for durations up to 36 hours, similar to the jack-down needs on the east coast for jack-up rigs.

Beaufort Sea operators did not identify wave spectra or other wave properties such as steepness and grouping as being required for operations. However, improvements in the accuracy of conventional forecasts (wave heights, periods and directions) particularly beyond 12 to 18 hours was noted as desirable.

Production Development

Development of oil or gas producing facilities is being contemplated on the Scotian Shelf, on the Grand Banks and in the Beaufort Sea. Depending upon the facility chosen in each area construction may involve heavy towage,

heavy lifts at sea, and pipelaying. All these activities are motion sensitive, making them subject to lost time for sea-states above certain thresholds. Contractors involved in these construction-related activities optimize operations carefully to minimize risks and downtime. Sea state forecasts play an important role in this process. According to J. Williams (Oceanroutes, pers. comm., 1987) forecast spectra and/or vessel motion response parameters are required in addition to routine wave height and period data. This practice has been introduced in the North Sea, for example, for heavy lifts onto platforms. A second example would be dynamic stress analysis for submarine pipelines during lay operations (e.g., Bryndum et al., 1982) for which barge motion parameters are required. Assuming that much the same construction technology would be used for Canadian fields one can envisage similar demands for detailed spectral wave forecasting during critical operations in the future. The specific forecast products would be tailored to user needs but would generally consist of one- or two-dimensional wave spectra; vessel heave, pitch or roll; or dynamic pipe stress envelopes every 1 to 3 hours for lead times out to 24 to 36 hours. The basic demand in terms of sea-state parameters is, however, for forecast directional wave spectra, or for one-dimensional spectra and dominant wave direction as a minimum.

3.3.2 Commercial Fishing and Tow Operators

The commercial fisheries are major industries on the Canadian east and west coasts. Both rely heavily on weather/sea-state forecasts provided by Environment Canada for the safety of their operations at sea. Probably the most comprehensive survey of user requirements in the fishery and tow boat industries was conducted jointly by AES, Vancouver and the Institute of Ocean Sciences (DFO), Sidney, B.C. who polled over 700 individuals and convened a number of public hearings for this purpose. Results of this survey were made available for the present study through AES, Vancouver.

A second survey, on marine hazards in B.C. coastal waters, was carried out by Seaconsult in 1987 to identify dangerous weather-related conditions and their relationship to forecasts. Responses were received from fishermen, tow boat operators, and master mariners in Coast Guard and Fisheries and Oceans, and the findings were incorporated into a guidance manual for west

coast mariners. A summary of the sea-state forecast requirements amalgamated from these two studies follows.

Marine area forecasts are used primarily to warn of dangerous sea-state, wind and weather conditions which occur most often in storms. The studies leave no doubt that sea-state forecasts are required and would be used by fishermen and tow boat skippers. The principal element is combined wave height. A discrimination between wind-sea and swell is also desirable; i.e. swell should be specified separately if it is present and its height should be forecast. Wave periods and directions were not identified as specific elements to be included in the forecast. However crossing seas, with swell and sea propagating in different directions, were considered hazardous leading to a requirement for swell direction where it is different from local wind-sea direction in the forecast.

Lead time is a critical factor in the marine forecasts. Six- to 12-hour lead times are necessary to recover gear and make a safe port in the event of a severe storm. Many west coast fishing vessels range in length from 12 to 18 m; for these craft dangerous sea-states would have combined sea significant wave heights in excess of 5 to 6 m with winds over 35 knots. These conditions occur frequently in winter storms along the exposed coast.

The consequence of a missed forecast is often loss of life and boats. Thus correct timing of the onset of severe wind and sea conditions is especially important. The worst situation is in storms that develop more rapidly than forecast and move ashore earlier than expected. Then skippers are left without adequate time to seek shelter.

Longer lead times of 36 to 48 hours are required by the offshore fishery on the east coast. Wave information is used in conjunction with the weather parameters to plan for fleet safety under severe conditions.

Marine forecasts are issued four times daily. On the Pacific coast, for example, the issue times are 0430, 1030, 1630, and 2230 PST. Users did not identify a requirement for more frequent updates and forecast dissemination, provided that severe weather warnings are issued in a timely manner. Because fishermen generally leave harbour by first light and need a forecast

earlier than 0430 PST, the following changes in issue times were proposed:

in summer: 0230 1000 1700 2200 PST

in winter: 0330 1000 1600 2100 PST

Two difficulties with forecasts were noted. The first concerned the precision of forecast parameters, specifically that descriptive wind terms (strong winds, gales, etc.) were too coarse and that 5-knot speed ranges are desirable. Quantitative wind forecasts are now routinely provided by the AES. The surveys did not indicate an equivalent precision for wave heights. It was noted, however, that most users would prefer forecasts of combined wave height in feet rather than given in whole metres. There is an implied increase in precision here from one metre to, perhaps, one-third to one-half metre. Forecasts should also be given in numeric parameters avoiding strictly descriptive terms for wind and sea-state.

The other concern had to do with spatial resolution--it was concluded that present marine areas (Bowie and Explorer, for which wave forecasts are available) are too large and that better discrimination of sea-states (and winds and weather) within each marine area is required. Sea-state forecasts are also required for the coastal marine areas. This leads to spatial resolution in wind and wave fields of the order of 50 km.

One problem to be addressed with higher resolution is the presentation of forecast material. Subdividing marine areas further tends to make voice broadcast unwieldy. More extensive use of facsimile equipment for graphical presentation of surface weather and wave information was considered advisable. Facsimile transmission has the advantage of giving marine users a clearer picture of developing storms and the movement of associated frontal systems as they approach coastal waters.

The B.C. coast is characterized by many localized hazards; these are described in "The Manual on Weather Hazards in British Columbia Coastal Waters" to be published by AES in 1987. With respect to ocean waves these hazards occur mainly when waves counter an opposing current, steepen and break. Often there is a strong wind at the same time so conditions are very dangerous for small craft. In many places bathymetric refraction, and wave

shoaling over shallows contribute to the problem. Wave height variations from severe to highly dangerous occur over scales of 2 to 5 km. Mariners identified the need for forecasts of these hazardous conditions. To satisfy this need imposes a new scale on wave modelling that incorporates detailed shallow water transformations and wave-current interactions.

It is expected that similar wave-related hazards are found along the east coast, and that the user requirements of inshore fishermen there are much the same as in B.C. waters.

3.3.3 Private Forecasting Firms

As noted earlier private forecasting firms supply such wave data products as directional spectra or vessel motion parameters to their clients. These parameters are calculated using spectral wave models applied on local area, high-resolution grids. Oceanroutes Inc., for example, uses a discrete spectral model for wave forecasting similar to that run operationally by the U.S. Navy at the Fleet Numerical Oceanography Center (FNOC), Monterey (see Clancy et al., 1986). Typical areas of application include the North Sea, and Bass Strait, South Australia (J. Williams, Oceanroutes, pers. comm., 1987). Depending on the precise nature of the local area model, it may require wave spectra derived from global models along open ocean boundaries.

The present practice is to acquire the boundary data from agencies such as FNOC which run global models operationally. In this respect the private forecasting firms become end-users who require wave spectra every 1 to 3 hours, out to 24 to 48 hours, at selected locations. In addition they require forecast wind fields.

3.3.4 Canadian Naval and Other Government Requirements

During this study a brief review of Canadian naval needs for sea-state forecast information was made with assistance from W. Lumsden of the Meteorological and Oceanographic Centre (METOC), Halifax. The objective of the review was to isolate the forecast elements requested of METOC by the navy, recognizing that METOC does not necessarily provide all of them at present. Where possible the use of the data is indicated but only in fairly general terms since a detailed examination of operational naval needs was beyond the study scope.

Naval forecast requirements relate mainly to surveillance and combat duties. Because large ocean areas are covered in planning and carrying out operations, forecast data are most conveniently presented in map form (Fig. 3.5). Such maps are routinely transmitted to ships at sea both by METOC in Canada and by FNOC in the United States.

General planning and route selection require combined sea significant wave height charts forecast out to 36 hours. A precision of 0.3 to 0.5 m in wave height is necessary. In addition to combined sea, information is wanted on both wind-sea (significant height, period and direction) and swell (significant height, period and direction).

Forecast data on wind-sea together with overwater wind speeds are related to acoustic noise in the ocean, affecting anti-submarine warfare. Swell height, period and direction are related to certain motion sensitive surface operations with submarines.

Mr. Lumsden did not identify a need for ocean wave spectra, either as these might be used for surface operations or for optimum ship track routing based on seakeeping ability. Nor was a requirement for other wave properties such as grouping, steepness or white capping frequency/coverage identified. Thus it appears at the time of this study that Canadian naval needs are met with basic wave height, period and direction data. However, naval activities also require other kinds of oceanographic data not normally associated with weather forecasting. These include sea surface temperature, 200-foot depth temperatures, and water feature (fronts) analysis.

Users have identified the need for improved predictions of peak combined sea conditions in storms although the desired accuracy was not quantified. The reliability of forecast sea-states as perceived by the user is governed by both absolute accuracy of each wave height field, and by the temporal resolution afforded by the forecast products. At present, twice-daily wave forecasts out to 36 hours are prepared by METOC in 12-hour increments and distributed to ships. The daily forecasting schedule showing data times and issue times is illustrated in the upper panel of Fig. 3.6. The lower panel shows lead times for which the wave predictions apply. The 12-hour spacing

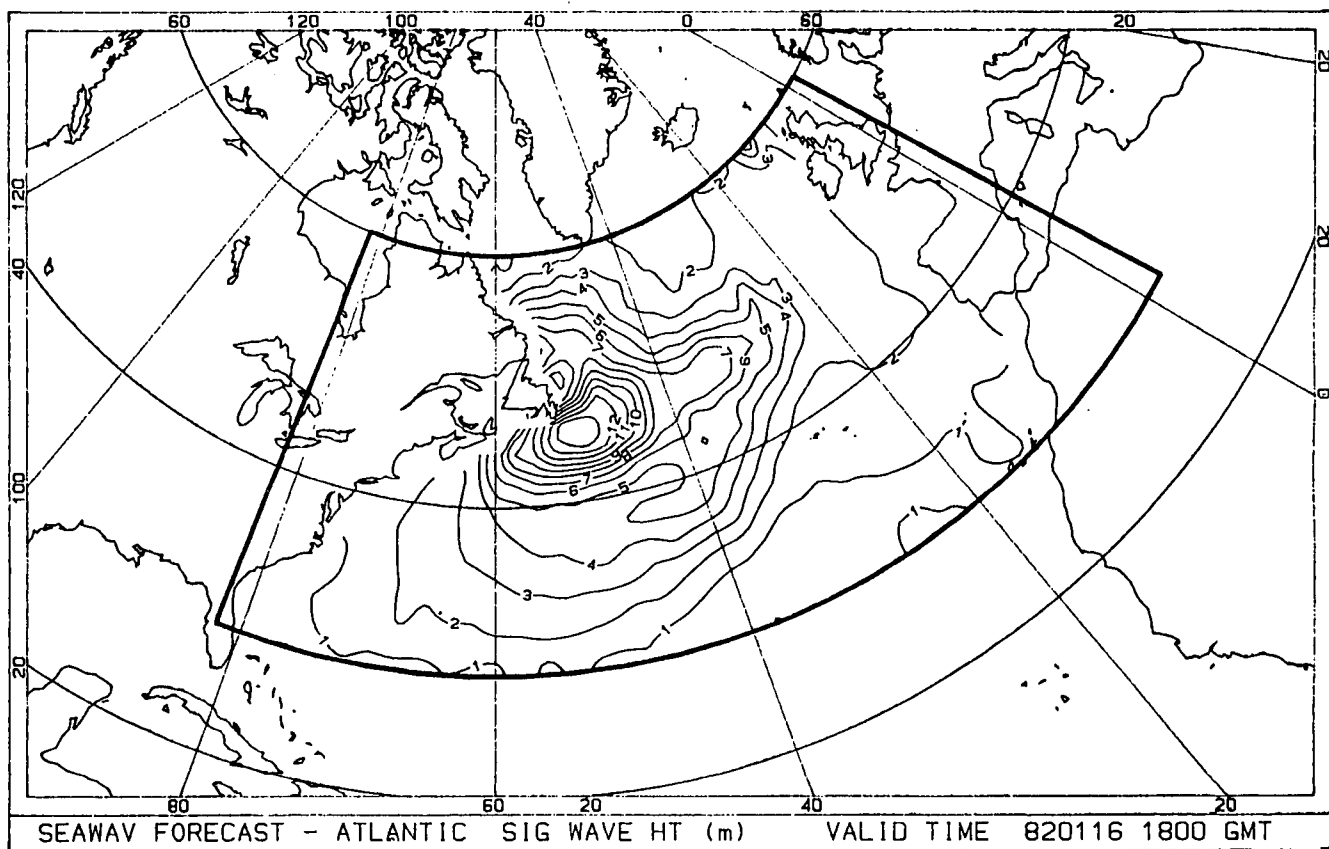
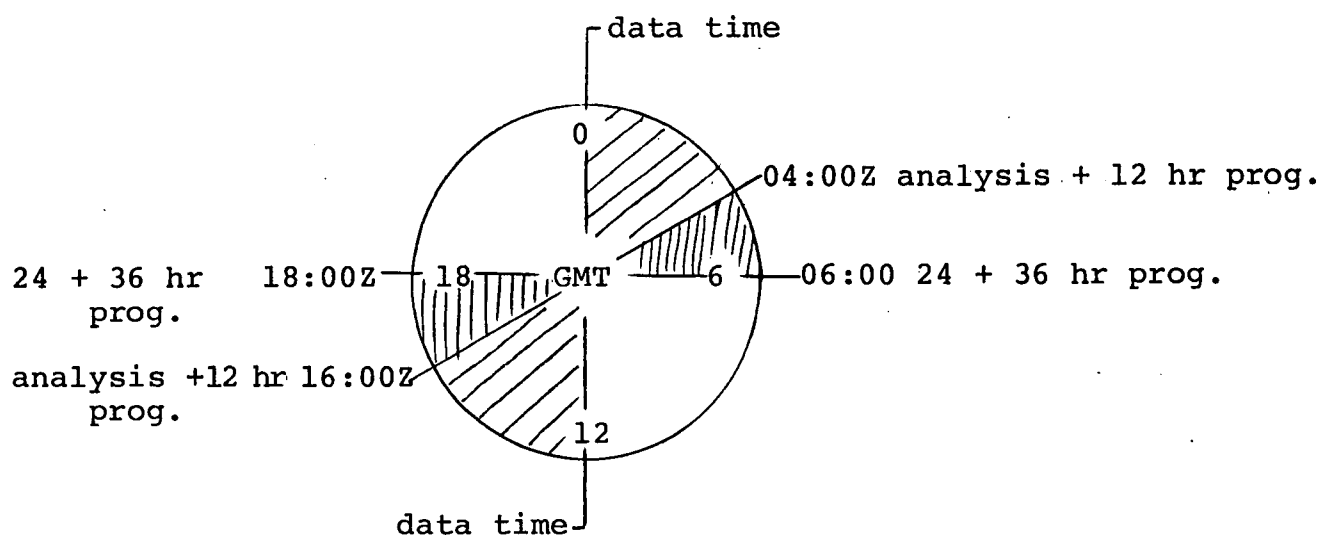
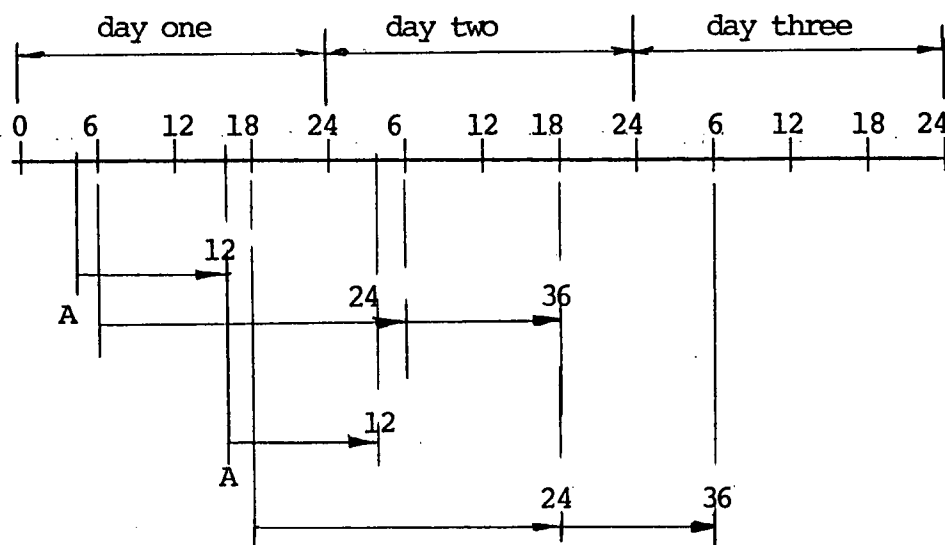


Fig. 3.5 Significant wave height field (produced by Seaconsult's SEAWAV® forecast system based on Resio's discrete spectral wave model WAVAD).



Daily forecasting schedule



A = analysis times

Prediction intervals in hours

Fig. 3.6 Illustration of the daily forecasting schedule and prediction lead times used by METOC for the Canadian Department of National Defence.

of the prognoses results in relatively poor resolution of sea-state changes. This can be reflected in the "valid times," defined as the interval centred on each prediction time during which wave heights may be expected to change by not more than some prescribed value, for example, 10% of the predicted height. During storms one may show, roughly, that (Carter, 1982)

$$H_s = 0.0146U^{1.286}D^{0.714} \quad (3.1)$$

where H_s is the significant wave height in metres for a duration D in hours, and U is the wind speed in m/s at 10-m elevation. For a wind of 30 m/s a 1-m change in $H_s = 10$ m requires a duration of about 3 hours under growing conditions. Under lighter winds of 15 m/s, a 10% change in $H_s = 5$ m would require about 5 hours. Thus we find that valid times are only a fraction of the interval between prediction times 12 hours apart. Outside of the valid times sea conditions are known only approximately by interpolation.

Naval users have not stated that better temporal resolution is deemed necessary, but indirectly infer that this is so by demanding reasonably accurate timing on peak sea-states. From the above example, it is clear that element forecasts must be presented on at least a 3-hour increment to achieve acceptable timing.

The Canadian Coast Guard has responsibility for search and rescue missions at sea, supported by air services from Department of National Defence. The sea-state forecast requirements for these operations require 12- to 24-hour prognoses of combined sea wave heights for assessing whether or not available search craft can function safely, and for making tactical decisions. Sea-state information is considered together with wind and weather for these purposes; the important aspect of the forecasting is timely and fairly accurate short-term predictions. As with the fishing community, underpredicted storm developments can put rescue craft in danger.

3.3.5 Recreational Boaters

The final user group considered here, briefly, is the recreational boating community. Information on their needs for weather and sea-state forecasting is contained in the AES/DFO and Seaconsult surveys referenced in the section on commercial fisheries. Boater needs focus primarily on timely warnings of

changes in weather that pose a hazard to small craft, and wind and wave forecasts out to 24 hours for planning routes and times of departure. Needs and opinions on weather/sea-state forecast requirements vary widely, however, depending upon boater knowledge, experience and skill, vessel type and size, and cruising areas. In surveys the recreational boaters are probably the group most critical of existing services by AES and yet one of the least specific about improvements that might actually be made.

It appears, however, that with respect to sea-state forecasts the required parameter is combined wave height when locally generated wind-seas dominate.

On the Pacific coast heavy swell occurs frequently. During fall and winter, 3- to 4-m swell with periods ranging from 14 to 22 s is typical (e.g., Hodgins et al., 1985). In summer, swell is also present but with generally lower heights. Away from the coast this swell in itself does not pose a significant hazard although it may inconvenience boating. Near the coast, however, swell interacts with strong tidal currents where it steepens and refracts, and these combined conditions are hazardous. Thus forecasts of swell heights and directions and the expected duration of swell is needed as an integral part of the marine area forecasts and warnings.

3.4 Summary

In summarizing user requirements for wave forecast data we have made several assumptions. First, it is accepted that in any forecasting service, public or private, updates and warnings are issued when weather and sea-state depart from the current prognosis and from expected development. The emphasis is on severe weather. Given the length of time required to run wave models now, updates or warnings may not be as quantitative as regularly scheduled forecasts that are prepared, for example, twice daily. Thus we look at user needs for wave information in terms of regularly scheduled forecasts, recognizing that all users demand weather warnings as an integral part of the service.

Second, it is assumed that special products such as motion response parameters, weather windows, optimum ship routes, seakeeping calculations and operations parameters would all be derived from basic outputs provided by wave models, by either a contractor or the end-user. We confine our

summary here to the basic wave outputs--heights, periods and directions, or spectra--and not to these additional products.

Third, in looking at user needs we have incorporated improvements to the present services provided either by AES or by private firms where these address known problems or represent obvious upgrades to the information contained in forecasts as they are issued now.

Offshore operators exploring for oil and gas require site-specific forecasts out to 48 hours providing wave heights, periods and directions for wind-sea, swell and combined sea and swell conditions. Hourly resolution of these parameters is required between 0 and 12 hours dropping back to six-hourly between 12 and 48 hours. Wave height accuracies of 15% (0 to 12 h) and 20% (12 to 48 h) are desirable, as are wave periods within about 2 s and directions specified on an eight-point compass.

One-dimensional spectra are considered necessary, at the same time-resolution as the above parameters, when drilling unit heave (or any other motion response parameter) has a large effect on drilling operations. This need leads to a separation in forecast requirements based on the rig type: spectra and heave are closely related to floating unit performance, especially drill ships, but are nearly irrelevant for jackup units, sacrificial beach islands and caissons during normal drilling operations. However, during construction or jack down, these fixed units are susceptible to wave-induced motion and, at these times, detailed wave forecasts out to 36 hours are required. Either wave spectra or height-period parameters, may be required depending on the contractor's needs. Construction requirements during production development may be expected to be similar, but spectral information will be more essential than the simpler height-period parameters.

In addition, regional sea-state forecasts in terms of combined heights are required between the supply base and the drilling unit for planning supply boat routes. Lead times of 12 to 24 hours are satisfactory with combined significant wave height accurate to within 20%. On the west coast, winter swell may constrain some operations and thus enter into the forecast requirement.

Wave properties such as steepness or grouping are not required.

The major benefits to forecast improvements in accuracy and resolution appear to relate mainly to optimizing operations to increase efficiency and not to a fundamental change in practice. If operators were to optimize emergency responses to take advantage of increased forecast accuracies, the result could be smaller margins on rig evacuation time, and an increase in the risk to safety.

Commercial fishermen depend heavily on weather forecast services for their safety at sea, and predictions of combined sea significant wave heights supplemented as necessary with swell heights and directions are required in coastal waters. The most important factor in sea-state forecasts is a 12-hour lead time since 12 hours is about the longest time that the smaller vessels require to bring gear aboard and reach a safe port. Thus, accurate combined sea prognoses (within 15%) out to about 12 to 18 hours are required to be included in regularly scheduled forecasts. Lead times of 36 to 48 hours are required by the offshore fishery.

Sea-state forecasts are required in coastal waters where sheltering, shallow water transformations, and local wind modifications affect the accuracy of wave predictions. Moreover, fishermen and tow operators require quantitative forecasts with wave heights specified in feet or metres, avoiding strictly descriptive words (e.g., gales) where the wind term implies a sea-state. Issue times matched to fishing operations are required which may vary from province to province and with the time of year. Finally it was found that because some present marine forecast areas are too large, further subdivision is required.

Private forecasting firms may run local area wave models to provide highly specialized products to some users. In general, deep water wave spectra along local area model boundaries (out to 48 h at one- to three-hourly time steps) are required. In the past these data have been obtained from national weather forecasting agencies (or military ones such as FNOC, Monterey) who run global or hemispherical atmospheric and wave models on coarse grids (of the order of 2.5° of latitude and longitude).

Naval requirements for wave data are satisfied by forecasts of wind-sea, swell and combined sea significant heights, periods and directions with lead times of 36 hours resolved every 3 hours. In general this information is required over large ocean areas leading to chart presentation rather than tabular listings. The three-hourly resolution represents a large change over the present four charts (analysis chart, 12 h, 24 h and 36 h prog charts); it reflects the stated need for better specification of the peak response in storms. Forecast wave spectra are not now required.

Canadian Coast Guard search and rescue missions at sea have requirements similar to commercial fisheries; i.e., 12- to 24-h prognoses of combined sea wave heights and swell characteristics, accurate enough to judge the safety and feasibility of rescue craft operations.

Recreational boater requirements centre on 24-hour prognoses of combined sea wave heights and predictions of swell heights, directions, and the expected duration of swell along exposed coastlines. In most coastal waters recreational boater needs would be adequately met with the same forecasts provided for commercial fishing operations.

4. WAVE MODELS

This section describes wave models in each of the three classes: parametric wave height, parametric spectral and discrete spectral. Aside from this stratification, the presentation largely follows historical developments in this field. The discussion is intended to be balanced, although it is sometimes limited by insufficient detail in the published literature. And it is inappropriate to de-emphasize the contributions of K. Hasselmann to parametric spectral modelling and of W. Pierson to discrete spectral modelling.

4.1 Parametric Wave Height Models

In this class, the wave models are based on the Sverdrup-Munk-Bretschneider (SMB) parametric equations (Bretschneider, 1970) that relate non-dimensional fetch (gF/U) to gH_s/U^2 , $gT_s/2\pi U$ and non-dimensional wind duration (gt_{dur}/U) where g is the gravitational acceleration constant and U is the mean surface wind speed. One application of the SMB equations, modified for variable wind speed and direction, is the model WAVSMB that was originally developed by Seaconsult for industrial hindcast applications in semi-enclosed basins like the Beaufort Sea.

The wind is divided by direction into a number of compass sectors (usually eight 45° units) and the geometrical fetch is determined in each of these sectors for the site(s) of interest.

Wave growth can take place so long as the wind is steady within a given sector; wave decay begins in that sector when the wind shifts to another sector, or the wind speed is less than the phase speed of the waves. Wave height decay is assumed to be proportional to $(1-t/T_d)$ where t is the time since decay started and T_d is the fetch length divided by the deep water wave group velocity (based on the initial wave period). At any time step, therefore, any of the sectors can contribute to the total wave height and are combined as

$$H_s = \left[\sum_{i=1}^N H_s(i)^2 \right]^{1/2} \quad (4.1)$$

where $i=1$ refers to the active generating sector and $i=2, \dots, N$ refer to the

sectors containing decaying wave heights. The wave period and directions are those associated with the largest $H_S(i)$.

A hindcasting application of WAVSMB was made in the Beaufort Sea with measured wave data for verification of the model. The map in Fig. 4.1 shows the hindcast site, its fetches and the locations of the wind and wave measurements. The results for a storm in August 1981 (Fig. 4.2) illustrate that the peak wave heights predicted by WAVSMB agree with the Waverider values at Station 196 (the hindcast point) to within 1% for the 1/10th ice cover fetch length. Following the storm peak, the discrepancy between the hindcasted and measured wave heights highlights a general difficulty of forecasting waves in the presence of pack ice. The ice edge definition is very imprecise to start with (obtained here from the weekly AES ice charts) and it can be very mobile under wind forcing (E. Hudson, AES Edmonton, pers. comm., 1984). In the August 1981 storm, the strongest winds were from across the ice (fetch sectors 7 and 8); this being the case, the fetch length could easily have diminished during the storm.

A wind-wave model similar to WAVSMB was constructed for Transport Canada (Baird, 1978). Figure 4.3 shows a one-month wave hindcast in Lake Superior by Baird's model compared with recorded wave heights. Based on many comparisons averaged over three hindcast years, Baird reported errors in H_S ranging from 10% to 25%.

The great advantage of the SMB equation models of the WAVSMB formulation is their computational simplicity and efficiency. Their application, however, is limited to deep water basins of small dimensions compared with the size of wind systems. For open ocean modelling, the solution technique must be altered to account for variable fetch lengths due to moving wind fields. A model of this type based on Wilson's (1963) "moving fetch" solution of the SMB equations has been designed for METOC, Halifax, by the MEP Company under contract to AES (MEP, 1982; 1983).

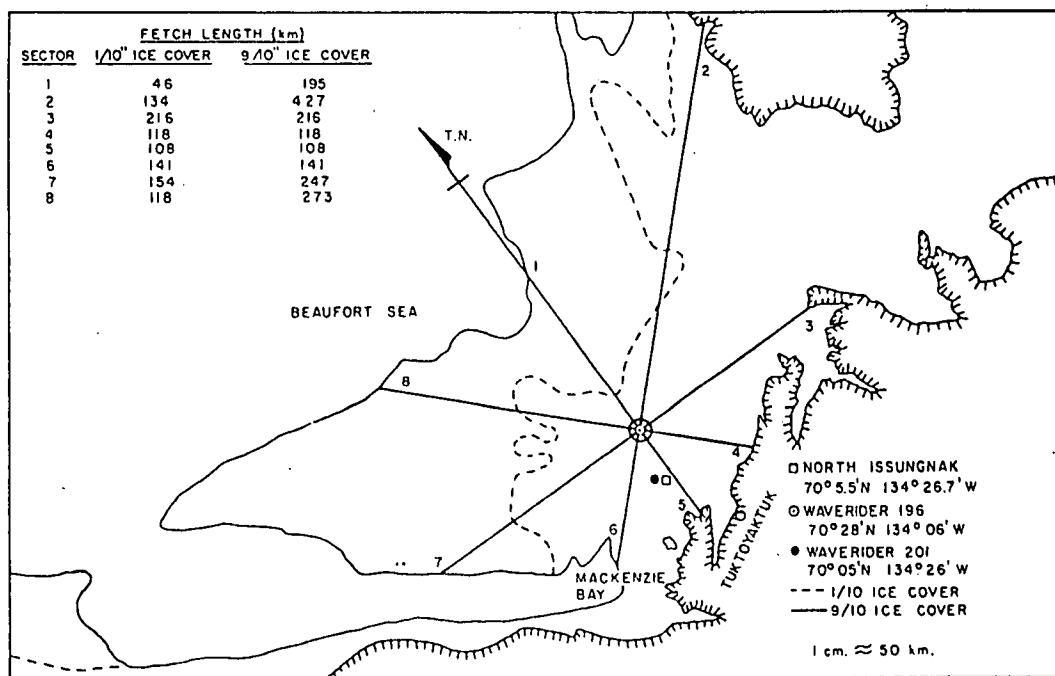
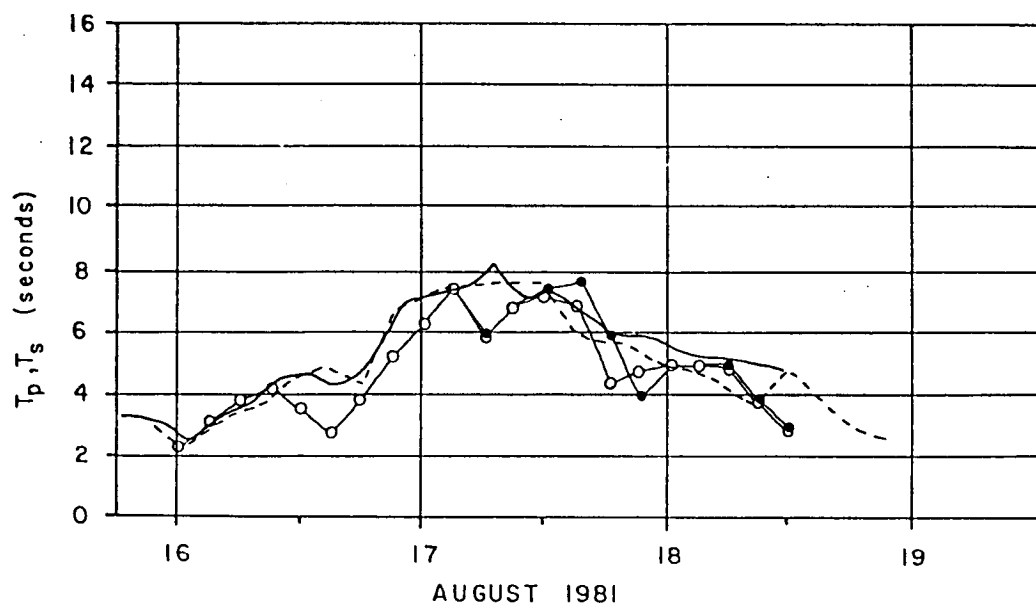
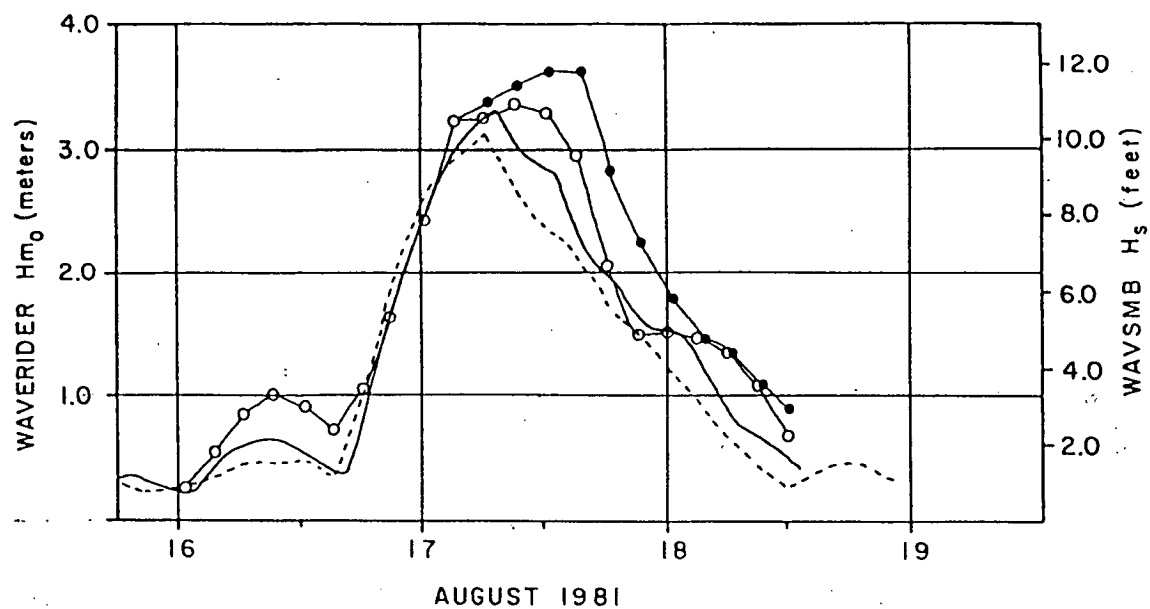


Fig. 4.1 Map showing locations of the hindcast site, the wind measuring station, and the Waverider buoys. The ice-limited fetch lengths are also shown.



- WAVERIDER 196 70°28'N 134°06'W
- WAVERIDER 201 70°05'N 134°26'W
- WAVSMB 1/10th ICE COVER
- WAVSMB 9/10th ICE COVER

Fig. 4.2 Time-series of predicted significant wave height (H_s) and period (T_s), together with measured characteristic wave height (H_{m0}) and peak period (T_p).

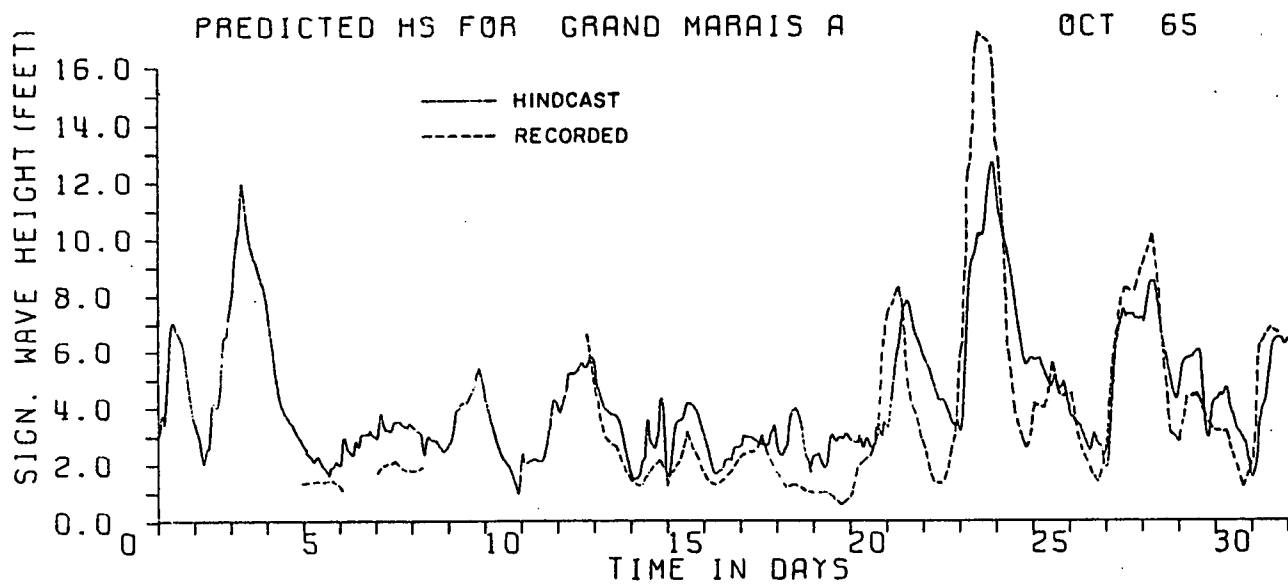


Fig. 4.3 Comparison of hindcast and recorded wave heights in Lake Superior in October 1965. (From Baird, 1978).

4.2 Parametric Spectral Wave Models

The basic concept in parametric spectral wave modelling is to solve a conservation of energy equation as a function of time, and to compute in this way the change in energy at the point of interest. From the solution $E(f)$, H_{m0} and T_p can be readily determined. The energy conservation equation in one dimension is (Hasselmann et al., 1976):

$$\frac{\partial}{\partial t} E(f) + \bar{c}_g \frac{\partial}{\partial x} E(f) = S \quad (4.2)$$

where $E(f) = \int F(f, \theta) d\theta$,

$$\bar{c}_g(f) = \frac{1}{E(f)} \int c_g' \cdot F(f, \theta) d\theta,$$

S represents the net energy source function and c_g' is the group velocity of the wave component parallel to the downwind sector at frequency f . In deep water $|c_g| = (8/3\pi) \cdot (g/4\pi f)$ and represents the directionally averaged group velocity, assuming the wave energy has a cosine-squared distribution about the wind. In order to integrate (4.2) the source function has to be specified; as noted previously, S_{n1} could in principle be calculated, but then S_{in} and S_{ds} still have to be specified empirically. Because it is not practical to evaluate S_{n1} directly in wave modelling applications, a specific spectrum is used to transform (4.2) into an easily integrated parametric form. Hasselmann et al. (1973, 1976) used the JONSWAP spectrum and that model, referred to as "Hasselmann's model" in this report, is discussed in the next subsection followed by a number of subsequent models developed by Hasselmann's coworkers. The GONO model (Subsection 4.2.3) uses a different spectral form, but the principle is similar.

4.2.1 Hasselmann's Model

This model was described in detail by Hasselmann et al. (1976) but its formulation followed from the earlier JONSWAP work. Essentially it is assumed that the parametric spectrum \hat{E} can be used to parameterize the wave-wave interaction term, S_{n1} (because this term is so important to the theory, it occupies a prominent position in the derivation of all the continuous spectral models). Further, it is assumed that if \hat{E} represents all wave spectra well that arise during integrations of the wave model, then \hat{E} can

also be used to parameterize all remaining terms in the energy balance equation. Making the substitution for \hat{E} in (4.2) yields

$$\frac{\partial a_i}{\partial t} + D_{ijk} \frac{\partial a_j}{\partial x} = T_i \quad (4.3)$$

where the propagation velocities, D_{ijk} , and the source terms, T_i , are functions of the five spectral parameters, a_i . The set $a = \{f_p, \alpha, \gamma, \sigma_a, \sigma_b\}$ is defined in (2.16).

Hasselmann et al. (1976) argue that of the five spectral parameters only the first two, f_p and α , are necessary because of the shape invariance of the spectrum: as a result a prognostic model for wave energy is presented in terms of $v = f_p U/g$ (non-dimensional f_p) and α . The resulting equations are similar in form to (4.3).

In order to solve these equations, empirical formulae are substituted for the wind input and dissipation processes, and the calculation is designed to ensure that the observed α to v relationship is reproduced by the model. Initial (usually $E=0$) and boundary conditions are also supplied.

Hasselmann et al. (1976) then go on to show that because the nonlinear term in the equation for α is dominant, and is balanced by the wind-generation term, a simple relation between α and v results

$$\alpha = 0.032 v^{0.66} \quad (4.4)$$

A power series expansion for α and v , substituted into the two-parameter prognostic equations yields a zero-order equation for v

$$\frac{1}{v} \frac{\partial v}{\partial \tau} + P \frac{\partial v}{\partial \eta} = - N v^{7/3} + \frac{1}{U} \frac{\partial U}{\partial \tau} + \frac{\partial U}{\partial \eta} \quad (4.5)$$

where $P = 0.95$,
 $N = 5.5 \times 10^{-4}$,
 $U =$ wind speed at 10 metres,
 with $|c_g| = 0.85 g/4\pi f_p$

Because the validity of this model (i.e., Equation 4.5) relies on a universally applicable α to ν relationship, Hasselmann et al. (1976) present the data shown in Fig. 4.4 to support the relationship (4.4): these data are from many different sources, including JONSWAP and hurricanes AVA and CAMILLE. In the 1976 paper, neither the two-parameter prognostic equations, nor the one-parameter ν equation, are solved using a specified wind field and the resulting spectra are not compared with observations. Hence the model is unverified, which is understandable because, in order to achieve good spectral comparisons, swell wave energy would have to be parameterized in \hat{E} . This requires a hybrid model in which the swell waves (defined in terms of non-dimensional frequency ν) are treated separately from the wind-sea. The development of the hybrid model was carried out jointly by the Max Plank Institute (MPI) in Hamburg, the Hydraulics Research Station (HRS) and the Institute of Oceanographic Sciences (IOS) in England, and reported by Guenther et al. (1979), Ewing et al. (1979) and Guenther and Rosenthal (1979). This work produced the NORSWAM model which was subsequently used for a major North Sea hindcast.

Extensions to Hasselmann's Work: HYPA and HYPAS

The logical extension to the one- and two-parameter models is one including all five JONSWAP coefficients. In principle this generalizes the model and should improve the shape of the predicted spectra. However, it is well known that the mean propagation direction of long waves lags changes in wind direction considerably. Thus, any attempt to reproduce directional spectra with a set of prognostic equations derived only from a one-dimensional spectrum could not be expected to perform well under most natural wind conditions. To improve the model in this respect a sixth prognostic variable, mean wave direction $\bar{\theta}$, which is a function of frequency, was added to the set. This set yields six prognostic transport equations to be solved at each time step, and is the basis of the HYPA model (Guenther et al., 1979) which was referred to in the SWAMP report (SWAMP, 1985).

The addition of mean wave direction as a prognostic parameter is an important step up from other one-parameter spectral models (Haug, 1968; Toba et al., 1985; Janssen et al., 1984) in which, with some loss by radiation into swell, wave directions at all frequencies in the wind-sea portion of

J, COMPOSITE DATA SET

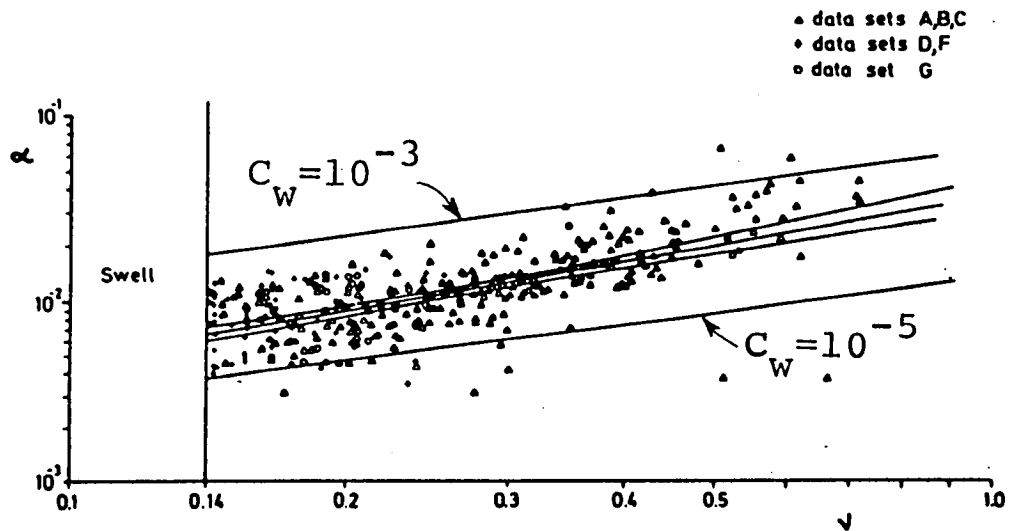


Fig. 4.4 Comparison of the α to ν relationship with wave data from many sources (see Hasselmann et al., 1976). The solid parallel lines correspond to wave-induced drag coefficients $C_W = 10^{-3}$ and $C_W = 10^{-5}$.

the spectrum are assumed to adjust instantaneously to the local wind direction. Inclusion of $\bar{\theta}$ allows HYPA to develop more varied spectral shapes and directional lag effects for non-uniform wind fields than the other, simpler formulations. Evidence that these directional effects in HYPA are actually correct is lacking, although they appear intuitively reasonable for idealized tests (SWAMP, 1985).

Swell, defined by those components that propagate faster than the wind speed, are treated as completely decoupled from the growing wind-sea portion. Components at large angles to the wind are also classed as swell, and HYPA transfers wind-sea energy into swell as a continuous function of the rate of change of wind direction. Provision is also made to absorb swell back into the wind-sea under certain conditions. Swell propagation is computed using characteristic ray paths.

HYPAS is a shallow water version of the model formulated on the same theoretical framework, but where a depth-dependent spectral form--the TMA spectrum (Bouws et al., 1985a)--is used in place of the JONSWAP form and the group velocity of waves is based on the dispersion relation for finite-depth water. The TMA spectrum degenerates to the JONSWAP equation in deep water and so is consistent in that respect with HYPA. The prognostic equations in HYPAS therefore contain different terms than in HYPA but are solved in a similar manner. A good scientific description of HYPAS has not yet been published (it is only given cursory treatment in the SWIM (1985) papers), and so details of the formulation are lacking. A comparison of predictions in deep and shallow water (significant wave height and mean crossing period) are shown in Fig. 4.5 for a storm sequence in the North Sea on November 20 to 26, 1981. The height predictions in deep water are not particularly good although all models (BMO and GONO are described below) collapse onto the measurements made in 27 m of water. Although the intent of this work (Bouws et al., 1985b) was a shallow water intercomparison, we note that in 27 m of water with $H_s = 5$ m and $T_p \approx 12$ s, $d/gT^2 = 0.019$ and the waves are about mid-way in the transitional range between deep and shallow water. The comparisons are thus not critical tests in the shallow water sense. Differences between models, and between predictions and measurements, have been explained by

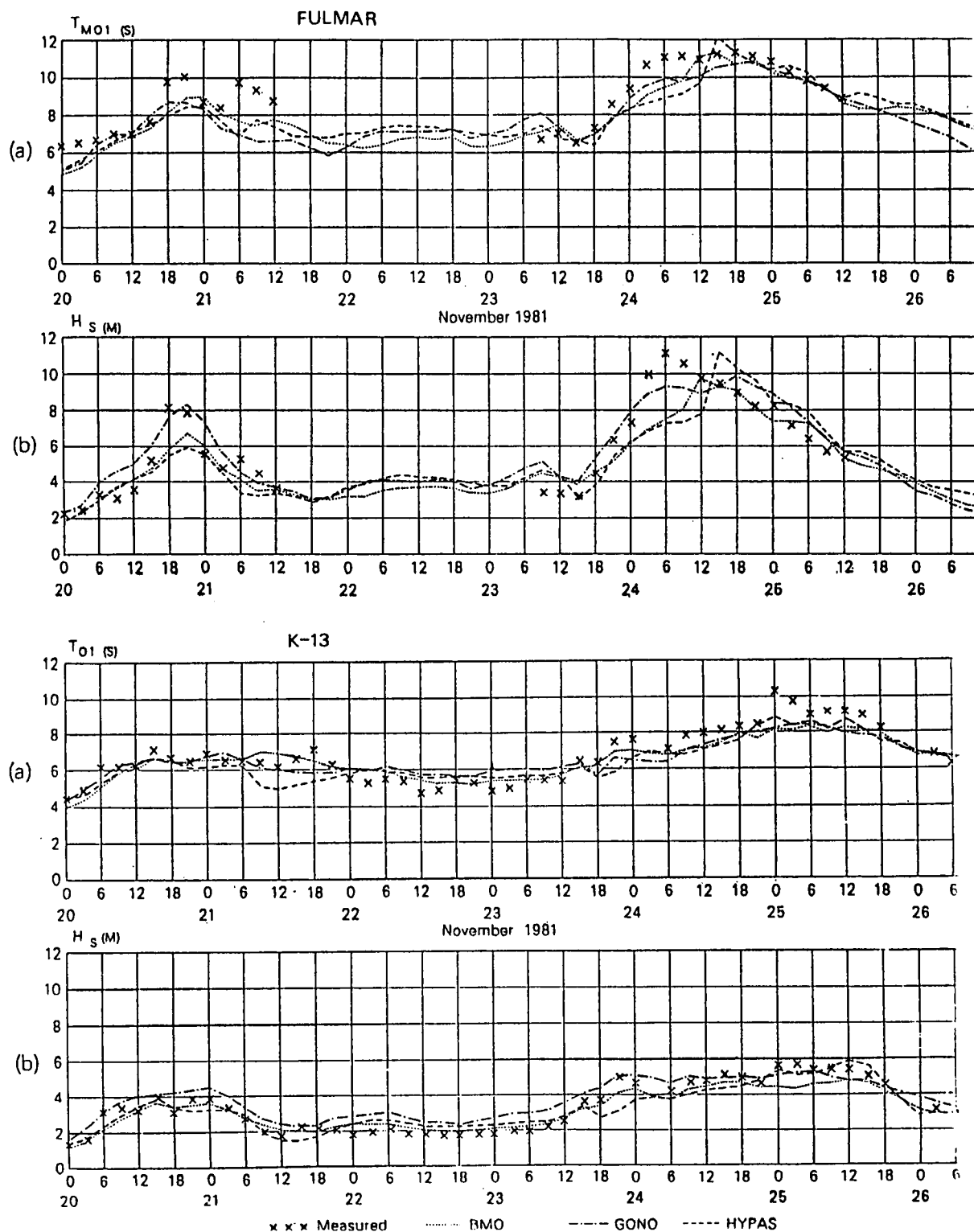


Fig. 4.5 Time-series plots of (a) mean zero-upcrossing period $T_{m0,2}$, (b) significant wave height H_s for the Fulmar and K-13 locations during the hindcast period November 20-26, 1981. Results from the three models are intercompared and verified against measured data. (From Bouws et al., 1985b).

wind field variations and the characteristics of each model with respect to non-stationary wind fields and swell, rather than in terms of shallow water, or the type of spectral representation used in each.

Third-Generation Models

The greatest restriction on HYPA (HYPAS) results is that the spectral shape is defined a priori and does not evolve to its final form as a balance of the source terms in the energy conservation equation. Thus although the predictions are in reasonable agreement with most measurements, for integral properties of the spectrum (H_s), verifications are seldom discussed in terms of two-dimensional spectral shape, or even in terms of how well the peak frequency is modelled. Moreover, the JONSWAP spectrum was derived from reasonably steady winds on restricted fetches; thus, HYPA and HYPAS do not necessarily generalize correctly to other wind fields, or even to open ocean conditions (JONSWAP may be too peaky, in general).

The objective of the third-generation models (a term coined, we believe, by K. Hasselmann in 1982) is to remove the restriction of a prescribed spectral shape, and to compute the complete spectrum explicitly as a superposition of the three source terms, S_{in} , S_{nl} , and S_{ds} , plus the propagation terms. The emphasis lies on the method of computing S_{nl} , since this term is responsible for redistributing energy within the spectrum, and hence for its shape under growing conditions. The central problem consists of finding efficient methods for computing the third-order wave-wave interactions expressed in the Boltzmann integral (Hasselmann, 1961).

Over the past twenty years this integral has been computed exactly (Hasselmann, 1963b; Sell and Hasselmann, 1972; Webb, 1978; Masuda, 1980), and in approximate forms (Longuet-Higgins, 1976; Fox, 1976; Dungey and Hui, 1979). A dispersion-operator approximation for small scattering angles was also used for the integration by Hasselmann and Hasselmann (1981) and Hasselmann et al. (1984). None of these approximate methods are considered accurate enough for typical wind-sea spectra (Komen et al., 1984); however, an alternative approach taking advantage of the symmetry properties of the wave number interactions in phase space (Hasselmann and Hasselmann, 1981; Hasselmann et al., 1984) is both sufficiently accurate and fast enough to

compute in a wave model. This method is, in fact, used in a third generation global wave model (Hasselmann and Hasselmann, undated; Komen, 1984) that is proposed for operational use in Europe commencing in about 1988.

Other efforts at parameterizing S_{n1} have been made to improve existing second generation models, particularly in the discrete spectral class (see below). The two most important are parameterizations using empirical orthogonal functions (EOF's) and the "discrete interaction approximation" (Hasselmann et al., 1984).

EOF's in terms of two shape parameters (peak enhancement factor γ and directional spread exponent s) have been derived from a database of 18 exact computations for various JONSWAP spectral distributions with γ varying from one to seven and a number of different s -values. The source function is then specified in terms of a mean \bar{S}_{n1} for the range of parameters (γ, s) considered and the sum of an expansion, truncated to five functions, representing the variability of S_{n1} about the ensemble mean. For the range of γ and s parameters considered this provides an effective method for estimating S_{n1} at each time step; it is implemented in the model published by Allender et al. (1985).

The discrete interaction approximation refers to an integration procedure similar to the exact computation in the symmetrical interaction phase space referred to above and in Komen et al. (1984), but where interactions are confined to the dominant neighbouring wavenumbers plus a finite distance set of more removed wavenumbers. In the approximate form the Boltzmann integral is taken over a two-dimensional continuum and four discrete frequencies instead of the five-dimensional interaction phase space.

The algebraic details of both approximate methods are complicated and will not be reproduced here. Hasselmann et al. (1984) have presented results from both methods to show how well they model the exact S_{n1} calculations for JONSWAP spectra. Figure 4.6 illustrates the fit obtained with each procedure; in the EOF case the spreading function was of the cosine- $2s$ form, a function not used in the EXACT- S_{n1} calculations from which the EOF's were originally derived, and, particularly at zero degrees (mean wave direction),

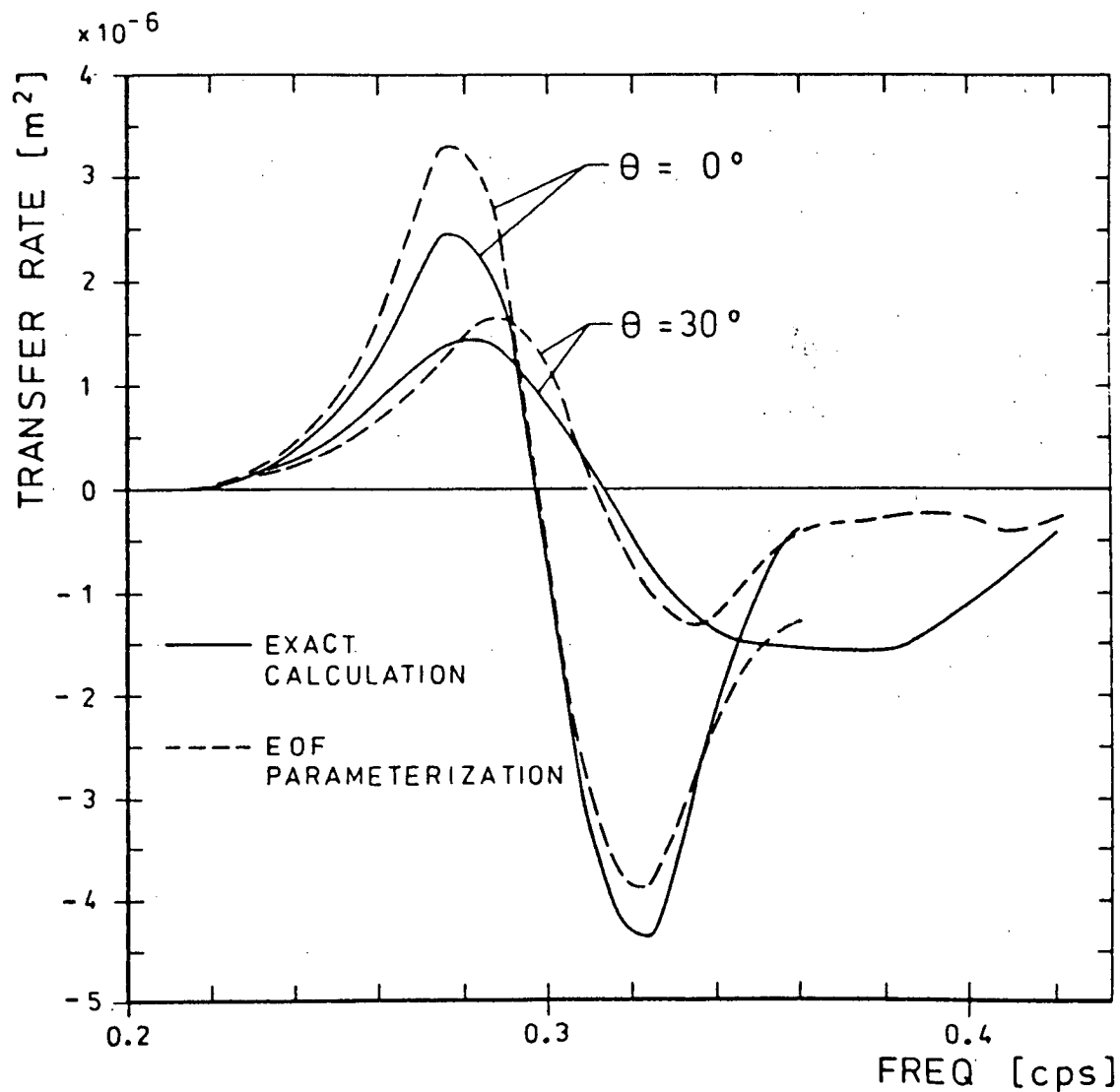


Fig. 4.6a Comparison of exact computations of the two-dimensional functions S_{n1} with the parameterized form derived from an EOF expansion corresponding to a spreading function of the cosine-2s form which was not a member of the EOF ensemble. The one-dimensional spectra are JONSWAP spectra.

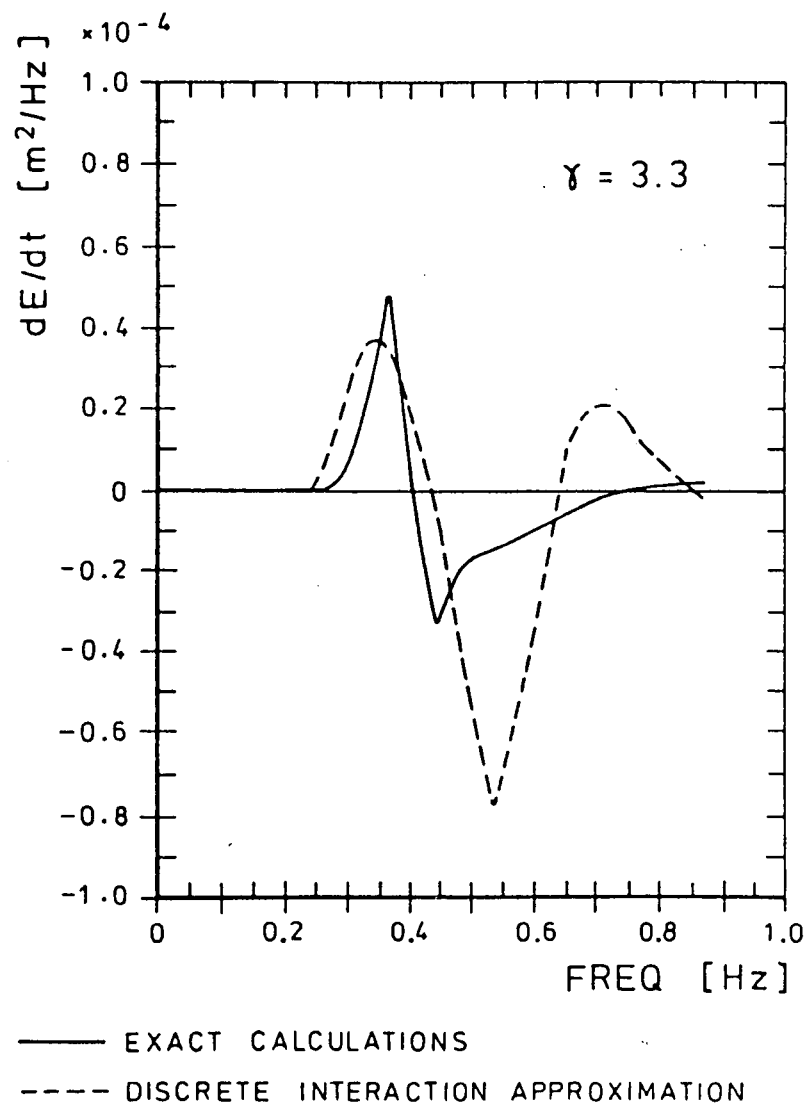


Fig. 4.6b Comparison of the exact one-dimensional distribution S_{n1} with the discrete interaction approximation for a JONSWAP spectrum.

the positive lobe is overestimated. Conversely, the discrete interaction approximation overpredicts the negative lobe but shows good agreement on the positive energy transfer rate side. Hasselmann et al. (1984) argue that the positive lobe is the more important since it controls the transfer of energy to lower frequencies and has an important bearing on how well T_p is predicted. Figure 4.7 shows a series of non-dimensional spectra at various fetches $x^* = gx/u_*^2$ ($f^* = u_* f_p/g$) computed with the EXACT- S_{nl} and the discrete approximation; there is good qualitative agreement in f^* and total energy as noted by Hasselmann et al. (1984).

Apparently Hasselmann and his co-workers have implemented the largest part of the nonlinear wave-wave interaction theory in computational methods that are matched to operational wave model requirements. Much testing still remains to show that these procedures actually reproduce oceanic wave spectra within the bounds of sampling error, particularly for directional spectra under rapidly changing wind fields. One theoretical example of such spectra is shown in Fig. 4.8. This work is tackling one of the most important aspects of wave prediction modelling, and may be expected to lead to much more general codes than earlier models based on highly empirical growth equations. However, it is fair to point out that one term remains that is very uncertain in all model codes, namely the dissipation term S_{ds} . Various researchers (e.g., Hasselmann et al., 1973) have attempted to compute it as a difference of the remaining terms in the energy balance equation, but this largely fails because of the uncertainty in estimates of S_{nl} and the divergence of propagating wave energy. Hasselmann et al. (1984), and Phillips (1980) in particular, comment on the difficulties of estimating both S_{ds} and S_{in} including three-dimensional effects of air flow over a wavy surface.

Thus, third-generation models should be an improvement on earlier codes from a theoretical standpoint, but it remains to be seen if this is borne out in practice given the empirical nature of the other terms.

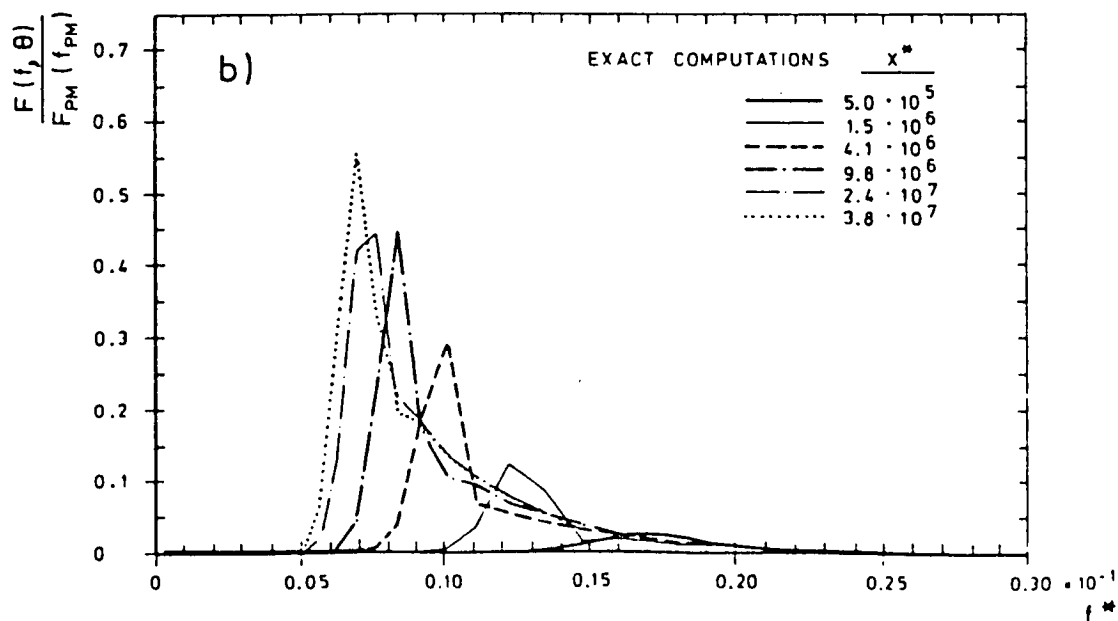
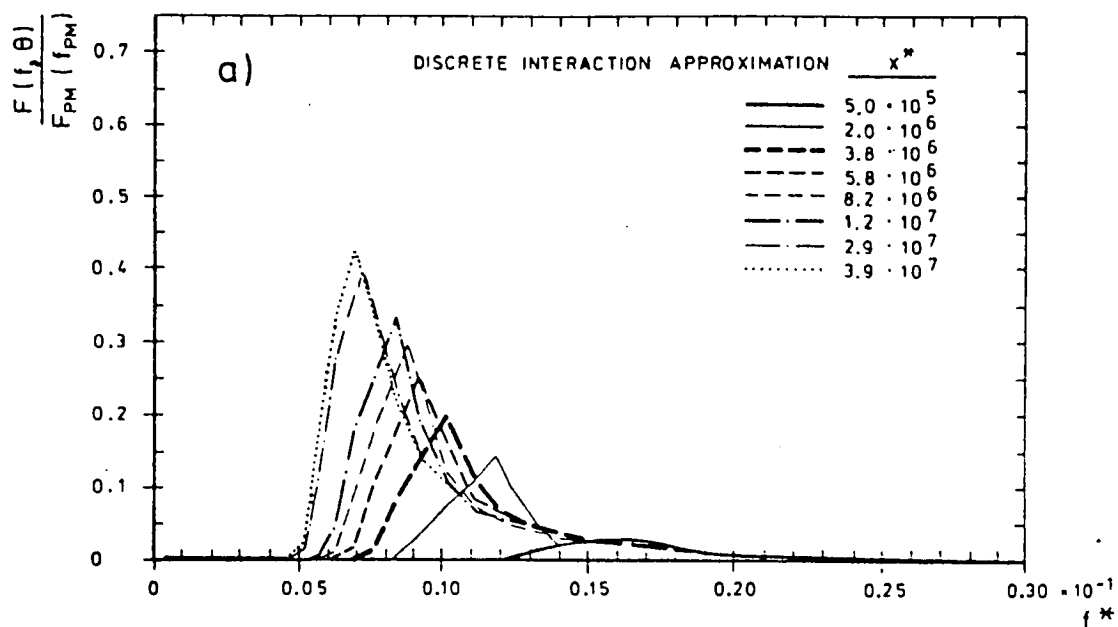


Fig. 4.7 Comparison of the growth of fetch-limited one-dimensional spectra computed using (a) the discrete interaction approximation and (b) the exact form of S_{n1} .

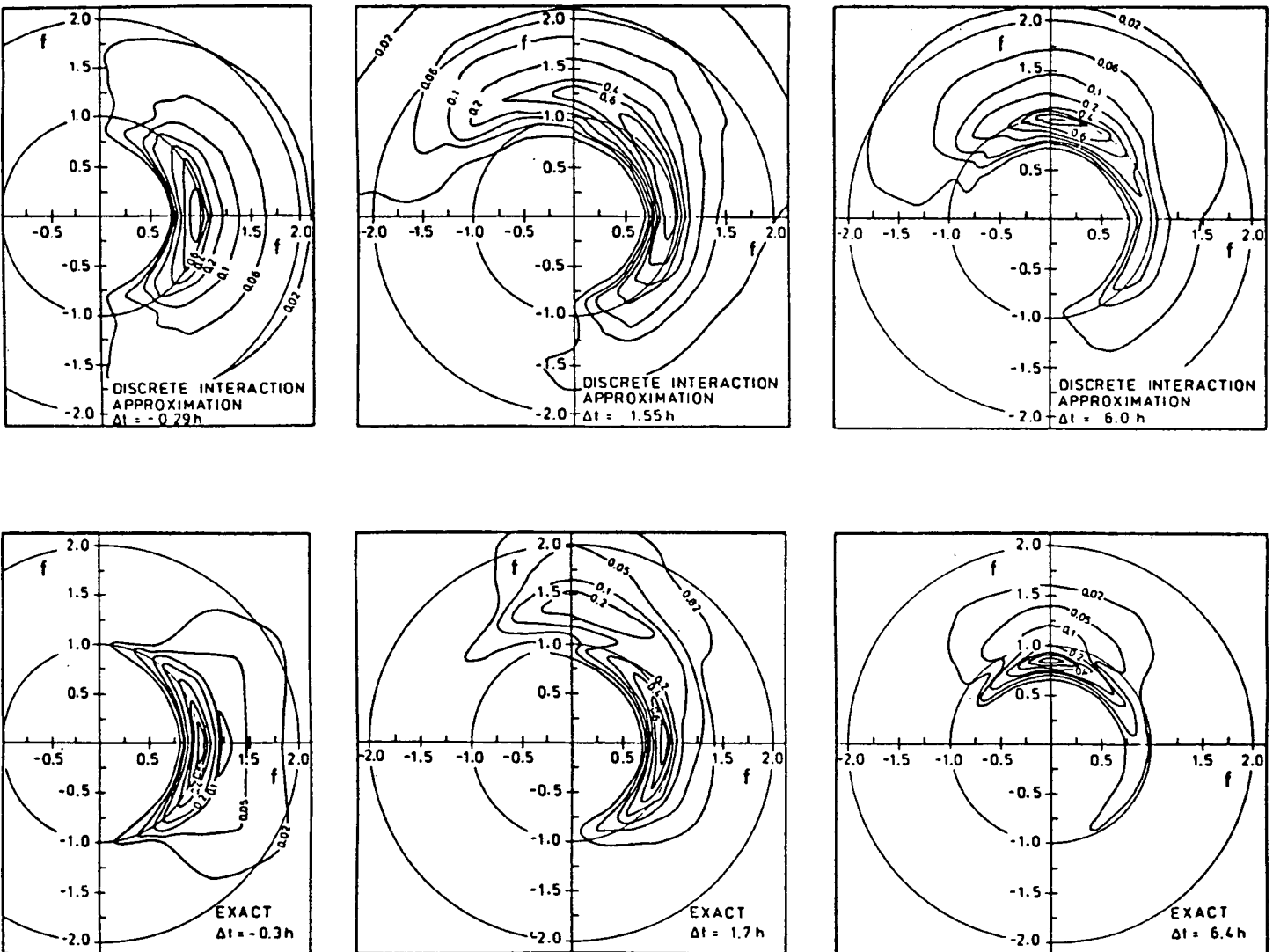


Fig. 4.8 Comparison of the response of a two-dimensional wave spectrum to a sudden 90° change in wind direction at time t_0 computed using the exact form and the discrete interaction approximation of S_{n1} . $\Delta t = t - t_0$, and t_0 is the time at which the peak frequency is just twice the fully developed peak frequency. The strength of the wind forcing remains constant ($u_* = 0.357$ m/s). (From Hasselmann et al., 1984).

4.2.2 NORSWAM: A Hybrid Model for Wind-Sea and Swell

As already noted, the parametric spectrum E is strictly valid for fetch-limited growing wind-seas, i.e. for winds such that $v > 0.13$. In other words, when $U < g(0.13)/f_p$ the phase velocity of waves at the spectral peak exceeds the wind velocity, and it is assumed that no energy is transmitted from the atmosphere to the sea waves. Thus the energy spectrum cannot be maintained at a level at which the wave-wave interaction term, S_{nl} , is effective and the wave field propagates freely as swell. The energy equation (4.2) could be solved for this condition, with $S \equiv 0$, by finite differences on a regular grid of points, or by representing the swell field on a set of characteristic rays. In NORSWAM the characteristic ray method (similar to that used by Barnett et al., 1969) has been implemented. For each swell frequency, f , the model is covered with a mesh of rays, and the swell energy is represented by discrete packets at points along each ray separated by a distance of $\Delta t \cdot c_g(f)$. These energy packets then propagate at their group velocities $c_g(f)$, which depend upon the packet frequency. Δt is the time step of the wind-sea and swell submodels.

NORSWAM uses one more free parameter, γ , in \hat{E} than those described above by Hasselmann et al. (1976) for the two-parameter model. This addition was found to be necessary to model the energy exchanges between the wind-sea and swell (HRS, 1977a; 1977b). Thus the hybrid model consists of a three-parameter (f_p, α, γ) continuous spectral wind-wave model based on Hasselmann's formulation, together with a characteristic ray swell model.

For hindcasts of extreme waves in the North Sea the grid shown in Fig. 4.9 was used. The characteristic ray sets are shown in Fig. 4.10. The swell wave frequency resolution was (0.05, 0.15 Hz) in 10 steps of 0.1 Hz on each ray. The input to the model consisted of the wind vector at 10 metres above the sea at each appropriate grid point shown in Fig. 4.9. Forty-two storms were selected in the hindcast and analyzed as described by Harding and Binding (1978). A sample wind field is shown in Fig. 4.11.

During verification trials, data from two stations, Stevenson and Famita (Fig. 4.9), were used to prove the model and to establish the optimum α to v relationship. This relationship is the most important aspect of the

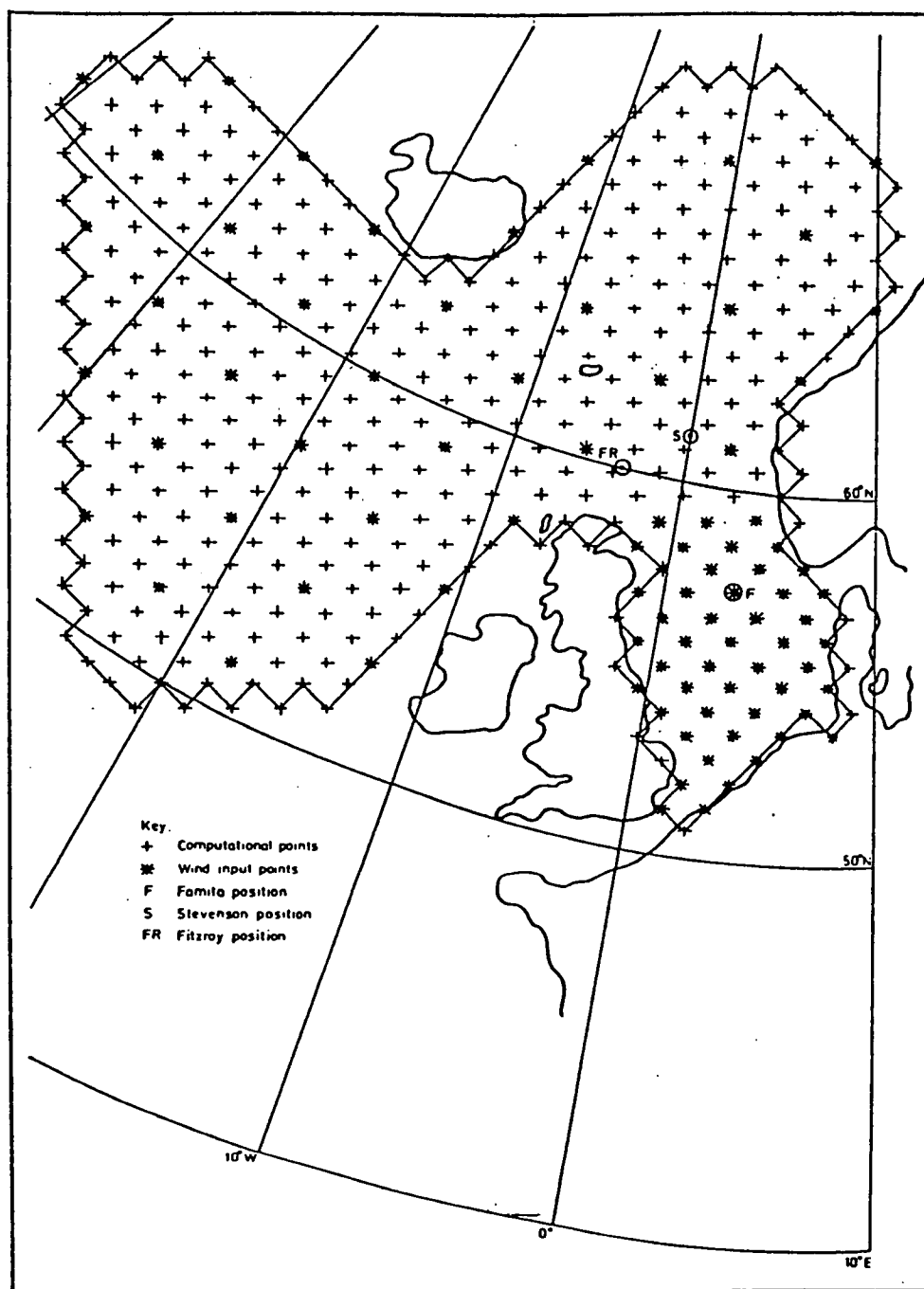


Fig. 4.9 Grid used in the numerical wave model. The wind field is defined on a 100-km grid within the North Sea and a 300-km grid elsewhere. Wave computations are made on the 100-km grid over the whole area. Wave measurements have been made at stations Famita, Fitzroy and Stevenson. (From HRS, 1977a).

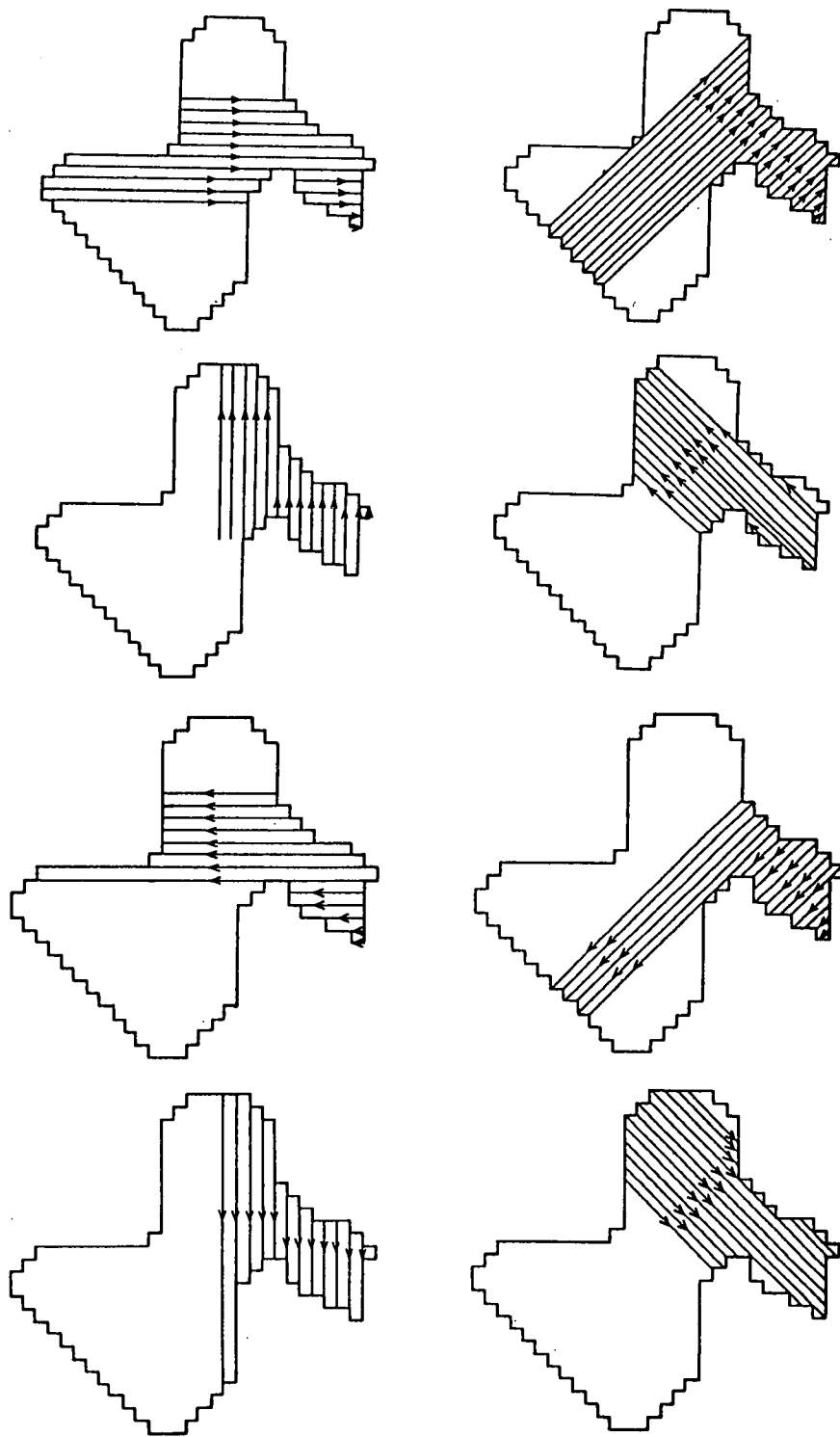


Fig. 4.10 Characteristic rays used in NORSWAM. (From HRS, 1977a).

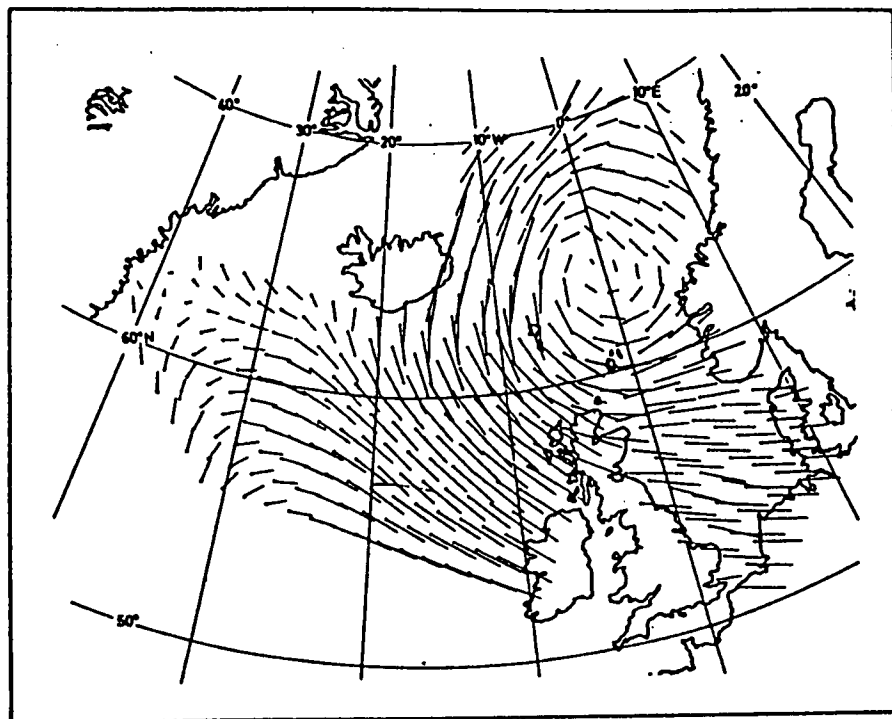


Fig. 4.11 Example of the wind field input to NORSWAM. The vectors show strength and direction of the wind. (From Guenther et al., 1979).

modelling approach and the result shown in (4.4) emerged from the NORSWAM study.

Sample spectral comparisons are shown in Fig. 4.12 at the Famita location for strong NW gales: the modelled energy content in the spectra is much greater than in the measured spectra, although the comparisons improve as the wind later begins to diminish. After 21:00 hours on October 20, 1970, the swell portion becomes increasingly important. For SE fetch-limited spectra (Fig. 4.13) the comparisons are generally good, but this is to be expected since these meteorological conditions correspond to those of JONSWAP, upon which the modelling philosophy is based.

The comparisons of significant wave height, H_s , (defined as H_{m0}) and the average wave period, T_z , are shown in Fig. 4.14 for two different sets of storms. Ewing et al. (1979) conclude that the model provides estimates of H_{m0} and T_z without bias and an rms error of about 0.7 metres.

A subsequent application of this model in the Severn Estuary has been reported by HRS (1981).

4.2.3 GONO: The Dutch Operational Forecast Model

GONO (Golven Noordzee, i.e. North Sea waves) is a coupled hybrid model in which wind-sea is modelled as an evolving parametric spectrum and swell is propagated by a ray tracing technique (Janssen et al., 1984). The invariant spectral form is the Kruseman spectrum:

$$E(f) = \begin{cases} 0 & f < f_{\min} \\ \frac{\hat{\alpha} g^2}{(2\pi)^4} \frac{1}{f_p^5} \frac{f - f_{\min}}{f_p - f_{\min}} & f_{\min} < f < f_p \\ \hat{\alpha} g^2 (2\pi)^{-4} f^{-5} & f > f_p \end{cases} \quad (4.6)$$

where f_{\min} = minimum frequency
 f_p = peak frequency
 $\hat{\alpha}$ = Phillips' parameter

$\hat{\alpha}$ is specified as an empirical function of the "stage of development" parameter ξ where

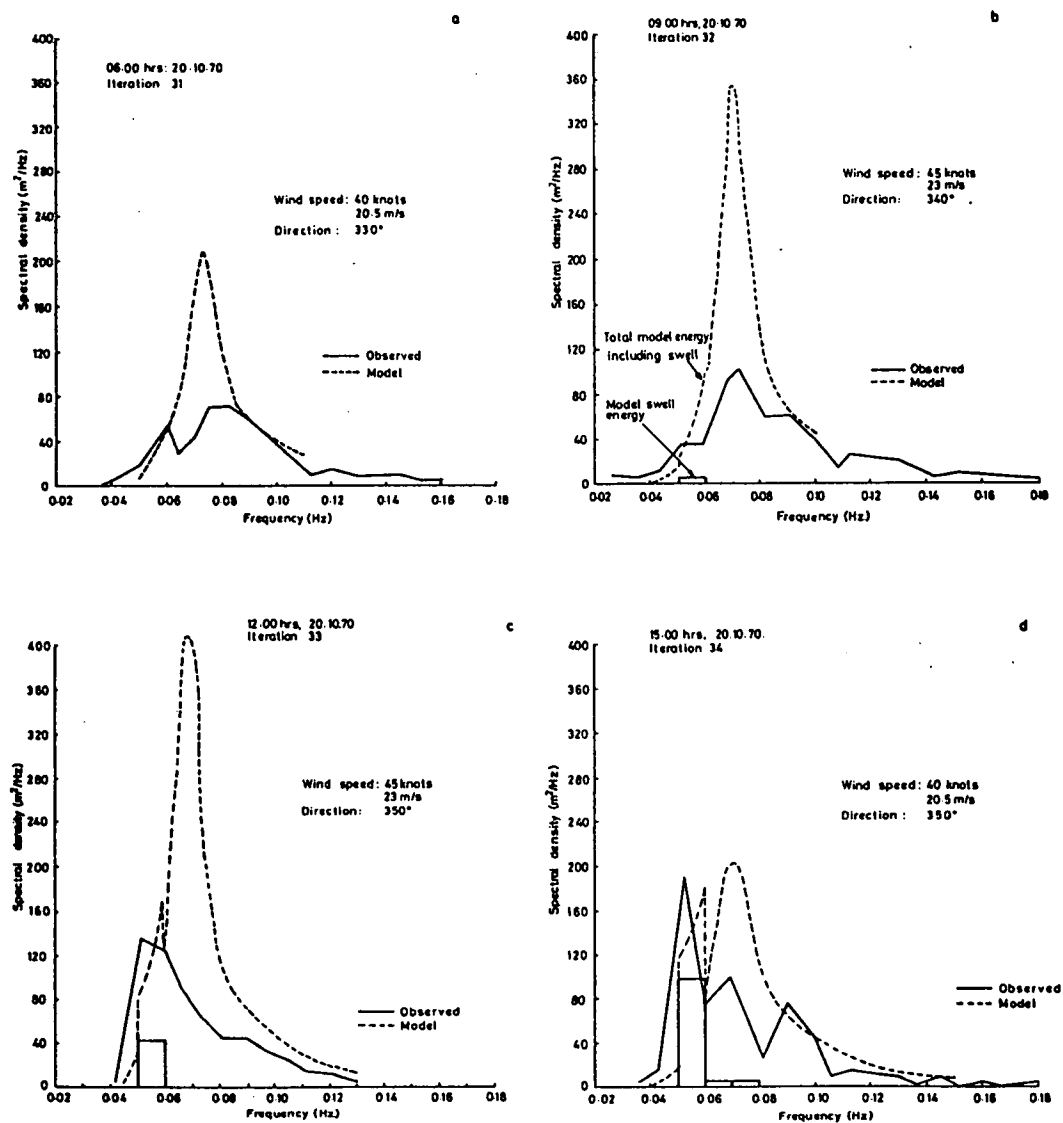
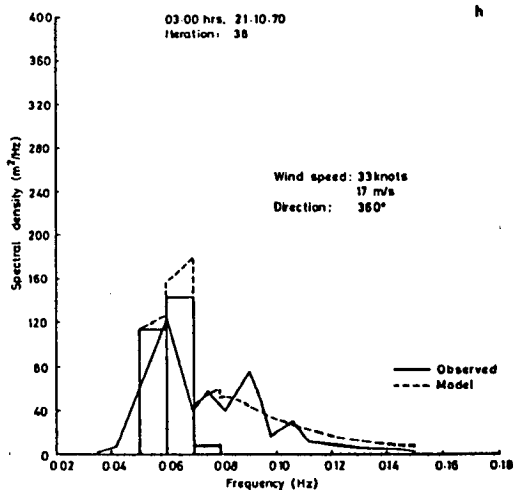
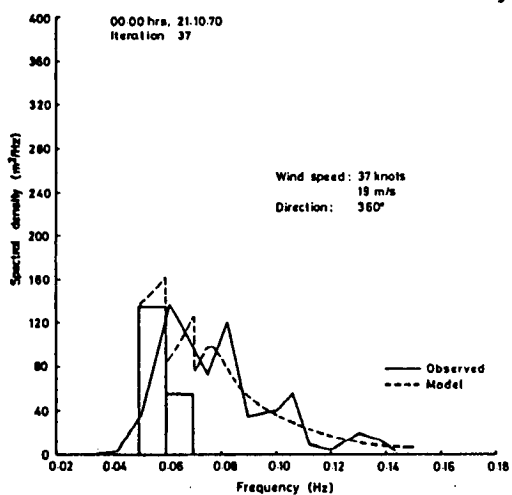
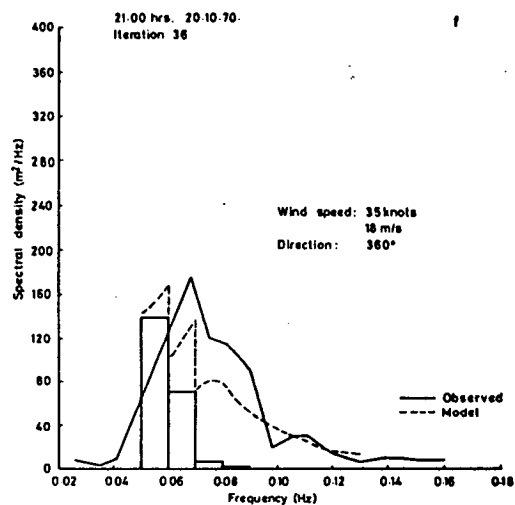
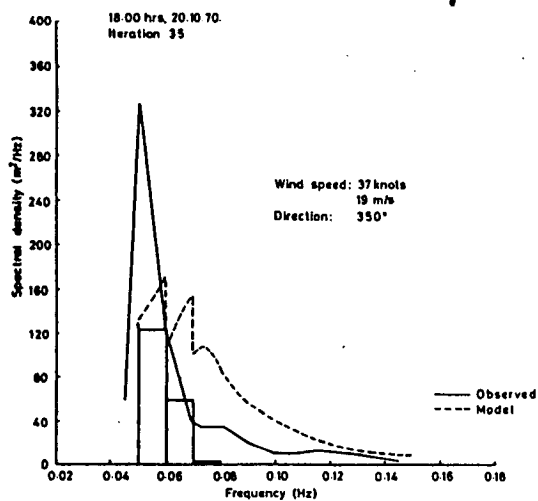
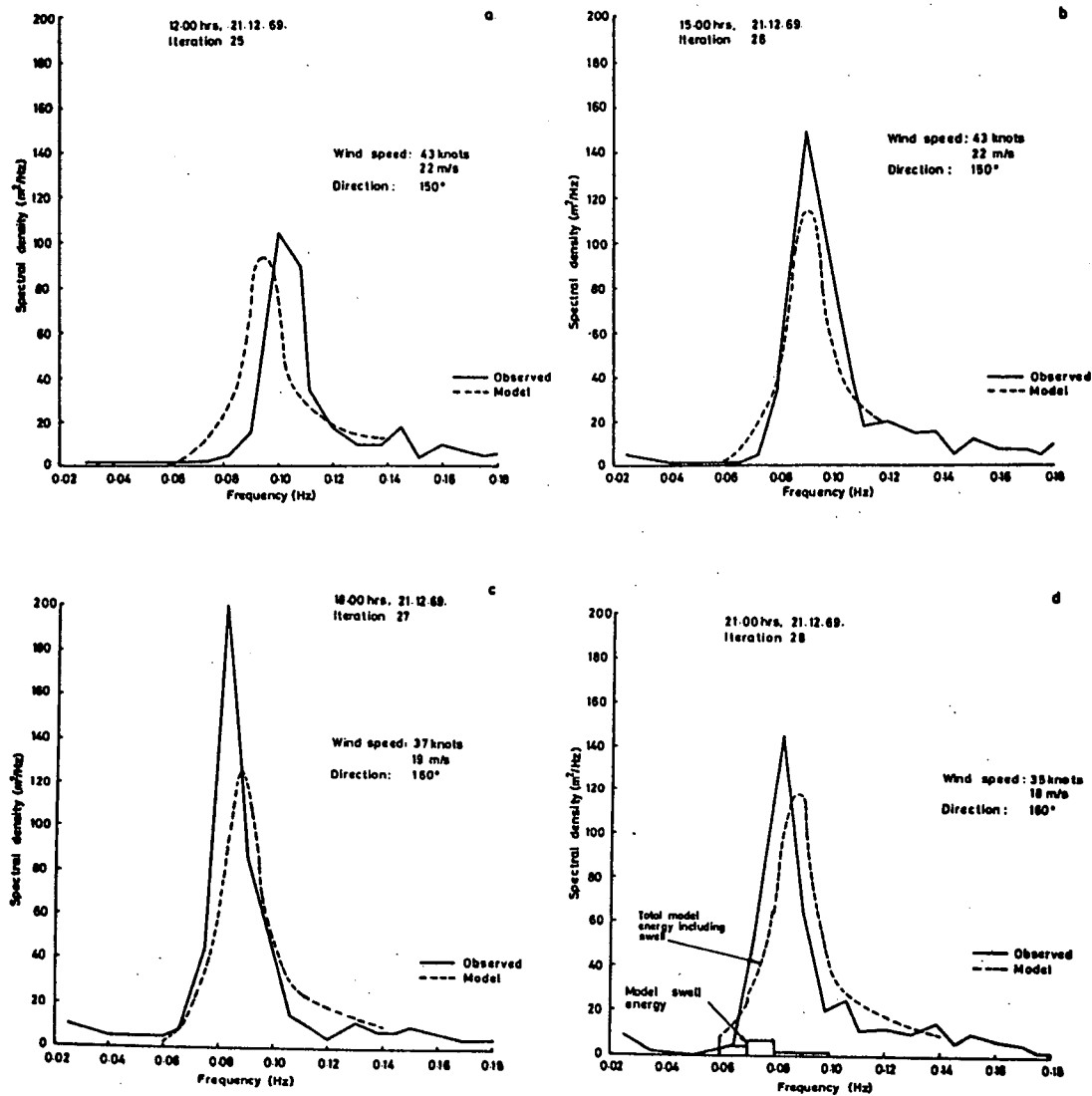


Fig. 4.12 Spectral comparisons between observed data and NORSWAM for NW winds. (From HRS, 1977a).



Storm 1 - Famita position

Fig. 4.12 Continued.



Storm 3 - Famita position

Fig. 4.13 Spectral comparisons between observed data and NORSWAM for SE winds. (From HRS, 1977a).

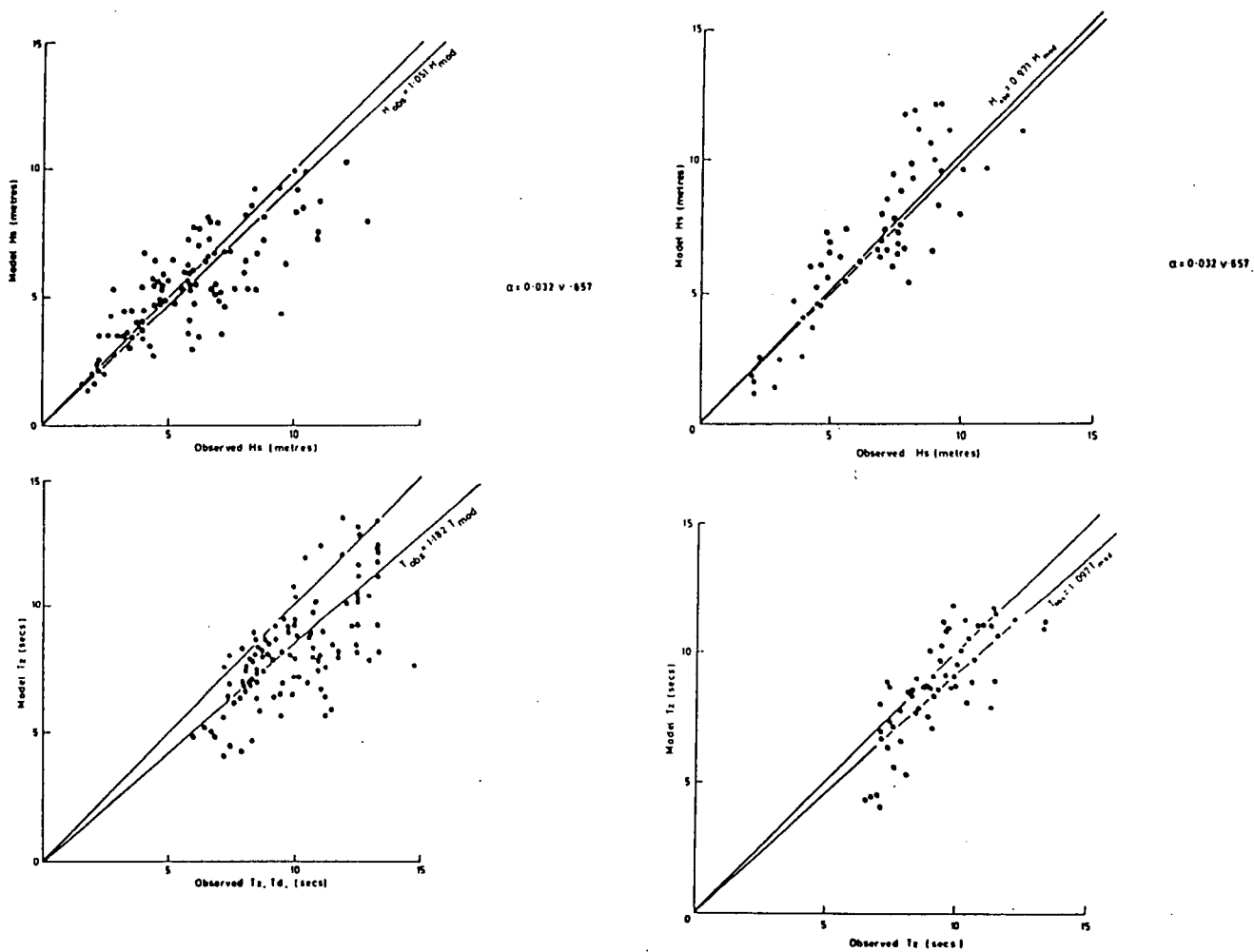


Fig. 4.14 Correlation of wave heights and periods at Stevenson for eight similar storms. (From HRS, 1977a).

$$\xi = \left[\frac{m_o}{m_o(\max)} \right]^{1/4} \quad (4.7)$$

Here $m_o(\max)$ is the maximum total energy possible for a given wind speed.

Janssen et al. (1984) report that (4.6) fits measured wave spectra as well as the JONSWAP spectrum (2.16), and was chosen for its simple analytical form. The directional spreading of $E(f)$ is assumed to be given by

$$F(f, \theta) = \frac{2}{\pi} \cos^2(\theta - \phi) E(f) \quad (4.8)$$

where ϕ is the wind direction and (4.8) is defined only for $|\theta - \phi| < \pi/2$.

Integrating the energy balance equation (2.17) with respect to frequency yields

$$\frac{\partial}{\partial t} E(\theta) + \nabla \cdot \bar{c}_g E(\theta) = \langle S \rangle_f \quad (4.9)$$

where \bar{c}_g is the average group velocity. Defining

$$\langle S \rangle_{f, \theta} = \int S \, df \, d\theta = \int [S_{in} + S_{nl} + S_{ds}] \, df \, d\theta \quad (4.10)$$

it is noted that since S_{nl} is energy conserving, it makes no contribution to $\langle S \rangle_{f, \theta}$. Further, it is argued that at infinite fetch, the total wind-sea energy is independent of position so that (4.9) may be integrated with respect to direction to yield

$$\frac{\partial}{\partial t} m_o = \langle S \rangle_{f, \theta} \quad (4.11)$$

or in dimensionless terms,

$$\frac{\partial \xi}{\partial \tau} = \frac{g}{U_{10}^3} \langle S \rangle_{f, \theta} = \hat{B} \quad (4.12)$$

A summary and definition list of commonly referenced non-dimensional wave parameters is compiled in Appendix 4.1.

Sanders (1976) developed a duration-limited growth curve (see Equation 4.13) based on a gale in the Norwegian Sea which is used to solve (4.12) for \hat{B} (see Equation 4.14):

$$\hat{H} = \tanh(at^b) \quad (4.13)$$

$$\hat{B} = \frac{ab}{8} \beta^2 \xi^2 (1 - \xi^4) \left\{ \frac{1}{2a} \ln \frac{1 + \xi^2}{1 - \xi^2} \right\}^{1-1/b} \quad (4.14)$$

where $\beta = 0.22$

$a = 6.1 \times 10^{-4}$

$b = 0.75$ and

\hat{H} = non-dimensional wave height, $4\sqrt{\epsilon}$.

Thus neither S_{in} nor S_{ds} need be specified explicitly.

The energy advection method is a first-order finite difference scheme (time-forward, upwinding). Only that portion of the directional spectrum aligned with the wind is subject to wind growth; the remainder is accounted for in the swell calculations.

GONO is the Dutch operational forecast model for the North Sea with a grid that covers the Irish Sea and extends north to the polar ice pack, thus covering the Norwegian Sea also (Fig. 4.15). A regular Cartesian grid (17 x 36) is overlaid on a stereographic projection giving a grid size of 75 km at 60°N. For computation of the surface winds, "frictional and inertial effects" are applied by unspecified methods to output from a four-layer, quasi-geostrophic, atmospheric model (Janssen et al., 1984). The model produces forecasts four times daily and operates with a 90-min time step. The output product is a map of contoured wave height superimposed on the forecast wind field as illustrated in Fig. 4.16. The full two-dimensional spectrum is calculated only on selected grid points where energies are specified in eight period bands (0-6, 6-8, ... 18-20 s) and six directional sectors.

In Fig. 4.16, four model verification points are identified: Europort, Ijmuiden and Pennzoil in relatively shallow water (20 to 25 m) near the coast, and Ekofisk in the mid-North Sea. Janssen et al. (1984) report that a verification program began in December 1979 with four variables being monitored--wind speed, wind direction, wave height and H_{10} defined as four times the square root of the variance in waves with periods exceeding 10 s. However, they also comment critically on the quality of the verification

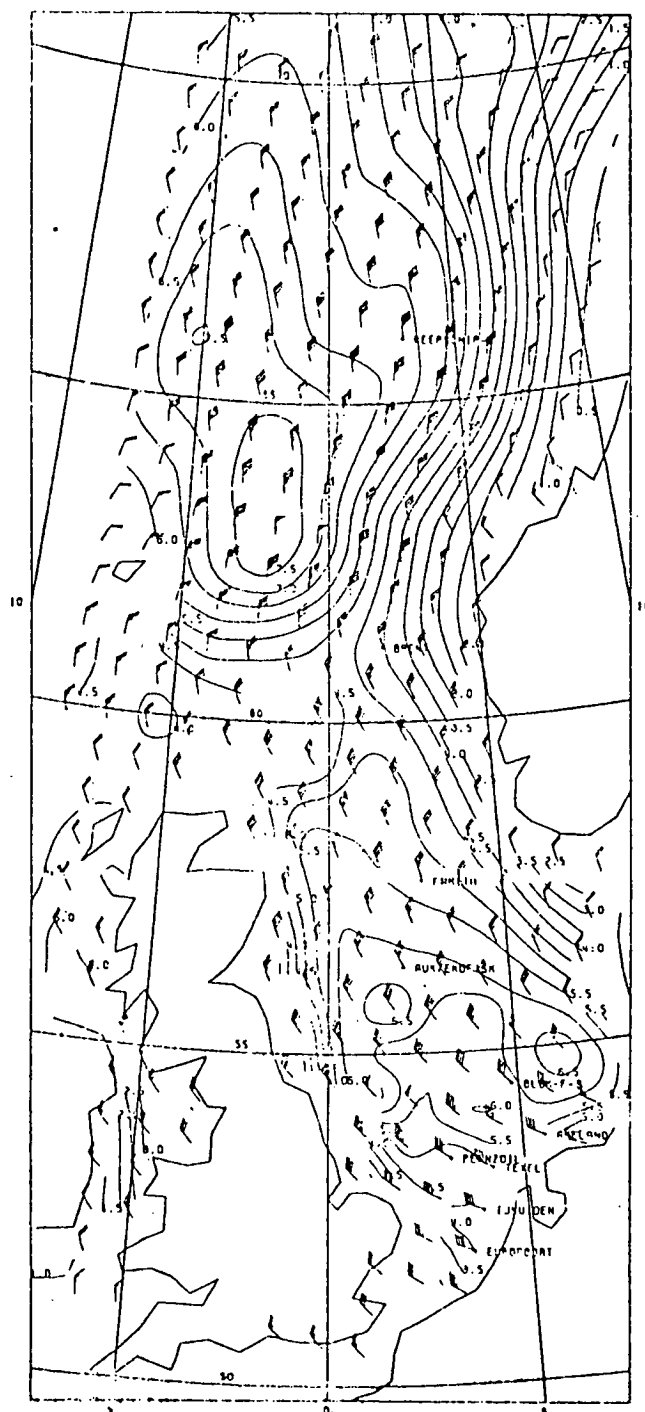


Fig. 4.16 Typical wave chart as produced by GONO. Computed lines of equal zero-moment wave height and computed winds in standard meteorological convention are indicated. Each cross bar equals 5 m/s, pennants = 25 m/s.

wind data--location of wind sensors, reduction factors for converting $U(z)$ to U_{10} , and data gaps. As a result, there is considerable uncertainty in the sources and apportioning of the observed errors.

Because GONO is run on a quite restricted region, the 500 grid points and 10 output points require only 35K of memory. Janssen et al. (1984) report that a 24-hour forecast (presumably four 6-h forecasts) with $\Delta t = 90$ min uses 10 min CPU on a Burroughs 6800.

4.2.4 Donelan's Model

Developed at the Canadian Centre for Inland Waters (CCIW) for wind-wave modelling on the Great Lakes, this model draws upon the key results from Hasselmann et al. (1973), combined with an original approach for the treatment of the transfer of wind momentum into the wave field. Donelan (1978a) stresses the point that the sea-state affects the drag of the wind on the water surface, and hence the transfer of momentum and energy from the wind to the waves depends upon the height and phase speed of the waves in addition to the wind speed. He emphasizes further that the wind stress is a vector quantity that can be added vectorially to the mean momentum of the moving wave field, a process which is physically more appealing than working in terms of a scalar property such as energy.

The conservation equation for the mean momentum of the waves is written in an analogous form to the energy conservation equation (4.2), i.e.,

$$\frac{\partial M_i}{\partial t} + \frac{\partial}{\partial x_j} (\bar{V}_j M_i) = \frac{1}{\rho g} (\tau_\eta)_i \quad ; i, j = 1, 2 \quad (4.15)$$

where M_i = total momentum vector,
 \bar{V}_j = group velocity,
 ρ = water density,
 τ_η = fraction of momentum flux producing wave growth and decay
 i, j = summation indices representing x,y coordinate directions.

This is the basic equation to be solved for a suitable parameterization of M_i . Donelan relates M_i to the wave spectrum $F(f, \theta)$, assuming an equipartition of kinetic and potential energies, by

$$|M| = \iint \frac{F(f, \theta)}{c(\theta)} df d\theta \quad (4.16)$$

$$\theta_0 = \frac{1}{|M|} \iint \frac{F(f, \theta)}{c(f)} df d\theta \quad (4.17)$$

where $c(f)$ = phase speed,
 θ_0 = mean propagation direction.

Relating the one-dimensional spectrum, $E(f)$, to $F(f, \theta)$, i.e. $E(f) = \int F(f, \theta) d\theta$, the group velocity is

$$|\bar{v}| = \frac{1}{|M|} \iint \frac{F(f, \theta)}{c(f)} \cdot v(f) \cos(\theta - \theta_0) df d\theta \quad (4.18)$$

where $v(f) = c(f)/2$.

Donelan (1978a) then uses the JONSWAP spectrum, \hat{E} , to relate the mean square water level displacement σ_η^2 , to the momentum and the peak phase speed,

$$\frac{\sigma_\eta^2}{|M|} = 0.86 c_p \quad (4.19)$$

since $\sigma_\eta^2 = \int E(f) df$. This result, plus a similar solution for $|\bar{v}|$ in terms of c_p , allows (4.15) to be recast into parametric form involving only σ_η^2 and c_p , the two dependent variables to be solved on a regular grid in x and y spatial coordinates. The prognostic equation is:

$$\frac{\partial A_i}{\partial t} + \frac{\partial}{\partial x_j} B_{ij} = \frac{-1}{\rho g} \cdot \tau_i \quad ; i, j = 1, 2 \quad (4.20)$$

where the elements of the A, B , and τ matrices are given in Table 4.1.

Thus, the JONSWAP results are used to link the momentum approach to the coupling of the wave field to the wind field; Donelan's model in its present form is then limited by two assumptions made by Hasselmann et al. (1973): (a) that an angular energy spreading function given by $\cos^2 (\theta - \theta_0)$ applies, and (b) that this spreading function is independent of wave frequency.

Table 4.1

Matrix Elements for Donelan's Model
Equation (4.20)

Element	i	j	Parameterization
A	1	-	$\frac{\sigma_{\eta}^2}{c_p} \cos \theta_o$
A	2	-	$\frac{\sigma_{\eta}^2}{c_p} \sin \theta_o$
B	1	1	$0.425(\sigma_{\eta}^2 \cos^2 \theta_o)$
B	1	2	$\frac{0.425}{2}(\sigma_{\eta}^2 \sin 2\theta_o)$
B	2	1	$\frac{0.425}{2}(\sigma_{\eta}^2 \sin 2\theta_o)$
B	2	2	$0.425(\sigma_{\eta}^2 \sin^2 \theta_o)$
τ	1	-	$(\tau_{\eta})_x$
τ	2	-	$(\tau_{\eta})_y$

Mitsuyasu et al. (1975), and Hasselmann et al. (1980) on independent data, have shown that the spreading function is a strong function of the non-dimensional frequency, f/f_p (as discussed in Subsection 2.2.2 and illustrated in Fig. 2.8).

Donelan has also indicated that spreading functions other than the cosine-squared relation may be more appropriate (Donelan, CCIW, pers. comm., 1981). As a result, areas of the model can be improved for future applications.

The main justification for approaching the problem through momentum transfer is that it allows the use of source terms, τ_i , that are aerodynamic forces produced by the form and skin drag of the wind, instead of totally empirical formulae that give an energy flux relative to a 10-m or 19.5-m reference wind speed. The problem which arises is that of the total momentum transferred to the sea surface, some fraction goes to add momentum to the waves and some fraction to the underlying currents. The fraction which actually adds to the growing wind waves is a factor to be determined in the modelling. Donelan (1978a, 1978b, 1979) has determined this fraction sufficiently well that it is not a limitation to the modelling approach.

To account for changing wind direction, two wave fields are also included: an "active" and a "fossil" field. These differ in direction by 90° or more, and account for the addition of momentum to the actively generated wave field by waves generated at earlier times.

Figure 4.17 shows a typical result for Lake Ontario during a four-day simulation: the agreement between Waverider and hindcast data is within about 10% (H_{m0}) at the time of maximum westerly winds on August 9, 1972. Two further comparisons are shown in Fig. 4.18 for significant wave height and peak period for oceanic conditions. There is general agreement in both wave height and period, but with considerable scatter at the larger values.

Schwab et al. (1984) published a second application of Donelan's model, this time to Lake Erie. In this case, verification data were available at two locations widely separated on the lake. One set of measurements, considered the more reliable of the two, was made at a fixed tower with an array of Zwarts gauges. Excellent agreement between predicted and measured

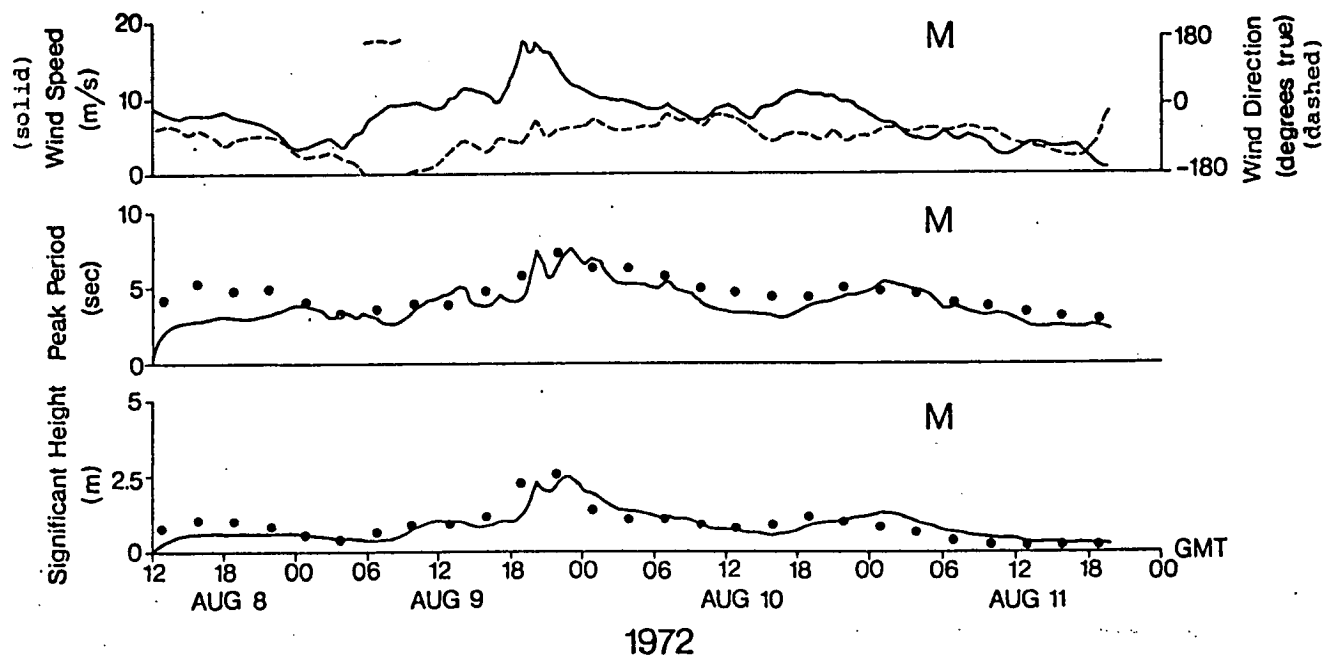


Fig. 4.17 Comparison of measured (•) and hindcast (-) wave heights and periods during a storm in Lake Ontario (Donelan's model). (From Donelan, 1978a).

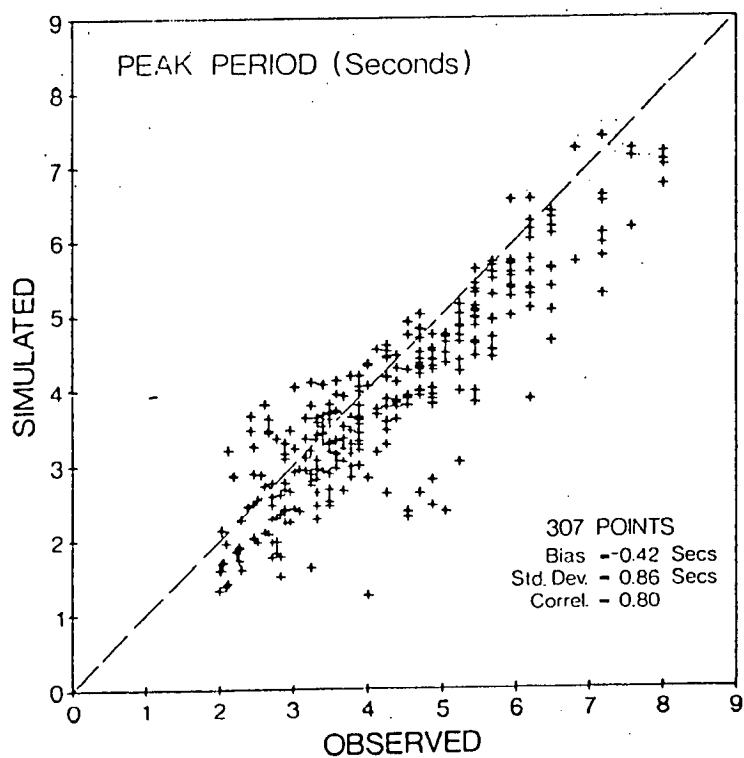
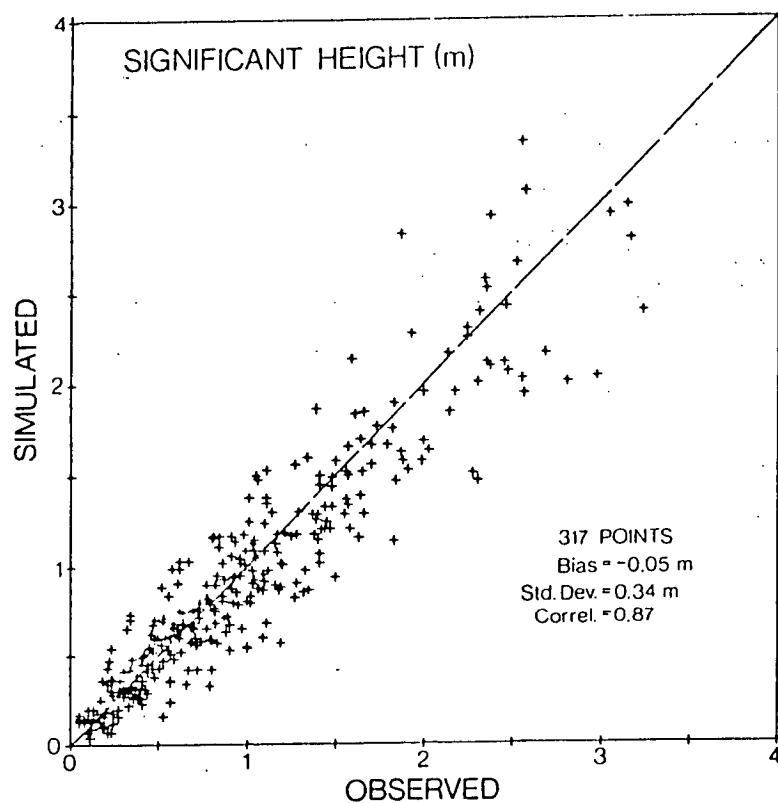


Fig. 4.18 Comparison of hindcast with observed wave heights and periods from Donelan's model. (Provided by Donelan).

significant wave heights was obtained over a two-month period, September and October 1981. Values of H_s ranged from 0.1 to 3 m, with a standard error of model prediction of 0.2 m. Over the measurement period, the computed and measured mean wave heights were 0.74 m versus 0.75 m and standard deviations were 0.55 m versus 0.52 m, based on 890 samples. Mean wave direction also showed good agreement with measurements.

Peak wave period predictions were not as good, with the model showing a bias to underestimating longer periods. The authors suggest that this problem may be related to the JONSWAP empirical relations used in the model and the excessive peakiness of the JONSWAP spectrum as full development is approached. This indicates that improvements are required in the model, particularly if it is applied to larger basins where higher waves with correspondingly larger periods may be expected.

Liu et al. (1984) published an account of applying the same model to Lake Michigan and comparing the predicted significant wave heights with synoptic wave measurements obtained from an airborne laser altimeter. Good agreement between predicted and measured heights was obtained, in a range $1 \text{ m} < H_s < 3.5 \text{ m}$.

Operational aspects of this model for the Great Lakes are discussed by Schwab et al. (1986) and Clodman (1983) has described some additional testing with recommendations for future applications.

4.2.5 The Ross Hurricane Model

The Ross model is a straightforward extension of the ideas presented by Hasselmann et al. (1976), to growing wind-seas under hurricane conditions (Ross, 1976; Ross and Cardone, 1978). Ross proposed that the advecting wave field in a hurricane can be determined by a local wind, and a fetch determined by the local radius of curvature of the wind field, which is proportional to the radial distance to the eye (r). The relevant non-dimensional terms are:

peak frequency	$\nu = U f_p / g$
total spectral energy	$\epsilon = m_0 g^2 / U^4$,
fetch	$\hat{x} = g r / U^2$.

Power law relations were established between these parameters for hurricanes AVA, CAMILLE, and ELOISE, and between the other JONSWAP spectral parameters in (2.16), to give the following prognostic equations

$$\left. \begin{aligned} \nu &= 0.97 \hat{x}^{-0.21} \\ \epsilon &= 2.25 \times 10^{-5} \hat{x} \\ \gamma &= 4.7 \hat{x}^{-0.13} \\ \alpha &= 0.035 \nu^{0.82} \end{aligned} \right\} \hat{x} \leq 3.0 \times 10^4$$

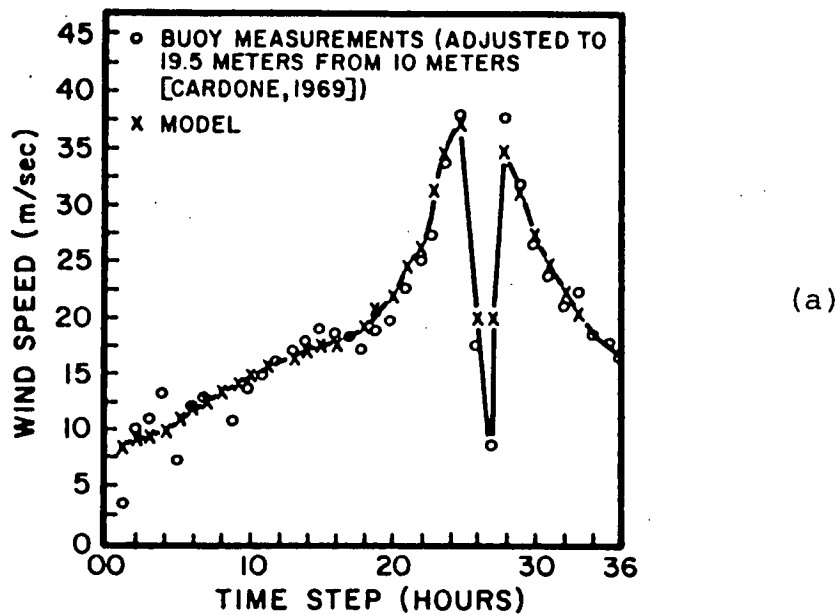
σ_a and σ_b were constants of about 0.1, independent of \hat{x} .

In the Ross and Cardone (1978) applications the wind input was derived from a hurricane model (Cardone et al., 1976). Results from the parametric model are limited to the three hurricanes named above, which were used in the calibration process, and as a result independent verifications are still required. The published comparisons with data from hurricane ELOISE and with Cardone's spectral model, are shown in Fig. 4.19 for NOAA data buoy EB10.

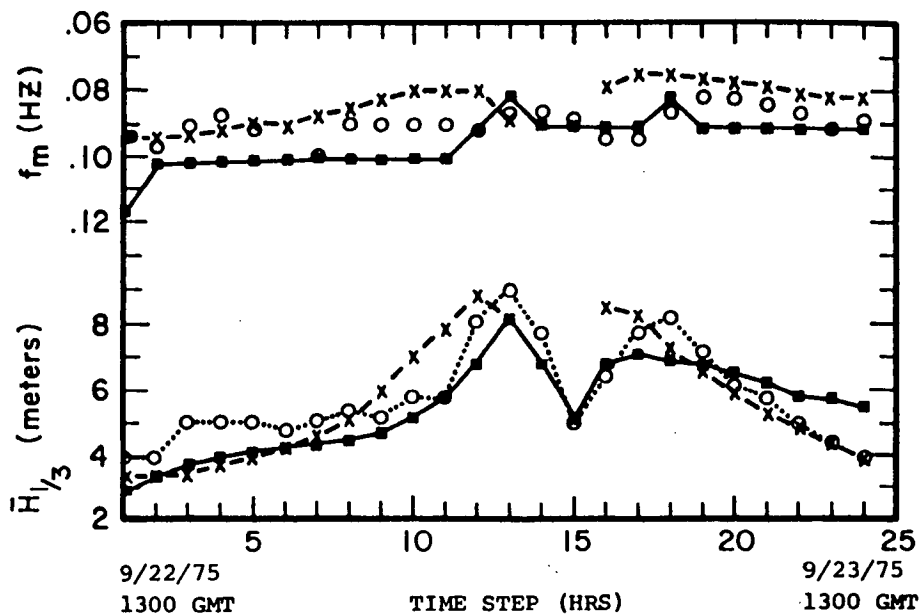
The Cardone spectral model (see discussion in the next subsection) provides generally better agreement with the observations, although the much simpler parametric model simulates the maximum wave heights to within ± 15 per cent.

Two spectral comparisons for hurricane BELLE are shown in Fig. 4.20 together with one time-series of H_{m0} . The maximum modelled spectra (at the storm peak) agree well with each other, and show peak spectral frequencies similar to the observed spectrum at EB15. At EB41, Cardone's spectral model clearly provides a better fit to the observed spectrum than does the parametric model; the reasons for this difference are not fully discussed by Ross and Cardone (1978). Also, the authors do remark on the poor performance of the simple parametric model for both very fast, and very slowly moving hurricane systems.

The Ross model has not been applied to extratropical storms over the ocean. The central problem in doing so, similar to that in attempting to use the SMB method or Baird's model, is one of determining the effective fetch. Off the east or west coasts of Canada, for example, the fetch may be governed mainly by the individual storm characteristics: its shape, trajectory and



(a)



(b)

Fig. 4.19 Comparison of modelled and measured wind speed (a) and modelled [x-parametric; ■-Cardone's spectral] significant wave height and peak spectral period with observed values [o] (b). (From Ross and Cardone, 1978).

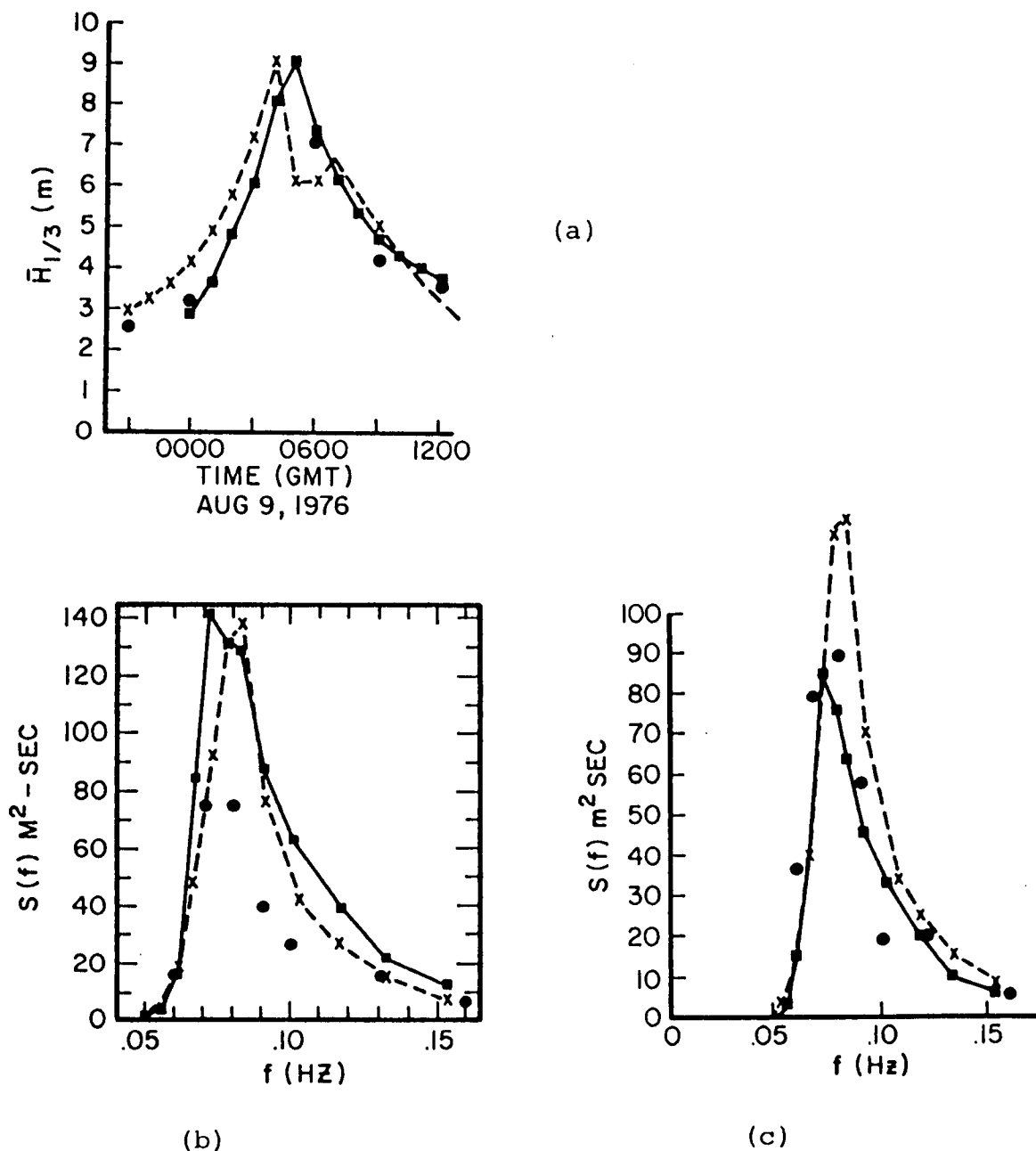


Fig. 4.20 Comparison of modelled [x-parametric, ■-Cardone's spectral] with measured [●] parameters during hurricane BELLE: (a) significant wave height at EB15, (b) maximum predicted spectra superimposed on maximum measured spectrum at EB15, and (c) maximum predicted spectra at EB41. (From Ross and Cardone, 1978).

evolution as it passes. The performance of the Ross model depends crucially on the proper choice of fetch at each point in time. In view of this difficulty, and because the other spectral models overcome it directly, the Ross model will not be considered further in this report.

4.2.6 The Norwegian Model

The Norwegian model is a continuous spectral model based on an empirical function for E derived by Neumann (see Kinsman, 1965, Section 8.4) in 1952 (Fig. 4.21). This model has been integrated with weather forecasting services since May 1967 to predict wave conditions along the Norwegian coast. A growing wind-sea is distinguished from swell generated by distant storms and the two wave systems are treated separately. The approach to formulating the model is described by Haug (1968) and follows the same principle used in Hasselmann's model.

The Neumann spectrum is used to derive an expression for the total energy content of waves at a point, given the wind speed and direction. The local change in energy is then found by solving a conservation equation like (4.2) with a two-stage (propagation and growth-decay processes) finite difference method.

The Neumann spectrum also allows the calculation of an average group velocity, c_g , for the wave energy flux, which is needed to solve the propagation stage. Once this stage is completed at each grid point, the wave growth is calculated with empirical formulae. The upper limit to wave growth is provided by the saturated Neumann spectrum.

The model also looks at swell energy (parameterized in a discrete spectrum) arriving at a point as a function of lags backward in time. Energy in eight compass octants is propagated along rays to the point of interest and used to construct a local swell spectrum. Thus the results are defined at each point as coming from a growing wind-sea spectrum (Neumann) or a propagating swell-sea spectrum. Once the wind stops building the wind-sea, there is usually a shift over to the swell-determined spectrum as is shown in Fig. 4.22.

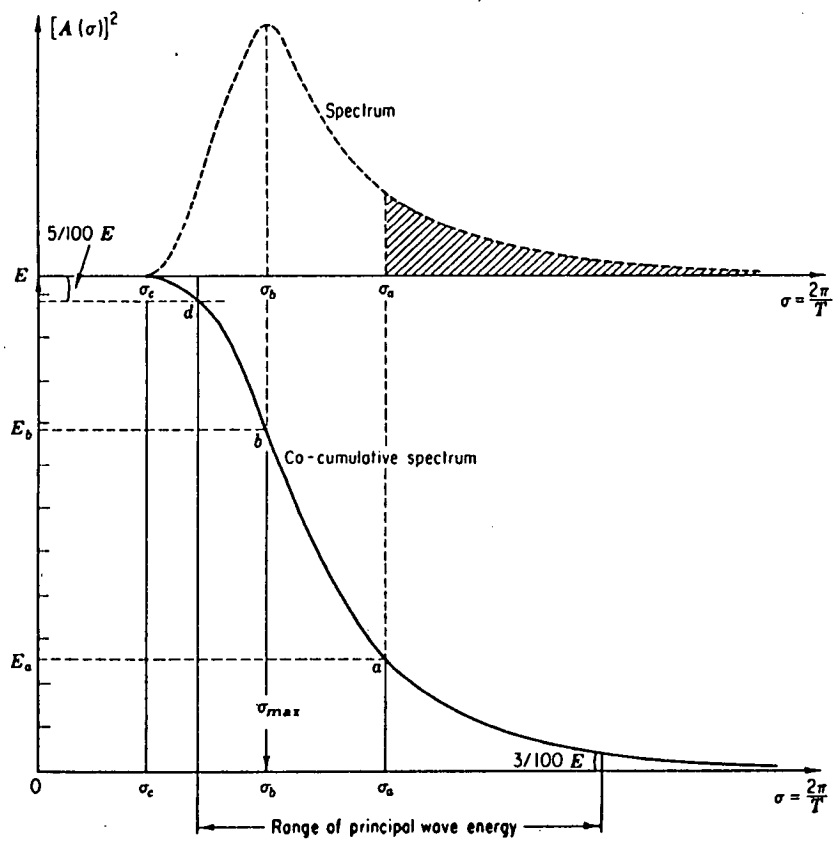


Fig. 4.21 The Neumann spectrum and co-cumulative spectrum. (From Pierson et al., 1955).

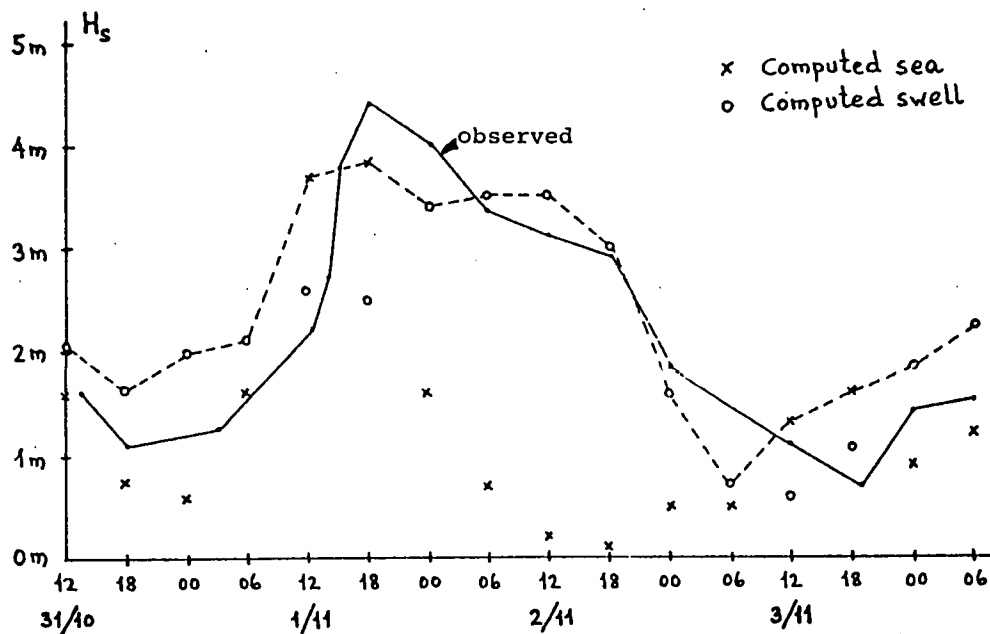


Fig. 4.22 Computed and observed significant wave heights for the period 31/10 to 03/11, 1966. (From Haug, 1968). Haug presents this figure in his paper without discussion. The dotted line connects the larger of the wind sea or swell to give, apparently, the wave height value.

Since 1972, verification trials have been run and the sensitivity of the results to more recent spectral functions (JONSWAP; Sanders, 1976) has been investigated (Røed and Guddal, undated; Haug and Guddal, 1981). Figure 4.23 shows a comparison between the different spectra for which the solution grid is shown in Fig. 4.24. A comparison of the model with observed wave data is shown in Fig. 4.25: the value of H_{m0} is substantially overestimated during this event, except perhaps on January 6 when, however, the timing is wrong. This bias can be explained by a spectrum which contains too much energy to be representative of the actual sea-states, and this supposition is supported by the comparison of the zero- and the first-order spectral moments (Fig. 4.25). Røed and Guddal conclude, however, that their results are more influenced by the accuracy of input winds than they are by the choice of the spectrum.

In March 1985, the Norwegian Meteorological Institute implemented a new wave model called WINCH which was developed by V. Cardone. It is reported (J. Guddal and M. Reistad, Norwegian Meteorological Institute, pers. comm., 1985) to be a discrete spectral model that is similar to Cardone's SAIL model (see Subsection 4.3.5).

4.3 Discrete Spectral Models

4.3.1 General Descriptions

The discrete spectral (DS) models, like the continuous parametric spectral models, represent the wave field in terms of an energy spectrum that is in a local balance with advected wave energy, energy growth due to the wind and dissipation due to white capping. The discrete models are unique in that they describe the two-dimensional spectrum in terms of a finite set of frequencies and directions.

The growth of energy in all bands lying at $\pm 90^\circ$ to the wind direction is determined through empirical growth formulae, normally represented (Pierson et al., 1966) as

$$S_{in} = (A + B.F)(1 - [F/F_\infty]^2) \quad (4.21)$$

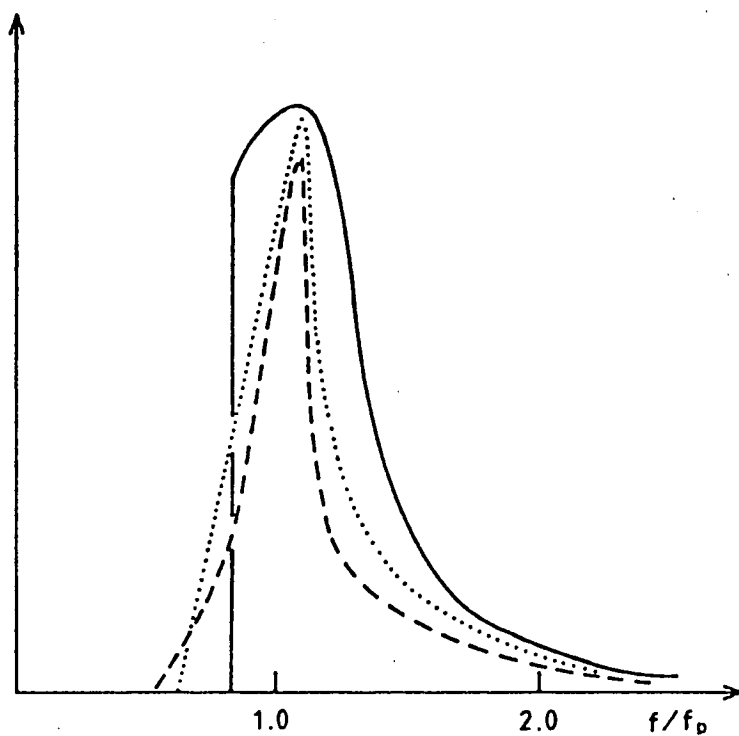


Fig.3. Wind sea energy spectra, normalized.

- a. ————— Neumann's spectrum (with "cut - off"
at a minimum frequency)
- b. - - - - - The JONSWAP spectrum.
- c. Sanders' spectrum.

Fig. 4.23 Schematic diagram comparing the Neumann, JONSWAP and Sanders' spectra. (From Røed and Guddal, undated).

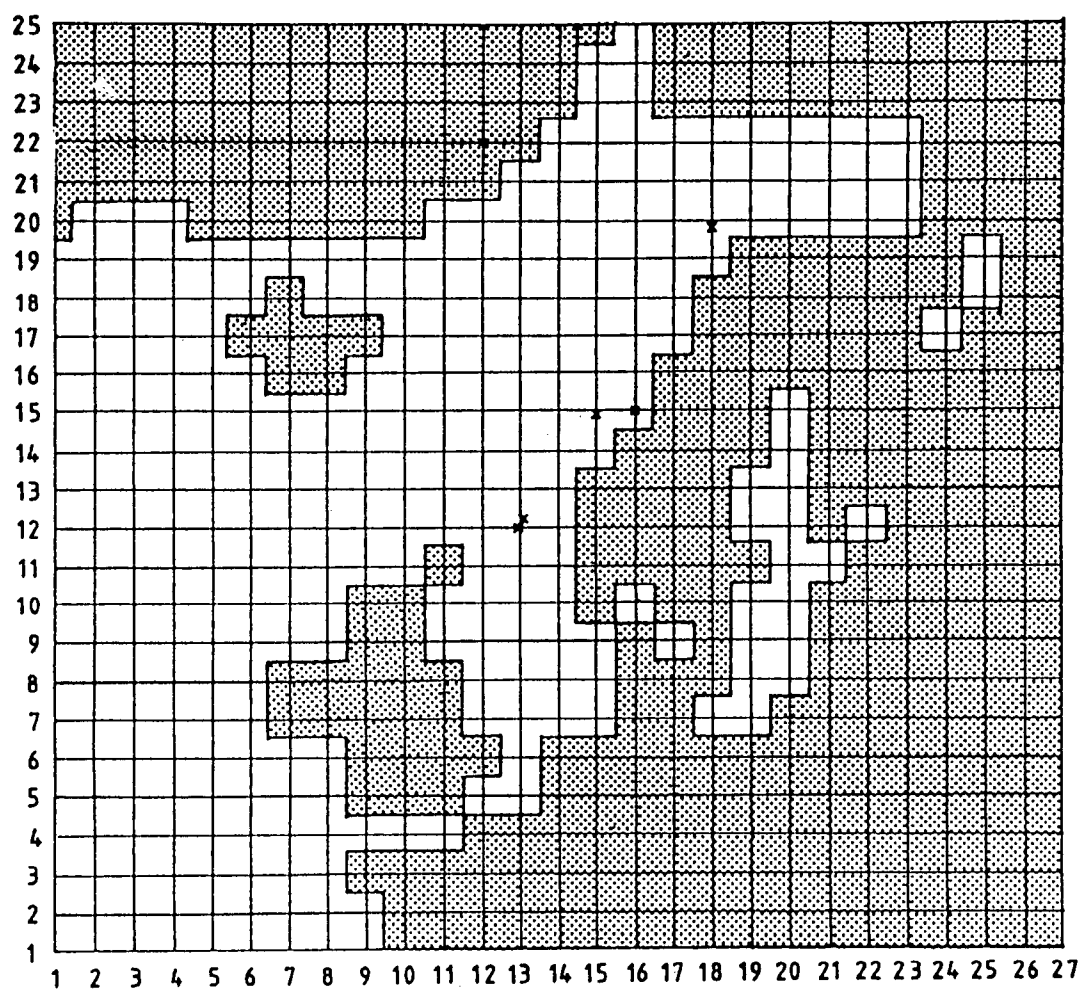


Fig. 4.24 Norwegian model grid showing land contours. Grid spacing is 150 km. (From Haug and Guddal, 1981).

A1: TROMSÖFLAKET 3/1 - 7/1 1977, Gridpkt. (18, 20)

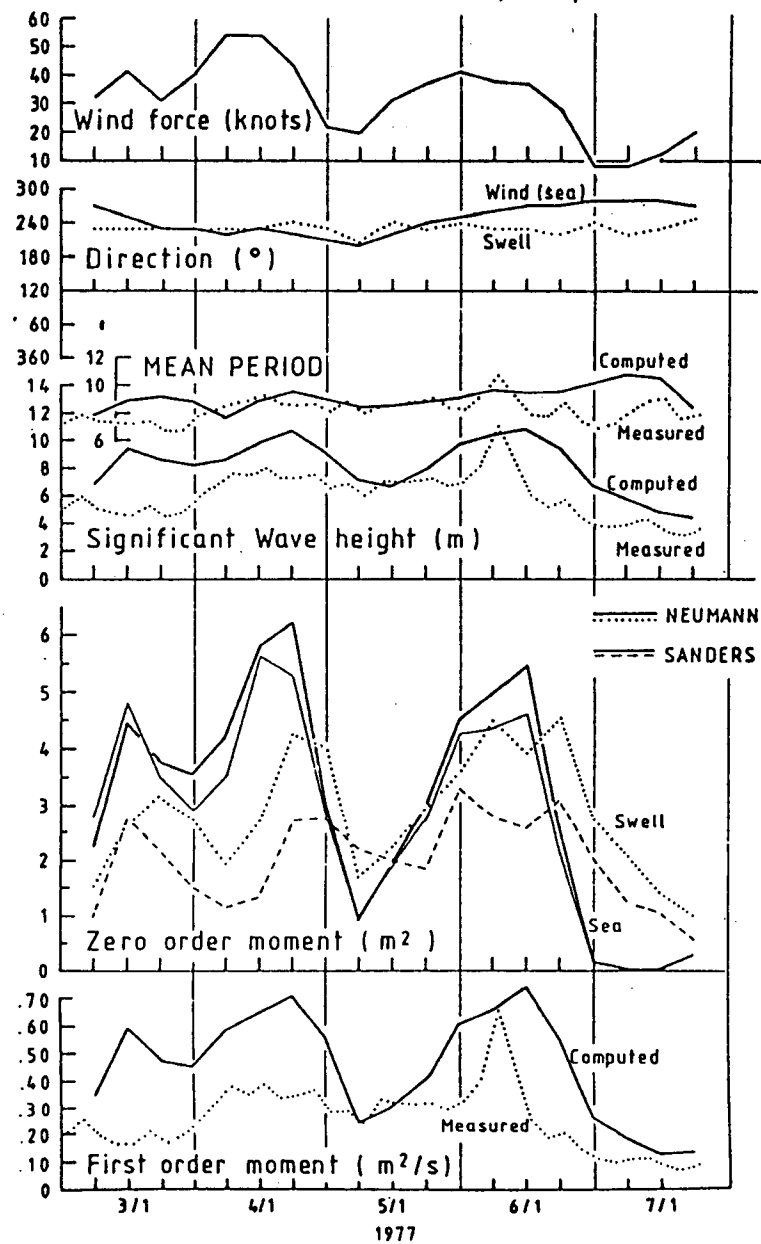


Fig. 4.25 Comparison of observed and computed wave heights (upper panel). Intercomparison of spectral moments (lower panel). (From Røed and Guddal, undated).

where A represents Phillips (1957) external turbulent pressure forcing, $B.F$ corresponds to Miles (1957) linear feedback mechanism and F_{∞} is a limiting fully-developed empirical spectrum. Both A and B are functions of frequency, direction and wind speed.

Energy dissipation (S_{ds}) is most often modelled as a "switch" function which prevents a growing sea-state spectrum from exceeding a theoretical saturation limit (e.g. the PM spectrum defined by (2.15)). If a calculated spectrum does not exceed the limiting value, no dissipation is required; if it does, then the calculated spectrum is set equal to the saturated limit (or perhaps some refinement that is a function of time) and the attendant loss of energy is assumed to be S_{ds} . One result of this approach is, however, to eliminate the "overshoot" effect (Barnett and Sutherland, 1968) in which the spectral energy in a growing wind-sea can exceed saturated levels prior to attaining equilibrium.

Those directional components of the spectrum that are travelling against the wind are subject to an empirical dissipation function.

The major differences in the discrete spectral models arise from the treatment of the nonlinear interaction term S_{nl} ; from a related topic, the assumptions concerning the coefficients A and B in (4.21); and from solution of the advection portion of the energy balance equation. The adopted magnitudes of A and B are empirically calibrated against field measurements of net observed wave growth. The A and B terms used in any application, therefore, are fitted constants that reflect not only the growth mechanism of Phillips and Miles, but also other mechanisms, frequently including the wave-wave interaction term S_{nl} .

Some models have always included a simplified parametric representation of S_{nl} (Barnett, 1968; Ewing, 1971; Resio, 1981) and some updated versions such as the DHI model (Brink-Kjaer et al., 1984) have incorporated this approach too, but the well-established operational models (SOWM, GSOWM, and ODGP) based on work by Pierson et al. (1966) do not.

The discrete spectrum is evaluated at each point of a regular grid superimposed on a distance-preserving projection of the region of interest

at each time step of the simulation. If individual storm events are modelled, the simulation time may be about six days, of which two to three days at the beginning of each run are used to calculate an initial wave field that is balanced with the wind field--a process called spin-up. Because the advective terms, $c_g \cdot \nabla F$, in the energy balance equation are especially important, considerable attention must be paid to their solution algorithm to avoid pseudo-dispersion of energy due to truncation error (see e.g., Roberts and Weiss, 1966). In many of the following models it is the method of treating wave energy propagation that, in the main, distinguishes one from another.

One of the serious drawbacks to parametric (continuous) spectral modelling with hybrid wind-sea and swell models is the difficulty of accurately considering the transition between sea and swell. This problem is greatly reduced in discrete spectral models since the two wave types are not treated independently.

4.3.2 The Gelci Model: DSA-5

The Gelci model is one of the earliest of the DS models, and it has evolved into a version that is now routinely applied for forecasting by the Direction de la meteorologie in Paris, in conjunction with weather forecasting services (Gelci and Chavy, 1978). The model was first published by Gelci et al. (1957) and was called the method of "densities spectro-angulaires" or DSA; in subsequent developments Gelci et al. (1964), Devillaz (1964) and Devillaz (1965) focused on the numerical properties of the scheme, particularly the energy advection term and control of numerical dispersion. Early results from individual storms over the Atlantic Ocean are discussed by Fons (1965) and by Gelci and Devillaz (1970).

In the DSA-5 model the energy balance equation is written as

$$\frac{\partial F}{\partial t} + c_g \cdot \nabla F = \Gamma [U, |\theta - \psi|, T] - \frac{AF}{T^4} m_0 \quad (4.22)$$

where F = the directional spectral energy density
 Γ = the growth function
 A = the damping coefficient = 18×10^{-9}
 θ = wave direction

ψ = wind direction

m_0 = the total energy summed over direction and period

T = wave period.

The principal difference between this model and the others to be discussed below is in the specification of the growth and damping functions. The growth function is defined by an empirical relation of the form

$$\Gamma [U, |\theta - \psi|, T] = G(\theta - \psi) \cdot P(U, T) \quad (4.23)$$

where G = a spreading function based on a cosine-squared law. The implementation of G in the model is done in discrete bands over direction as shown in Fig. 4.26.

The spreading function also changes with wave period, to produce a reduction of spreading on the growth function for wave periods of 7 s and less (Fons, 1965). The growth function, P , is given by

$$P(U, T) = \frac{4.30T^2}{U^3} (U - 2T)^3 \quad (4.24)$$

where the numerical constants have been determined by calibration trials (Queffeulou, 1980).

The propagation of wave energy from one step to the next is done by a process of letting each component F propagate for the time step, Δt , at its deepwater group velocity, and then distributing, by interpolation, the energy from the end-point of this propagation vector, to the nearest grid points. In general the end-point of the propagation vector will not coincide exactly with a grid point. This method produces a lateral dispersion of energy which is fictitious, but which also appears to not influence the final results to a detectable degree.

The DSA-5 model is solved on a uniform grid (Fig. 4.27) of 30 by 50 mesh points at a spacing of 90 nautical miles. The plane of the grid is tangent to the earth's surface at 45°N 40°W. The spectrum, F , is represented by 6 period bands with $\Delta T = 3$ s ranging from 2.5 to 20.5 s. The directional resolution is by 16 bands of 22.5°: the wind input U is also organized into the same 16 directional sectors. U is specified as the surface wind speed

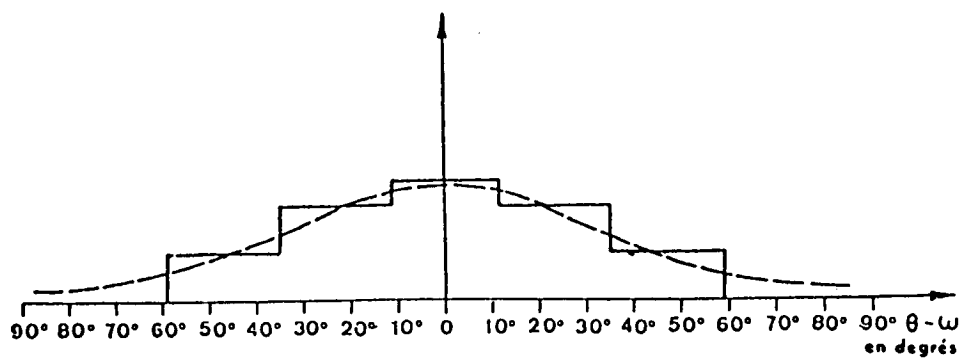


Fig. 4.26 Comparison of the DSA-5 spreading function (solid line) with the cosine-squared law. (From Fons, 1965).

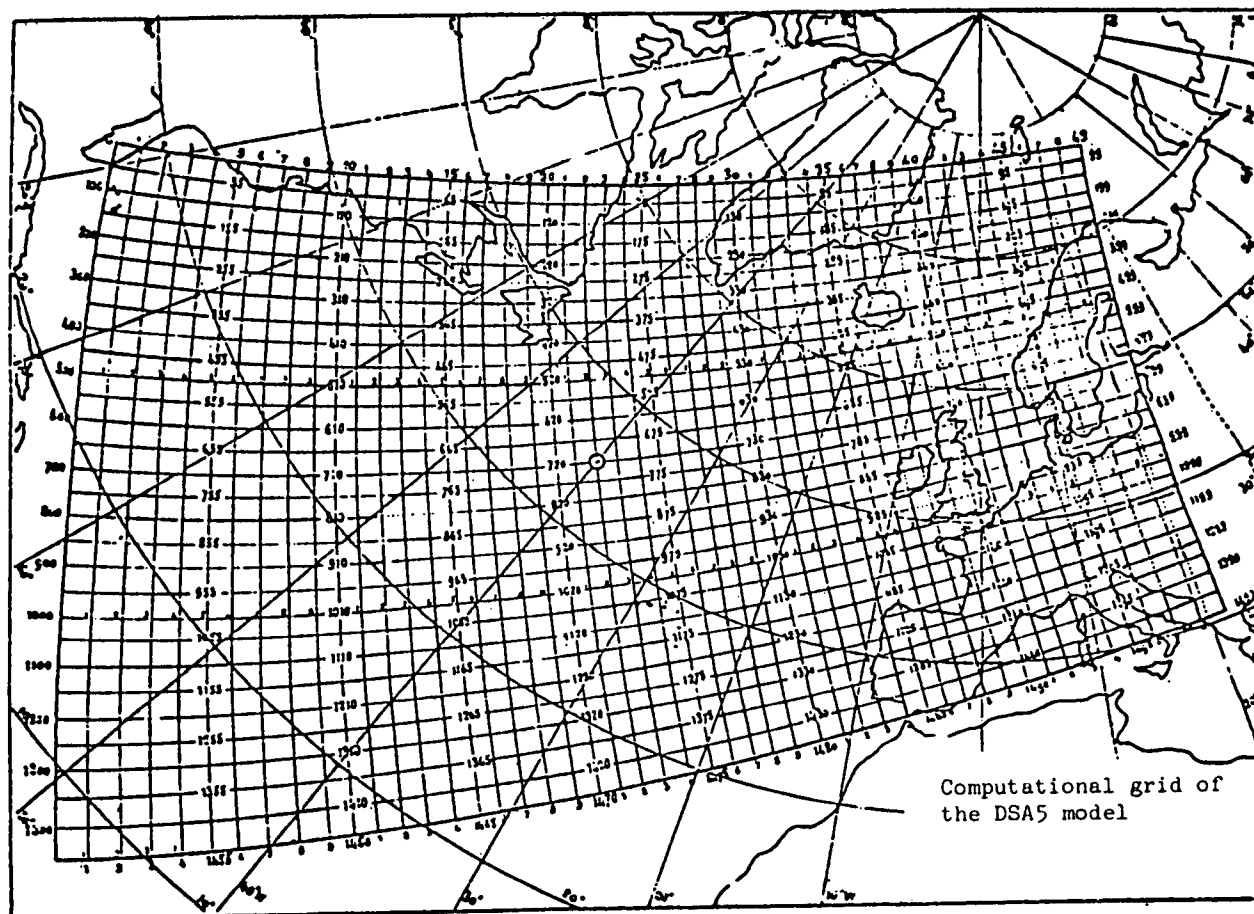


Fig. 4.27 DSA-5 model grid for the North Atlantic Ocean. (From Gelci and Chavy, 1978).

in knots, although a reference height is not reported. The time step of the model is 3 hours. The growth and decay of energy at each grid point is computed first in the model, followed by the energy propagation scheme at each new time level (Queffeulou, 1980).

Some early comparisons between DSA-5 hindcasts and wave measurements, reported by Fons (1965) and Gelci and Chavy (1978), show both some good, and some poor, agreements for individual storms. The more recent work by Queffeulou (1980), where the DSA-5 predictions are compared with SEASAT altimeter data over the mid-Atlantic Ocean is more interesting. Table 4.2 summarizes the key results for wave heights ranging from 0 to 9 m. A similar comparison with visually observed waves at 45°N 16°W is shown in Table 4.3. These results have been summarized in Fig. 4.28 in terms of the difference between model and observed values: a definite bias toward underestimating the large wave heights is present in the model. This is shown also in the time-series comparison of $H_{1/3}$ at 45°N 16°W for January and February 1974 (Fig. 4.29). The SEASAT and DSA-5 predictions are correlated in Fig. 4.30 for 379 points derived from 57 satellite passes. The bias is not evident here although there is considerable scatter in the data, indicating at times quite poor comparisons.

4.3.3 The PTB Model: Pierson's Contribution

The Pierson-Tick-Baer (PTB) model reached an advanced stage of development in 1964 and was reported to the U.S. Navy in 1966 (Pierson et al., 1966). The structure of the model is essentially that given in Subsection 4.3.1. It drew on the work of Inoue (1966) to incorporate the combined linear-exponential growth function given in (4.21) and it assumed that growth produced in this manner would account for all the important processes in the evolution of the growing wind-sea spectrum. Growth was limited by the PM spectrum.

The growth functions for S_{in} in (4.21) are

$$S_{in}(f_i) = A(U) \cdot [1-R^2]^{3/2} + [1-R^2] \cdot B(U, f_i) E(f_i) \quad (4.25)$$

Table 4.2

**Comparison of DSA-5 Significant Wave Height
Predictions with SEASAT Altimeter Wave Data**

H 1/3 SEASAT	0m - 1m	2m	3m	4m	5m	6m	7m	8m	9m
N	4	65	86	93	66	26	19	11	7
$\bar{\Delta}$ (m)	0.85	0.73	0.17	-0.30	-0.51	-1.12	-1.79	-3.00	-2.29
σ (m)	0.20	0.50	0.79	0.98	1.32	1.13	1.70	1.15	1.14

N = number of points.

$\bar{\Delta}$ = mean difference, where $\Delta = H_{1/3} \text{ DSA-5} - H_{1/3} \text{ SEASAT}$.

σ = standard deviation of the differences.

Source: Queffeulou, 1980.

Table 4.3

**Comparison of DSA-5 Significant Wave Height
Predictions with Visual Wave Observations at
45°W 16°N**

H Observed (m)	N	$\bar{\Delta}$ (m)	σ (m)
0 - 2	134	0.3	0.4
2 - 4	140	-0.1	0.8
4 - 6	61	-0.7	0.8
6 - 8	46	-1.3	0.9
8 - 10	14	-3.0	1.1
10 - 12	20	-4.2	1.2
>12	9	-3.6	1.3
>10	29	-4.7	1.4

(Symbols defined as in Table 4.2)

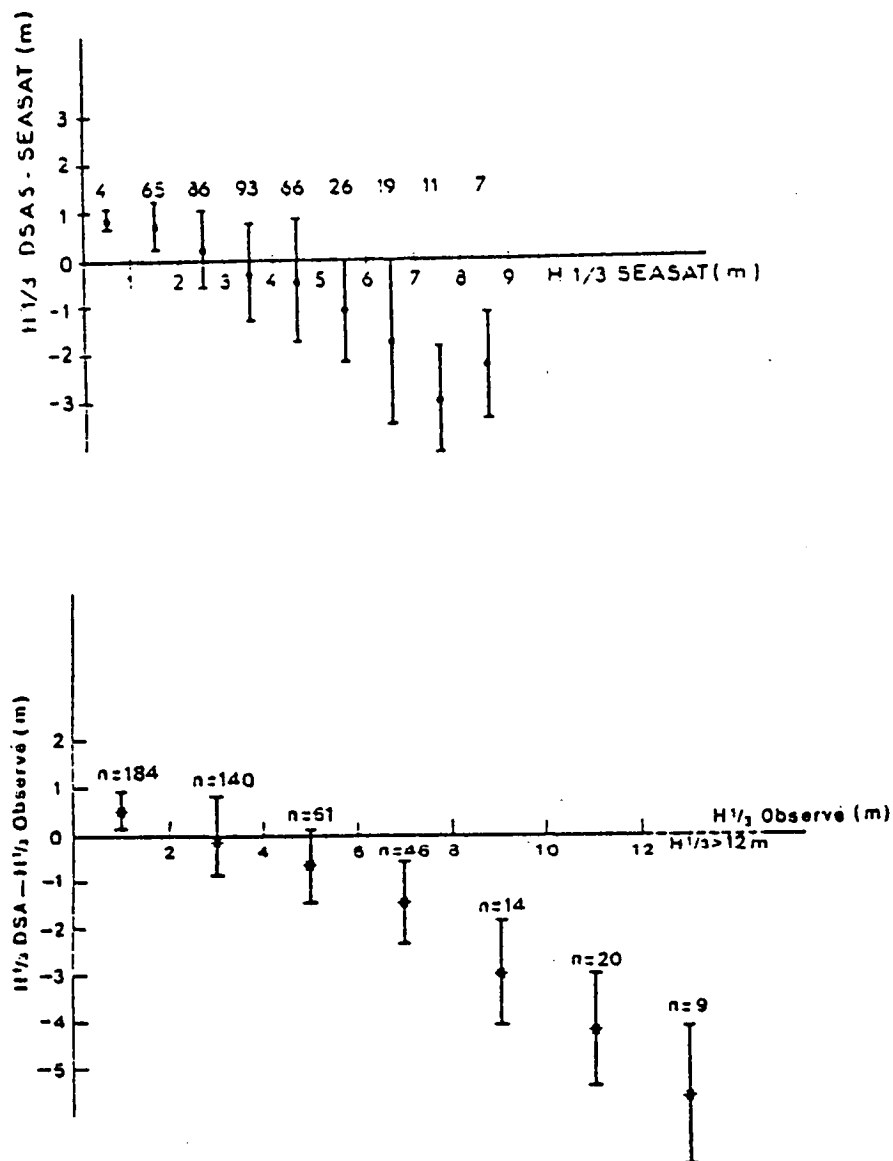


Fig. 4.28 Variation of the difference between DSA-5 significant wave height predictions and SEASAT altimeter data (top panel) and visual wave observations (lower panel) as a function of observed wave height. (From Queffeulou, 1980).

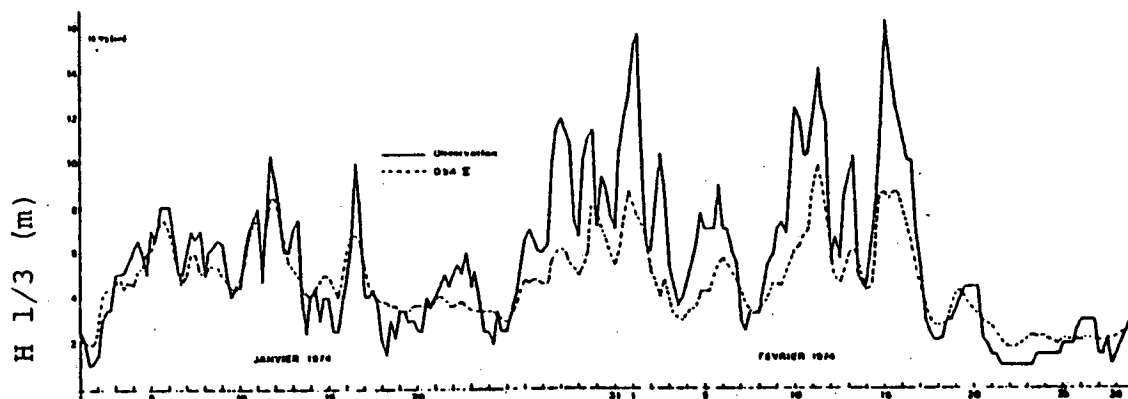


Fig. 4.29 Comparison of $H_{1/3}$ from the DSA-5 model (dotted line) with visual observations at $45^{\circ}\text{N } 16^{\circ}\text{W}$ (solid line). (From Queffeulou, 1980).

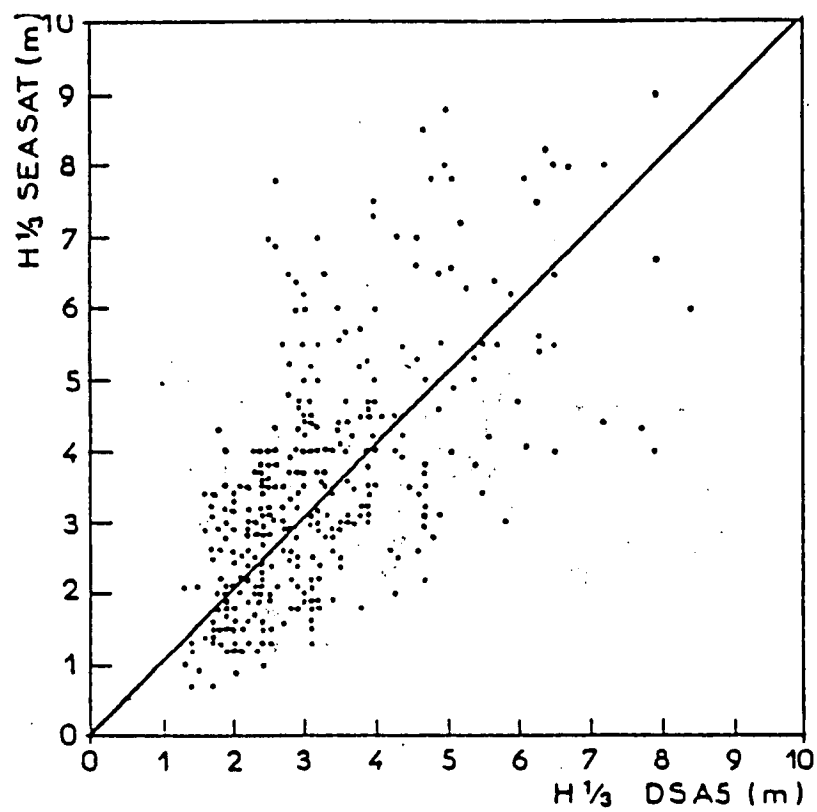


Fig. 4.30 Correlation of $H_{1/3}$ SEASAT with $H_{1/3}$ DSA-5 model. (From Queffeulou, 1980).

where

$$R = E(f_i)/E_\infty(f_i)$$

$$E(f_i) = \int_{\pi/2}^{\pi/2} F(f_i, \theta) d\theta$$

$$A(U) = 1.4 \times 10^{-8} U^3$$

$$B(U, f_i) = 6.27(U/c)^2 \exp[-0.017(c/U)^4] \cdot 2\pi \Delta f$$

c = wave component phase speed = $g/2\pi f_i$

f = frequency band centred at f_i .

$S_{in}(f_i)$ is interpreted as the growth of the one-dimensional spectral component centred at frequency f_i . The numerical coefficients for the A and B functions are for energy in ft^2/hour , U is at 19.5 m above the sea surface and both U and c have units of knots. Wave growth is calculated at each model grid point and then distributed over a directional swath covering $\pm 90^\circ$ to the wind direction for each frequency f_i using the spreading function developed in SWOP (Coté et al., 1960). The calculation is repeated for the parameter range of f_i (15 bands in this model).

Wave dissipation, S_{ds} , is assumed to take place on wave components travelling against the wind. The change in component energy is given by

$$F(f_i, \theta_j)_{t+\Delta t} = F(f_i, \theta_j)_t \left\{ \exp[-78 \sqrt{E(f_i)} \cdot f_i^4] \right\}^N \quad (4.26)$$

where Δt = time step = 2 hours,

$$N = \begin{cases} 4 & \text{if } \theta_j \text{ opposite to wind direction,} \\ 3.5 & \text{if } \theta_j \pm 15^\circ \text{ to wind} \\ 3 & \text{if } \theta_j \pm 30^\circ \text{ to wind} \\ \vdots & \\ 0 & \text{if } \theta_j \pm 90^\circ \text{ to wind.} \end{cases}$$

The main application of the PTB model was to global wave forecasting, primarily for military and civilian ship routing applications. A special lattice of triangular elements (Fig. 4.31) was designed which could be subdivided into a grid whose points would be joined by great circles--this allows propagation of wave energy along grid lines. Pierson et al. (1966) used the icosahedral-gnomonic projection (Fig. 4.31), which has the property

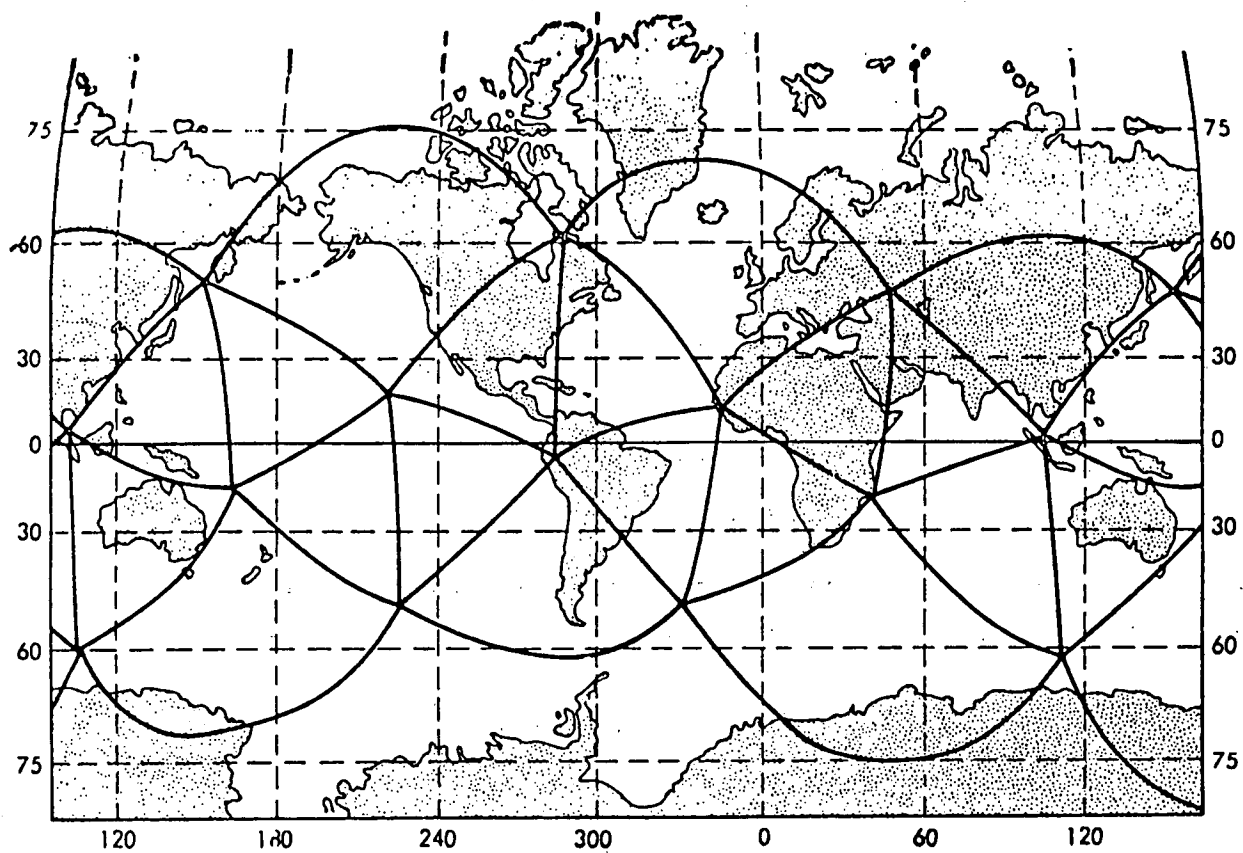


Fig. 4.31 The locations on a Mercator Projection of the triangles that constitute the icosahedral-gnomonic projection. (From Pierson et al., 1966).

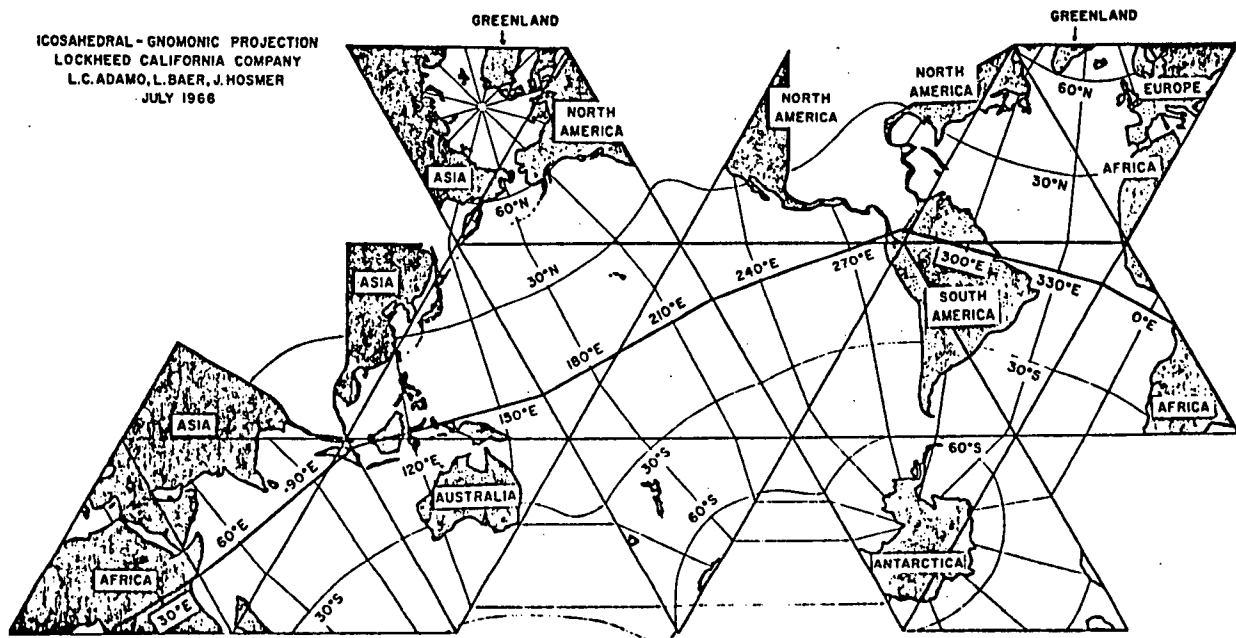


Fig. 4.32 Partitioning of the world oceans on the icosahedral-gnomonic projection. (From Pierson et al., 1966).

of straight-line great circles, to derive the oceanic partitioning shown in Fig. 4.32 for the numerical model. Each major triangular element was then subdivided and solved separately. Data transfer across the boundaries in this type of partitioning presents many numerical problems (Pierson et al., 1966; S. Lazanoff, FNOC, pers. comm., 1981) and slows execution speed considerably over that for a single grid covering one ocean.

Energy is propagated within the grid points for each frequency component, along the 12 directional components, at the deep water group velocity. The algorithm (Baer, 1962) essentially looks backward in time and outward in space for each required frequency component and finds the correct energy increment to bring forward to the calculation point by considering the time required for propagation. This calculation necessitates some interpolation amongst the grid points to derive the required energy value. The distortion of scale caused by the projection must be taken into account for the propagation path lengths and together with the interpolation requirements, makes this type of "jump" scheme quite complicated to program.

Pierson et al. (1966) do not present any verification data. Trials were, however, conducted by Lazanoff and Stevenson (1975, 1978) and are discussed in the next subsection.

4.3.4 SOWM and GSOWM: The FNOC Models

In April 1972 the PTB model was implemented for the Mediterranean Sea and brought up to operational status to provide twice daily analyses and forecasts out to 36 hours (Lazanoff et al., 1973). This model entered routine use by the global forecasting arm of the U.S. Navy Weather Service. Following this the PTB model (Pierson et al., 1966), on the icosahedral-gnomonic projection, was tested on a northern hemispherical grid and implemented for routine use, under the name Spectral Ocean Wave Model (SOWM), in 1974 (Lazanoff and Stevenson, 1975; 1978).

Resolution in SOWM is 15 frequencies and 12 directions. Wind fields for analysis are blended using surface pressure analysis charts and ship's observations (see Lazanoff and Stevenson, 1975 for details). Figure 4.33 shows a typical mapping of ship-observed winds received at FNOC, Monterey, together with the surface pressure analysis in Fig. 4.34. From these

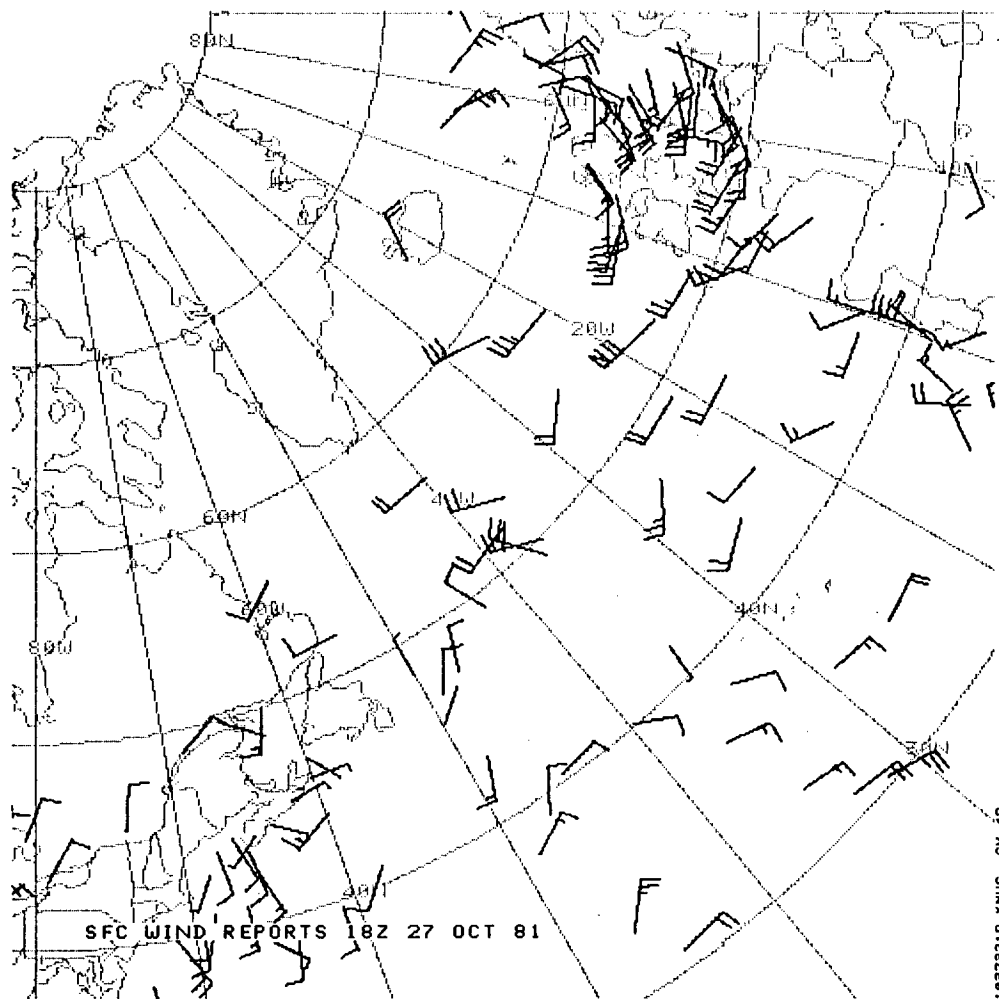


Fig. 4.33 Typical surface wind reports from ships at sea input to the wind field analysis for SOWM. (Provided by FNOC).

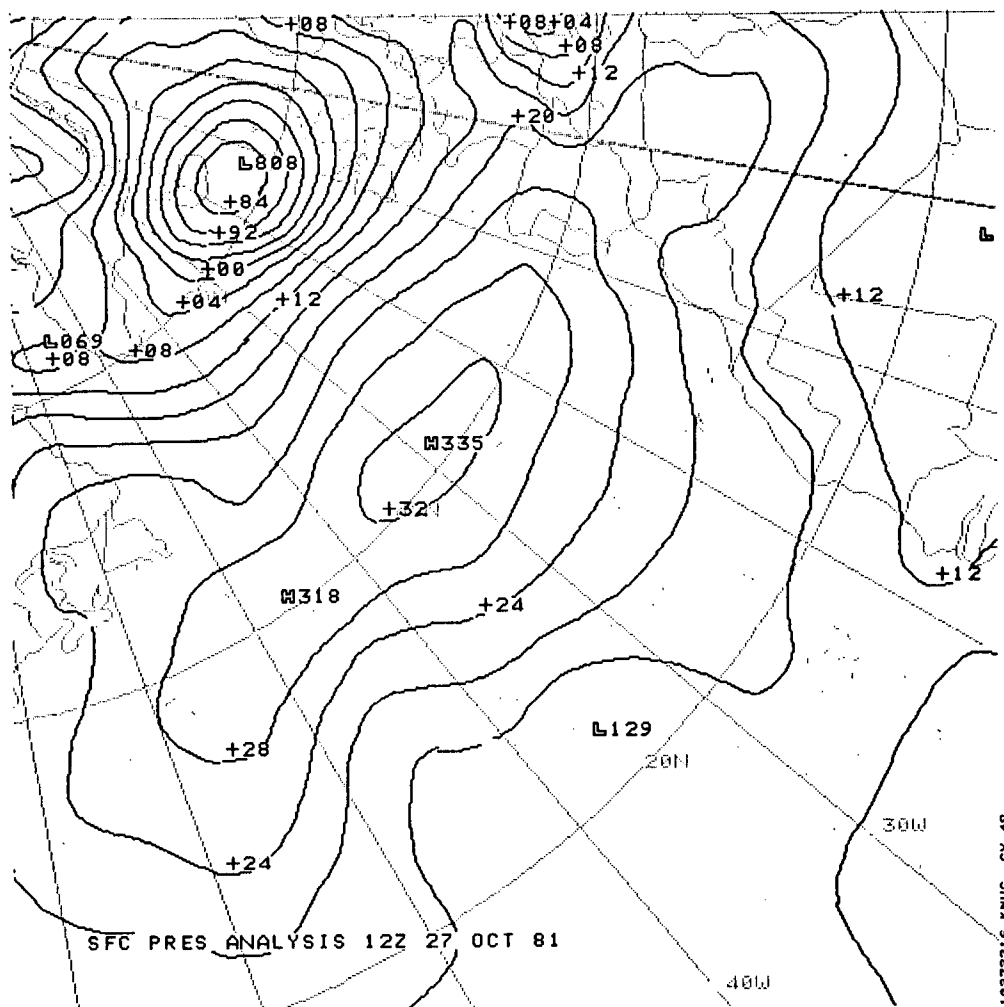


Fig. 4.34 Typical surface pressure analysis from which wind fields are derived for input to SOWM. (Provided by FNOG).

pressure analyses, the surface wind fields at 19.5 m are calculated and entered into SOWM. The model produces contoured maps of significant wave height (Fig. 4.35) over the analysis area, as well as other data products.

To date the best verification trials are those reported by Lazanoff and Stevenson (1975). Spectral comparisons were made for a number of North Pacific storms and typical examples of a wind field and spectral comparison are shown in Fig. 4.36 and 4.37 respectively at Ocean Station PAPA. The significant wave height is under-predicted (by 19%), as is the wind speed (by about 16%), and the measured spectral energy is typically higher at both the peak frequency (~ 0.075 Hz) and at higher frequencies (> 0.09 Hz) for this storm.

At FNOC, the operation of SOWM is intimately connected with the running of a global numerical primitive equation meteorological model (GPEM) which provides suitable wind fields (Mihok and Kaitala, 1976) to the wave model. A PBL submodel is used to reduce geostrophic winds to the 19.5-m reference level winds, based on two external parameters: a surface Rossby number and a stability parameter (see Mihok and Kaitala, 1976). The GPEM provides the prognosis winds out to 72 hours, which in turn permits a simultaneous wind-wave prediction. These machine-based procedures for obtaining wind fields (as noted above, analysis fields are a combination of pressure charts, and observed winds, blended by a computer algorithm) have made a 20-year wave spectral climatology for the Northern Hemisphere possible (Lazanoff and Stevenson, 1978) on the icosahedral-gnomonic projection. To date the most extensive verification trials available for these data are those reported by Lazanoff and Stevenson (1975) (S. Lazanoff, FNOC, pers. comm., 1981).

Lazanoff and Stevenson (1975) point out that the main difficulty with SOWM is the transfer of wave energy from one triangular ocean area to another, within the icosahedral-gnomonic projection. This projection, and resulting method of partitioning the world oceans, originated with the original PTB model formulation, and is justified there on the basis that it provides an optimal representations of great circles (along which wave energy propagates) in terms of straight line segments. Lazanoff (FNOC, pers. comm., 1981) indicates, however, that the spatial partitioning was required

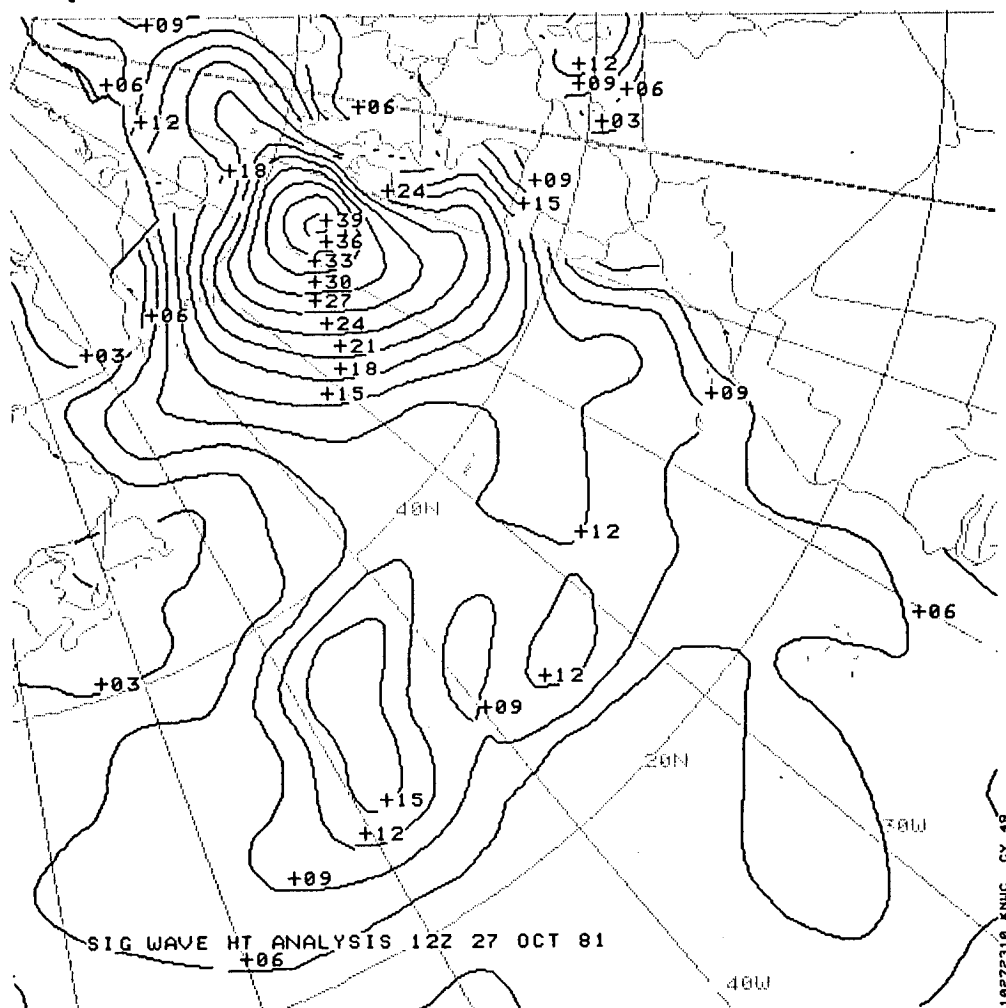


Fig. 4.35 Significant wave height field corresponding to the surface pressure analysis shown in Fig. 4.34. (The intermediate step--the wind field--was not available; however, a typical example is shown in Fig. 4.36). (Provided by FNOC).

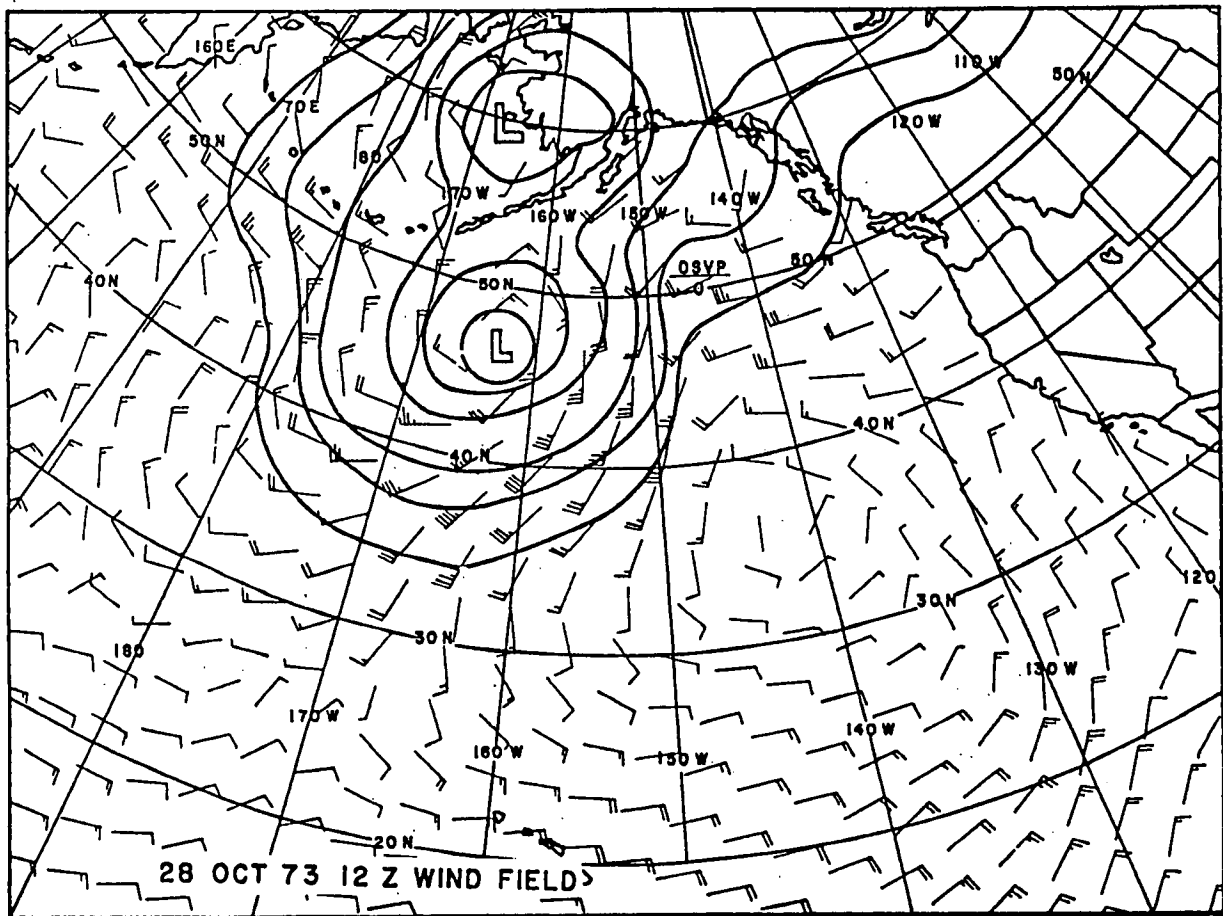


Fig. 4.36 Typical wind field input to SOWM. (From Lazanoff and Stevenson, 1975).

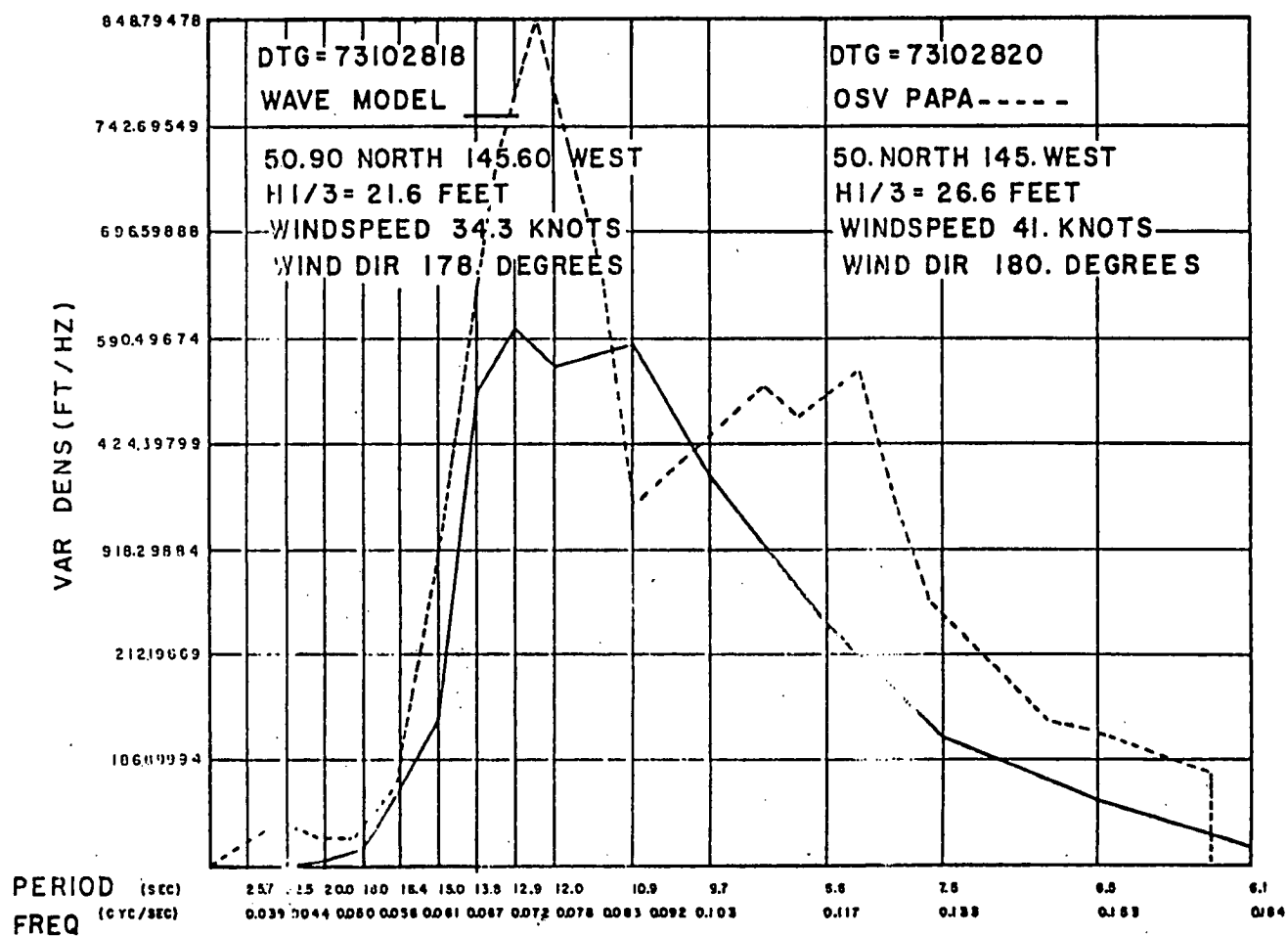


Fig. 4.37 Spectral comparison during a North Pacific storm in October, 1973. The wind field is shown in Fig. 4.36. (From Lazanoff and Stevenson, 1975).

to make the model fit into the computer available in 1966-1970, and that this was an equally important, although infrequently stated, reason for the great-circle argument. Recent computer developments (primarily increasingly effective use of core storage) have essentially eliminated the need to partition the major oceans, and FNOC, with a view to improving their wave modelling capability, have had Cardone implement a version of the PTB model on a regular Cartesian grid covering the earth's surface: this model is called the Global Spectral Ocean Wave Model (GSOWM). A typical input wind field (Northern Hemisphere) for GSOWM is shown in Fig. 4.38, which also shows the earth's projection that is used in the model: this projection provides good equatorial mapping, but produces large distortions of distance at higher latitudes. The significant wave height field in centimetres, corresponding to the winds in Fig. 4.38, is shown in Fig. 4.39.

4.3.5 Cardone's Influence: The ODGP and Subsequent Models

Vincent Cardone occupies a prominent position in the application and subsequent development of the PTB model. He graduated, as a student of Willard Pierson, from New York University having completed a thesis on the specification of wind fields in the marine boundary layer for input to numerical wave generation models (Cardone, 1969). As part of the Ocean Data Gathering Program (ODGP) (Ward, 1974) the PTB model was applied to the Gulf of Mexico, and carefully calibrated with the extensive tropical hurricane wind and wave data that were collected in that study (Cardone et al., 1975; Cardone et al., 1976). The PTB model formulation was essentially that published by Pierson et al. (1966), including the jump propagation scheme (Baer, 1962) but with modification to the growth term, S_{in} . The icosahedral-gnomonic projection was also used here. The most important storm events for calibration were hurricane CAMILLE and tropical storm FELICE.

The growth term was modified to correct over-specification of the low-frequency components and to calculate the growth of each spectral directional component individually rather than the growth of the one-dimensional spectral variance (Equation 4.25). The PM spectrum was also modified to include a wind speed dependence at high frequencies (Cardone et al., 1976; Stacy, 1973). The exact forms of the modified terms are not

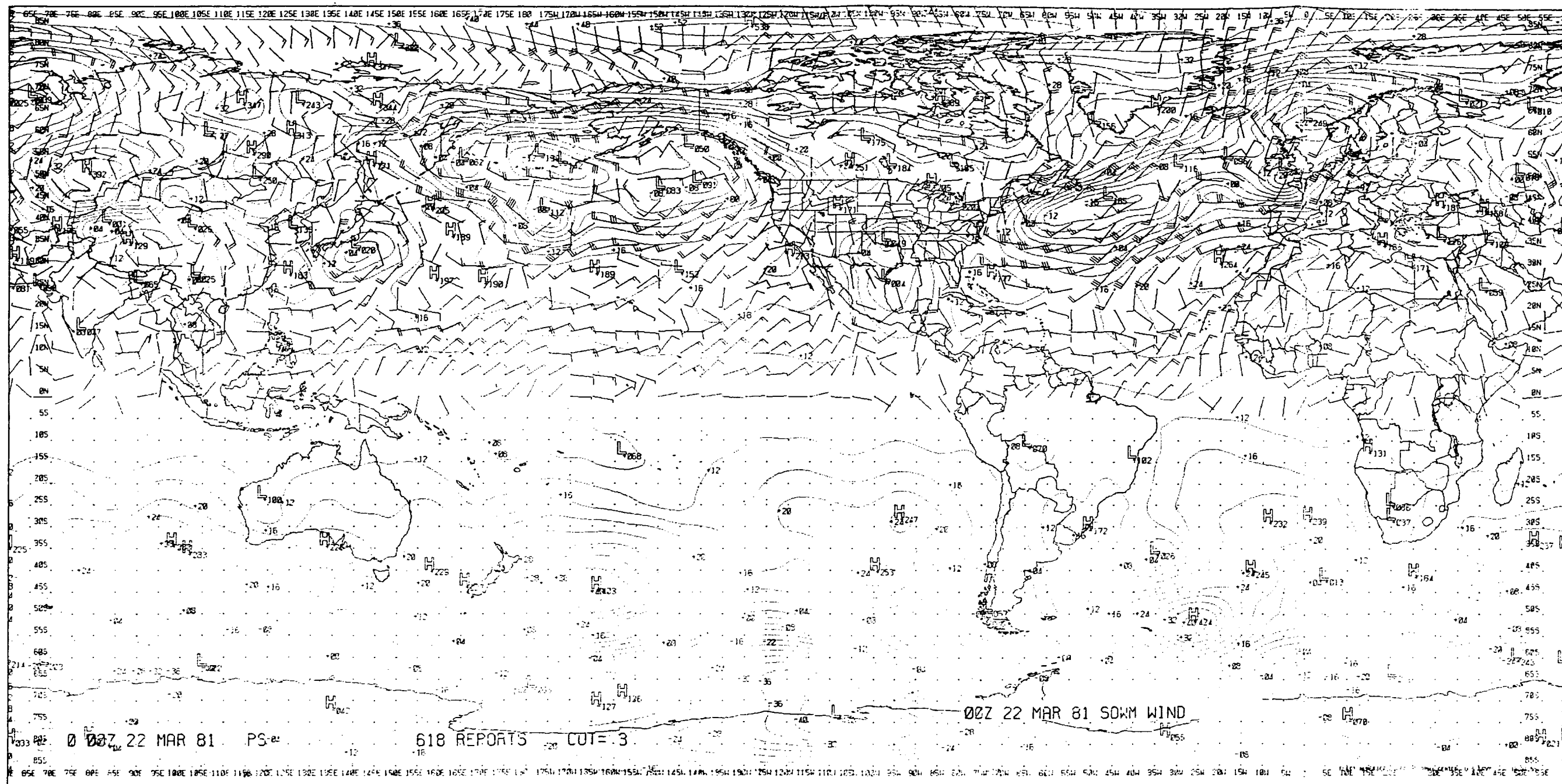


Fig. 4.38 Typical wind field used as input to GSOWM (northern hemisphere simulation). (Provided by FNOC).

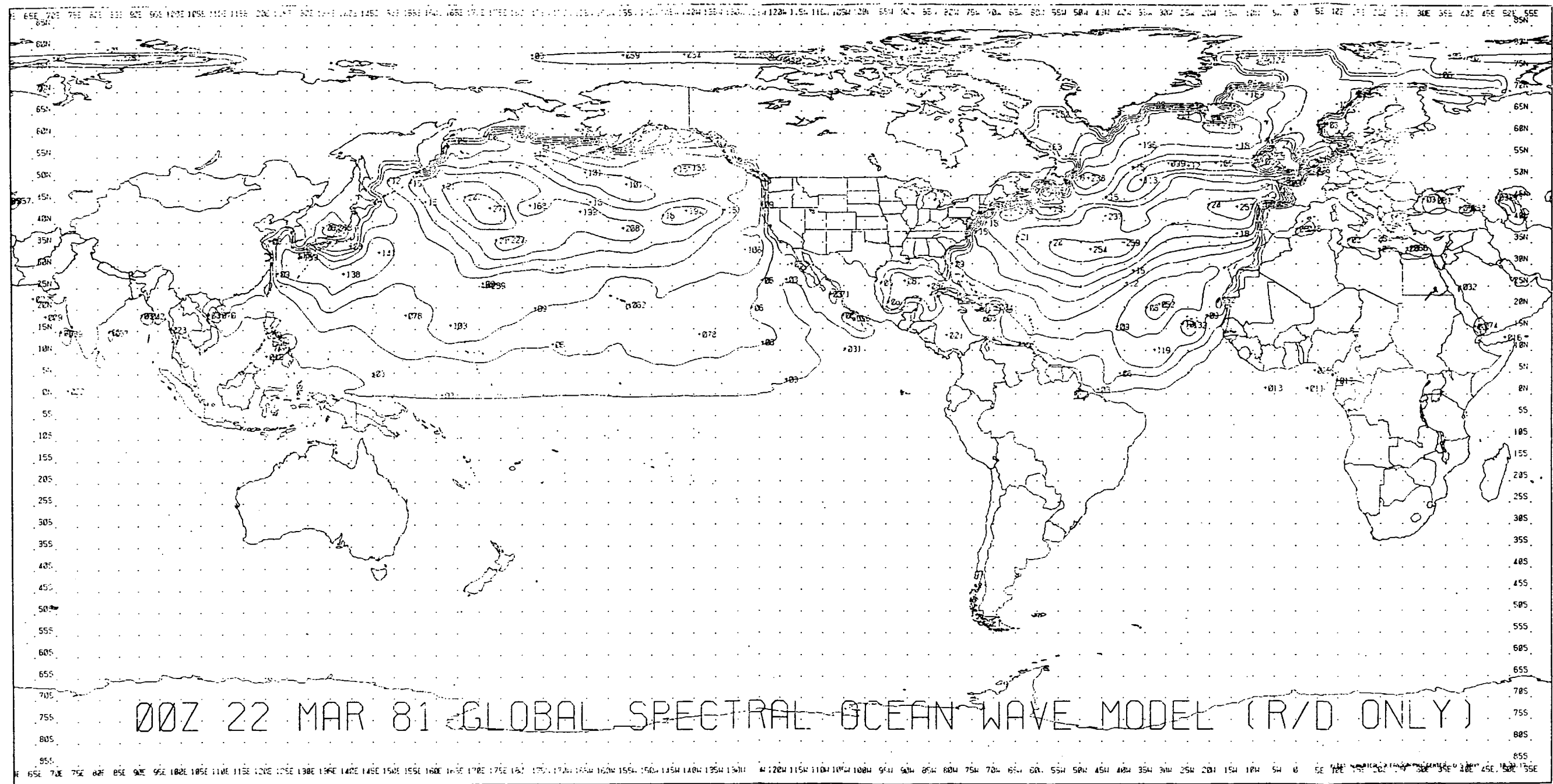


Fig. 4.39 Typical significant wave height field (cm) from GSOWM. (Provided by FNOC).

published (Cardone et al., 1976), but are thought to be necessary due to the intensity of wind in the hurricanes.

The Gulf of Mexico grid is shown in Fig. 4.40. The modelled and observed (Patterson, 1974) CAMILLE winds at one station are shown in Fig. 4.41a, together with the observed and hindcasted wave height time-series at three neighbouring stations in Fig. 4.41b. The CAMILLE storm maximum wave heights at the six ODGP stations are compared (model versus observation) in Fig. 4.42, together with a typical spectral comparison in Fig. 4.43. These comparisons show that under very strong winds, characterizing a tropical storm, and producing waves exceeding 60 to 70 feet (maximum) the PTB model, as modified and calibrated by Cardone, performs well in terms of both wave height and spectra. The CAMILLE data show significant wave height (storm maxima) agreement within about 5% at the stations with the three largest measured waves.

Following the ODGP model developments, the new version of the PTB formulation was applied to hindcast studies in the Gulf of Alaska Pilot Study (GAPS). This was an oil industry study (Shell Oil Co. as operator) and the final results are proprietary to the sponsoring group of companies. The emphasis of the study was on hindcasting wave heights produced by extratropical storms (Cardone et al., 1979) and the results were compared, for a number of storms, with Waverider data collected around the perimeter of the Gulf of Alaska. In general it was found that the DS model performed about as well as it did in the ODGP trials (W. Spring, Mobil Oil Co., pers. comm., 1981) and that provided the wind fields were reasonably accurate, the wave heights would be well modelled. For more details on the individual storm results, access to the final GAPS report prepared by Cardone (Oceanweather, Inc.) would be required.

Following GAPS, a major shift in emphasis, away from the PTB formulation and embodying a parametric growth model to include nonlinear wave-wave interactions, was undertaken by Cardone in conjunction with NOAA. These developments led to the SAIL model, standing for Sea-Air Interaction Laboratory model. The SAIL model incorporates parts of the PTB-type models, particularly B-term growth in (4.21) and the treatment of a discrete

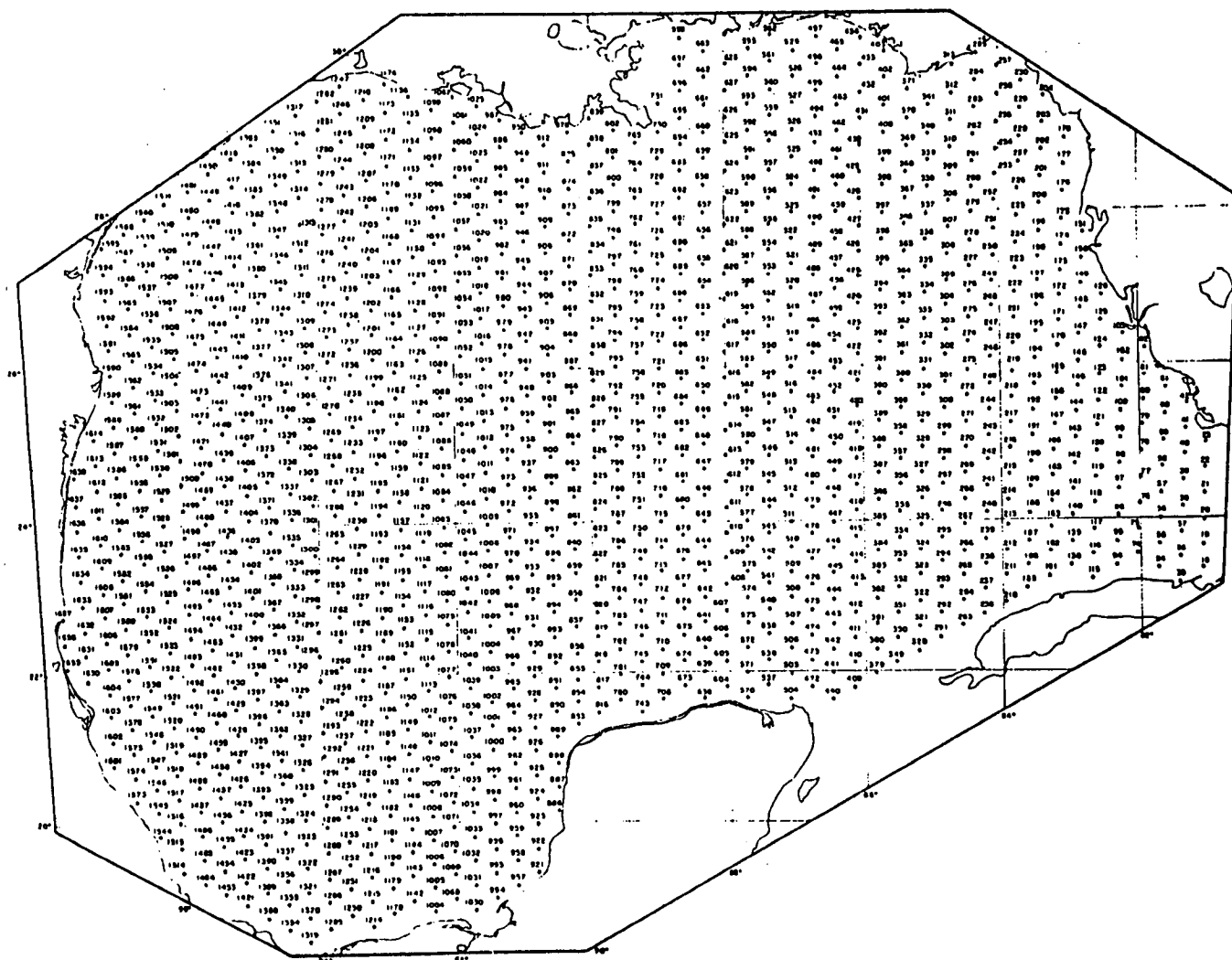
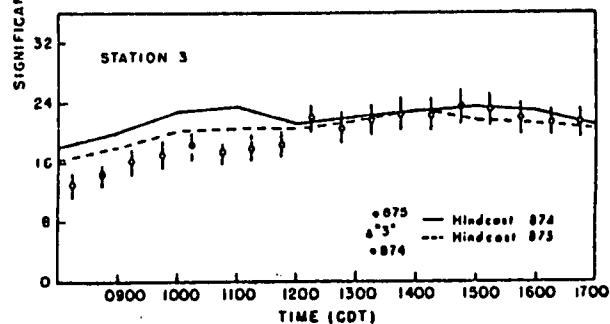
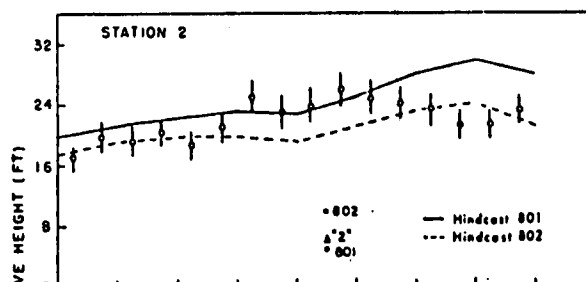
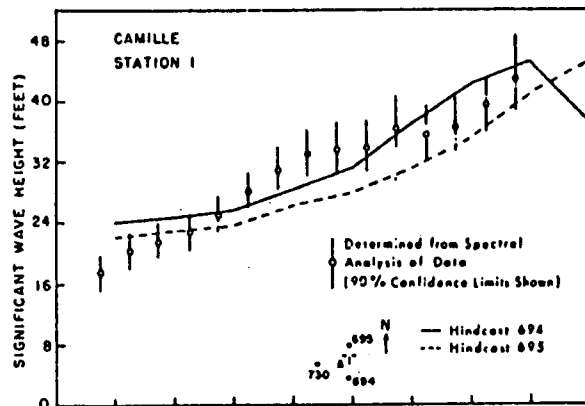
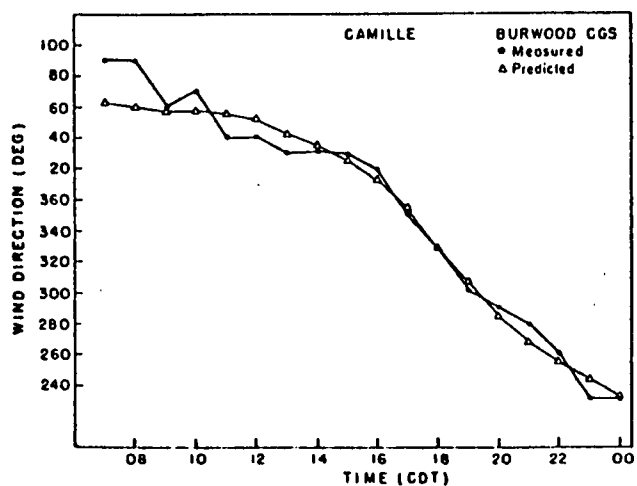
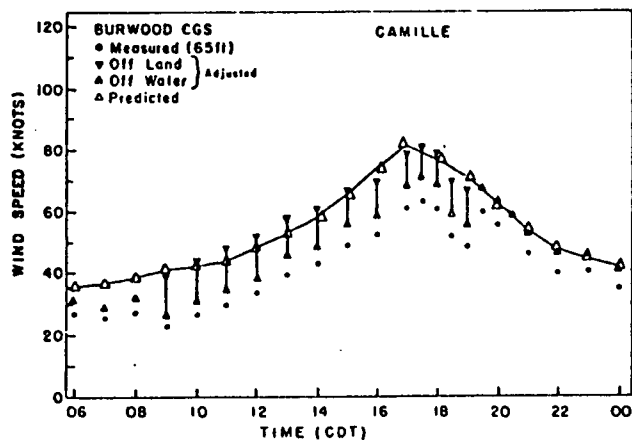


Fig. 4.40 Grid system used in the PTB wave hindcast model in the Gulf of Mexico (ODGP). (From Cardone et al., 1976).



(a)

(b)

Fig. 4.41 Comparisons during hurricane CAMILLE: (a) predicted and measured wind at Burwood, and (b) hindcast and measured significant wave heights at ODGP stations 1, 2 and 3. (From Cardone et al., 1976).

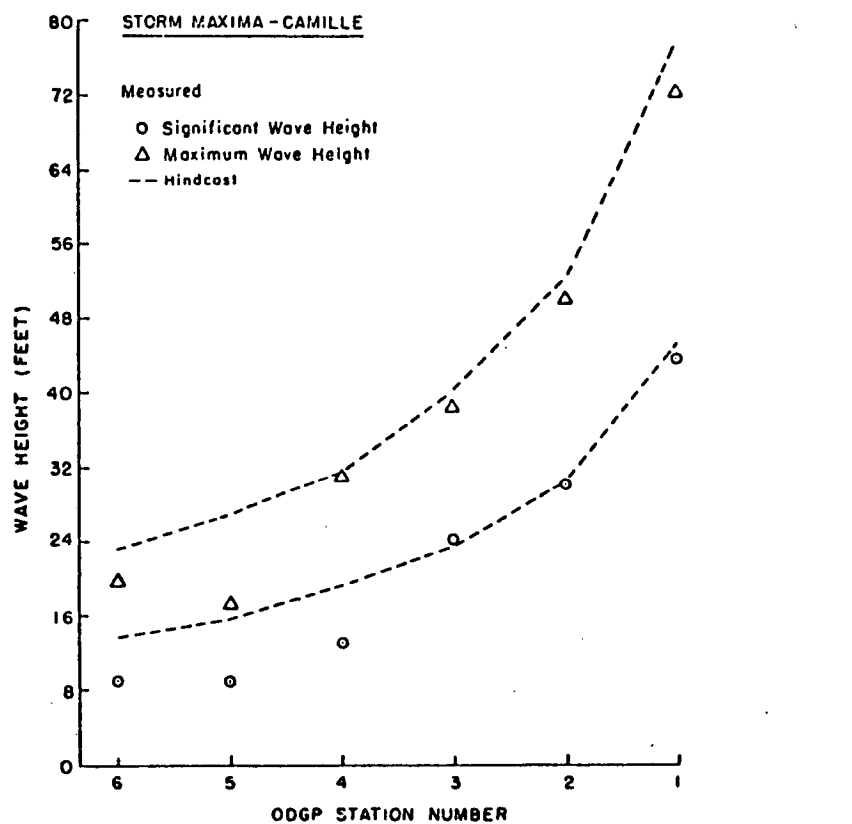


Fig. 4.42 Hindcast and measured significant and maximum wave heights at each ODGP station (storm maxima) during hurricane CAMILLE. (From Cardone et al., 1976).

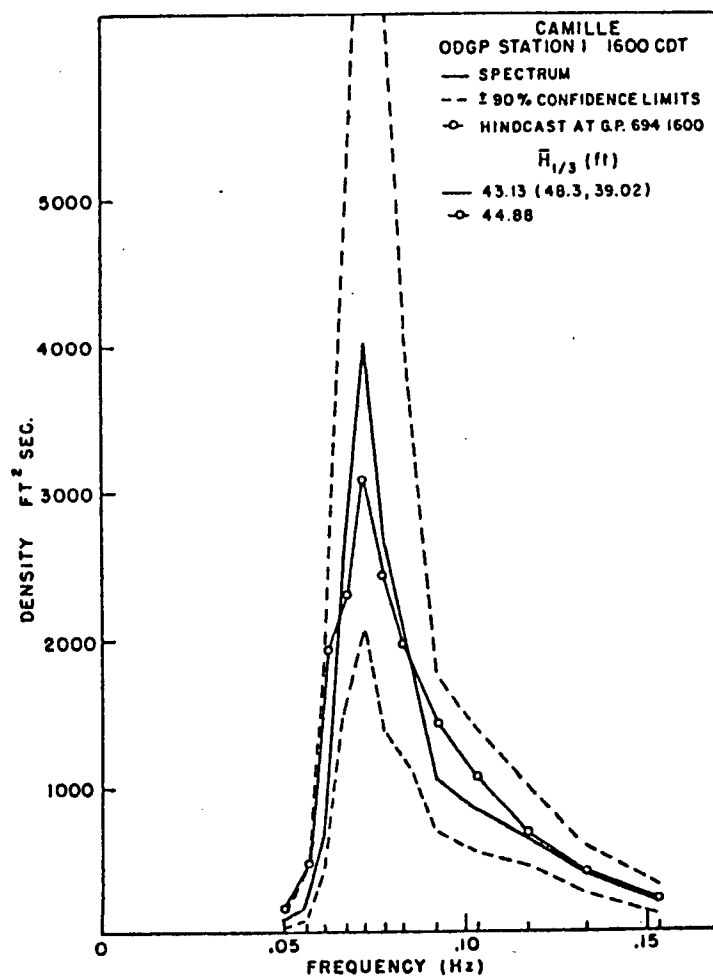


Fig. 4.43 Hindcast and measured maximum one-dimensional spectra at ODGP station 1 during hurricane CAMILLE. (From Cardone et al., 1976).

spectrum in which the energy in each frequency band is propagated at its own group velocity. It also uses a parametric growth approach, relating total non-dimensional energy to non-dimensional fetch (see Greenwood et al., 1982). This leads to a comparatively complicated process for wave growth. In each frequency bin, B-term growth (i.e. growth proportional to $F[f, \theta]$) is computed. Following this, parametric wave growth is carried out using a PM reference spectrum. This latter growth incorporates enhancement of the spectral peak energies and so models overshoot. On the forward face of the spectrum, for frequencies less than the PM peak frequency, growth is limited by the PM spectrum as in earlier DS models.

For frequencies above the PM peak frequency, the B-term growth can move the computed spectrum away from an f^{-5} variation. To return the spectrum to this observed variation, a second peak frequency (i.e., above the PM peak) is computed and all energies for frequencies above both peaks are adjusted to give an accepted parametric form. This adjustment process, where the wave energy content is forced to agree with a parametric spectral shape, is termed "equilibrium range relaxation."

One of the difficulties with other DS models applied in rapidly turning winds is that because the finite time step is large (of the order of 1 h) growth is too slow to allow the high-frequency energy to come into equilibrium with the instantaneous local wind direction. In the SAIL model additional adjustments are made at each time step to ensure that energy in the "equilibrium range" is in balance with the wind direction. Energies on the forward face of the spectrum undergo partial adjustment, termed "directional relaxation."

Greenwood et al. (1982) indicate that the parametric growth and the directional relaxation term are tunable factors, as in fact is the B-term growth coefficient. Thus the model has (at least) three calibration coefficients, which raises the difficulty of achieving the correct, unique set of parameters in any one hindcast with only one-dimensional spectra for verification. This problem is common to many hydrodynamic models which have a number of free parameters to be adjusted against limited data. In their paper Greenwood et al. (1982) comment that growth properties were, in fact,

sensitive to the directional relaxation algorithm. Duration-limited growth for a steady 20 m/s wind is shown in Fig. 4.44 computed with the SAIL model: the overshoot is clearly seen.

Cardone was also involved in implementing the PTB model at the U.S. Navy facility in Monterey, where it evolved into a routine wave forecasting program as discussed in the previous subsection. As a result of Cardone's extensive experience with the Navy and NOAA modelling efforts on the one hand, and with the oil industry hindcast programs on the other, he has become a central figure identified with wind and wave hindcasting techniques in the United States. His work has demonstrated that DS models, which either ignore the wave-wave interaction process so central to Hasselmann's theories, or include it in a simple parametrical growth form, and which bases wave growth on an empirical coupling between discrete energy packets in the spectrum and the wind speed, can successfully model sea-states.

In March 1985, the Norwegian operational wave model described in Subsection 4.2.7 was replaced by a discrete spectral model named WINCH which was developed by V. Cardone based on the SAIL model (J. Guddal and M. Reistad, Norwegian Meteorological Institute, pers. comm., 1985). The model operates with 15 frequency bands (0.04 Hz to 0.23 Hz) and 24 (15°) directional bands on the grid shown in Fig. 4.45. At this time, no other wave model details are available, but as WINCH is being used to generate a 30-year (1955 to 1984) hindcast, some interesting verifications with North Sea and Norwegian Sea Waverider data may be expected.

4.3.6 The Resio Model

What is called here, the "Resio Model" evolved from a modelling program on the Great Lakes carried out by the U.S. Army Waterways Experiment Station (WES). The purpose of this study was to provide design wave information for each of the Great Lakes using numerical DS models (Resio and Vincent, 1976). Resio considered the various growth, decay and nonlinear wave-wave interaction terms carefully and the final modelling results presented in that study were based on a model similar to Barnett's (1968) model (Resio, 1980). Samples of storm maxima and a full range of hindcast wave heights compared with measurements are shown in Fig. 4.46 for two stations in Lake Erie.

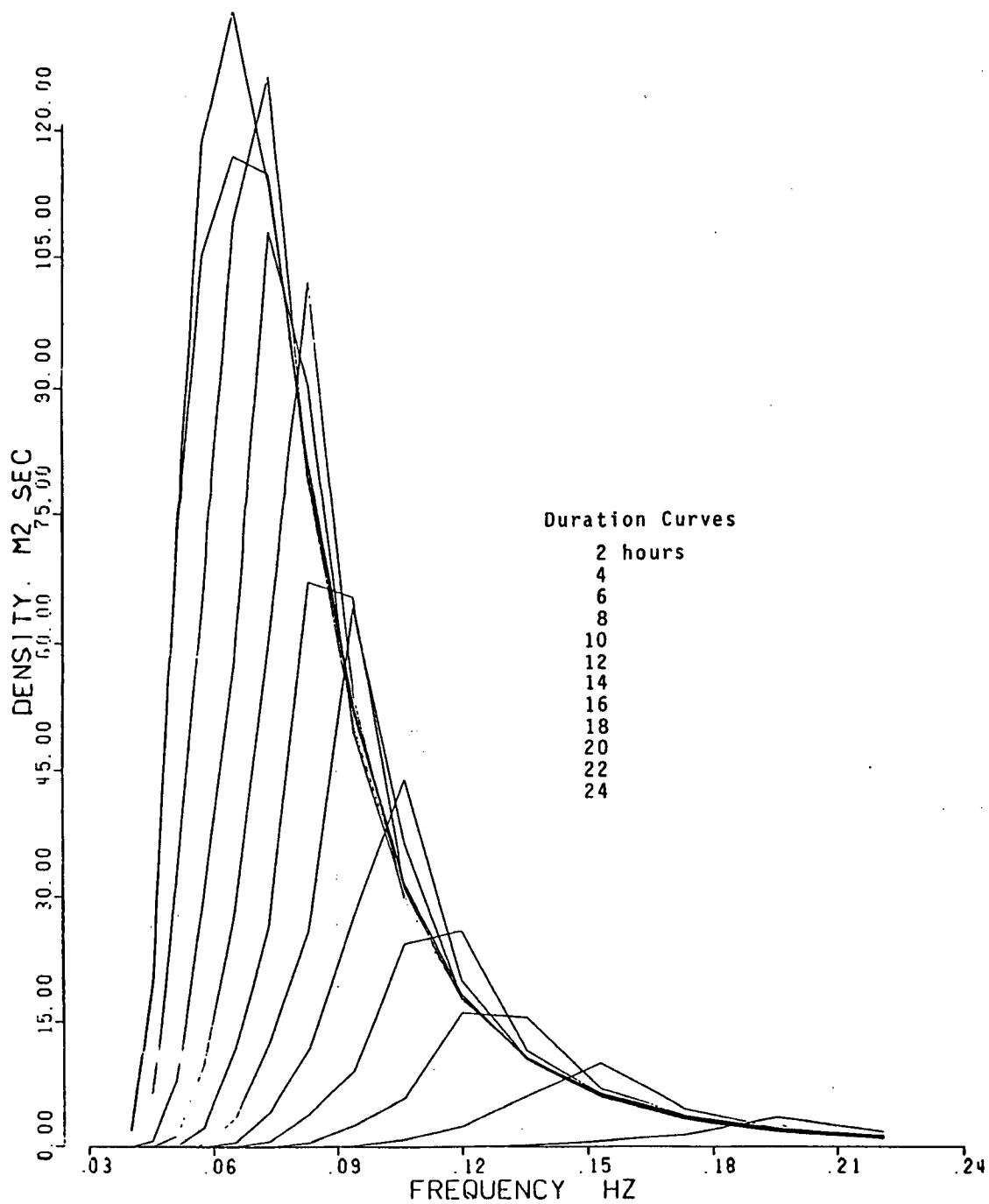


Fig. 4.44 Duration limited spectra from the SAIL model for a steady 20 m/s wind speed. (Provided by V. Cardone).

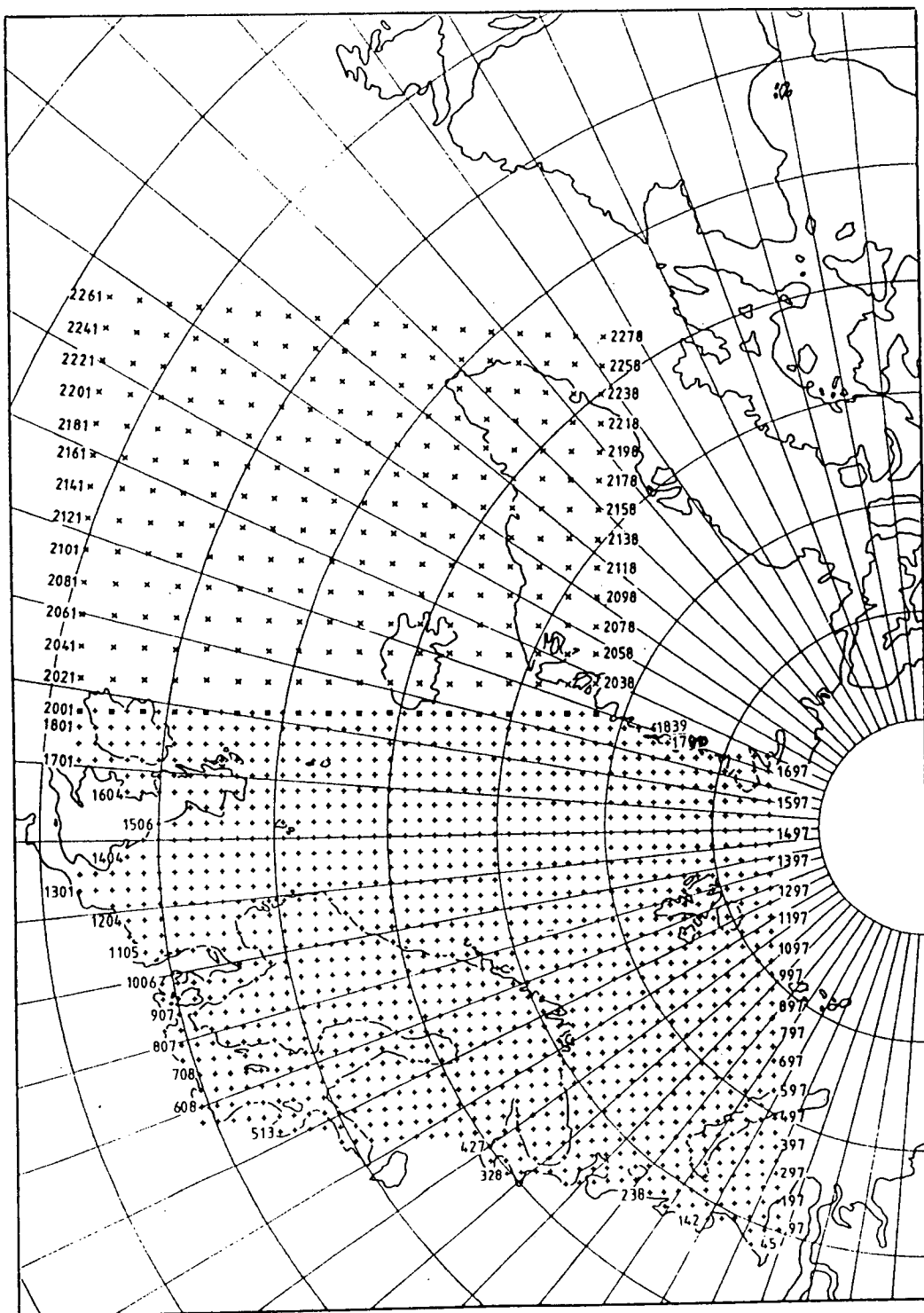
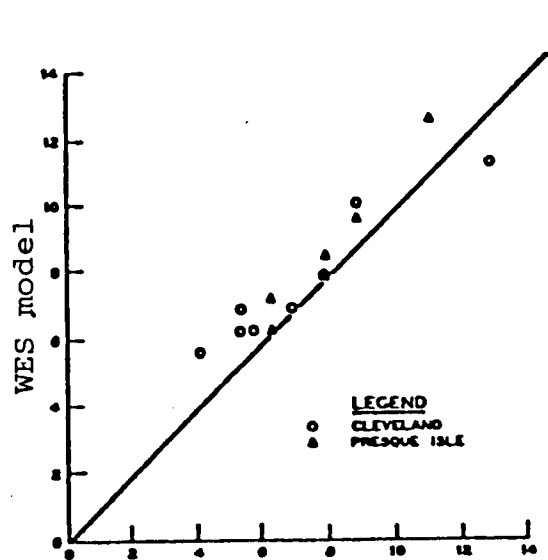
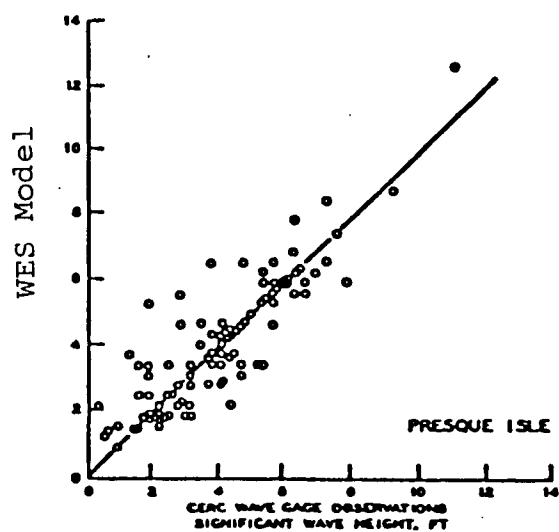
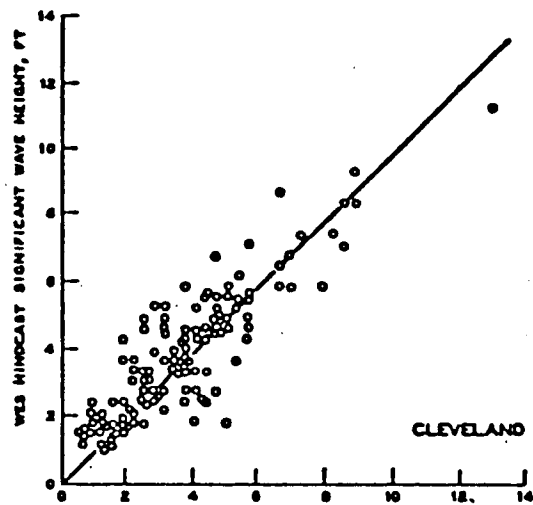


Fig. 4.45 WINCH model grid. (Provided by Norwegian Meteorological Institute).



Observed

(a)



(b)

Fig. 4.46 Correlation of measured and WES predicted wave heights: (a) storm maxima and (b) full-range values. (From Resio, 1980).

A parallel program at WES sought to develop a wave climate for the U.S. Atlantic seaboard (Vincent and Resio, 1979). This program, the Wave Information Study (WIS), resulted in a 20-year wind climatology over the Atlantic Ocean which was in turn used to generate the wave climatology. The model grid is shown in Fig. 4.47. A comparison between hindcast significant wave heights with measured values at several stations off Nova Scotia and Newfoundland (see Fig. 4.48) for individual severe storms are reported by Baird and Readshaw (1981). Figure 4.49 shows the correlation of storm maxima exceeding 5 m; however, Baird and Readshaw point out that several factors affect the comparison, including separation of hindcast and measurement locations, inaccuracies in the wind fields, and the coarse spatial resolution in the hindcast grid, and that these may be more important than the model formulation itself.

Later developments in the model emphasize the role of the wave-wave interaction terms. Hasselmann et al. (1973) and Resio (1981, 1982) have shown theoretically and empirically that in deep water the balance among the source/sink terms involves primarily the wind input S_{in} and the wave-wave interactions S_{nl} . There is also a growing resource of measurements to give empirical evidence that this is also so in shallow water (Bouws et al., 1985a). Further evidence of the suitability of the Resio (1986a) formulation for the wave-wave interaction mechanism comes from a recent study sponsored by the ESRF Waves Committee (Hodgins et al., 1986) in which the transformation of deep water waves into shallow water as predicted by WAVAD (which is the name of the present (1986) operational version of Resio's model) was compared with measurements in 12 m of water on Sable Island Bank with a directional wave buoy during winter storms in 1984-85. Preliminary results (discussed more fully in Subsection 4.3.10 in comparison with the uncoupled propagation model SPECREF) indicate that the agreement is quite acceptable, within about 10% in total energy and significant wave height but somewhat low in peak period.

In WAVAD, the energy spectrum is considered to be composed of three segments as shown in Fig. 4.50: the forward face at frequencies below f_p , an intermediate range where S_{in} is operational and the high frequency tail of the spectrum. The high frequency tail (region III) is regarded as fully

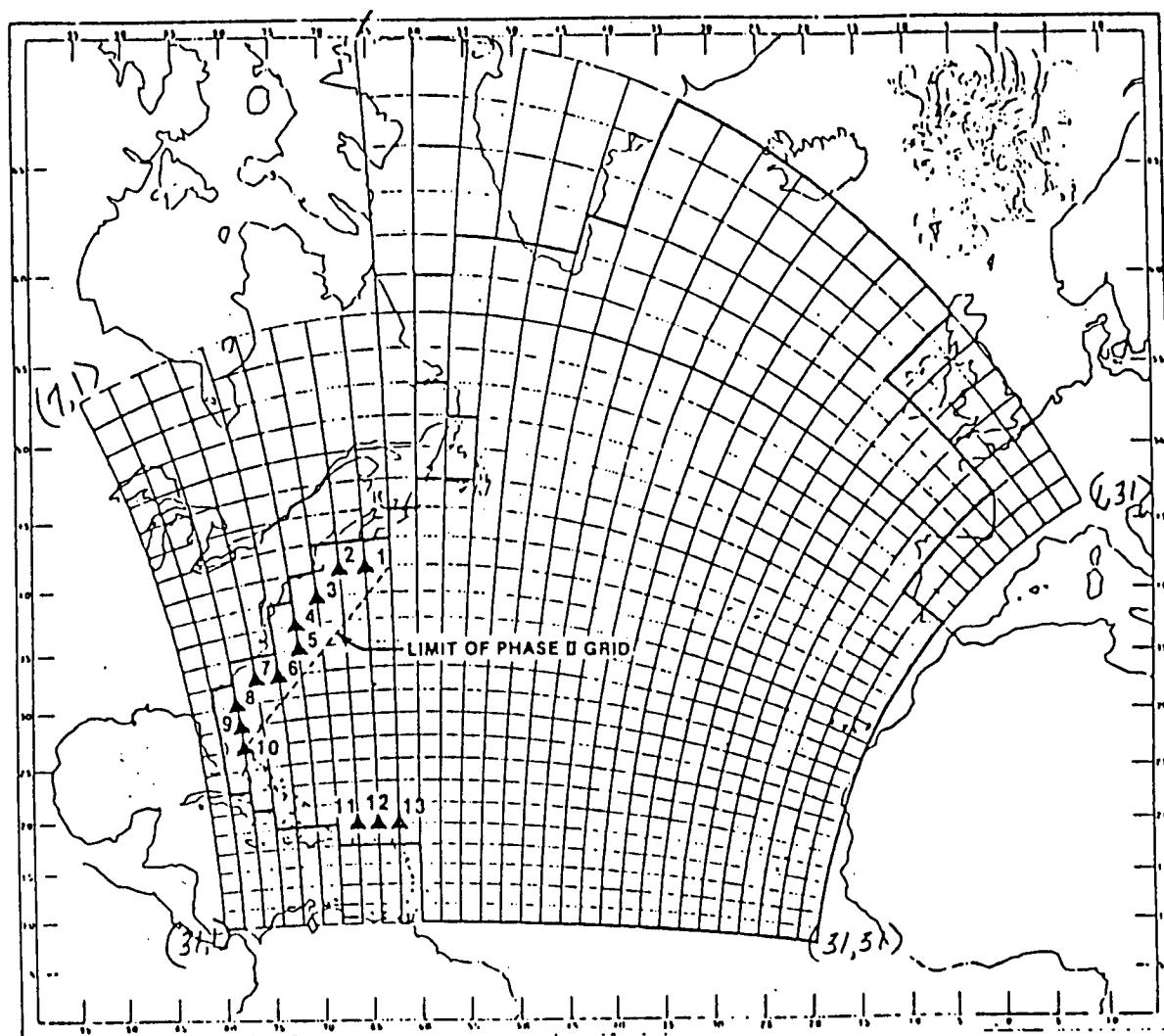


Fig. 4.47 WES model grid for the North Atlantic Ocean. (From Vincent and Resio, 1979).

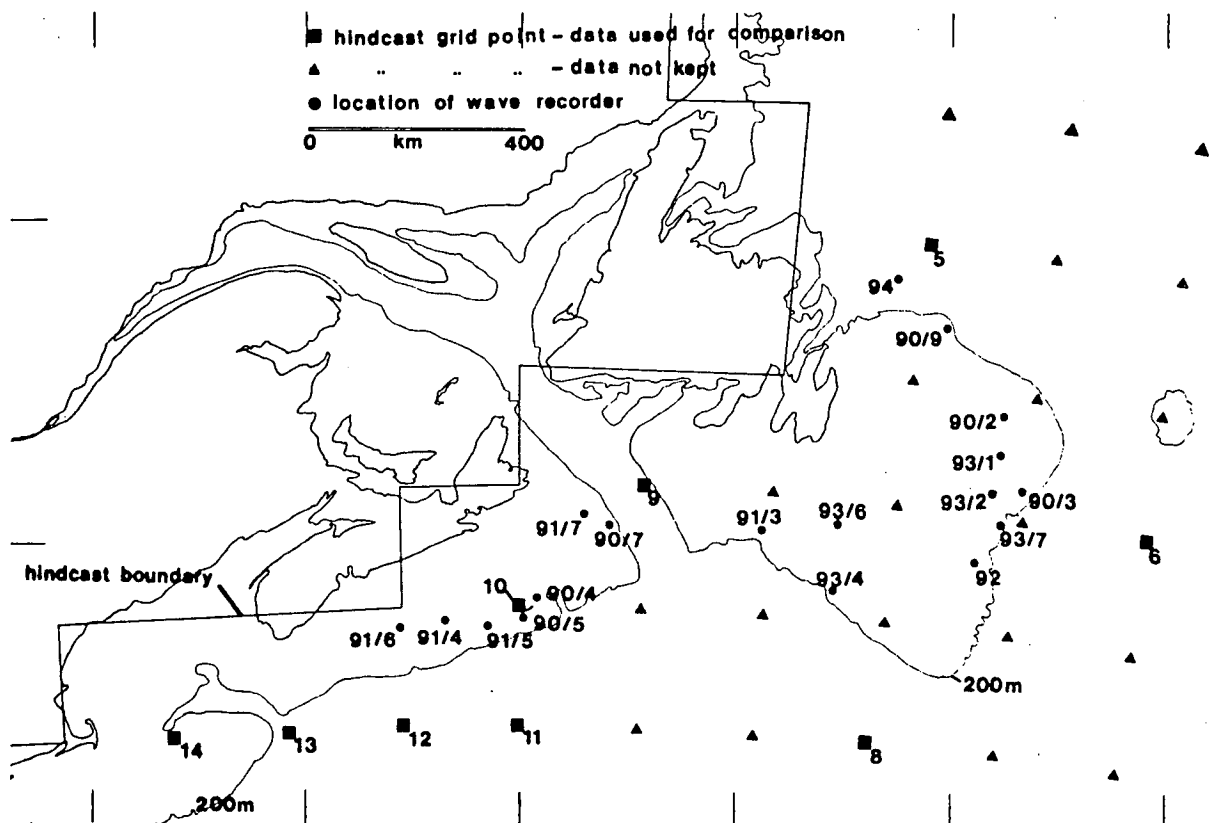


Fig. 4.48 Waverider and hindcast comparison points used by Baird and Readshaw, 1981.

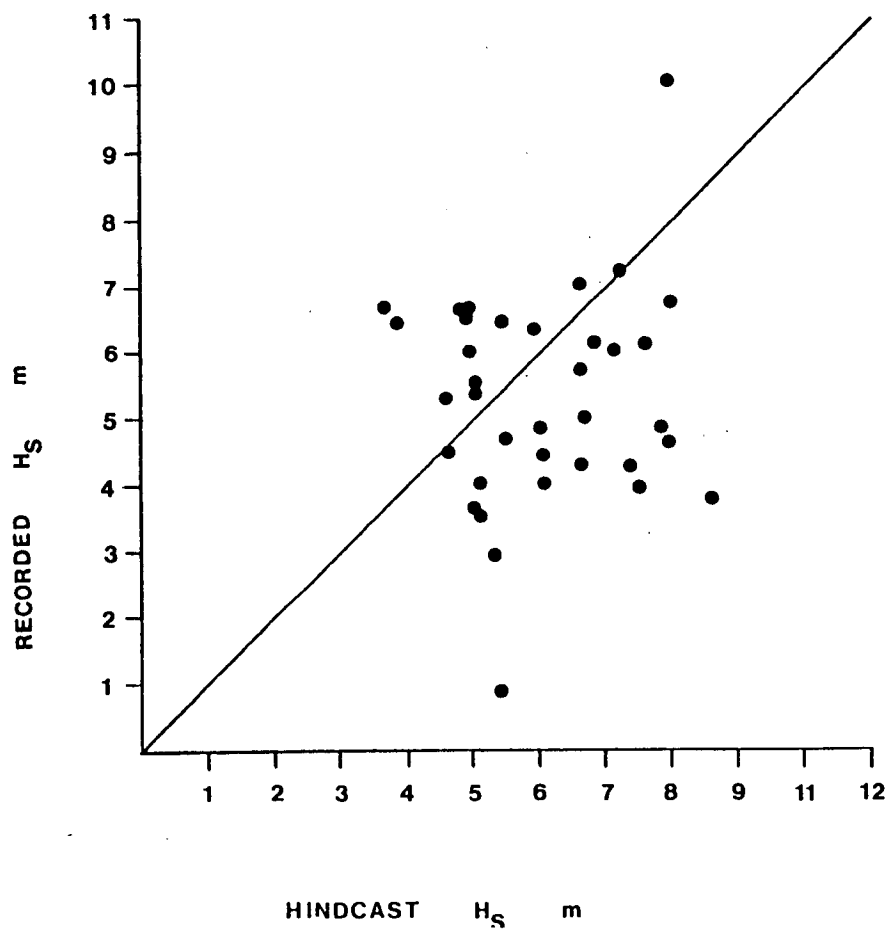


Fig. 4.49 Correlation of hindcast (WES model) with storm maxima (Waverider data) off Nova Scotia and Newfoundland. (From Baird and Readshaw, 1981).

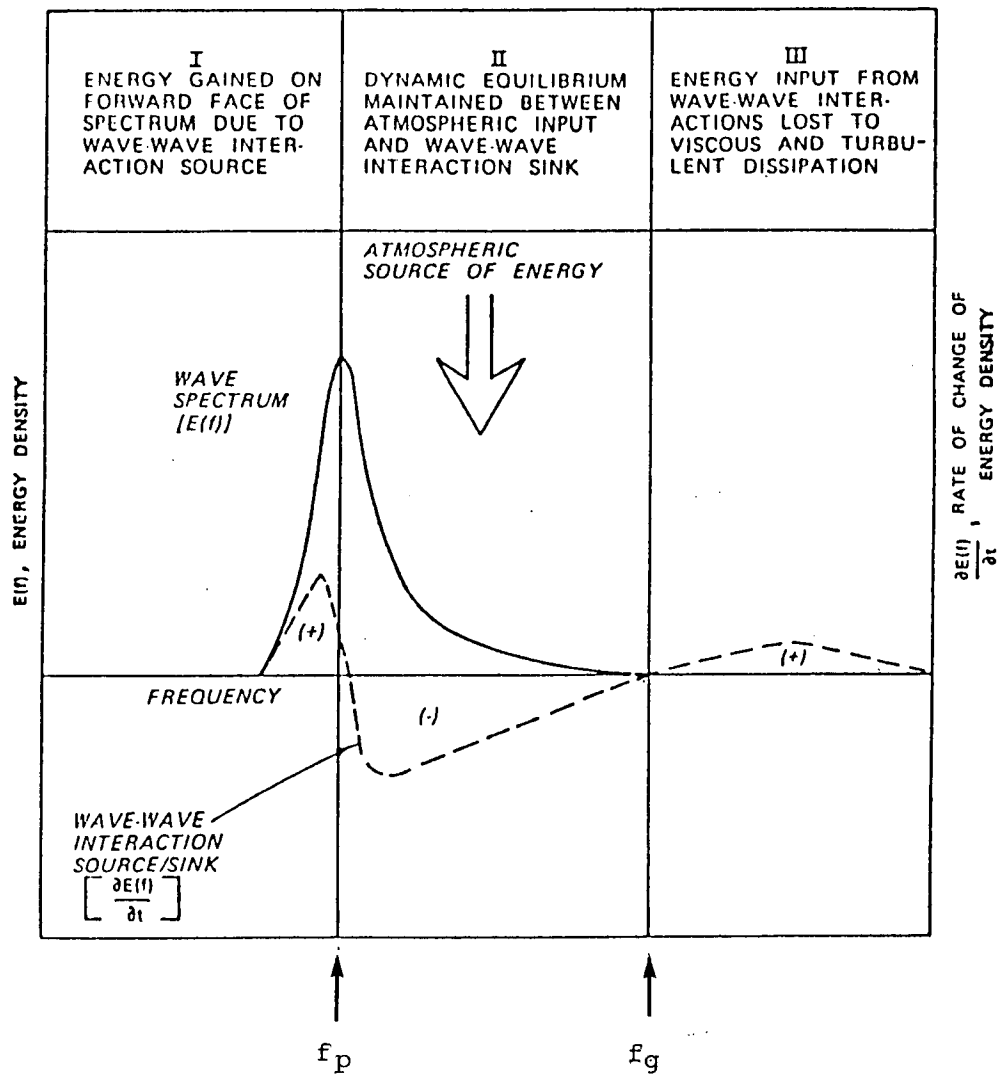


Fig. 4.50 Energy regimes within a spectrum during active wave growth. (From Resio, 1982).

saturated at all times and governed by the $E(f) \propto f^{-5}$ power law. This part of the energy spectrum is also referred to as the Phillips equilibrium range where energy input is balanced by dissipation through whitecapping and wave breaking.

Modern hypotheses (Resio, 1986a; Kitaigorodskii, 1983) argue that the source of energy to region III is not from the local wind, but from resonant nonlinear wave-wave interactions originating from region II. The transition between regimes II and III in deep water is approximately (Kitaigorodskii, 1983)

$$\tilde{\omega}_g = \frac{2\pi f_g U_a}{g} \approx \frac{\beta}{\alpha_u} \quad (4.27)$$

where α_u is approximately 4.4×10^{-3} ,
 β is approximately 1.5×10^{-2} , and
 U_a is the average wind speed.

Thus f_g is about $5.32/U_a$. For a moderate wind of 20 knots ($U_a = 10$ m/s) then f_g is about 0.5 Hz or $T_g = 2$ s. Because this cutoff is at such a high frequency, $E(f_g) \ll E(f_p)$ and the contribution of region III to the total spectral energy will be negligible.

Resio (1986a) and Kitaigorodskii (1983) hypothesize that region II also has an equilibrium shape characterized by a power law, support for which has been found by Kitaigorodskii in experimental data from several sources:

$$E(\omega) = \alpha_u g U_a \omega^{-4} \quad (4.28)$$

where α_u is a non-dimensional constant ($\approx 4.4 \times 10^{-3}$),
 g is the gravitational constant,
 U_a is the mean wind speed ($u_*/U_a \approx 1/30$), and
 ω is angular frequency ($2\pi f$).

In other words, the saturated shape of this part of the spectrum is invariant, but the energy content depends directly on mean local wind speed. The limits of the range are f_p and f_g , and as such they have dynamic definitions that depend, for the most part, on local wind speed. This central region of the energy spectrum has been designated by Kitaigorodskii

(1983) as Kolmogoroff's equilibrium range in recognition of the parallels between Kitaigorodskii's theories of energy transfer from low to high frequencies in wave spectra and Kolmogoroff's theory of a turbulent energy cascade from low to high frequencies.

In WAVAD, the wind energy input to region II is defined as

$$S_{in} = \lambda \frac{\rho_a}{\rho_w} C_D \frac{U_{10}^3}{g} \quad (4.29)$$

where λ is a partitioning coefficient expressing the fraction of wind momentum that enters the wave field,

ρ_a is air density,

ρ_w is water density,

C_D is the surface drag coefficient,

U_{10} is the 10-m elevation wind speed, and

g is the gravitational constant.

Hasselmann et al. (1973) concluded that the minimum atmospheric momentum flux into the wave field is of the order of 10 to 40% of the total momentum transfer across the air-sea interface, but it may be up to 100% if dissipation is important. Resio (1986a) argues that the partitioning coefficient is more reasonably about 60%.

The drag coefficient has the form proposed by Large and Pond (1981) with slightly different coefficients:

$$C_D = (0.75 + 0.054 U_{10}) \times 10^{-3} \quad (4.30)$$

Resio (1986a) has assumed that where bottom effects are negligible S_{in} is exactly balanced by S_{nl} when the energy spectrum is saturated in region II. Based on this equilibrium balance and an approximate integration of the collision (Boltzmann) integral, the expression for the total energy flux rate in terms of spectral parameters is given as

$$S_{nl} = \frac{\epsilon \sqrt{g} E_o^3 k_p^{4.5}}{\tanh^{3/4}(k_p d)} \quad (4.31)$$

where ϵ is a non-dimensional constant

(evaluated numerically to be of the order of 100),

g is the gravitational constant,

E_0 is the total spectral energy in the domain $f_p < f < \infty$,

k_p is the peak wave number ($4\pi^2 f_p^2 / g$ in deep water), and

d is the local water depth.

When the wind-wave system is not in balance, $S_{in} - S_{nl}$ provides a net source or sink of energy to or from the Kolmogoroff range.

Energy growth on the forward face of the spectrum (region I in Fig. 4.50) is defined as a fixed proportion of S_{nl} , the remainder of which is dissipated by implicit transfer to the permanently saturated spectral region III. The shape of the forward face is presumed to have an evolutionary rather than an equilibrium form (Resio, 1986a). The rate of energy transfer among the frequencies is viewed as an analogue of heat transfer in a medium of constant conductivity. In deep water, this idea yields

$$E(f) = E(f_p) \exp[-\delta(f/f_p)^{-4}] \quad (4.32)$$

where δ is a dimensionless constant.

Other energy source-sink terms included in WAVAD are shoaling, refraction and bottom interaction effects.

In this model, solutions to the energy balance equation are obtained using a fractioned step procedure (Yanenko, 1971) by recasting the governing equation as

$$\left(\frac{\partial}{\partial t} + C_g \cdot \nabla \right) E = 0 \quad (4.33)$$

$$\frac{\partial E}{\partial t} = S_{in} + S_{nl} + S_b \quad (4.34)$$

Equation (4.33) is solved using characteristic rays, reverse-propagated from each grid point at the new time level to intersect the solution for E at the previous time level. Following Longuet-Higgins (1957) with

$$\frac{C_g}{4\pi^2 f} E(f, \theta) = \text{constant} \quad (4.35)$$

as the quantity conserved along each characteristic in the absence of source-sink terms, this equation is then solved along each ray for given (f, θ) , taking the old-time level value for E as the initial value.

In the second step the propagated spectrum at the new time level is modified to account for energy input, changes in spectral shape due to nonlinear fluxes and bottom friction losses.

Using historical wave measurements from four different locations (Duck, North Carolina; Hiezu Coast, Japan; Nishikinohama Coast, Japan; and Melkbosstrand, South Africa), Resio (1986b) has verified the performance of the shallow water implementation of WAVAD for a wide variety of energy source-sink conditions. In Table 4.4, which presents his summary of these test cases, the four righthandmost columns give the relative importance of shoaling, refraction, wind input and nonlinear interactions in each spectral test case. In case 1, for example, as the wind input diminishes with time, the S_{n1} term quickly becomes negligible and shoaling begins to be the dominant source of wave growth. Columns 2 and 3 give the simultaneous H_g values at the deeper H_1 location and the shoreward shallow H_2 site. It is the difference between these H_g values that is attributed to the various $S(f)$ terms in the last four columns.

The WAVAD prediction of H_g at site H_2 is given in column 4 and is almost always within 10% of the measured value without any apparent bias. In the two examples that exceed the 10% deviation, the relative importance of the $S(f)$ terms is about the same but certainly not uniquely so. These results indicate very acceptable performance by WAVAD over a broad range of physical prototype conditions.

Other applications of this model have included a hindcast performed using a nested shallow water grid for the Canadian northeast Pacific coast (Hodgins and Nikleva, 1986) and an extensive test in the Beaufort Sea in an application where ice edge evolution and bottom effects are important considerations.

Table 4.4

**Comparison of Predicted and Observed Wave Heights
as a Function of
Modelled Energy Source Terms in Resio's WAVAD**

Date-Time	H ₁	H ₂	H _{pred}	Dev	% Dev	%1	%2	%3	%4	
8210100100	1.8	1.8	1.8	.0	-.1	-4.5	.0	49.7	-45.8	- Case 1
8210101300	2.4	2.6	2.8	.2	7.8	54.1	.0	30.6	-15.3	
8210110100	2.1	2.7	2.6	-.1	-3.7	59.0	.0	31.7	-9.3	
8210111300	2.0	2.6	2.4	-.2	-6.1	83.7	.0	10.5	-5.8	
8210120100	2.0	2.4	2.5	.1	5.3	91.9	.0	1.9	-6.2	
8210121300	2.4	3.1	3.0	-.1	-3.3	93.1	.0	.6	-6.3	- Case 2
8210121900	2.2	3.1	2.8	-.3	-9.9	94.9	.0	.7	-4.4	
8210241300	4.1	3.4	3.5	.0	1.1	.9	-.9	42.5	-55.7	
8210251300	3.6	3.2	3.6	.4	13.5	50.4	-11.7	.1	-37.9	
8410060700	1.1	1.0	1.0	.0	-3.0	-.9	.0	48.0	-51.1	
8410061900	1.4	1.2	1.3	.1	5.7	-12.2	-.4	41.8	-45.5	- Case 3
8410070700	1.5	1.4	1.5	.0	2.1	-18.3	-.9	50.0	-30.9	
6412021405	1.9	1.8	2.0	.1	6.1	59.1	-22.2	.0	-18.7	
6412021434	2.4	2.1	2.4	.3	12.0	61.4	-16.4	.1	-22.1	
6412021527	2.0	2.0	2.1	.1	4.3	69.6	-14.6	.2	-15.6	
6410021546	1.9	1.9	1.9	-.1	-2.9	-63.5	-18.8	.3	-17.4	- Case 4
6401311620	.8	.7	.6	.0	-2.2	-.9	-.2	37.6	-61.4	
6401311710	.8	.8	.8	.0	6.6	-.5	-.6	52.6	-46.4	
6901160000	1.7	1.5	1.5	.1	4.0	-44.6	-31.3	15.3	-8.9	
6905130000	3.4	3.1	3.3	.2	6.4	27.4	-13.6	.3	-50.8	
6905290000	2.7	2.4	2.6	.2	8.4	17.4	-49.3	.1	-33.2	- Case 5
6908190000	3.4	3.0	3.0	.0	-.5	-59.3	-2.2	1.4	-37.0	
6910070000	2.1	2.2	2.3	.1	3.4	81.9	-5.4	7.1	-5.6	
6911180000	4.4	3.5	3.6	.2	4.5	17.4	-15.7	6.3	-60.6	
7001270000	2.7	2.6	2.5	-.1	-3.6	-7.7	-69.8	5.9	-16.6	

KEY

- H₁ measured wave height (m) at site 1 (deeper)
H₂ measured wave height (m) at site 2 (shallower)
H_{pred} predicted wave height (m) at site 2
Dev H_{pred} - H₂ (m)
% Dev 100 x (H_{pred} - H₂)/H₂
%1 percentage of change due to shoaling
%2 percentage of change due to refraction
%3 percentage of change due to wind input
%4 percentage of change due to nonlinear interactions

4.3.7 The DHI System 20 Model

The System 20, or S20, model has been developed over the past 10 years by the Danish Hydraulic Institute for commercial wave hindcast studies. Early versions were closely related to the PTB-SOWM and Inoue (1966) formulations, in which wave growth took place independently in each (f, θ) band up to a wind-dependent PM spectrum. Hindcasts in Canadian waters using this older model were described by Abbott (1978) for Davis Strait, and by Hodgins et al. (1981) for a Beaufort Sea study commissioned by ESSO Resources Canada Limited. Between 1982 and 1983 the S20 model was reformulated to incorporate wave-wave interaction terms, and growth rates approximately 1.87 times faster than the JONSWAP results given in Hasselmann et al. (1976).

The approach to specifying wave growth is similar to that given by Resio (1981). However, a prescribed saturation spectrum is retained here--the PM spectrum in deep water, and a modified form,

$$E_{PM} \cdot \frac{(\tanh kd)^2}{\left(1 + \frac{2kd}{\sinh kd}\right)}$$

in intermediate water, consistent with the Kitaigorodskii et al. (1975) predictions. In shallow water an addition factor of $4d/L_0$, where L_0 is the wave length in deep water and d is the local water depth, is applied. Thus, the model incorporates the theory of wave-wave interaction giving forward face growth in agreement with observations, while preserving an accepted spectral shape in the saturated range.

Brink-Kjaer et al. (1984) point out that dissipation is specified in the swell range. The functional form, for depths less than 200 m, is

$$- \propto \frac{H_{m0}^2 f^2}{d}$$

but the coefficient of proportionality is not given. This decay rate is also applied to overdeveloped (i.e. above the PM spectrum) components. Within one time step the maximum rate will bring the energy of a particular component down to E_{PM} . In earlier versions of the model, the spreading function was of the cosine-squared form. This relation appears to be

retained in the newer versions also, constant across all frequencies.

As in the other DS model applications, the wave energy spectrum is discretized in terms of a number of frequencies and directions at each node of the regular grid, and energy balance equation (2.17) is numerically integrated in time over all space points. Through partial differentiation it is rewritten in two parts: a transport stage and a growth/decay stage. The transport calculation is done first to propagate wave energy at the former time level (from a region surrounding the point of interest in space) to the present time level. Then the growth and decay terms are evaluated to modify the energy at the new time level, found from the first stage calculation.

The numerical solution technique for the transport stage in the S20 model makes use of a high order difference scheme to avoid false numerical dispersion of energy which would result from simpler schemes (Roberts and Weiss, 1966). It utilizes the group velocity, at which the wave energy is transported to establish a Lagrangian explicit difference scheme. In the deep water version, the group velocity is constant for each spectral component and the wave energy propagates along straight lines.

Thus at each grid point the energy at the old time level (which is everywhere known) at a position $\int_0^{\Delta t} -\vec{c}_g \cdot d\vec{s}$ is moved to the point at the new time level. Interpolation for the energy value at a position $P(\Delta x, \Delta y)$ with respect to the grid point is carried out with the following third-order polynomial

$$\begin{aligned} F(\Delta x, \Delta y) = & k_1 \\ & + k_2 \frac{\Delta x}{\Delta s} + k_3 \frac{\Delta y}{\Delta s} \\ & + k_4 \left\{ \frac{\Delta x}{\Delta s} \right\}^2 + k_5 \frac{\Delta x}{\Delta s} \frac{\Delta y}{\Delta s} + k_6 \left\{ \frac{\Delta y}{\Delta s} \right\}^2 \\ & + k_7 \left\{ \frac{\Delta x}{\Delta s} \right\}^3 + k_8 \left\{ \frac{\Delta x}{\Delta s} \right\}^2 \frac{\Delta y}{\Delta s} + k_9 \frac{\Delta x}{\Delta s} \left\{ \frac{\Delta y}{\Delta s} \right\}^2 + k_{10} \left\{ \frac{\Delta y}{\Delta s} \right\}^3 \\ & + k_{11} \left\{ \frac{\Delta x}{\Delta s} \right\}^3 \frac{\Delta y}{\Delta s} + k_{12} \frac{\Delta x}{\Delta s} \left\{ \frac{\Delta y}{\Delta s} \right\}^3 \end{aligned}$$

where the 12 coefficients k_i are fitted to the energy values in the 12 grid points surrounding P (Fig. 4.51). Due to the discretization of frequency, and hence of the propagation speed, and direction of propagation, the energy reaching a grid point originates from a discrete element of area. An average value for the energy of this area is calculated in the S20 model and moved to the grid point considered (this is shown schematically in Fig. 4.52). For a point in the vicinity of open model boundaries, missing values for the 12-point interpolation scheme are found by a mirror condition across the boundary.

Brink-Kjaer et al. (1984) have reported an extensive series of model verifications using the new code. The model grids are shown in Fig. 4.53 together with measurement verification points. During November 1981, two especially severe storms were recorded. The comparison of predicted and measured significant wave heights is shown in Fig. 4.54; the agreement is excellent, supporting the faster growth rate (than JONSWAP) programmed into this model. A comparison of storm peak values of H_{m0} for 18 separate storms and several locations is shown in Fig. 4.55. Once again, agreement with measurements, up to H_{m0} values exceeding 10 m, is excellent. Here the correlation coefficient was 0.97 and the standard deviation in H_{m0} was 0.46 m for a set of verification data that is one of the most extensive yet reported.

4.3.8 The British Meteorological Office (BMO) Model

Golding's model (Golding 1978; 1983), also referred to as the BMO model, is a discrete spectral model of the PTB formulation. It includes empirical functions for growth and decay, and a procedure to account for nonlinear interactions. The propagation term is integrated with a modified Lax-Wendroff scheme (attributed to Gadd, 1978); tests of the procedure: accuracy were reported in Golding (1978) and Vincent and Resio (1979).

The growth term coefficients are given by

$$A = \begin{cases} \frac{6 \times 10^{-8}}{2\pi f_{\max}} U^2 \cos(\theta - \psi) & \text{for } f = f_{\max}, |\theta - \psi| < 90^\circ \\ 0 & \text{otherwise} \end{cases} \quad (4.36)$$

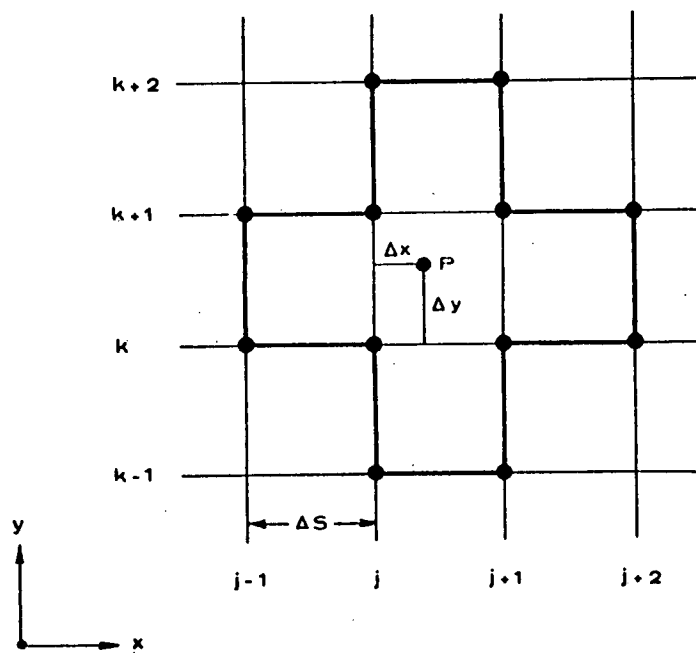


Fig. 4.51 The 12-point interpolation scheme for the energy at any point P within the S20 grid. (Provided by DHI).

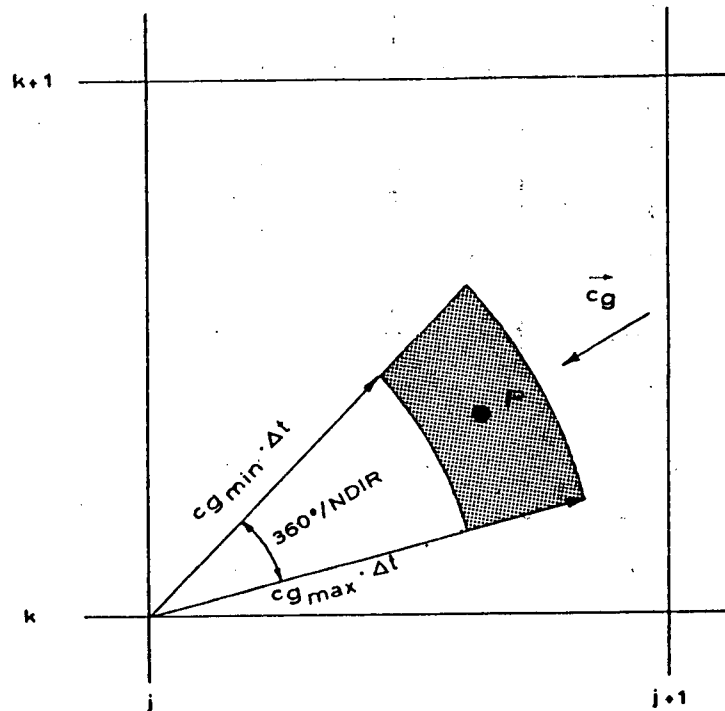


Fig. 4.52 Energy from the shaded area is advanced in the S20 transport scheme to the new time level. (Provided by DHI).

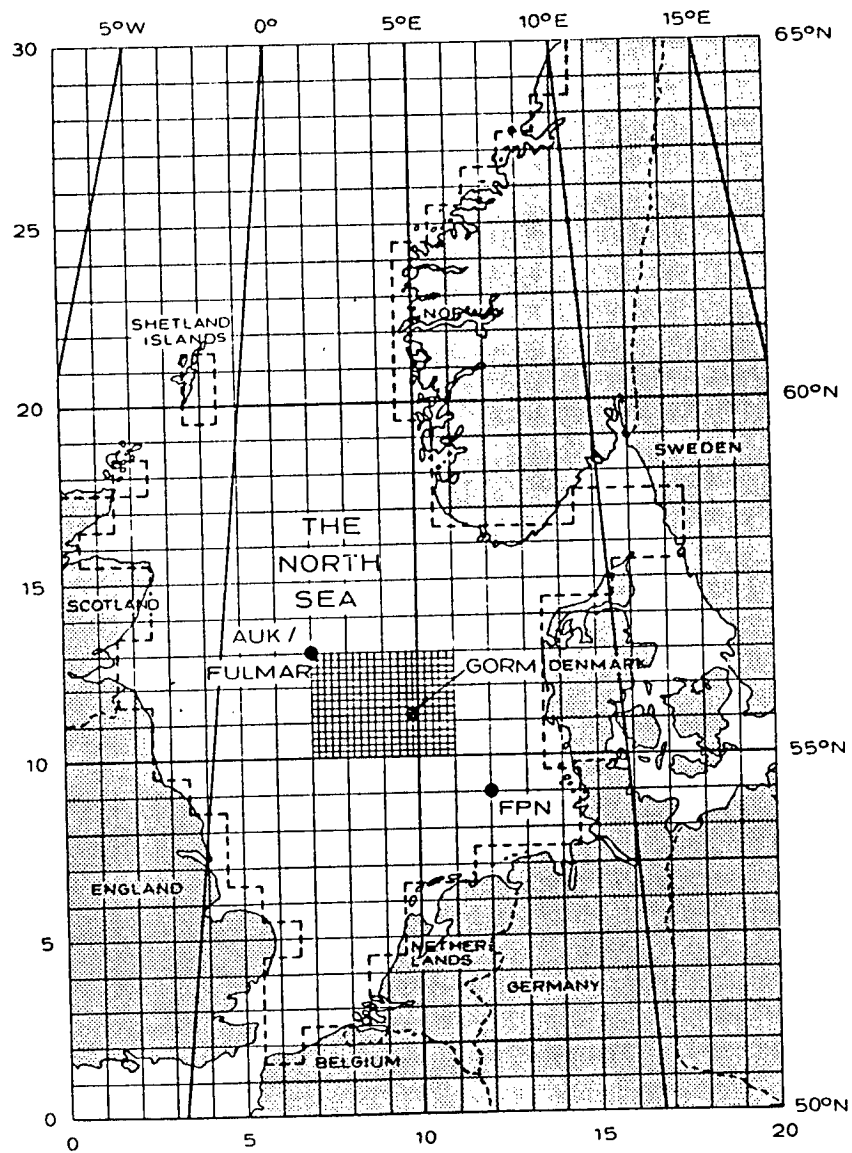


Fig. 4.53 Model grid for the DHI S20 application to the North Sea. (From Brink-Kjaer et al., 1984).

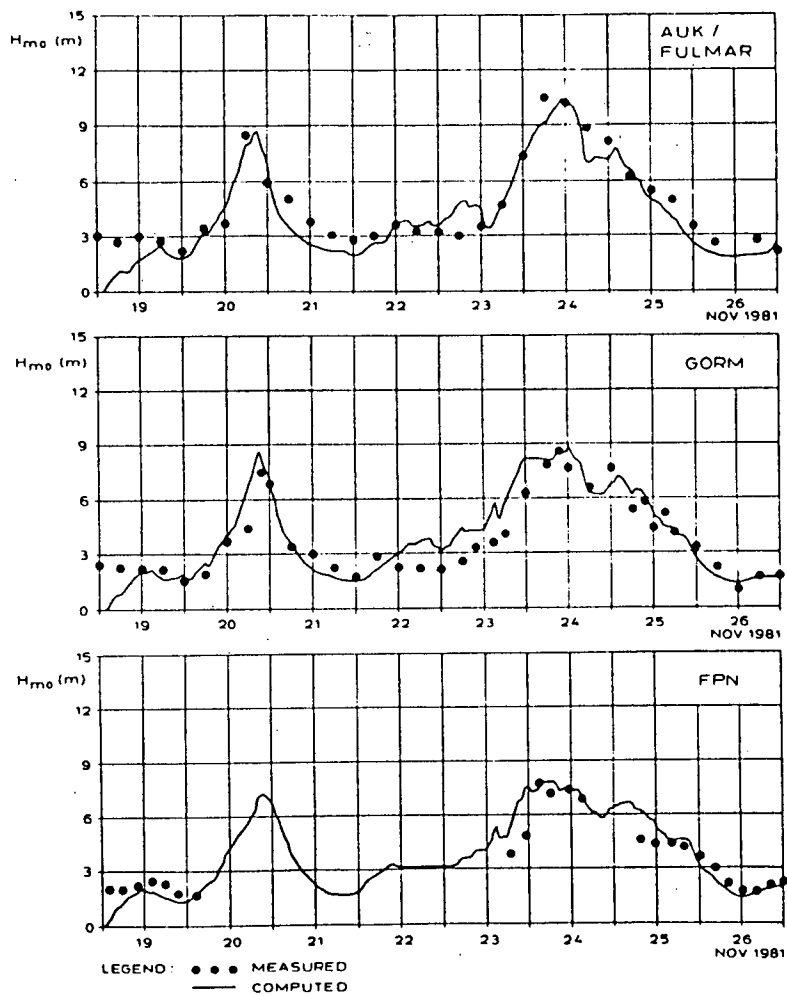


Fig. 4.54 Time-series comparison of significant wave height measured during the November 1981 storm with the S20 prediction. (From Brink-Kjaer et al., 1984).

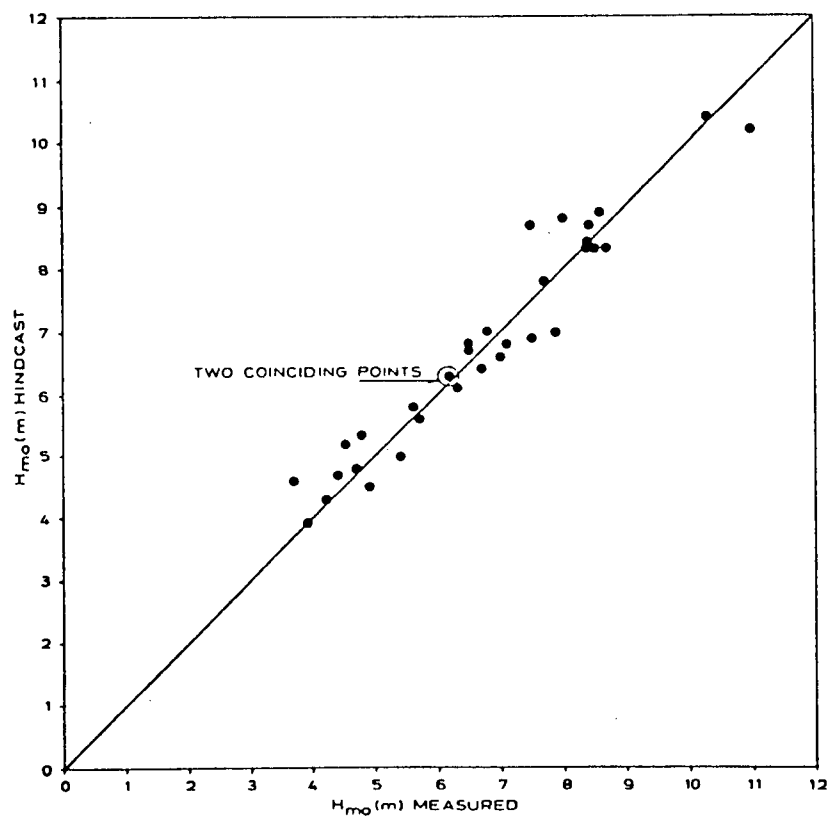


Fig. 4.55 Correlation of measured versus predicted storm maximum significant wave heights for 18 separate events in the North Sea. (From Brink-Kjaer et al., 1984).

where f_{\max} is the highest frequency component represented and (U, ψ) is the wind vector at 19.5 m, and

$$B = \begin{cases} 6 \times 10^{-2} \frac{2\pi\rho_a f}{\rho_w} ([U \cos(\theta - \psi)/c] - 1) & \text{if } U \cos(\theta - \psi)/c > 1 \\ 0 & \text{otherwise} \end{cases} \quad (4.37)$$

where c is the phase speed of waves of frequency f (normally $g/(2\pi f)$). This formulation follows from the findings of Snyder et al. (1981) that the linear term (A) becomes unimportant soon after the initiation of wave growth.

Dissipation is parameterized following Hasselmann (1974) as

$$S_{ds} = 4 \times 10^{-4} f^2 F(f, \theta) m_0^{1/4} \quad (4.38)$$

As this dissipation does not exactly balance the energy input when the fully developed spectrum is reached, the total energy in the spectrum is explicitly limited to the total energy in the saturated PM spectrum, but the distribution of that energy among the frequencies is not imposed by this condition.

The three numerical coefficients in (4.36), (4.37) and (4.38) were tuned together to reproduce the JONSWAP growth curve as a function of duration, giving

$$\begin{aligned} \epsilon &= 0.887 \times 10^{-4} \xi && \text{for fetch-limited growth} \\ \epsilon &= 1.165 \times 10^{-6} \tau^{1.493} && \text{for duration-limited growth} \end{aligned}$$

The nonlinear transfer processes are modelled implicitly by adjusting the shape of the wind-sea portion of the spectrum to be that of a JONSWAP spectrum. This is an intuitively satisfying approach, but the limitations of it lie in the difficulty in separating wind-sea from swell energy and in the accuracy of the diagnostic relations for the JONSWAP shape parameters. Golding (1983) defines the spectral separation for wind-sea as

$$\begin{aligned} f &\geq 0.8 f_p \\ |\phi - \psi| &\leq 90^\circ \end{aligned} \quad (4.39)$$

However, because only the total energy in the combined spectrum is known, f_p must be determined by successive approximations beginning with the lowest possible value, the peak of the PM spectrum.

Using (4.39), the total energy in the wind-sea spectrum $m_o(w)$ is determined. The JONSWAP spectrum is then specified by formulae which approximate the single-parameter model of Hasselmann et al. (1976) for small values of $m_o(w)/m_o(\text{PM})$ and tend towards the PM values as $m_o(w) \rightarrow m_o(\text{PM})$:

$$\begin{aligned} f_p &= [(10^{-4} + 7 \times 10^{-4}(\gamma-1)\sigma)/m_o(w)]^{0.25} \\ \gamma &= 1.0 + 2.3[1 - (m_o(w)/m_o(\text{PM}))^2] \\ \sigma &= 0.08 \end{aligned} \quad (4.40)$$

Shallow water effects are included in the model by adding the refraction term $\partial[(c_g \nabla \theta)F]/\partial \theta$ to the propagation terms of the energy balance equation. $c_g \nabla \theta$ is formulated in terms of the orthogonal bottom slopes on the model grid and the linear wave dispersion relation. The bottom slopes are approximated by centred differences at each grid point, and the complete refraction term is solved in a first-order upstream difference form in θ . Each component (f, θ) is solved independently. Frictional dissipation due to bottom roughness has also been included with the approximate form described by Collins (1972). This term is discussed in more detail in Subsection 4.3.10 for the decoupled propagation models.

The starting point of each forecast period is an accurate diagnosis of the prevailing wave conditions based on specification of the actual wind field over the preceding 12 hours derived from the mass field analysis updated with surface wind observations. Forecast winds are obtained from the British operational 10-level forecast model up to 36 hours ahead. Until 1982, the 900 mb values were reduced to 19.5 m with empirical relationships based on results of Findlater et al. (1966):

$$\begin{aligned} V_o/V_{900} &= a V_{900}^2 + b V_{900} + c \\ \theta_o &= \theta_{900} + d \end{aligned}$$

The constants a , b , c and d are reported (Golding, 1983) to depend on the "lapse rate" between 950 mb and the surface.

The surface temperature is obtained from the model's two lowest layers and the sea surface temperature as

$$T_o = \begin{cases} T_{950} + 0.5 h_{950} \gamma_d \\ 0.1(T_{950} + 0.5 h_{950} \gamma_{900}) + 0.9 T_s \\ T_s \end{cases}$$

where h_{950} is the height of the 950 mb surface
 γ_d is the dry adiabatic lapse rate
 γ_{900} is the lapse rate between T_{850} and T_{950} .

With the introduction of a new atmospheric model in September 1982 incorporating a detailed boundary layer specification, the foregoing empirical reduction has been eliminated.

The model is configured as a coarse grid (300-km grid spacing at 60°N) covering the Atlantic and Pacific Oceans north of 20°N with a nested fine grid (Fig. 4.56) covering the continental shelf. The coarse grid model is a deep water version used for ship routing forecasts and to provide input boundary conditions to the fine mesh model. The continental shelf model presently has a grid length of 50 km (reduced from 100 km prior to August 1982) overlayed on a polar stereographic projection and uses the following spectral discretization: 12 directions (30° spacing) and 11 frequencies (0.05, 0.06, 0.072, 0.086, 0.014, 0.124, 0.148, 0.178, 0.214, 0.256, 0.308 Hz).

The model was transferred from an IBM 360/195 computer to a Cyber 205 machine in September 1982. The operational time step has not been reported, but forecasts are run from T-12 to T+36 hours and are archived.

Comparisons between wave model results and measured wave data have been reported by Houghton (1984), but the evolution of the wind and wave models makes long-term comparisons difficult. Table 4.5 from Houghton lists the significant developments in the modelling and archiving procedures. Monthly mean and rms errors for three west coast sites are presented in Fig. 4.57. At the more exposed locations (South Uist and Isles of Scilly), the monthly mean errors are less than about ± 0.4 m and are largely trendless. Over the entire comparison period, the absolute mean error is 0.05 m and the rms

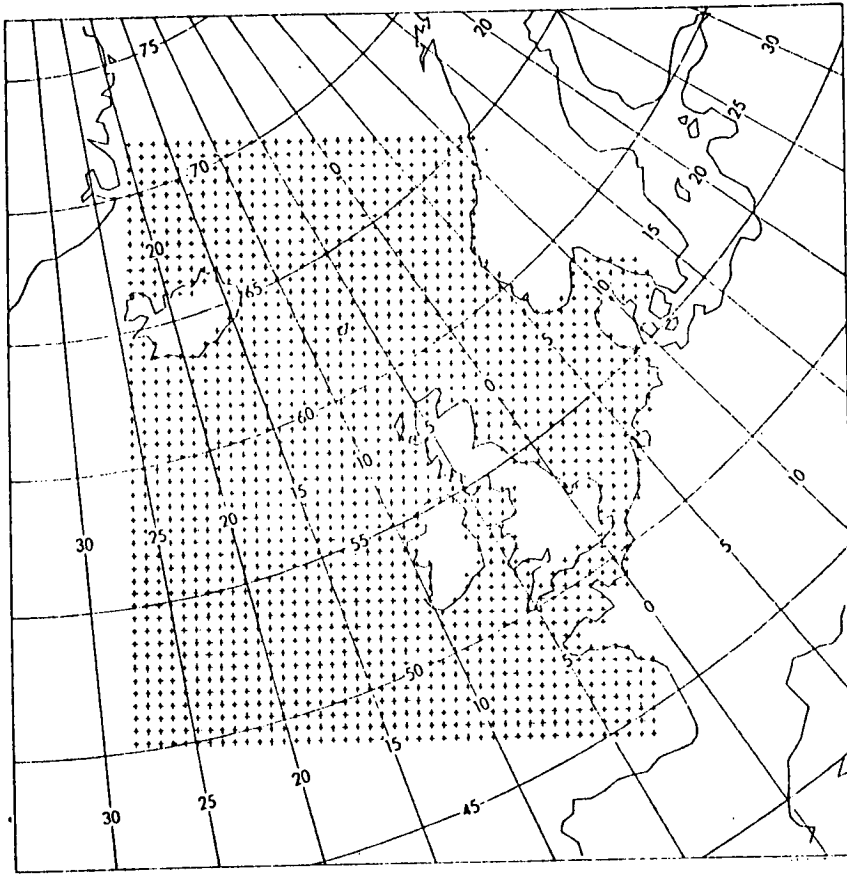


Fig. 4.56 Grid points of the BMO fine mesh wave model. (From Golding, 1983).

Table 4.5

Principal Dates in the Development of the BMO Model

Date	Development	Effect
1978-07-18	Surface wind analysis introduced	Better hindcast winds
1978-09-26	Shallow-water friction term introduced	Lower wave heights in shallow water
1979-10-23	Wave growth includes JONSWAP spectrum	More realistic wave growth
	11 frequencies	Higher resolution wave spectrum
1980-03-18	Dissipation coefficient increased	Greater attenuation of swell and slower wave growth
1981-04-14	Modification of archived spectrum representation	More accurate storage of high-frequency wave energy components

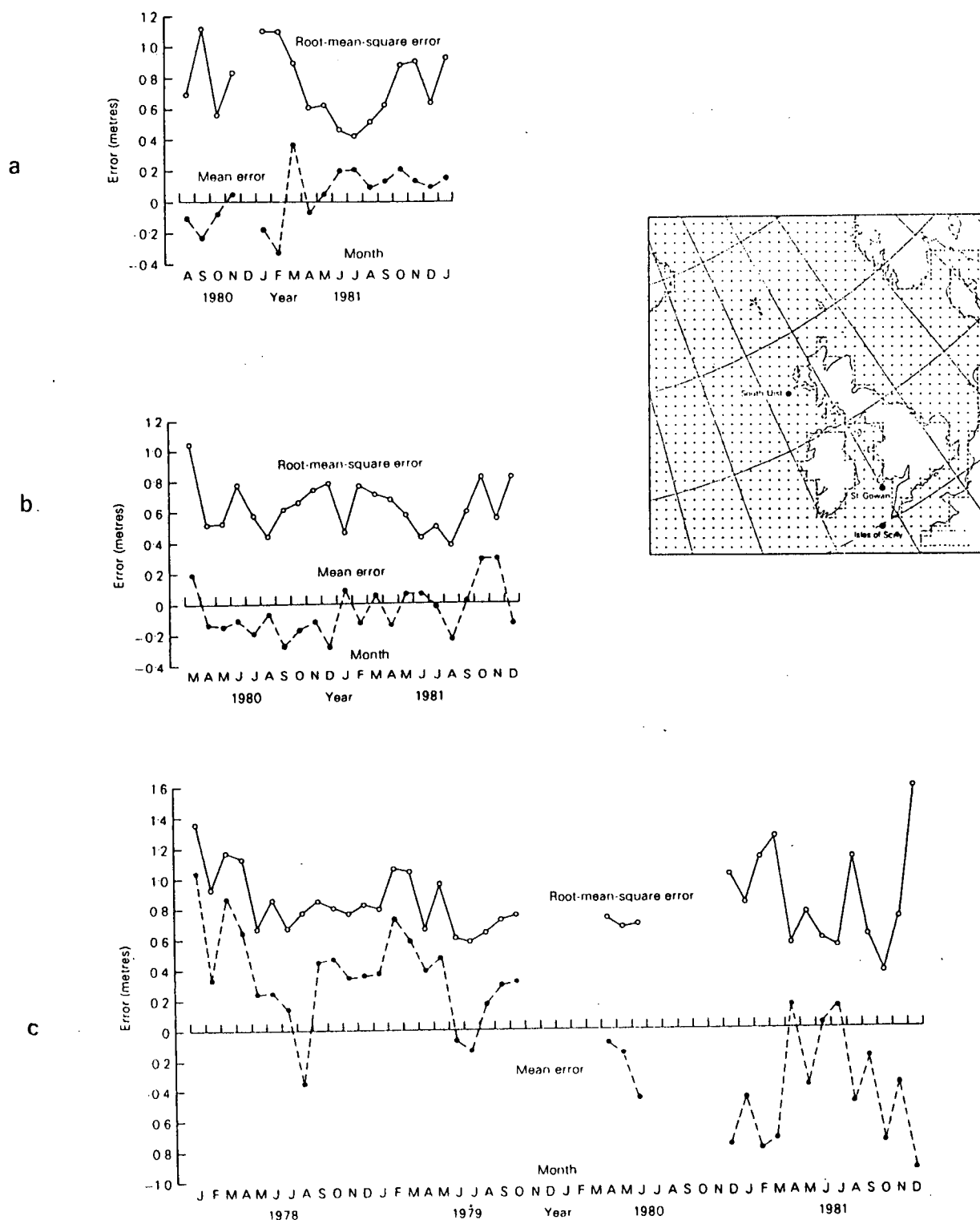


Fig. 4.57 Monthly mean and rms errors at (a) South Uist, (b) Isles of Scilly and (c) St. Gowan. (From Houghton, 1984).

error is less than 0.75 m. The larger errors and the overall and seasonal trends in the St. Gowan results are attributed to modelling changes associated with calculating wind-sea for high winds at short fetches: the smaller errors in summer are coincident with primarily swell waves propagating from the long fetch to the southwest.

Time-series comparisons shown in Fig. 4.58, illustrate the wave models' performance: plate (a) shows all the measured data and plate (b) contains only 00 and 12 GMT measurements corresponding to the wave model times. In general the phase and amplitudes of the measured variations are well modelled. It seems likely that the comparison would have been somewhat improved if Houghton had calculated a running average of the measured data over 6 or 12 hours.

4.3.9 Japanese Models: Isozaki and Uji

The Isozaki and Uji (1973) model is a DS model of the PTB type containing linear-exponential growth, frictional dissipation during propagation and damping by opposing winds. The PM spectrum is used as a bound on wave growth as in the other models in this class. The frictional dissipation term has the form

$$S_{ds} = -D f^4 \cdot F \quad (4.41)$$

where D is a constant. This form of dissipation damps out the high frequency wave components quickly while leaving the low frequency components comparatively unaffected. In this way it is intended to model the wave-wave interaction processes.

Wave energy is also dissipated by opposing winds in a form similar to that used in the DHI S20 model, i.e.,

$$S_{ds} = -(B + D \cdot f^4) F \quad (4.42)$$

where B is the exponential growth coefficient and D is the previously defined constant.

The energy balance equation is solved with a finite difference scheme, the most important part of which deals with the propagating wave energy. Isozaki and Uji (1973) describe this as a combination finite difference

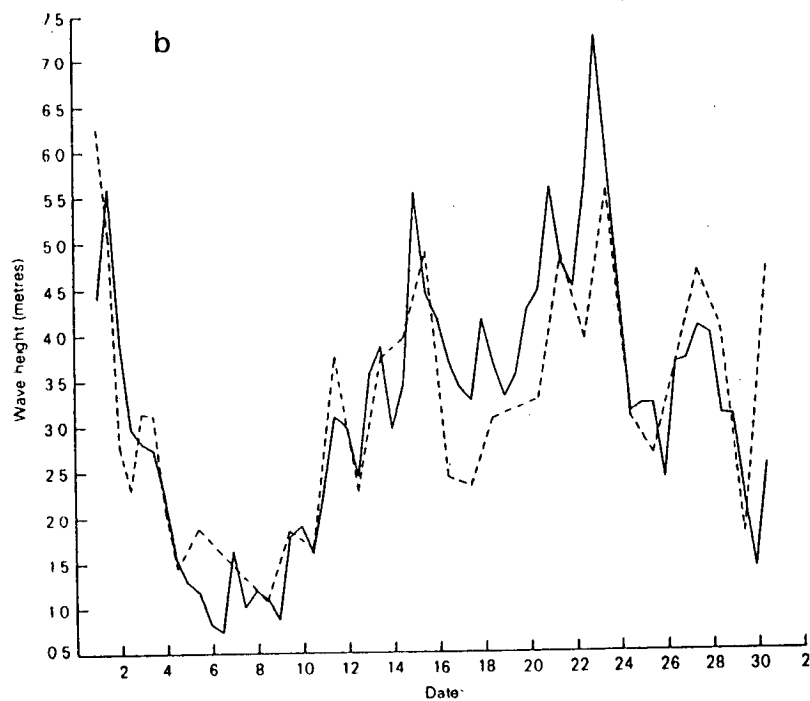
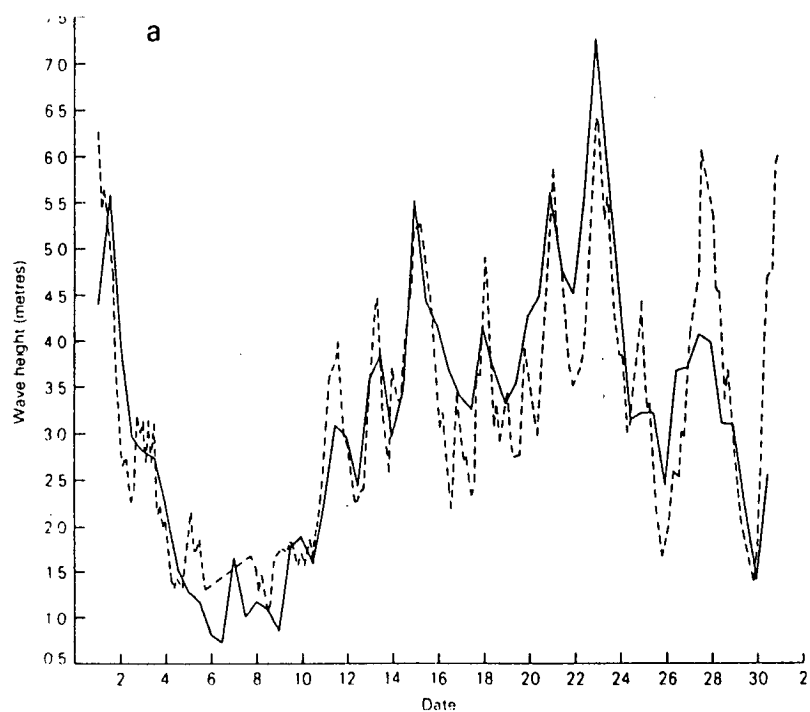


Fig. 4.58 Time-series wave heights at South Uist for November 1980 (a) using all data and (b) using only 00 and 12 GMT data. (— model data and --- measured data). (From Houghton, 1984).

scheme and "jump" technique like that used by Pierson et al. (1966).

The December 16 to 18, 1959 storm was hindcast by Isozaki and Uji, with the grid shown in Fig. 4.59. The spacing is 120 n.m. The spectrum was resolved with frequencies ranging from 0.04 Hz to 0.20 Hz in 0.01-Hz steps and 16 directional components. The significant wave heights (model versus measured) are shown in Fig. 4.60. The one-dimensional spectra are compared in Fig. 4.61. Isozaki and Uji (1973) report one other application of their model to the Japan Sea, with results of similar quality to those presented here.

4.3.10 Two Decoupled Propagation Models--VENICE and SPECREF

Many of the above models emphasize the importance of the nonlinear wave-wave interactions that are responsible for redistributing energy between frequencies in the spectrum. In the numerical simulation of this process the energy at each discrete frequency at one time step is related to the energy distribution at the next time step by an explicit relation. In this way the evolution of the spectrum is coupled in time-frequency space. If instead one is content to predict the result of the nonlinear processes in a more empirical fashion, decoupled models can be formulated wherein the time evolution of energy at each frequency is linearly independent of that at every other frequency. Two examples of this type of model solved using ray methods have been developed: one called the VENICE model, published by Cavaleri and Rizzoli (1981), has been applied to the Adriatic and Tyrrhenian Seas around Italy and a second, called SPECREF, originating from Seaconsult (Hodgins et al., 1986), has been applied in Canadian shelf waters primarily for simulating shallow water modification of deep water wave conditions. These models have two particular advantages. First, they very accurately account for depth-induced refraction which is usually the dominant transformation process in shallow water, and second, because of their decoupled formulation, they are readily applied to one or a few arbitrary points of interest rather than to all points of a mesh. This last aspect affords considerable economy and at the same time yields a complete directional spectrum.

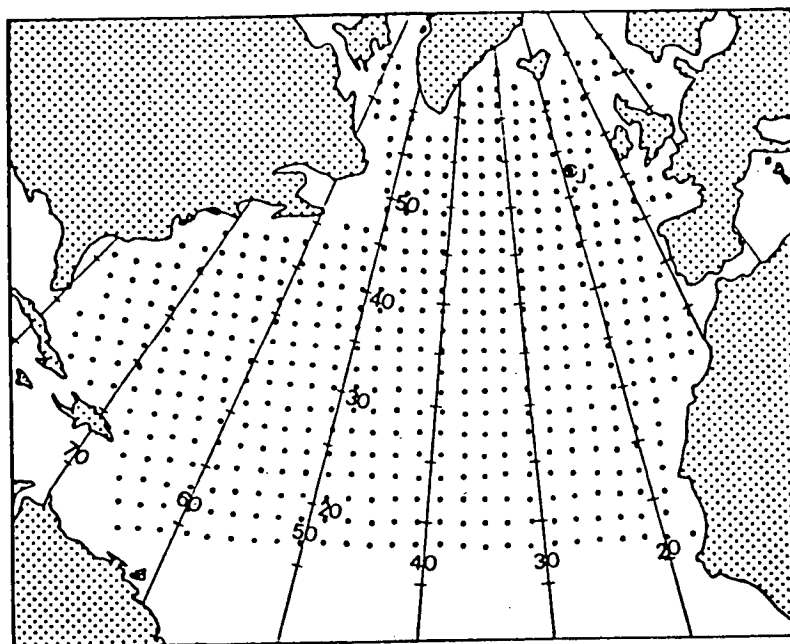


Fig. 4.59 North Atlantic Ocean model grid used by Isozaki and Uji (1973).

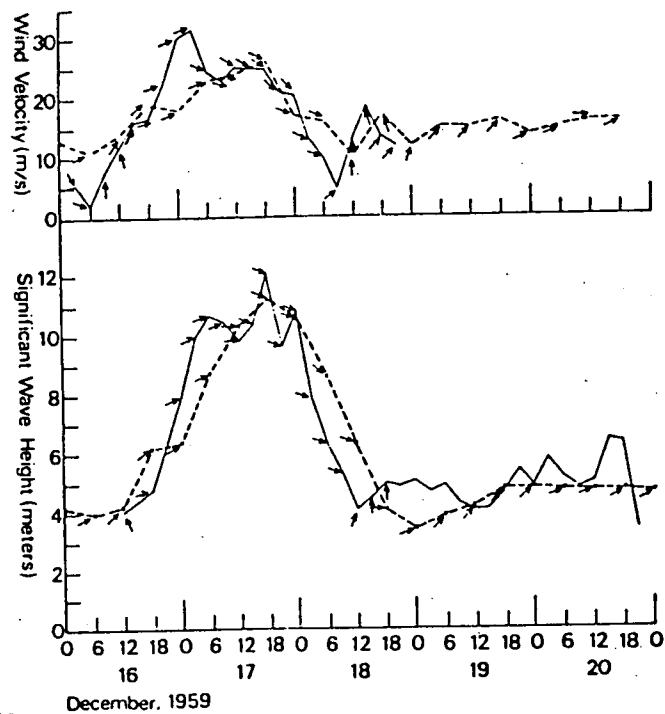


Fig. 4.60 Comparison of modelled (dashed line) versus measured (solid line) wind speed and significant wave height. The arrows indicate wind speed and direction. (From Isozaki and Uji, 1973).

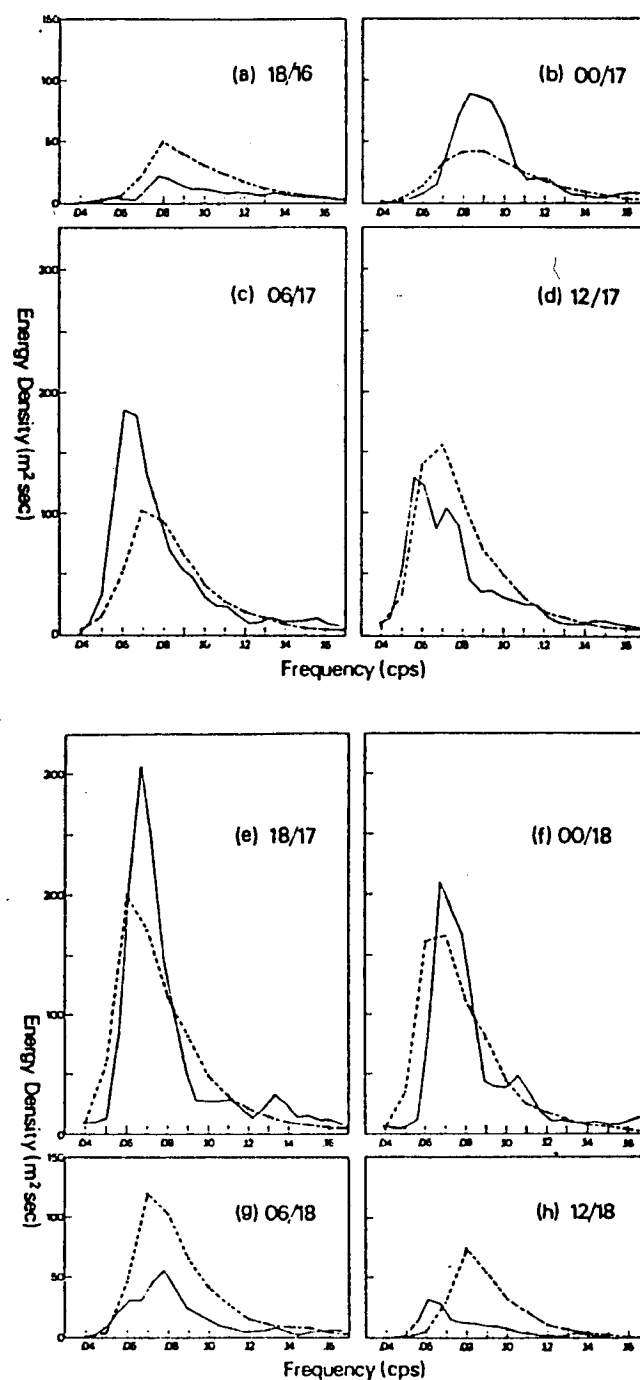


Fig. 4.61 Comparison of predicted (dashed line) and observed (continuous line) one-dimensional wave spectra at the station "J" during December 1959. (From Isozaki and Uji, 1973).

Both models are similar in principle. For a given location the energy conservation equation is solved in two stages

$$\frac{\partial F}{\partial t} = -\mathbf{c}_g \cdot \nabla F \quad (4.43)$$

$$\frac{\partial F}{\partial t} = S(f, \theta, \mathbf{x}, t) \quad (4.44)$$

The first stage solution (propagation) is solved by the method of characteristics which is done by constructing wave ray diagrams outward from the point of interest according to refraction principles. For arbitrary depth $d(\mathbf{x})$, the rays satisfy the relations (Collins, 1972)

$$\frac{d\mathbf{x}}{dt} = \mathbf{c}_g = \frac{\partial \omega}{\partial \mathbf{k}} \quad (4.45)$$

$$\frac{d\mathbf{k}}{dt} = - \frac{\partial \omega}{\partial \mathbf{x}} \quad (4.46)$$

where $\mathbf{x} = (x, y)$ are the two space coordinates, $\mathbf{k} = (k_x, k_y)$ are the wave number components, and $\omega = 2\pi f$ is the circular frequency. Longuet-Higgins (1957) has shown that along a ray $F(\mathbf{k})$ remains constant provided that $S \equiv 0$; then it is possible to write the expression (see, for example, Abernethy and Gilbert, 1975)

$$F(\mathbf{k}) = \frac{c_g}{2\pi k} F(f, \theta) = \text{constant} \quad (4.47)$$

where c_g and k represent the modulus of \mathbf{c}_g and \mathbf{k} respectively. Since $k = \omega/c = 2\pi f/c$ this becomes

$$F(\mathbf{k}) = \frac{c \cdot c_g}{4\pi^2 f} F(f, \theta) \quad (4.48)$$

where c is the phase speed.

For the condition $S \neq 0$ corresponding to wave growth by wind, and energy dissipation by bottom friction and/or wave breaking, the second stage solution is obtained by integrating (4.44) along each wave ray, noting that $\partial/\partial t = c_g \partial/\partial s$ where s is the distance along the ray. The resulting

expression is

$$\frac{\partial F(\mathbf{k})}{\partial s} = \frac{1}{c_g} S \quad (4.49)$$

which becomes upon substituting (4.48)

$$\frac{\partial}{\partial s}(c \cdot c_g F(f, \theta_b)) = \frac{4\pi^2 f \cdot S}{c_g} \quad (4.50)$$

where θ_b denotes the direction of the wave ray at the boundary of the solution domain. This equation, integrated with respect to distance along each ray, is the basic expression for the evolution of energy. The two models differ primarily in the formulation of S . The integration must be carried out for all rays and all frequencies at each time step.

Cavaleri's VENICE Model

In Cavaleri's model growth and dissipation are considered to affect energy packets running along each ray at the group velocity. A time-stepping integration procedure is then used to solve for the contribution for each term in S corresponding with the equation

$$\frac{\partial F}{\partial t} \approx \frac{\Delta F}{\Delta t} = S \quad (4.51)$$

The following processes are included:

Wave growth: this is modelled with the conventional Phillips-Miles formula

$$S = A + BF$$

$$\text{where} \quad A(k) \approx \frac{80 \rho_a^2 \omega}{\rho_w^2 g^2 k^2} C_d^2 U^4 \quad (4.52)$$

$$\text{and} \quad B = \frac{5 \rho_a}{\rho_w} f \left\{ \frac{U \cos \psi}{c} - 0.90 \right\} \quad (4.53)$$

In these expressions ρ_a , ρ_w , $C_d (=0.0012)$ and ψ denote air and water densities, surface wind drag coefficient and the angle between the local wind and the wave ray respectively.

Energy saturation: the original spectral form proposed by Phillips (1958) is used to limit wave growth, with the Phillips parameter α taken as constant. This limit is applied in the model in terms of a PM spectrum multiplied by a cosine-fourth spreading function to give F_{∞} .

Wave breaking: Cavaleri also includes an explicit wave breaking term of the form

$$S(k) = -\eta\omega^2 F(k) \quad (4.54)$$

where the coefficient η was evaluated in the JONSWAP experiment. Use of this term is somewhat redundant when combined with A + BF growth up to a saturated limit. As noted by Cavaleri and Rizzoli (1981) use of this term provided slower growth rates (as would be expected) than without it, but with little effect on the final values of H_{m0} predicted at the site of interest under strong wind conditions.

Bottom friction: energy loss due to bottom friction is modelled using the linearized expression derived by Collins (1972)

$$s = - \frac{C_f g k c_g}{2\pi\omega^2 \cosh^2(kd)} \langle u \rangle \cdot F(f, \theta) \quad (4.55)$$

where the time-averaged wave velocity $\langle u \rangle$ is given by

$$\langle u \rangle = \left\{ \sum_f E(f) \frac{g^2 k^2}{\omega^2 \cosh^2(kd)} \cdot \Delta f \right\}^{1/2} \quad (4.56)$$

Evaluation of the summation in this last equation requires knowledge of the one-dimensional frequency spectrum at each point along the ray. Since this is not known Cavaleri uses an approximate form for $E(f)$ given by the JONSWAP spectrum scaled using the local 10-metre wind speed and the non-dimensional fetch for the computation point in question. This type of approximation is effective where the wave rays terminate on land and $E(f) \equiv 0$ there. It would not work well for open ocean boundaries where $E(f)$ may be the largest on the boundary, and diminishing in energy toward the shallow water point.

Applications: Cavaleri and Rizzoli (1981) discuss two applications in the Adriatic Sea with directional spectral measurements at a tower in 16 m of water near Venice. Time-series of measured and computed values of H_{m0} ($=H_s$) are shown for two storms in Fig. 4.62; spectral comparisons are shown in Fig. 4.63 for six times during the high wave events. We note, however, that H_{m0} peaked at about 2 m during each measurement period, which is rather low. Results for a much more severe storm in the Tyrrhenian Sea were presented also (Fig. 4.64): Cavaleri and Rizzoli found rms errors in H_{m0} , referred to the measured data, of 0.5 to 0.6 m or about 15 to 20%, over the peak of the storm.

The SPECREF Model

SPECREF, standing for spectral refraction (Hodgins, 1986; Hodgins et al., 1986), embodies mechanisms for energy input from the wind, frequency- and depth-dependent saturation limits to growth, and energy dissipation due to bottom friction. The energy balance equation is solved to give the directional wave frequency spectrum $F(x, f, \theta)$ at a specified location x for an arbitrary depth field resolved on a regular Cartesian grid. The following assumptions are invoked:

- (a) the dominant source-sink mechanisms are wind input and bottom friction; the effect of nonlinear energy fluxes between different frequencies is adequately parameterized by the saturation spectrum,
- (b) wave-current interactions are ignored,
- (c) wave diffraction and wave reflection are negligible,
- (d) energy losses due to opposing winds are negligible, and
- (e) energy is limited by the depth-dependent saturation law (Kitaigorodskii et al., 1975).

Under these constraints, the governing equation is

$$\left(\frac{\partial}{\partial t} + \mathbf{c}_g \cdot \nabla\right) F = S_{in} + S_b \quad (4.57)$$

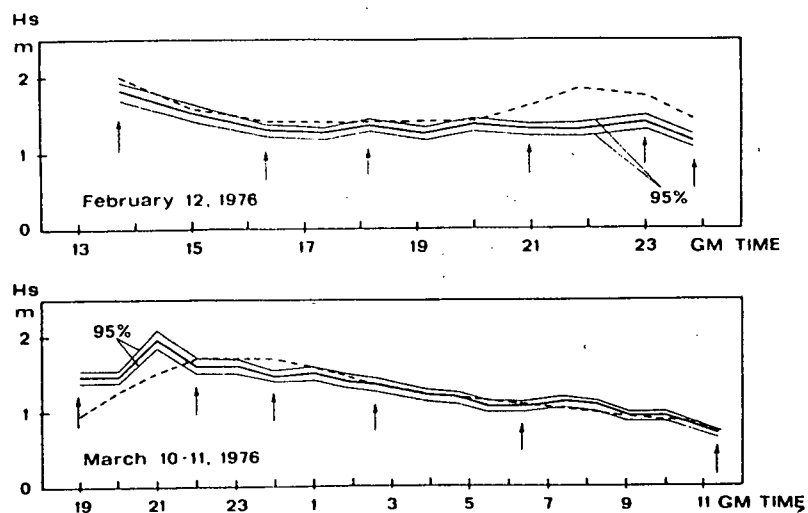
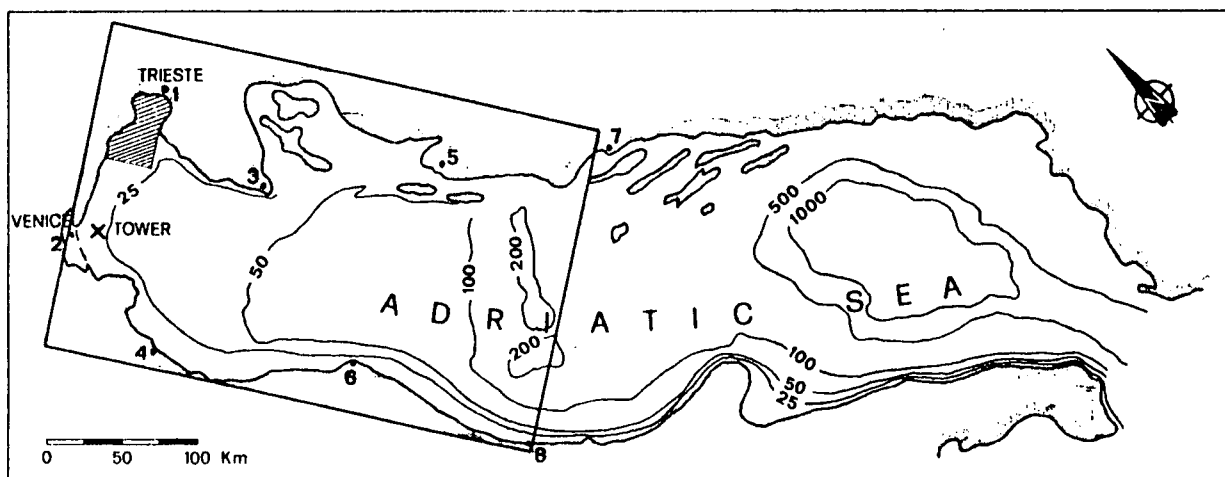


Fig. 4.62 Observed (continuous) and computed (dashed line) significant wave heights at the tower (above) for records of February 12, 1976, and March 10, 1976; 95% confidence limits are shown. Arrows indicate the records whose spectra are shown in Fig. 4.63.

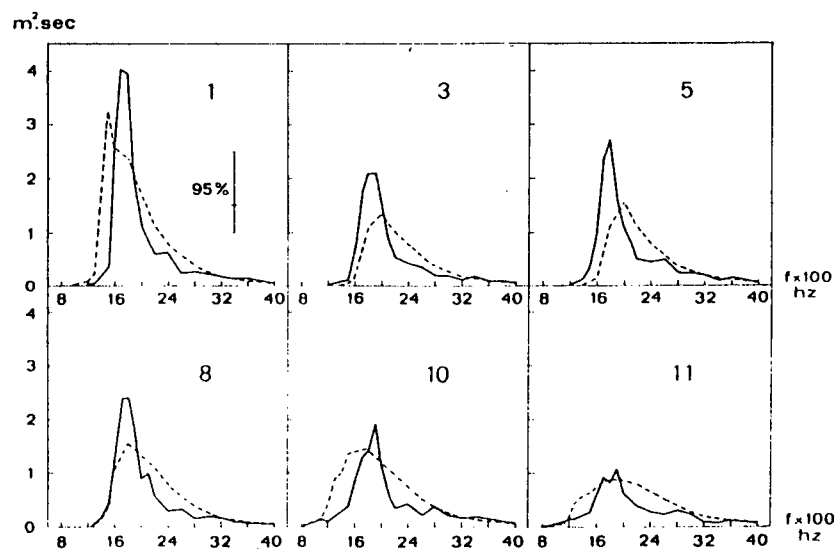


Fig. 4.63 Spectra of six records (see Fig. 4.62) during February 12, 1976 storm; 95% confidence limits are shown beside the spectrum of record number 1. Dashed lines show the hindcast spectra from the model.

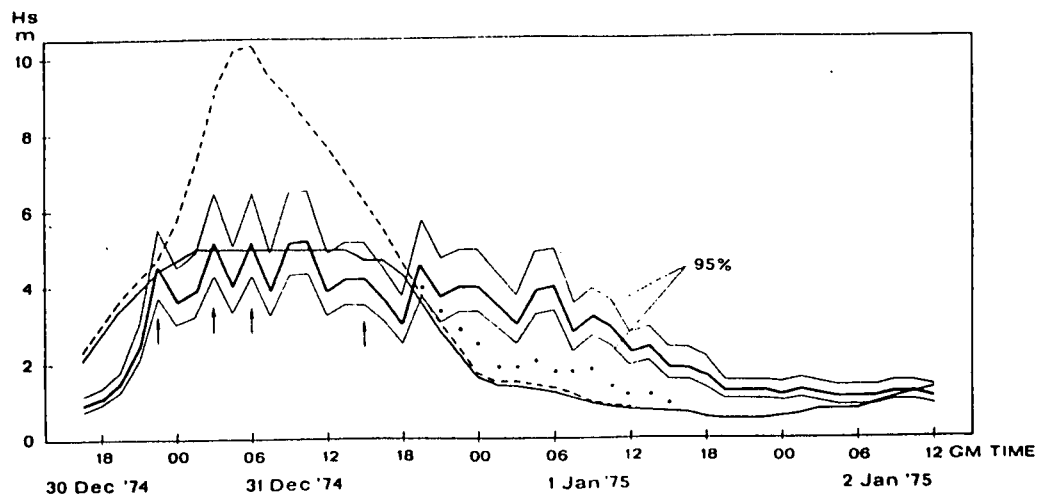
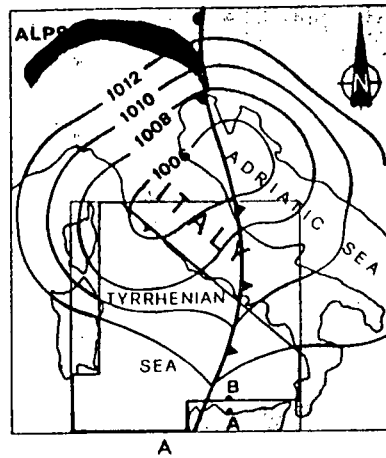


Fig. 4.64 Observed (heavy line) and computed (thin line) significant wave height in the Tyrrhenian Sea (Point A). The dashed line refers to computations in deep water (Point B).

Wave growth: the exponential wave growth term B.F has been incorporated, with the form for B proposed by Barnett (1968)

$$B = \begin{cases} K \cdot f \left(\frac{\rho_a}{\rho_w} \right) \left[\frac{U \cos \beta}{c} - 0.90 \right], & \frac{U \cos \beta}{c} > 0.90 \\ 0, & \frac{U \cos \beta}{c} \leq 0.90 \end{cases} \quad (4.58)$$

where K is an empirical coefficient

U is wind speed at 10 m

β is the angle between the wind and wave directions

c is wave phase speed ($gk^{-1} \tanh(kh)$), and

ρ_a, ρ_w are air and water densities respectively.

Barnett found $K = 5$ gave the best fit to data; however, more recent work by Dobson and Elliott (1978) and Snyder et al. (1978) suggest this value to be slightly high.

The linear wave growth term based on the Phillips resonant mechanism has not been included since its contribution is small once the wave field is formed.

Dissipation: bottom friction is one mechanism included in the model to explicitly remove energy from the wave field. The formulation is identical to the VENICE model:

$$S_b = \frac{-C_f g k c_g}{2\pi\omega^2 \cosh^2(kh)} \cdot F(f, \theta) \langle u \rangle \quad (4.59)$$

where C_f = nondimensional drag coefficient

$$c_g = \frac{1}{2} \left[1 + \frac{2kh}{\sinh(2kh)} \right] c$$

$$\langle u \rangle = \left[\sum E(f) \frac{g^2 k^2}{\omega^2 \cosh^2(kh)} \Delta f \right]^{1/2}$$

and
$$E(f) = \frac{F(f_i, \theta_i)}{F_o(f_i, \theta_j)} \cdot E_o(f)$$

with the subscript o denoting deep water.

Propagation and Refraction: with $S = 0$, (4.57) can be written as a homogeneous transport equation in wave energy with characteristics given by the set of wave rays radiating outward from the location \mathbf{x} for all (f, θ) . If these characteristic curves are known then the energy conservation equation may be written as $dF/dt = S$ where the time integration is along each characteristic for (f, θ) . Following Longuet-Higgins (1957),

$$\frac{cc_g}{4\pi^2 f} F(f, \theta) = \text{constant} \quad (4.60)$$

is the quantity conserved along each characteristic in the absence of source-sink terms, and noting the equivalence of time-space integration given by $ds = c_g dt$ then the applicable energy conservation equation becomes

$$\frac{d}{ds} \left(\frac{cc_g F}{4\pi^2 f} \right) = \frac{1}{c_g} [S_{in} + S_b] \quad (4.61)$$

The numerical solution is computed in two steps. First the characteristic wave rays are calculated using linear refraction theory over the specified $h(\mathbf{x})$ for a discrete set of frequencies and directions. The rays are reverse-traced until they intersect an open sea boundary or land. Second, (4.61) is integrated along each ray for given f_i and θ_j at the point of interest in shallow water using a forward stepping procedure.

The boundary conditions are supplied at the end of each characteristic ray, either from measured, hindcast or parametric directional spectra in deep water, or $S(\mathbf{x}, f, \theta) = 0$ for land points.

Saturation limit: finally the depth-dependent saturation mechanism is used as an upper bound on wave energy to the right of f_m in the form proposed by Kitaigorodskii et al. (1975)

$$E_k(f) = \alpha g^2 (2\pi)^{-4} f^{-5} \phi(kh) \quad (4.62)$$

where α = Phillips' equilibrium range parameter,

$$\phi(kh) = \frac{\sinh^3(kh)}{[\cosh(kh)(kh + \sinh(kh)\cosh(kh))]} \quad (4.63)$$

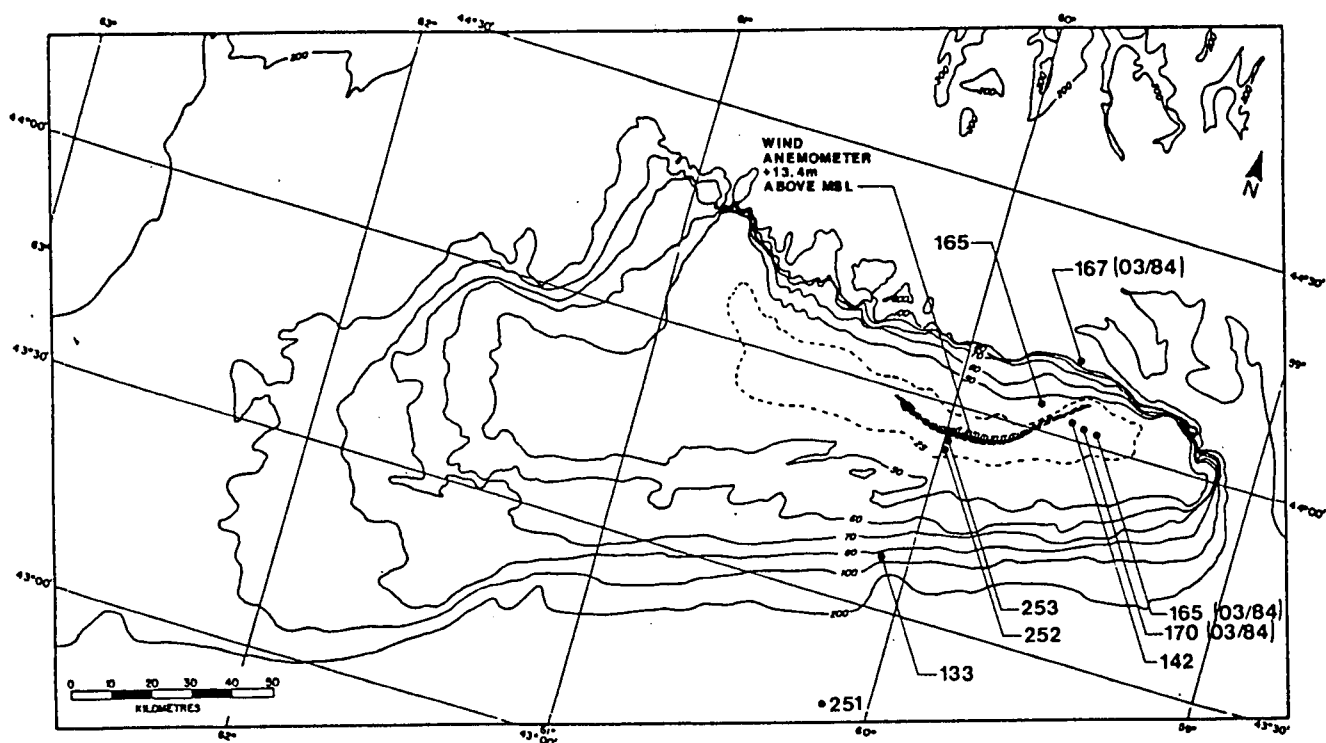
To the left of f_m , on the forward face, energies are unbounded and are controlled there by a balance between wind input and bottom friction.

Applications: SPECREF and Resio's WAVAD (see Subsection 4.3.6) were both used to hindcast the storms between December 23, 1984 and January 26, 1985 on Sable Island Bank (Hodgins et al., 1986). The measured data resources for this model intercomparison are shown in Fig. 4.65. WAVAD was used to generate boundary conditions $F(f, \theta)$ for the shallow water modelling such that both models were hindcasting on the same grid domain (Fig. 4.66) with the same bathymetry, wind input and deep water boundary spectra.

For four hindcast storms, the performance of the two models in terms of H_s in deep (>25 m) and shallow water is shown in Fig. 4.67. The statistics show that both models are characterized by rms errors of about 1 m in H_s and scatter indices of 15 to 20%. WAVAD shows a bias high of about $1 \Delta f$ in f_m with a standard deviation of $2 \Delta f$ -bins. SPECREF is more accurate in this respect being unbiased in f_m and a standard deviation of $1.6 \Delta f$ -bins. Both models exhibit mean directional errors of less than one $\Delta \theta$ -bin; in the case of SPECREF this amounts to about 8° compared with 18° for WAVAD.

In this application, the decoupled model was slightly more accurate than the coupled formation, at least in terms of wave parameters frequently used in engineering practice; both models, however, gave results that would be considered accurate enough for forecasting use.

The reason for the similarity in behaviour of the two models lies in the dominant role of the saturation spectrum in the overall energy balance. For the storm conditions modelled here the wave spectra appear to be governed by an equilibrium range for frequencies higher than f_m , resulting from a balance between energy input from the boundaries and locally by the wind, and the losses due to wave breaking.



LEGEND

STN. NO	INSTRUMENT	WATER DEPTH (m)
165	WR (ND)	34
165 (03/84)	WR (ND)	21
167 (03/84)	WR (ND)	160
170 (03/84)	WR (ND)	22
142	WR (ND)	16
133	WR (ND)	85
251	WRPS (ND)	200
252	WAVEC (D)	22
253	WAVEC (D)	12

WR - WAVERIDER[®]
 ND - NONDIRECTIONAL
 D - DIRECTIONAL
 WRPS - SATELLITE BUOY
 WAVEC[®] - HEAVE-PITCH-ROLL BUOY

NOTE: 03/84 DENOTES BUOY POSITION FOR THE
 HINDCAST STORM OF MARCH 29-31, 1984.
 ALL OTHER STATION NUMBERS PERTAIN
 TO THE 1984-85 FIELD PROGRAM.

Fig. 4.65 Disposition of wave and wind instrumentation providing data for the wave model intercomparisons. (From Hodgins et al., 1986).

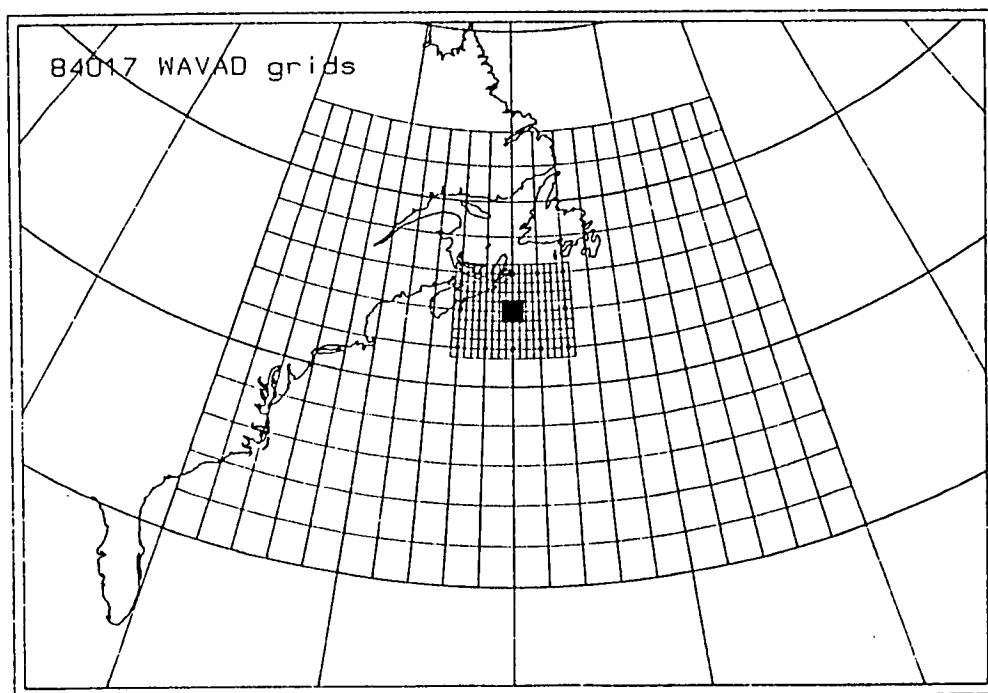
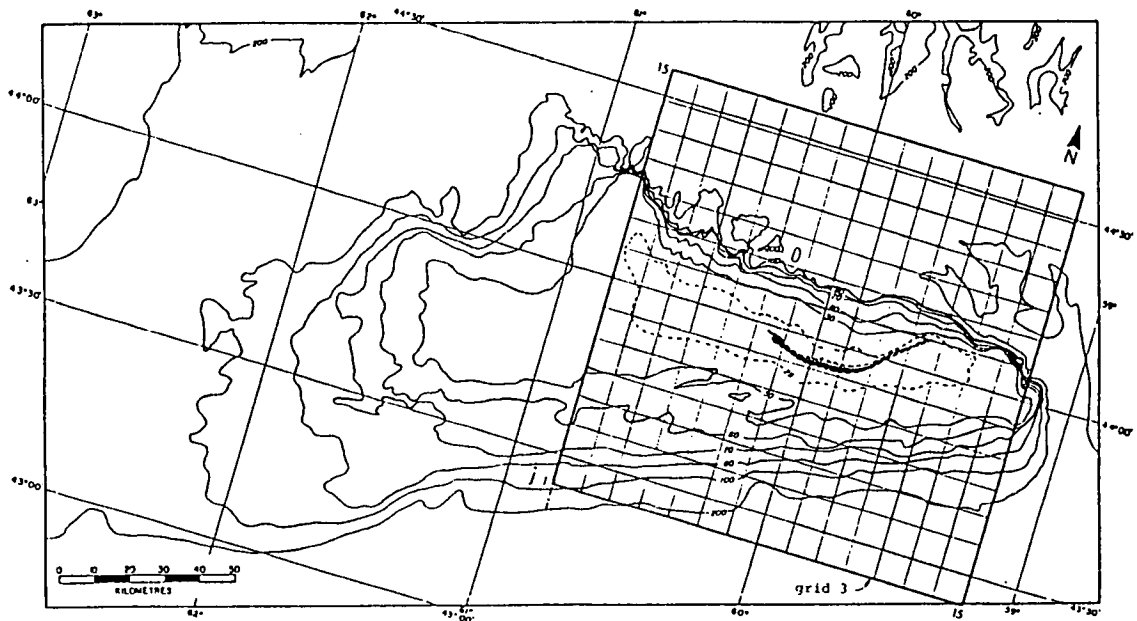


Fig. 4.66 SPECREF grid (upper panel) and the system of nested WAVAD grids (lower panel). The innermost WAVAD grid domain is the same as the SPECREF grid.

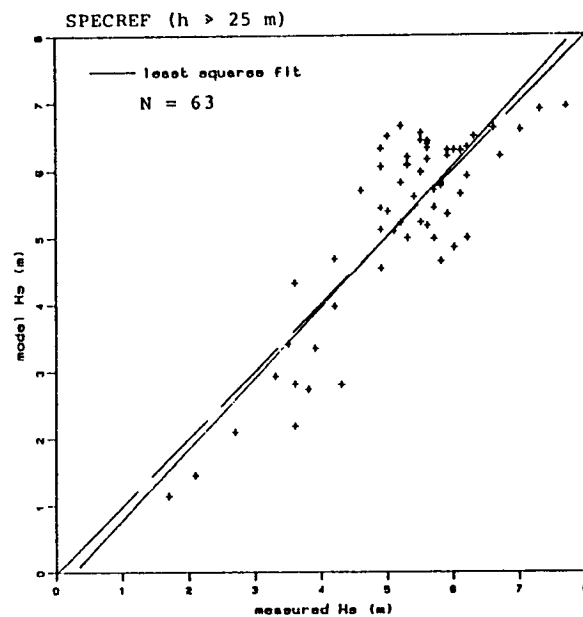
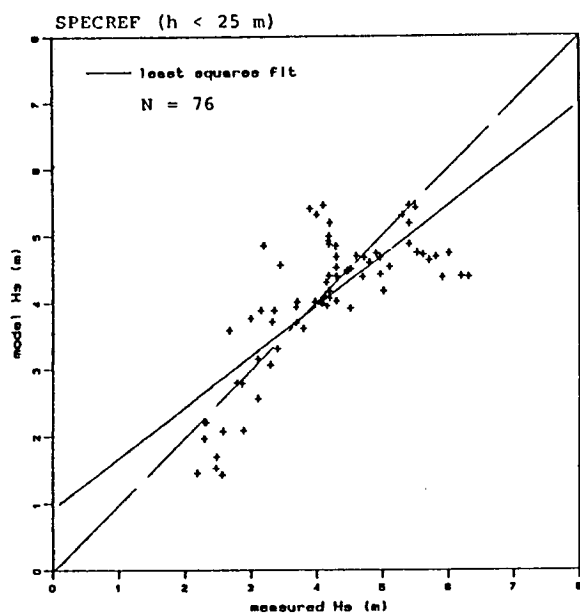
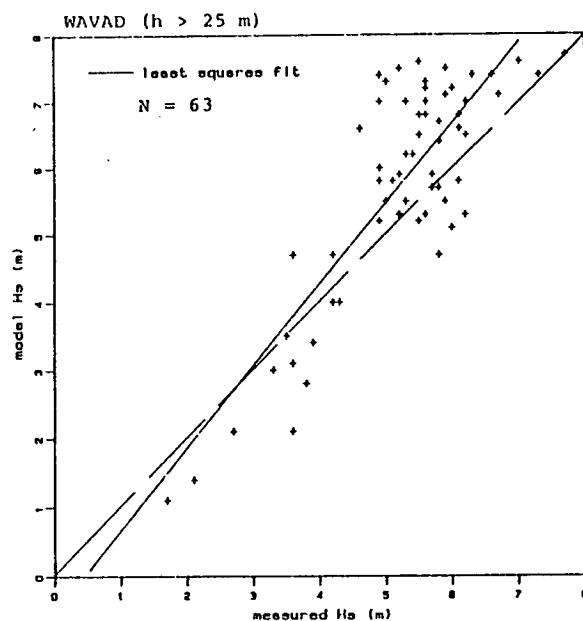
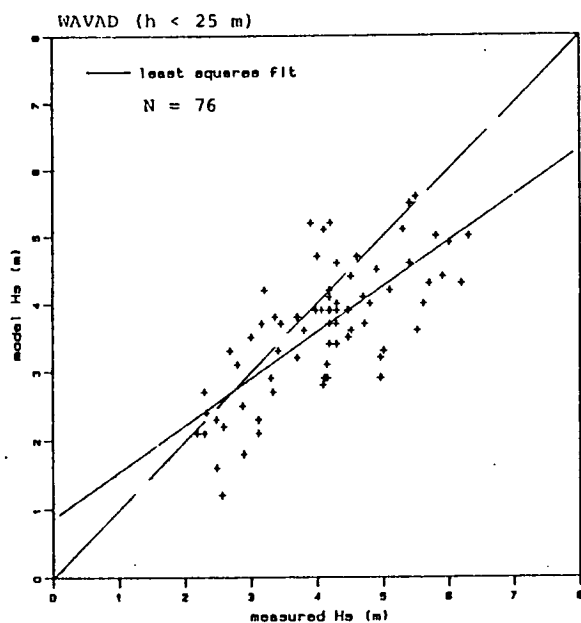


Fig. 4.67 Regressions of H_s -predicted onto H_s -measured for deep ($h > 25$ m) and shallow ($h < 25$ m) water on Sable Island Bank for the four hindcast storms for WAVAD (upper panels) and SPECREF (lower panels). (From Hodgins et al., 1986).

4.4 Wave Model Specifications

There are three basic wave model classes:

- (1) parametric wave height models based on SMB parametric equations;
- (2) parametric spectral wind-sea models based on an invariant spectral form, generally coupled with a swell propagation algorithm which the SWAMP Group (1985) call coupled hybrid (CH) models; and
- (3) discrete spectral wind-sea and swell models which have either
 - (a) a fully coupled discrete (CD) formulation of $S(f, \theta)$ in which energy may be exchanged between frequencies or
 - (b) a decoupled propagation (DP) formulation in which each energy packet travels along its own ray path at its group velocity subject only to energy input from the wind and dissipation due to shallow water effects.

In Canada, the Department of National Defence forecasting organization, located at METOC in Halifax, uses the SMB empirical approach married to a swell propagation scheme. Since the early 1970's, all the northern European and American forecasting agencies have been using either CH or CD models. Increasingly, the trend is towards the coupled discrete models due primarily to the difficulty of handling the transition between wind-sea and swell in the CH models.

The recent commercial hindcasts of Canadian waters have almost always been performed with discrete spectral models as illustrated in Table 4.6. Two exceptions are the 1980 SMB-based hindcast for the Beaufort Sea performed for Gulf Canada Resources Inc. and the ongoing testing of Donelan's parametric spectral model in the Beaufort Sea for AES, Downsview.

It seems, therefore, that discrete spectral modelling is a generally accepted method to most accurately hindcast significant wave height, peak period and mean wave direction. If this is so for hindcasting in which every effort is made to provide the best calibrated wind fields, it follows that it is also the preferred method for wave forecasting. Resio and Vincent (1979) have argued, correctly, that the most accurate wave model should be applied, especially if wind field errors may be large. Since wind input and wave model errors are generally additive, reducing either one will

Table 4.6

**Recent Canadian Hindcast Studies Using
Discrete Spectral Wave Models**

Location	Model	Type	Client
Scotian Shelf	WAVAD	CD	Mobil Oil Canada, Ltd.
	WAVAD	CD	ESRF
	SPECREF	DP	ESRF
	ODGP	CD	ESRF/DFO/DND
	ODGP	CD	ESRF
Grand Banks	ODGP	CD	Mobil Oil Canada, Ltd.
	ODGP	CD	ESRF/DFO/DND
Beaufort Sea	DHI S20	CD	Esso Resources Canada Limited
	WAVAD	CD	Esso Resources Canada Limited
	WAVAD	CD	DFO (MEDS)
	Donelan's	CH	AES
Kugmallit Bay	SPECREF	DP	DFO (IOS)
Pacific Coast	WAVAD	CD	DFO (IOS)/AES (Vancouver)
	SPECREF	DP	DFO (IOS)/AES (Vancouver)/TC
Strait of Georgia	Donelan's	CH	DFO (IOS)/AES (Vancouver)/TC

in most cases automatically reduce the total rms error in the wave field.

4.4.1 Model Domain

The coastal wave modelling regime must cover a considerable portion of the adjacent ocean in order to encompass the entire domain of active weather systems that impact on the coast. When swell is a significant source of energy, it must also model wave propagation from very distant storms. On the east coast of Canada, swell from storms in the eastern Atlantic is not generally considered important enough to model the entire North Atlantic Ocean. Because wave models are best implemented on latitude-longitude grids, a reasonable domain for the Scotian Shelf, Grand Banks and Labrador Sea would stretch from northern Florida (30°N) to the south end of Davis Strait (64°N) and from the eastern Florida coast (80°W) to midway between Greenland and Iceland (30°W).

In semi-enclosed or enclosed waters like the Gulf of St. Lawrence, the Great Lakes, Hudson Bay and the open water zone of the Beaufort Sea, the entire water body must be mapped with appropriate boundary conditions supplied where they connect to other water bodies.

On the west coast, swell is a much more important component since waves from extra-tropical cyclones tend to travel east and northeast across the Pacific to impinge on the B.C. coastline. Attempts at accurate west coast wave forecasting ought, therefore, to consider the entire North Pacific Ocean, at least north of about 30°N .

4.4.2 Shallow Water Regions

In Canadian waters, deep water wave modelling approximations are adequate for the northeast Pacific Ocean west of the shelf break, much of the northwest Atlantic Ocean and the Labrador Sea. On the Grand Banks with a water depth of roughly 80 m only the longest period waves will refract, but since the Bank is a fairly level plain the refraction will be weak. The most common long waves will be southwesterly swell arriving from the Scotian Shelf area. Since these waves cross the shelf break on the SW edge of the Grand Banks at about 90° , refractive effects will be minimized.

On the Scotian Shelf, the bathymetry is much more complex. In particular,

portions of Sable Island Bank are much shallower than the Grand Banks and here shallow water effects can be quite important. Refraction of 12-s WSW waves in the vicinity of Sable Island is illustrated in Fig. 4.68 to show wave energy (hence height) concentrating south of the eastern end of the island.

On the west coast, the Pacific Ocean swell can be greatly modified by bathymetry. Figure 4.69 shows the effect on 16-s waves from the south entering Queen Charlotte Sound and bending westward towards the east coast of the Queen Charlotte Islands.

4.4.3 Grid and Spectral Resolution

The choice of grid size must adequately resolve both the land boundaries and the forcing (wind) field. Usually the oceanic wave models use about a $2^\circ \times 2^\circ$ latitude-longitude grid which corresponds approximately to the resolution provided by wind models such as the CMC hemispheric spectral model. This definition provides a north-south spacing of about 220 km and an east-west increment of about 200 km at 30°N decreasing to about 140 km at 60°N . The extent to which Canada's coastlines are represented by the $2^\circ \times 2^\circ$ grid is shown in Fig. 4.70.

In the shallow water regimes like the Beaufort Sea, resolution of the bathymetry for bottom dissipation and of landforms for sheltering govern the requisite grid scale. Typically 10 to 20 km is used in the Beaufort Sea, 30 km is adequate for the nearshore west coast of B.C., but grids as fine as 1 to 5 km may be necessary if very accurate representations are required for places like Sable Island, Northumberland Strait, the St. Lawrence River estuary or the Strait of Georgia.

Spectral resolution is typically in terms of about 16 to 24 equal direction bands to provide 22.5° to 15° increments. Frequency discretization and the frequency cutoffs need to be considered quite carefully in order to represent high energy sea-states as well as possible.

The high frequency cutoff is usually between 0.5 Hz (2 s) and 0.2 Hz (5 s). The low frequency cutoff depends on physically realistic swell frequencies that must be resolved. For open ocean modelling, 0.033 Hz (30 s) would be

Waves from WSW

T = 12.4s

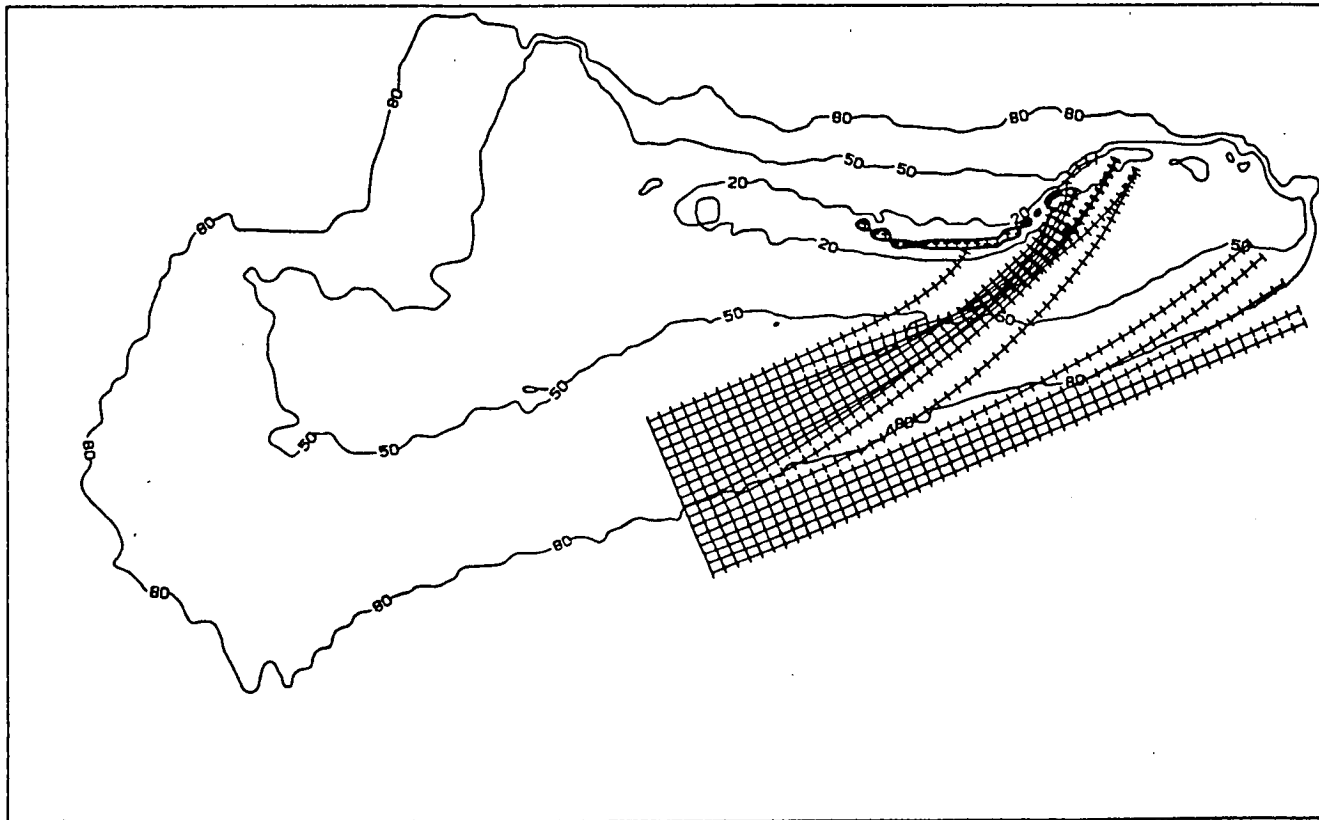


Fig. 4.68 Wave refraction of 12.4-s period waves approaching Sable Island from the WSW. (From Hodgins et al., 1986).

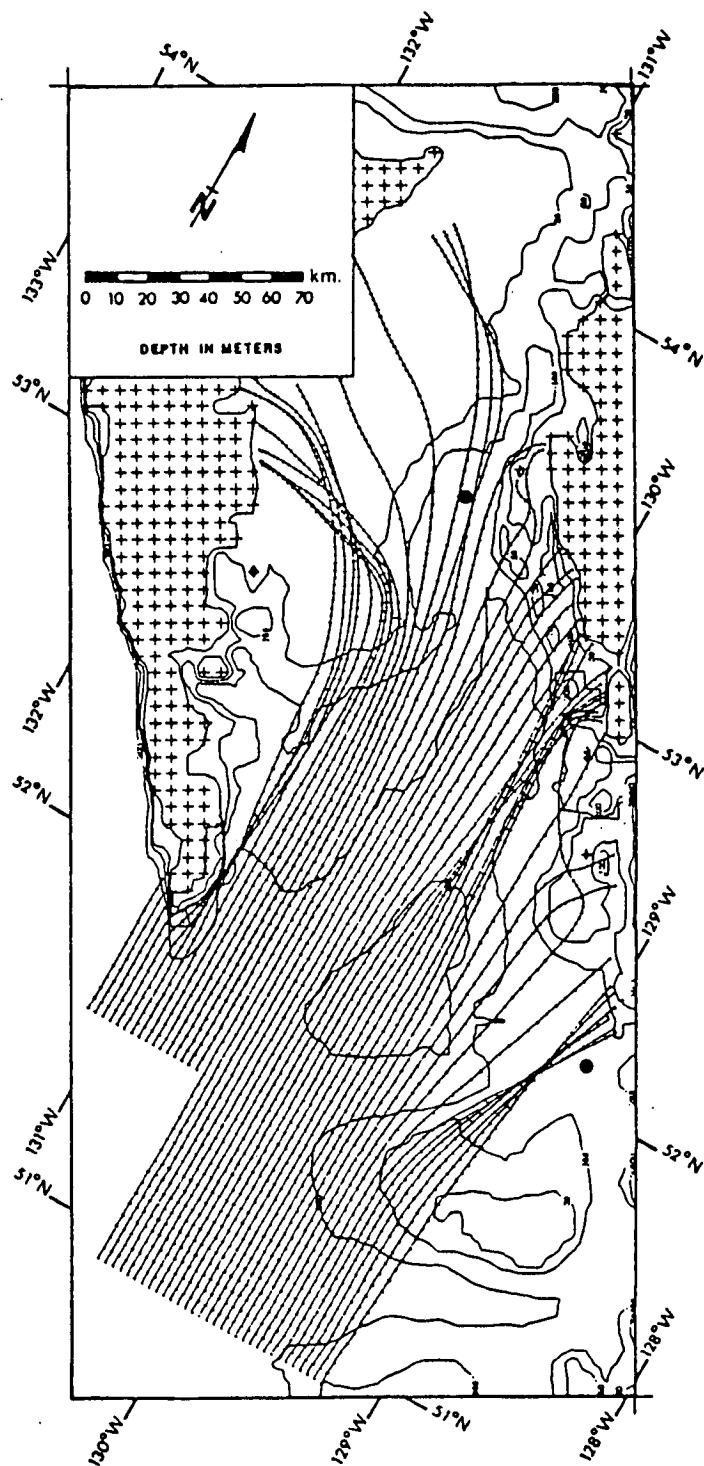


Fig. 4.69 Refraction of 16-s waves entering Queen Charlotte Sound and Hecate Strait from the south and impinging on the east coast of the Queen Charlotte Islands. (From Hodgins et al., 1985).

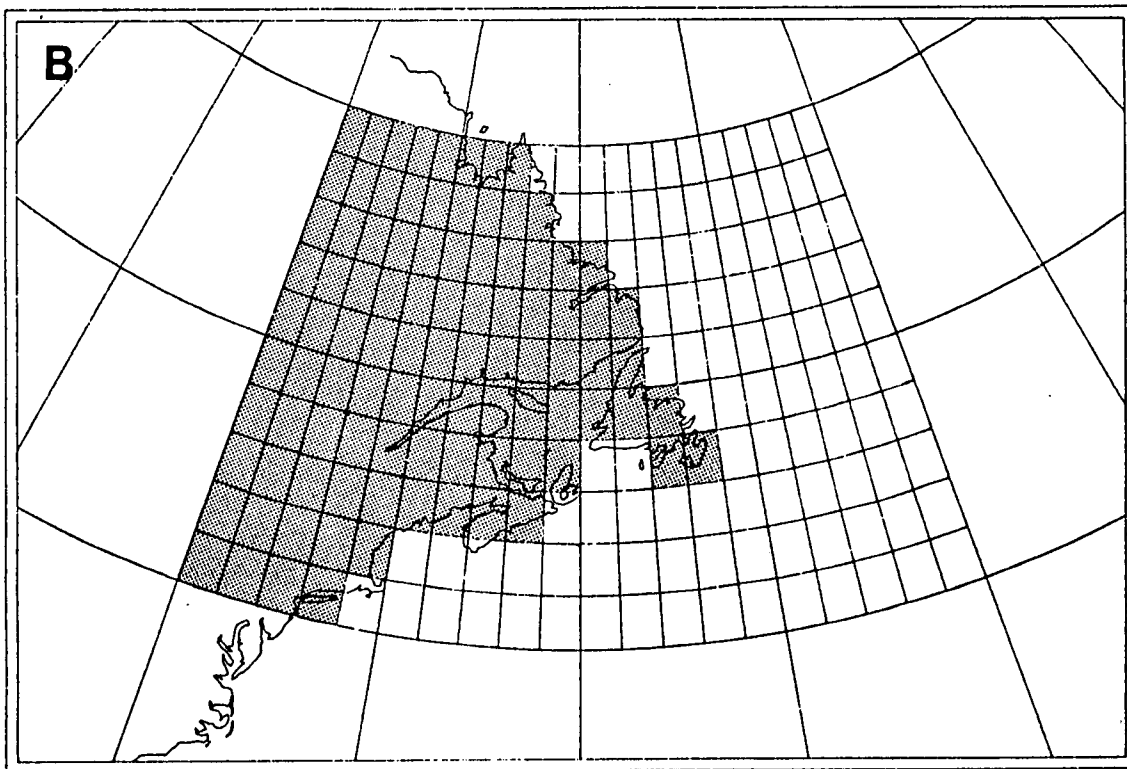
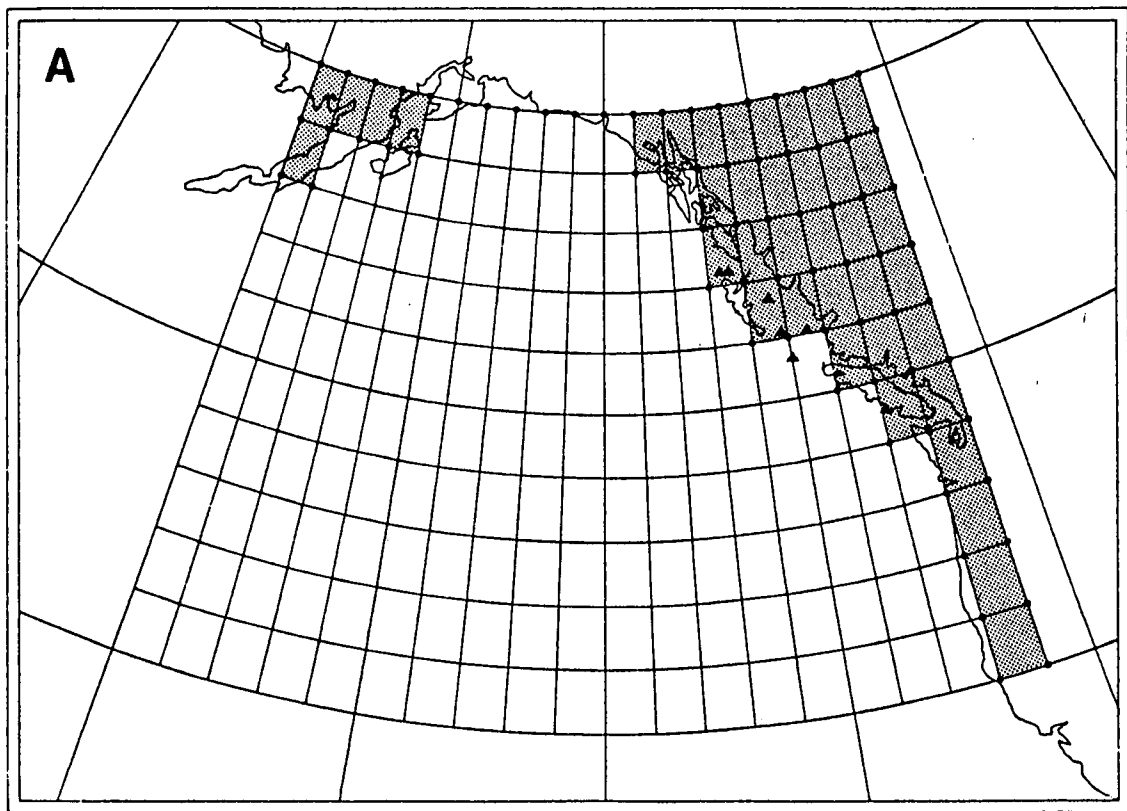


Fig. 4.70 Canada's west (A) and east (B) coasts resolved by a $2^\circ \times 2^\circ$ latitude-longitude deep water wave modelling grid.

appropriate whereas in semi-enclosed basins 0.5 Hz (20 s) should suffice.

Many models are run with equal frequency band definitions which corresponds to the spectral resolution obtained by Fourier analysis methods on wave measurements. The disadvantage is that the more energetic the sea-state is, the more poorly resolved is the peak of the energy spectrum in terms of wave period. An alternative is, therefore, to define the frequency bands in terms of equal period increments. This alternative provides that the forward face of the spectrum is better resolved than in the empirical equilibrium and saturated ranges, and subtle shifts in peak frequency cannot result in gross changes in peak period. A compromise can be based on the definition that $f_i:f_{i+1} = \text{constant}$. These three methods are defined in Table 4.7.

4.4.4 Time-Step of Integration

Once the grid size and the longest resolvable wave are specified, the maximum time step is imposed by the Courant condition for computational stability of the wave propagation scheme. For most models this means that the fastest wave may not traverse a length exceeding the smallest model grid element in one time step. If the domain is a $2^\circ \times 2^\circ$ grid extending to 64°N , then the smallest grid length is 97 km (2° longitude at 64°N). If the longest wave has a period of 33 s, its group velocity will be $gT/4\pi$ or 26 m/s based on linear wave theory and deep water approximations. Thus the maximum time step will be 3,730 s or, conveniently, one hour.

4.4.5 Possible Models

The user requirements for combined sea significant wave height, period and direction and for spectra are most reliably met by running coupled discrete (CD) spectral wave models in deep water and by either a CD model incorporating bottom effects or a decoupled propagation (DP) model in shallow water regimes. DP models are more cost-effective if a set of site-specific forecasts is required, but information for mapping (contours of H_s for example) is usually better obtained from a grid-based CD solution. However, bathymetric resolution can be finer in DP models than in CD ones without such a severe impact on computational effort since the time step is independent of the grid size.

Table 4.7

Three Frequency Resolution Definitions

	Equal Freq. $\Delta f=0.01$ Hz		Equal Period $\Delta T=1$ s		$f(i):f(i+1) = 0.9$	
Band	Central f	Central T	Central f	Central T	Central f	Central T
1	.055	18.2	.050	20.0	.050	20.0
2	.065	15.4	.053	19.0	.056	18.0
3	.075	13.3	.056	18.0	.062	16.2
4	.085	11.8	.059	17.0	.069	14.6
5	.095	10.5	.063	16.0	.076	13.1
6	.105	9.5	.067	15.0	.085	11.8
7	.115	8.7	.071	14.0	.094	10.6
8	.125	8.0	.077	13.0	.105	9.6
9	.135	7.4	.083	12.0	.116	8.6
10	.145	6.9	.091	11.0	.129	7.7
11	.155	6.5	.100	10.0	.143	7.0
12	.165	6.1	.111	9.0	.159	6.3
13	.175	5.7	.125	8.0	.177	5.6
14	.185	5.4	.143	7.0	.197	5.1
15	.195	5.1	.167	6.0		
16			.200	5.0		

To be a prime candidate for Canadian wave forecasting, a model should have the following credentials. It must be

- based on sound physics as understood at the present time: where empirical laws are required, publications should document and justify the parameters and coefficients;
- available to the forecast agency with adequate documentation and/or backup support;
- rigorously verified in several geographical locations and meteorological conditions with demonstrably adequate error characteristics not only in H_s and T_p but also in two-dimensional spectral shape;
- preferably successfully applied in Canadian waters, at least in hindcast mode, for a variety of severe meteorological and geographical tests;
- capable of shallow water wave modification due to shoaling, refraction and bottom dissipation (at least).

Table 4.8 summarizes all of the reviewed models in terms of these characteristics. The resulting short list of possibly suitable models that are available and have enough other desirable qualities to warrant consideration are listed in Table 4.9. Each has some limitation, or at least raises some reservation, about its immediate applicability.

Resio's WAVAD

In our opinion, the most promising model is Resio's WAVAD code because of these factors: the high level of physics explicitly and empirically embodied including detailed consideration of spectral shape, the incorporation of shallow water modifications, the number of Canadian hindcast verifications under fairly severe constraints (NE Pacific, Beaufort Sea, Sable Island), and the availability in Canada of users with first hand experience in adapting and running the model providing direct familiarity with the code and documentation. To our knowledge, WAVAD is the only CD model on the short list that has undergone detailed hindcast examination of its two-dimensional spectral shape in shallow water.

Table 4.8

Summary of Key Wave Model Characteristics

Model	Source/Contact*	Primary Application	Deep or Shallow	Canadian Application	Published Verifications	Available	Desirable
Parametric							
SMB formulations	Seaconsult	OH	D	Y	N	Y	N
	Baird	OH	D	Y	Y	?	N
	MEP	OF	D	Y	N	?	N
Parametric Spectral and Coupled Hybrid							
Hasselmann's	Max-Plank	R	D	N	N	Y	N
NORSWAM	Max-Plank	R	D	Y	Y	Y	N
HYPAS	Max-Plank	R	D	N	Y	?Y	N
HYPAS	Max-Plank	R,OF	D/S	N	Y	?Y	N
GONO	KNMI	OF	D/S	N	Y	?N	N
Donelan's	GLERL	R	D	Y	Y	Y	QY
Donelan's	Seaconsult	OH,OF	D	Y	Y	Y	QY
Ross Hurricane	?	R	D	N	QY	?N	N
Norwegian	NMI	OF	D	N	Y	?N	N
Coupled Discrete Spectral							
DSA-5	DM, Paris	OF	D	N	Y	?N	N
PTB	NYU	R,OF	D	N	Y	?N	N
SOWM	FNOC	OF	D	N.Hemisphere	Y	Y	N
GSOWM	FNOC	OF	D	Global	Y	?N	QY
ODGP	Oceanweather	OH,OF	D	Y	Y	QY	QY
SAIL	Oceanweather	R,OH	D	N	QY	?N	N
WINCH	NMI	OF	D	N	N	?N	N
WAVAD	OCTI,Seaconsult	OH	D/S	Y	Y	Y	Y
S-20	DHI	OH	D/S	QY	Y	Y	QY
Golding's	BMO	OF	D/S	N	Y	N	N
Japanese	MRI	OF	D	N	Y	?N	N
VENICE	ISDGM	OH,OF	S	N	Y	?N	N
SPECREF	Seaconsult	OH,OF	S	Y	Y	Y	QY

Key: OH - Operational Hindcast
 OF - Operational Forecast
 R - Research
 D - deep water
 D/S- deep and shallow water
 S - shallow water

Y - yes
 QY - qualified yes
 N - no
 ? - not known

?Y - probably yes
 ?N - probably no
 * - see Appendix 4.2

Table 4.9

Short List of Models for Canadian Wave Forecasting

Desirable Models	Minimum Computer	Incorporating Shallow Water Effects	Limitations/Reservations
WAVAD	high-end microcomputer (e.g. Intel 310, Cromenco System 3)	Yes	Slow execution if nested grids are required to resolve bathymetry, geography. Requires further code optimization to improve speed performance for forecast mode.
DHI S-20	probably mini-computer (e.g. VAX)	Yes	No first-hand experience with the present model version. No known forecast applications.
ODGP	mini-computer (e.g. VAX)	No	Deep water formulation only. Limited parameterization of wave physics and hence may require site-specific calibrations. Difficult to apply on west coast because of shallow water and complex geography, in the Beaufort Sea because of long shallow shelf, in Hudson Bay because of shallow water and lack of calibration data.
SPECREF	high-end microcomputer (e.g. Intel 310, HP1000, Microvax)	Yes	Specific point model that is suitable for regional grid-based applications. Requires $S(f, \theta)$ boundary condition.
Donelan's	high-end microcomputer (e.g. Intel 310, HP1000, Microvax)	No	Deep water formulation only. Verification is underway. Suitable for enclosed basins if swell is negligible, although shallow water wave propagation may need to be added.

DHI System-20

In principle, the DHI System-20 model in its newest version should be about equivalent with WAVAD, but it has not been used in Canadian waters and so has not undergone the Sable Island shallow water verification test that WAVAD (and SPECREF) has.

Cardone's ODGP

Cardone's ODGP model is of some interest, primarily because it is used in operational forecast mode on the east coast. However, its representation of wave physics is very empirical, it does not account for shallow water wave modification processes, there are no known verifications of its deep water two-dimensional spectral shape, it is not generally applicable in the shallow Beaufort Sea and it has not been applied on the west coast. Moreover, access to this model may be restricted by exclusive licensing arrangements now in place. A decoupled, one-dimensional shallow water transformation algorithm (Eid et al., 1987) was developed for the CASP forecast experiment that used a single ODGP deep water spectrum as input at the deep water end of a uniformly-sloped shelf (i.e., propagation perpendicular to idealized parallel depth contours). This simple expedient method of modifying near-coastal waves means that ODGP is not a shallow water forecast model in the sense that WAVAD, S-20 and others are.

Seaconsult's SPECREF

The appeal of SPECREF as a decoupled propagation model is that it is well-tested in Canadian waters (Beaufort Sea, Sable Island and elsewhere), it is a well-developed algorithm incorporating all the source-sink terms that such models can embody, it is a single-author code which is a distinct advantage for implementation and modification, and the software has undergone a series of upgrades to improve computational efficiency so that it runs comfortably on a microcomputer.

Donelan's Model

Donelan's parametric spectral model should be considered for enclosed basins where swell is negligible, but it would be essential to incorporate shallow water transformations to apply the model realistically in areas like Hudson Bay or the Beaufort Sea. The parametric formulation is computationally more

efficient than a coupled discrete model such as WAVAD, but swell must truly be negligible for the concept to be suitable.

Each of these models has well-established credentials and each could play a role in wave forecasting for Canadian waters assuming that where sea ice influences the open water generation area, the ice edge is adequately defined and treated like an equivalent land boundary.

None of the above models treat the physics of wave growth, energy redistribution among different frequency components, or wave energy dissipation within the marginal ice zone. Consequently, they are not suitable for predicting sea-state conditions inside unconsolidated ice fields, and they all would be in error if wave energy were transmitted through strips or patches of ice into open water. There are two areas that require investigation with respect to improving the models to give a more realistic treatment of marginal ice zone wave conditions:

- (1) a better understanding of the behaviour of waves that are generated in, or propagated through, unconsolidated ice of varying concentrations by observational studies coupled with theoretical studies; and
- (2) methods to give a rational parameterization of marginal ice features and concentrations that simultaneously satisfy the wave modelling requirements in terms of minimum resolvable grid scales, and are achievable by AES Ice Branch given their resources in remote sensing, modelling, data assimilation and forecasting.

5.0 WIND FIELD SPECIFICATION FOR WAVE FORECASTING

5.1 Wind Requirements for Wave Modelling

The models described in the previous section that fall into the parametric spectral or discrete spectral classes require a description of the two-dimensional wind field $U(x,y,t)$ representing overwater wind at an elevation close to the sea surface. This wind enters the term S_{in} given in (2.19) specifying the flux of energy into the wave field, and may also enter into terms representing energy loss as waves propagate into opposing winds. Parametric wave models in the SMB class likewise require overwater wind speed and direction although a lack of precision as to reference height is noted in the literature. In this model class the relationship between wind input and the resulting wave height and period is purely empirical.

The source term S_{in} is specified in a variety of ways in the different spectral models, and there is no universal rule for wind specifications suitable for all models. In most cases the physics of wave growth is related to two mechanisms: (i) a random wind excitation term referred to as the Phillips resonance mechanism and (ii) the Miles instability mechanism. These terms generally appear in S_{in} in the form $A+B.E$ where A and B are semi-empirical coefficients derived from measurements of wave growth.

A and $B.E$ represent the resonant and instability mechanisms respectively. The influence of A is generally very small for oceanic wave forecasting since this term mainly serves to initiate wave growth from a calm sea, and is ignored in many models. Cardone (1980) summarizes two components entering into the A coefficient: the convection velocity at which the atmospheric turbulent pressure fluctuations are transported downwind, and the intensity of the turbulent fluctuations. In the absence of prognostic data on turbulence in the boundary layer, the A term has been scaled in terms of the mean wind speed at some, generally imprecisely, specified height above the waves raised to powers ranging from 4 to 6 (e.g. Priestley, 1965; Barnett, 1968). The scaling is completed by a constant of proportionality chosen to give the correct growth rate.

The wind dependence for the instability term usually follows the theoretically predicted form. Based on logarithmic wind profiles and Miles'

(1957) quasi-linear theory, the growth rate nondimensionalized by frequency should be a universal function of the ratio between friction velocity u_* and the wave phase speed c , and of another nondimensional number involving the Monin-Obukhov stability length scale L . In practice most models scale this growth in accordance with only u_*/c (Cardone, 1980). The friction velocity is defined as

$$u_*^2 = \frac{\tau}{\rho_a} \quad (5.1)$$

where τ is the surface stress and ρ_a is the density of air.

The friction velocity u_* is most often estimated using the bulk aerodynamic drag coefficient CD and the mean wind U_z at some reference height z above sea level (usually 10 m). CD is itself a function of the mean wind speed, and of atmospheric stability (see e.g. Garratt, 1977; Smith, 1980; Large and Pond, 1981; and Donelan, 1982). Byrne (1982), Geernaert et al. (1986), and Hsu (1986), among others have also examined the dependence of CD on sea-state, including the effects of atmospheric stability.

Consequently the wind requirements for wave modelling include some measure of stability in addition to the mean wind U_z . For example, the variation of drag coefficient for neutral stability, CDN , may be specified for oceanic conditions (Large and Pond, 1981); an estimate of u_* for arbitrary stabilities thus requires a value of the drag coefficient CD for in situ stability. By way of an example, Large and Pond give

$$CD = CDN [1 + (CDN)^{1/2} \kappa^{-1} \ln(z/10) - \psi_m(z/L)] \quad (5.2)$$

where κ is von Karman's constant (0.4) and ψ_m is a function depending on the sign of z/L (Paulson, 1970). z/L may be related to a bulk Richardson Number

$$Ri(\Delta T) = \frac{-gz\Delta T}{U_z^2 T_o^2} \left(1 + T_o^2 \frac{\Delta Q}{\Delta T} 1.72 \times 10^{-6} \right), \quad (5.3)$$

the drag coefficient CD , and the Stanton Number CT (air-sea heat flux) (Large and Pond, 1981) through

$$\frac{z}{L}(\Delta T) = \kappa C T C D^{-3/2} R i(\Delta T) \quad (5.4)$$

In these expressions T represents temperature with T_0 being a local average, and Q denotes absolute humidity. Taking

$$\Delta T = T_s - T \quad \text{and}$$

$$\Delta Q = Q_s - Q$$

(where T_s , Q_s represent sea surface temperature and humidity respectively) provides an estimate of z/L . The approximation involved in using air temperatures in place of potential temperature in (5.3) gives rise to errors of less than 5% in CD according to Large and Pond (1981).

Thus, in practical terms boundary layer stability may be taken into account with data on the mean wind, air temperature, and air humidity at some reference height, sea surface temperature, and the humidity of the air just above the water surface. Most wave models contain an algorithm to evaluate u_* , or alternatively the neutral 10-m wind, given these data.

5.2 CMC's Spectral Hemispheric Forecast Model

Since 1962 the Canadian Meteorological Centre (CMC) in Montreal has employed a succession of numerical weather prediction (NWP) models to aid in the forecast of regional weather. The operational large-scale forecast model is a spectral primitive equation model defined over the northern hemisphere. This model first became operational in February 1976 but has been upgraded several times. The most recent significant change was the implementation of a high-resolution version in June 1984 when the Cray computer became available at CMC.

In addition to the operational spectral model, a finite element small-area regional model has been developed at Recherche en Prevision Numerique (RPN) in Montreal. This model supplements the long-range forecasts of the spectral model with shorter, higher spatial resolution forecasts. The finite element model is now being run twice daily and was used to provide weather forecasts during the Canadian Atlantic Storm Project (CASP) in the winter of 1985-86.

The purpose of NWP models is to provide temporal and spatial arrays of prognostic variables such as pressure, wind velocity, temperature and humidity at several levels in the atmosphere for use in the preparation of weather forecasts. For wave forecasting, the vertical profile of the near-surface wind could be constructed from forecast fields of wind, temperature, air density, and surface roughness length, but in practice only the wind vector at the lowest available elevation is used. Although both of the NWP models used by CMC can provide data for use by a wave forecast model, only the hemispheric spectral model has been considered in this study.

5.2.1 The Governing Equations

The primitive governing equations of the spectral hemispheric model embody conservation of mass, Newton's second law of motion, the first law of thermodynamics, and the gas law relating density, temperature and pressure. These principles are expressed in five equations defining the time dependence of the prognostic variables: vertical component of vorticity, horizontal divergence, absolute temperature, surface pressure, and dew point depression. All other atmospheric variables, including wind, are derived from these five parameters. The equations themselves and the numerical solution techniques are described in detail by Daley et al. (1976) and by Creswick (1983).

The coordinate system used in the spectral model consists of latitude and longitude in the horizontal, and σ -units in the vertical where $\sigma(z)$ is the ratio of pressure at an elevation z to the surface pressure. Thus, a constant value of σ will correspond to an elevation that varies spatially and temporally as the pressure field evolves (see Fig. 5.1 for example). σ can be related to elevation by using the hydrostatic approximation to give

$$z = \frac{(1-\sigma)p_s}{g\rho_a} \quad (5.5)$$

where p_s = surface pressure ($[1.01 \pm 0.05] \times 10^5$ Pa)

g = gravitational acceleration

ρ_a = density of air (assumed independent of z within 100 m of the surface; 1.3 ± 0.1 kg/m³).

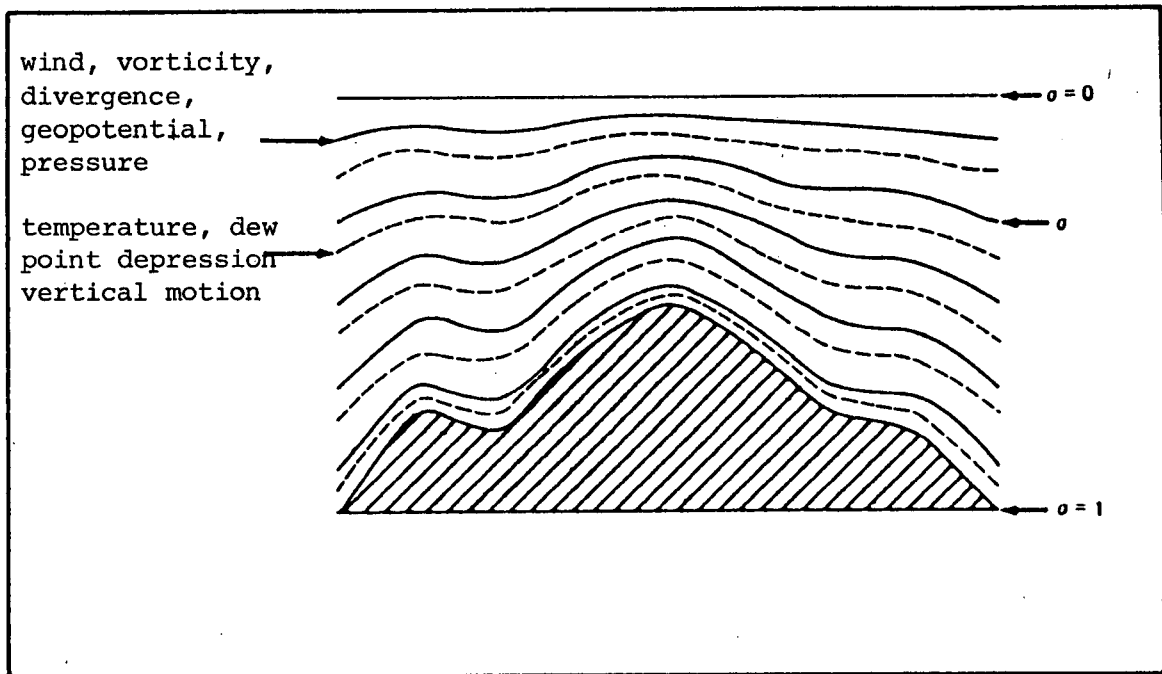


Fig. 5.1 Schematic representation of the vertical structure of the model ($N = 5$, equally spaced in σ) showing the distribution of model variables.

At $\sigma = 0.998$, for example, $z = (16 \pm 10)$ m which is a reasonable choice for input to wave models that typically require wind at 10 or 19.5 m.

5.2.2 The Spectral Solution Method

The numerical solution of the governing equations employs a spectral transform technique described by Creswick (1983) as follows:

"Since the atmosphere is a continuous fluid, it is best represented in a mathematical model by continuous analytic functions. The most convenient for the spherical earth are spherical harmonics series. Spherical harmonics are two-dimensional functions having the form of trigonometric functions in the east-west direction and of associated Legendre [functions] of the first kind in the north-south [direction]. This is termed spectral representation since it represents a set of discrete wave-lengths. The number of terms included in the series is limited by the available computer and must be truncated at some wave number. The truncation may be either rhomboidal, that is, with the same maximum wave number in both directions, or triangular, in which case the sum of the zonal and meridional wave numbers is held to a maximum, which results in uniform resolution over the globe...

"When the spectral series are substituted for the variables in the primitive equations, we obtain a separate algebraic equation for the time tendency of the amplitude of each spectral component of each variable...

"... It [is] now feasible to compute the terms of the primitive equations at grid points with horizontal derivatives calculated analytically from the spectral series. The tendencies of the model variables at the grid points are then transformed into a spectral series to obtain the tendencies of the spectral coefficients of the variables. In order to avoid aliasing, i.e. the interpretation of inadequately sampled short waves as being of a much longer wave length, we must use considerably more (by a factor of about two) grid points than we have terms in the spectral series. The results of the calculation are the same as from a fully spectral calculation but with far less effort, and computing time is just as fast as for a finite-difference model of comparable resolution."

The equations are solved to fourth-order accuracy on a spatial array of equally spaced longitudes and "almost-equally-spaced" latitudes, according to a formula discovered by Gauss, so that only half as many points are required for a given level of accuracy in calculating the spectral coefficients. The present model uses a computational grid of dimension 180 by 45 in the east-west and north-south directions respectively and triangular truncation with 59 wavenumbers.

A semi-implicit leap-frog scheme with a time step of 20 min is used to numerically integrate the governing equations. After each 3-h period of model simulation time all of the grid-point fields are saved for forecast dissemination, later analysis, or to restart the model for continued computation.

5.2.3 Boundary Conditions and Initialization

Because the model is defined on a hemispheric domain, an open boundary condition is required at the equator. Symmetry in all variables is assumed here thus eliminating fluxes across the equator. This condition leads to the generation of spurious waves at low latitudes that eventually corrupt the entire model solution, and thereby limit the effective duration of a prognosis to less than 5 days.

The model is initialized from objective analyses which are on the same horizontal grid as the spectral model. However, the variables must be vertically interpolated from isobaric to σ -surfaces. Vorticity and divergence are calculated from horizontal wind components which in spectral form are related by algebraic rather than differential equations.

At the boundary between the model atmosphere and the earth or ocean, fluxes of momentum, heat, and moisture are required. These appear in the vertical flux gradient terms of the governing equations. Surface fluxes are calculated using "nowcast" values for surface roughness length, sea surface temperatures, ice cover, snow cover, surface albedo, deep soil temperature, soil moisture, and soil heat conductivity--all of which are kept constant throughout the forecast.

5.2.4 Model Output

User-accessible output products are derived from the raw model output in one or two steps. If the user cannot use parameters at one of the model's σ -levels, the data are interpolated to specific isobaric surfaces using methods outlined by Creswick (1983). Horizontal wind components on the Gaussian grid are calculated spectrally from the forecast vorticity and divergence and may be requested at a σ -level. The forecast products are then extracted on the user's grid by cubic interpolation. The grid may be Cartesian on a polar stereographic projection, latitude-longitude or an arbitrary sequence of specific locations.

5.3 Implications for Wave Modelling

There are a number of consequences of the spectral wind model formulation for wave modelling applications which are highlighted in this section.

5.3.1 Horizontal Resolution

Horizontal resolution in CMC's spectral model has been investigated by Verret (1984) who presents arguments to show that the minimum resolved meteorological wavelength is about 690 km at 60°N, increasing to 976 km at 45°N and 1175 km at 30°N which is approximately 12° of longitude at all latitudes. This implies that a latitude-longitude grid of 1° to 2° would suffice to resolve the prognostic wind field with a minimum resolution of 6 to 12 points per meteorological wavelength. As resolution of the CMC wind field product improves, wave model grids must then be refined to incorporate the increased meteorological information.

Since all fine detail is removed by spectral truncation, local topographic effects (like Sable Island) are missing and the smallest synoptic-scale meteorological systems (meso-scale features) are virtually eliminated. As a result, there is a tendency for forecast systems associated with narrow jet streams to move much too slowly whereas patterns that are quasi-stationary are predicted to move. The report that "verification statistics confirm that the average position error is zero" (Creswick, 1983) provides no solice for wave forecasters.

5.3.2 Vertical Resolution

Near-surface vertical resolution in the model has improved greatly over the years from a minimum of $\sigma = 0.99$ ($z \approx 80$ m) in 1983 to $\sigma = 0.998$ ($z \approx 15$ m) in 1985 to, reportedly, $\sigma = 1$ ($z \approx 5$ m) in 1986. Generally speaking, if a wind at an effective elevation between 10 and 20 m can be extracted directly from the spectral model, application of a boundary-layer wind profile model to the CMC forecasts should not be warranted for wave modelling needs. This hypothesis is examined in the next chapter wherein the $\sigma=0.998$ output wind is compared directly with a 10-m reference elevation wind. The precise details of how the $\sigma=0.998$ wind is calculated within the CMC forecast process is not important, so long as it is consistent, since the objective is to use this level for wave model input without modification.

A problem may arise near sharp, steep coastlines, however, since the expected truncation procedure at the $\sigma = 1$ (surface) level highly smooths the topographic land-sea interface.

6.0 EVALUATION OF CMC FORECAST WINDS

CMC forecast wind data were obtained twice daily from September 9, 1985 to February 28, 1986 on two 1° by 1° rectangular grids, one centred at Sable Island (44°N 60°W) and the other near Hibernia (47°N 48.5°W) as shown in Fig. 6.1. Three-hourly forecasts were obtained for 00 to 30 hours commencing at both 00Z and 12Z. The forecast variables obtained were wind vector components, air temperature, dew point depression and atmospheric pressure at $\sigma = 0.998$, about 10 m above the sea surface. Sea surface temperature, which is constant through the forecast period, was also included.

The intention of this CMC forecast data evaluation was to establish error statistics based on the best available wind measurements, and then to place these error characteristics in the context of wave forecasting.

6.1 Measured Wind Data Resources

For the Canadian east coast offshore regions there are only two sources of reliable wind measurements: the AES approved meteorological instrumentation and recording procedure (MANMAR) on the oil drilling rigs and the permanent Environment Canada weather station on Sable Island. Both these data resources have some undesirable characteristics which require correction, calibration, or at least recognition.

6.1.1 Offshore Oil Rig Data

The rig anemometers are mounted 50 to 100 m above sea level on the drilling derrick or on one of the jack-up legs. In these positions, the measurements are subject to some air turbulence created by flow past the structures. In addition, particularly on floating rigs, the elevation of the wind measurement may vary with ballasting changes. Nevertheless, these data are more representative of overwater winds than samples taken from land-based towers.

During this study data were available from six offshore operators (Mobil Oil Canada, Ltd.; Petro-Canada Inc.; Canterra Energy Ltd.; Husky/Bow Valley; Shell Canada; and Gulf Oil Canada) operating at 16 different wellsite locations. Of these sites, the only significant amounts of data that were recorded close to one of the CMC grid locations are from Mobil's West

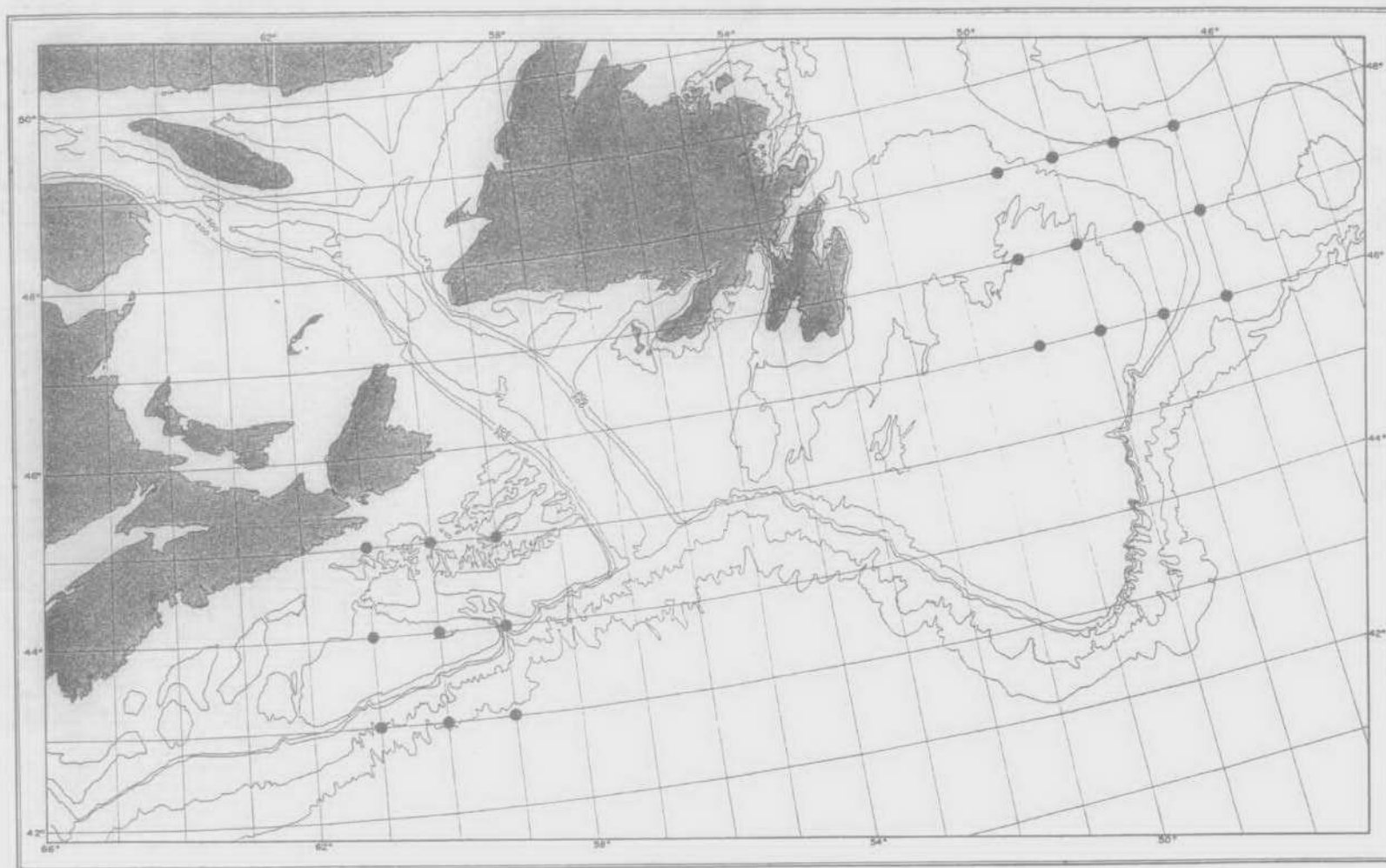


Fig. 6.1 Locations of CMC wind forecast data.

Olympia O-51 site just north of Sable Island and from Husky/Bow Valley's Whiterose L-61 location on the northeast edge of the Grand Banks. The West Olympia data were selected for the intercomparison because they had been collected early in the CMC data acquisition phase of this project and thus they were available for analysis as the forecast fields were being accumulated. Furthermore, this site at 44°01'N 59°53'W is essentially coincident with both the CMC grid point at 44°N 60°W and the Sable Island weather station at 43°56'N 60°02'W. This coincidence allowed an almost ideal intercomparison of CMC forecasts, overwater winds and near-surface land-based measurements.

If spatial variability could be accounted for, or neglected, the rig wind time-series from Whiterose J-49 and Whiterose L-61 (when it becomes available) should provide a good Grand Banks verification data set. The West Olympia data were recorded at three-hourly intervals aboard the Rowan Gorilla jack-up rig which is illustrated in Fig. 6.2. The anemometer height was deduced to be 113 m based on information provided by the Port Meteorological Officer in Halifax. The data, as measured, are presented in Fig. 6.3. All measured wind speeds are less than 50 knots and there are no particularly well-defined, severe storm events. The wind direction tends to be westerly most of the time.

6.1.2 Sable Island Climatological Station Data

Environment Canada through AES, Bedford, maintains a climatological station on Sable Island from which hand-recorded hourly records of wind speed, direction, air temperature and surface pressure were obtained for the period September 1985 to the end of February 1986. Wind data are sampled by a U2A anemometer mounted on a standard 10.1-m tower about 13 m above mean sea level (MSL) at the position indicated in Fig. 6.4. Since the surrounding sand dunes exceed 10 m above MSL within about 300 m on the north side of the tower, the measured winds are believed to contain some distortion due to boundary layer flow over these landforms. In addition, the predominance of westerly winds imposes flow along, rather than across, the island most of the time.

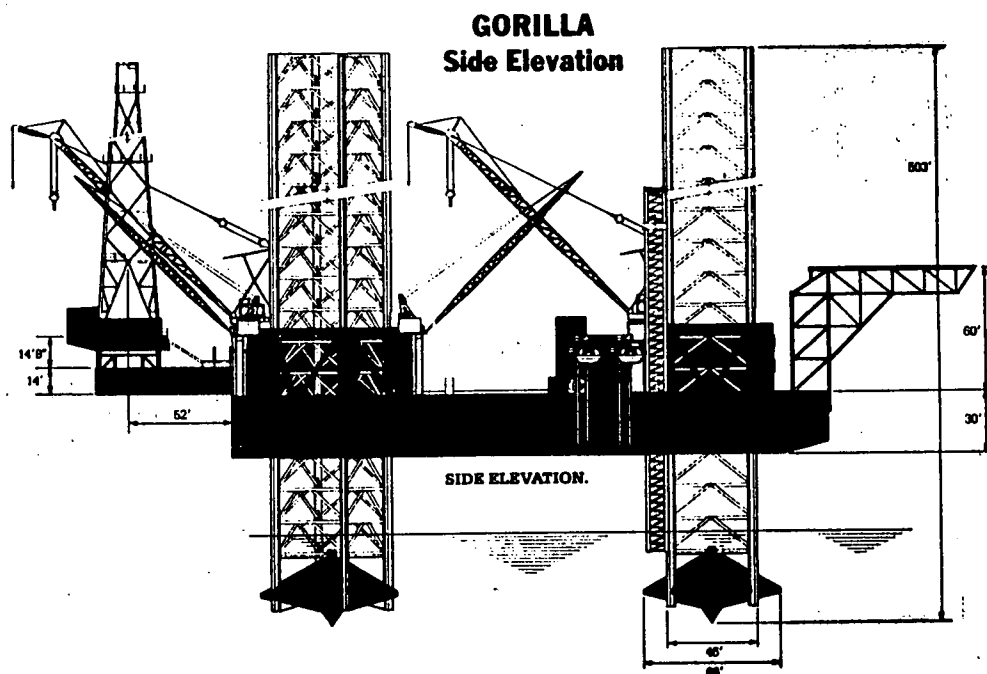


Fig. 6.2 Schematic diagram of the Rowan Gorilla jack-up drilling rig.

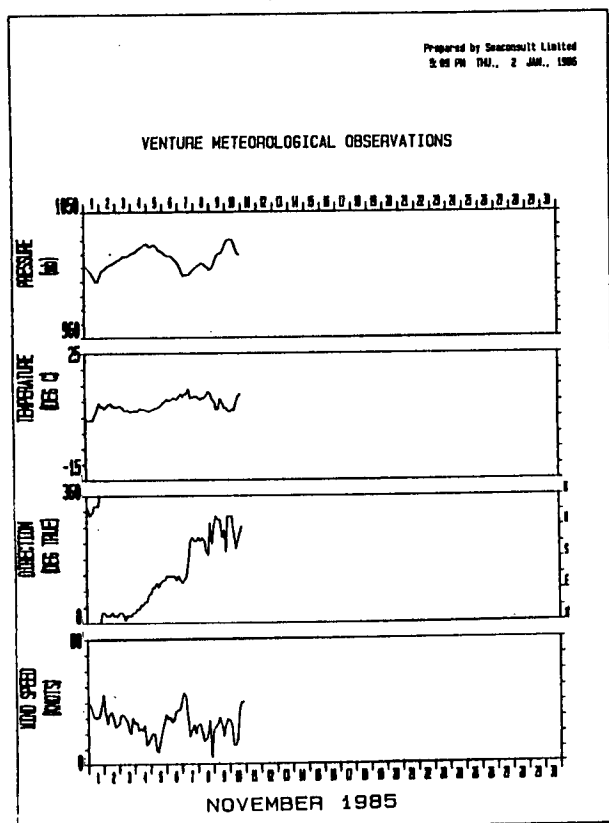
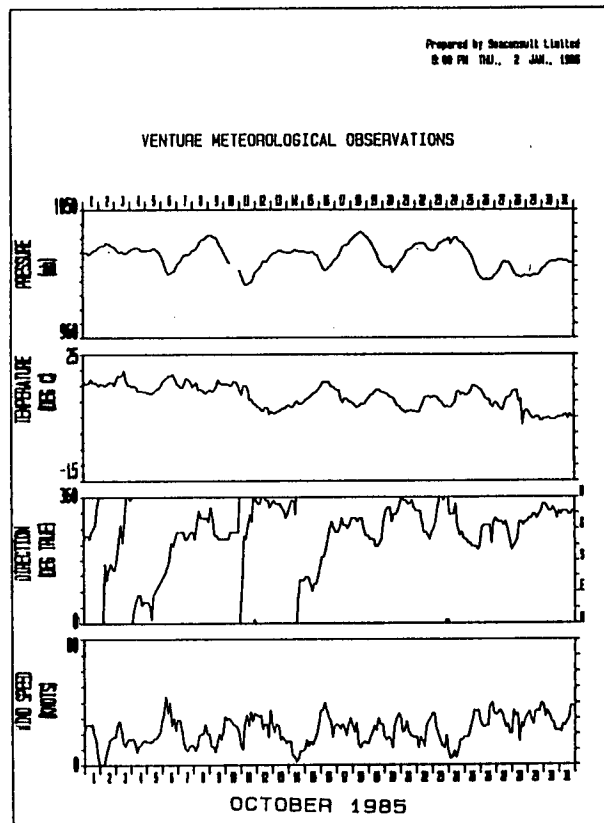
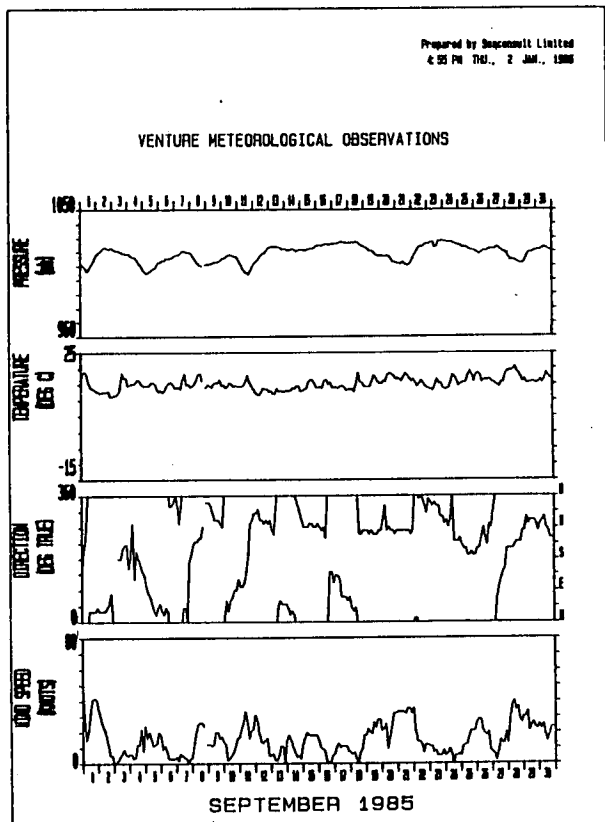


Fig. 6.3 West Olympia O-51 (Rowan Gorilla) meteorological data from September 1 to end of the drilling program, November 10, 1985.

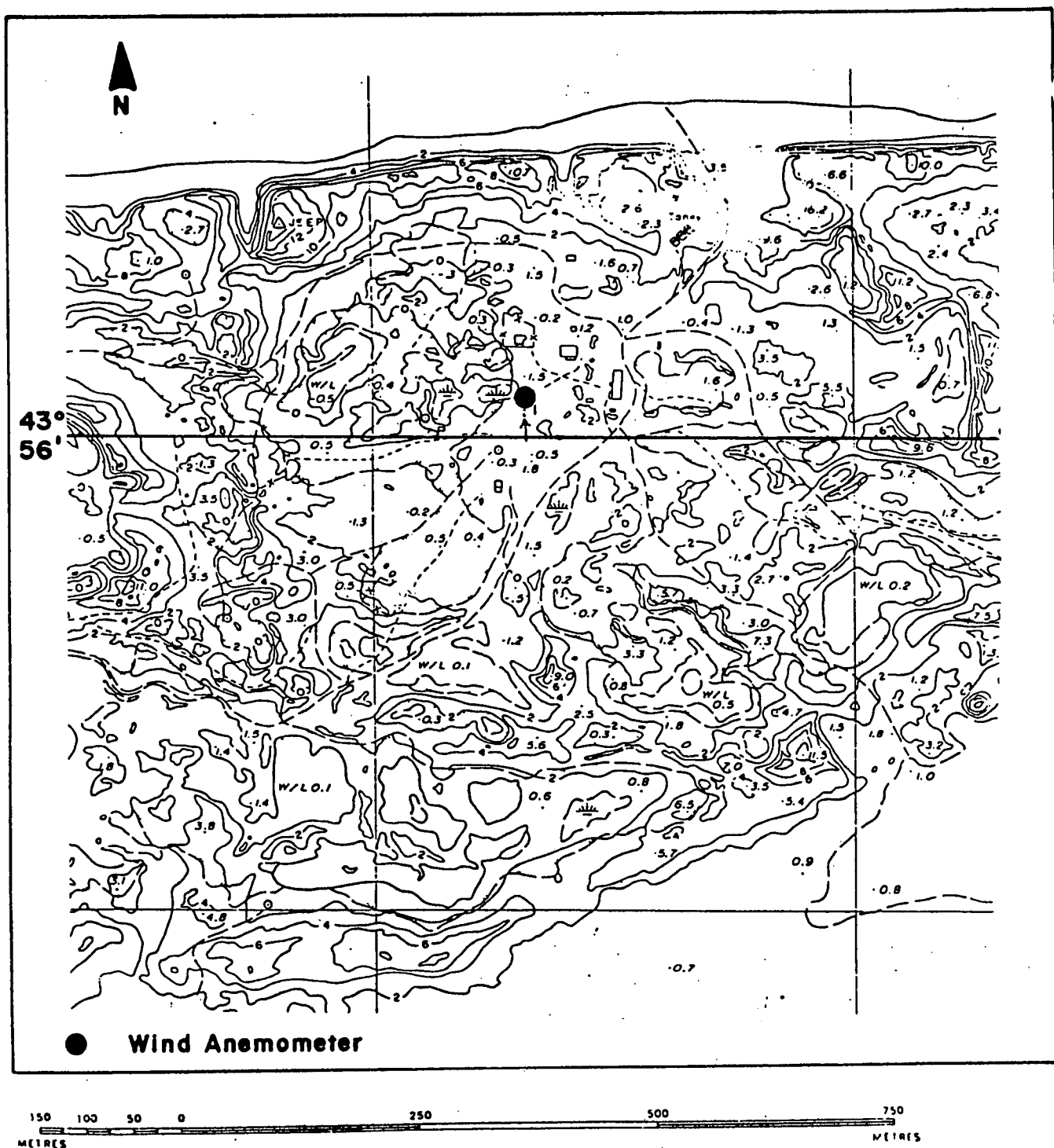


Fig. 6.4 Location of the wind anemometer on Sable Island and the surrounding topography.

The five months of Sable Island meteorological data are presented as a time-series in Fig. 6.5. During the first three months, the wind speed and direction data evolve very similarly to the rig winds plotted in Fig. 6.4, but the speeds are considerably smaller at the Sable Island site, rarely exceeding 30 knots.

6.2 CMC Forecasts Compared With Rig Winds

6.2.1 Data Presentation Formats

Three data products were prepared to facilitate intercomparison of vector winds and the errors in the forecasts. These products are

- 1) superimposed time-series plots of measured and forecast wind speed, direction, surface pressure and air temperature as well as time-series of error in speed and error in direction;
- 2) scatterplots of
 - forecast versus measured speed,
 - speed error versus measured speed,
 - direction error versus measured speed,
 - speed error versus direction error; and
- 3) verification tables of
 - speed error versus direction error,
 - measured speed versus speed error,
 - measured speed versus direction error.

The time-series plots show clearly the error characteristics for individual storm events and highlight the circumstances that produced large forecasting errors. They also illustrate that, in general, wind measurements contain higher frequency, small-scale variability than is present in the numerical forecasts.

The scatterplots summarize the error biases and trends in speed and direction as a function of wind speed. The verification tables quantify the information in the scatter plots. They permit calculation of the percentage of acceptably correct forecasts at different thresholds of required accuracy in wind speed or direction.

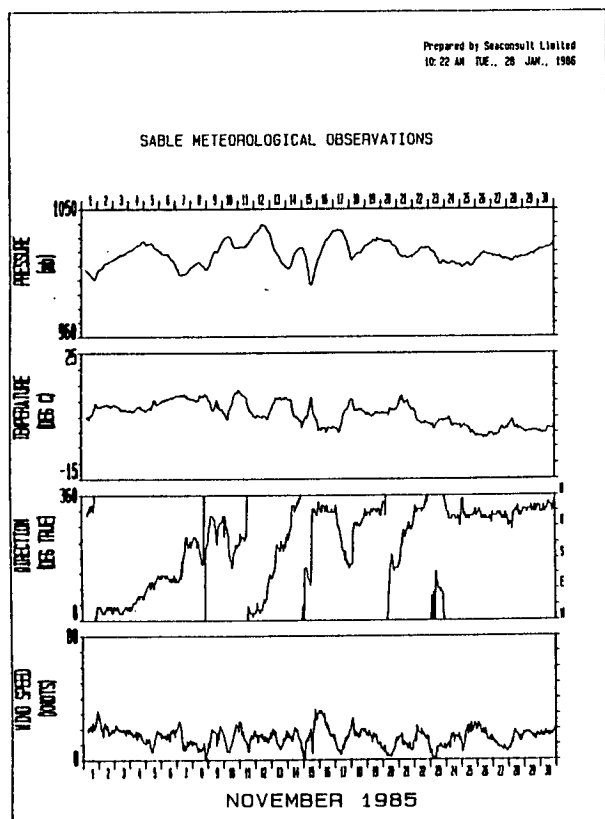
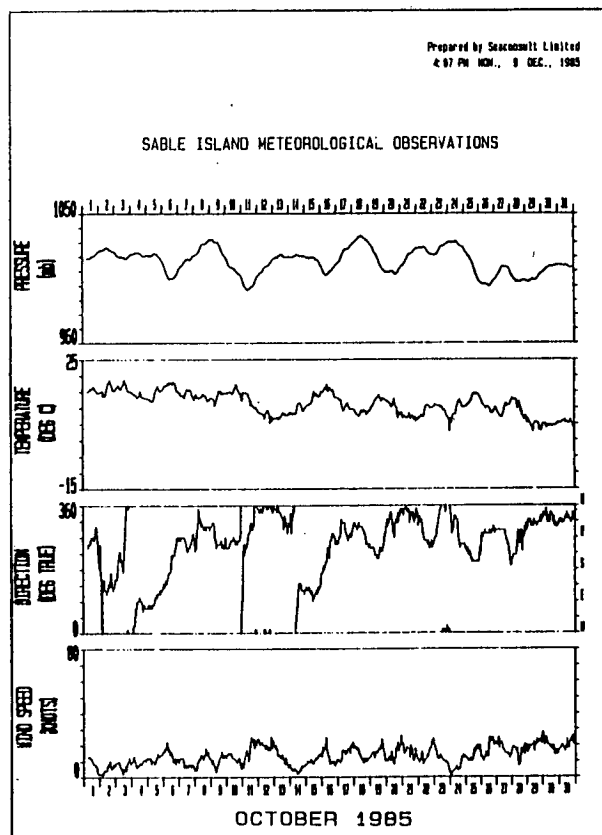
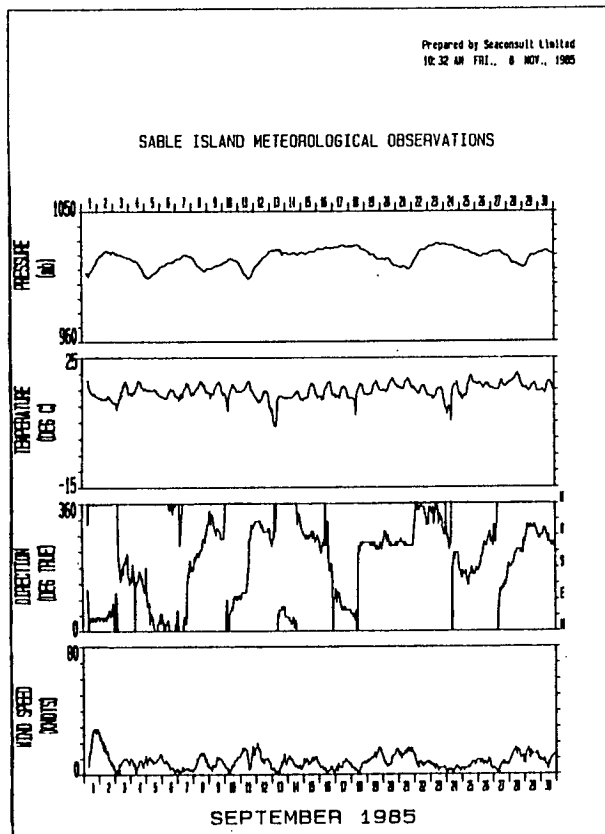
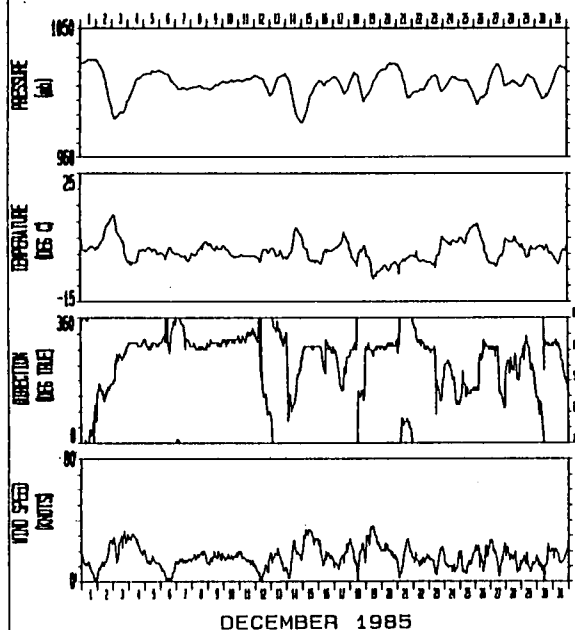


Fig. 6.5 Time-series of meteorological parameters at Sable Island from September 1985 to February 1986.

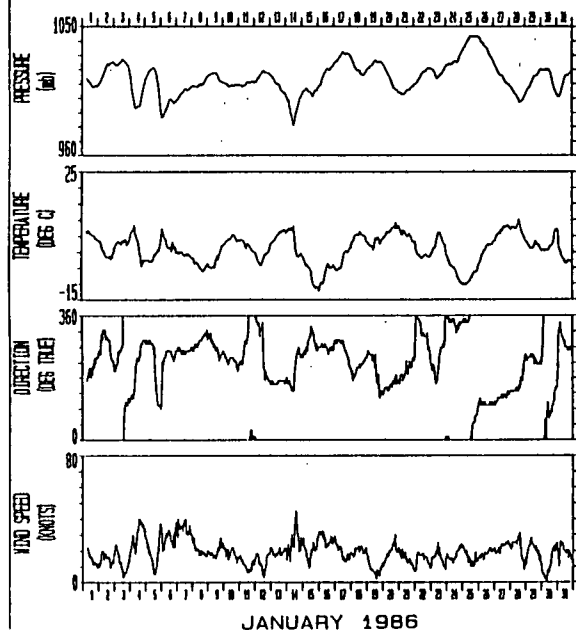
Prepared by Seascope Limited
10:27 AM TUE., 28 JAN., 1986

SABLE METEOROLOGICAL OBSERVATIONS



Prepared by Seascope Limited
11:07 AM THU., 13 MAR., 1986

SABLE ISLAND METEOROLOGICAL OBSERVATIONS



Prepared by Seascope Limited
8:00 AM TUE., 25 APR., 1986

SABLE ISLAND METEOROLOGICAL OBSERVATIONS

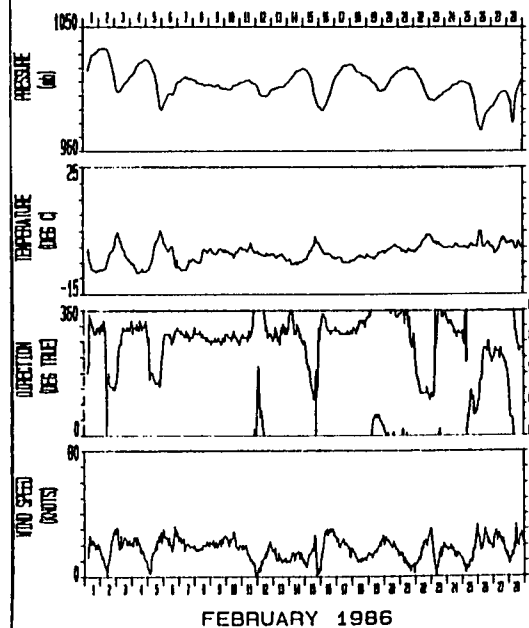


Fig. 6.5 Continued.

The scatterplots and verification tables were constructed for the 00-, 12- and 24-hour forecasts (F(00), F(12), F(24)) only. The correspondence between observation time and forecast time is illustrated in Fig. 6.6.

Four statistical error parameters were also calculated for the 00-, 12- and 24-hour forecasts. Defining the set of N observations of a parameter as O_i and the corresponding forecast parameter values as F_i , then the following definitions are obtained.

$$1) \quad \text{mean error or bias, } \bar{E} = \sum_i (O_i - F_i) / N$$

The mean error describes the average bias or offset in the forecast. A positive mean error indicates that, on average, the forecast is lower than the measurements; a negative mean error indicates that the forecast overpredicts the observations.

$$2) \quad \text{absolute error, } |E| = \sum_i |O_i - F_i| / N$$

The absolute error expresses the average magnitude of the forecast error, neglecting whether it over- or under-predicts the measurement.

$$3) \quad \text{root mean squared (rms) error, } E_{\text{rms}} = \left[\sum_i (O_i - F_i)^2 / N \right]^{1/2}$$

The rms error indicates the average dispersion in the individual errors E_i . If the bias is zero, the rms error is equivalent to the standard deviation of E.

$$4) \quad \text{scatter index, } SI = (E_{\text{rms}} / \bar{O}) * 100\%$$

The scatter index is an attempt to standardize the rms error to permit comparisons between data sets. \bar{O} is the average parameter value where $\bar{O} = \sum O_i / N$.

\bar{E} , $|E|$ and E_{rms} were calculated for wind speed and direction, surface pressure and air temperature. SI was determined for wind speed only.

OBSERVATION TIME		Day	1	2	3	4	5	6				
		Hour	00	12	00	12	00	12	00	12	00	12
Day	Hour	FORECAST TIME										
1	00	00										
	03	03										
	06	06										
	09	09										
	12	12 00										
	15	15 03										
	18	18 06										
	21	21 09										
2	00	<u>24 12 00</u>			F(24), F(12), F(00) for Day 2 @ 00Z							
	03	27 15 03										
	06	30 18 06										
	09	21 09										
	12	<u>24 12 00</u>			F(24), F(12), F(00) for Day 2 @ 12Z							
	15	27 15 03										
	18	30 18 06										
	21	21 09										
3	00	<u>24 12 00</u>			F(24), F(12), F(00) for Day 3 @ 00Z							
	03	27 15 03										
	06	30 18 06										
	09	21 09										
	12	24 12 00										
	15	27 15 03										
	18	30 18 06										
	21	21 09										
4	00	24 12 00										
	03	27 15 03										
	06	30 18 06										
	09	21 09										
	12	24 12 00										
	15	27 15 03										
	18	30 18 06										
	21	21 09										
5	00	24 12 00										
	03	27 15 03										
	06	30 18 06										
	09	21 09										
	12	24 12										
	15	27 15										
	18	30 18										
	21	21										
6	00	24										

Fig. 6.6 Relationship of forecast times F(00), F(12) and F(24) to observation times for calculation of error statistics.

6.2.2 Reduction of Rig Winds to Near-Surface

The profile of wind velocity as a function of elevation above the sea surface depends on the free atmosphere wind (above the planetary boundary layer), the potential temperature difference $\Delta\theta$ and the mean potential temperature $\bar{\theta}$ between the top of the boundary layer and the sea surface. Of the latter two parameters, $\Delta\theta$ is the more important and characterizes the air column stability. In practice $\Delta\theta$ ranges from about -10° for strongly unstable air masses to about $+10^\circ$ in very stable situations. $\Delta\theta = 0^\circ$ describes neutral stability.

The solution for the near-surface wind speed at a specified elevation is taken from Delage (1984) and corresponds to the procedure used in the CMC spectral wind model (Girard, CMC, pers. comm., 1985). The advantage of this method over many others is the independence of the solution from the boundary layer height h which is notoriously difficult to estimate. The solution for the surface wind angle is more awkward in that it does require a value for h , which is estimated assuming a barotropic atmosphere (Yamada, 1976).

To reduce the rig winds (which are measured at some intermediate level between the sea surface and the top of the boundary layer) to a near-surface (10-m elevation) wind, a look-up table of speed and direction adjustment factors was constructed as functions of air column stability and wind speed at the rig anemometer elevation. In doing so it was assumed that $\Delta\theta$ could be adequately approximated by the difference in rig measured air temperature and sea temperature, thereby ignoring pressure effects. The angular change in wind direction was presumed to vary linearly with elevation since only the surface deflection angle could be estimated directly. Results from the wind speed adjustment algorithm based on Delage (1984) compared favourably with tables constructed by Smith (1981).

Figure 6.7 compares the "as measured" 113-m elevation rig winds and the reduced 10-m wind time-series. The speed correction is often of the order of 10 to 20 knots for peak wind speeds. The plot of $\Delta\theta$ (second panel from top) illustrates that the air column stability changes, fairly abruptly, around October 11 from neutral or moderately stable to generally moderately

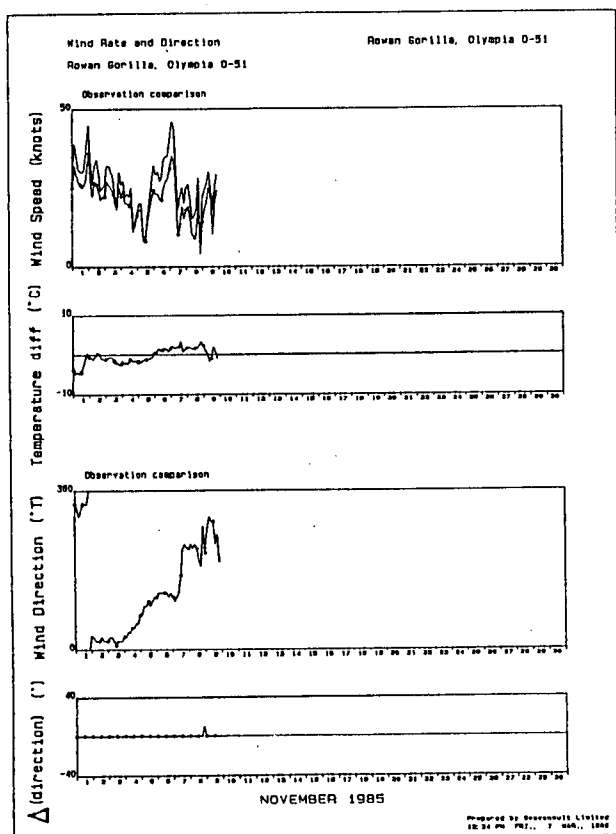
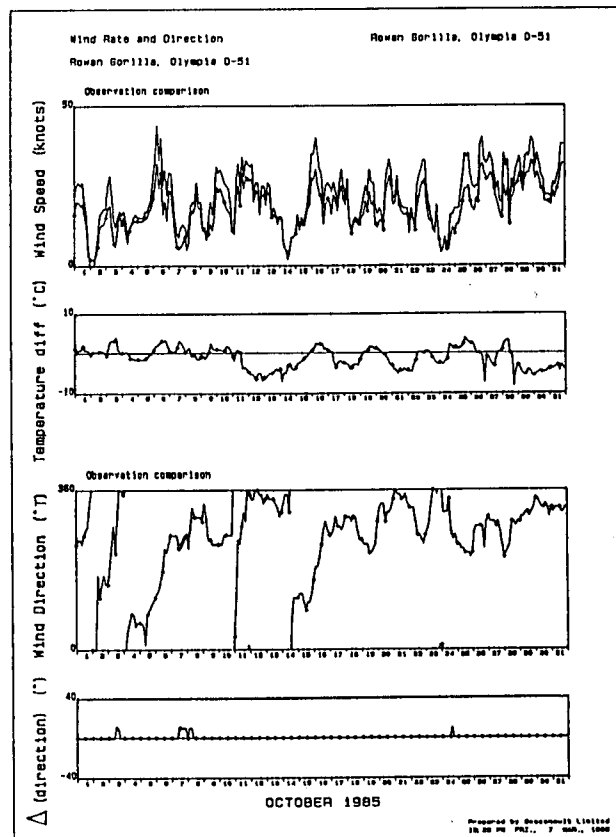
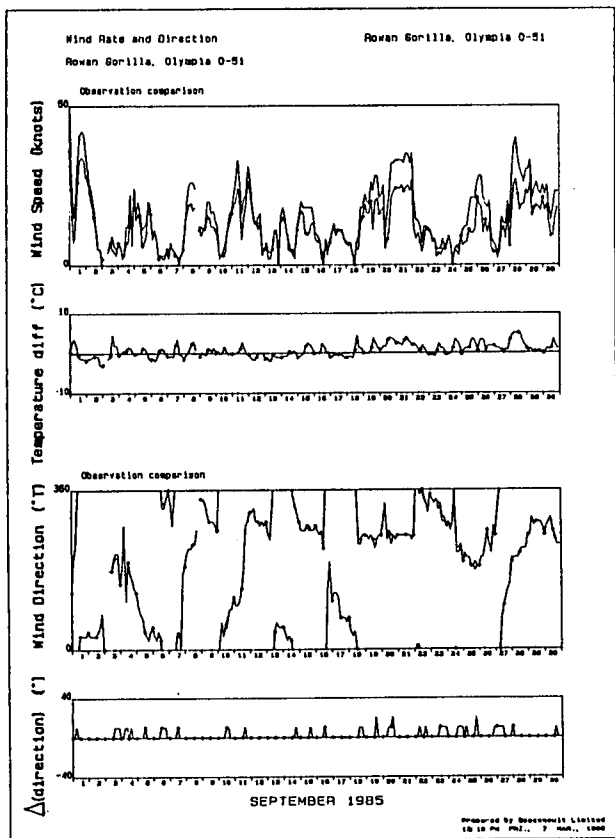


Fig. 6.7 Superposition of Rowan Gorilla rig winds as measured at 113 m elevation and the time-series of 10 m reduced winds.

or highly unstable conditions. During the more stable period, wind direction corrections are about 15° , but are negligible for unstable air masses.

6.2.3 Discussion of Comparisons

All the data comparison products constructed from the CMC forecasts and the Rowan Gorilla, West Olympia 0-51 rig measurements are presented in Appendix 6.1. In this section some of those products are reproduced to illustrate specific findings.

Figure 6.8 contains the time-series comparisons of the Rowan Gorilla rig winds, reduced to 10-m elevation, and the CMC forecasts for 00, 03, 06 and 09 hours at sigma level 0.998. Large negative speed errors (i.e., CMC forecast exceeding the rig measurement) tend to occur following peak storm winds which suggests that wind speeds occasionally decay faster in reality than in the CMC model. This type of error is as great as 20 knots and is evident on September 22, 28 and on October 6. Positive errors are not quite as large in magnitude and tend to occur during storm development, preceding peak wind speeds. Such errors occurred, for example, on September 27, October 11 and October 15. Because these two error characteristics do not usually occur during the same storm event, simple timing errors in the forecasts are not indicated.

For the most part directional errors in the 00 hour forecasts are small. When they are not, the wind speed is generally less than 10 knots.

Considering only the 00 hour forecasts, Fig. 6.9 presents the standard error statistics for wind speed, direction, surface pressure and air temperature as well as the scatterplots. This figure illustrates a number of additional characteristics of the CMC 00 hour forecast winds:

- 1) there is a small (<1 knot) negative bias in the CMC winds (i.e., the CMC forecast speeds are slightly high on average);
- 2) the directional bias is about -9° (i.e., on average CMC winds are rotated about 9° clockwise from measurements);
- 3) CMC surface pressure bias is about 1 mb low and CMC air

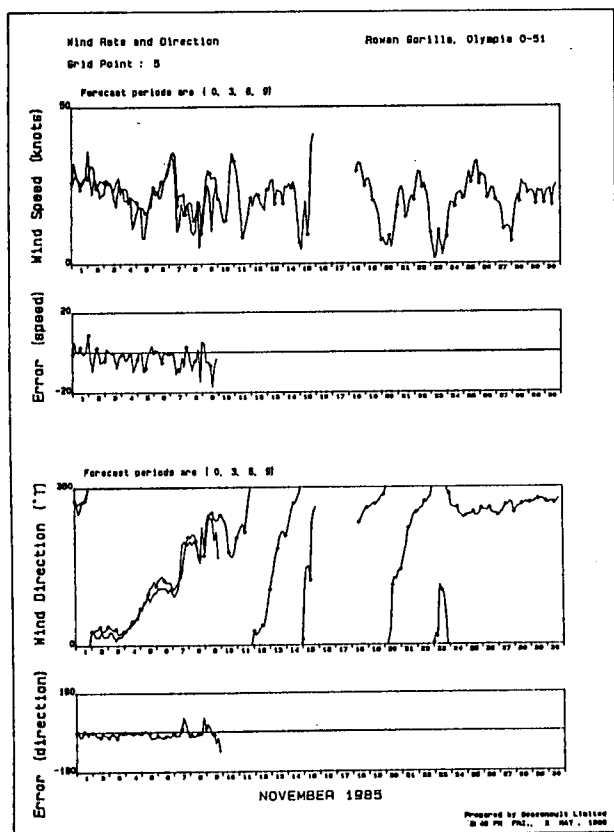
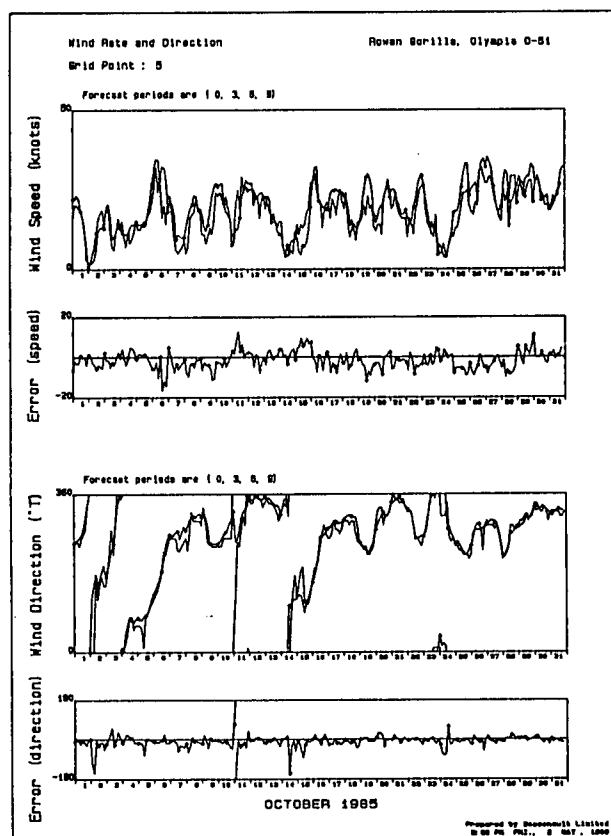
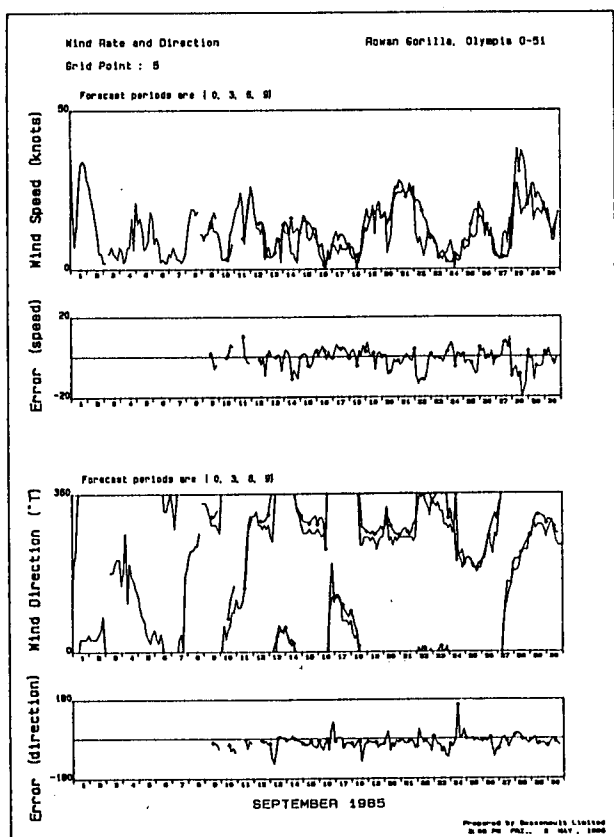


Fig. 6.8 Time-series comparisons of the Rowan Gorilla rig winds with CMC 00, 12 and 24 hour forecast winds.

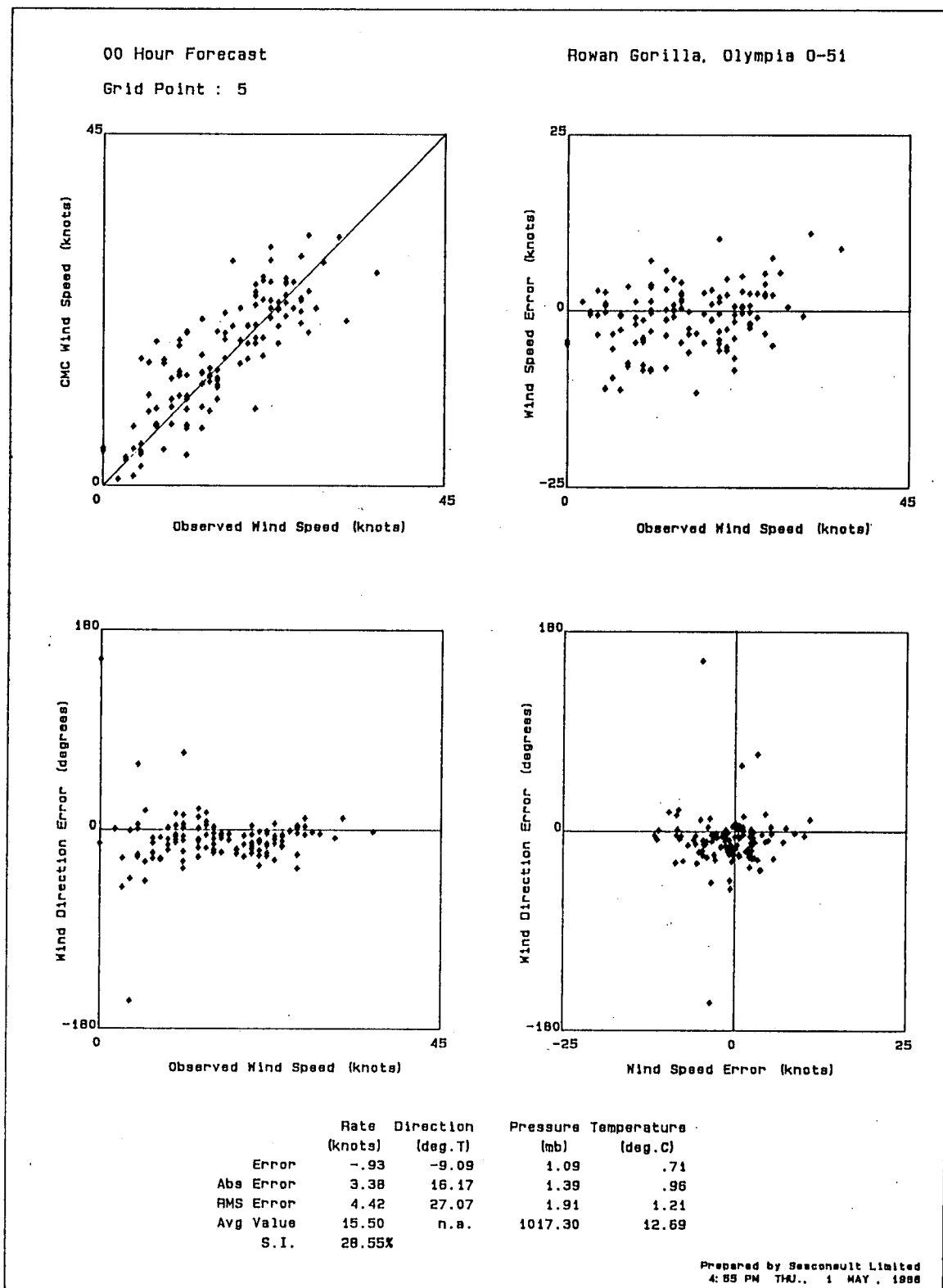


Fig. 6.9 Scatterplots and standard error statistics for the CMC 00 hour forecasts in relation to the Rowan Gorilla rig winds.

temperature bias is about 1°C low; and

- 4) the positive errors in wind speed tend to increase with greater wind speed, but the negative errors are largely independent of wind speed.

Figure 6.10 compares the error statistics for F(00), F(12) and F(24) and illustrates an expected deterioration in forecast accuracy with length of forecast period. Each of the error statistics \bar{E} , $|E|$ and E_{rms} increases by about 1 knot for each 12 hours of forecast lead time. The rms direction errors increase from 27° at 00 h to 37° at 24 h. The verification tables (in Appendix 6.1) show that the number of times the forecast is within ± 2.5 knots and $\pm 22.5^\circ$ drops from 40% at 00 h to 21% at 12 h to 14% at 24 h, but this is partially explained by the increasing bias in speed as the forecast lead time increases.

On a monthly basis, the mean wind speed error increases uniformly from September to November for each forecast interval as shown in Fig. 6.11. The mean direction error decreases uniformly over the same period. Because September and November are not complete data months, no definite conclusions should be drawn from the monthly statistics.

In general, the forecast speed errors out to 24 hours characterized by E_{rms} = 4 to 7 knots, including a bias of -1 to -3 knots, are probably acceptable for wave forecasting applications. Removing the average bias from the forecast values decreases the largest rms error to 6 knots. The directional errors may be more significant, especially in coastal areas where bathymetric refraction and landform sheltering considerations rely on accurate directional wave input.

6.3 CMC Forecasts Compared With Sable Island Winds

Because direct comparisons with offshore measured winds were severely limited by the amount of continuous, well-located rig data that was available during the study period, the Sable Island wind records were analyzed to try to overcome this deficiency.

6.3.1 CMC Versus Sable Island for Rig Period

Initially, the analyses described in subsection 6.2 were repeated by

00 Hour Forecast

	Rate (knots)	Direction (deg.T)	Pressure (mb)	Temperature (deg.C)
Error	-.93	-9.09	1.09	.71
Abs Error	3.38	16.17	1.39	.98
RMS Error	4.42	27.07	1.91	1.21
Avg Value	15.50	n.a.	1017.30	12.69
S.I.	28.55%			

12 Hour Forecast

	Rate (knots)	Direction (deg.T)	Pressure (mb)	Temperature (deg.C)
Error	-1.98	-12.94	.10	.04
Abs Error	4.22	22.54	1.40	.92
RMS Error	5.49	31.61	1.99	1.17
Avg Value	15.57	n.a.	1017.27	12.65
S.I.	35.27%			

24 Hour Forecast

	Rate (knots)	Direction (deg.T)	Pressure (mb)	Temperature (deg.C)
Error	-2.77	-11.32	-.36	-.19
Abs Error	5.20	24.67	1.97	1.14
RMS Error	6.59	36.73	2.64	1.43
Avg Value	15.57	n.a.	1017.27	12.65
S.I.	42.33%			

Fig. 6.10 Standard error statistics for the CMC F(00), F(12) and F(24) data in relation to the Rowan Gorilla rig winds.

Rowan Gorilla, Olympia 0-51
Grid Point : 5
00 Hour Forecast
Month : September

	Rate (knots)	Direction (deg.T)	Pressure (mb)	Temperature (deg.C)
Error	- .65	-9.69	1.43	.56
Abs Error	3.27	19.39	1.56	1.00
RMS Error	4.56	31.26	1.70	1.20
Avg Value	11.78	n.a.	1018.45	15.12
# of pts	40	40	40	40
S.I.	38.68%			

Rowan Gorilla, Olympia 0-51
Grid Point : 5
12 Hour Forecast
Month : September

	Rate (knots)	Direction (deg.T)	Pressure (mb)	Temperature (deg.C)
Error	- .68	-18.45	.37	.18
Abs Error	3.97	30.15	1.00	1.08
RMS Error	5.26	38.91	1.30	1.37
Avg Value	11.78	n.a.	1018.45	15.12
# of pts	39	39	39	39
S.I.	44.61%			

Rowan Gorilla, Olympia 0-51
Grid Point : 5
24 Hour Forecast
Month : September

	Rate (knots)	Direction (deg.T)	Pressure (mb)	Temperature (deg.C)
Error	-1.23	-21.61	-.49	.15
Abs Error	4.98	34.89	1.70	1.33
RMS Error	6.21	48.19	2.18	1.65
Avg Value	11.78	n.a.	1018.45	15.12
# of pts	38	38	38	38
S.I.	52.68%			

Rowan Gorilla, Olympia 0-51
Grid Point : 5
00 Hour Forecast
Month : October

	Rate (knots)	Direction (deg.T)	Pressure (mb)	Temperature (deg.C)
Error	- .97	-8.87	.86	.93
Abs Error	3.36	15.39	1.35	1.05
RMS Error	4.29	26.99	2.14	1.33
Avg Value	17.50	n.a.	1016.94	11.45
# of pts	62	62	62	62
S.I.	24.49%			

Rowan Gorilla, Olympia 0-51
Grid Point : 5
12 Hour Forecast
Month : October

	Rate (knots)	Direction (deg.T)	Pressure (mb)	Temperature (deg.C)
Error	-2.27	-10.64	-.35	.16
Abs Error	3.94	20.17	1.59	.81
RMS Error	5.03	29.55	2.32	1.03
Avg Value	17.65	n.a.	1016.89	11.37
# of pts	61	61	61	61
S.I.	28.52%			

Rowan Gorilla, Olympia 0-51
Grid Point : 5
24 Hour Forecast
Month : October

	Rate (knots)	Direction (deg.T)	Pressure (mb)	Temperature (deg.C)
Error	-3.11	-6.35	-.65	-.14
Abs Error	4.79	21.54	2.06	1.00
RMS Error	6.17	32.18	2.90	1.24
Avg Value	17.65	n.a.	1016.89	11.37
# of pts	61	61	61	61
S.I.	34.95%			

Rowan Gorilla, Olympia 0-51
Grid Point : 5
00 Hour Forecast
Month : November

	Rate (knots)	Direction (deg.T)	Pressure (mb)	Temperature (deg.C)
Error	-1.43	-8.47	1.09	.29
Abs Error	3.68	11.73	1.18	.55
RMS Error	4.59	14.28	1.43	.69
Avg Value	20.96	n.a.	1014.73	8.86
# of pts	18	18	18	18
S.I.	21.89%			

Rowan Gorilla, Olympia 0-51
Grid Point : 5
12 Hour Forecast
Month : November

	Rate (knots)	Direction (deg.T)	Pressure (mb)	Temperature (deg.C)
Error	-3.94	-8.55	1.08	-.72
Abs Error	5.79	13.59	1.62	.97
RMS Error	7.30	16.47	2.04	1.15
Avg Value	20.96	n.a.	1014.73	8.86
# of pts	17	17	17	17
S.I.	34.84%			

Rowan Gorilla, Olympia 0-51
Grid Point : 5
24 Hour Forecast
Month : November

	Rate (knots)	Direction (deg.T)	Pressure (mb)	Temperature (deg.C)
Error	-4.98	-6.15	.98	-1.14
Abs Error	7.17	13.04	2.19	1.24
RMS Error	8.60	17.28	2.64	1.52
Avg Value	20.96	n.a.	1014.73	8.86
# of pts	17	17	17	17
S.I.	41.04%			

Fig. 6.11 Monthly error statistics for the CMC F(00), F(12) and F(24) data in relation to the Rowan Gorilla rig winds.

substituting unmodified Sable Island winds recorded from September 9 to November 10, 1985 for the measured rig winds. Figure 6.12 summarizes the results of this analysis for the 00 hour forecast. The speed bias is -6 knots (versus -1 knot for the reduced rig winds) and the scatter index is 61%. Both $|E|$ and E_{rms} are between 1.5 and 1.7 times the equivalent values for the reduced rig winds. The direction errors are also somewhat greater, although pressure and temperature errors are slightly smaller in the Sable Island data.

This evidence suggests that the Sable Island wind data are biased low with respect to CMC forecasts and to the rig winds. It also indicates a greater degree of scatter for both speed and direction in the Sable Island data.

6.3.2 Calibration of Sable Island Winds

The Sable Island winds were compared directly with the three-hourly Rowan Gorilla 10-m reduced winds. In Fig. 6.13, the Sable Island winds are the "observed" (i.e., reference) data set. This illustration shows that the two wind speed measures are fairly well correlated, although the scatter is large (SI = 50%).

For the most part, the directions agree reasonably well: 88% of the data pairs are within $\pm 22.5^\circ$. Almost all of the exceptions occur at Sable Island wind speeds below 10 knots. The fact that MANMAR observations (both rig and Sable) have a directional precision of only 10° also contributes to the magnitude of these errors.

Two simple regression models were investigated to calibrate the Sable Island wind speeds with the rig data. The first one was a non-directional linear regression yielding the relationship

$$R_{rig} = 1.15 R_{Sable} + 2.5$$

Since the correlation coefficient R^2 is only 0.79 for these 555 data pairs, an alternative directional regression analysis was done. The amount of available data restricted this approach to only the four quadrants centred on north, east, south and west.

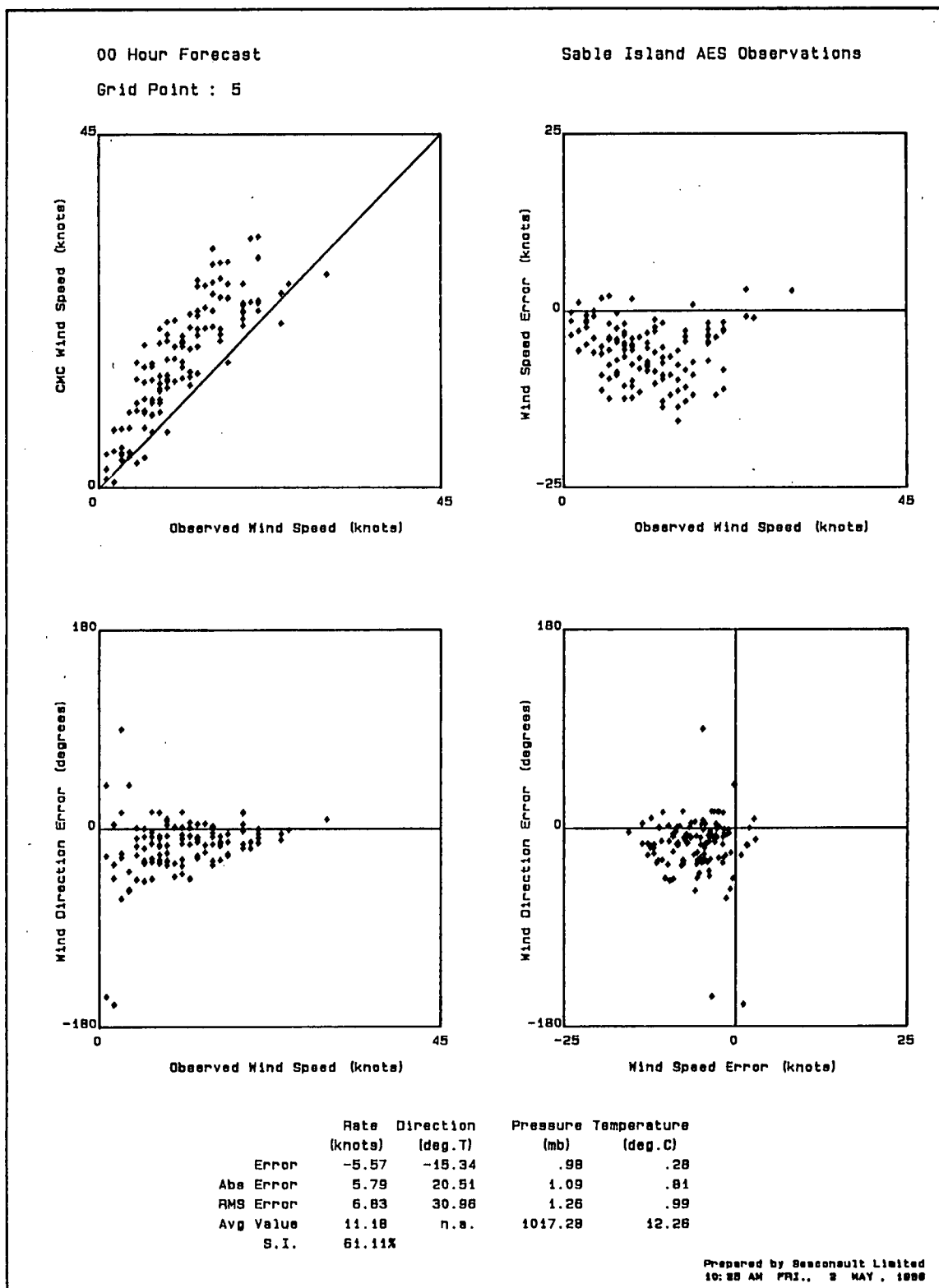


Fig. 6.12 Unmodified Sable Island data compared with CMC 00 hour forecast.

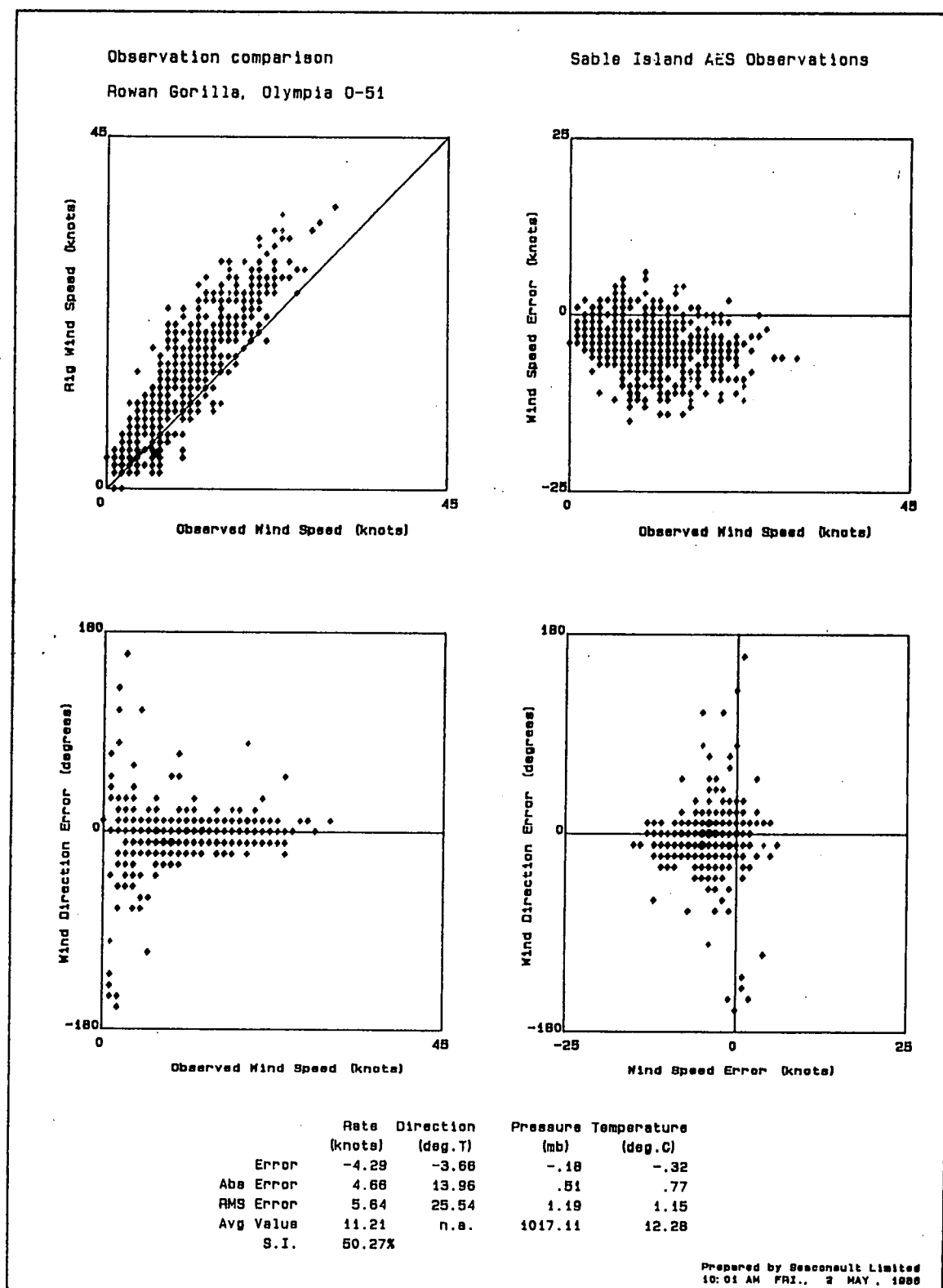


Fig. 6.13 Unmodified Sable Island data compared with 10-m reduced rig winds.

The results (in terms of R^2) are not uniformly better than the non-directional model, but since the biases (intercepts) and scaling factors (slopes) are so different, it appears that directional considerations are important. The following relationships were used, therefore, to obtain the calibrated Sable Island wind speeds R_C :

Direction	Regression Equation	R^2	No. of Samples
North	$R_C = 1.12 R_{Sable} + 1.9$	0.90	140
East	$R_C = 1.33 R_{Sable} + 0.5$	0.83	93
South	$R_C = 1.37 R_{Sable} + 1.1$	0.73	85
West	$R_C = 1.08 R_{Sable} + 3.7$	0.71	237

Figure 6.14 contains the error statistics of the calibrated Sable Island wind speeds as a function of forecast period. Comparison with the rig wind errors in Fig. 6.10 confirms that the adjusted Sable Island winds have approximately the same error values at F(00), F(12) and F(24). The bias in the adjusted Sable data is about 0.5 knots greater, the scatter index is about 1% greater, but the absolute error is a little less. The calibration is, therefore, essentially successful and allows more reliable statistics to be calculated from the full 6 months of Sable Island measurements and CMC forecasts from September 1985 through February 1986.

6.3.3 CMC Versus Adjusted Sable Island Winds

Following adjustment of the Sable Island wind records on the directional basis given above, the error characteristics of the CMC forecasts were calculated for the 6-month period from September 1985 to February 1986. These statistics are presented on a monthly basis in Fig. 6.15. The F(00) bias increases from -2 knots (CMC overpredicts) in September to over 4 knots (CMC underpredicts) in February. All 00 hour forecast wind speed errors are at their minimum in November.

The longer range forecasts have quite different monthly error trends. CMC overpredicts in all months except February in the 12- and 24-hour prognoses and it is greatest in November. The scatter indices were much larger in September than in any other month, but the E_{rms} values peak in December.

00 Hour Forecast

	Rate (knots)	Direction (deg.T)	Pressure (mb)	Temperature (deg.C)
Error	-1.40	-15.34	.98	.28
Abs Error	3.15	20.51	1.09	.81
RMS Error	3.91	30.96	1.26	.99
Avg Value	15.36	n.a.	1017.28	12.26
S.I.	25.46%			

12 Hour Forecast

	Rate (knots)	Direction (deg.T)	Pressure (mb)	Temperature (deg.C)
Error	-2.50	-16.69	-.00	-.42
Abs Error	4.16	28.81	1.24	.89
RMS Error	5.66	41.96	1.61	1.11
Avg Value	15.44	n.a.	1017.25	12.21
S.I.	36.69%			

24 Hour Forecast

	Rate (knots)	Direction (deg.T)	Pressure (mb)	Temperature (deg.C)
Error	-3.31	-17.84	-.46	-.61
Abs Error	5.09	30.89	1.87	1.12
RMS Error	6.68	46.07	2.39	1.42
Avg Value	15.44	n.a.	1017.25	12.21
S.I.	43.29%			

Fig. 6.14 Standard error statistics for the CMC F(00), F(12) and F(24) data in relation to the adjusted Sable Island winds (rig period: September to November 1985).

Adjusted Sable Island Observations (Directional Regression)
Grid Point : 5
00 Hour Forecast
Month : September

	Rate (knots)	Direction (deg.T)	Pressure (mb)	Temperature (deg.C)
Error	-1.88	-25.44	1.32	-1.11
Abs Error	3.22	28.26	1.32	.89
RMS Error	4.12	37.77	1.45	1.09
Avg Value	11.60	n.a.	1018.23	14.47
# of pts	40	40	40	40
S.I.	35.51%			

Adjusted Sable Island Observations
Grid Point : 5
12 Hour Forecast
Month : September

	Rate (knots)	Direction (deg.T)	Pressure (mb)	Temperature (deg.C)
Error	-1.84	-26.15	.24	-.53
Abs Error	3.64	39.39	.93	1.01
RMS Error	5.44	49.20	1.14	1.29
Avg Value	11.60	n.a.	1018.23	14.47
# of pts	39	39	39	39
S.I.	46.8%			

Adjusted Sable Island Observations
Grid Point : 5
24 Hour Forecast
Month : September

	Rate (knots)	Direction (deg.T)	Pressure (mb)	Temperature (deg.C)
Error	-2.51	-27.40	-.59	-.49
Abs Error	4.14	42.84	1.65	1.23
RMS Error	5.92	54.62	2.09	1.60
Avg Value	11.60	n.a.	1018.23	14.47
# of pts	38	38	38	38
S.I.	51.07%			

Adjusted Sable Island Observations
Grid Point : 5
00 Hour Forecast
Month : October

	Rate (knots)	Direction (deg.T)	Pressure (mb)	Temperature (deg.C)
Error	-1.09	-10.00	.83	-.54
Abs Error	3.07	17.07	.97	.80
RMS Error	3.72	29.19	1.12	.96
Avg Value	17.39	n.a.	1016.90	11.26
# of pts	62	62	62	62
S.I.	21.40%			

Adjusted Sable Island Observations
Grid Point : 5
12 Hour Forecast
Month : October

	Rate (knots)	Direction (deg.T)	Pressure (mb)	Temperature (deg.C)
Error	-2.42	-11.79	-.39	-.20
Abs Error	4.03	25.05	1.40	.78
RMS Error	5.39	40.96	1.78	.97
Avg Value	17.52	n.a.	1016.84	11.17
# of pts	61	61	61	61
S.I.	30.78%			

Adjusted Sable Island Observations
Grid Point : 5
24 Hour Forecast
Month : October

	Rate (knots)	Direction (deg.T)	Pressure (mb)	Temperature (deg.C)
Error	-3.26	-13.40	-.68	-.51
Abs Error	5.10	26.56	2.00	.98
RMS Error	6.61	43.66	2.56	1.26
Avg Value	17.52	n.a.	1016.84	11.17
# of pts	61	61	61	61
S.I.	37.75%			

Adjusted Sable Island Observations
Grid Point : 5
00 Hour Forecast
Month : November

	Rate (knots)	Direction (deg.T)	Pressure (mb)	Temperature (deg.C)
Error	-.90	-10.98	1.10	.42
Abs Error	2.91	13.32	1.23	.82
RMS Error	3.79	16.76	1.53	1.01
Avg Value	18.96	n.a.	1018.36	5.78
# of pts	55	55	55	55
S.I.	19.99%			

Adjusted Sable Island Observations
Grid Point : 5
12 Hour Forecast
Month : November

	Rate (knots)	Direction (deg.T)	Pressure (mb)	Temperature (deg.C)
Error	-3.77	-11.06	.12	-.79
Abs Error	4.81	17.79	1.43	1.02
RMS Error	5.95	25.99	1.81	1.29
Avg Value	18.96	n.a.	1018.36	5.78
# of pts	54	54	54	54
S.I.	31.39%			

Adjusted Sable Island Observations
Grid Point : 5
24 Hour Forecast
Month : November

	Rate (knots)	Direction (deg.T)	Pressure (mb)	Temperature (deg.C)
Error	-4.04	-7.76	-.63	-1.18
Abs Error	5.66	20.24	2.23	1.44
RMS Error	6.74	30.73	3.00	1.69
Avg Value	18.96	n.a.	1018.36	5.78
# of pts	54	54	54	54
S.I.	35.56%			

Fig. 6.15 Monthly error statistics for the CMC F(00), F(12) and F(24) data in relation to the adjusted Sable Island winds.

Adjusted Sable Island Observations (Directional Regression)
Grid Point : 5
00 Hour Forecast
Month : December

	Rate (knots)	Direction (deg.T)	Pressure (mb)	Temperature (deg.C)
Error	1.84	-12.62	.70	.12
Abs Error	4.41	15.54	1.32	.90
RMS Error	5.64	19.79	1.60	1.19
Avg Value	20.77	n.a.	1011.35	.79
# of pts	62	62	62	62
S.I.	27.17%			

Adjusted Sable Island Observations
Grid Point : 5
12 Hour Forecast
Month : December

	Rate (knots)	Direction (deg.T)	Pressure (mb)	Temperature (deg.C)
Error	-2.24	-12.39	-.78	-1.46
Abs Error	5.51	23.84	1.74	1.66
RMS Error	7.04	36.61	2.46	2.04
Avg Value	20.80	n.a.	1011.52	.79
# of pts	61	61	61	61
S.I.	33.83%			

Adjusted Sable Island Observations
Grid Point : 5
24 Hour Forecast
Month : December

	Rate (knots)	Direction (deg.T)	Pressure (mb)	Temperature (deg.C)
Error	-3.19	-12.52	-1.46	-1.97
Abs Error	6.49	23.96	2.62	2.06
RMS Error	7.97	39.01	3.67	2.56
Avg Value	20.80	n.a.	1011.52	.79
# of pts	61	61	61	61
S.I.	38.33%			

Adjusted Sable Island Observations
Grid Point : 5
00 Hour Forecast
Month : January

	Rate (knots)	Direction (deg.T)	Pressure (mb)	Temperature (deg.C)
Error	1.64	-14.62	.62	-.16
Abs Error	5.24	17.18	1.12	1.12
RMS Error	6.58	22.28	1.42	1.53
Avg Value	24.53	n.a.	1014.01	.84
# of pts	48	48	48	48
S.I.	26.81%			

Adjusted Sable Island Observations
Grid Point : 5
12 Hour Forecast
Month : January

	Rate (knots)	Direction (deg.T)	Pressure (mb)	Temperature (deg.C)
Error	-2.80	-18.42	-.64	-.82
Abs Error	5.30	22.86	1.74	1.26
RMS Error	7.05	31.28	2.56	1.58
Avg Value	24.51	n.a.	1014.05	.78
# of pts	47	47	47	47
S.I.	28.77%			

Adjusted Sable Island Observations
Grid Point : 5
24 Hour Forecast
Month : January

	Rate (knots)	Direction (deg.T)	Pressure (mb)	Temperature (deg.C)
Error	-2.55	-17.08	-.93	-.99
Abs Error	5.69	23.33	2.32	1.45
RMS Error	7.02	33.39	3.08	1.82
Avg Value	24.51	n.a.	1014.05	.78
# of pts	46	46	46	46
S.I.	28.63%			

Adjusted Sable Island Observations
Grid Point : 5
00 Hour Forecast
Month : February

	Rate (knots)	Direction (deg.T)	Pressure (mb)	Temperature (deg.C)
Error	4.16	-7.85	.78	.46
Abs Error	4.77	17.94	1.25	.97
RMS Error	6.08	24.59	1.61	1.25
Avg Value	21.97	n.a.	1008.65	-1.92
# of pts	53	53	53	53
S.I.	27.66%			

Adjusted Sable Island Observations
Grid Point : 5
12 Hour Forecast
Month : February

	Rate (knots)	Direction (deg.T)	Pressure (mb)	Temperature (deg.C)
Error	.40	-8.85	-1.30	-.31
Abs Error	4.44	25.22	1.85	1.07
RMS Error	6.51	37.55	2.65	1.33
Avg Value	22.08	n.a.	1008.59	-1.89
# of pts	52	52	52	52
S.I.	29.49%			

Adjusted Sable Island Observations
Grid Point : 5
24 Hour Forecast
Month : February

	Rate (knots)	Direction (deg.T)	Pressure (mb)	Temperature (deg.C)
Error	1.28	-12.41	-3.07	-.57
Abs Error	5.31	32.77	3.34	1.38
RMS Error	7.95	48.97	4.60	1.67
Avg Value	22.08	n.a.	1008.59	-1.89
# of pts	52	52	52	52
S.I.	36.01%			

Fig. 6.15 Continued.

For all three forecast periods, the directional bias in September (about -25°) far exceeds the calculated values in the other months. As the time-series plots in Appendix 6.3 show, this trend persisted throughout September and the first three days of October. The improved directional comparison for the rest of October suggests that any inherent bias in the Sable data is probably small, at most of the order of 3° to 4° as shown in Fig. 6.13.

The global (6-month) set of error statistics are presented in Fig. 6.16 for the 00 hour forecasts. On this time frame, the average bias is less than 1 knot, E_{rms} is 5 knots and the scatter index is about 27%. These are essentially the same values that were obtained from the comparison with reduced rig winds (Fig. 6.9), although the sign of the bias is reversed. The directional error statistics are also similar for the two data sets. The complete set of statistical comparisons is found in Appendix 6.3.

6.4 Assessment of CMC Wind Fields for Wave Forecasting

6.4.1 Access

The wind forecast model is run twice daily on CMC's Cray computer using a Cyber machine as input and output controller. Generally the data are available within three to four hours after the 00 hour "nowcast" time (i.e., by 04Z and 16Z daily). However, external users do not have direct access to the forecast products. Instead, in discussion with CMC personnel, the user defines his data requirements in terms of forecast variables, grid locations, σ -level or elevation and forecast times. A CMC programmer then defines a user-specific utility routine to extract, interpolate and reformat the data to be stored in a specific file on the Cyber system. It is the user's responsibility to access and transfer this file of information to the computer of his choice. In practice, this "choice" is limited by the available communicating hardware and software.

First, a physical connection is made between the Cyber computer (REMOTE) and the user's machine (LOCAL). The most economical method over any significant distance is a packet switching network such as Datapac. Second, a logical connection must be made involving a login procedure on REMOTE to effect data communications over the physical link. Once the login procedure is complete, the data transfer can be performed in a number of ways with

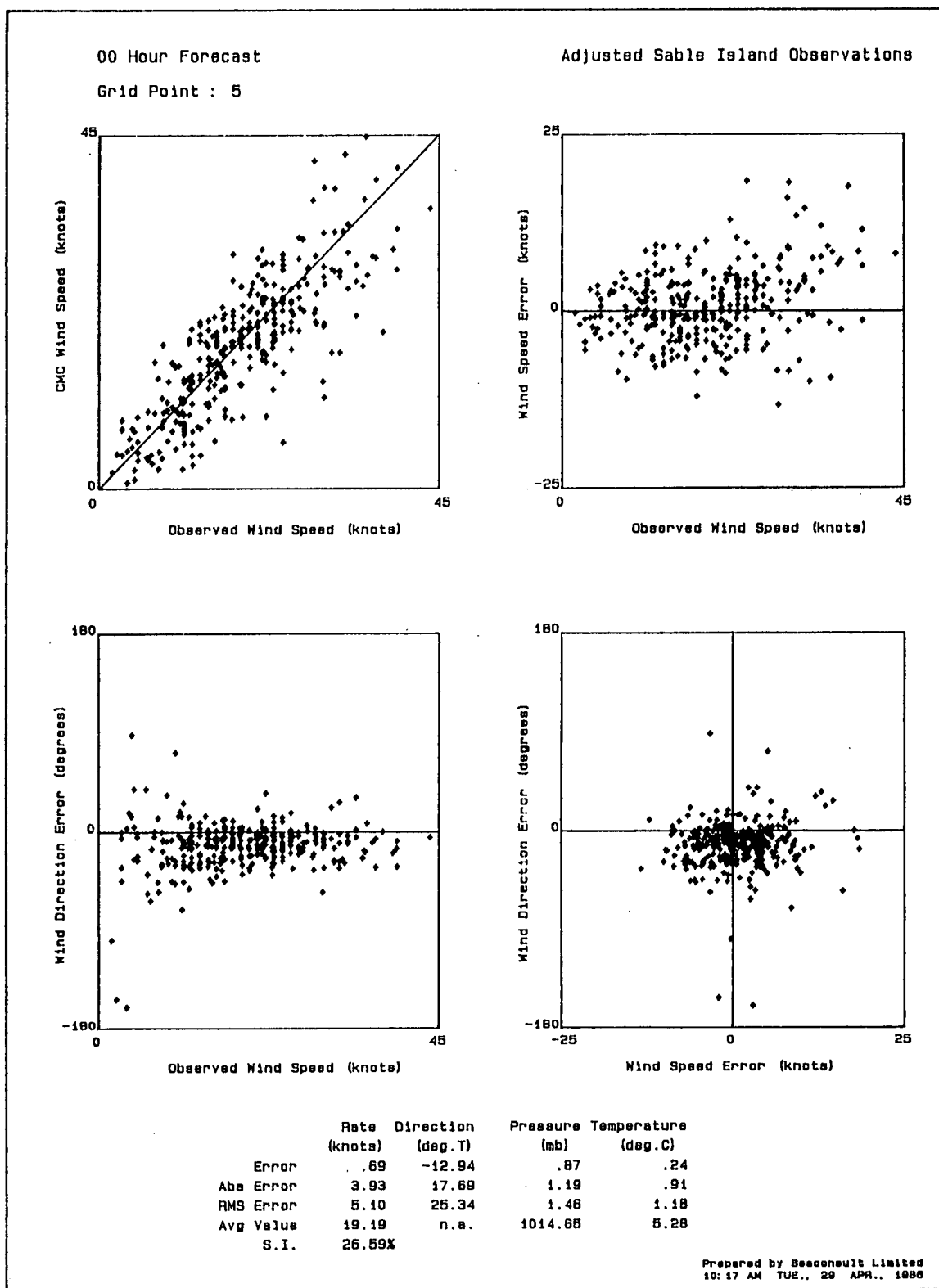


Fig. 6.16 Scatterplots and standard error statistics for the CMC 00 hour forecasts in relation to the adjusted Sable Island winds from September 1985 to February 1986.

varying degrees of cost, speed and integrity assurance.

In this study the physical connection was made using Datapac 3101 service via the public dial ports to the Cyber at CMC Montreal using a Network User Identifier (NUI) to reverse the Datapac charges to the caller. A Remote Micro Facility (RMF) was obtained from CMC to effect the logical connection. The RMF is a CDC product which allows for transfer of binary and text files between a microcomputer and a Cyber. This software is available for IBM PC's running PC-DOS and a wide variety of 8080/Z80-based machines running CP/M (few of which, however, could ever cope with wave forecasting software). In this case, an IBM-XT was used with the physical link to the PC through a serial port. A second physical-logical connection was made between the IBM-XT and the ultimate destination computer using a hardwired cable for the physical link and the KERMIT communications package to effect the logical connection.

In general terms, the procedure to acquire the CMC data is as follows. After invoking the RMF from the DOS command level on LOCAL (IBM-XT) and obtaining the RMF> prompt, the steps are 1) terminal emulation mode is entered, 2) the COM1 port of LOCAL is connected to a modem, 3) the Datapac herald is raised through a dial port, 4) the user's NUI is made active, 5) the CMC Datapac address is called, and 6) the REMOTE (Cyber) login procedure is followed. When the login is complete, terminal emulation is exited and the RMF is used as a file server. At this stage any number of files may be sent or received. Once the transfers are complete, terminal emulation mode is re-entered, the Cyber session is logged out and the Datapac connection is terminated.

The transfer of data across this link takes approximately 30 min for 130 kbytes and 10 min for 20 kbytes. The effective transfer rate is then near 600 baud for 130 kbytes but less than 300 baud for 20 kbytes. These differences arise from the differing file sizes, the efficiency with which Datapac fills its packets and possibly the retransmission (error) requirements. Using these examples as guides, then a 25x25 grid of speed and direction data (compressed into 2 characters per variable) will require about 1.5 min to transfer each forecast field. If six-hourly fields from

F(00) to F(48) were transmitted, about 15 min should suffice to accomplish the complete downloading of data from CMC to a PC computer (given a similar error transmission rate).

Transmission error checking requires cooperating software on both the sending REMOTE machine and the receiving LOCAL device. In this application there were two steps in the physical transfer involving quite different qualities of physical facility.

The Datapac link between the CMC node and the St. John's Datapac port utilizes the X.25 communications protocol and provides essentially error-free transmission. From the regional Datapac port to the LOCAL machine, standard telephone circuitry is used and over this segment the RMF is the primary quality-control facility. There is acknowledgement of each packet sent by Datapac, block counting and cyclic redundancy checking. Details of these features may be available from CMC.

Both transmission speed and quality assurance can be obtained (at a cost) with upgraded Datapac service through dedicated leased telephone lines or through upgrading the LOCAL user with X.25 protocol software and the necessary associated hardware to a Datapac node (i.e., equivalent to the CMC REMOTE).

This portion of the data acquisition is reasonably efficient and certainly cost-effective. However, it is both inefficient and costly to have to maintain the intermediate PC computer solely to communicate with CMC. To provide good service to potential users, an upgrade to the CMC communications software (RMF) is required to permit transfer of equivalent quality directly to "mainframe" micro-computers such as the Hewlett-Packard HP1000, the VAX family of machines and INTEL 80286/80386 processors on which wave forecast software may be run.

6.4.2 Timeliness

As it was arranged during this experiment, the CMC forecast products become available all at one time and can be downloaded to the LOCAL computer within about four hours after time 00 ("nowcast"). Thus, in real-time, it is already four hours into the forecast period before the wave forecast

procedure can be initiated. A reasonably fast deep-water spectral forecast can be performed at about one forecast hour every minute on a 15x15 point 2° latitude by 2° longitude grid size and a 1-hour time step. The earliest that all the 48-hour forecasts can be available will be of the order of six hours into the forecast period (Fig. 6.17, OPTION A). This situation cannot be viewed as satisfactory as it provides no prognosis at all for the first six hours of the forecast (which are probably the most accurately modelled) and only six hours lead time for the 12-hour forecast.

Some improvement can be achieved by disseminating the early forecast times as soon as they are available (F(12) after roughly five hours real-time, F(24) after 5.5 hours, and so on as illustrated by OPTION B in Fig. 6.17). Even more timeliness can be achieved by running the wind and wave models in parallel rather than sequentially. For an organization other than CMC to do this, the wind prognosis data would have to be disseminated as it is generated semi-continuously. If this were done, it seems feasible to issue a complete 48-hour wind and wave forecast by about 04:30 GMT (as proposed in Fig. 6.17, OPTION C) with the 12- and 24-hour wave prognoses available by 04 GMT. For shallow water models, timing would be even more critical as run times are significantly longer.

6.4.3 Reliability

After some initial start-up problems with the CMC data logging utility program, the forecast products were available throughout the six months except for the following periods:

November 16 00Z to November 18 12Z	(2.5 days)	reason unknown
January 02 12Z to January 07 12Z	(5.0 days)	downloading loss
January 11 12Z to January 12 00Z	(0.5 days)	reason unknown
January 17 12Z to January 19 00Z	(1.5 days)	reason unknown
February 05 12Z to February 06 00Z	(0.5 days)	reason unknown
February 23 12Z to February 24 12Z	(1.0 days)	reason unknown.

This represents a surprisingly high average failure rate of one or two days per month over the 5.5 month data acquisition period. Some losses may have been due to installation of an uninterruptable power supply at CMC, and thus our experience may be atypical. In the winter months, there is roughly a two-day periodicity to the wind speed signal (see Appendix 6.3 time-series

OPTION A

00Z 02 04 06 08 10 12 . . .

▲ winds disseminated; wave model initiated

▲ waves disseminated

Lag: -----> 04-----> 06-> 07-> 08 hours

OPTION B

00Z 02 04 06 08 10 12 . . .

▲ winds disseminated; wave model initiated

▲ 12-hour waves disseminated

▲ 24-hour waves disseminated

▲ 36, 48-hour waves disseminated

Lag: -----> 04-----> 06-> 07-> 08 hours

OPTION C

00Z 02 04 06 08 10 12 . . .

▲ 12,24-hour winds disseminated; wave model initiated

▲ 36-hour winds disseminated

▲ 48-hour winds disseminated

▲ 12, 24-hour waves disseminated

▲ 36-hour waves disseminated

▲ 48-hour waves disseminated

Lag: -----> 02-> 03-> 04-> 05-> 06 hours

Fig. 6.17 Possible schemes for dissemination of wind and wave forecasts.

plots for confirmation). So if the forecast wind data should be unavailable for two consecutive days, it is reasonably certain that a storm event (of some unspecified magnitude) will have been missed, which is unacceptable for a prognostic product on which lives and livelihood may depend. Even one day of downtime means that a winter storm may not be adequately forecast. Figure 6.18 illustrates this point: if two consecutive forecasts (i.e. one day) are unavailable, then the best forecast of the event peak pictured on day 04 hour 00 may be as old as 36 hours for which prognostic skill is poor.

If the wave forecast model had similar reliability characteristics that are statistically independent of the wind model performance then the wave model product would be "unavailable" every time the wind model failed and a similar number of times when only the wave model failed to run successfully. Every effort must be made to limit the failure rate of each model so that the user community is virtually guaranteed that no more than one-half day of forecast will be missed at a time.

6.4.4 Implications of Wind Field Errors

Bias

Since any wave model is driven directly by wind, any bias in wind speed will generate a corresponding bias in wave height. In principle either the wind input or the wave model itself could be calibrated to compensate for speed and direction bias if these statistics are uniform in space and time. However, as shown in Fig. 6.15 these errors vary with month from -2 knots to +4 knots in speed and -8° to -25° in direction. With this much variability in the mean error of 6 months of data at a single location, a general calibration to other than the long-term mean (which is apparently near zero anyway, at least near Sable Island) is impractical.

Standard Error Statistics

Standard statistics of the wind error characteristics are largely meaningless in the context of implying performance of a wave forecast model. They mask all the time and space dependencies in the two-dimensional temporal flow field that are critical to the behaviour of a model of a physical process like wind or wave field evolution.

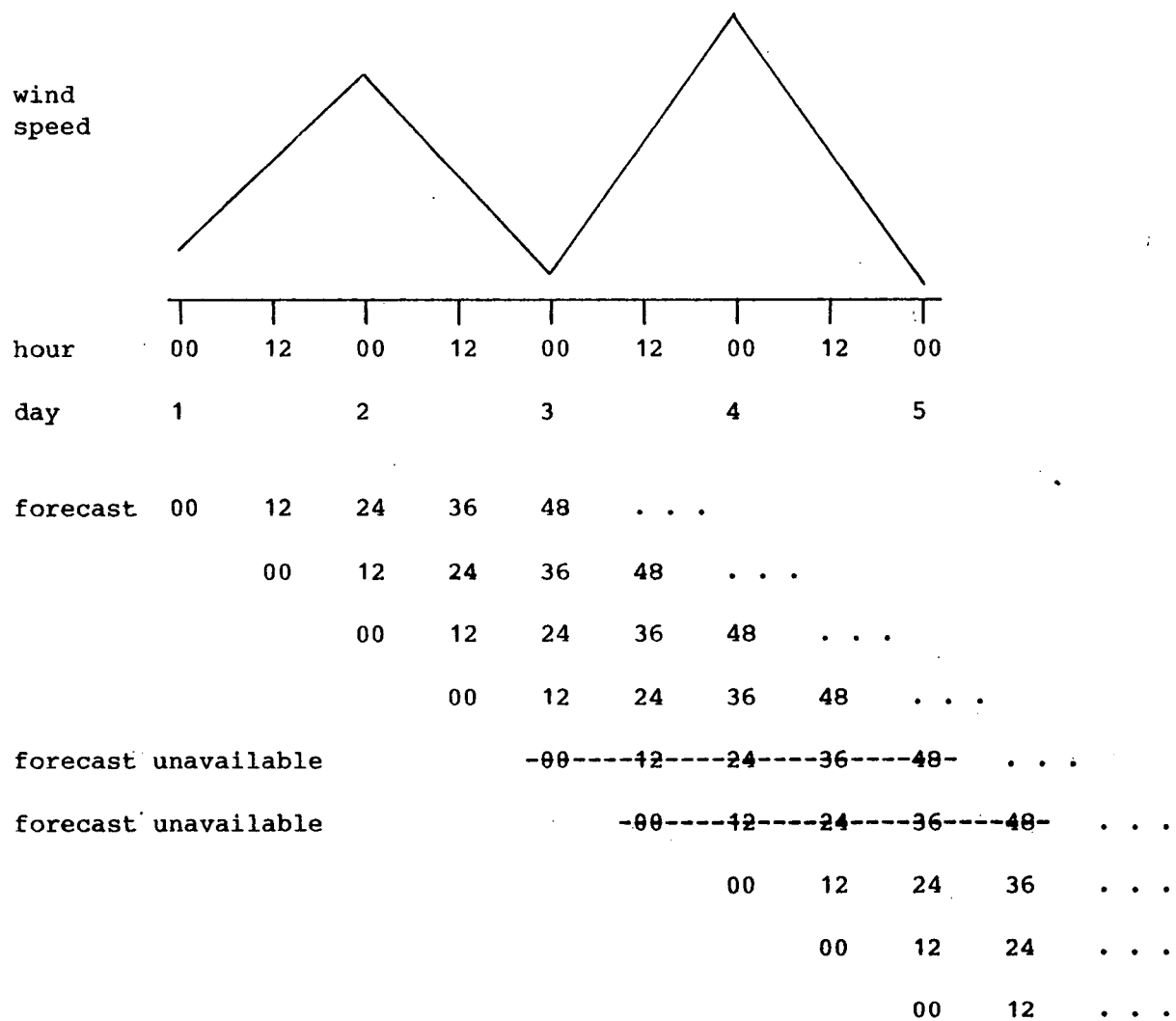


Fig. 6.18 Illustration of the consequences of missing two successive forecast intervals.

The only possible use for such gross measures of error is performance intercomparisons such as at different sites within the same model domain, or the same point from different models, or (as used in this study) different time frames at the same grid location. In all cases great care must be taken in selecting comparative data sets to avoid introduction of extraneous variations such as comparing "slightly" different locations from two different models and then incorrectly attributing all the calculated differences to the model formulations.

Resolution in Time and Space

As discussed in Section 5, it must always be kept in mind that a request to CMC for fine spatial resolution of the wind fields is achieved by straightforward interpolation and does not imbed any additional small-scale features that could be resolved on the requested grid. Over-specification of the wave model grid will, for the most part, only increase computation time without improving performance characteristics. In forecast mode, the only places that fine spatial resolution can be important in wave modelling are in topographic sheltering and bathymetric refraction zones.

For most Canadian coastal waters, a 1° or 2° latitude-longitude deep water wave model domain should be quite adequate and this resolution matches that of the CMC wind model very closely. The output of such a deep water wave forecast may provide boundary conditions to a shallow water module for nearshore areas--two such models were tested on Sable Island Bank and the results have been reported by Hodgins et al. (1986). In many situations, the shallow water solution will be dominated by boundary conditions other than wind input at the surface. In that case, the lack of small-scale features in the CMC forecast winds is not necessarily a serious limitation for wave forecasting on the continental shelves. If topographic modification of the wind field is important as it is near the mountainous islands and fjords of Canada's west coast, then the CMC forecast product will have inadequate horizontal resolution and the implication is that any derivative wave forecast will be poor in such areas.

Time resolution must normally be frequent enough to satisfy numerical stability criteria, that is the fastest (longest period) wave may not

traverse one grid element in one time step. Thus, for example, a 33-s wave will have a group velocity of $gT/4\pi$ or 26 m/s. If the smallest grid element is about 100 km then the maximum time step is about one hour. Although the CMC wind model has a time step of 20 min, the output is saved only every three hours of simulation time and must be linearly interpolated in time for input to a wave model. Considering even the three-hourly winds plotted in Appendix 6.1, it is readily apparent that the measured wind signal has considerably more variability from observation to observation than the CMC forecast product has. Since the sea-state is thought to be essentially in equilibrium with the local wind, a measured wave signal will respond to and reflect that wind variability whereas a wave forecast from the smoother CMC wind cannot.

6.5 Wind and Wave Modelling Strategy

The wave model specifications discussed in Section 4 show that, over Sable Island Bank and along the west coast, shallow water wave models with spatial resolutions of the order of 2 to 20 km will be required. Boundary data from large-scale deep water ocean wave models must be supplied to these localized fine grid models. Other local area wave models (for example, in Bay of Fundy, the Gulf of St. Lawrence and Davis Strait) must also be interfaced with deep ocean models.

Hudson Bay, the Beaufort Sea and the Strait of Georgia differ in that they are fully enclosed seas. An interface with either Pacific Ocean or Atlantic Ocean coarse grid models is not necessary. The major factor controlling sea state will be the overwater wind fields, assuming that where sea ice is important, its distribution is known.

A conceptual framework for numerical sea state prediction in Canadian waters that shows the relationship between oceanic coarse grid models and a series of nested, independent local area wave models is outlined in Fig. 6.19. The starting point is the numerical weather prediction model run by CMC. This model would generate grid-point overwater winds at grid spacings matched to two deep water coarse grid wave models--one for the northwest Atlantic Ocean and one for the Pacific Ocean.

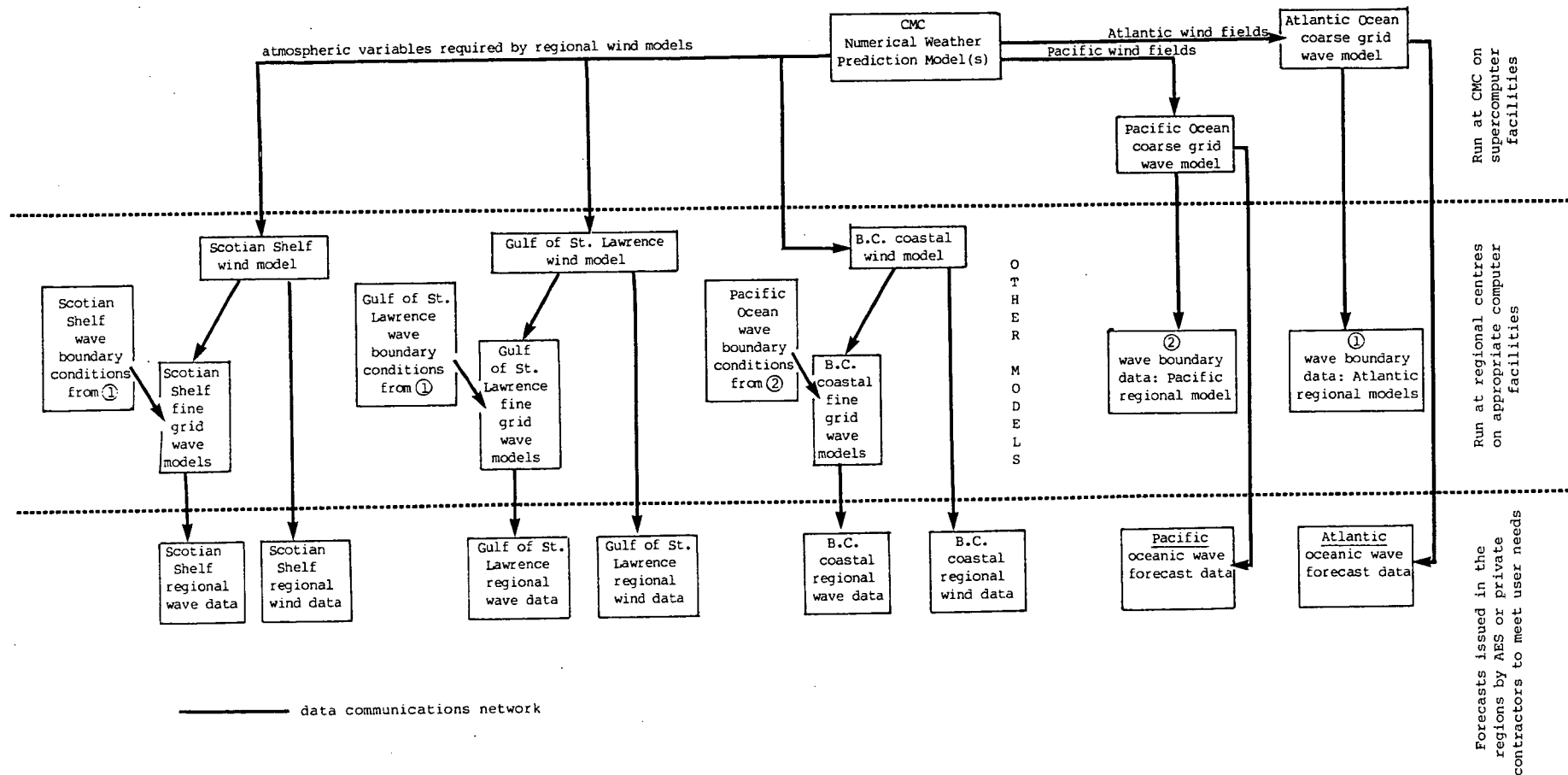


Fig. 6.19 Conceptual framework for wave forecasting in Canadian waters.

These coarse grid models provide prognosis wave fields suitable for naval and ship routing requirements directly, and would provide boundary conditions for a series of fine grid wave models. For example, the Atlantic model would supply boundary spectra to several nested coastal models for the Scotian Shelf, over the Grand Banks, in the Gulf of St. Lawrence, or in Davis Strait. On the west coast, one nested model covering the continental shelf would satisfy user needs there.

The CMC winds would also be input to a series of local area wind models that supply grid-point winds to the fine grid wave models. Along the B.C. coast, for example, such a small scale wind model would incorporate orographic effects and the changes in wind speed and direction associated with fronts crossing the nearshore waters. These wind submodels add information to the CMC winds at scales not represented in the hemispheric weather model that are important input to the fine grid wave models.

Three outputs would be provided from this approach. First, the standard meteorological forecast now disseminated by CMC would be obtained. Second, an ocean wide wind and wave forecast would follow from the coarse grid runs. These data would be suitable for vector and contour plots of wind, and of wave heights and wave directions with labelled wave periods. These products could be easily transmitted to users in digital format for in situ computer interpretation, or by facsimile in hardcopy form. Third, a series of regional wave forecasts would be produced. In these the number of output points and format of the prognosis fields could be tailored to specific user requirements. The type of spectral wave model used from one region to another may vary in response to a particular end user and may depend on the local factors affecting wave growth.

Timing is the most critical aspect of producing regional forecasts with this approach. To give the accuracy expected by most users for 12- to 24-hour forecasts, the regional wave calculations must be complete within six hours of data time. Realistically, this speed would only be achieved by running the models in parallel; that is, hemispheric winds would be input to coarse grid wave models and local wind models at several times during the main CMC run. The objective would be to have the coarse grid wave data and fine grid

wind inputs ready for regional wave models by about three hours after data time. This type of output procedure differs from that provided by CMC in this study.

Achieving this objective would leave approximately three hours to run regional wave models and prepare forecast products for dissemination. Coupled discrete spectral wave models (e.g., WAVAD, ODGP, etc.), optimized for a particular deep water grid, run sufficiently fast on minicomputers to meet the target completion time. This appears to be true also for high-end 16- to 32-bit microcomputers, and would be met with full 32-bit machines. The speed is achieved for the smaller machines by sufficient on-board RAM (3 to 8 Mbytes) to execute in core.

Microcomputer execution times for a coupled spectral wave model run in the hindcast mode with full shallow-water transformations (e.g., WAVAD) are typically about six hours for 48-hour predictions over a domain with approximately 500 water points. These benchmarks are for an Intel 80286/80287 processor running at 8 MHz. The hindcast mode requires extensive output which slows execution. A forecast optimized code running on a full 32-bit machine appears to be capable of meeting the three hour requirement for execution time, but this has not been confirmed through actual tests.

Less complicated models such as decoupled spectral codes or Donelan's model would easily run in the 3-hour time frame.

The largest unknown factor in this scheme is the time required to execute local area wind models. However, like the deep water wave models, these wind fields can be prepared in parallel with the spectral weather model run if CMC organizes staged outputs during execution.

In summary, it is feasible to provide wave forecasts meeting known user needs through numerical wave modelling, especially if the wave models are run on large mainframes or supercomputers (Cray, Cyber 205). It appears to be true also when the models are run on minicomputers or high-end microcomputers, although use of coupled-discrete shallow water wave models will require code optimization and implementation on 32-bit processors.

These conclusions do not apply to third-generation wave models (WAM, for example) which need a supercomputer.

There do not appear to be any constraints imposed by communications or computing power that restrict operational wave forecasting to large government or industry organizations. Provided that CMC can organize the required wind outputs and make them accessible over national networks, the wave models can be run by regional governmental agencies or by private firms.

7.0 CONCLUSIONS

On the basis of the material presented, there are a number of important conclusions that influence, or lead to, recommendations for proceeding towards a Canadian wave forecasting strategy.

- (1) Spectral rather than parametric (e.g., SMB) wave models should be used for all future wave forecasting because all the important wave parameters required by engineers, mariners and other users can be readily estimated from spectra. In fact, the spectra themselves are important primary input for many coastal engineering and naval architecture structural response functions.
- (2) Correct modelling of spectral shape will, in general, depend on the accuracy with which the non-linear wave-wave interaction term is formulated because it is believed to be the principal mechanism by which wave energy grows at frequencies below the spectral peak.
- (3) Oil and gas operators want to have site-specific hourly forecasts out to 12 hours and six-hourly prognoses between 12 and 48 hours for wave height (± 15 to 20%), period (± 2 s) and direction ($\pm 22.5^\circ$); if heave is important to the particular rig or vessel, then one-dimensional spectra are required at the same forecast times.
- (4) Rig supply vessel operators require regional combined sea-state forecasts of wave height ($\pm 20\%$) for 12- and 24-hour lead times or longer as dictated by transitting times.
- (5) Commercial fishermen require regional coastal wave forecasts of combined sea wave height ($\pm 15\%$) out to about 18 hours for areas where shallow water and topographic effects can be very important. In off-shore areas 36- to 48-hour combined wave height forecasts are needed.
- (6) Naval requirements are for three-hourly height, period and direction on a large regional basis out to 36 hours.
- (7) Other user needs are met if the most stringent of the foregoing requirements is satisfied. One exception may be the Great Lakes where user requirements have not been identified.

- (8) Coupled discrete wave models are the most generally applicable modelling technique; parameteric spectral wind-wave models should only be considered in restricted areas where swell is negligible.
- (9) Important wave model developments are underway within the WAM Group, although it is still too early to estimate the degree of success that they may achieve. Their objective is to build a forecast model that will compute the complete wave energy spectrum as the superposition of the three energy source-sink terms without recourse to imposing an empirical spectral shape. The key to success is believed to lie in development of an efficient algorithm to compute the non-linear wave-wave interactions.
- (10) For the Pacific and Atlantic Oceans a coarse grid deep water spectral wave model will be required to satisfy regional needs for the Navy and transitting vessels like supply boats, and to provide boundary condition energy spectra to local area (usually shallow water) models.
- (11) Coupled spectral models that now exist, either as hindcast or forecast codes, have been proven to be suitable for Canadian waters; the prime candidates are Resio's WAVAD, the DHI's System-20 and perhaps Cardone's ODGP model although Seaconsult's SPECREF and Donelan's GLERL model should also be considered for special cases.
- (12) There is no up-to-date, comprehensive, generally comprehensible description of the CMC spectral wind model or its products; this deficiency can lead to treating the forecast winds without due attention to their limitations.
- (13) Historically and demographically the CMC mandate has been primarily weather forecasting over land and at high altitude for aviation users; only recently has the importance of accurate near-surface overwater winds to wave modelling become apparent.
- (14) The effective spatial resolution of the CMC wind model is on a par with other national weather service models, but it is much too coarse to accurately resolve mesoscale features in the wind fields or to portray the local topographic influence at land-sea boundaries.

- (15) Compared with rig winds on the Scotian Shelf near Sable Island, the CMC forecast is biased high by 1 knot at analysis time and increasing to 3 knots for the 24-hour forecast; rms error increases from more than 4 to almost 7 knots through the 24-hour forecast period; rms directional error exceeds 22.5° at 00, 12- and 24-hour forecast times.
- (16) Because the Sable Island winds are biased more than 4 knots lower than 10-m reduced rig winds and the rms error is 6 knots, the Sable Island anemometer is unrepresentative of overwater winds over Sable Island Bank.
- (17) For a large domain forecast (e.g., the north Pacific Ocean), the 12- to 24-hour forecast winds would have to be available from CMC about two hours earlier than they are at present if a micro- or minicomputer were to be used for wave forecast modelling.
- (18) Since the CMC wind field bias varies from month to month, a general wave model calibration to compensate is impractical.
- (19) Standard error measures (rms error, scatter index, etc.) calculated at a point are almost meaningless as measures of two-dimensional time-varying wind or wave model performance since spatial homogeneity is not quantified nor is the temporal amplitude-phase response assessed; as a result, no definitive conclusion can be drawn concerning the consequences for wave modelling of the CMC wind field errors.
- (20) Because much of the Canadian expertise in practical spectral wave modelling (both hindcasting and forecasting) is in the private sector, every effort should be made to build on this foundation to satisfy our domestic needs for wave forecasting.

8.0 RECOMMENDATIONS

Eleven recommendations follow on how to meet user requirements for wave forecasts. These recommendations deal first with regional needs, and then with areas of research necessary to solve particular problems.

- (1) The most pressing need for an ongoing, large regional wave forecast capability is for the B.C. coastal waters for which, at present, there are no numerical prognoses. To meet the needs of commercial fishermen and other B.C. mariners, a shallow-water, coastal forecast is required; such prognoses could also be structured to provide the information required by offshore operators when exploratory drilling is resumed on the west coast. Recommendation: a deep water coarse grid spectral wave model should be implemented for the North Pacific Ocean, coupled with a coastal forecasting scheme; priority regions are Dixon Entrance, Hecate Strait, Queen Charlotte Sound, west coast of the Charlottes, west coast of Vancouver Island, Queen Charlotte Strait and Juan de Fuca Strait.
- (2) On the east coast, the regional requirements of the commercial fishery and similar wave forecast users have not been as clearly articulated as the west coast ones. On the other hand, the oil and gas sector has a fairly sustained need for localized wellsite forecasts on both the Grand Banks and the Scotian Shelf, although the number of wellsites and operators tends to fluctuate too much to support a private Canadian forecast industry. Detailed deep water regional wave forecasts are not at present available along the eastern seaboard, let alone verified shallow water prognoses for the Scotian Shelf. Recommendations: a deep-water coarse grid spectral wave model should be implemented for the North Atlantic Ocean. Nested regional wave models should then be developed to meet the enhanced forecast requirements of the oil and gas sector, fisheries, Coast Guard and other end users.
- (3) The framework for numerical wave prediction presented in Subsection 6.5 envisages the operation of local area wind models as a necessary intermediate step between the CMC hemispheric wind forecasts and the fine grid wave model prognoses. These small area wind models are intended to correct the smoothed CMC winds for important frontal effects and

orographic modifications. Recommendation: **research and development of appropriate local area wind models must be undertaken as part of the process of implementing regional wave models in all areas.**

- (4) Effective wave forecasting will require wind prognoses from CMC commencing within 1.0 to 1.5 hours of data time. The method of data transfer from CMC to Seaconsult in this study--in one batch about 3.5 hours after data time--is generally unsatisfactory. Recommendation: **CMC should disseminate the 3-hourly analysis and prognosis wind fields to users as grid point wind output files on a semi-continuous basis as the numerical weather model is running.**
- (5) Sea-state predictions are sensitive to errors in the wind fields used to drive the model. Objective analysis techniques to incorporate observed meteorological parameters into initial atmospheric fields are well-developed at CMC as part of running the spectral weather model. Similar concepts to assimilate direct wind reports into analysis surface wind fields, and sea-state measurements into initial wave fields, are receiving growing attention. In the next decade when orbiting satellites equipped with active and passive microwave sensors enter service, wind and wave data assimilation will become increasingly important. Recommendation: **research into data assimilation (wind, wave and sea ice) algorithms for spectral wave modelling should be undertaken in conjunction with model implementation. Present knowledge is deficient in these areas and the offshore data buoys are an important data resource that is not fully utilized.**
- (6) The accuracy of shallow water wave forecasts from local area wave models will depend on the ability of the deep water coarse grid models to predict directional wave spectra. Few verifications of modelled directional spectra have been reported, mainly because of the limited database. Recommendation: **verification of deep water directional spectra must be carried out as part of developing operational models. However, most of the existing directional wave database is distorted (and hence inappropriate) because of proximity to land. It should be expanded in deeper water on both coasts.**

- (7) Sea ice is a major determinant of sea state in the Beaufort Sea and, at certain times of the year, in Hudson Bay and along the east coast. The growth and damping of waves in the marginal ice zone and the transmission of wave energy through low concentration strips and patches are aspects of wave modelling that are at present ignored in spectral and parametric formulations. Recommendation: a study is required to synthesize what is presently known about these aspects of wave prediction, leading to a rational set of experiments or measurements to provide basic data for incorporation into models. Theoretical approaches should also be considered.
- (8) In the Beaufort Sea, Hudson Bay, the Gulf of St. Lawrence and the Labrador Sea, time and space resolution of the marginal ice zone provided by AES Ice Branch is inadequate for wave modelling at sites close to the moving, unconsolidated ice pack. This ice is too dynamic over the time scale of a storm to neglect the changes in concentration and geometry. Recommendation: a study should be undertaken to define the requirements for ice forecast parameters as input to wave modelling in terms of data that are available now and over the next few years as AES Ice Branch automates their procedures, and in terms of other alternatives in remotely sensed data. This study would be tied into recommendation (7) to define the sea ice parameters for wave modelling.
- (9) The CMC forecast wind fields for the open oceanic areas contain errors that can be quantified at a point in terms of long term mean trends, and these errors increase with increasing forecast lead time. These statistics provide only a crude estimate of overall model performance and do not characterize the error in terms of the two important properties--spatial coherence (at a point in time) and amplitude-phase response (at a point in space). Recommendation: a meaningful definition of error should be adopted for parameters (like winds and waves) that vary in time and in two spatial dimensions; methods of calculation should be standardized, clearly documented and widely disseminated.

- (10) The CMC wind forecast models are complex, evolving formulations that are poorly described for potential users. Recommendation: CMC personnel should produce a definitive descriptive document covering model formulation, limitations, output products, verification studies, notational definitions, and forecast philosophy, and should implement a procedure that is designed to keep users informed of changes.
- (11) A recent, comprehensive survey of west coast user requirements for meteorological forecasting has led to many new recommendations concerning wave forecasting. Recommendation: a similar user survey, concentrating on other than the oil and gas industry, should be conducted on the east coast with a view to defining the minimum regional wave forecasting requirements and to setting staged goals that would achieve that standard. Unique needs in the Great Lakes, Beaufort Sea and other arctic waters should then be included as a final step in setting a national set of standards covering all our important waterways.

REFERENCES

- Abbott, M.B., 1978. "New Development in Short-Wave Computation." Dock & Harbour Authority, LIX (691/692).
- Abernethy, C.L. and G. Gilbert, 1975. "Refraction of Wave Spectra." Hydraulics Rescuret Station, Wallingford, Report No. INT 117.
- Allender, J.H., T.P. Barnett and M. Lybanon, 1985. "The DNS Model: an Improved Spectral Model for Ocean Wave Prediction," in Ocean Wave Modeling. Plenum, New York, 235-248.
- Baer, L., 1962. "An Experiment in Numerical Forecasting of Deep-Water Ocean Waves." Report No. LMSC-801296, Lockhead California Study.
- Baird, W.F., 1978. "Wave Climate Analysis for Selected Locations in the Gulf of St. Lawrence and Lake Superior." Marine Directorate Report, Public Works, Canada.
- Baird, W.F. and J.S. Readshaw, 1981. "A Comparison of Hindcast and Recorded Wave Data". Contractor Report No. 1., Marine Environmental Data Service, Fisheries and Oceans, Canada, 23 pp. + Appendices.
- Barnett, T.P., 1968. "On the Generation, Dissipation, and Prediction of Ocean Wind Waves." J. Geophys. Res., 73(2), 513-529.
- Barnett, T.P. and A.J. Sutherland, 1968. "A Note on an Overshoot Effect in Wind-Generated Waves." J. Geophys. Res., 73(22), 6879-6885.
- Barnett, T.P. and J.C. Wilkerson, 1967. "On the Generation of Ocean Wind Waves as Inferred from Airborne Radar Measurements of Fetch-Limited Spectra." J. Marine Res., 25, 292-328.
- Barnett, T.P., C.H. Holland and P. Yager, 1969. "A General Technique for Wind-Wave Prediction with Application to the South China Sea." Unpublished Report, Westinghouse Ocean Res. Lab., San Diego, Ca.
- Battjes, J.A., 1981. "Effects of Shortcrestedness on Wave-Load on Long Structures." Presented at Wave and Wind Directionality Conf., September 29 - October 1, Paris.
- Borgman, L.E., 1969. "Directional Spectra Models for Design Use." Proc. Offshore Tech. Conf., Paper no. OTC 1069, 721-746.
- Bouws, E., H. Guenther, W. Rosenthal and C.L. Vincent, 1985a. "Similarity of the Wind Wave Spectrum in Finite Depth Water. Part 1: Spectral Form." J. Geophys. Res., 90, 975-986.
- Bouws, E., J. Ephraums, J. Ewing, P. Francis, H. Guenther, P. Janssen, G. Komen, W. Rosenthal, W. de Voogt, 1985b. Shallow Water Intercomparison of Wave Models Parts I, II, III, in The Ocean Surface: Wave Breaking, Turbulent Mixing and Radio Probing (Ed. Y. Toba and H. Mitsuyasu). Reidel Publishing Company, Dordrecht, 201-220.

- Bretschneider, C.L., H.L. Crutcher, J. Darbyshire, G. Neumann, W.J. Pierson, H. Walden and B.W. Wilson, 1962. "Data for High Wave Conditions Observed by the O.W.S. 'Weather Reporter' in December, 1959." Deut. Hydrog. Zeit., 15, 243-255.
- Brink-Kjaer, O., J. Knudsen, G.S. Rodenhuis and M. Rugbjerg, 1984. Extreme Wave Conditions in the Central North Sea. 16th Annual Offshore Tech. Conf., OTC 4809.
- Bryndum, M.B., R.S. Colquhoun and A. Verwey, 1982. "Dynamic Lay Stresses for Pipelines." Proc. Offshore Tech. Conf., Paper OTC 4267, 469-473.
- Byrne, H.M., 1982. "Variations in the Atmospheric Drag Coefficient due to Changes in Sea State." Proc. Oceans '82, Sept. 20-22, 1982. Washington, 445-452.
- Cardone, V.J., 1969. "Specification of the Wind Distribution in the Marine Boundary Layer for Wave Forecasting." Report Tr-69-1, School of Engineering and Science, New York University, 131 pp.
- Cardone, V.J., 1980. "Windfields for Wave Models." Transcript of Workshop on Wind-wave Hindcasting and Forecasting Models. U.S. Dept. of Commerce, NOAA, 33-82.
- Cardone, V.J., W.J. Pierson and E.G. Ward, 1975. "Hindcasting the Directional Spectra of Hurricane-Generated Waves." Proc. Offshore Tech. Conf., Paper OTC 2332.
- Cardone, V.J., W.J. Pierson and E.G. Ward, 1976. Hindcasting the Directional Spectra of Hurricane-Generated Waves." J. Petroleum Tech., 4, 385-394.
- Cardone, V.J., A.J. Broccoli, C.V. Greenwood and J.A. Greenwood, 1979. "Error Characteristics of Extratropical Storm Windfields Specified from Historical Data." Proc. Offshore Tech. Conf., Paper OTC 3598, 2103-2108 + figures.
- Carter, D.J.T., 1982. "Prediction of Wave Height and Period for a Constant Wind Velocity Using the JONSWAP Results." Ocean Engng., 9(1), 17-33.
- Cartwright, D.E., 1963. "The Use of Directional Spectra in Studying the Output of a Wave Recorder on a Moving Ship," in Ocean Wave Spectra. Prentice-Hall, Englewood Cliffs, 203-218.
- Cavaleri, L. and P.M. Rizzoli, 1981. "Wind Wave Prediction in Shallow Water: Theory and Applications." J. Geophys. Res., 86, 10961-10973.
- Clancy, R.M., J.E. Kaitala, and L.F. Zambresky, 1986. "The Fleet Numerical Oceanography Center Global Spectral Ocean Wave Model." Bull. Am. Meteor. Soc., 67(5), 498-512.
- Clodman, S., 1983. "Testing and Future Applications of the Donelan Numerical Lake Wave Model." Unpublished Manuscript, Int. Report MSRB-83-4, Atmospheric Environment Service, Downsview, Canada, 20 pp.

- Collins, J.I., 1972. "Prediction of Shallow-Water Spectra." J. Geophys. Res., 77, 2693-2707.
- Cote, L.J., J.O. Davis, W. Marks, R.J. McGough, E. Mehr. W.J. Pierson, J.F. Ropek, G. Stephenson and R.C. Vetter, 1960. "The Directional Spectrum of a Wind Generated Sea as Determined from Data Obtained by the Stereo Wave Observation Project." Meteorological Papers, New York University, College of Engineering, 2(6), 88 pp.
- Creswick, W.S., 1983. "The CMC Operational Spectral Forecast Model." CMC Info., 1(2), 22-38.
- Daley, R., C. Girard, J. Henderson and I. Simmonds, 1976. "Short-term Forecasting with a Multi-level Spectral Primitive Equation Model, Parts I and II." Atmosphere, 14(2), 98-134.
- Delage, Y., 1984. "Surface Turbulent Flux Formulation in Stable Conditions for Atmospheric Circulation Models." Reprint submitted to J. Atmos. Sci. (and later published in 1985 under same title in Monthly Weather Review, 113, 89-98.)
- Dello Stritto, F.J., J.R. Benoit and J.A.N. Ransom, 1985. "Wind-Related Needs of Offshore Industry: A Select Review." Proceedings Int'l Workshop on Offshore Winds and Icing, Halifax, NS.
- Devillaz, E., 1964. "Traitement Numerique de l'Etat de la Mer. Le Modele DSA 5." Notes de l'establissement d'Etudes et de Recherches Meteorologiques, No. 179, Paris.
- Devillaz, E., 1965. "Traitement Numerique de l'Etat de la Mer. Dispersion Artificielle et Premiers Resultats du Modele DSA-5-M." Note de l'Etablissement d'Etudes et de Recherches Meteorologiques, No. 211, Paris.
- Dobson, F.W. and J.A. Elliott, 1978. "Wave-Pressure Correlation Measurements Over Growing Sea Waves with a Wave Follower and Fixed-Height Pressure Sensors," in Turbulent Fluxes Through the Sea Surface, Wave Dynamics, and Prediction (Ed. A. Favre and K. Hasselmann), Plenum, New York, 421-432.
- Donelan, M.A., 1978a. "A Simple Numerical Model for Wave and Wind Stress Prediction." Unpublished Manuscript, Environment Canada, CCIW, Burlington, 11 pp. + Tables and Figures.
- Donelan, M.A., 1978b. "Whitecaps and Momentum Transfer," in Turbulent Fluxes Through the Sea Surface, Wave Dynamics, and Prediction (Ed. A. Favre and K. Hasselmann). Plenum, 273-287.
- Donelan, M.A., 1979. "On the Fraction of Wind Momentum Retained by Waves," in Marine Forecasting, Proc. 10th Intern. Liege Colloquium on Ocean Hydrodynamics. Elsevier, 141-159.

- Donelan, M.A., 1982. "The Dependence of the Aerodynamic Drag Coefficient on Wave Parameters." Proc. Conf. on Meteorology and Air-sea Interaction of the Coastal Zone, The Hague, 381-387.
- Dungey, J.C. and W.H. Hui, 1979. "Nonlinear Energy Transfer in a Narrow Gravity-wave Spectrum." Proc. R. Soc. Lond. A, 368, 239-265.
- Eid, B.M., V.J. Cardone, J.A. Greenwood and J. Saunders, 1987. "Real-time Spectral Wave Forecasting Model Test During CASP." Proc. International Workshop on Wave Hindcasting and Forecasting, Environmental Studies Revolving Funds Report No. 065, 183-195.
- Ewing, J.A., 1971. "A Numerical Wave Prediction Method for the North Atlantic Ocean." Deut. Hydrol. Zeit., 24(6), 241-261.
- Ewing, J.A. 1973. "Mean Length of Runs of High Waves." J. Geophys. Res., 78, 1933-1936.
- Ewing, J.A., T.J. Weare and B.A. Worthington, 1979. "A Hindcast Study of Extreme Wave Conditions in the North Sea." J. Geophys. Res., 84(C9), 5739-5747.
- Findlater, J., T.N.S. Harrower, G.A. Howkins, and H.L. Wright, 1966. "Surface and 900 mb Wind Relationships." Met. O. Sci. Pap. 23, HMSO, London.
- Fons, C., 1965. "Prevision de la Houle. La Methode des Densites Spectro-Angulaires No. 5 (DSA 5)." Notes Techniques, Travaux Meteorologiques, 15-33.
- Forristall, G.Z., 1978. "On the Statistical Distribution of Wave Heights in a Storm." J. Geophys. Res., 83, 2353-2358.
- Forristall, G.Z., 1984. "The Distribution of Measured and Simulated Wave Heights as a Function of Spectral Shape." J. Geophys. Res., 89(C6), 10547-10552.
- Fox, M.J.H., 1976. "On the Nonlinear Transfer of Energy in the Peak of a Gravity-wave Spectrum." Proc. R. Soc. Lond. A, 348, 467-483.
- Funke, E.R. and E.P.D. Mansard, 1979. "On the Synthesis of Realistic Sea-States in a Laboratory Flume." Tech. Report LTR-HY-66, Hydraulics Laboratory, National Research Council, Canada, 55 pp. + Appendices.
- Gadd, A.J., 1978. "A Numerical Advection Scheme with Small Phase Speed Errors." Quart. J. Royal Met. Soc., 104, 583-594.
- Garratt, J.R., 1977. "Review of Drag Coefficients Over Oceans and Continents." Mon. Wea. Rev., 105, 915-929.
- Geernaert, G.L., K.B. Katsaros and K. Richter, 1986. "Variation of the Drag Coefficient and its Dependence on Sea State." J. Geophys. Res., 91(C6), 7667-7679.

- Gelci, R. and P. Chavy, 1978. "Seven Years of Routine Numerical Wave Prediction by DSA-5 Model," in Turbulent Fluxes Through the Sea Surface, Wave Dynamics and Prediction (Ed. A. Farve and K. Hasselmann). Plenum, 565-591.
- Gelci, R. and E. Devillaz, 1970. "Le Calcul Numerique de l'Etat de la Mer." Houille Blanche, 25, 157-180.
- Gelci, R., H. Cazale and J. Vassal, 1957. "Prevision de la Houle. La Methode des Densites Spectro-Angulaires." Bulletin d'Information, Comite Central d'Oceanographie et d'Etude des Cotes, 8, 416-435.
- Gelci, R., E. Devillaz and P. Chavy, 1964. "Evolution de l'Etat de la Mer. Calcul Numerique des Advection." Note de l'Etablissement d'Etude et de Recherches Meteorologiques, No. 166, Paris.
- Goda, Y., 1970. "Numerical Experiments on Wave Statistics with Spectral Simulation." Rep. Port and Harbour Res. Inst., Japan, 9(3), 320-337.
- Goda, Y., 1976. "On Wave Groups." Proc. Behavior of Offshore Structures, BOSS '76, Trondheim, Vol. I, 115-128.
- Golding, B.W., 1978. "A Depth-Dependent Wave Model for Operational Forecasting," in Turbulent Fluxes Through the Sea Surface, Wave Dynamics and Prediction (Ed. A. Favre and K. Hasselmann). Plenum, New York, 593-606.
- Golding, B.W., 1983. "A Wave Prediction System for Real-Time Sea State Forecasting." Quart. J.R. Met. Soc., 109, 393-416.
- Greenwood, J.A., V.J. Cardone and L.M. Lawson, 1982. "Intercomparison Test Version of the SAIL Wave Model." (preprint) To appear Proc. IUCRM Meeting held in May, 1981, Miami, Fl.
- Guenther, H. and W. Rosenthal, 1979. "Application of the Parametrical Surface Wave Prediction Model to Rapidly Varying Wind Fields During JONSWAP 1973." J. Geophys. Res., 84(C8), 4855-4863.
- Guenther, H., W. Rosenthal, T.J. Weare, B.A. Worthington, K. Hasselmann and J.A. Ewing, 1979. "A Hybrid Parametrical Wave Prediction Model." J. Geophys. Res., 84(C9), 5727-5737.
- Harding, J. and A.A. Binding, 1978. "The Specification of Wind and Pressure Fields over the North Sea and Some Areas of the North Atlantic During 42 Gales from the Period 1966 to 1976." Report No. 55, Institute of Oceanographic Sciences, Unpublished Manuscript, 31 pp.
- Hasselmann, D.E., M. Dunckel and J.A. Ewing, 1980. "Directional Wave Spectra Observed During JONSWAP 1973" J. Phys. Oceanogr., 10(8), 1264-1280.
- Hasselmann, K., 1961. "On the Nonlinear Energy Transfer in a Gravity-wave Spectrum, 1, General Theory." J. Fluid Mech., 12, 481-500.

- Hasselmann, K., 1962. "On the Non-Linear Energy Transfer in a Gravity-Wave Spectrum. 1. General Theory." J. Fluid Mech., 12, 481-500.
- Hasselmann, K., 1963a. "On the Non-Linear Energy Transfer in a Gravity-Wave Spectrum. 2. Conservation Theorems, Wave-Particle Correspondence, Irreversibility." J. Fluid Mech., 15, 273-281.
- Hasselmann, K., 1963b. "On the Non-Linear Energy Transfer in a Gravity-Wave Spectrum. 3. Computation of the Energy Flux and Swell-Sea Interaction for a Neumann Spectrum." J. Fluid Mech., 15, 385-398.
- Hasselmann, K., 1974. "On the Spectral Dissipation of Ocean Waves due to White-capping." Bdy.-Layer Met., 6, 107-127.
- Hasselmann, K., T.P. Barnett, E. Bouws, H. Carlson, D.E. Cartwright, K. Enke, J.A. Ewing, H. Gienapp, D.E. Hasselmann, P. Kruseman, A. Meerburg, P. Mueller, D.J. Olbers, K. Richter, W. Sell, and H. Walden, 1973. "Measurements of Wind-Wave Growth and Swell Decay During the Joint North Sea Wave Project (JONSWAP)." Deut. Hydrog. Zeit., Reihe A., Nr. 12, 96 pp.
- Hasselmann, K., D.B. Ross, P. Mueller and W. Sell, 1976. "A Parametric Wave Prediction Model." J. Phys. Oceanogr., 6, 200-228.
- Hasselmann S. and K. Hasselmann, undated. "A Global Wave Model." Unpublished manuscript of the Max-Planck-Institute fuer Meteorologie, Hamburg.
- Hasselmann, S. and K. Hasselmann, 1981. "Integrations of the Spectral Transport Equation With Exact and Parametrical Computation of the Nonlinear Energy Transfer." Proc. Symp. Wave Dynamics and Radio Probing of Ocean Surface, Miami, Fl., 1981.
- Hasselmann, S., K. Hasselmann, J.H. Allender and T.P. Barnett, 1984. "Improved Methods of Computing and Parameterizing the Nonlinear Energy Transfer in a Gravity Wave Spectrum." Preprint provided by the authors.
- Haug, O., 1968. "A Numerical Model for Prediction of Sea and Swell." Meteorologische Annaler, 5(4), 139-161.
- Haug, O. and J. Guddal, 1981. "Hindcasting the Wind and Wave Climate of Norwegian Waters." Unpublished Manuscript, Project Report B1810.7279, Det Norske Meteorologiske Institute.
- Hodgins, D.O., 1984. "Weather Forecasting Services for the Canadian Offshore. Part 2: Assessment of Adequacy." A Report to the Royal Commission on the Ocean Ranger Marine Disaster by Seaconsult Limited, St. John's.
- Hodgins, D.O., 1986. "Evaluation of Two Shallow Water Wave Models on Sable Island Bank, Canada." Proc. Int'l Workshop on Wave Hindcasting and Forecasting, Sept. 23-26, 1986. Halifax, Canada.

- Hodgins, D.O. and K.F. Harry, 1984. "Weather Forecasting Services for the Canadian Offshore. Part 1: Organization of Responsible Agencies and Current Practice." A Report to the Royal Commission on the Ocean Ranger Marine Disaster by Seaconsult Limited, St. John's.
- Hodgins, D.O. and S. Hodgins, 1983. "East Coast Wave Climatology. Phase I Report." Prepared for Petro-Canada Exploration Inc. by Seaconsult Marine Research Ltd., Vancouver.
- Hodgins, D.O. and S. Nikleva, 1986. "On the Impact of New Observing Sites on Severe Sea State Warnings for the B.C. Coast." Unpublished technical report prepared for Fisheries & Oceans Canada by Seaconsult Marine Research Ltd., Vancouver.
- Hodgins, D.O., P.H. LeBlond and O. Brink Kjaer, 1981. "A Hindcast Study of Extreme Water Levels in the Beaufort Sea.: Prepared for Esso Resources Canada Limited by Seaconsult Marine Research Ltd., Vancouver.
- Hodgins, D.O., P.H. LeBlond, D.S. Dunbar and C.T. Niwinski, 1985. "A Wave Climate Study of the Northern British Columbia Coast, Vol. II." Unpublished technical report prepared for Fisheries and Oceans Canada by Seaconsult Marine Research Ltd., Vancouver.
- Hodgins, D.O., C.T. Niwinski and D.T. Resio, 1986. "Comparison and Validation of Two Shallow-Water Spectral Wave Models." Draft report prepared for The Environmental Studies Revolving Funds, Ottawa by Seaconsult Marine Research Ltd., Vancouver.
- Holthuijsen, L.H., 1981. "Wave Directionality Inferred from Stereo Photos." Presented at Directional Wave Spectra Applications '81, 14-16 Sept., Berkeley.
- Houghton, I., 1984. "A Long Time-series Verification of Hindcasts from the Meteorological Office Wave Model Archive." The Met. Mag., Met. O. 964, 113(1348), 317-329.
- Hsu, S.A., 1986. "A Mechanism for the Increase of Wind Stress (Drag) Coefficient With Wind Speed Over Water Surfaces: A Parametric Model." J. Phys. Oceanogr., 16(1), 144-150.
- Hsiung, C.C. and A.F. Aboul-Azm, 1982. "Iceberg Drift Affected by Wave Action." Ocean Engng., 9(5), 433-439.
- Huntington, S.W., 1981. "Wave Loading in Short-Crested Seas." Presented at Wave and Wind Directionality Conf., Sept. 29-Oct. 1, Paris.
- Huntington, S.W. and G. Gilbert, 1979. "Extreme Forces in Short-Crested Seas." Proc. Offshore Tech. Conf., Paper No. OTC 3595, 2075-2081.
- Hydraulics Research Station (HRS), 1977a. "Numerical Wave Climate Study for the North Sea (NORSWAM)." Report No. EX 775, 17 pp. + Tables and Figures.

- Hydraulics Research Station (HRS), 1977b. "Numerical Wave Climate Study for the North Sea (User Manual)." Report No. EX 776, 14 pp. + Tables and Figures.
- Hydraulics Research Station (HRS), 1981. "Severn Tidal Power, Hindcasting Extreme Waves." Report No. EX 978, 21 pp. + Tables and Figures.
- Inoue, T., 1966. "On the Growth of the Spectrum of a Wind Generated Sea According to a Modified Miles-Phillips Mechanism". GSL Report TR-66-6, School of Engineering and Science, New York University.
- Isozaki, I. and T. Uji, 1973. "Numerical Prediction of Ocean Wind-Waves." Papers in Meteorology and Geophysics, 24(2), 207-231.
- Janssen, P.A.E.M., G.J. Komen and W.J.P. de Voogt, 1984. "An Operational Coupled Hybrid Wave Prediction Model." J. Geophys. Res., 89(C3), 3635-3654.
- Jones, W.L., F.J. Wentz and L.C. Schroeder, 1980. "Microwave Scatterometer Measurements of Oceanic Wind Vector," in Oceanography from Space. Proceedings of a COSPAR/SCOR/IUCRM Symposium, Venice, Italy.
- Kinsman, B., 1965. Wind Waves. Prentice-Hall, Englewood Cliffs, 676 pp.
- Kitaigorodskii, S.A., 1962. "Applications of the Theory of Similarity to the Analysis of Wind-generated Wave Motion as a Stochastic Process." Izv., Geophys. Ser. Acad. Sci. U.S.S.R., 1, 105-17.
- Kitaigorodskii, S.A., 1983. "On the Theory of the Equilibrium Range in the Spectrum of Wind-Generated Gravity Waves". J. Phys. Oceanogr., 13(5), 816-827.
- Kitaigorodskii, S.A., V.P. Krasitskii and M.M. Zaslavskii, 1975. "On Phillips' Theory of Equilibrium Range in the Spectra of Wind-Generated Gravity Waves." J. Phys. Oceanogr., 5, 410-420.
- Komen, G.J., 1984. "The Wave Modelling (WAM) Project: Proposal for the Development and Operational Implementation of a Third Generation Ocean Wave Model." First draft, unpublished manuscript, De Bilt, The Netherlands.
- Komen, G.J., S. Hasselmann and K. Hasselmann, 1984. "On the Existence of a Fully Developed Windsea Spectrum." J. Phys. Oceanogr., 14, 1271-1285.
- Kotsch, W.J., 1983. Weather for the Mariner, 3rd ed. Naval Institute Press, Annapolis, Maryland.
- Lake, B.M. and H.C. Yuen, 1978. "A New Model for Nonlinear Wind Waves. Part I. Physical Model and Experimental Evidence." J. Fluid Mech., 88, 33-62.

- Lake, B.M., H.C. Yuen, H. Rungaldier and W.E. Ferguson, 1977. "Nonlinear Deep-water Waves: Theory and Experiment. Part 2. Evolution of a Continuous Wave Train." J. Fluid Mech., 83, 49-74.
- Large, W.G. and S. Pond, 1981. "Open Ocean Momentum Flux Measurements in Moderate to Strong Winds." J. Phys. Oceanogr., 11(3), 324-336.
- Lazanoff, S.M. and N.M Stevenson, 1975. "An Evaluation of a Hemispheric Operatiuonal Wave Spectral Model." Fleet Numerical Weather Central Technical Report No. 75-3, 102 pp.
- Lazanoff, S.M. and N.M Stevenson, 1978. "A Twenty Year Northern Hemisphere Wave Spectral Climatology," in Turbulent Fluxes Through The Sea Surface, Wave Dynamics and Prediction (Eds. A. Favre and K. Hasselmann). Plenum, New York, 547-563.
- Lazanoff, S.M., N.M. Stevenson and V.J. Cardone, 1973. "A Mediterranean Sea Wave Spectral Model." Fleet Numerical Weather Central Technical Note 72-1, 49 pp.
- LeBlond, P.H., 1984. Final Report of the Investigation on the Storm of October 11-12, 1984 on the West Coast of Vancouver Island. Ministry of the Environment, Victoria, B.C.
- Liu, P.C., D.J. Schwab and I.R. Bennett, 1984. "Comparison of a Two-dimensional Wave Prediction Model with Synoptic Measurements in Lake Michigan." J. Phys. Oceanogr., 14(9), 1514-1518.
- Longuet-Higgins, M.S., 1952. "On the Statistical Distribution of the Heights of Sea Waves." J. Marine Res., 11, 245-266.
- Longuet-Higgins, M.S., 1957. "On the Transformation of a Continuous Spectrum by Refraction." Proc. Camb. Phil. Soc., 53, 226-229.
- Longuet-Higgins, M.S., 1976. "On the Non-linear Transfer of Energy in the Peak of a Gravity Wave Spectrum." Proc. R. Soc. Lond. A, 347, 311-328.
- Longuet-Higgins, M.S., 1980. "On the Distribution of the Heights of Sea Waves: Some Effects of Nonlinearity and Finite Band Width." J. Geophys. Res., 85(C3), 1519-1523.
- Longuet-Higgins, M.S., D.E. Cartwright and N.D. Smith, 1961. "Observations of the Directional Spectrum of Sea Waves Using the Motions of a Floating Buoy," in Ocean Wave Spectra, Prentice-Hall, Englewood Cliffs, 111-132.
- Masuda, A., 1980. "Nonlinear Energy Transfer Between Wind Waves." J. Phys. Oceanogr., 10, 2082-2093.
- Melville, W.K., R.J. Rapp and E. Chan, 1985. "Wave Breaking, Turbulence and Mixing," in The Ocean Surface: Wave Breaking, Turbulent Mixing and Radio Probing, Ed. Y. Toba and H. Mitsuyasu. D. Reidel Publishing Company, Boston, 413-418.

- MEP, 1982. "Development of an Ocean Wave Forecasting System." Unpublished report by The MEP Company, Downsview to The Atmospheric Environment Service, Downsview.
- MEP, 1983. "Testing and Refinement of the Parametric Wind-Wave Model." Unpublished report by The MEP Company, Markham to The Atmospheric Environment Service, Downsview.
- Mihok, W.F. and J.E. Kaitala, 1976. "U.S. Navy Fleet Numerical Weather Central Operational Five-Level Global Fourth-Order Primitive-Equation Model." Monthly Weather Review, 104(12), 1527-1550.
- Miles, J.W., 1957. "On the Generation of Surface Waves by Shear Flows." J. Fluid Mech., 3, 185-204.
- Mitsuyasu, H., 1981. "Directional Spectra of Ocean Waves in Generation Area." To Appear Proc. Directional Wave Spectra Applications '81. Berkeley, 14-16 September, 1981.
- Mitsuyasu, H. and S. Mizuno, 1971. "Experimental Study of Wave Decay Caused by Opposing Winds." Proc. 18th Conf. Coastal Engineering, 37-42.
- Mitsuyasu, H., F. Tasai, T. Suhara, S. Mizuno, M. Ohkuso, T. Honda and K. Rikiishi, 1975. "Observations of the Directional Spectrum of Ocean Waves using a Cloverleaf Buoy." J. Phys. Oceanogr., 5, 750-760.
- Mountain, D.G., 1980. "On Predicting Iceberg Drift." Cold Reg. Sci. Technol., 1, 273-282.
- Nagai, K., 1973. "Runs of the Maxima of the Irregular Sea." Coastal Eng. in Japan, 16, 13-18.
- Nolte, K.G. and F.H. Hsu, 1973. "Statistics of Ocean Wave Groups." Proc. Offshore Tech. Conf., Paper No. OTC 1688, 637-656.
- Nordco, 1983. "Forecast Program Report, Nautilus C-92." Unpublished report prepared for Mobil Oil Canada, Ltd. by NORDCO Ltd., St. John's.
- Ochi, M.K. and C. Tsai, 1983. "Prediction of Occurrence of Breaking Waves in Deep Water." J. Phys. Oceanogr., 13, 2008-2019
- Patterson, M.M., 1974. "Oceanographic Data from Hurricane Camille." Proc. Offshore Tech. Conf., Paper No. OTC 2109.
- Paulson, C.A., 1970. "Representation of Wind Speed and Temperature Profiles in the Unstable Atmospheric Surface Layer." J. Appl. Meteor., 9, 857-861.
- Phillips, O.M., 1957. "On the Generation of Waves by Turbulent Wind." J. Fluid Mech., 2, 417-445.
- Phillips, O.M., 1958. "The Equilibrium Range in the Spectrum of Wind-Generated Waves." J. Fluid Mech., 4, 426-434.

- Phillips, O.M., 1980. "Wave Generation, Propagation and Dissipation Theory." Transcript of Workshop on Wind-wave Hindcasting and Forecasting Models, U.S. Dept. of Commerce, NOAA, 6-32.
- Pierson, W.J. and W. Marks, 1952. "The Power Spectrum Analysis of Ocean-Wave Records." Trans. Amer. Geophys. Un., 33(6), 834-844.
- Pierson, W.J. and L. Moskowitz, 1964. "A Proposed Spectral Form for Fully-Developed Wind Sea Based on the Similarity Theory of S.A. Kitaigorodskii." J. Geophys. Res., 69, 5181-5190.
- Pierson W.J., G. Neumann and R.W. James. 1955. "Practical Methods for Observing and Forecasting Ocean Waves by Means of Wave Spectra and Statistics." U.S. Navy Hydrographic Office Pub. No. 603, 284 pp.
- Pierson, W.J. and L.J. Tick and L. Baer, 1966. "Computer Based Procedures for Preparing Global Wave Forecasts and Wind Data Analyses Capable of Using Wave Data Obtained by a Spacecraft." Sixth Naval Hydrodynamics Symp. Office of Naval Research, Washington, D.C., 499-532.
- Priestley, J.T., 1965. "Correlation Studies of Pressure Fluctuation on the Ground Beneath a Turbulent Boundary Layer." Natl. Bur. Std. NBS Report 8942, U.S. Department of Commerce, 92 pp.
- Queffeulou, P., 1980. "Contribution a l'etude des etats de mer de l'Atlantique Nord. Evaluation et exploitation de mesures satellitaires SEASAT et du modele d'analyse et de prevision DSA 5." Docteur Ingenieur These, Universite de Bretagne Occidentale, 143 pp.
- Resio, D.T., 1980. "Deepwater Models." Proc. of Workshop on Wind-Wave Hindcasting and Forecasting Models, June 3-5, 1980, Gaithersburg, Maryland, 83-140.
- Resio, D.T., 1981. "The Estimation of Wind-Wave Generation in a Discrete Spectra Model." J. Phys. Oceanogr., 11, 510-525.
- Resio, D.T., 1982. "Wave Prediction in Shallow Water." Proc. 14th Annual Offshore Tech. Conf., OTC 4242, Vol. 2, 147-152.
- Resio, D.T., 1986a. "Wave Transformations Related to Nonlinear Fluxes. Part 1: Theory." Submitted to ASCE J. Waterway, Port, Coastal and Ocean Engineering.
- Resio, D.T., 1986b. "Wave Transformations Related to Nonlinear Fluxes. Part 2: Field Comparisons." Submitted to ASCE J. Waterway, Port, Coastal and Ocean Engineering.
- Resio, D.T. and C.L. Vincent, 1976. "Design Wave Information for the Great Lakes, Technical Report No. 1, Lake Erie." U.S. Army Engineer Waterways Experiment Station, Report WES-TR-H-76-1-1, 57 pp. + Appendices.

- Resio, D.T. and C.L. Vincent, 1979. "A Comparison of Various Numerical Wave Prediction Techniques." Proc. 11th Annual Offshore Technology Conf., OTC 3642, 2471-2478.
- Roberts, K.V. and N.O. Weiss, 1966. "Convective Difference Schemes." Math. of Computation, 20, 272-299.
- Røed, L.P. and J. Guddal, Undated. "Calibration Experiments with the Norwegian Wave Forecasting Model. Part A - Main Report." Unpublished Manuscript, Project Report: Wave Data for Wave Power Plant Projects, Det Norske Meteorologiske Institutt, 22 pp. + Figures.
- Ross, D.B., 1976. "A Simplified Model for Forecasting Hurricane Generated Waves (Abstract)." Bull. A.M.S., January, 113. Presented at Conferences on Atmospheric and Oceanic Waves, Seattle, Washington, March 29 to April 2, American Meteorological Society.
- Ross, D.B. and V. Cardone, 1978. "A Comparison of Parametric and Spectral Hurricane Wave Prediction Products," in Turbulent Fluxes Through the Sea Surface, Wave Dynamics, and Prediction (Ed. A. Favre and K. Hasselmann). Plenum, New York, 647-665.
- Rye, H., 1974. "Wave Group Formation Among Storm Waves." Proc. 14th Coastal Eng. Conf., 164-183.
- St. Denis, M. and W.J. Pierson, 1953. "On the Motion of Ships in Confused Seas." Trans. NAME, 61, 280-357.
- Sanders, P., 1976. "A Growth-Stage Scaling Model for the Wind-Driven Sea." Sonderdruck aus der Deutsche Hydrographische Zeitschrift, Band 29.
- Sarpkaya, T. and M. Isaacson, 1981. Mechanics of Wave Forces on Offshore Structures. Van Nostrand Reinhold Co., New York, 651 pp.
- Schwab, D.J., J.R. Bennett, P.C. Liu and M.A. Donelan, 1984. "Application of a Simple Numerical Wave Prediction Model to Lake Erie." J. Geophys. Res., 89(C3), 3586-3592.
- Schwab, D.J., J.R. Bennett and E.W. Lynn, 1986. "A Two-dimensional Lake Wave Prediction System." Environmental Software, 1(1), 4-9.
- Seaconsult, 1984. "Simulations of Oil Spill Trajectory Motion for the Hibernia P-15 Site." Unpublished report prepared for Mobil Oil Canada, Ltd. by Seaconsult Limited, St. John's.
- Seakem and Seaconsult, 1983. "A Wave Climate Study of Northern British Columbia Coast." Progress Report No. 3, DSS contract no. 51SS-FP-802-2-2034. Prepared by Seakem Oceanography, Sidney, BC and Seaconsult Marine Research Ltd., Vancouver, BC for the Marine Environmental Data Service, Ottawa.

- Sell, W. and K. Hasselmann, 1972. "Computations of Non-Linear Energy Transfer for JONSWAP and Empirical Wind Wave Spectra." Unpublished Manuscript, Inst. Geophys., University of Hamburg.
- Smith, S.D., 1980. "Wind Stress and Heat Flux Over the Ocean in Gale Force Winds." J. Phys. Oceanogr., 10, 709-726.
- Smith, S.D., 1981. "Factors for Adjustment of Wind Speed Over Water to a 10-metre Height." Bedford Institute of Oceanography, Report Series BI-R-81-3.
- Snyder, R.L. and C.S. Cox, 1966. "A Field Study of the Wind Generation of Ocean Waves." J. Marine Res., 24, 141-178.
- Snyder, R.L., R.B. Long, F.W. Dobson, and J.A. Elliott, 1978. "The Bight of Abaco Pressure Experiment," in Turbulent Fluxes Through the Sea Surface, Wave Dynamics, and Prediction (Ed. A. Favre and K. Hasselman). Plenum, New York, 433-444.
- Snyder, R.L., F.W. Dobson, J.A. Elliott and R.B. Long, 1981. "Array Measurements of Atmospheric Pressure Fluctuations Above Surface Gravity Waves." J. Fluid Mech., 102, 1-59.
- Stacy, R.A., 1973. "High-Frequency Gravity Waves in Hurricanes." MS Thesis, New York University.
- Stewart, R.H., 1980. "Ocean Wave Measurement Techniques." Air-Sea Interaction, Instruments and Methods (Ed. Dobson, F., L. Hasse and R. Davis,). Plenum, New York, 447-470.
- SWAMP Group, 1985. Ocean Wave Modeling. Plenum, New York.
- SWIM Group, The (Bouws, E., J. Ephraums, J. Ewing, P. Francis, H. Guenther, P. Janssen, G. Komen, W. Rosenthal, W. de Voogt), 1985. "Shallow Water Intercomparison of Wave Models Parts I, II, III," in The Ocean Surface: Wave Breaking, Turbulent Mixing and Radio Probing (Ed. Y. Toba and H. Mitsuyasu). Reidel Publishing Company, Dordrecht, 201-220.
- Tayfun, M.A., 1981. "Distribution of Crest-to-Trough Wave Heights." ASCE J. Waterway, Port, Coastal and Ocean Div., 107(WW3), 149-158.
- Toba, Y., 1978. "Stochastic form of the Growth of Wind Waves in a Single-Parameter Representation with Physical Implications." J. Phys. Oceanogr., 8, 494-507.
- Toba, Y., S. Karvai and P.S. Joseph, 1985. "The TOHOKU Wave Model," in Ocean Wave Modeling. Plenum, New York, 201-210.
- Verret, R., 1984. "A Matter of Resolution." CMC Info., II(1), 2-31.
- Vincent, C.L. and D.T. Resio, 1979. "A Discussion of Wave Prediction in the Northwest Atlantic Ocean," in Marine Forecasting, Predictability, and Modelling in Ocean Hydrodynamics. Elsevier, 71-90.

- Walsh, E.J., E.A. Uliana and B.S. Yapple, 1978. "Ocean Wave Heights Measured by a High-Resolution Pulse-Limited Radar Altimeter." Boundary-Layer Meteorology, 13, 263-276.
- Walsh, E.J., D.W. Hancock, D.E. Hines, and J.E. Kenney, 1981. "Remote Sensing of Directional Wave Spectra Using Surface Contour Radar." Presented at Directional Wave Spectra Applications '81, 14-16 Sept., Berkeley.
- Ward, E.G., 1974. "Ocean Data Gathering Program - An Overview." Proc. Offshore Tech. Conf., Paper OTC 2108-B.
- Webb, D.J., 1978. "Nonlinear Transfer Between Sea Waves." Deep-Sea Res., 25, 279-298.
- Wilson, B.W., 1963. "Deep Water Wave Generation by Moving Wind Systems." Trans. Am. Soc. Civil Eng., 128, Paper No. 3416.
- Wilson, J.R. and W.F. Baird, 1972. "A Discussion of Some Measured Wave Data." Proc. 13th Coastal Eng. Conf., Vancouver.
- Yamada, T., 1976. "On the Similarity Functions A, B, and C of the Planetary Boundary Layer." J. Atmos. Sci., 33(5), 781-793.
- Yanenko, N.N., 1971. The Method of Fractional Steps. Springer.

APPENDICES

Appendix 4.1

Non-Dimensional Parameters

The literature of wind-wave modelling makes frequent reference to several non-dimensional parameters. For a convenient summary, the most common ones are defined here:

Non-Dimensional Fetch: $\hat{x} = \frac{gF}{U_{10}^2}$

Non-Dimensional Peak Frequency: $\nu = \frac{U_{10} f_p}{g}$

Non-Dimensional Wave Height: $\hat{H} = \frac{gH_{m0}}{U_{10}^2} = \frac{gH_s}{U_{10}^2}$

Non-Dimensional Time: $\tau = \frac{gt}{U_{10}}$

Non-Dimensional Total Energy: $\epsilon = \frac{g^2 m_0}{U_{10}^2} = \frac{\hat{H}^2}{16}$

Non-Dimensional Period: $\hat{T} = \frac{gT}{2\pi U_{10}}$

where g is gravitational constant H_{m0} is significant wave height

F is fetch length t is time

U_{10} is 10 m wind speed m_0 is zero'th order spectral moment
($\int E(f) df$)

f_p is peak frequency T is wave period

Appendix 4.2
List of Contacts for Wave Model Information

Reference Key	Address	Contact	Model(s)
BAIRD	W.F. Baird & Assoc. 150-38 Antares Dr. Ottawa, ON K2E 7V2	J. Readshaw (613) 225-6560	SMB
BMO	Meteorological Office Met O 26, Room R204 London Road Bracknell, Berks. U.K. RG12 2SZ	Dr. P.E. Francis 0344 (Bracknell) 420242 ext. 2698	BMO
DHI	Danish Hydraulics Inst. Agern Alle 5 DK-2970 Horsholm Denmark	Torben Sorensen Director	S-20
DM, Paris	Direction de la Meteorologie Nationale Ministere des Travaux Publics et des Transports Secretariat General a l'Aviation Civile Paris, France	E. Devillaz	DSA-5
FNOC	The Fleet Numerical Oceanography Center Data Integration Dept. Monterey, CA 93943	Ms. L.F. Zambresky	SOWM; GSOWM
GLERL	Great Lakes Environ- mental Research Lab. 2300 Washtenaw Ave. Ann Arbor, Michigan 48104	D.J. Schwab	Donelan's Model
ISDGM	Istituto per lo Studio della Dinamica delle Grandi Masse Consiglio Nazionale delle Richerche 30125 Venice, Italy	L. Caveleri	VENICE
KNMI	KNMI P.O. Box 201 3730 AE De Bilt The Netherlands	Dr. G.J. Komen	GONO

Reference Key	Address	Contact	Model(s)
MAX-PLANK	Max-Plank Institut Fuer Meteorologie Bundesstr. 55 2000 Hamburg 13 Fed. Rep. of Germany	Prof. K. Hasselmann Telex Nr. 211092	Hasselmann's Model;NORSWAM; HYPA;HYPAS; WAM
MEP	The MEP Company 100-7050 Woodbine Ave. Markham, ON L3R 4G8	Dr. B. Weisman (416) 477-0870	SMB (METOC)
MRI	Meteorological Research Institute Ibarakiken 305 Japan	T. Uji	MRI
NMI	Norwegian Met. Instit. Vervarslinga pa Vestlandet Allegt. 70 N-5000 Bergen, Norway	J. Guddal M. Reistad	WINCH; Original Norwegian Model
NYU	CUNY Institute of Marine and Atmospheric Sciences City College of New York New York 10031	W.J. Pierson	PTB
Oceanweather	Oceanweather Inc. 1-5 River Road Cos Cob, CT 06807	Dr. V. Cardone (203) 661-3091	ODGP; SAIL
OCTI	Offshore & Coastal Technologies Inc. 911 Clay Street Vicksburg, MS 39180	Dr. D.T. Resio (601) 638-8484	WAVAD
Seaconsult	Seaconsult Marine Research Ltd. 820-1200 W73rd Ave. Vancouver, BC V6P 6G5	Dr. D.O. Hodgins (604) 266-9135	WAVAD;SPECREF; SMB;Donelan's

Appendix 6.1

Comparison of Rowan Gorilla 10-m Reduced Winds With CMC Forecasts.

Time-series plots of wind speed and direction

00,03,06,09 h forecasts: September, October, November 1985
12,15,18,21 h forecasts: September, October, November 1985
21,24,27,30 h forecasts: September, October, November 1985

Time-series plots of pressure and air temperature

00,03,06,09 h forecasts
12,15,18,21 h forecasts September, October, November 1985
21,24,27,30 h forecasts

Scatterplots and error statistics

00 h forecast
12 h forecast September to November 1985 inclusive
24 h forecast

Verification Tables

00 h forecast
12 h forecast September to November 1985 inclusive
24 h forecast

Monthly error statistics

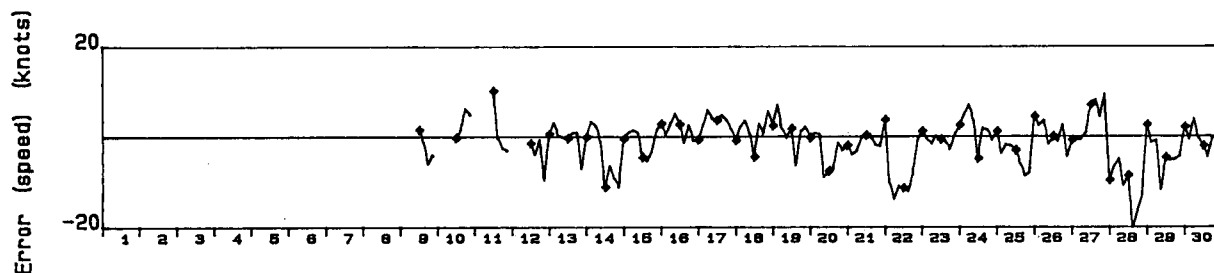
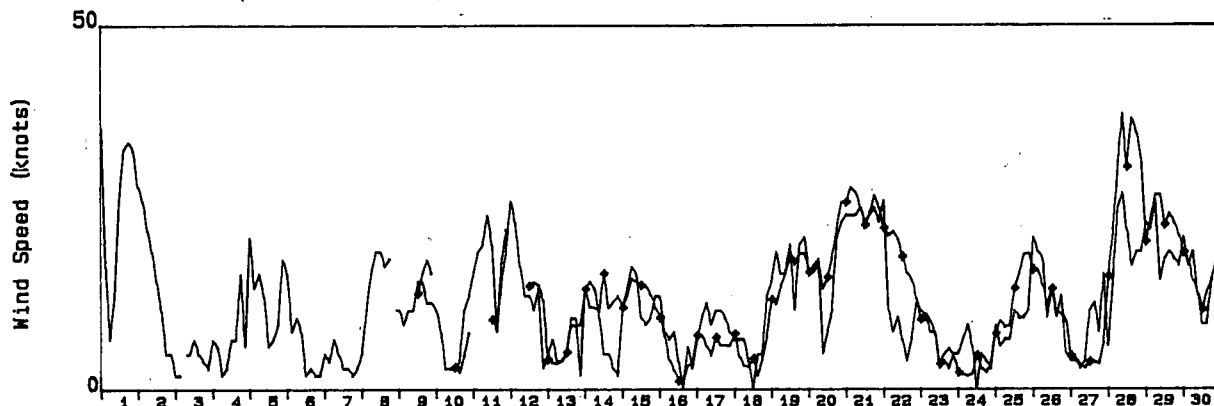
00 h forecast
12 h forecast September, October, November 1985
24 h forecast

Wind Rate and Direction

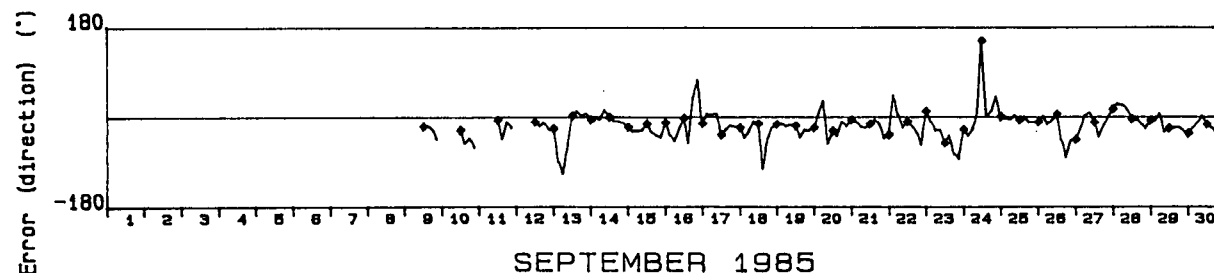
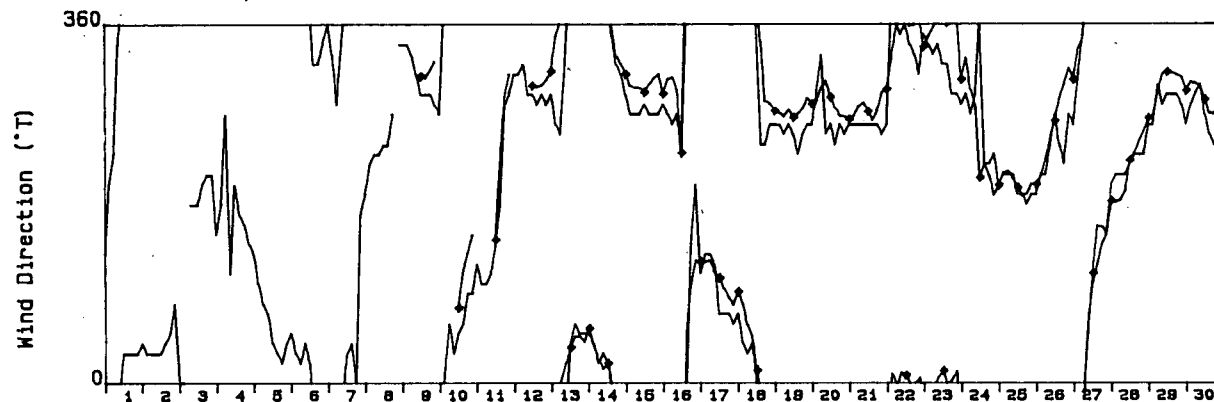
Rowan Gorilla, Olympia 0-51

Grid Point : 5

Forecast periods are (0, 3, 6, 9)



Forecast periods are (0, 3, 6, 9)



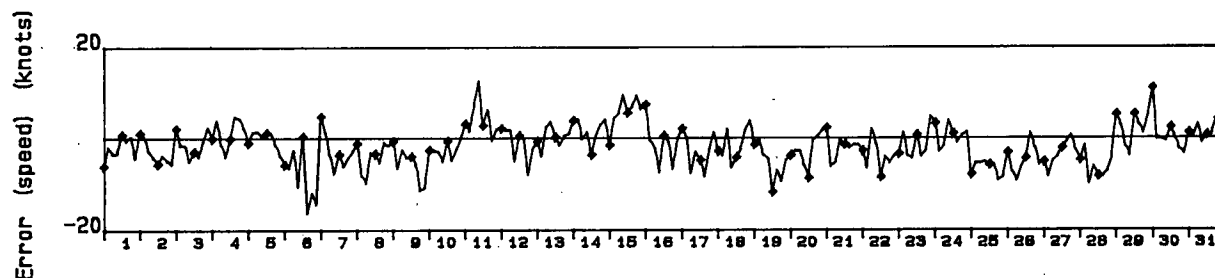
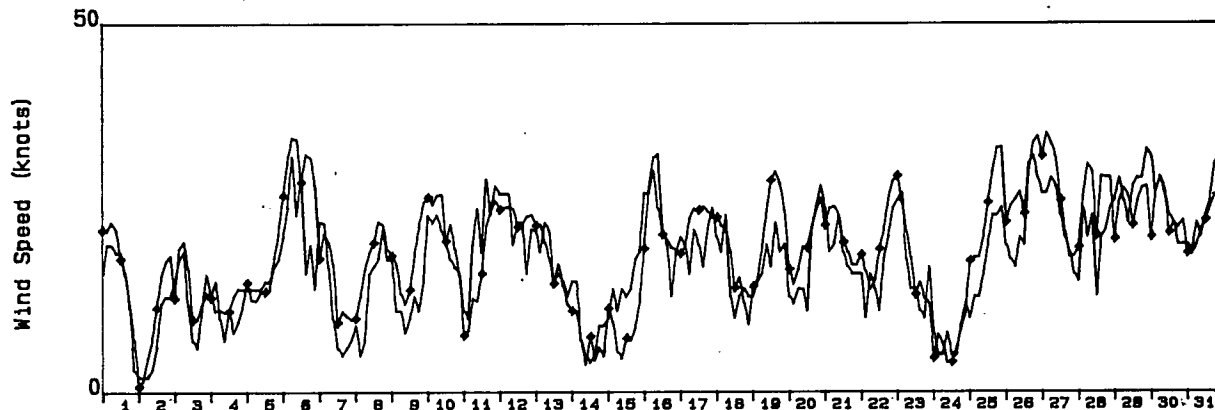
SEPTEMBER 1985

Wind Rate and Direction

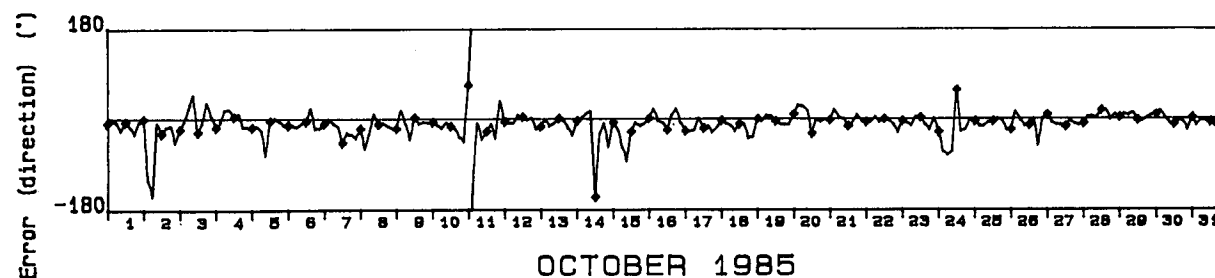
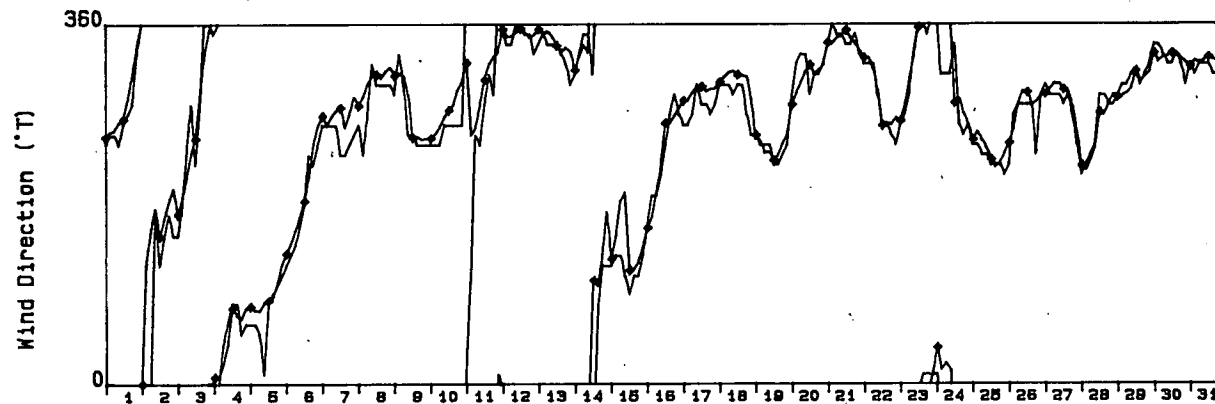
Rowan Gorilla, Olympia 0-51

Grid Point : 5

Forecast periods are (0, 3, 6, 9)



Forecast periods are (0, 3, 6, 9)



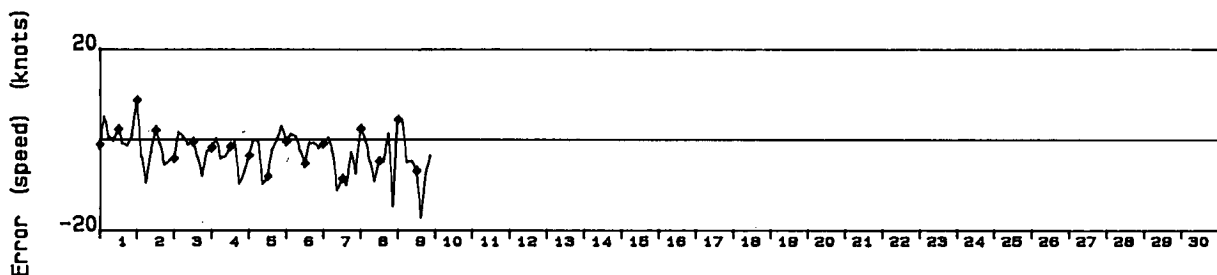
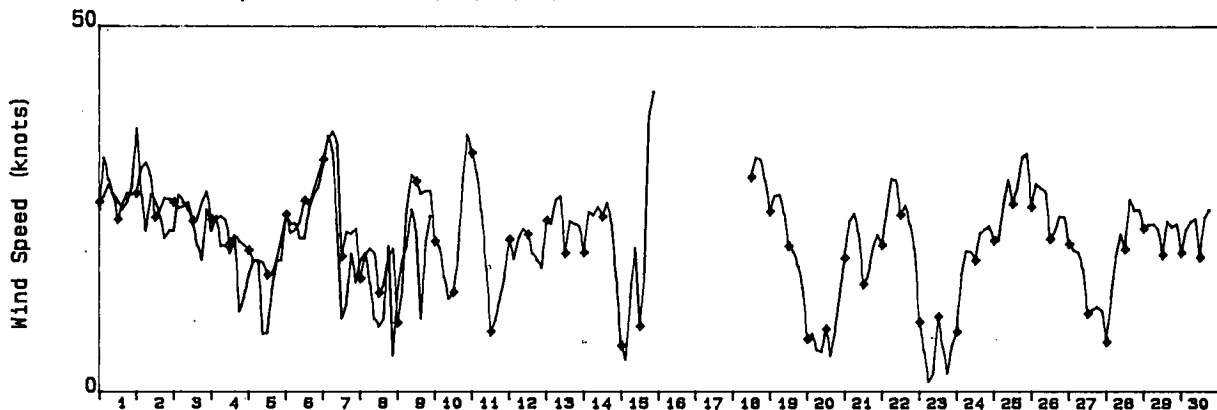
OCTOBER 1985

Wind Rate and Direction

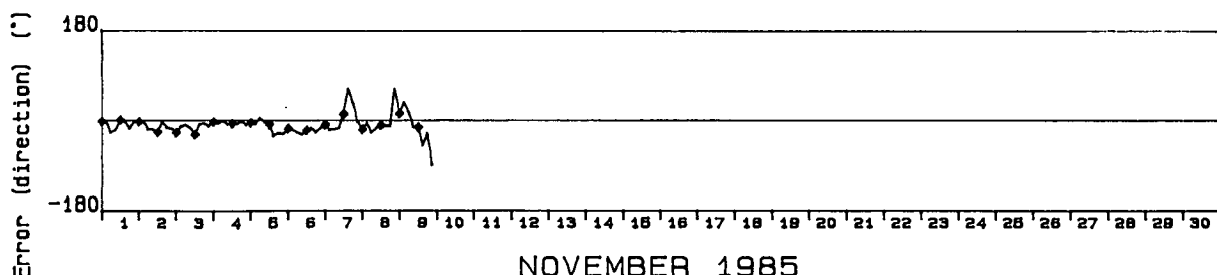
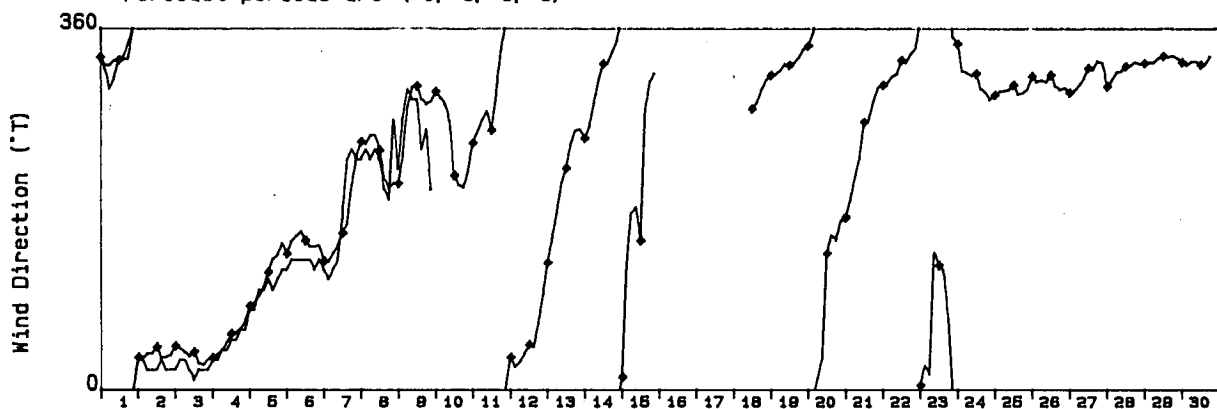
Rowan Gorilla, Olympia 0-51

Grid Point : 5

Forecast periods are (0, 3, 6, 9)



Forecast periods are (0, 3, 6, 9)



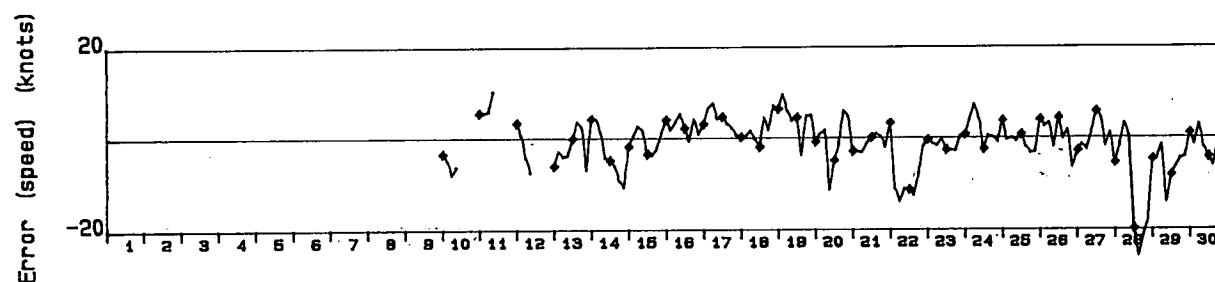
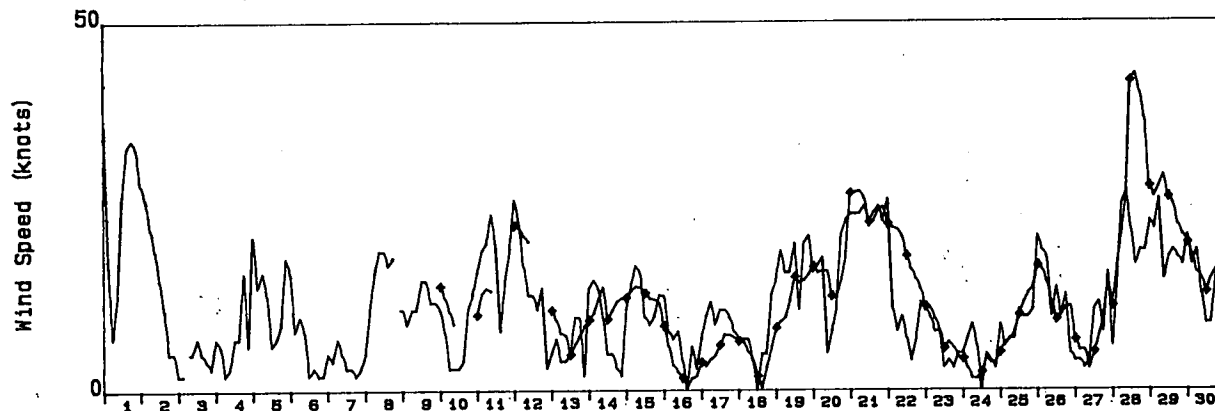
NOVEMBER 1985

Wind Rate and Direction

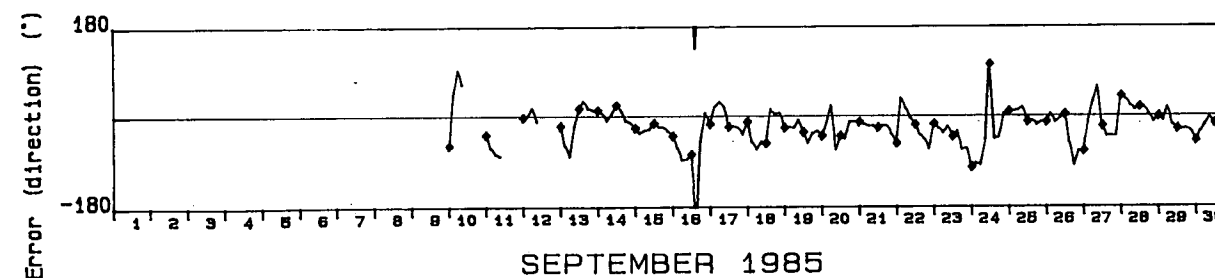
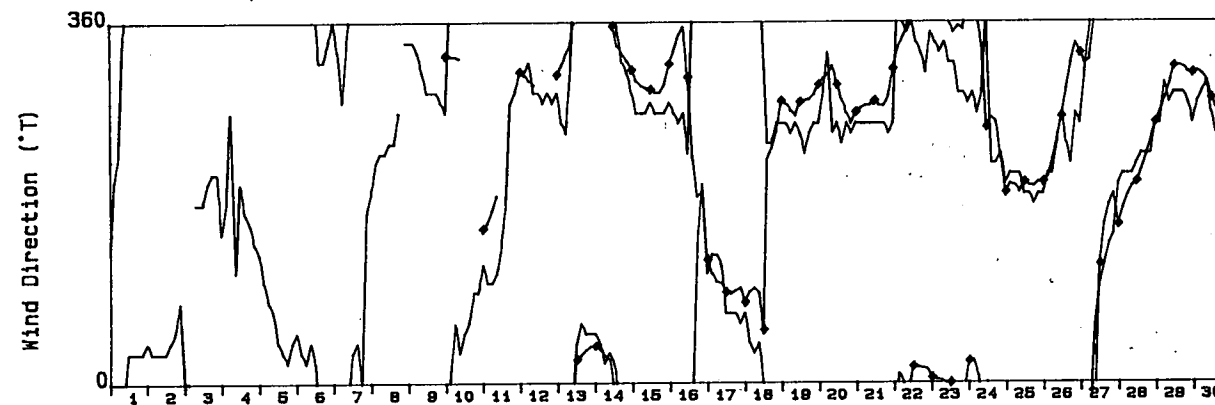
Rowan Gorilla, Olympia 0-51

Grid Point : 5

Forecast periods are (12, 15, 18, 21)



Forecast periods are (12, 15, 18, 21)



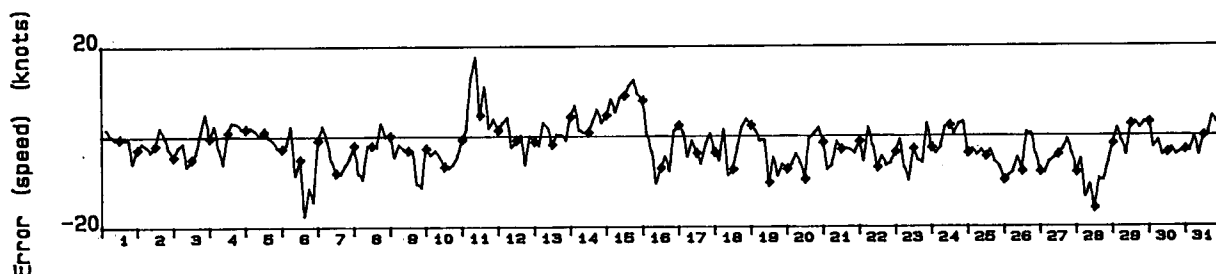
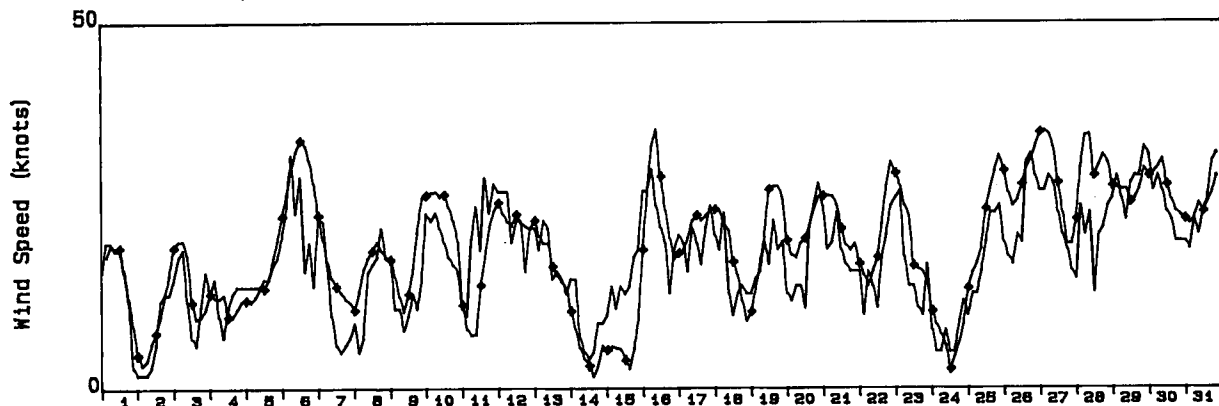
SEPTEMBER 1985

Wind Rate and Direction

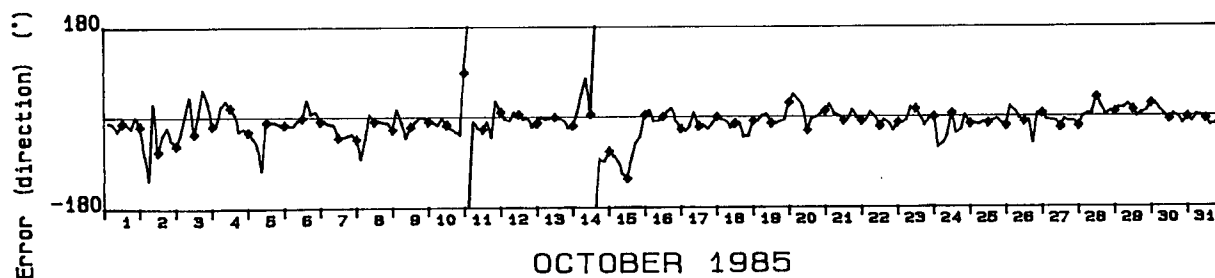
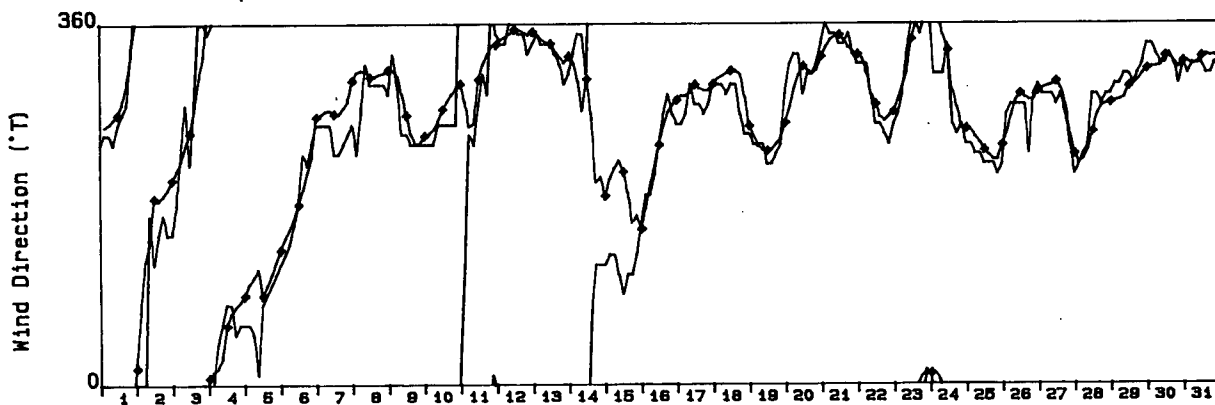
Rowan Gorilla, Olympia 0-51

Grid Point : 5

Forecast periods are (12, 15, 18, 21)



Forecast periods are (12, 15, 18, 21)



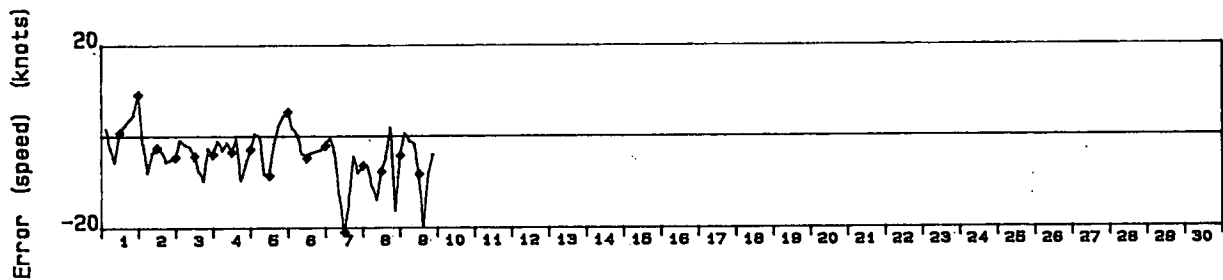
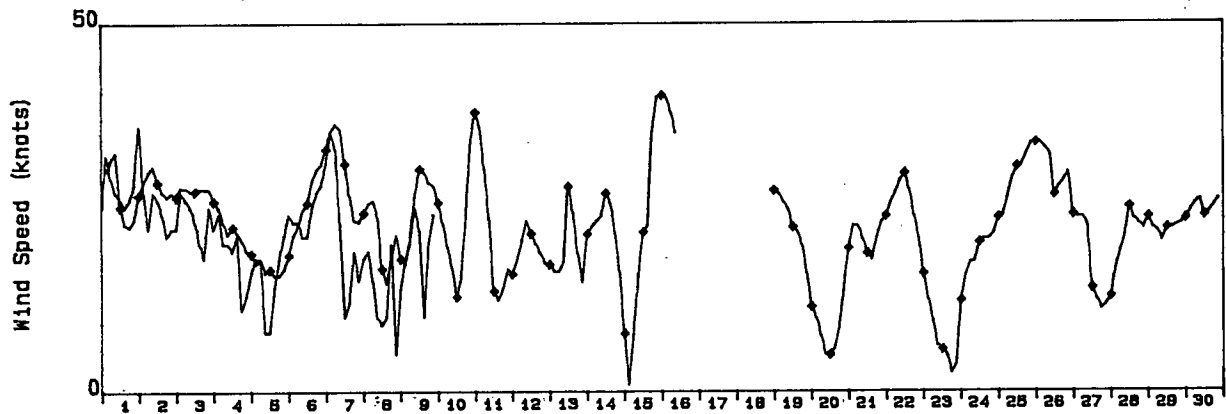
OCTOBER 1985

Wind Rate and Direction

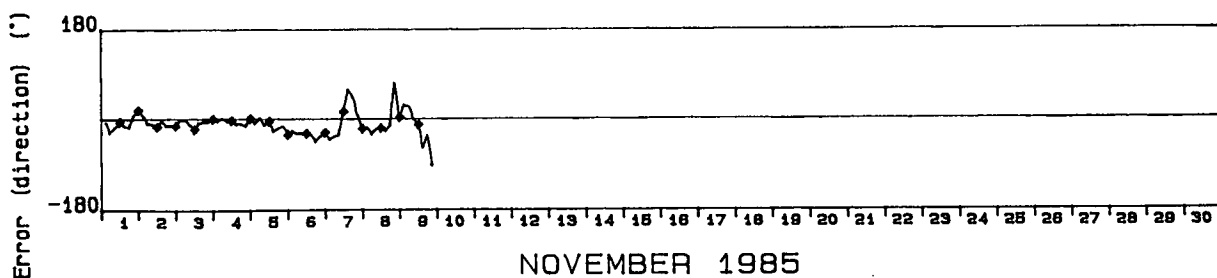
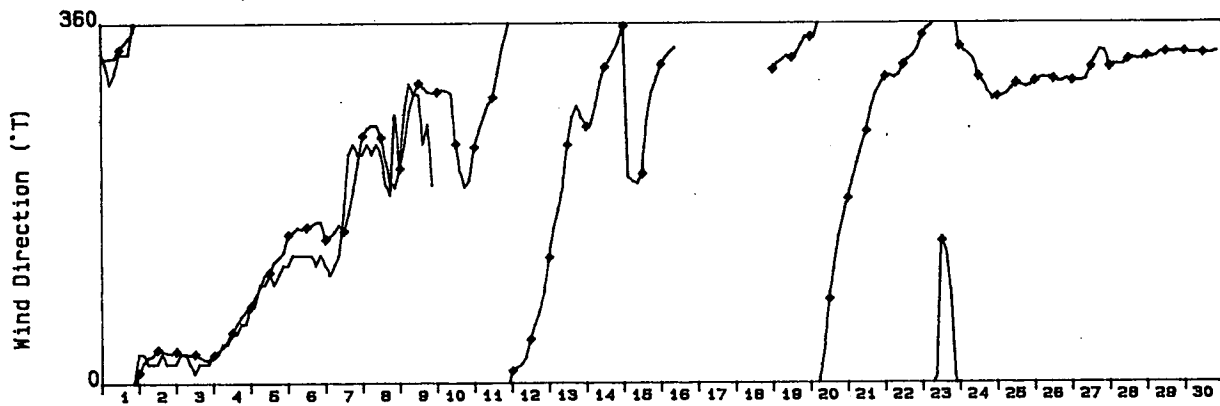
Rowan Gorilla, Olympia 0-51

Grid Point : 5

Forecast periods are (12, 15, 18, 21)



Forecast periods are (12, 15, 18, 21)



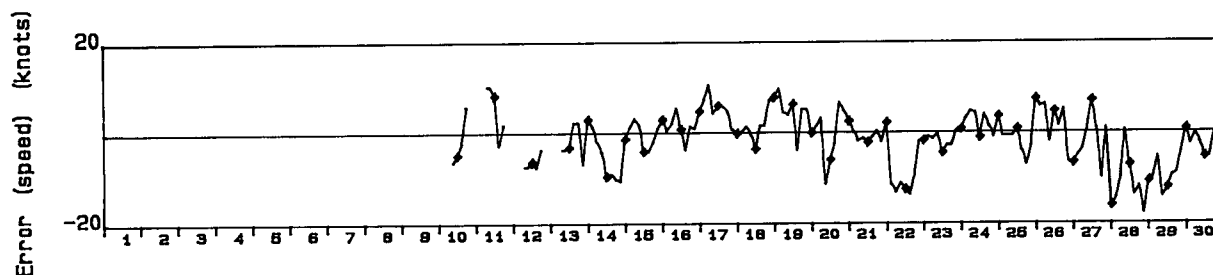
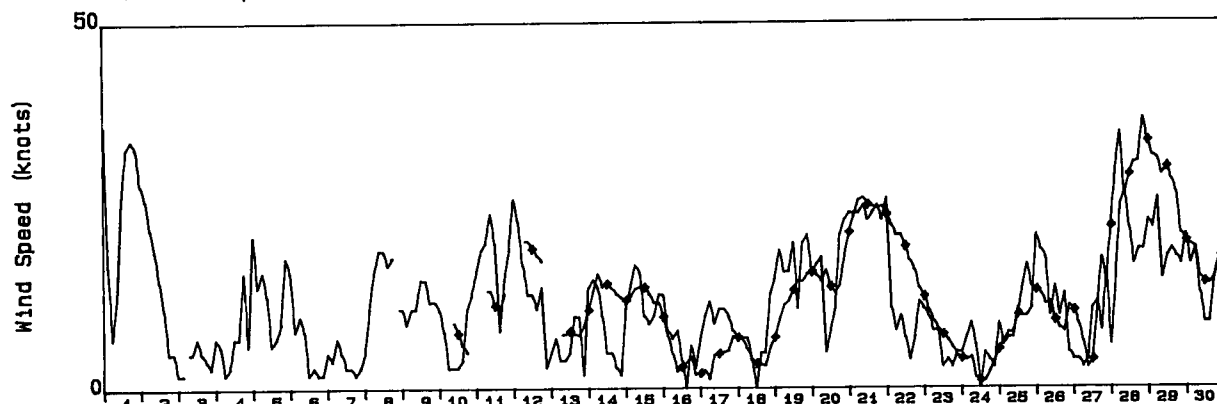
NOVEMBER 1985

Wind Rate and Direction

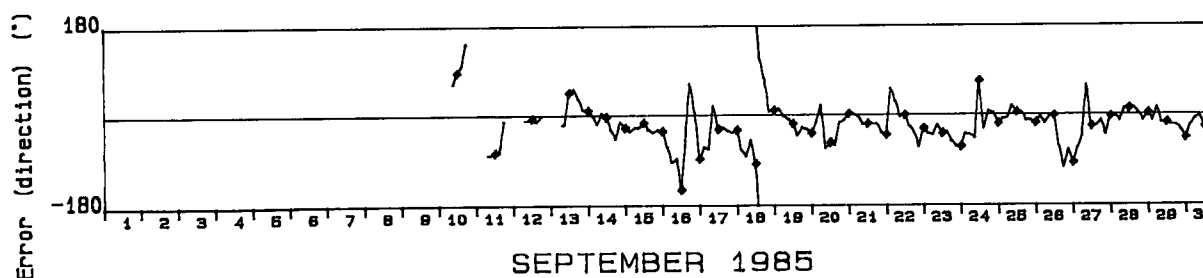
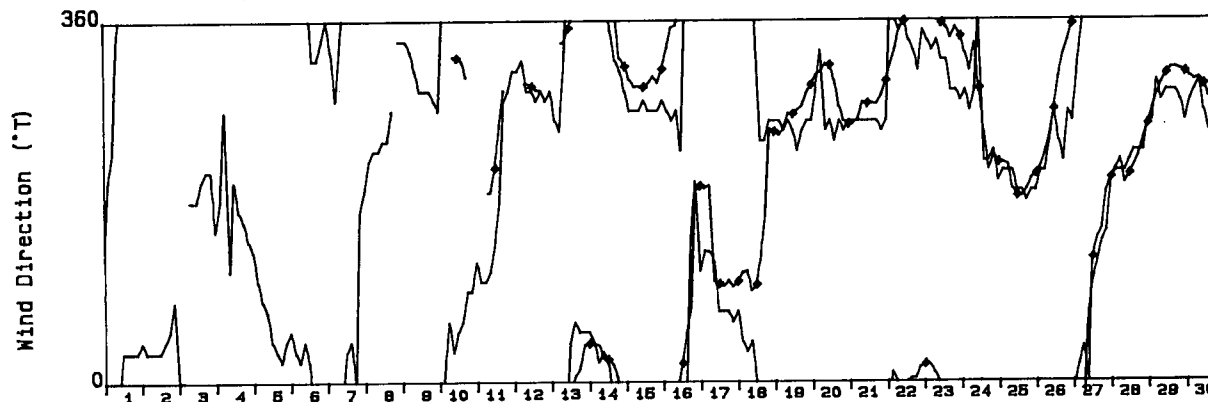
Rowan Gorilla, Olympia O-51

Grid Point : 5

Forecast periods are (21, 24, 27, 30)



Forecast periods are (21, 24, 27, 30)



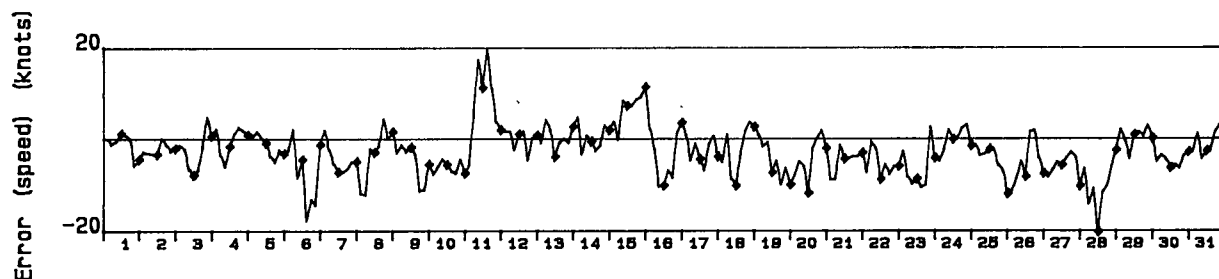
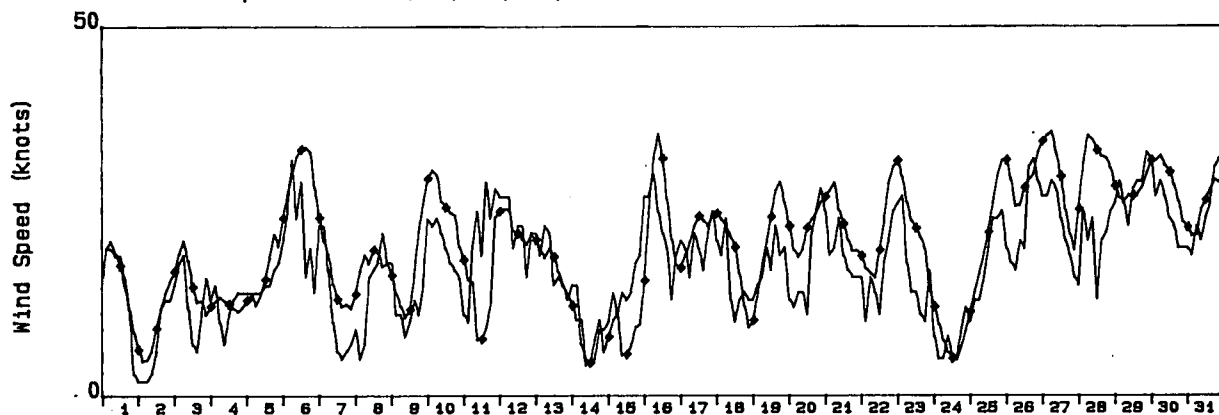
SEPTEMBER 1985

Wind Rate and Direction

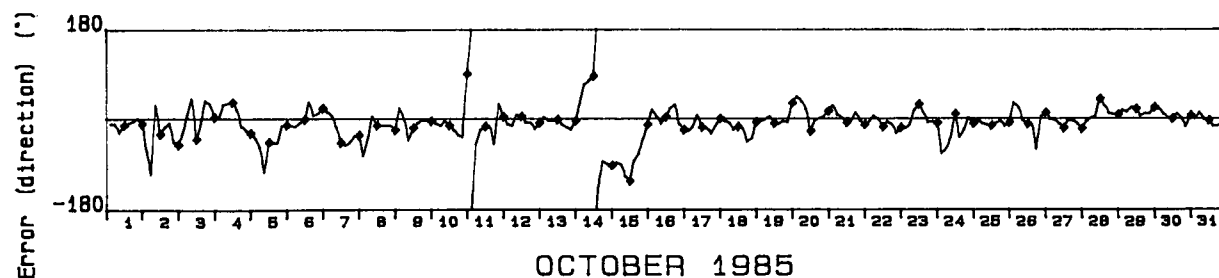
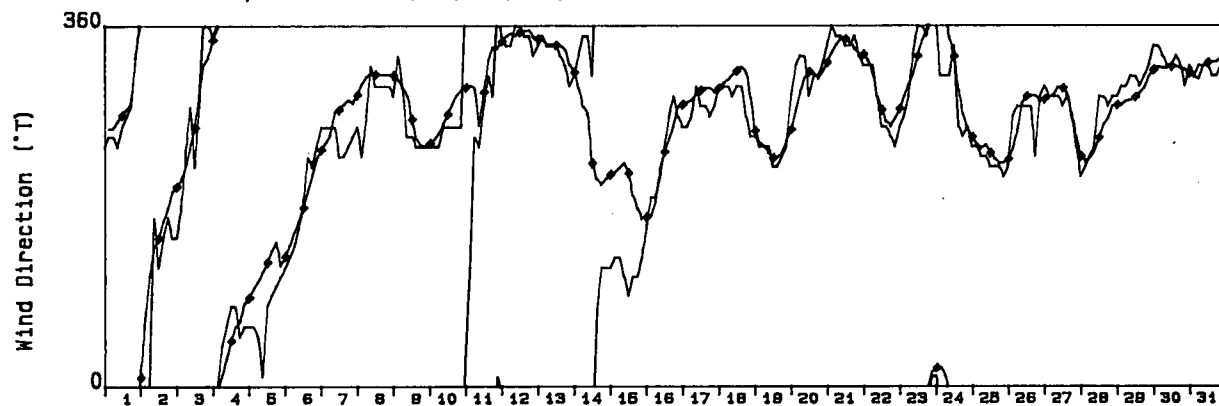
Rowan Gorilla, Olympia 0-51

Grid Point : 5

Forecast periods are (21, 24, 27, 30)



Forecast periods are (21, 24, 27, 30)



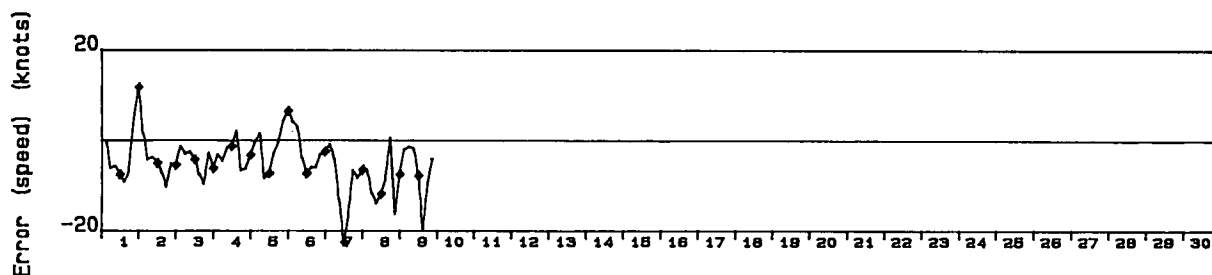
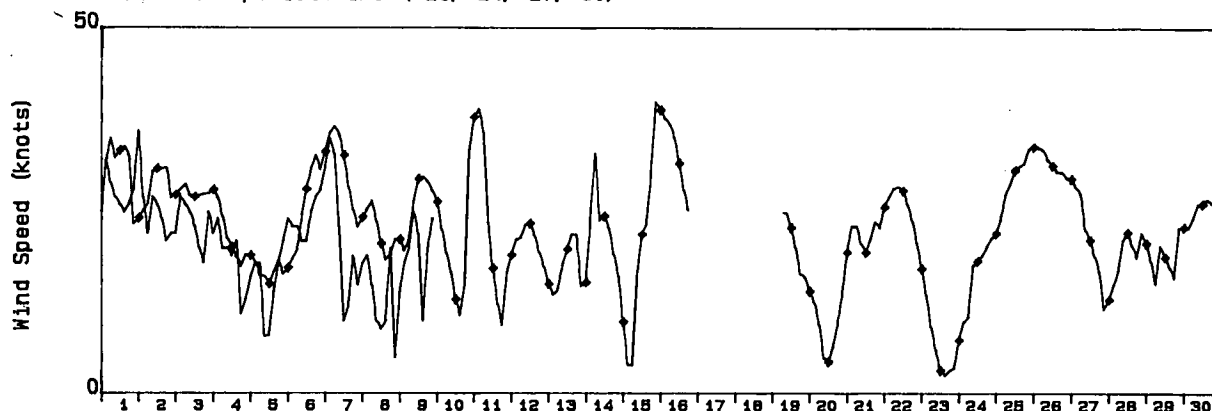
OCTOBER 1985

Wind Rate and Direction

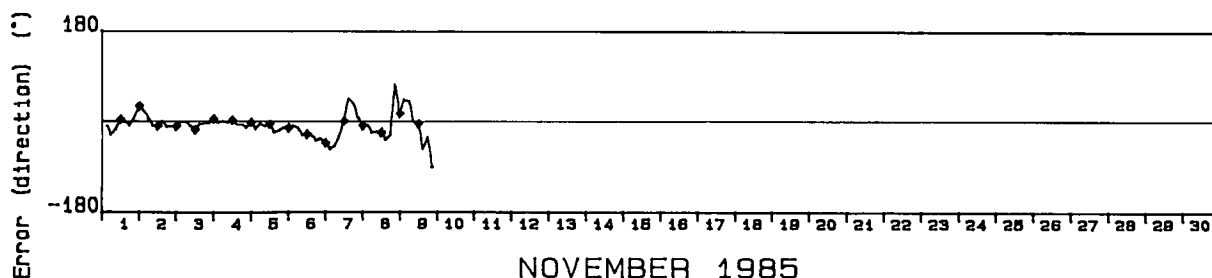
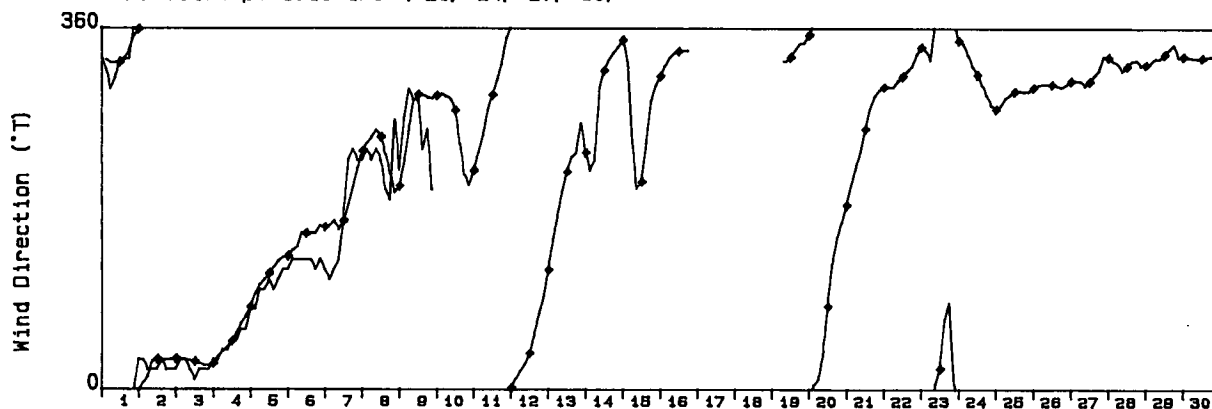
Rowan Gorilla, Olympia O-51

Grid Point : 5

Forecast periods are (21, 24, 27, 30)



Forecast periods are (21, 24, 27, 30)



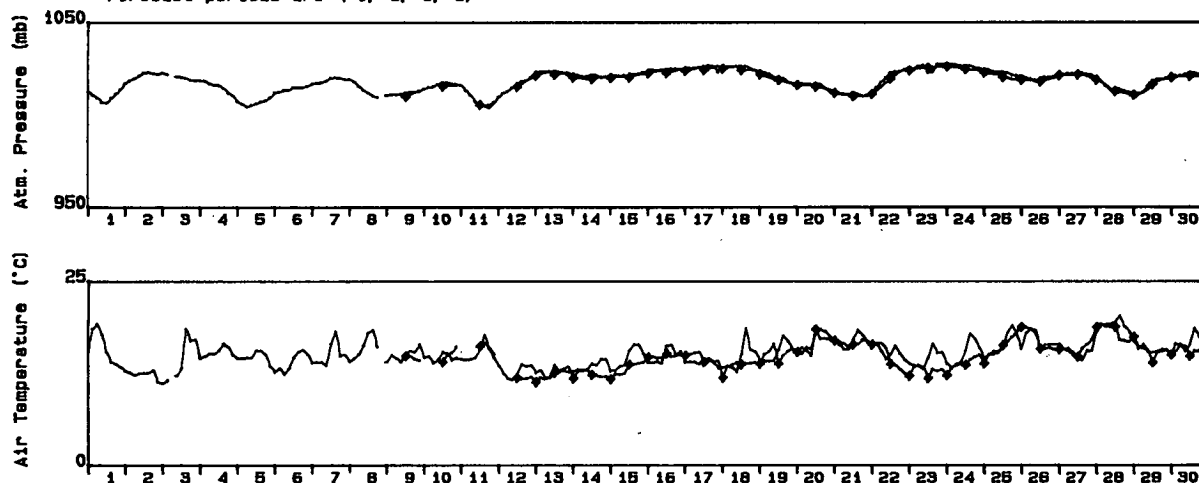
NOVEMBER 1985

Pressure and Air Temperature

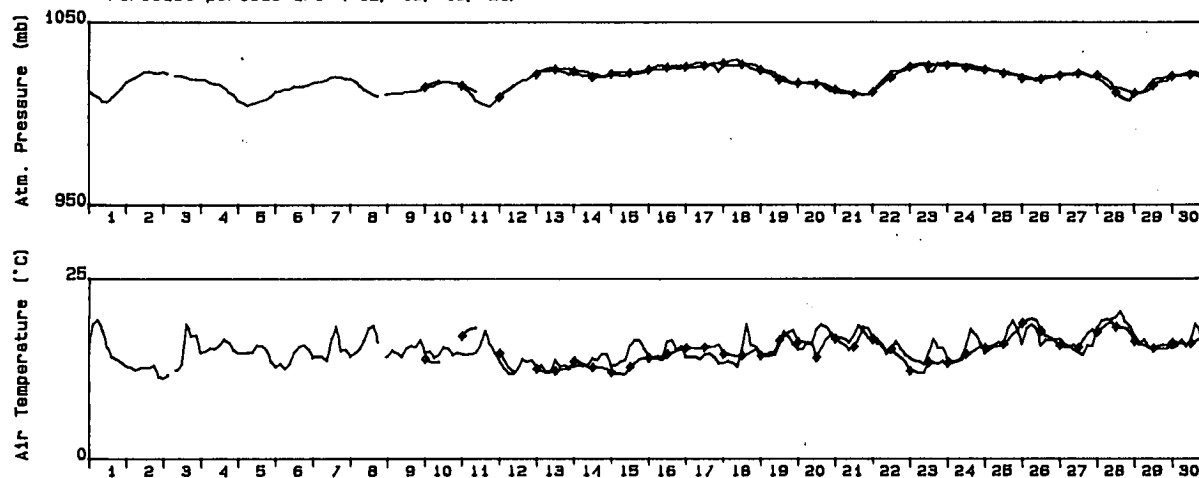
Rowan Gorilla, Olympia 0-51

Grid Point : 5

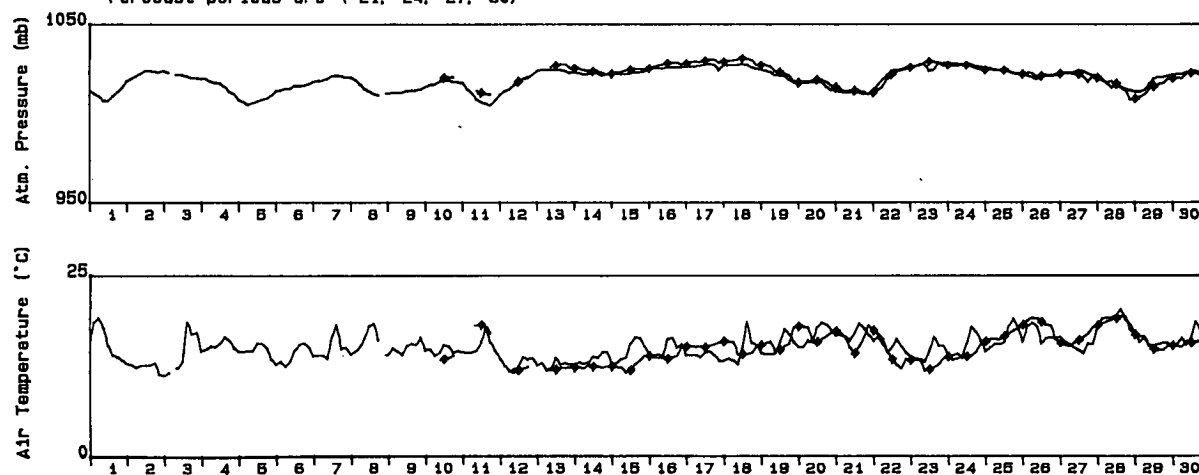
Forecast periods are (0, 3, 6, 9)



Forecast periods are (12, 15, 18, 21)



Forecast periods are (21, 24, 27, 30)



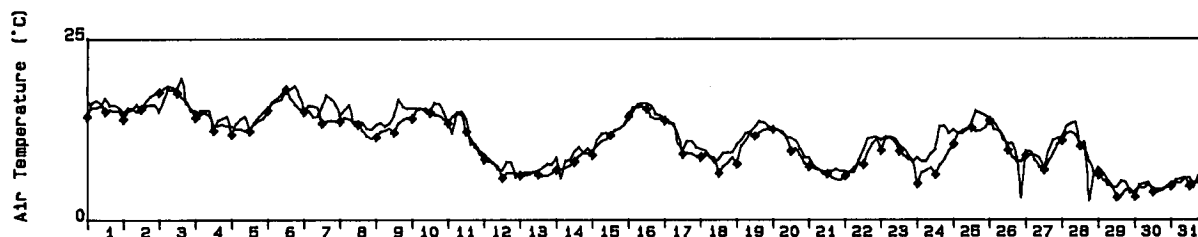
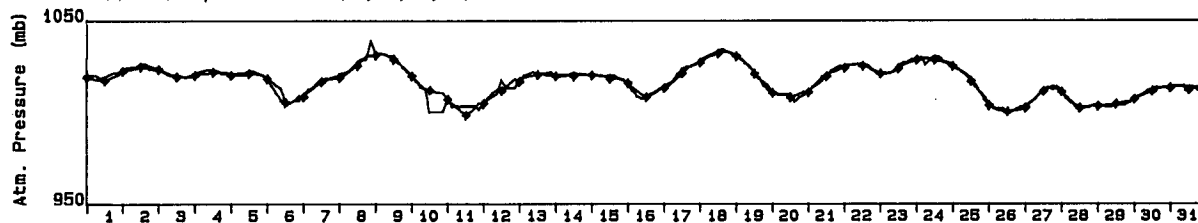
SEPTEMBER 1985

Pressure and Air Temperature

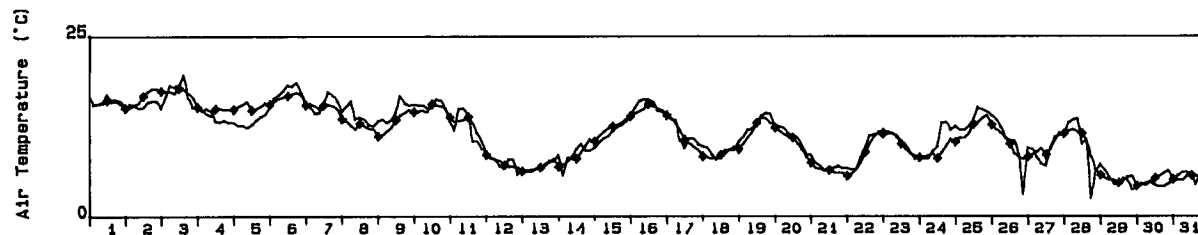
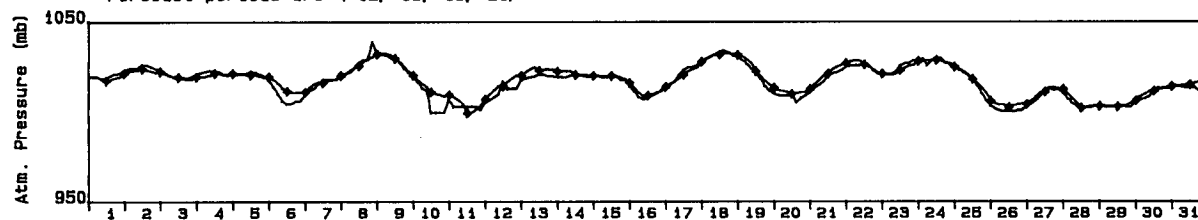
Rowan Gorilla, Olympia 0-51

Grid Point : 5

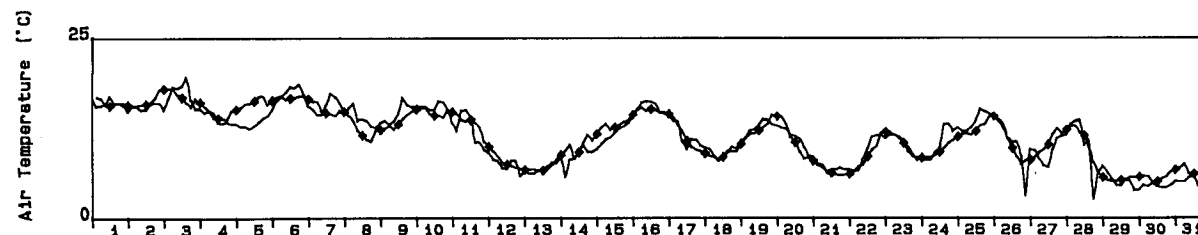
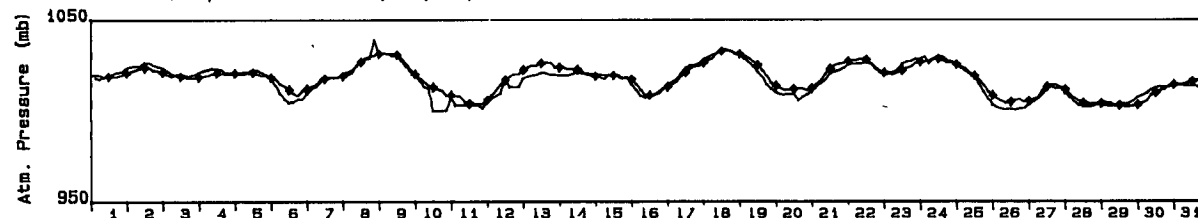
Forecast periods are (0, 3, 6, 9)



Forecast periods are (12, 15, 18, 21)



Forecast periods are (21, 24, 27, 30)



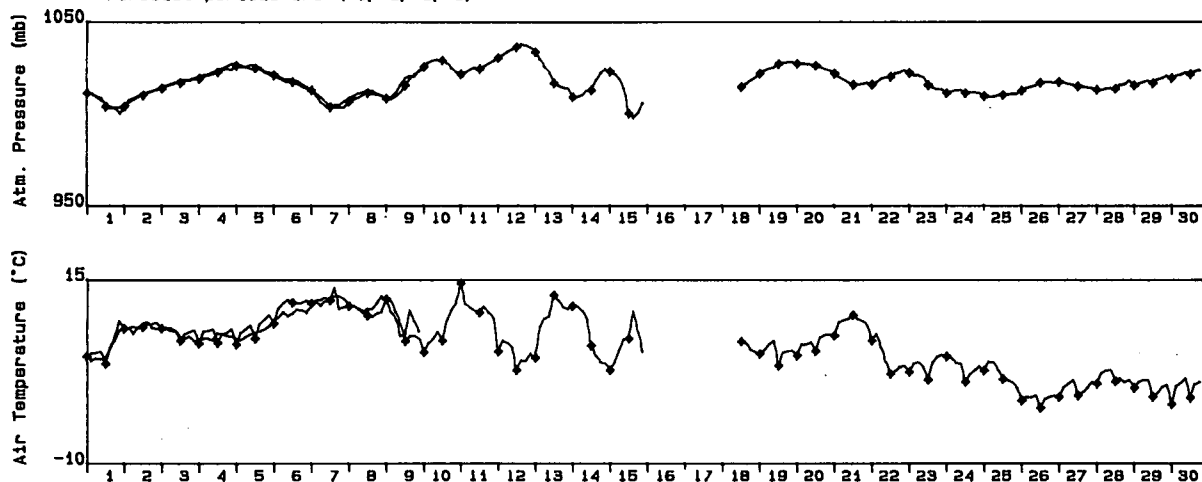
OCTOBER 1985

Pressure and Air Temperature

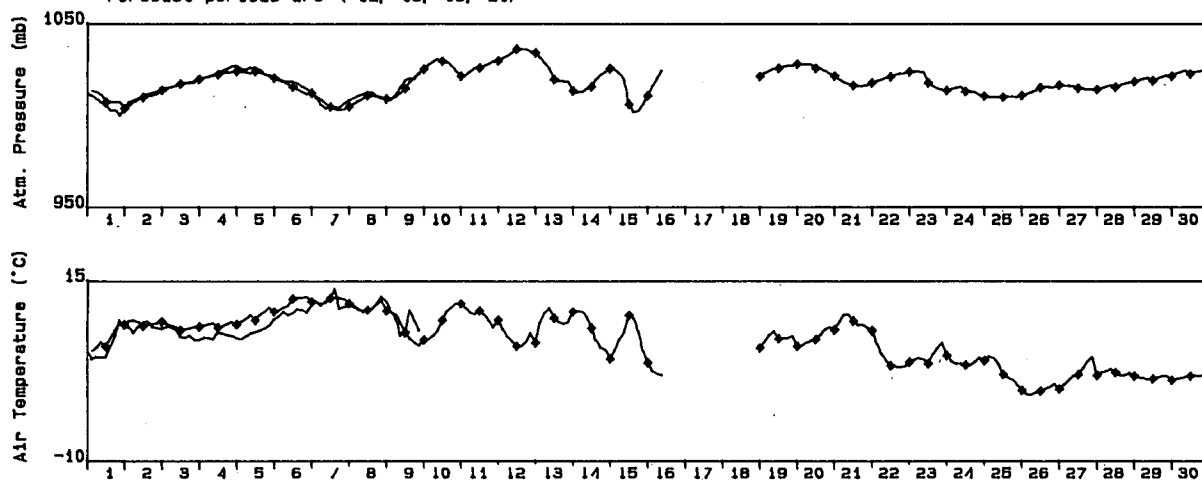
Rowan Gorilla, Olympia 0-51

Grid Point : 5

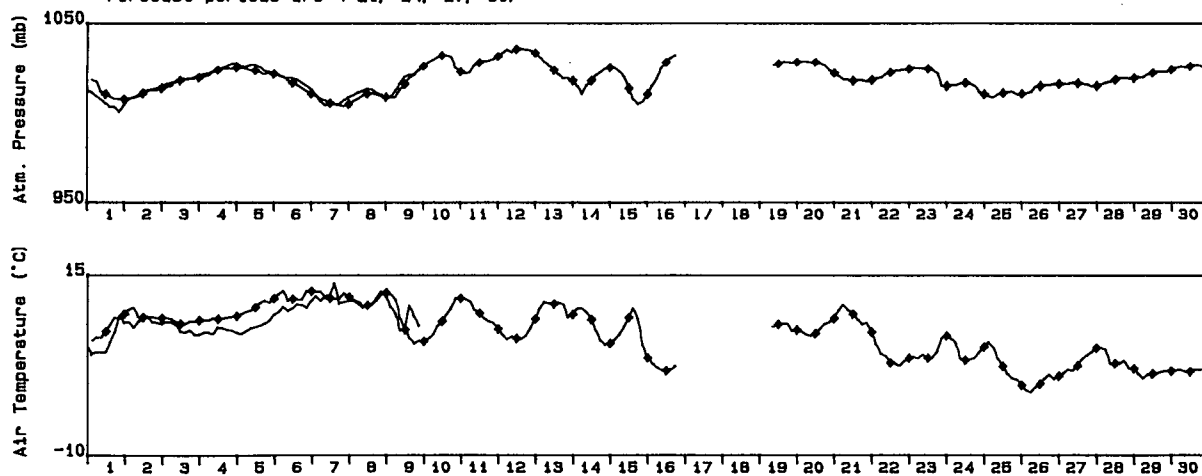
Forecast periods are (0, 3, 6, 9)



Forecast periods are (12, 15, 18, 21)



Forecast periods are (21, 24, 27, 30)

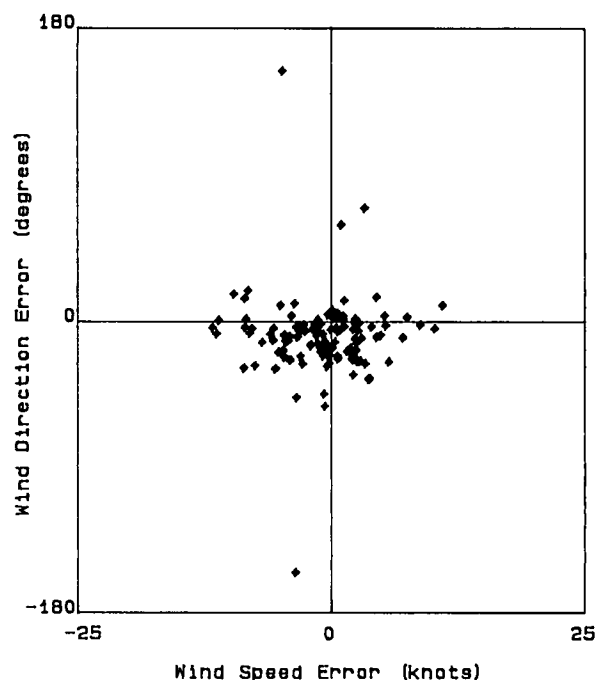
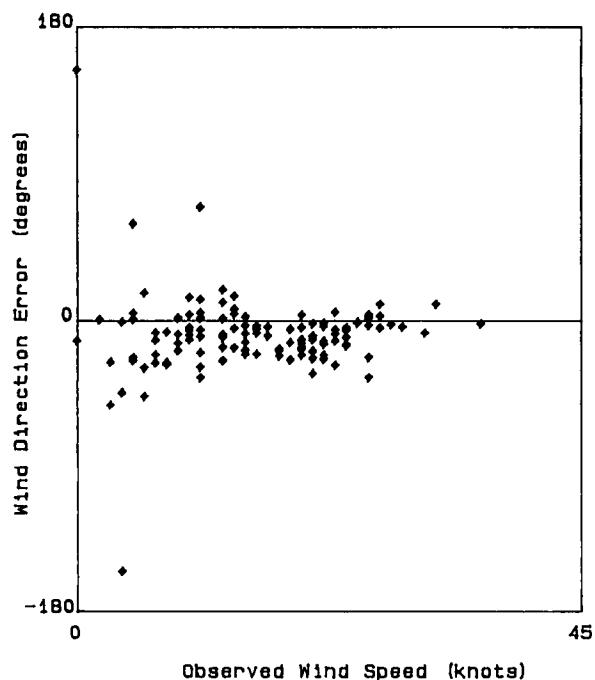
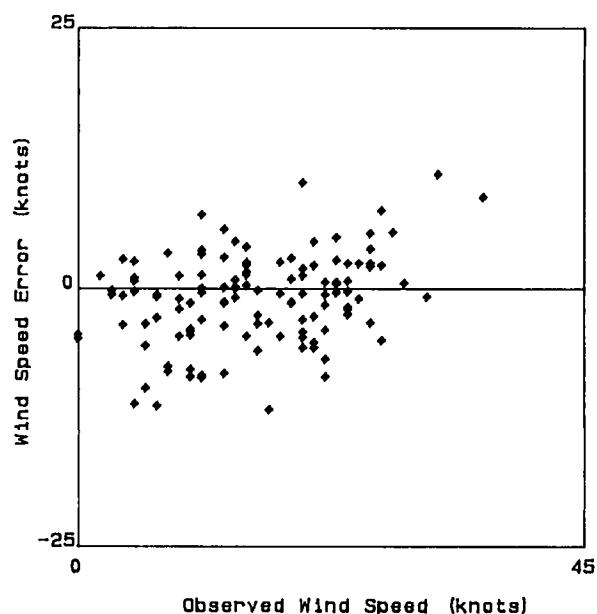
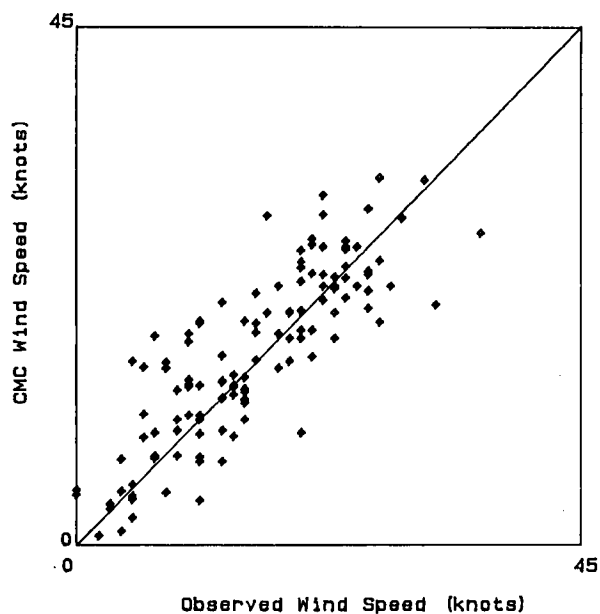


NOVEMBER 1985

00 Hour Forecast

Rowan Gorilla, Olympia 0-51

Grid Point : 5

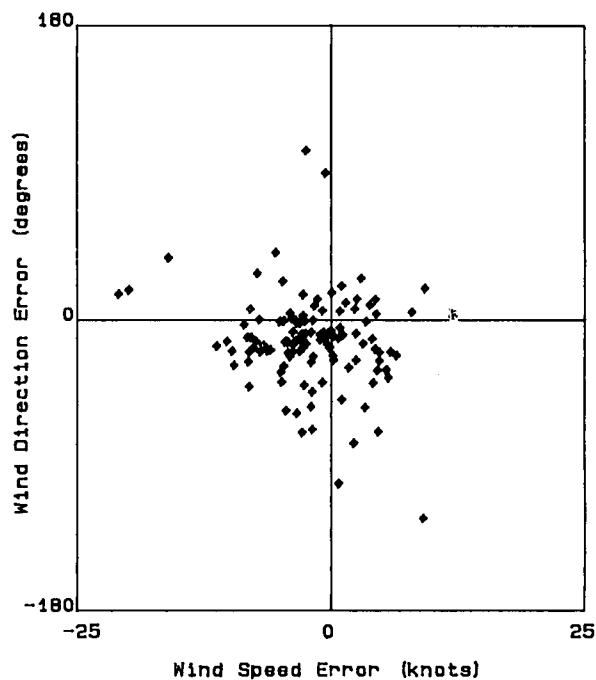
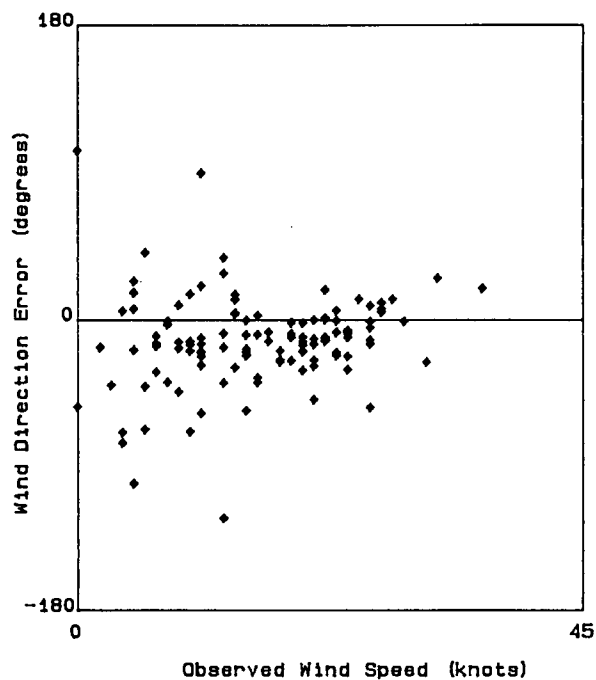
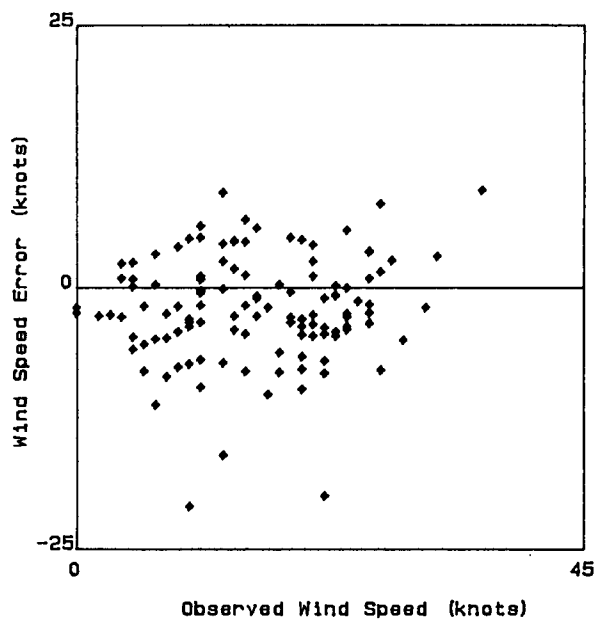
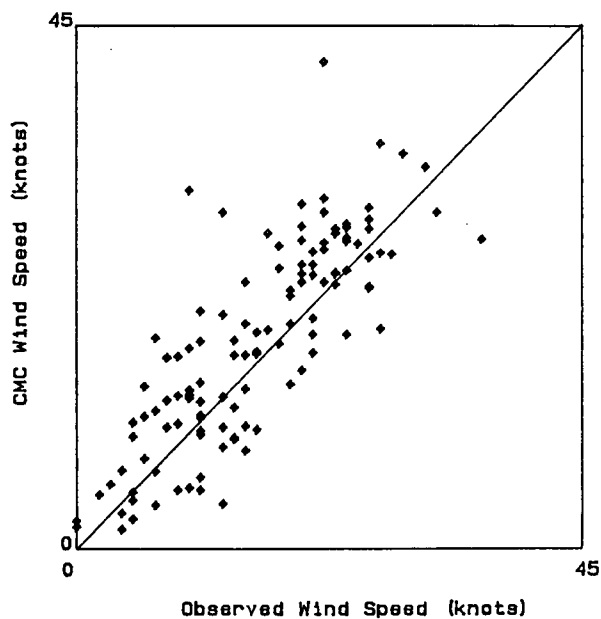


	Rate (knots)	Direction (deg.T)	Pressure (mb)	Temperature (deg.C)
Error	-.93	-9.09	1.09	.71
Abs Error	3.38	16.17	1.39	.96
RMS Error	4.42	27.07	1.91	1.21
Avg Value	15.50	n.a.	1017.30	12.69
S.I.	28.55%			

12 Hour Forecast

Rowan Gorilla, Olympia 0-51

Grid Point : 5

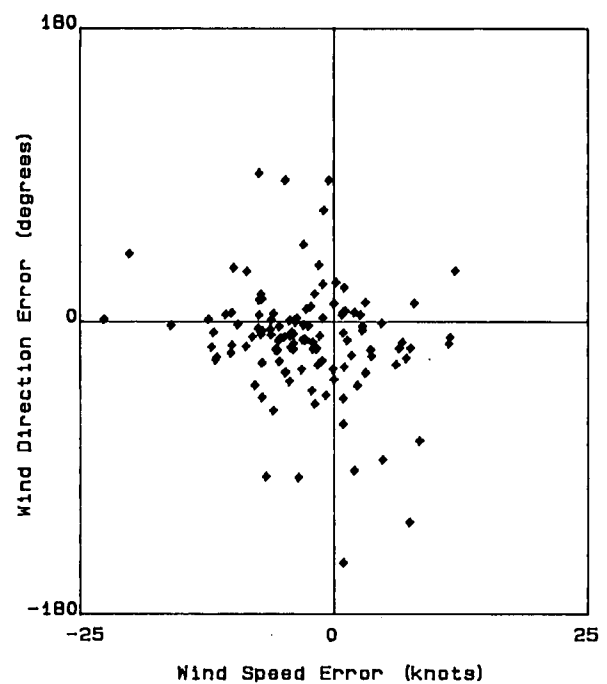
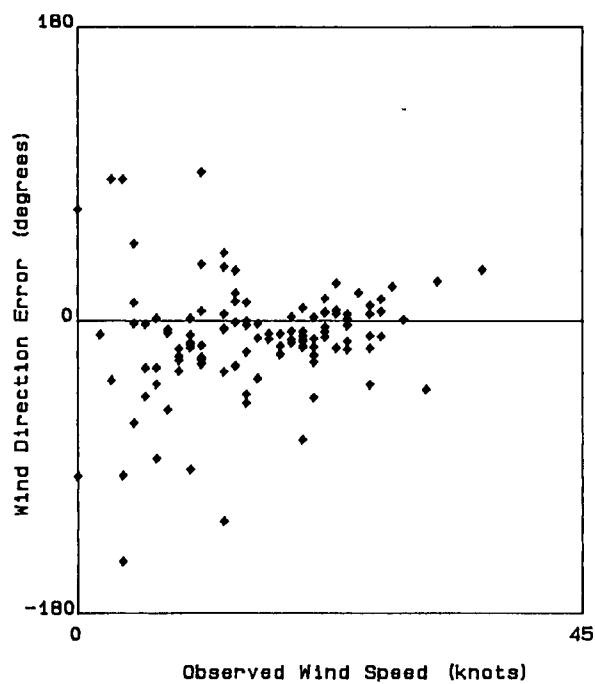
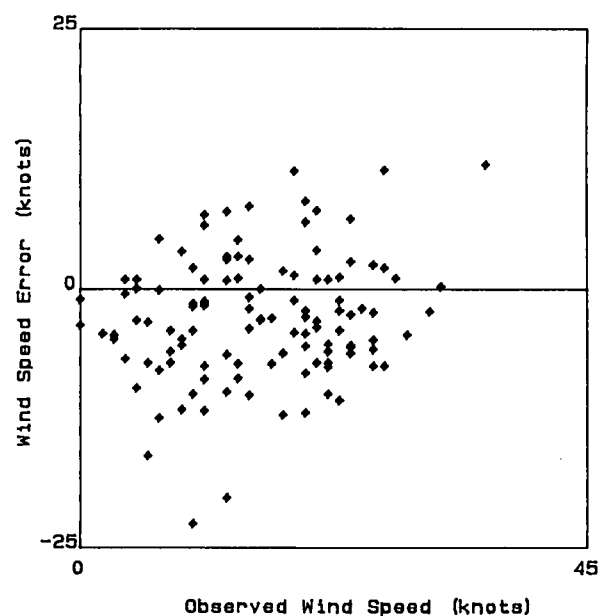
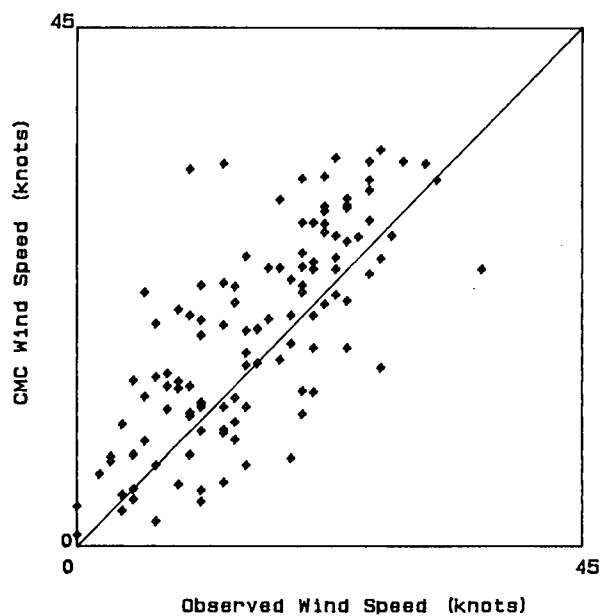


	Rate (knots)	Direction (deg.T)	Pressure (mb)	Temperature (deg.C)
Error	-1.98	-12.94	.10	.04
Abs Error	4.22	22.54	1.40	.92
RMS Error	5.49	31.61	1.99	1.17
Avg Value	15.57	n.a.	1017.27	12.65
S.I.	35.27%			

24 Hour Forecast

Grid Point : 5

Rowan Gorilla, Olympia 0-51



	Rate (knots)	Direction (deg.T)	Pressure (mb)	Temperature (deg.C)
Error	-2.77	-11.32	-.36	-.19
Abs Error	5.20	24.67	1.97	1.14
RMS Error	6.59	36.73	2.64	1.43
Avg Value	15.57	n.a.	1017.27	12.65
S.I.	42.33%			

Verification Tables
Rowan Gorilla I MANMAR Observations
00 Hour Forecast
Grid Point : 5
Period : Sept. '85 to Feb. '86

Error of speed vs error of direction

		Speed error (knots)										Total	% Occ.
		-27.5	-22.5	-17.5	-12.5	-7.5	-2.5	2.5	7.5	12.5	17.5		
		-22.5	-17.5	-12.5	-7.5	-2.5	2.5	7.5	12.5	17.5	22.5		
Dir. error (deg.)													
(-157.5, -112.5)						1						1	1
(-112.5, -67.5)												0	0
(-67.5, -22.5)					2	4	8	6				20	17
(-22.5, 22.5)					10	24	48	11	3			96	80
(22.5, 67.5)							1					1	1
(67.5, 112.5)								1				1	1
(112.5, 157.5)						1						1	1
(157.5, 202.5)												0	0
Total		0	0	0	12	30	57	18	3	0	0	120	
% Occurrence		0	0	0	10	25	48	15	3	0	0		

Speed vs error of speed

		Speed (knots)								Total	% Occ.
		0	5	10	15	20	25	30	35		
		5	10	15	20	25	30	35	40		
Speed error (knots)											
(-27.5, -22.5)										0	0
(-22.5, -17.5)										0	0
(-17.5, -12.5)										0	0
(-12.5, -7.5)										12	10
(-7.5, -2.5)			5	5	1	1				12	10
(-2.5, 2.5)		3	4	5	6	10	2			30	25
(2.5, 7.5)		4	8	11	11	16	6	1		57	48
(7.5, 12.5)		1	2	6	2	3	4			18	15
(12.5, 17.5)						1		1	1	3	3
(17.5, 22.5)										0	0
Total		8	19	27	20	31	12	2	1	120	
% Occurrence		7	16	23	17	26	10	2	1		

Speed vs error of direction

		Speed (knots)								Total	% Occ.
		0	5	10	15	20	25	30	35		
		5	10	15	20	25	30	35	40		
Dir. error (deg.)											
(-157.5, -112.5)		1								1	1
(-112.5, -67.5)										0	0
(-67.5, -22.5)		3	7	3	1	4	2			20	17
(-22.5, 22.5)		3	11	23	19	27	10	2	1	96	80
(22.5, 67.5)			1							1	1
(67.5, 112.5)				1						1	1
(112.5, 157.5)		1								1	1
(157.5, 202.5)										0	0
Total		8	19	27	20	31	12	2	1	120	
% Occurrence		7	16	23	17	26	10	2	1		

Verification Tables
Rowan Gorilla I MANMAR Observations
12 Hour Forecast
Grid Point : 5
Period : Sept. '85 to Feb. '86

Error of speed vs error of direction

Speed error (knots)

	-27.5	-22.5	-17.5	-12.5	-7.5	-2.5	2.5	7.5	12.5	17.5	Total	% Occ.
	-22.5	-17.5	-12.5	-7.5	-2.5	2.5	7.5	12.5	17.5	22.5		
Dir. error (deg.)												
(-157.5, -112.5)								1			1	1
(-112.5, -67.5)					1	2	1				4	3
(-67.5, -22.5)				3	6	10	6				25	21
(-22.5, 22.5)		2		9	32	24	11	2			80	68
(22.5, 67.5)			1		3		1				5	4
(67.5, 112.5)						2					2	2
(112.5, 157.5)											0	0
(157.5, 202.5)											0	0
Total	0	2	1	12	42	38	19	3	0	0	117	
% Occurrence	0	2	1	10	36	32	16	3	0	0		

Speed vs error of speed

Speed (knots)

	0	5	10	15	20	25	30	35	Total	% Occ.
	5	10	15	20	25	30	35	40		
Speed error (knots)										
(-27.5, -22.5)									0	0
(-22.5, -17.5)			1		1				2	2
(-17.5, -12.5)			1						1	1
(-12.5, -7.5)		4	1	3	3	1			12	10
(-7.5, -2.5)	3	7	9	5	16	2			42	36
(-2.5, 2.5)	4	6	8	7	7	5	1		38	32
(2.5, 7.5)		2	6	4	3	3	1		19	16
(7.5, 12.5)			1			1		1	3	3
(12.5, 17.5)									0	0
(17.5, 22.5)									0	0
Total	7	19	27	19	30	12	2	1	117	
% Occurrence	6	16	23	16	26	10	2	1		

Speed vs error of direction

Speed (knots)

	0	5	10	15	20	25	30	35	Total	% Occ.
	5	10	15	20	25	30	35	40		
Dir. error (deg.)										
(-157.5, -112.5)			1						1	1
(-112.5, -67.5)	2	1	1						4	3
(-67.5, -22.5)	2	5	5	6	5	1	1		25	21
(-22.5, 22.5)	2	11	17	13	25	11		1	80	68
(22.5, 67.5)		2	2				1		5	4
(67.5, 112.5)	1		1						2	2
(112.5, 157.5)									0	0
(157.5, 202.5)									0	0
Total	7	19	27	19	30	12	2	1	117	
% Occurrence	6	16	23	16	26	10	2	1		

Verification Tables
Rowan Gorilla I MANMAR Observations
24 Hour Forecast
Grid Point : 5
Period : Sept. '85 to Feb. '86

Error of speed vs error of direction

Speed error (knots)

	-27.5	-22.5	-17.5	-12.5	-7.5	-2.5	2.5	7.5	12.5	17.5	Total	% Occ.
	-22.5	-17.5	-12.5	-7.5	-2.5	2.5	7.5	12.5	17.5	22.5		
Dir. error (deg.)												
(-157.5, -112.5)						1	1				2	2
(-112.5, -67.5)					2	1	1	1			5	4
(-67.5, -22.5)				2	7	11	3				23	20
(-22.5, 22.5)	1		1	12	31	16	10	3			74	64
(22.5, 67.5)		1		2	1	3		1			8	7
(67.5, 112.5)					2	2					4	3
(112.5, 157.5)											0	0
(157.5, 202.5)											0	0
Total	1	1	1	16	43	34	15	5	0	0	116	
% Occurrence	1	1	1	14	37	29	13	4	0	0		

Speed vs error of speed

Speed (knots)

	0	5	10	15	20	25	30	35	Total	% Occ.
	5	10	15	20	25	30	35	40		
Speed error (knots)										
(-27.5, -22.5)			1						1	1
(-22.5, -17.5)			1						1	1
(-17.5, -12.5)		1							1	1
(-12.5, -7.5)		4	5	2	5				16	14
(-7.5, -2.5)	5	8	4	7	14	5			43	37
(-2.5, 2.5)	3	3	9	6	6	5	2		34	29
(2.5, 7.5)		2	7	1	5				15	13
(7.5, 12.5)				2	1	1		1	5	4
(12.5, 17.5)									0	0
(17.5, 22.5)									0	0
Total	8	18	27	18	31	11	2	1	116	
% Occurrence	7	16	23	16	27	9	2	1		

Speed vs error of direction

Speed (knots)

	0	5	10	15	20	25	30	35	Total	% Occ.
	5	10	15	20	25	30	35	40		
Dir. error (deg.)										
(-157.5, -112.5)	1		1						2	2
(-112.5, -67.5)	2	1	1		1				5	4
(-67.5, -22.5)	1	8	7	3	2	1	1		23	20
(-22.5, 22.5)	1	8	13	15	27	10			74	64
(22.5, 67.5)		1	4		1		1	1	8	7
(67.5, 112.5)	3		1						4	3
(112.5, 157.5)									0	0
(157.5, 202.5)									0	0
Total	8	18	27	18	31	11	2	1	116	
% Occurrence	7	16	23	16	27	9	2	1		

Rowan Gorilla, Olympia 0-51

Grid Point : 5

00 Hour Forecast

Month : September

	Rate (knots)	Direction (deg.T)	Pressure (mb)	Temperature (deg.C)
Error	- .65	-9.69	1.43	.56
Abs Error	3.27	19.39	1.56	1.00
RMS Error	4.56	31.26	1.70	1.20
Avg Value	11.78	n.a.	1018.45	15.12
# of pts	40	40	40	40
S.I.	38.68%			

Rowan Gorilla, Olympia 0-51

Grid Point : 5

00 Hour Forecast

Month : October

	Rate (knots)	Direction (deg.T)	Pressure (mb)	Temperature (deg.C)
Error	-.97	-8.87	.86	.93
Abs Error	3.36	15.39	1.35	1.05
RMS Error	4.29	26.99	2.14	1.33
Avg Value	17.50	n.a.	1016.94	11.45
# of pts	62	62	62	62
S.I.	24.49%			

Rowan Gorilla, Olympia 0-51

Grid Point : 5

00 Hour Forecast

Month : November

	Rate (knots)	Direction (deg.T)	Pressure (mb)	Temperature (deg.C)
Error	-1.43	-8.47	1.09	.29
Abs Error	3.68	11.73	1.18	.55
RMS Error	4.59	14.28	1.43	.69
Avg Value	20.96	n.a.	1014.73	8.86
# of pts	18	18	18	18
S.I.	21.89%			

Rowan Gorilla, Olympia 0-51

Grid Point : 5

12 Hour Forecast

Month : September

	Rate (knots)	Direction (deg.T)	Pressure (mb)	Temperature (deg.C)
Error	-.68	-18.45	.37	.18
Abs Error	3.97	30.15	1.00	1.08
RMS Error	5.26	38.91	1.30	1.37
Avg Value	11.78	n.a.	1018.45	15.12
# of pts	39	39	39	39
S.I.	44.61%			

Rowan Gorilla, Olympia 0-51

Grid Point : 5

12 Hour Forecast

Month : October

	Rate (knots)	Direction (deg.T)	Pressure (mb)	Temperature (deg.C)
Error	-2.27	-10.64	-.35	.16
Abs Error	3.94	20.17	1.59	.81
RMS Error	5.03	29.55	2.32	1.03
Avg Value	17.65	n.a.	1016.89	11.37
# of pts	61	61	61	61
S.I.	28.52%			

Rowan Gorilla, Olympia 0-51
 Grid Point : 5
 12 Hour Forecast
 Month : November

	Rate (knots)	Direction (deg.T)	Pressure (mb)	Temperature (deg.C)
Error	-3.94	-8.55	1.08	-.72
Abs Error	5.79	13.59	1.62	.97
RMS Error	7.30	16.47	2.04	1.15
Avg Value	20.96	n.a.	1014.73	8.86
# of pts	17	17	17	17
S.I.	34.84%			

Rowan Gorilla, Olympia 0-51
 Grid Point : 5
 24 Hour Forecast
 Month : September

	Rate (knots)	Direction (deg.T)	Pressure (mb)	Temperature (deg.C)
Error	-1.23	-21.61	-.49	.15
Abs Error	4.98	34.89	1.70	1.33
RMS Error	6.21	48.19	2.18	1.65
Avg Value	11.78	n.a.	1018.45	15.12
# of pts	38	38	38	38
S.I.	52.68%			

Rowan Gorilla, Olympia 0-51
 Grid Point : 5
 24 Hour Forecast
 Month : October

	Rate (knots)	Direction (deg.T)	Pressure (mb)	Temperature (deg.C)
Error	-3.11	-6.35	-.65	-.14
Abs Error	4.79	21.54	2.06	1.00
RMS Error	6.17	32.18	2.90	1.24
Avg Value	17.65	n.a.	1016.89	11.37
# of pts	61	61	61	61
S.I.	34.95%			

Rowan Gorilla, Olympia 0-51
 Grid Point : 5
 24 Hour Forecast
 Month : November

	Rate (knots)	Direction (deg.T)	Pressure (mb)	Temperature (deg.C)
Error	-4.98	-6.15	.98	-1.14
Abs Error	7.17	13.04	2.19	1.24
RMS Error	8.60	17.28	2.64	1.52
Avg Value	20.96	n.a.	1014.73	8.86
# of pts	17	17	17	17
S.I.	41.04%			

Appendix 6.2

Comparison of Unmodified Sable Island 10-m Winds With CMC Forecasts for Rig Period.

Time-series plots of wind speed and direction

00,03,06,09 h forecasts: September, October, November 1985
12,15,18,21 h forecasts: September, October, November 1985
21,24,27,30 h forecasts: September, October, November 1985

Time-series plots of pressure and air temperature

00,03,06,09 h forecasts
12,15,18,21 h forecasts September, October, November 1985
21,24,27,30 h forecasts

Scatterplots and error statistics

00 h forecast
12 h forecast September, October, November 1985 inclusive
24 h forecast

Verification Tables

00 h forecast
12 h forecast September, October, November 1985 inclusive
24 h forecast

Monthly error statistics

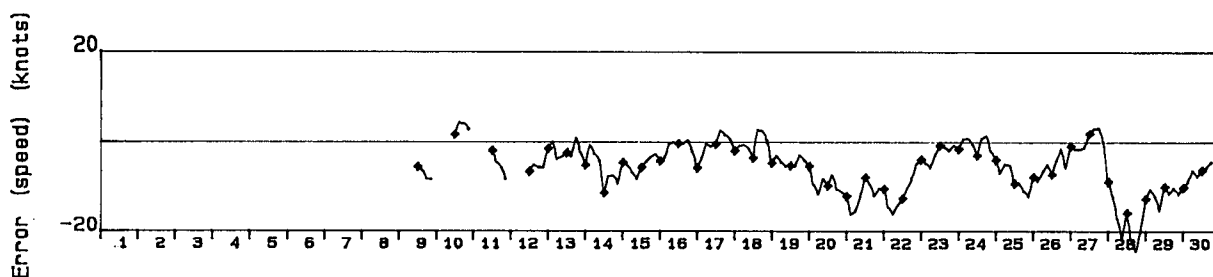
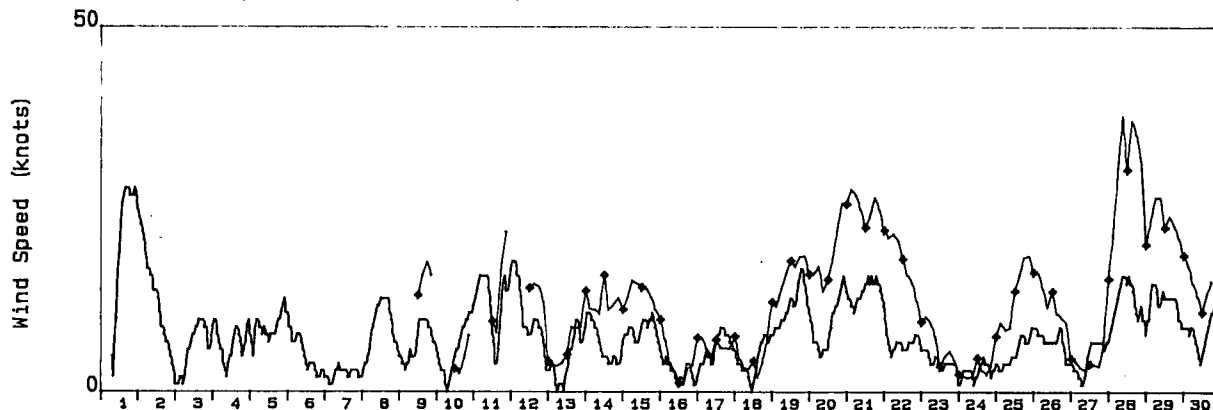
00 h forecast
12 h forecast September, October, November 1985
24 h forecast

Wind Rate and Direction

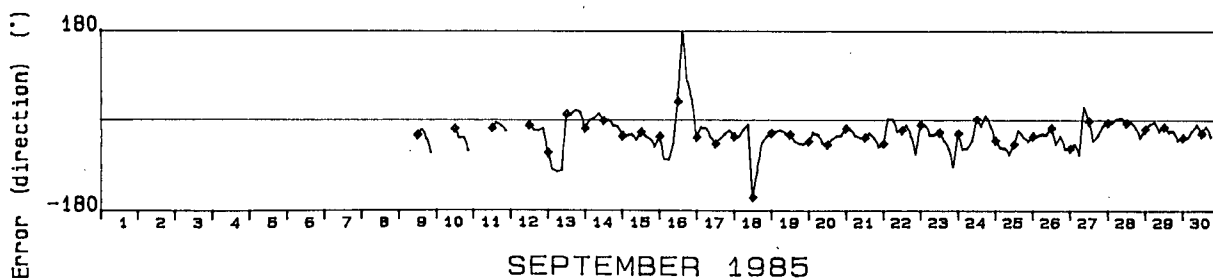
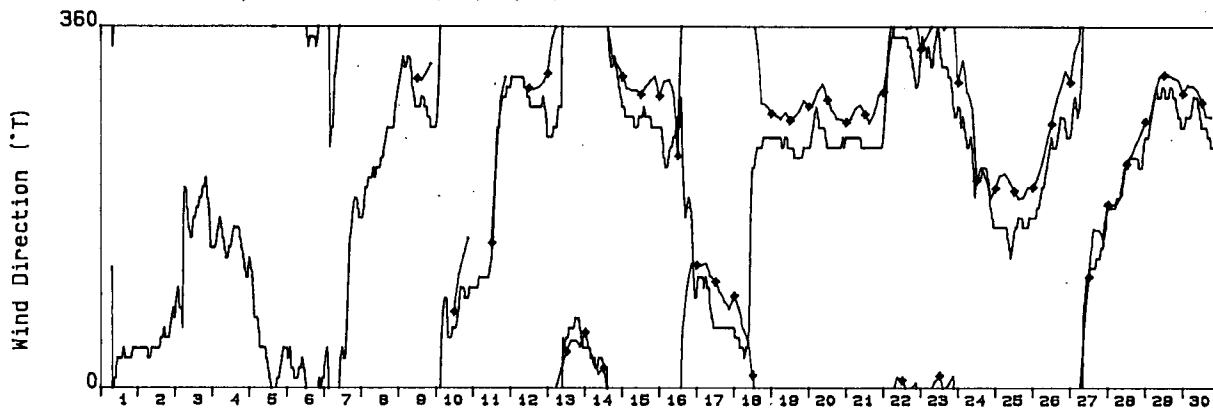
Sable Island AES Observations

Grid Point : 5

Forecast periods are (0, 3, 6, 9)



Forecast periods are (0, 3, 6, 9)



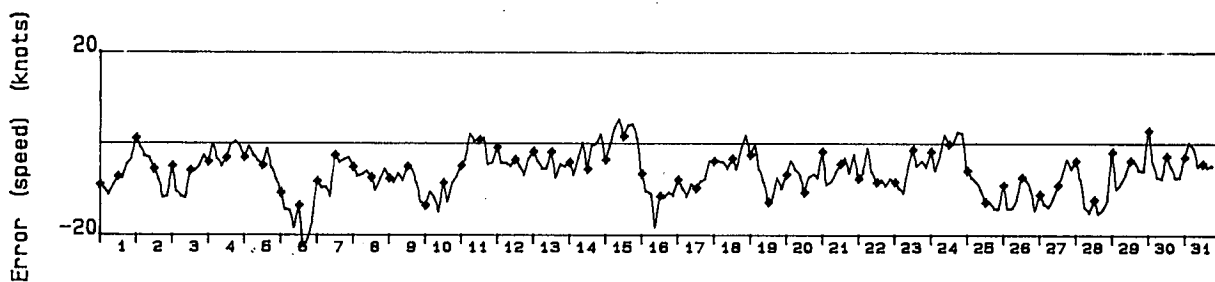
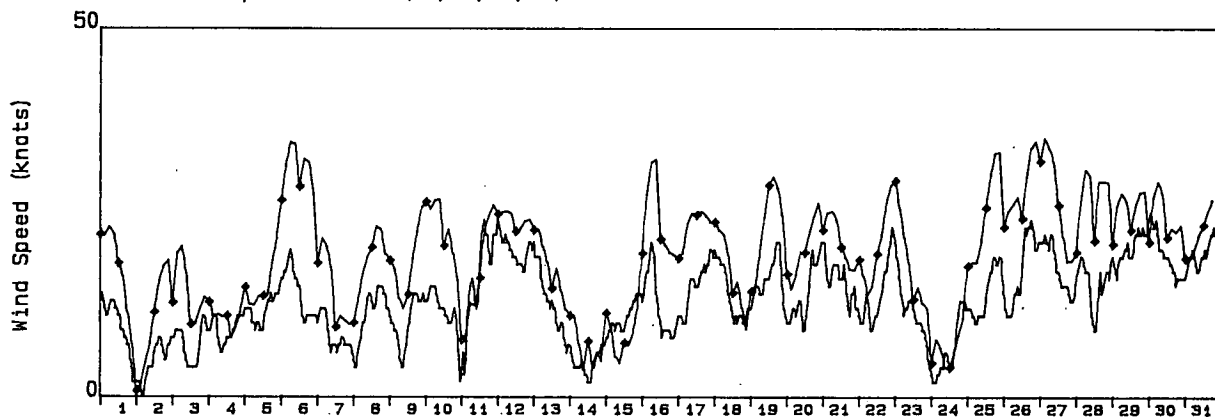
SEPTEMBER 1985

Wind Rate and Direction

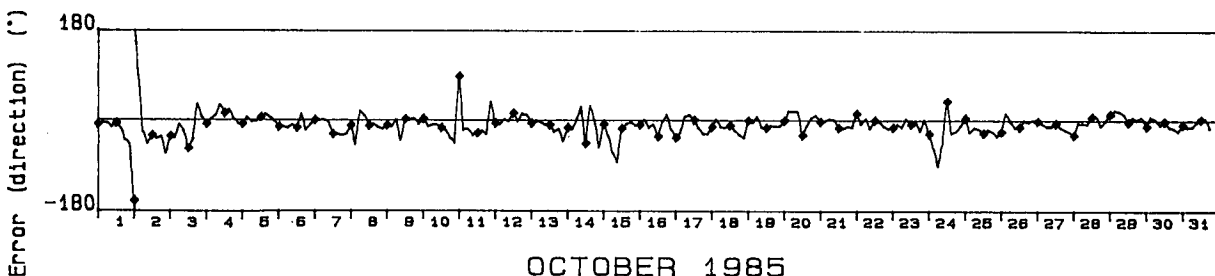
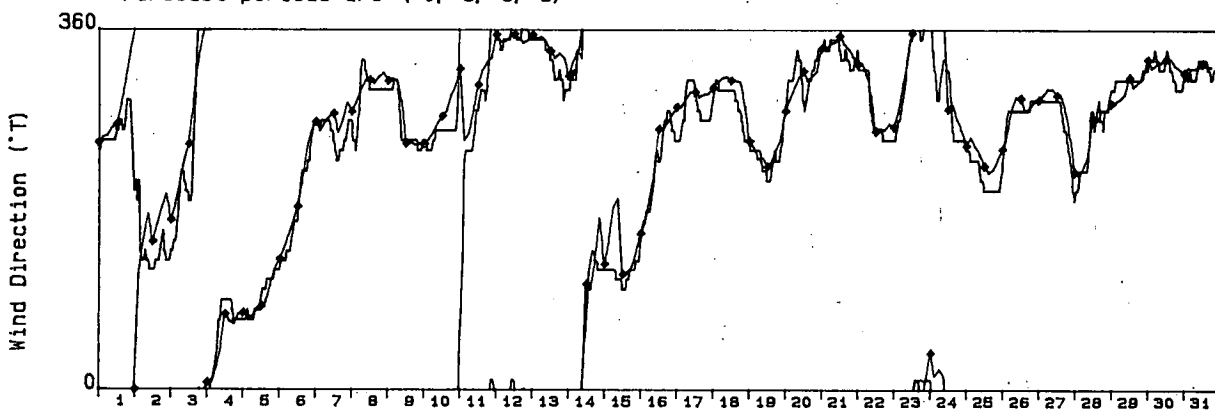
Sable Island AES Observations

Grid Point : 5

Forecast periods are (0, 3, 6, 9)



Forecast periods are (0, 3, 6, 9)



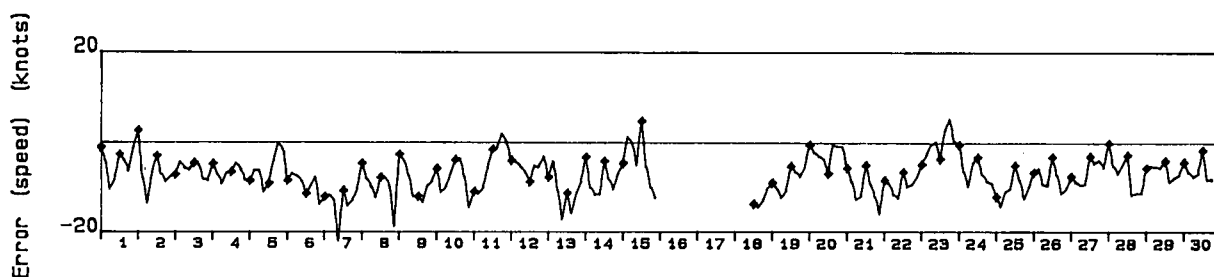
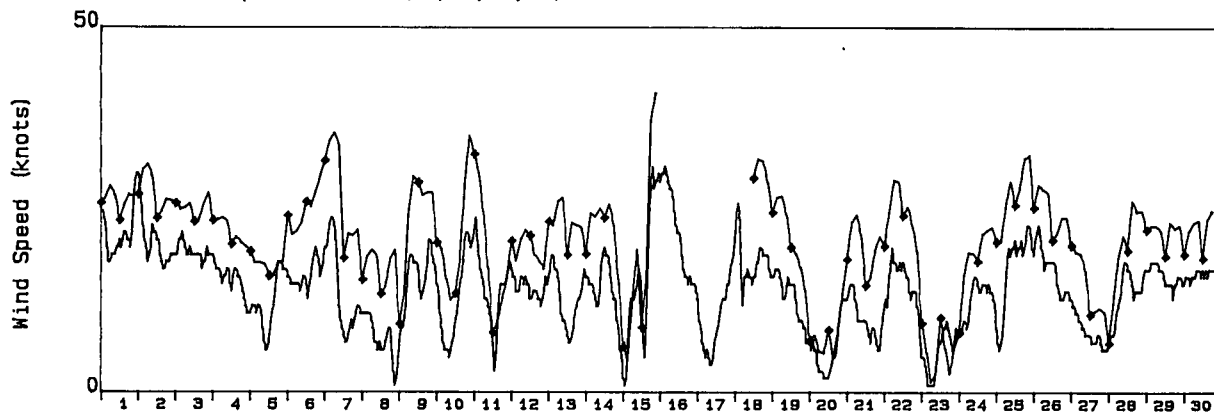
OCTOBER 1985

Wind Rate and Direction

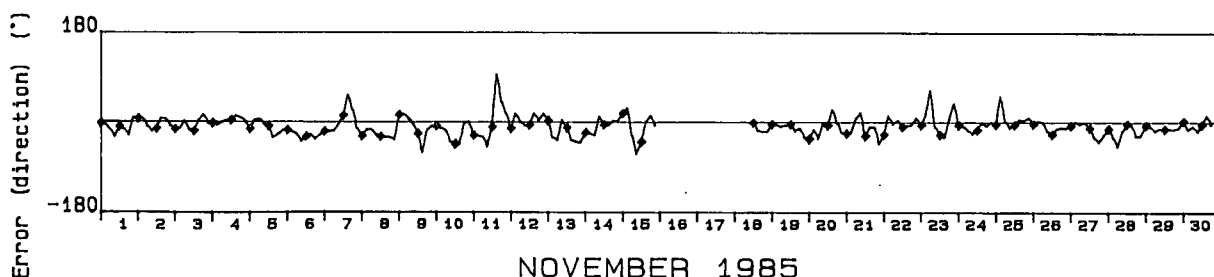
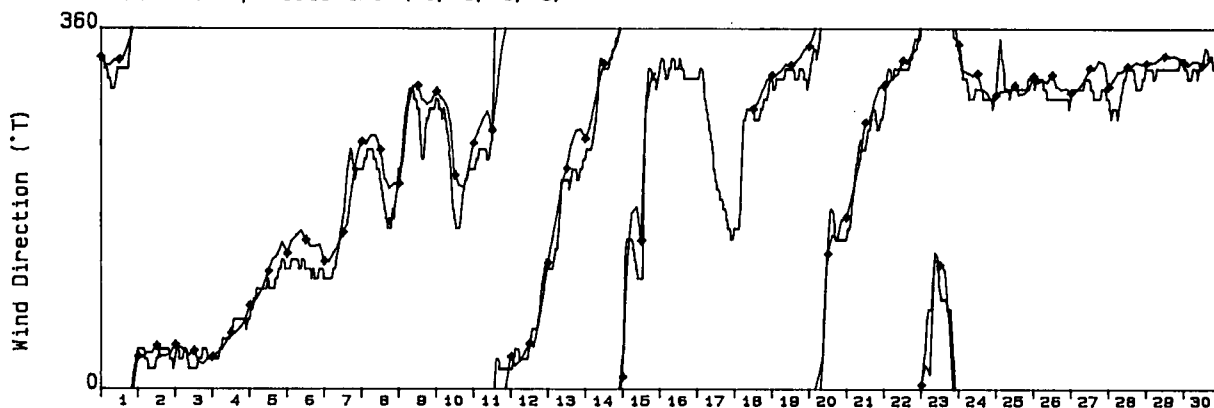
Sable Island AES Observations

Grid Point : 5

Forecast periods are (0, 3, 6, 9)



Forecast periods are (0, 3, 6, 9)



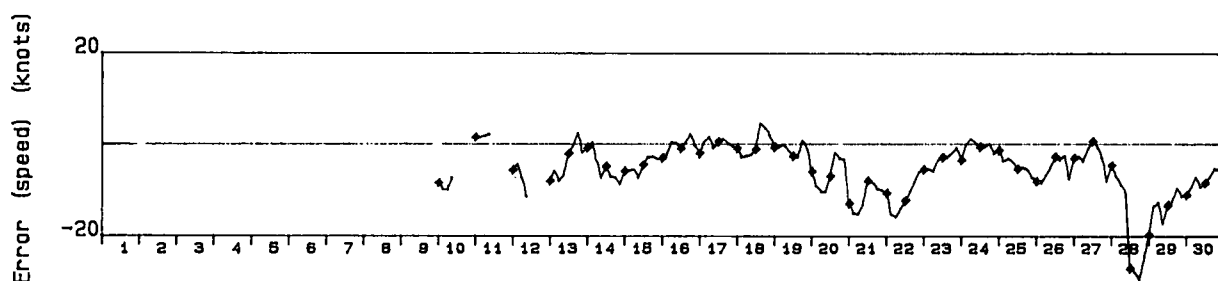
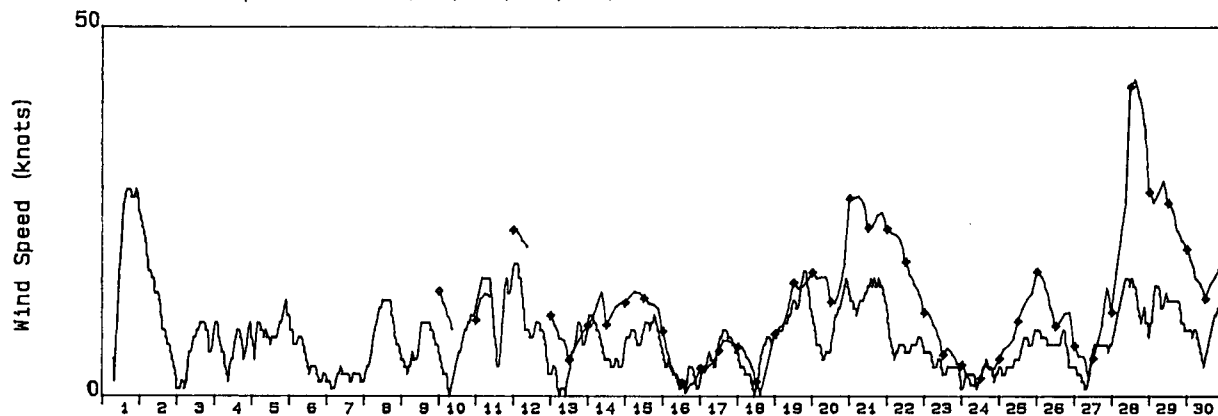
NOVEMBER 1985

Wind Rate and Direction

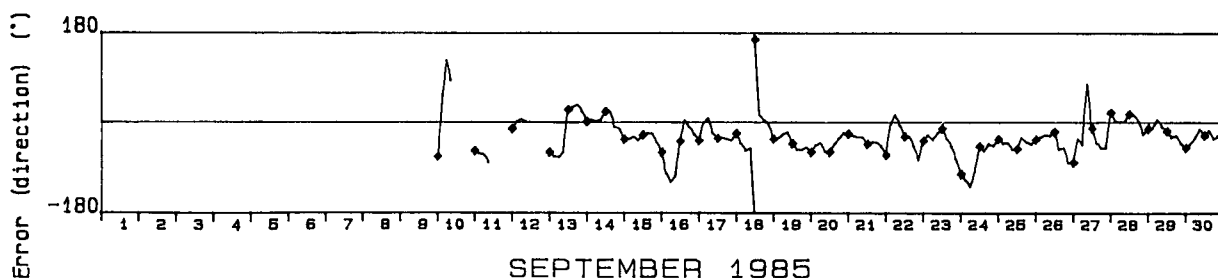
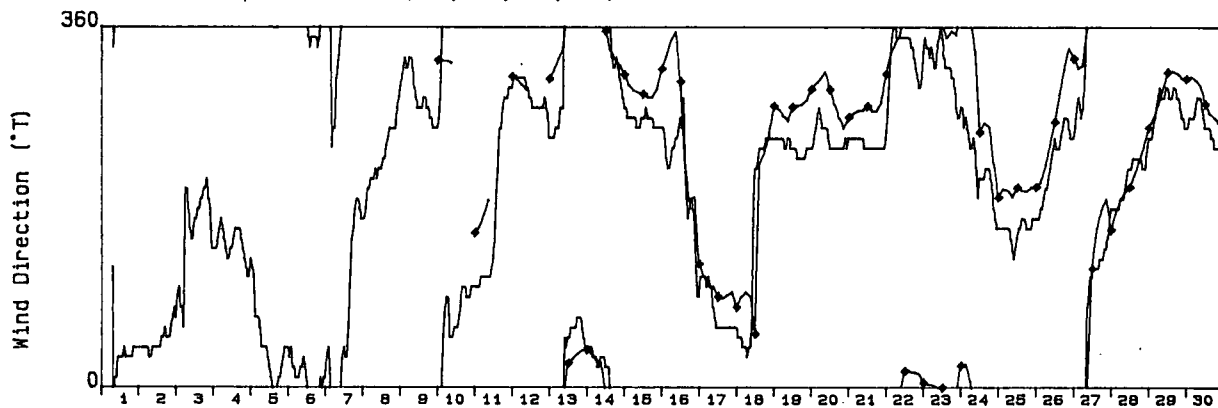
Sable Island AES Observations

Grid Point : 5

Forecast periods are (12, 15, 18, 21)



Forecast periods are (12, 15, 18, 21)



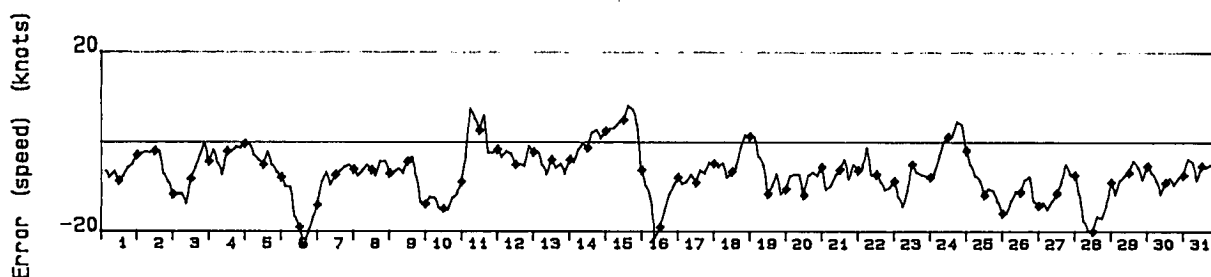
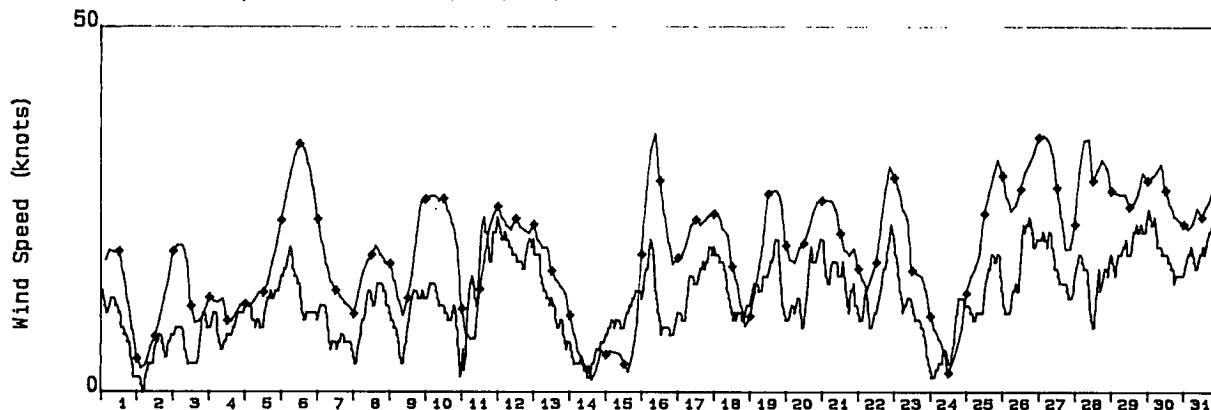
SEPTEMBER 1985

Wind Rate and Direction

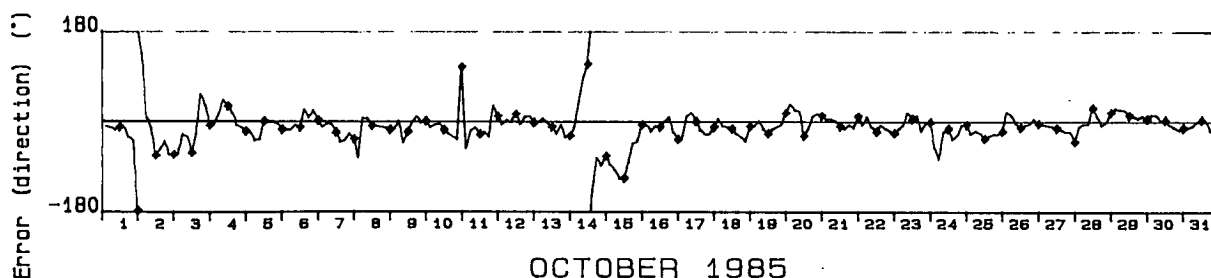
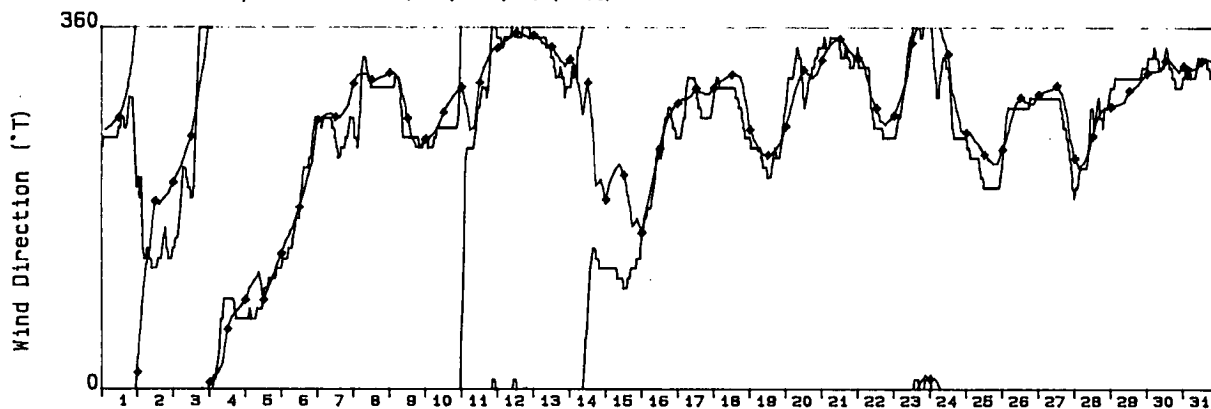
Sable Island AES Observations

Grid Point : 5

Forecast periods are (12, 15, 18, 21)



Forecast periods are (12, 15, 18, 21)



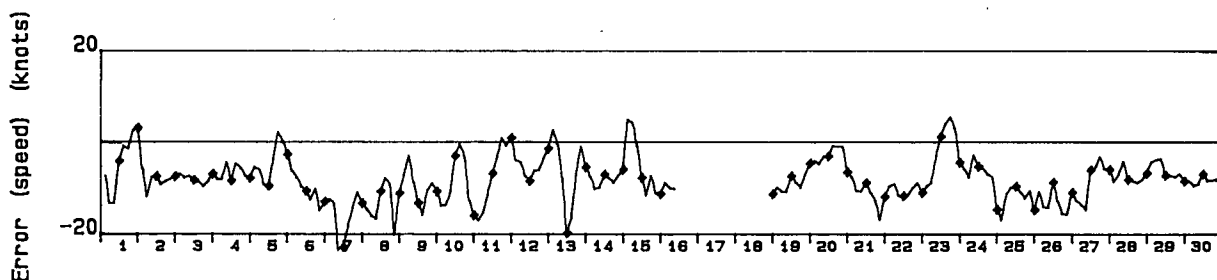
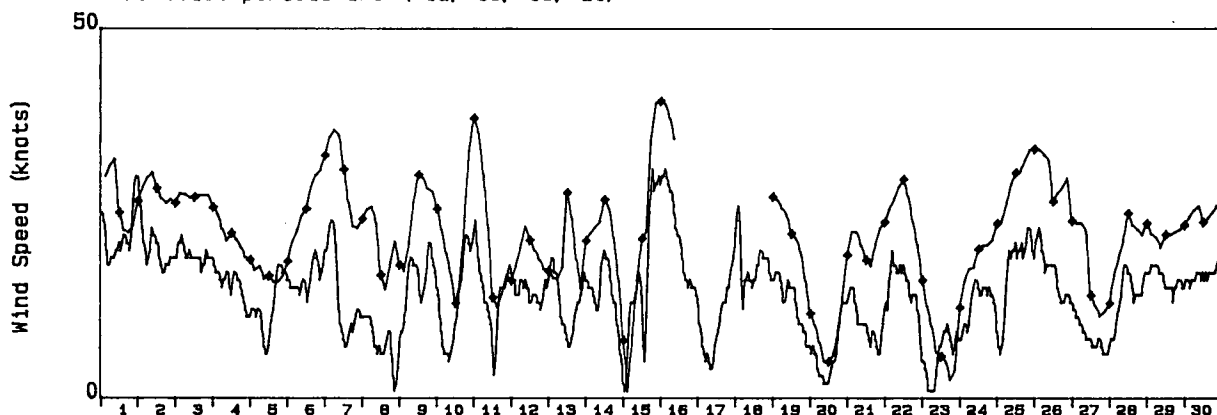
OCTOBER 1985

Wind Rate and Direction

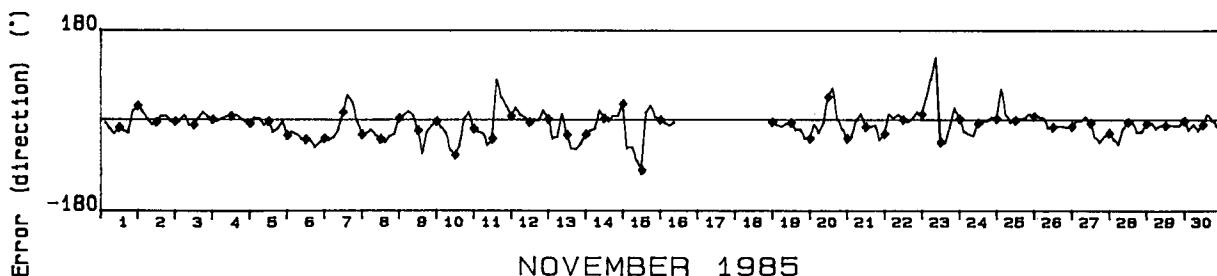
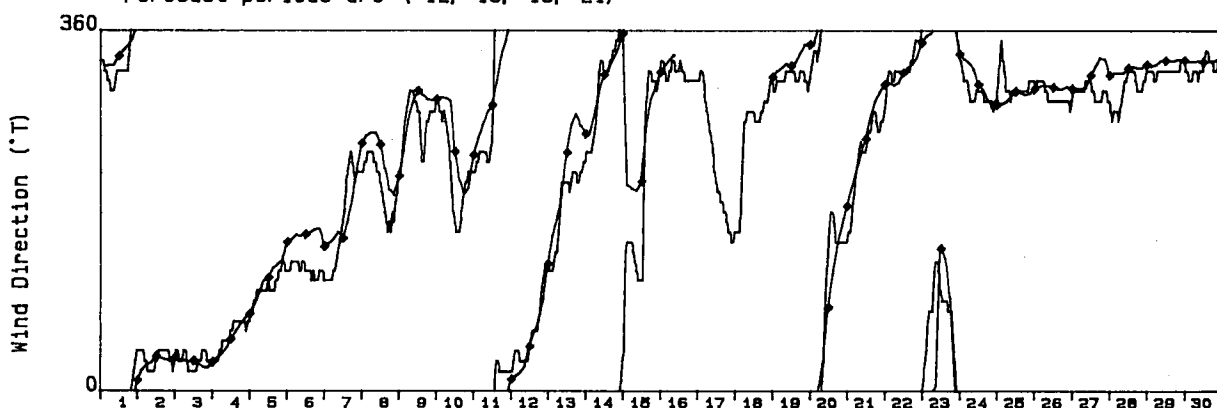
Sable Island AES Observations

Grid Point : 5

Forecast periods are (12, 15, 18, 21)



Forecast periods are (12, 15, 18, 21)



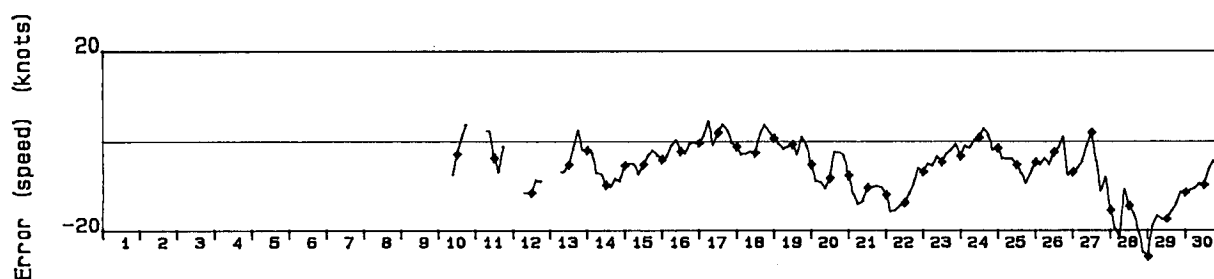
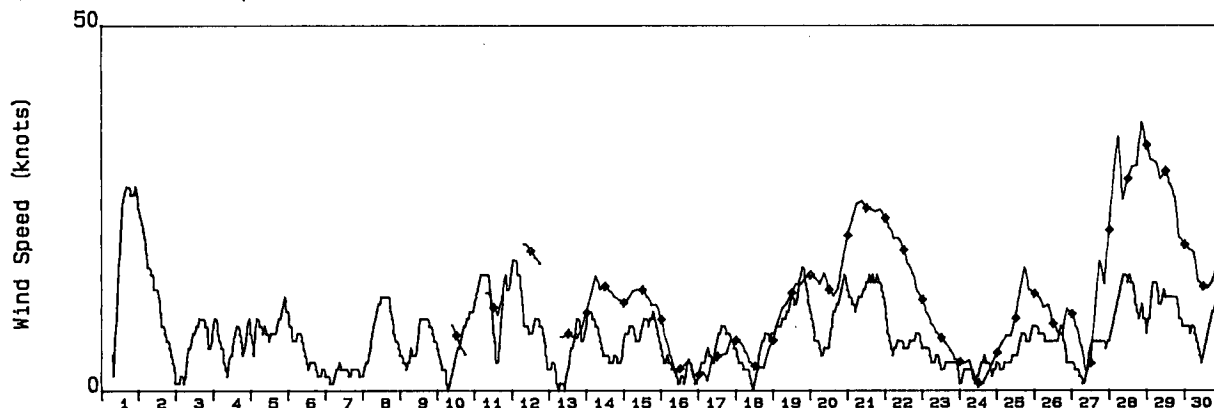
NOVEMBER 1985

Wind Rate and Direction

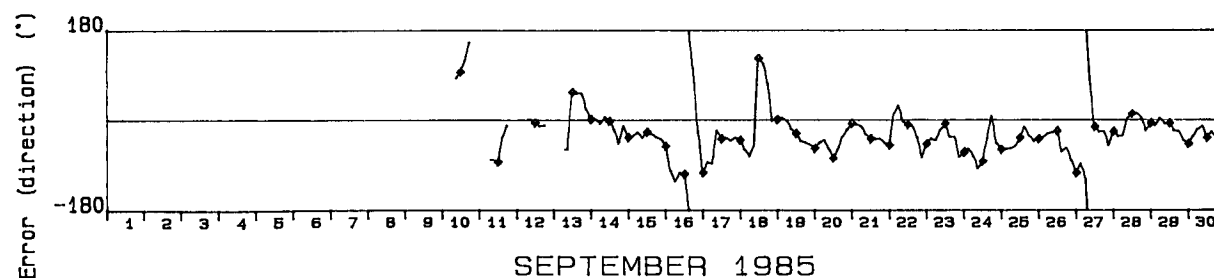
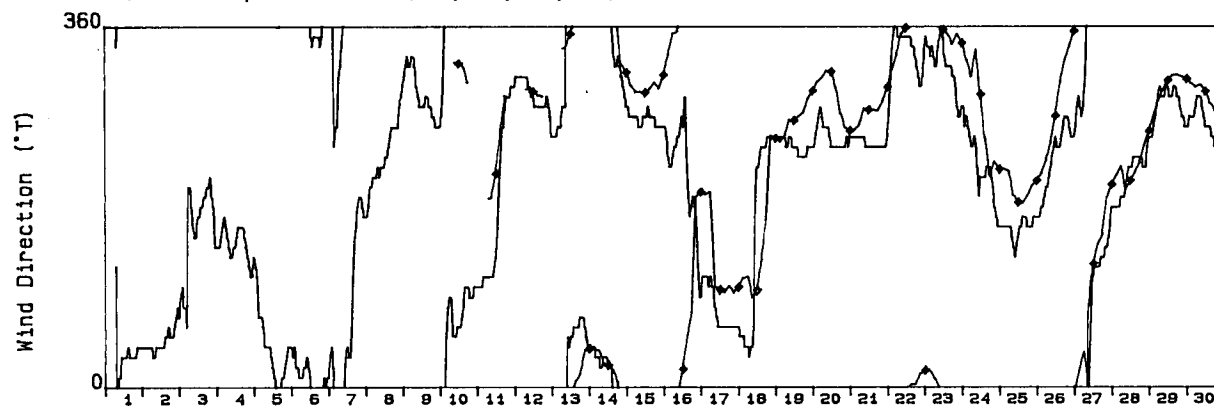
Sable Island AES Observations

Grid Point : 5

Forecast periods are (21, 24, 27, 30)



Forecast periods are (21, 24, 27, 30)



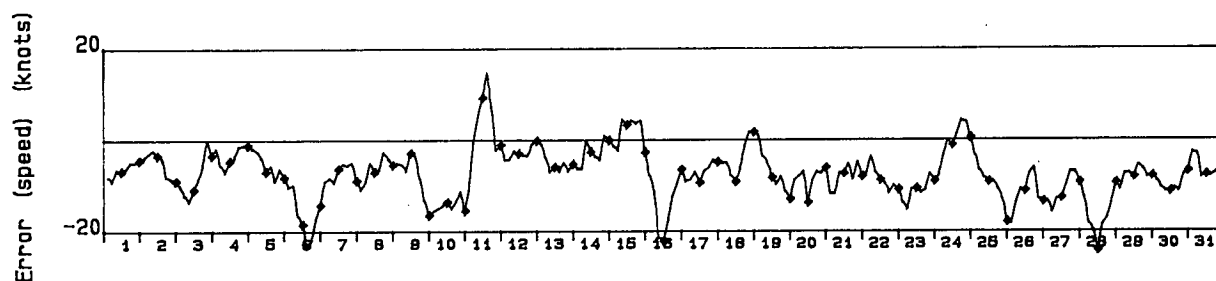
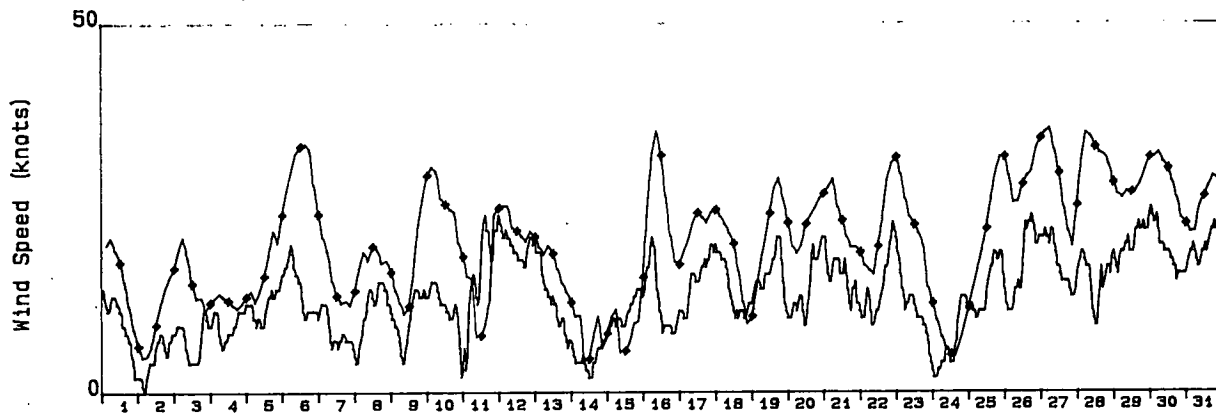
SEPTEMBER 1985

Wind Rate and Direction

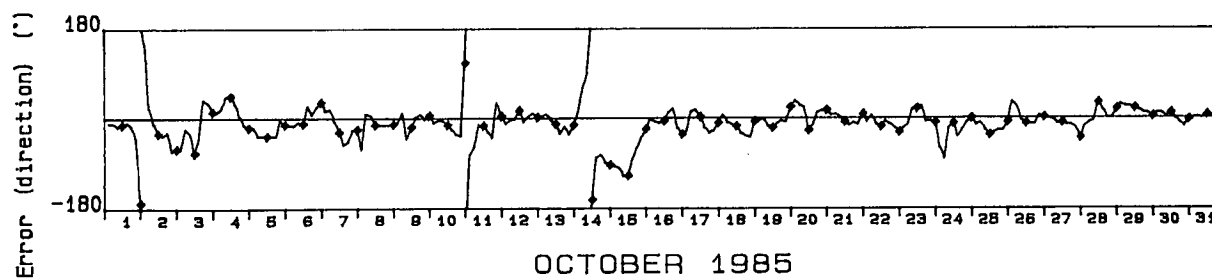
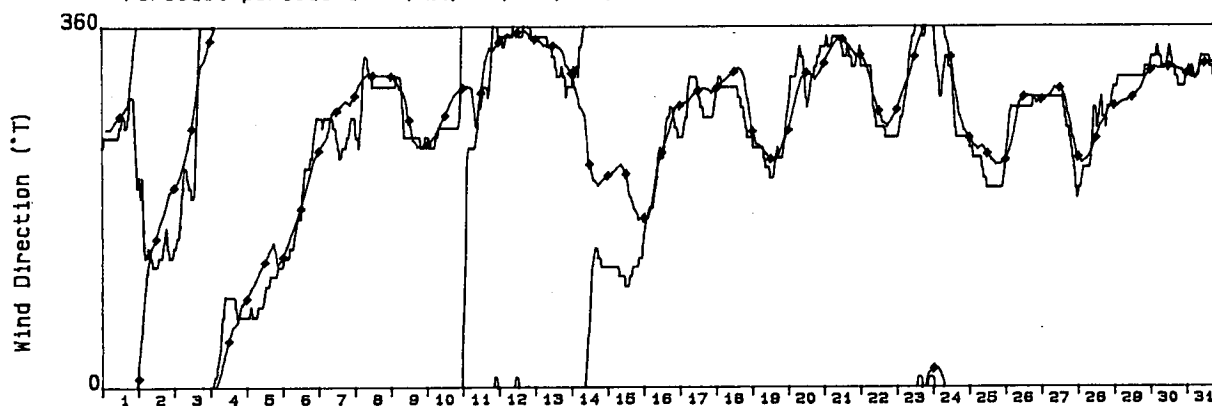
Sable Island AES Observations

Grid Point : 5

Forecast periods are (21, 24, 27, 30)



Forecast periods are (21, 24, 27, 30)



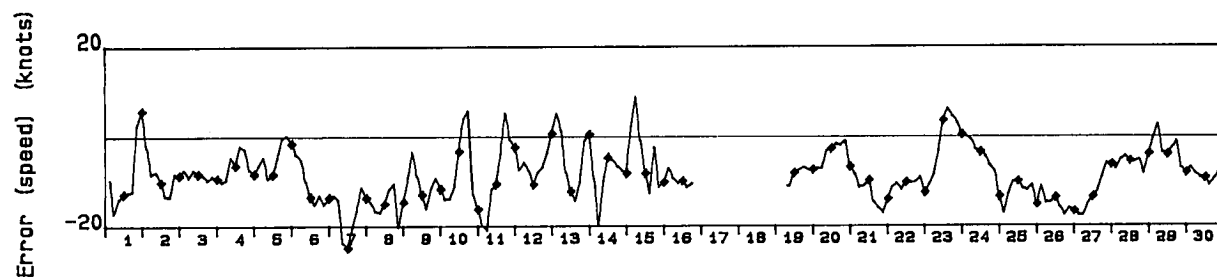
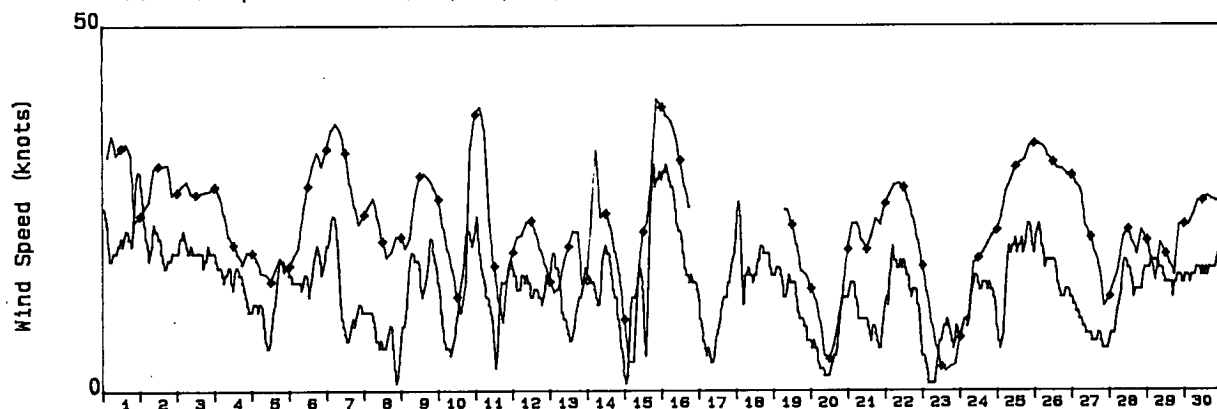
OCTOBER 1985

Wind Rate and Direction

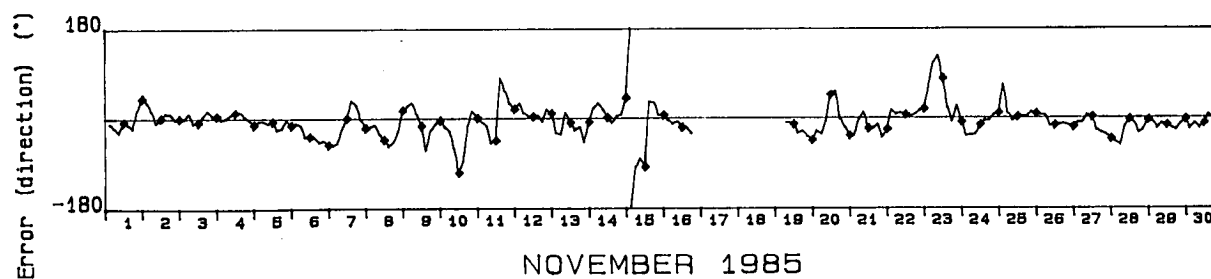
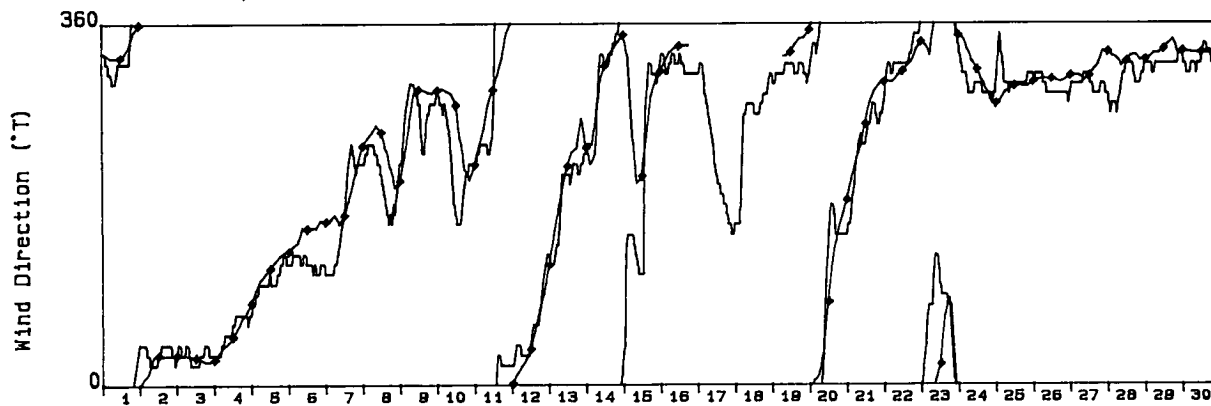
Sable Island AES Observations

Grid Point : 5

Forecast periods are (21, 24, 27, 30)



Forecast periods are (21, 24, 27, 30)



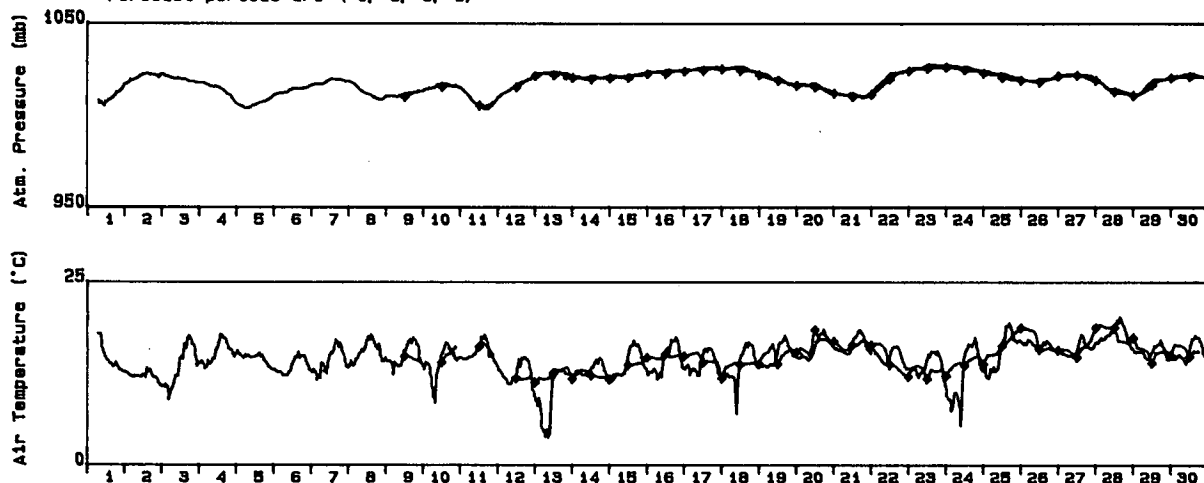
NOVEMBER 1985

Pressure and Air Temperature

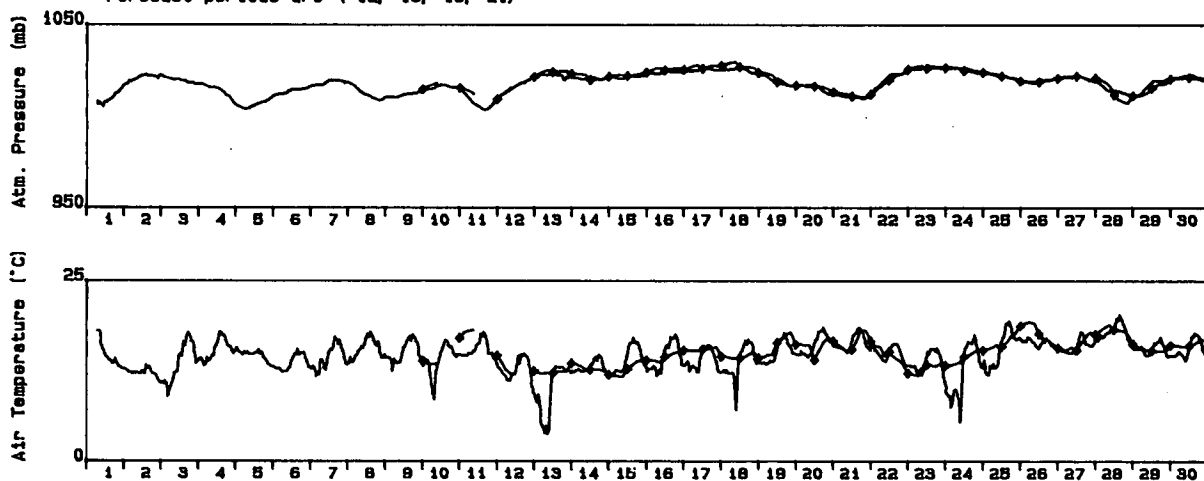
Sable Island AES Observations

Grid Point : 5

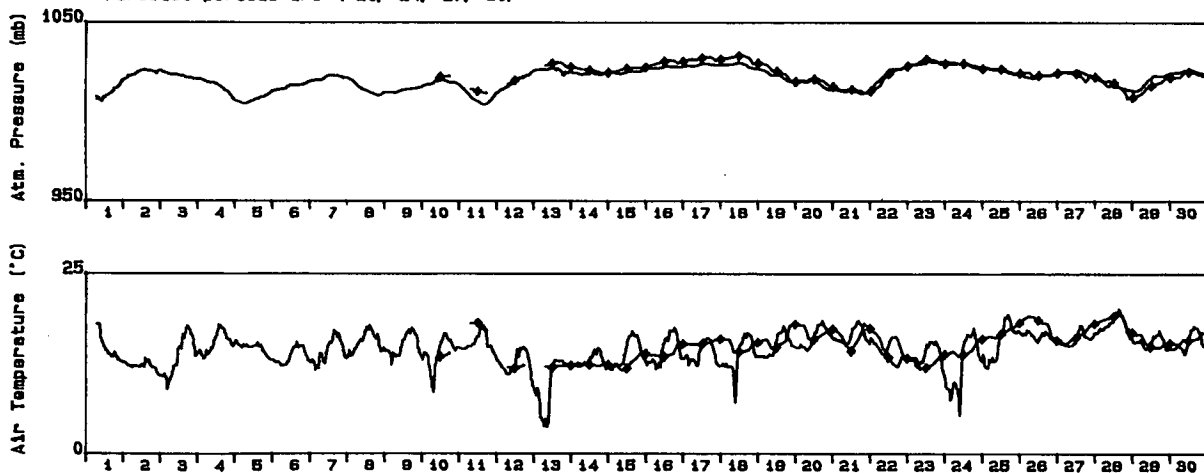
Forecast periods are (0, 3, 6, 9)



Forecast periods are (12, 15, 18, 21)



Forecast periods are (21, 24, 27, 30)



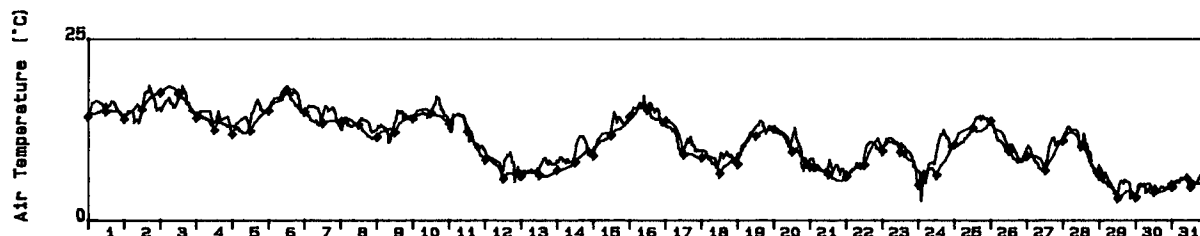
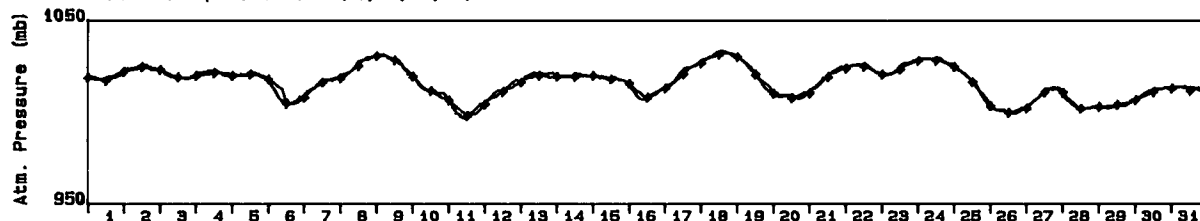
SEPTEMBER 1985

Pressure and Air Temperature

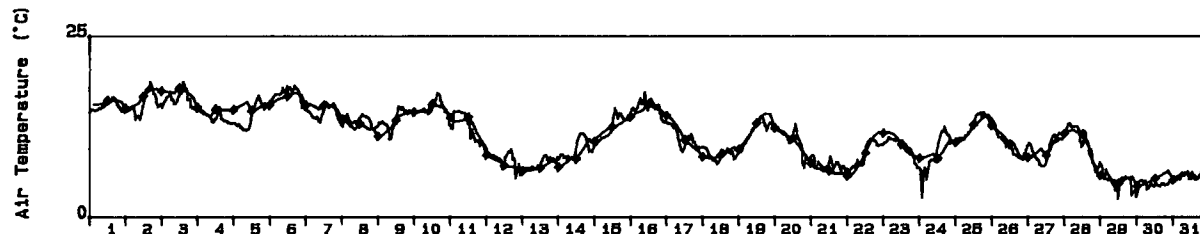
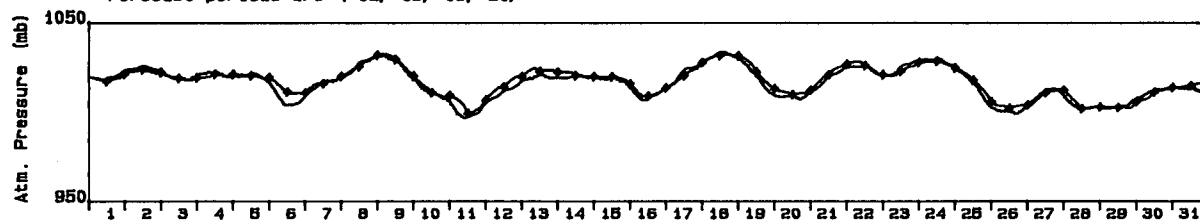
Sable Island AES Observations

Grid Point : 5

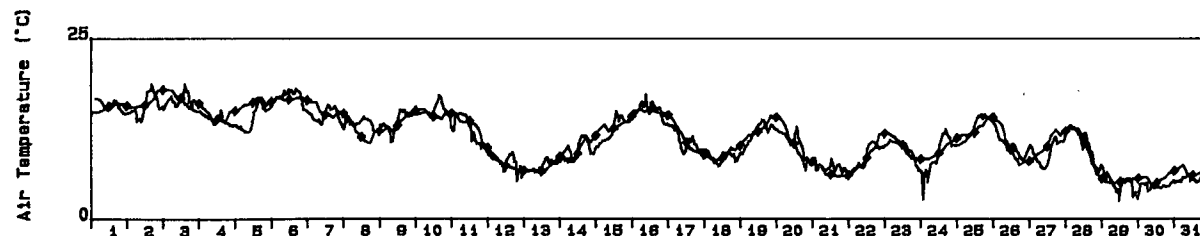
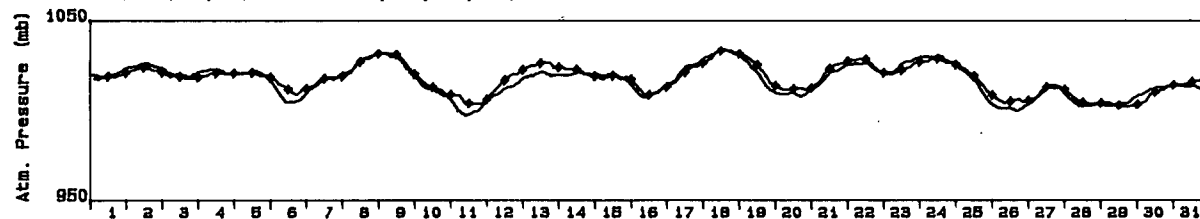
Forecast periods are (0, 3, 6, 9)



Forecast periods are (12, 15, 18, 21)



Forecast periods are (21, 24, 27, 30)



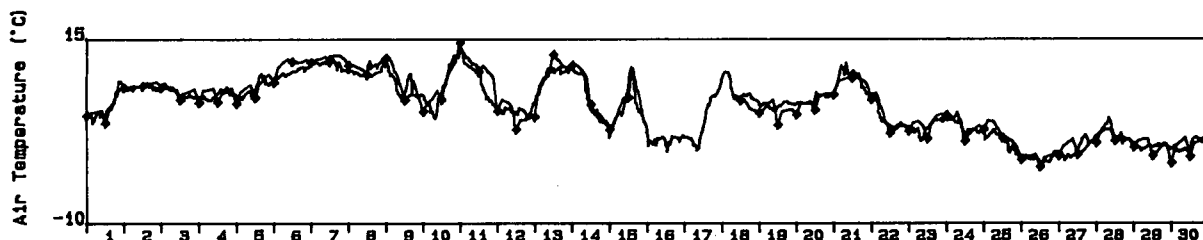
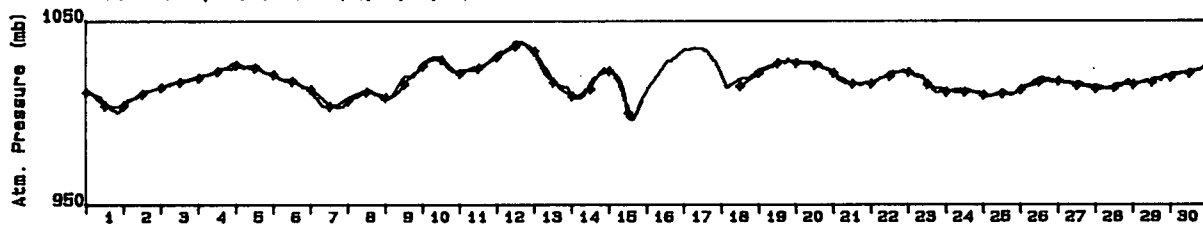
OCTOBER 1985

Pressure and Air Temperature

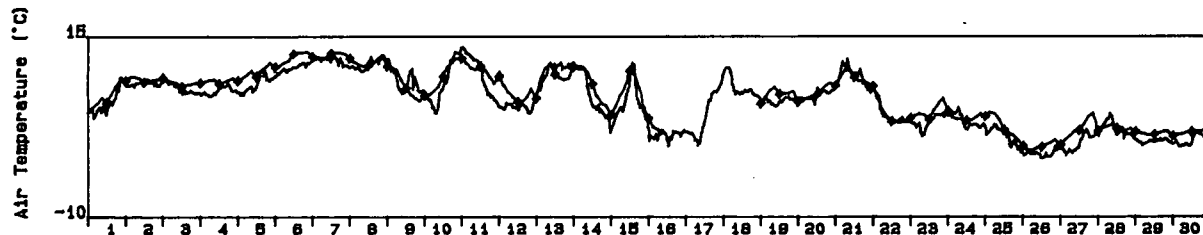
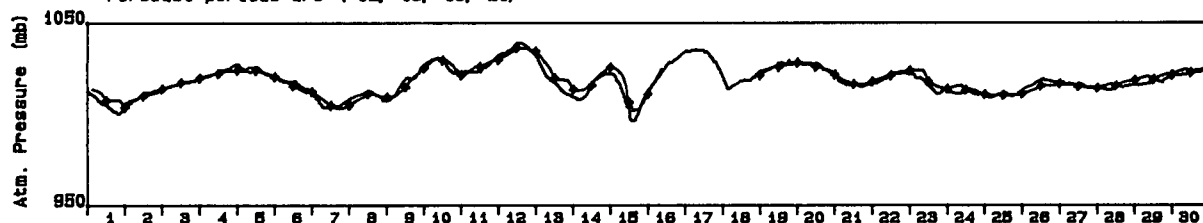
Sable Island AES Observations

Grid Point : 5

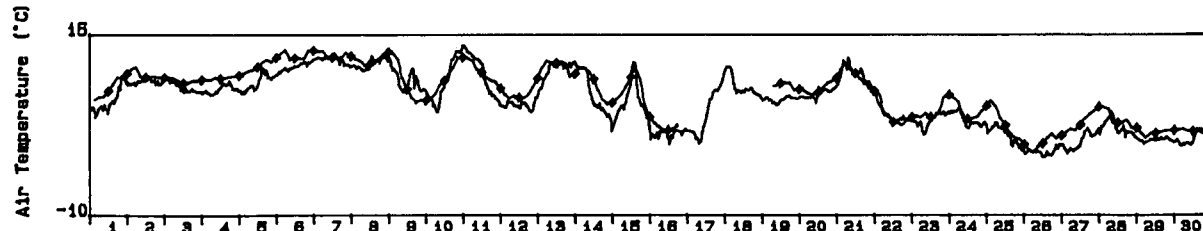
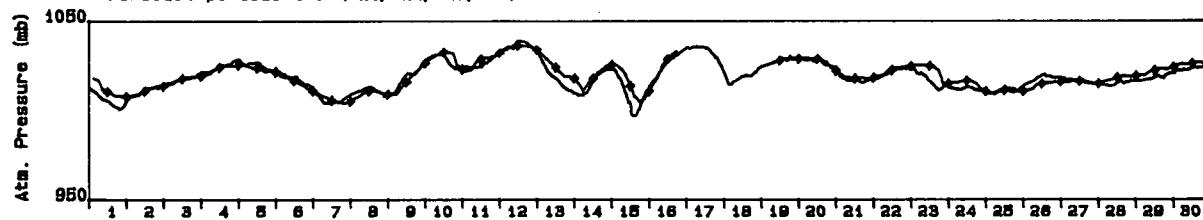
Forecast periods are (0, 3, 6, 9)



Forecast periods are (12, 15, 18, 21)



Forecast periods are (21, 24, 27, 30)

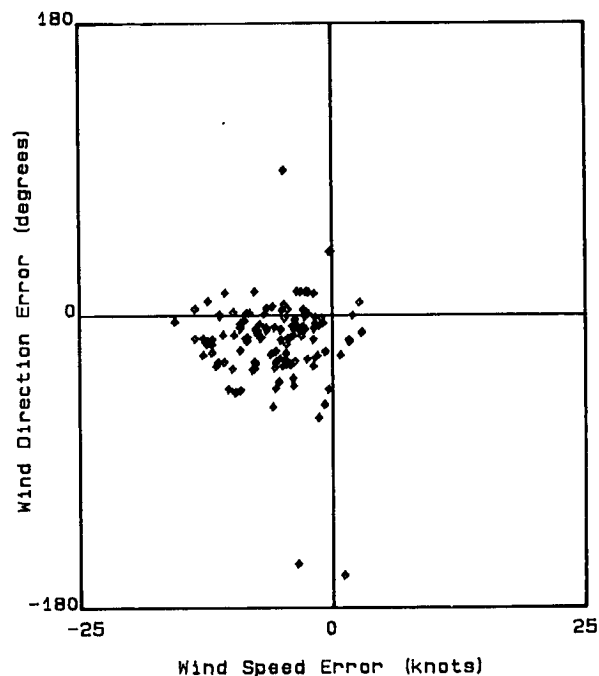
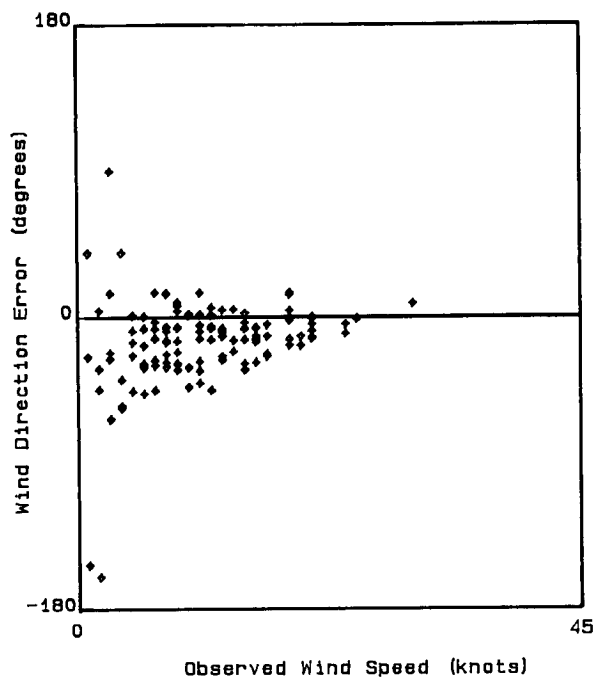
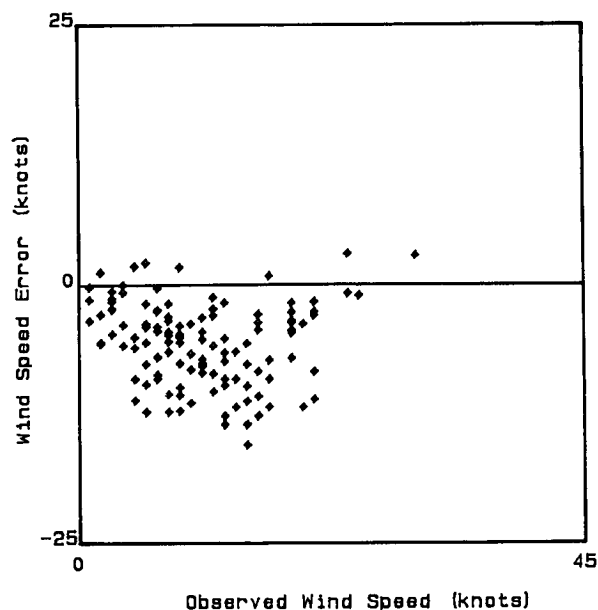
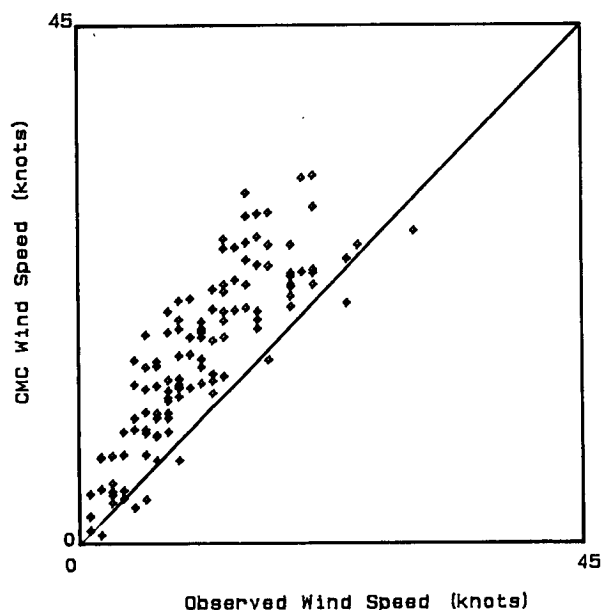


NOVEMBER 1985

00 Hour Forecast

Grid Point : 5

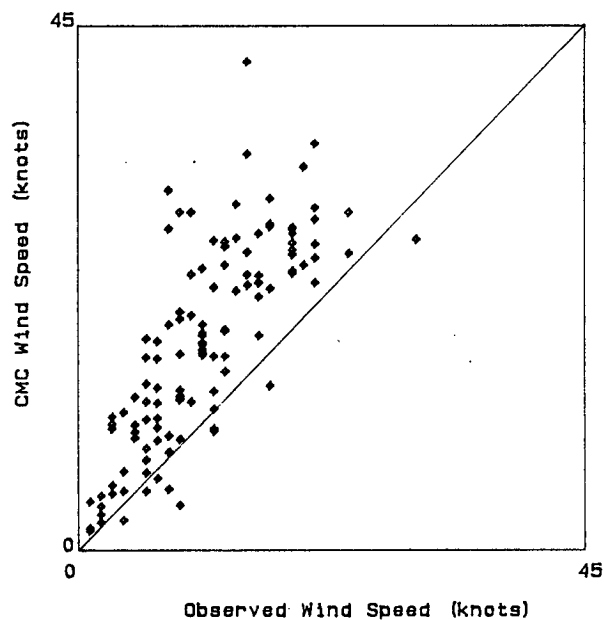
Sable Island AES Observations



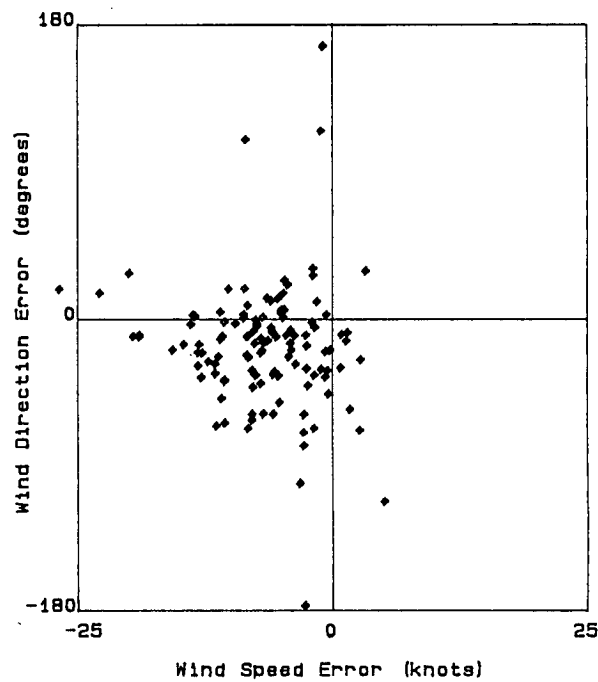
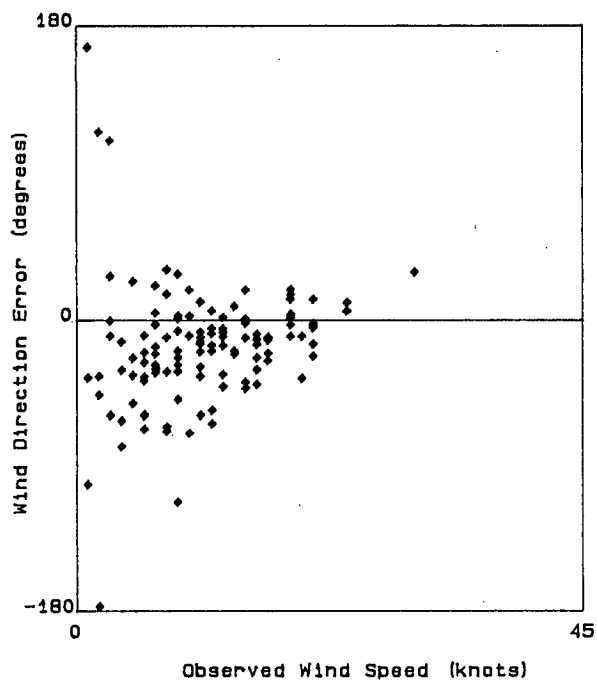
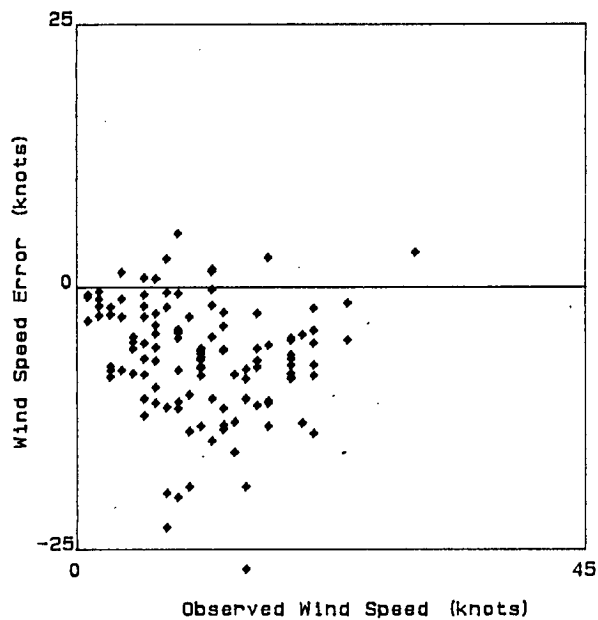
	Rate (knots)	Direction (deg.T)	Pressure (mb)	Temperature (deg.C)
Error	-5.57	-15.34	.98	.28
Abs Error	5.79	20.51	1.09	.81
RMS Error	6.83	30.96	1.26	.99
Avg Value	11.18	n.a.	1017.28	12.26
S.I.	61.11%			

12 Hour Forecast

Grid Point : 5



Sable Island AES Observations

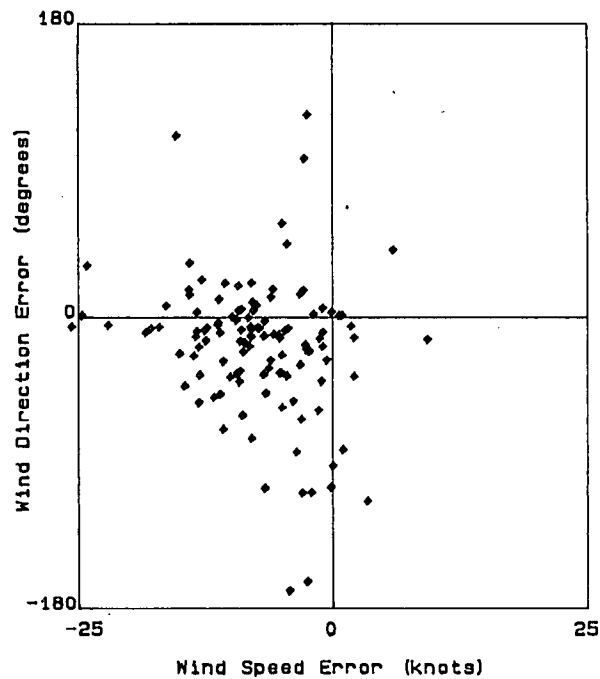
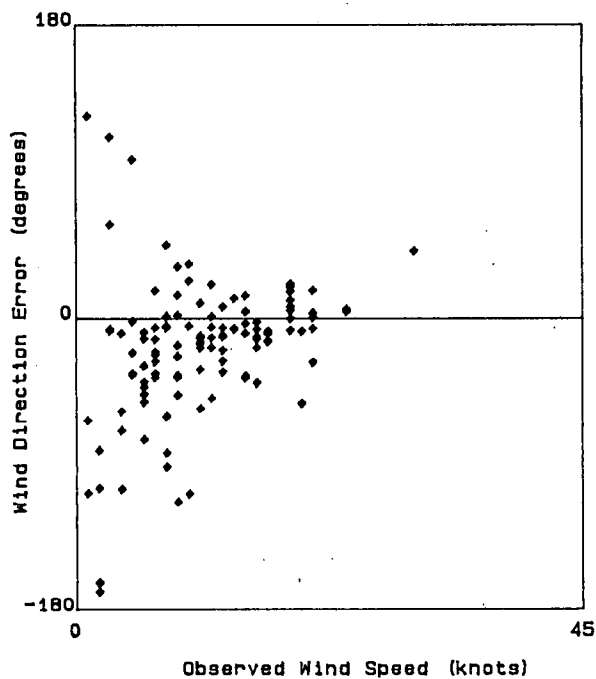
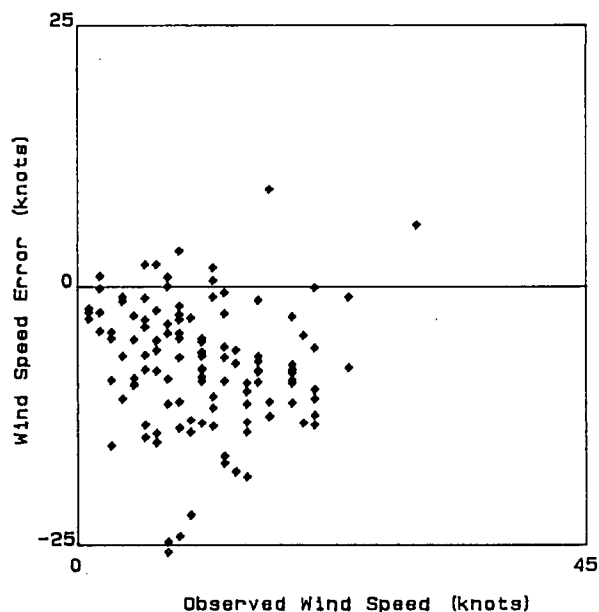
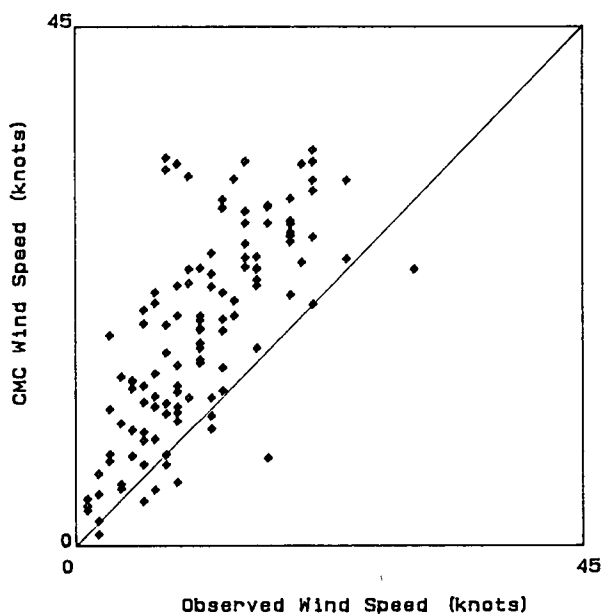


	Rate (knots)	Direction (deg.T)	Pressure (mb)	Temperature (deg.C)
Error	-6.69	-16.69	-0.00	-.42
Abs Error	7.03	28.81	1.24	.89
RMS Error	8.65	41.96	1.61	1.11
Avg Value	11.25	n.a.	1017.25	12.21
S.I.	76.91%			

24 Hour Forecast

Grid Point : 5

Sable Island AES Observations



	Rate (knots)	Direction (deg.T)	Pressure (mb)	Temperature (deg.C)
Error	-7.47	-17.84	-4.46	-6.61
Abs Error	7.93	30.89	1.87	1.12
RMS Error	9.59	46.07	2.39	1.42
Avg Value	11.25	n.a.	1017.25	12.21
S.I.	85.25%			

Verification Tables
 Sable Island AES Observations
 00 Hour Forecast
 Grid Point : 5
 Period : Sept. '85 to Nov. '85

Error of speed vs error of direction

Speed error (knots)

	-27.5	-22.5	-17.5	-12.5	-7.5	-2.5	2.5	7.5	12.5	17.5	Total	% Occ.
	-22.5	-17.5	-12.5	-7.5	-2.5	2.5	7.5	12.5	17.5	22.5		
Dir. error (deg.)												
(-157.5, -112.5)					1						1	1
(-112.5, -67.5)											0	0
(-67.5, -22.5)			1	12	16	9					38	31
(-22.5, 22.5)			4	24	36	13	2				79	65
(22.5, 67.5)						2					2	2
(67.5, 112.5)					1						1	1
(112.5, 157.5)											0	0
(157.5, 202.5)						1					1	1
Total	0	0	5	36	54	25	2	0	0	0	122	
% Occurrence	0	0	4	30	44	20	2	0	0	0		

Speed vs error of speed

Speed (knots)

	0	5	10	15	20	25	30	35	Total	% Occ.
	5	10	15	20	25	30	35	40		
Speed error (knots)										
(-27.5, -22.5)									0	0
(-22.5, -17.5)									0	0
(-17.5, -12.5)			2	3					5	4
(-12.5, -7.5)		13	13	7	3				36	30
(-7.5, -2.5)	7	20	12	12	3				54	44
(-2.5, 2.5)	9	7	3	2	3	1			25	20
(2.5, 7.5)					1		1		2	2
(7.5, 12.5)									0	0
(12.5, 17.5)									0	0
(17.5, 22.5)									0	0
Total	16	40	30	24	10	1	1	0	122	
% Occurrence	13	33	25	20	8	1	1	0		

Speed vs error of direction

Speed (knots)

	0	5	10	15	20	25	30	35	Total	% Occ.
	5	10	15	20	25	30	35	40		
Dir. error (deg.)										
(-157.5, -112.5)	1								1	1
(-112.5, -67.5)									0	0
(-67.5, -22.5)	9	16	8	5					38	31
(-22.5, 22.5)	2	24	22	19	10	1	1		79	65
(22.5, 67.5)	2								2	2
(67.5, 112.5)	1								1	1
(112.5, 157.5)									0	0
(157.5, 202.5)	1								1	1
Total	16	40	30	24	10	1	1	0	122	
% Occurrence	13	33	25	20	8	1	1	0		

Verification Tables
 Sable Island AFS Observations
 12 Hour Forecast
 Grid Point : 5
 Period : Sept. '85 to Nov. '85

Error of speed vs error of direction

		Speed error (knots)										Total	% Occ.
		-27.5	-22.5	-17.5	-12.5	-7.5	-2.5	2.5	7.5	12.5	17.5		
		-22.5	-17.5	-12.5	-7.5	-2.5	2.5	7.5	12.5	17.5	22.5		
Dir. error (deg.)	(-157.5, -112.5)							1				1	1
	(-112.5, -67.5)					3		1				4	3
	(-67.5, -22.5)			2	16	11	9	1				39	33
	(-22.5, 22.5)	2	3	8	16	28	9					66	55
	(22.5, 67.5)		1			1	2	1				5	4
	(67.5, 112.5)				1							1	1
	(112.5, 157.5)						1					1	1
	(157.5, 202.5)					1	1					2	2
Total		2	4	10	33	44	22	4	0	0	0	119	
% Occurrence		2	3	8	28	37	18	3	0	0	0		

Speed vs error of speed

		Speed (knots)								Total	% Occ.
		0	5	10	15	20	25	30	35		
		5	10	15	20	25	30	35	40		
Speed error (knots)	(-27.5, -22.5)		1		1					2	2
	(-22.5, -17.5)		2	1	1					4	3
	(-17.5, -12.5)			7	1	2				10	8
	(-12.5, -7.5)	4	10	7	11	1				33	28
	(-7.5, -2.5)	4	15	10	10	5				44	37
	(-2.5, 2.5)	8	7	5		2				22	18
	(2.5, 7.5)		2		1			1		4	3
	(7.5, 12.5)									0	0
	(12.5, 17.5)									0	0
	(17.5, 22.5)									0	0
Total		16	37	30	25	10	0	1	0	119	
% Occurrence		13	31	25	21	8	0	1	0		

Speed vs error of direction

		Speed (knots)								Total	% Occ.
		0	5	10	15	20	25	30	35		
		5	10	15	20	25	30	35	40		
Dir. error (deg.)	(-157.5, -112.5)		1							1	1
	(-112.5, -67.5)	2	1	1						4	3
	(-67.5, -22.5)	6	19	7	6	1				39	33
	(-22.5, 22.5)	3	13	22	19	9				66	55
	(22.5, 67.5)	1	3					1		5	4
	(67.5, 112.5)	1								1	1
	(112.5, 157.5)	1								1	1
	(157.5, 202.5)	2								2	2
Total		16	37	30	25	10	0	1	0	119	
% Occurrence		13	31	25	21	8	0	1	0		

Verification Tables
 24 Hour Forecast
 Sable Island AES Observations
 Grid Point : 5
 Period : Sept.'85 to Nov.'85

Error of speed vs error of direction

Speed error (knots)

	-27.5	-22.5	-17.5	-12.5	-7.5	-2.5	2.5	7.5	12.5	17.5	Total	% Occ.
	-22.5	-17.5	-12.5	-7.5	-2.5	2.5	7.5	12.5	17.5	22.5		
Dir. error (deg.)												
(-157.5, -112.5)							1				1	1
(-112.5, -67.5)				2	3	4					9	8
(-67.5, -22.5)			5	8	12	4					29	25
(-22.5, 22.5)	2	3	10	25	16	11		1			68	58
(22.5, 67.5)	1		2		2		1				6	5
(67.5, 112.5)			1		1						2	2
(112.5, 157.5)					1						1	1
(157.5, 202.5)					2						2	2
Total	3	3	18	35	37	19	2	1	0	0	118	
% Occurrence	3	3	15	30	31	16	2	1	0	0		

Speed vs error of speed

Speed (knots)

	0	5	10	15	20	25	30	35	Total	% Occ.
	5	10	15	20	25	30	35	40		
Speed error (knots)										
(-27.5, -22.5)		3							3	3
(-22.5, -17.5)			2	1					3	3
(-17.5, -12.5)	1	5	6	4	2				18	15
(-12.5, -7.5)	2	8	7	14	4				35	30
(-7.5, -2.5)	7	15	10	3	2				37	31
(-2.5, 2.5)	5	7	4	1	2				19	16
(2.5, 7.5)		1					1		2	2
(7.5, 12.5)				1					1	1
(12.5, 17.5)									0	0
(17.5, 22.5)									0	0
Total	15	39	29	24	10	0	1	0	118	
% Occurrence	13	33	25	20	8	0	1	0		

Speed vs error of direction

Speed (knots)

	0	5	10	15	20	25	30	35	Total	% Occ.
	5	10	15	20	25	30	35	40		
Dir. error (deg.)										
(-157.5, -112.5)		1							1	1
(-112.5, -67.5)	5	3	1						9	8
(-67.5, -22.5)	2	17	5	3	2				29	25
(-22.5, 22.5)	3	15	21	21	8				68	58
(22.5, 67.5)	1	2	2				1		6	5
(67.5, 112.5)	1	1							2	2
(112.5, 157.5)	1								1	1
(157.5, 202.5)	2								2	2
Total	15	39	29	24	10	0	1	0	118	
% Occurrence	13	33	25	20	8	0	1	0		

Sable Island AES Observations
Grid Point : 5
00 Hour Forecast
Month : September

	Rate (knots)	Direction (deg.T)	Pressure (mb)	Temperature (deg.C)
Error	-5.48	-25.44	1.32	-.11
Abs Error	5.67	28.26	1.32	.89
RMS Error	6.85	37.77	1.45	1.09
Avg Value	7.96	n.a.	1018.23	14.47
# of pts	40	40	40	40
S.I.	86.03%			

Sable Island AES Observations
Grid Point : 5
00 Hour Forecast
Month : October

	Rate (knots)	Direction (deg.T)	Pressure (mb)	Temperature (deg.C)
Error	-5.47	-10.00	.83	.54
Abs Error	5.69	17.07	.97	.80
RMS Error	6.72	29.19	1.12	.96
Avg Value	12.90	n.a.	1016.90	11.26
# of pts	62	62	62	62
S.I.	52.12%			

Sable Island AES Observations
Grid Point : 5
00 Hour Forecast
Month : November

	Rate (knots)	Direction (deg.T)	Pressure (mb)	Temperature (deg.C)
Error	-6.05	-11.68	.79	.24
Abs Error	6.33	15.66	1.01	.70
RMS Error	7.14	18.76	1.25	.87
Avg Value	15.55	n.a.	1015.60	8.72
# of pts	20	20	20	20
S.I.	45.90%			

Sable Island AES Observations
Grid Point : 5
12 Hour Forecast
Month : September

	Rate (knots)	Direction (deg.T)	Pressure (mb)	Temperature (deg.C)
Error	-5.52	-26.15	.24	-.53
Abs Error	5.70	39.39	.93	1.01
RMS Error	7.95	49.20	1.14	1.29
Avg Value	7.96	n.a.	1018.23	14.47
# of pts	39	39	39	39
S.I.	99.78%			

Sable Island AES Observations
Grid Point : 5
12 Hour Forecast
Month : October

	Rate (knots)	Direction (deg.T)	Pressure (mb)	Temperature (deg.C)
Error	-6.80	-11.79	-.39	-.20
Abs Error	7.24	25.05	1.40	.78
RMS Error	8.56	40.96	1.78	.97
Avg Value	13.03	n.a.	1016.84	11.17
# of pts	61	61	61	61
S.I.	65.68%			

Sable Island AES Observations
Grid Point : 5
12 Hour Forecast
Month : November

	Rate (knots)	Direction (deg.T)	Pressure (mb)	Temperature (deg.C)
Error	-8.76	-13.01	.72	-.87
Abs Error	9.11	19.17	1.36	1.02
RMS Error	10.21	25.95	1.82	1.15
Avg Value	15.55	n.a.	1015.60	8.72
# of pts	19	19	19	19
S.I.	65.68%			

Sable Island AES Observations
Grid Point : 5
24 Hour Forecast
Month : September

	Rate (knots)	Direction (deg.T)	Pressure (mb)	Temperature (deg.C)
Error	-6.07	-27.40	-.59	-.49
Abs Error	6.39	42.84	1.65	1.23
RMS Error	8.40	54.62	2.09	1.60
Avg Value	7.96	n.a.	1018.23	14.47
# of pts	38	38	38	38
S.I.	105.50%			

Sable Island AES Observations
Grid Point : 5
24 Hour Forecast
Month : October

	Rate (knots)	Direction (deg.T)	Pressure (mb)	Temperature (deg.C)
Error	-7.63	-13.40	-.68	-.51
Abs Error	8.12	26.56	2.00	.98
RMS Error	9.64	43.66	2.56	1.26
Avg Value	13.03	n.a.	1016.84	11.17
# of pts	61	61	61	61
S.I.	73.99%			

Sable Island AES Observations
Grid Point : 5
24 Hour Forecast
Month : November

	Rate (knots)	Direction (deg.T)	Pressure (mb)	Temperature (deg.C)
Error	-9.74	-12.98	.50	-1.15
Abs Error	10.36	20.90	1.89	1.32
RMS Error	11.49	33.08	2.35	1.54
Avg Value	15.55	n.a.	1015.60	8.72
# of pts	19	19	19	19
S.I.	73.89%			

**Appendix 6.3 Comparison of Adjusted Sable Island Winds With CMC
Forecasts.**

Time-series plots of wind speed and direction

00,03,06,09 h forecasts: September 1985 to February 1986
12,15,18,21 h forecasts: September 1985 to February 1986
21,24,27,30 h forecasts: September 1985 to February 1986

Time-series plots of pressure and air temperature

00,03,06,09 h forecasts
12,15,18,21 h forecasts September 1985 to February 1986
21,24,27,30 h forecasts

Scatterplots and error statistics

00 h forecast
12 h forecast September 1985 to February 1986 inclusive
24 h forecast

Verification Tables

00 h forecast
12 h forecast September 1985 to February 1986 inclusive
24 h forecast

Monthly error statistics

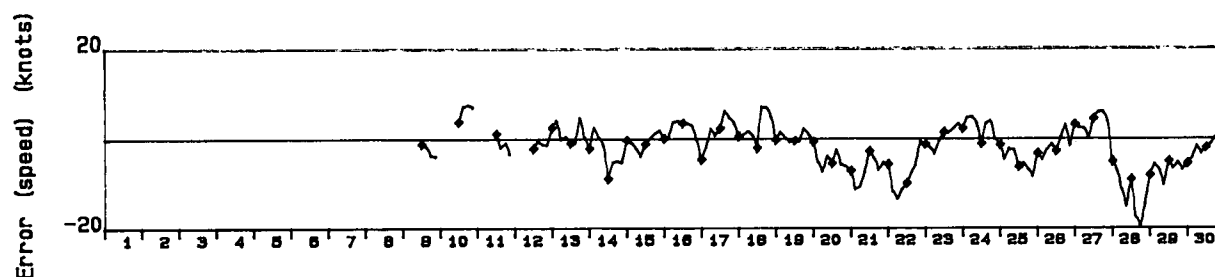
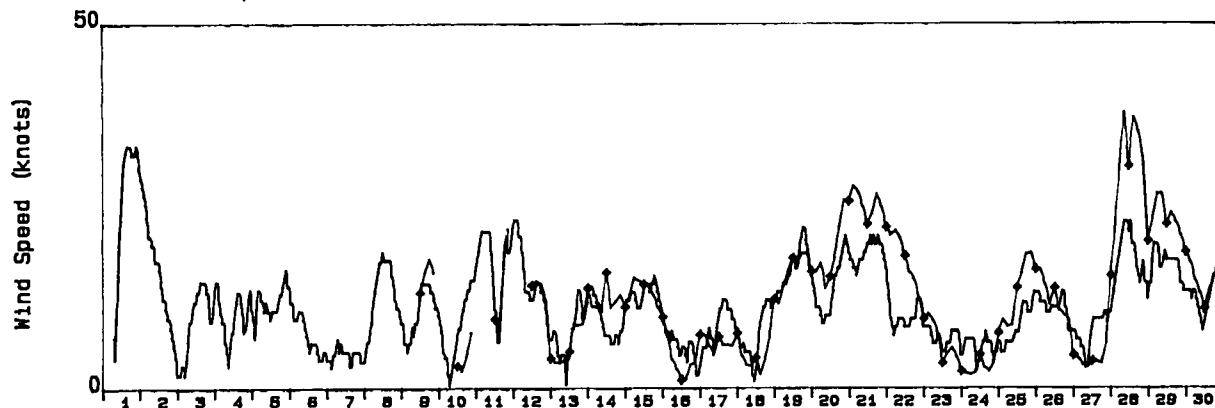
00 h forecast
12 h forecast September 1985 to February 1986
24 h forecast

Wind Rate and Direction

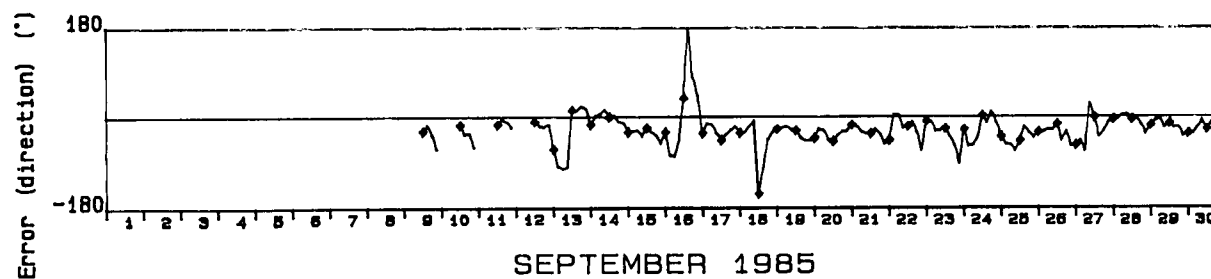
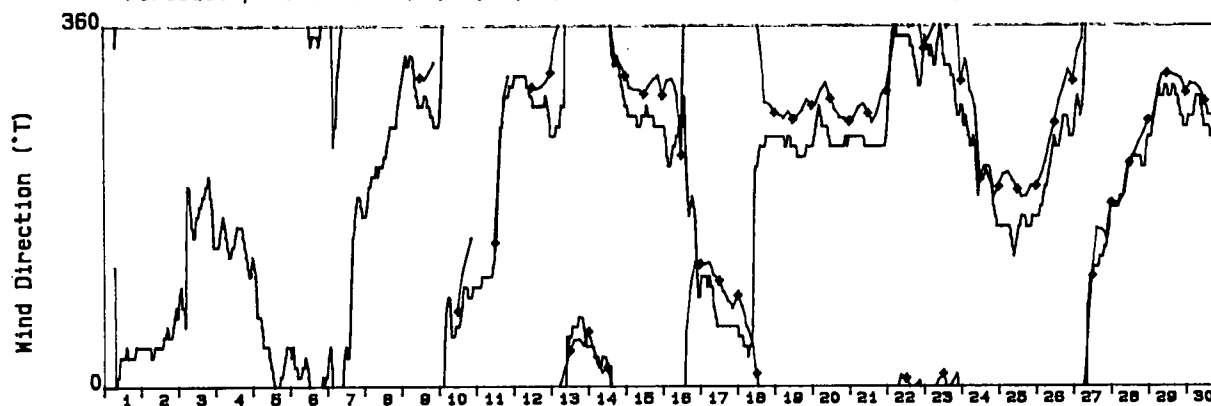
Adjusted Sable Island Observations

Grid Point : 5

Forecast periods are (0, 3, 6, 9)



Forecast periods are (0, 3, 6, 9)



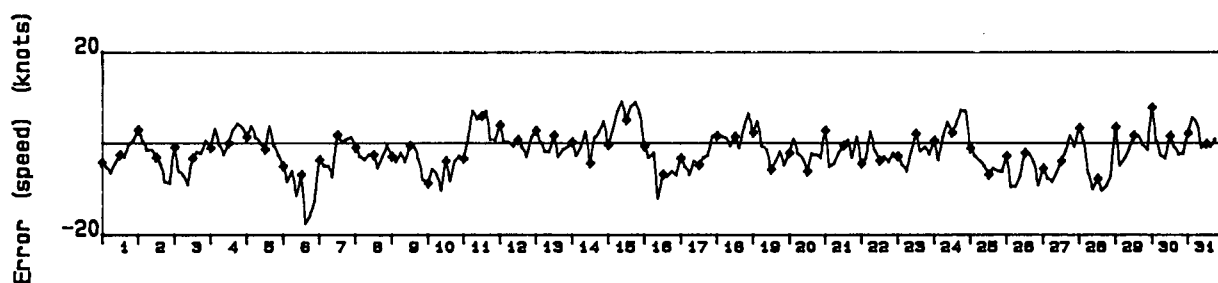
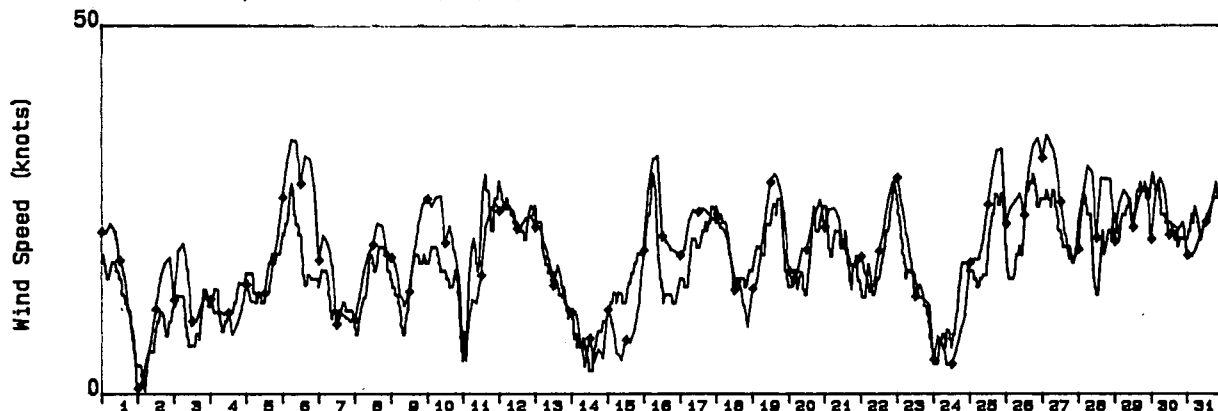
SEPTEMBER 1985

Wind Rate and Direction

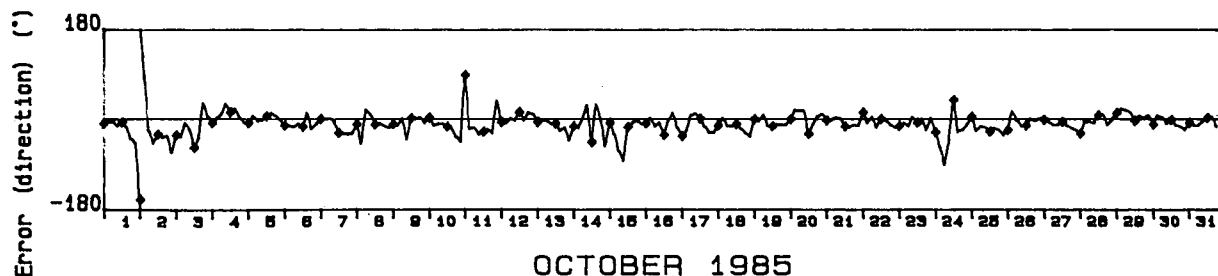
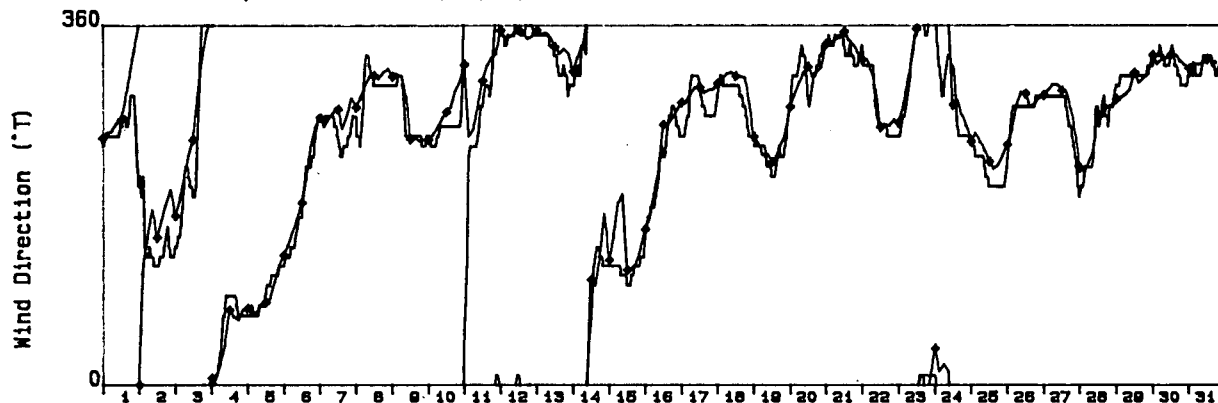
Adjusted Sable Island Observations

Grid Point : 5

Forecast periods are (0, 3, 6, 9)



Forecast periods are (0, 3, 6, 9)



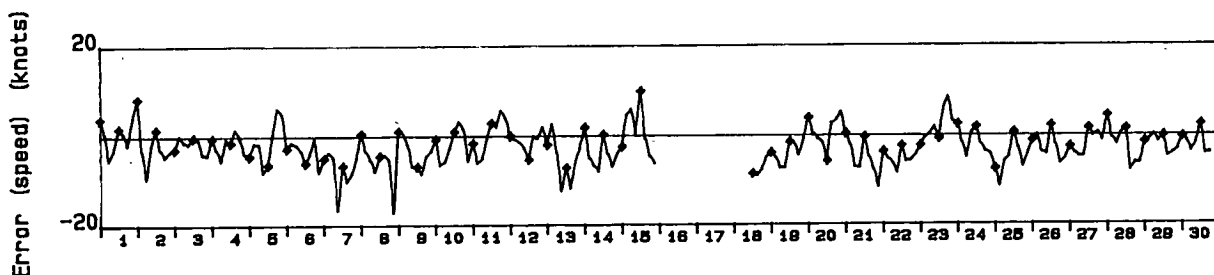
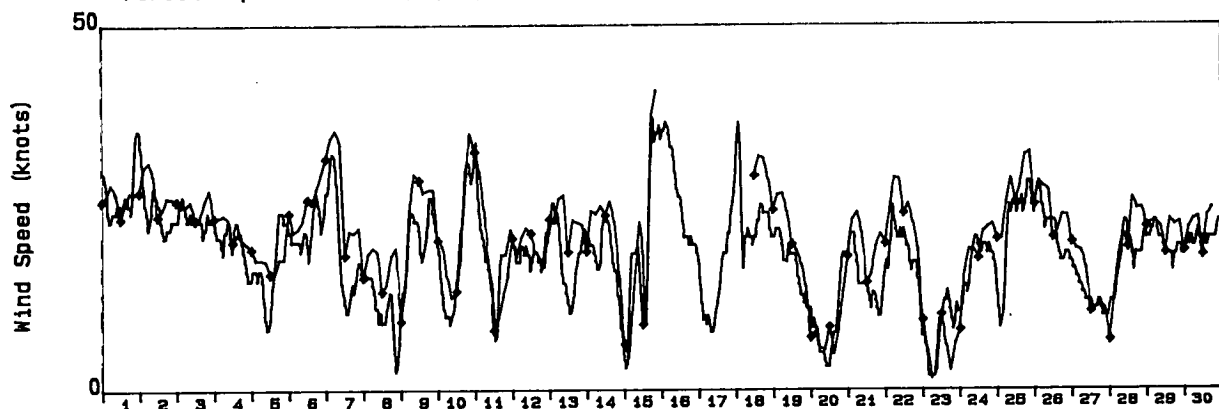
OCTOBER 1985

Wind Rate and Direction

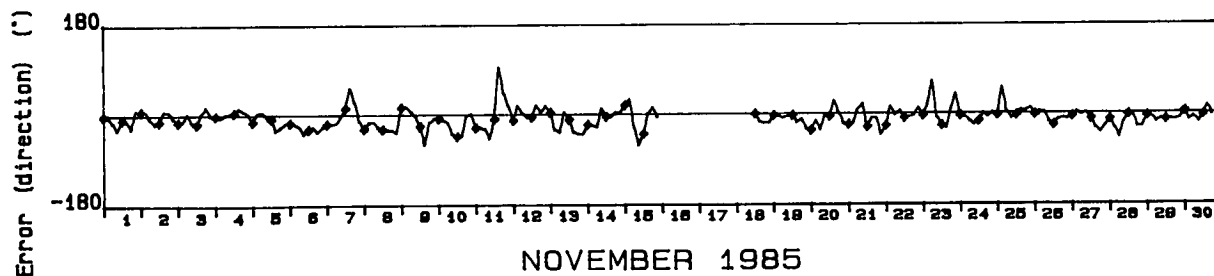
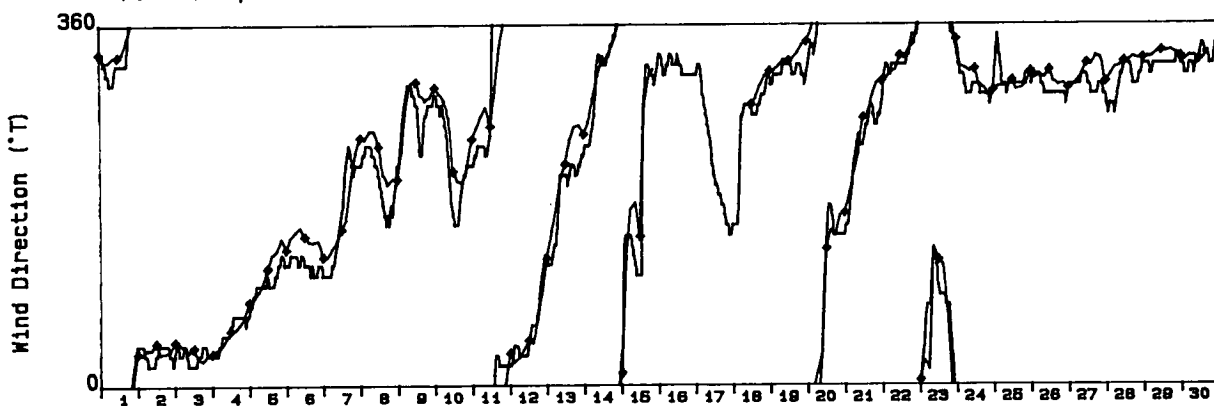
Adjusted Sable Island Observations

Grid Point : 5

Forecast periods are (0, 3, 6, 9)



Forecast periods are (0, 3, 6, 9)



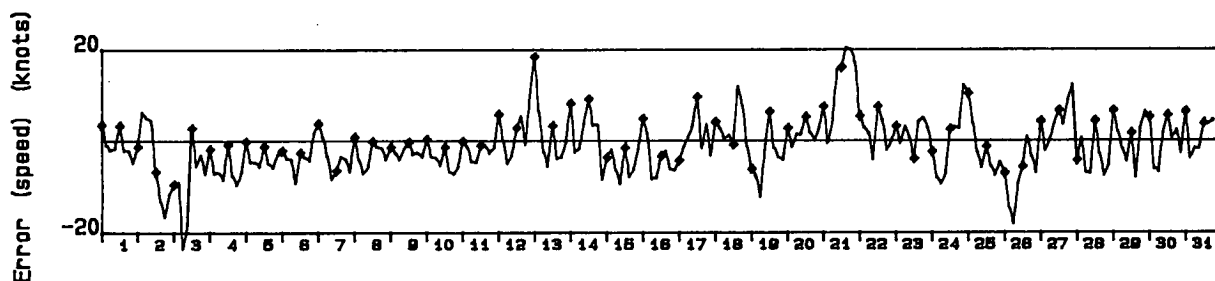
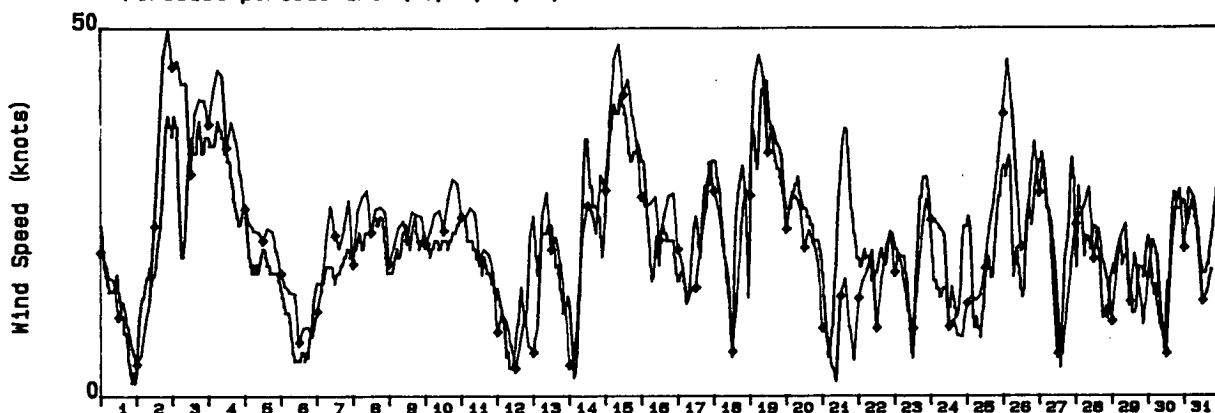
NOVEMBER 1985

Wind Rate and Direction

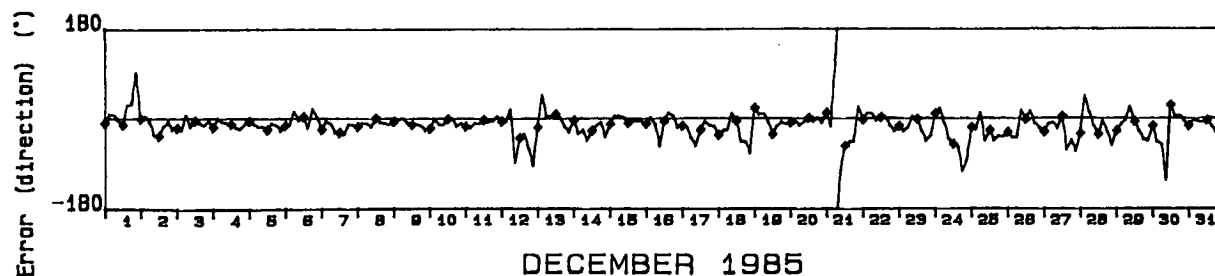
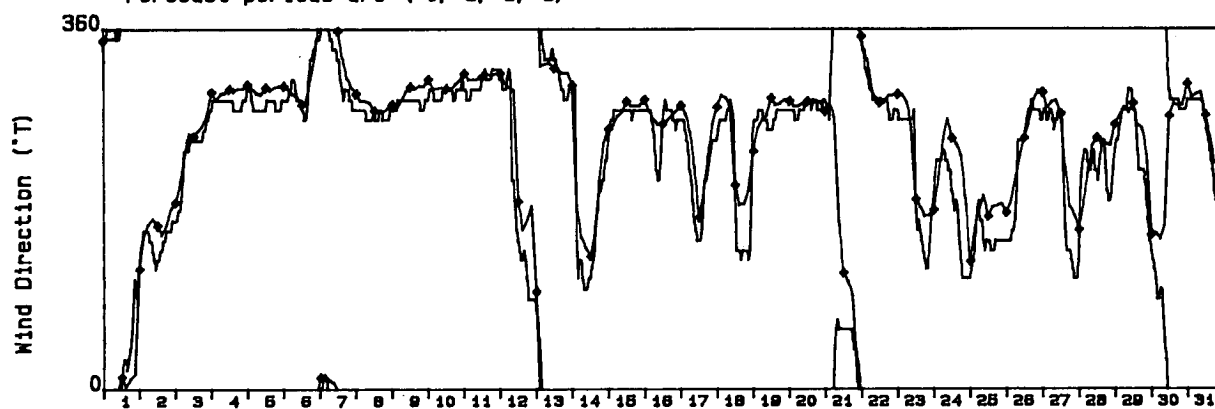
Adjusted Sable Island Observations

Grid Point : 5

Forecast periods are (0, 3, 6, 9)



Forecast periods are (0, 3, 6, 9)



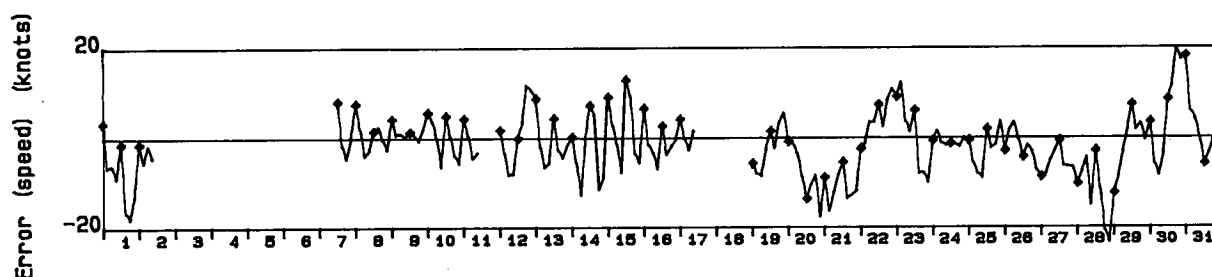
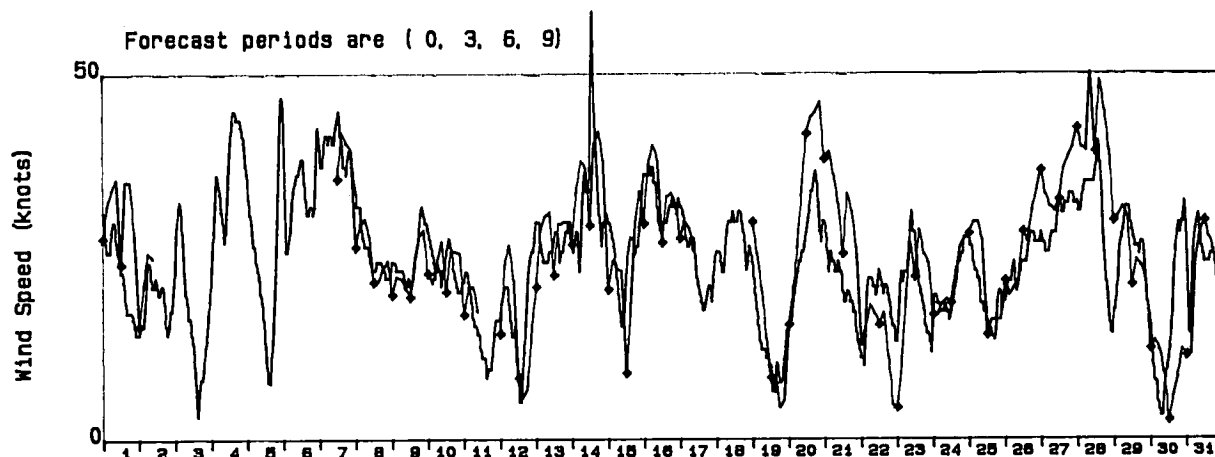
DECEMBER 1985

Wind Rate and Direction

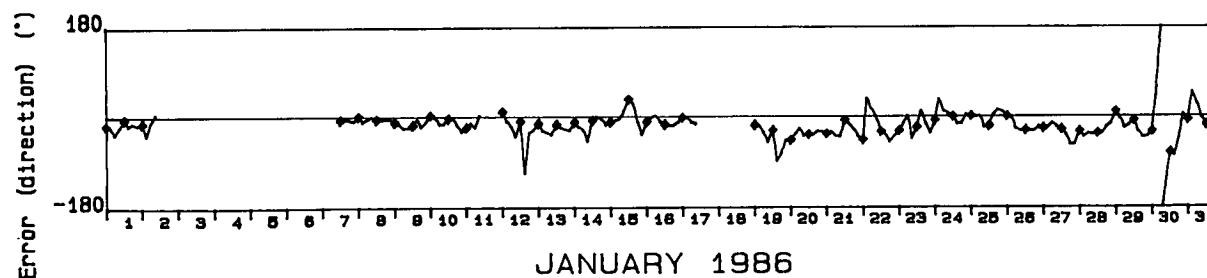
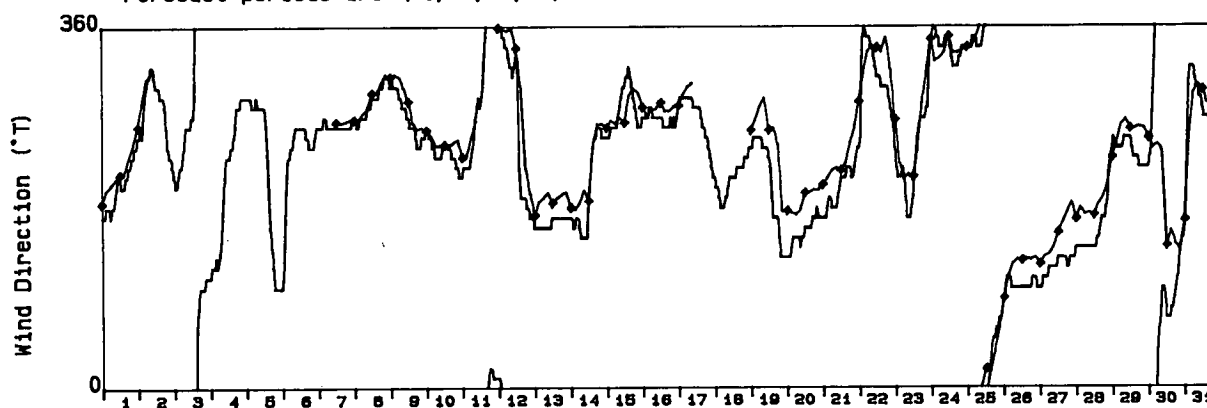
Adjusted Sable Island Observations

Grid Point : 5

Forecast periods are (0, 3, 6, 9)



Forecast periods are (0, 3, 6, 9)



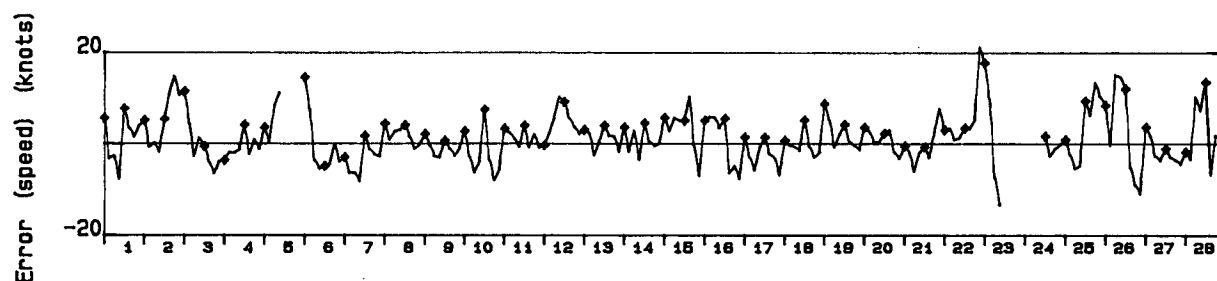
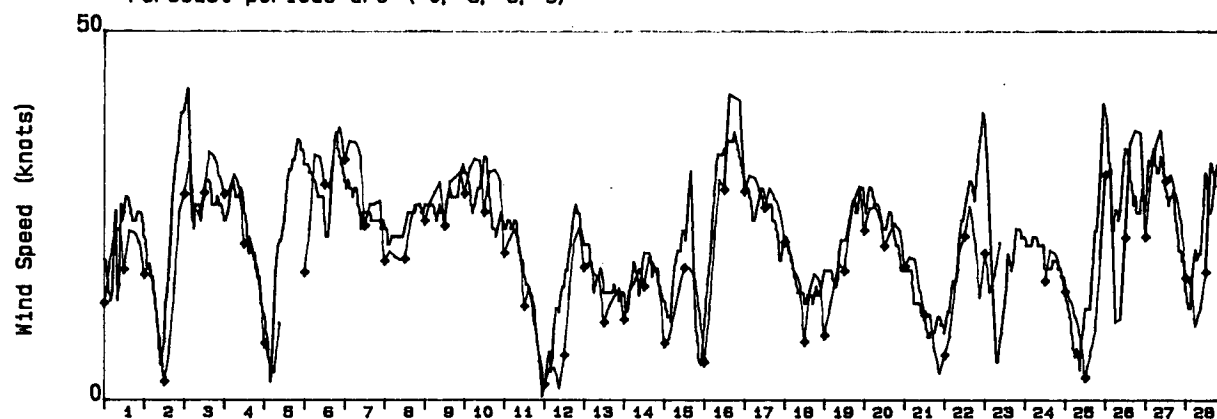
JANUARY 1986

Wind Rate and Direction

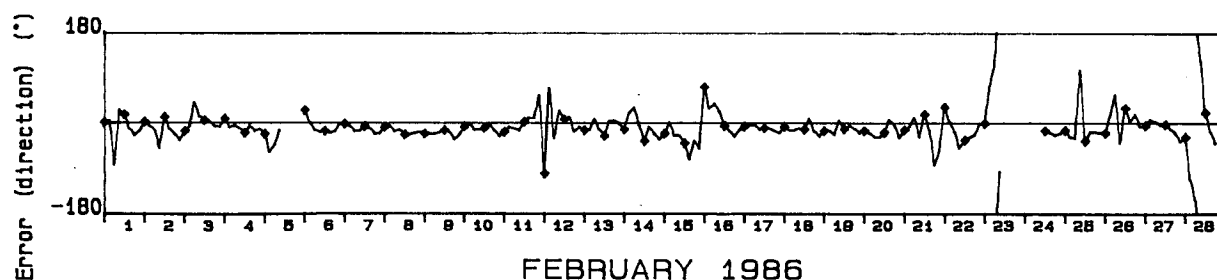
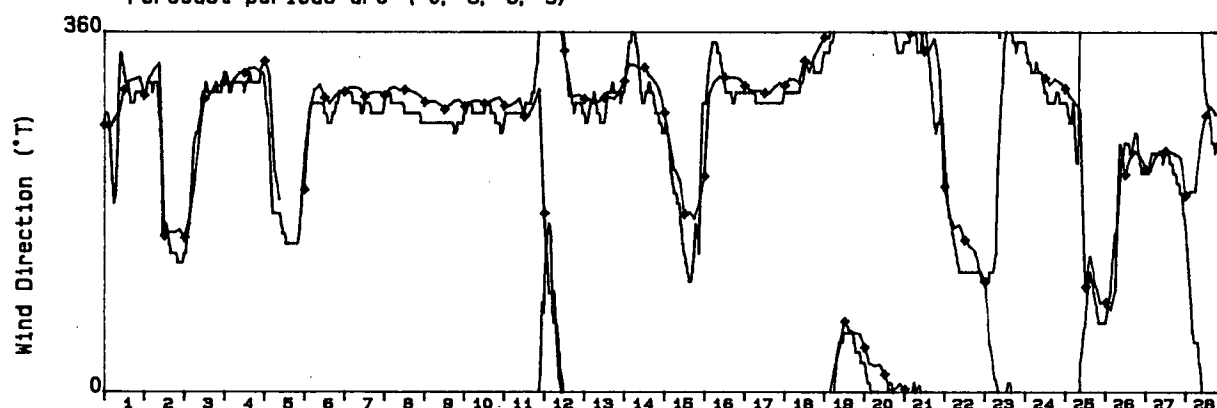
Adjusted Sable Island Observations

Grid Point : 5

Forecast periods are (0, 3, 6, 9)



Forecast periods are (0, 3, 6, 9)



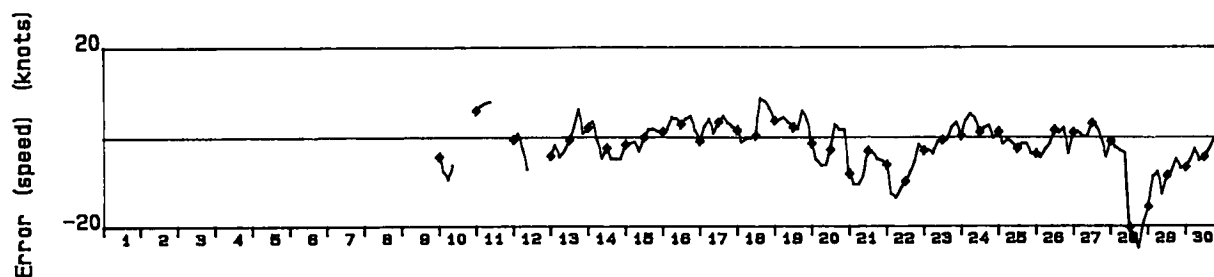
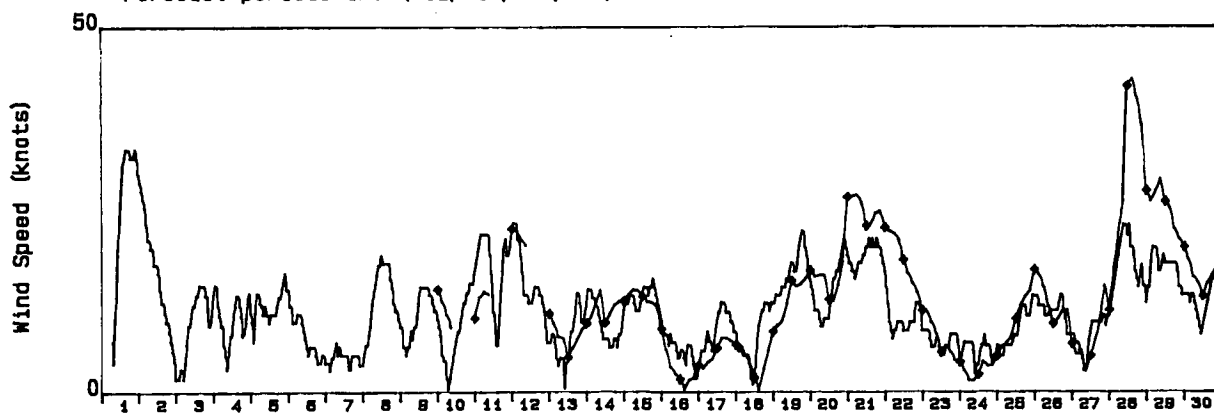
FEBRUARY 1986

Wind Rate and Direction

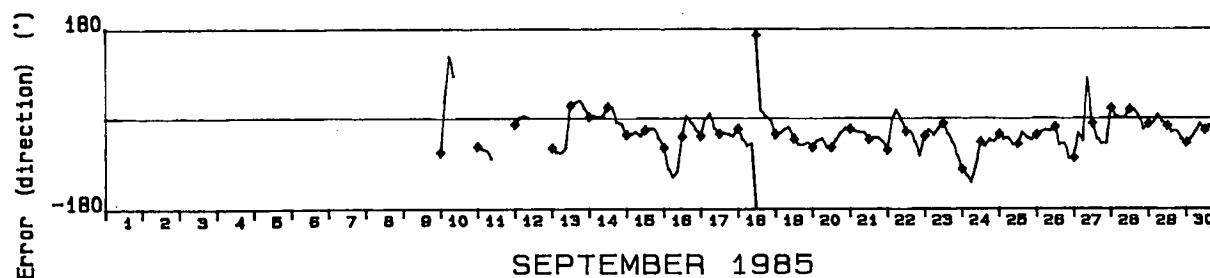
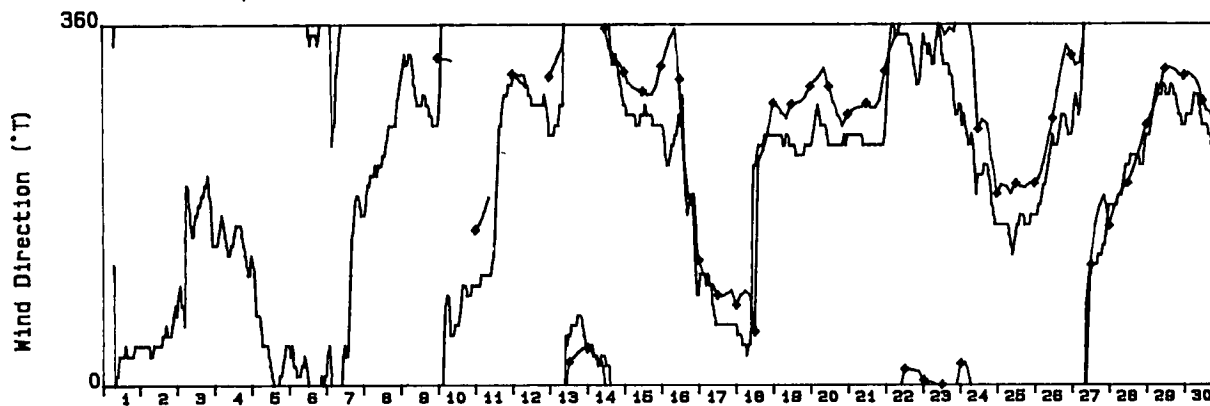
Adjusted Sable Island Observations

Grid Point : 5

Forecast periods are (12, 15, 18, 21)



Forecast periods are (12, 15, 18, 21)



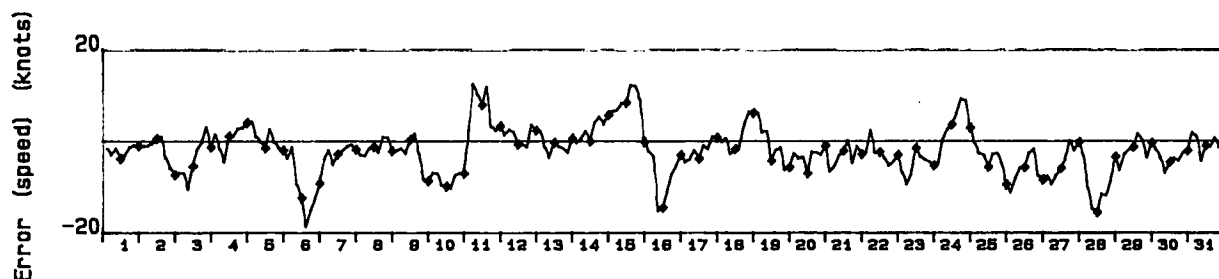
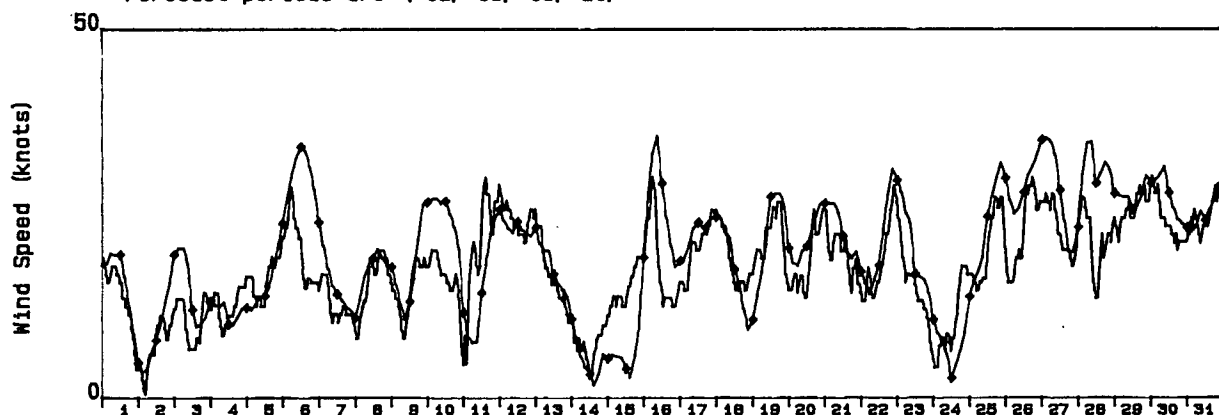
SEPTEMBER 1985

Wind Rate and Direction

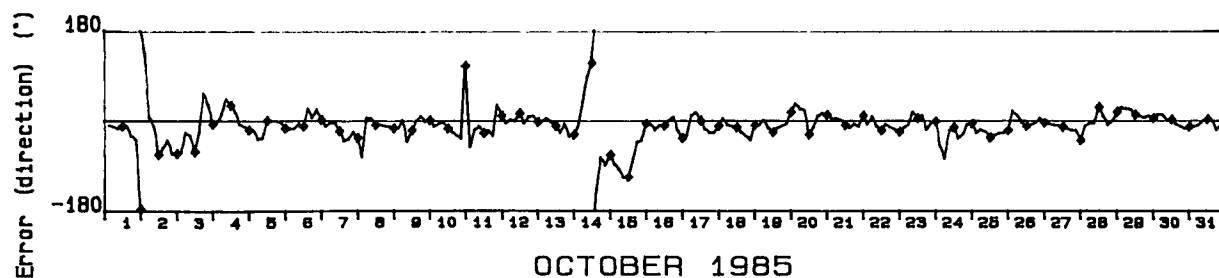
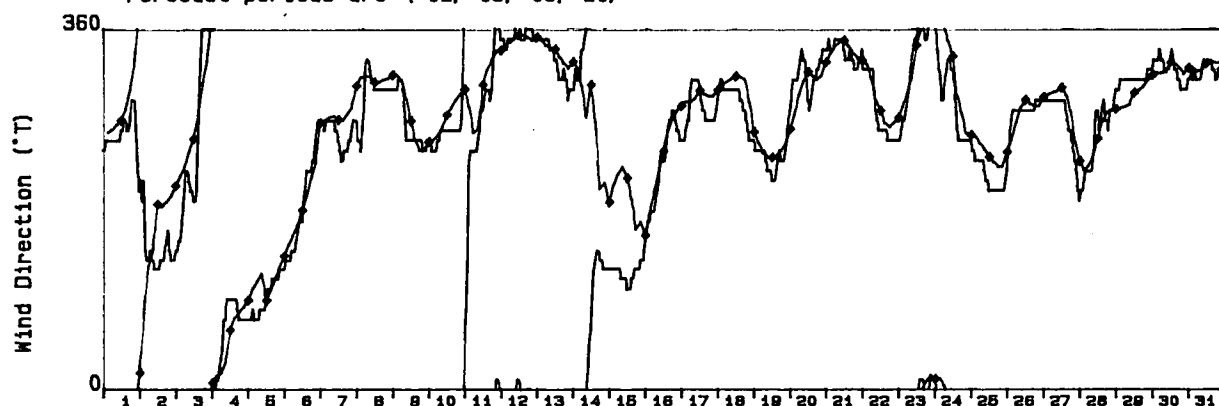
Adjusted Sable Island Observations

Grid Point : 5

Forecast periods are (12, 15, 18, 21)



Forecast periods are (12, 15, 18, 21)



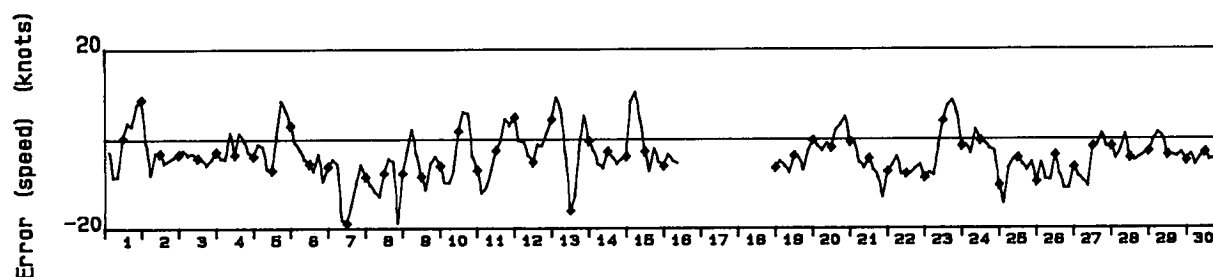
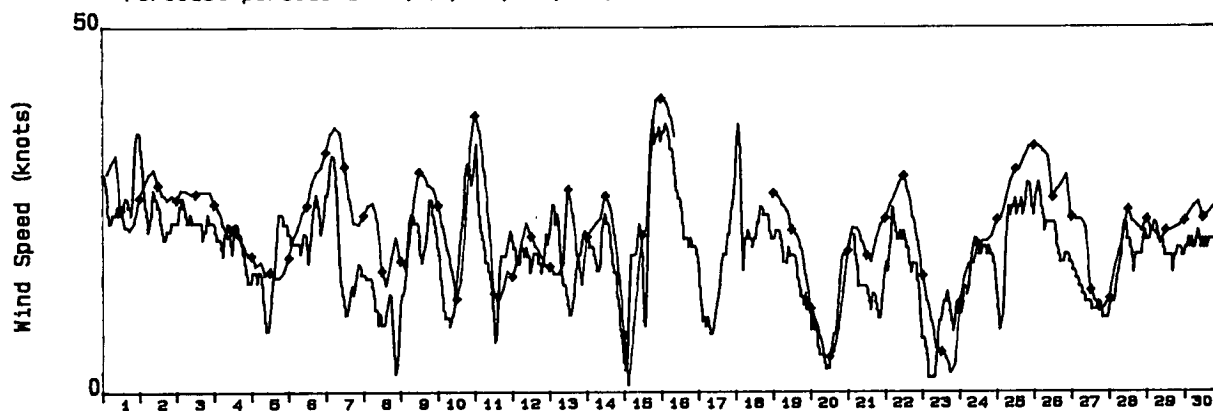
OCTOBER 1985

Wind Rate and Direction

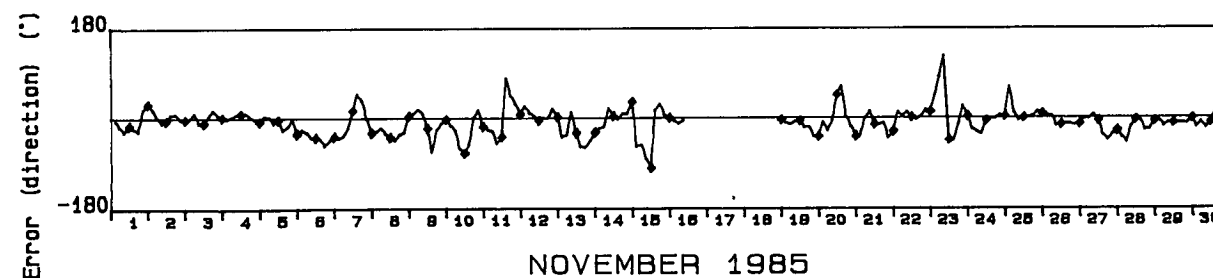
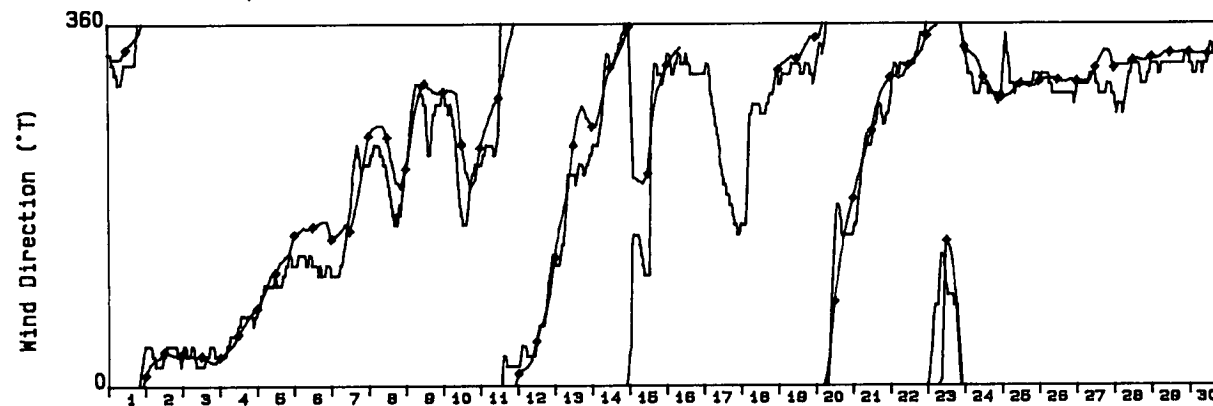
Adjusted Sable Island Observations

Grid Point : 5

Forecast periods are (12, 15, 18, 21)



Forecast periods are (12, 15, 18, 21)



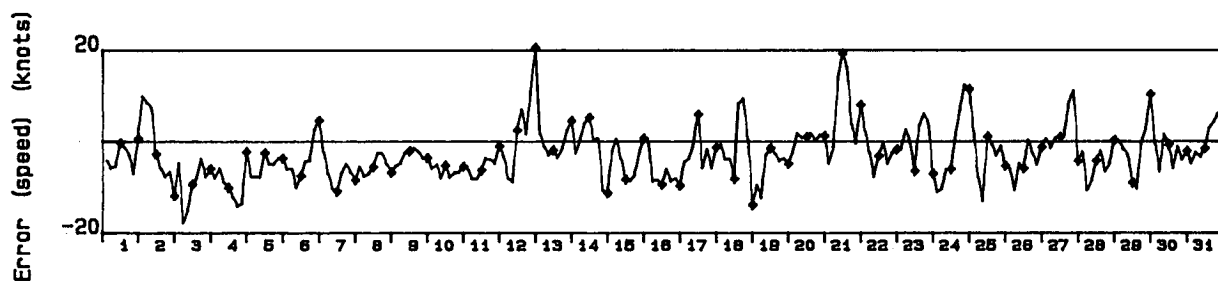
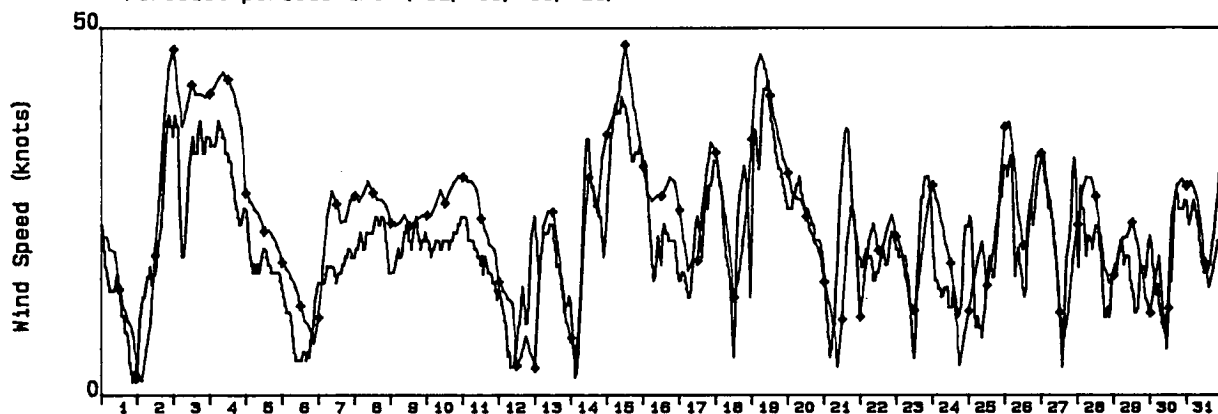
NOVEMBER 1985

Wind Rate and Direction

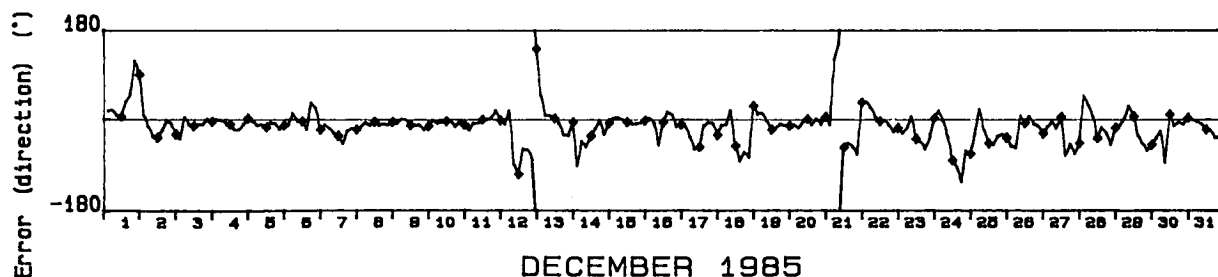
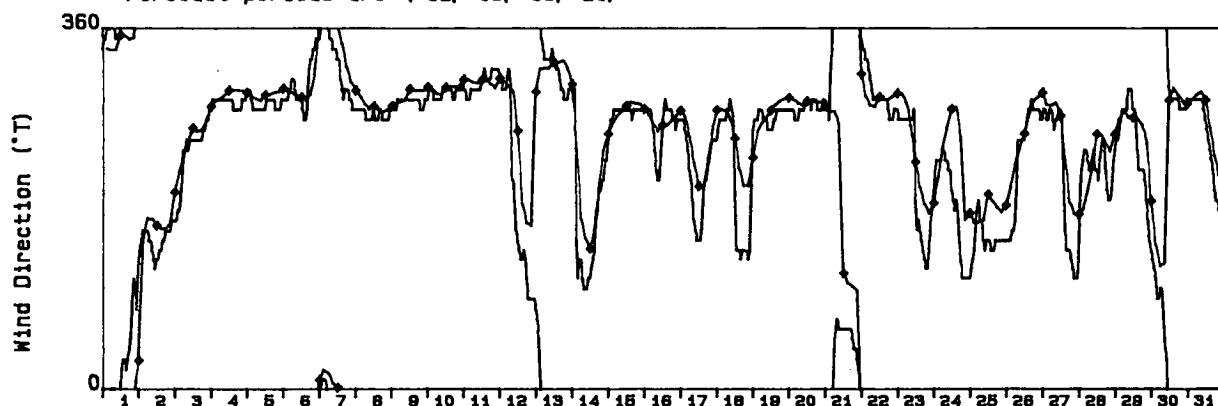
Adjusted Sable Island Observations

Grid Point : 5

Forecast periods are (12, 15, 18, 21)



Forecast periods are (12, 15, 18, 21)



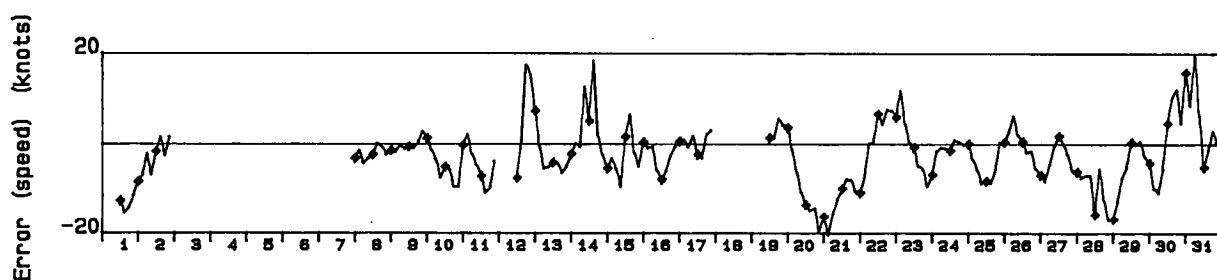
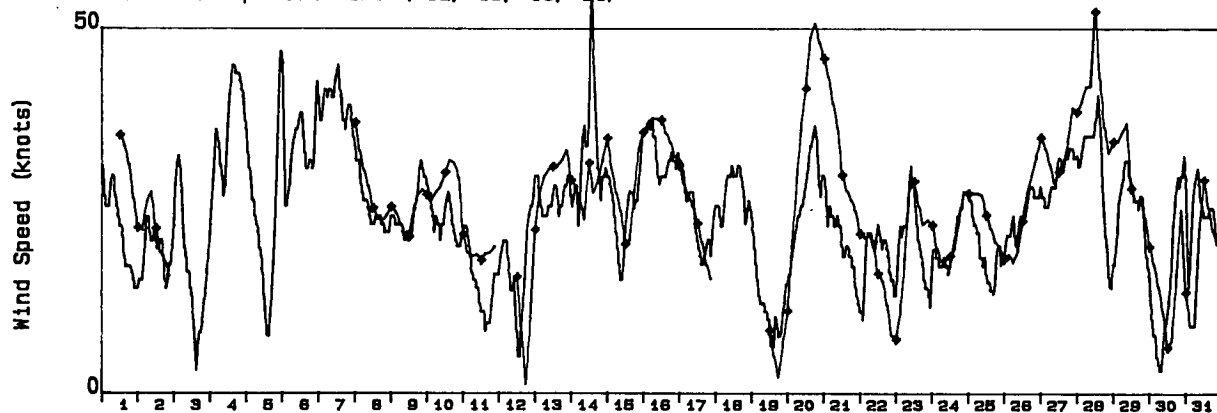
DECEMBER 1985

Wind Rate and Direction

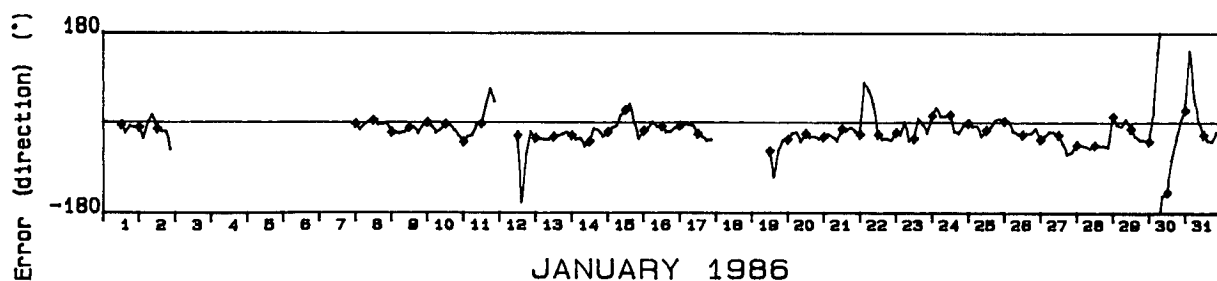
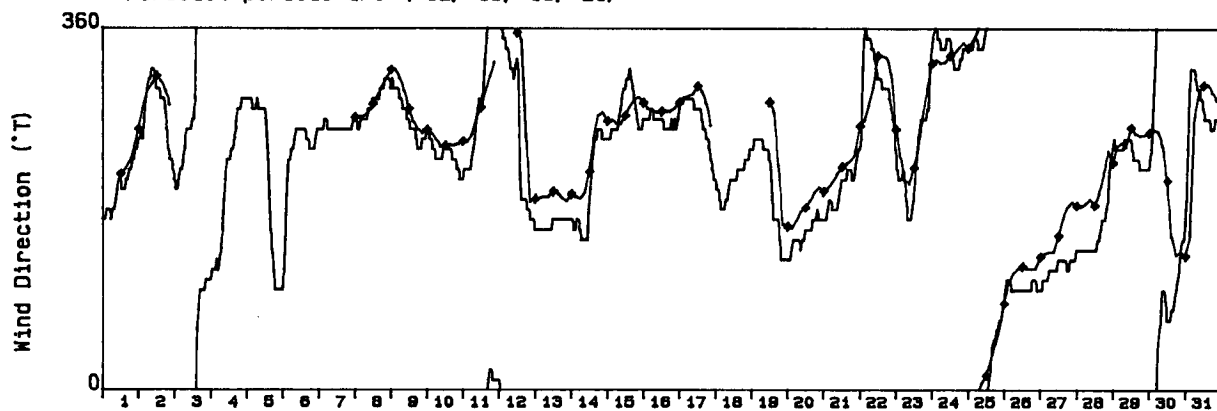
Adjusted Sable Island Observations

Grid Point : 5

Forecast periods are (12, 15, 18, 21)



Forecast periods are (12, 15, 18, 21)



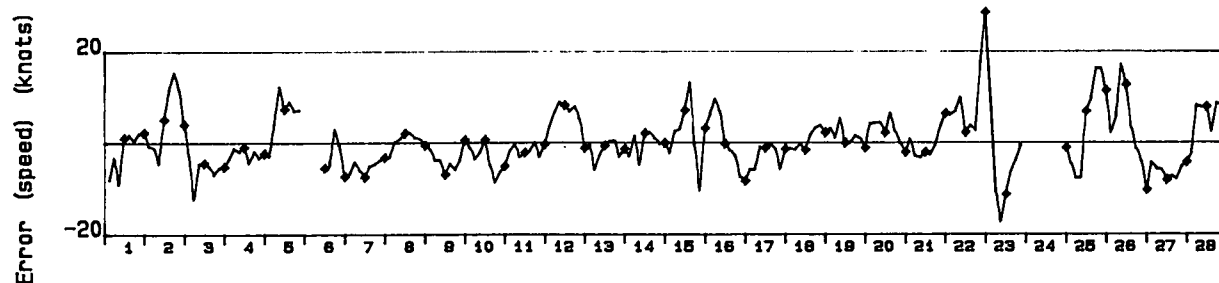
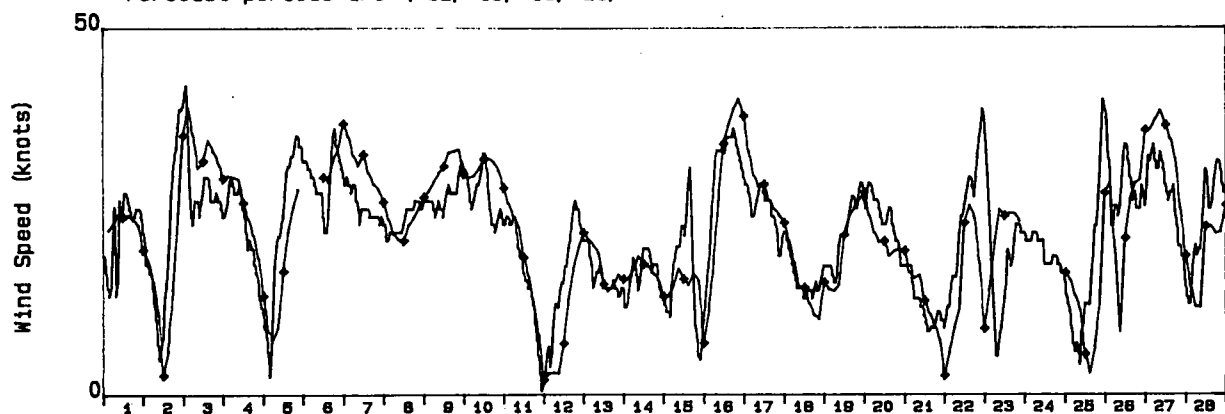
JANUARY 1986

Wind Rate and Direction

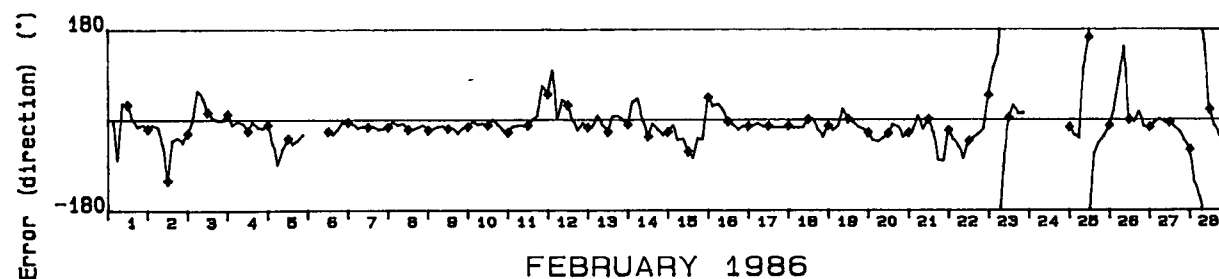
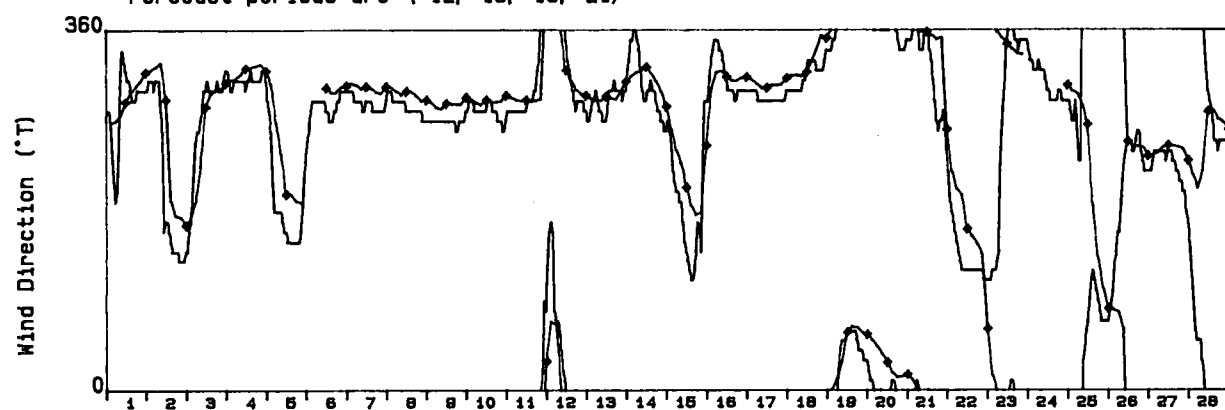
Adjusted Sable Island Observations

Grid Point : 5

Forecast periods are (12, 15, 18, 21)



Forecast periods are (12, 15, 18, 21)



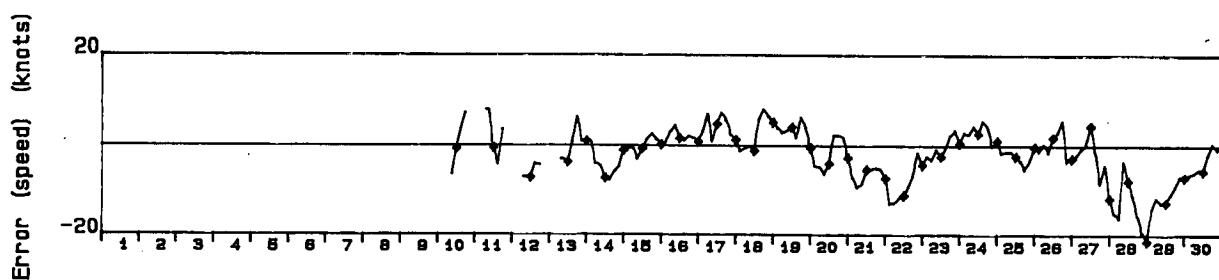
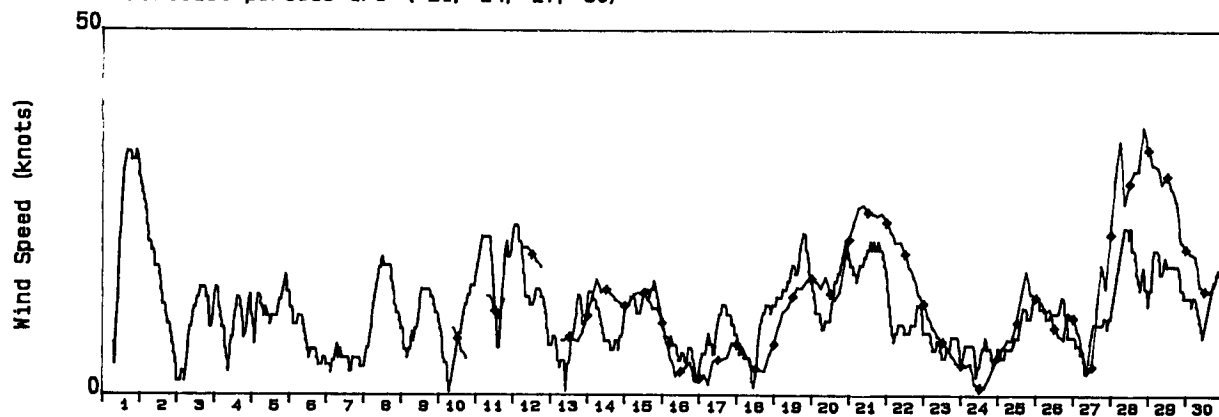
FEBRUARY 1986

Wind Rate and Direction

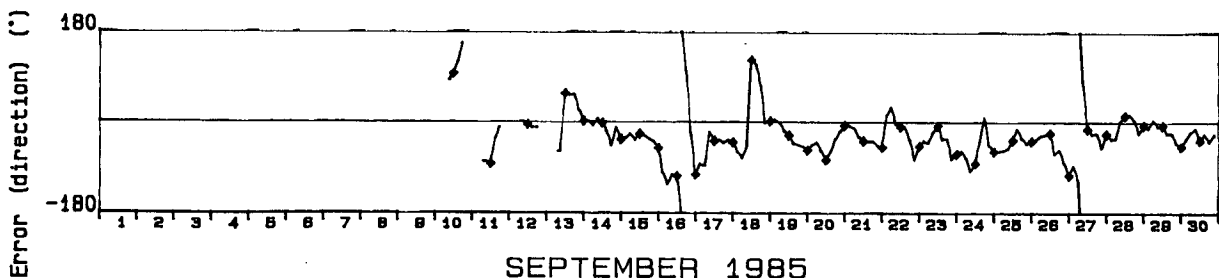
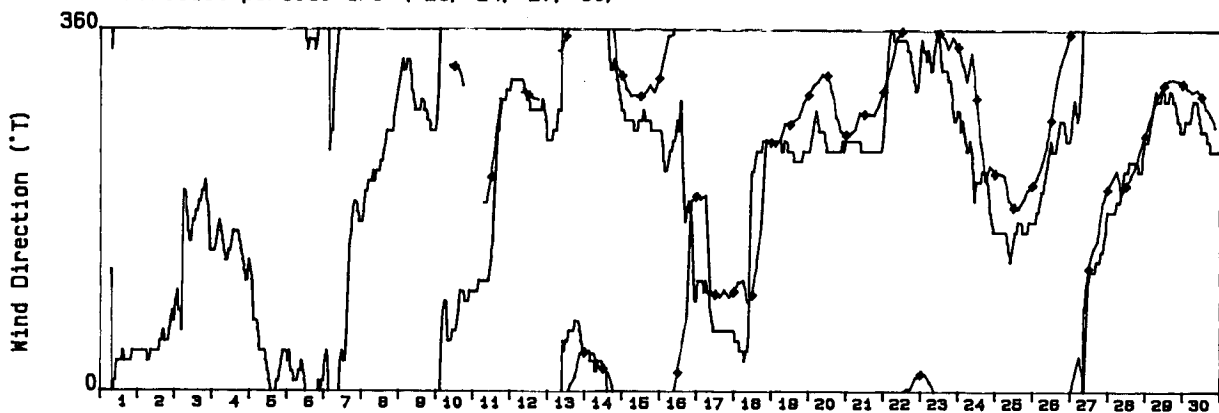
Adjusted Sable Island Observations

Grid Point : 5

Forecast periods are (21, 24, 27, 30)



Forecast periods are (21, 24, 27, 30)



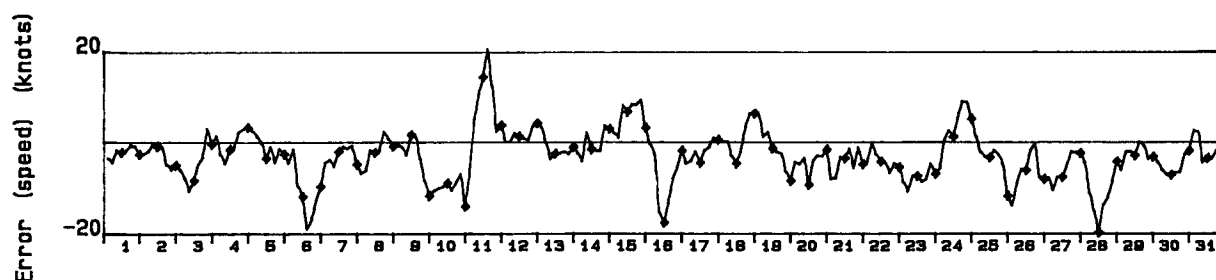
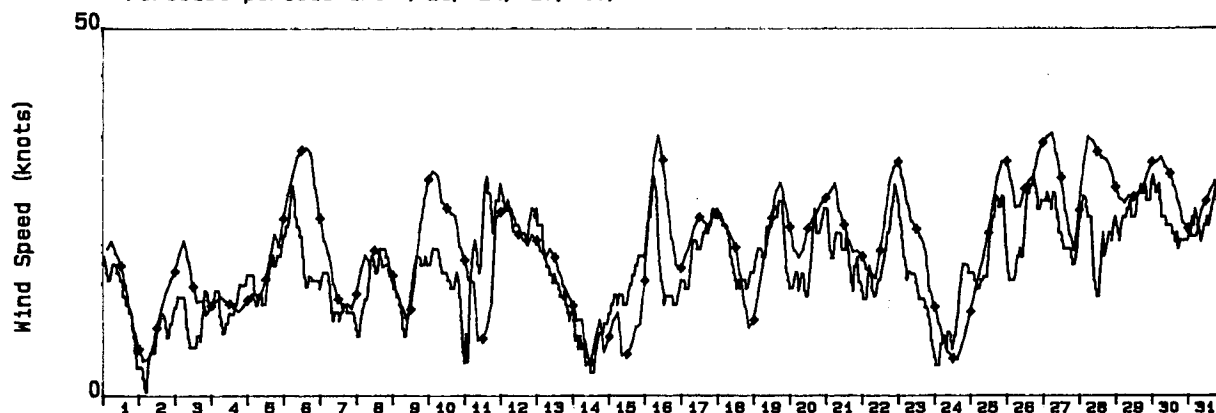
SEPTEMBER 1985

Wind Rate and Direction

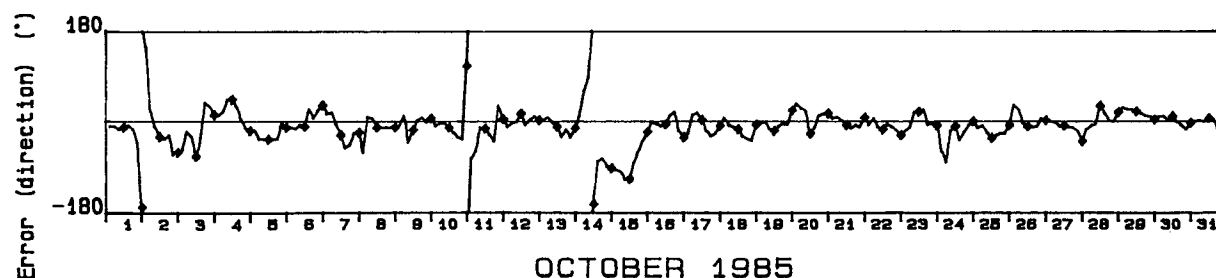
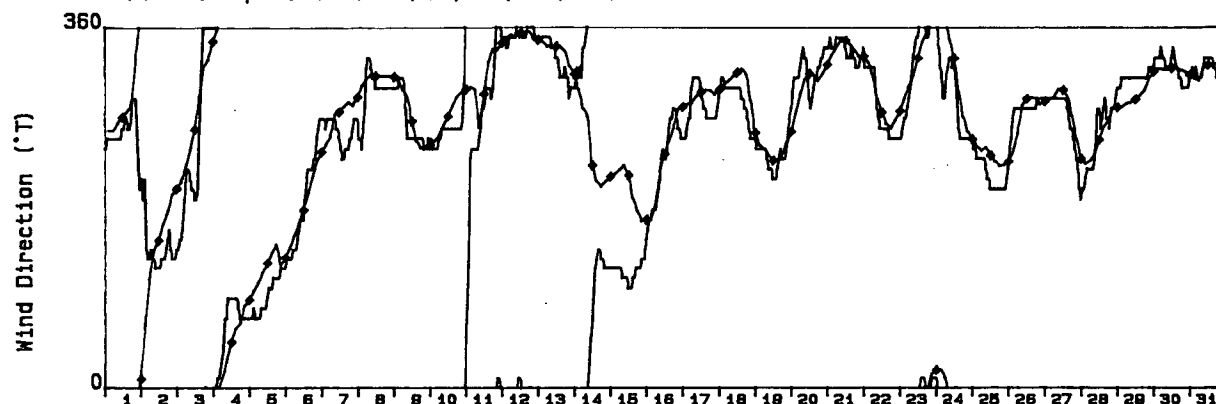
Adjusted Sable Island Observations

Grid Point : 5

Forecast periods are (21, 24, 27, 30)



Forecast periods are (21, 24, 27, 30)



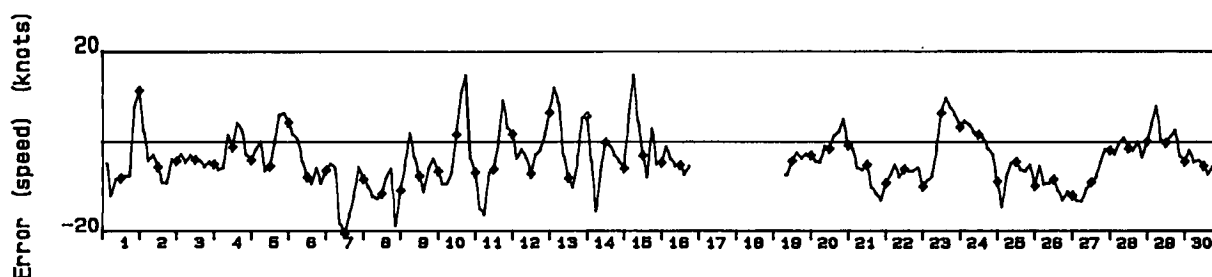
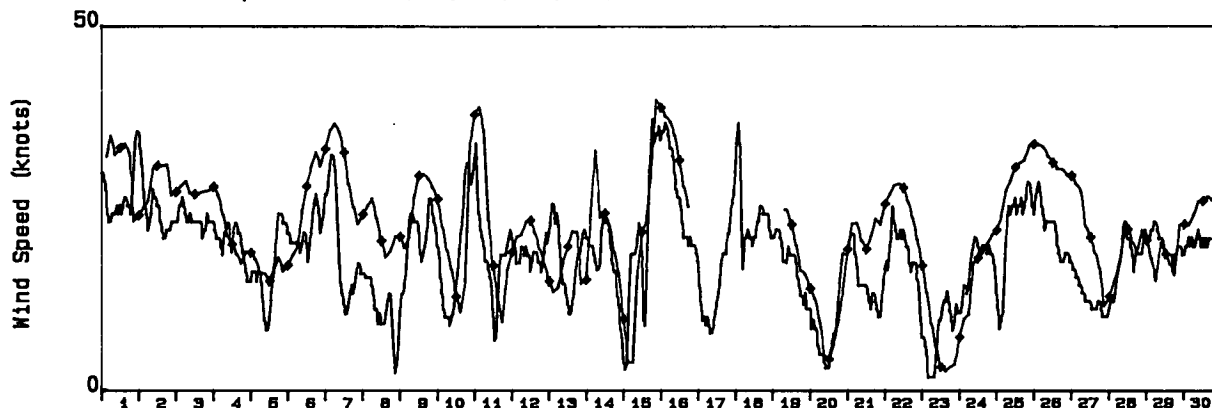
OCTOBER 1985

Wind Rate and Direction

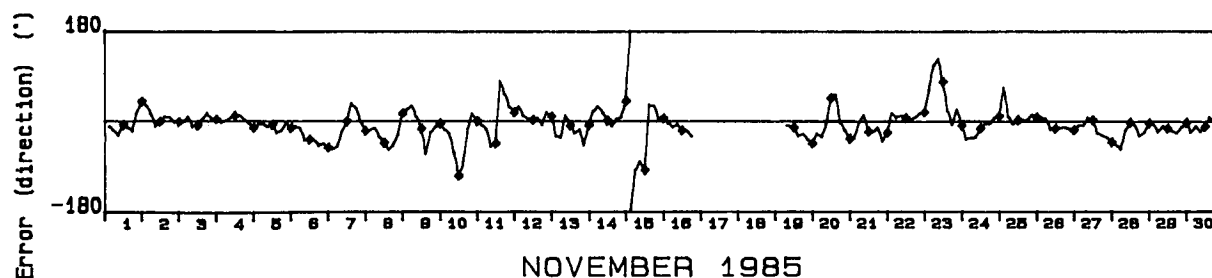
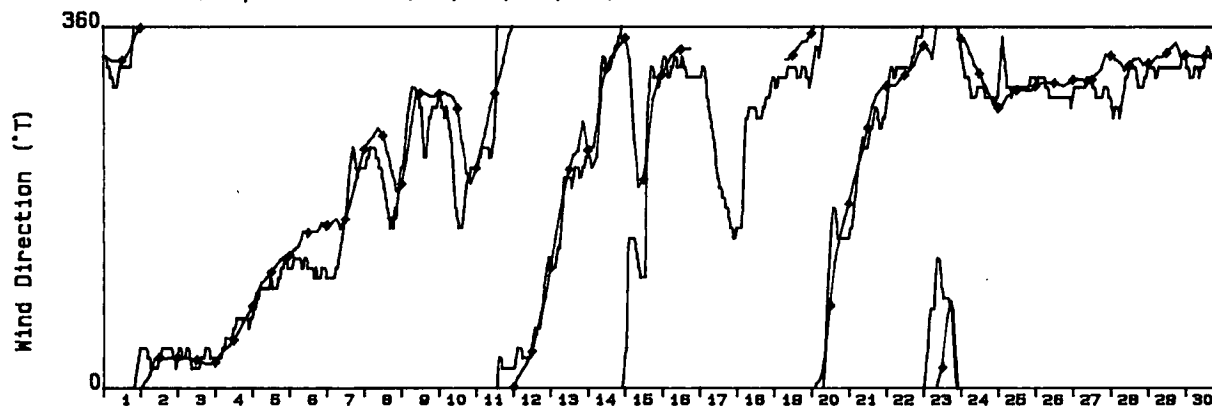
Adjusted Sable Island Observations

Grid Point : 5

Forecast periods are (21, 24, 27, 30)



Forecast periods are (21, 24, 27, 30)



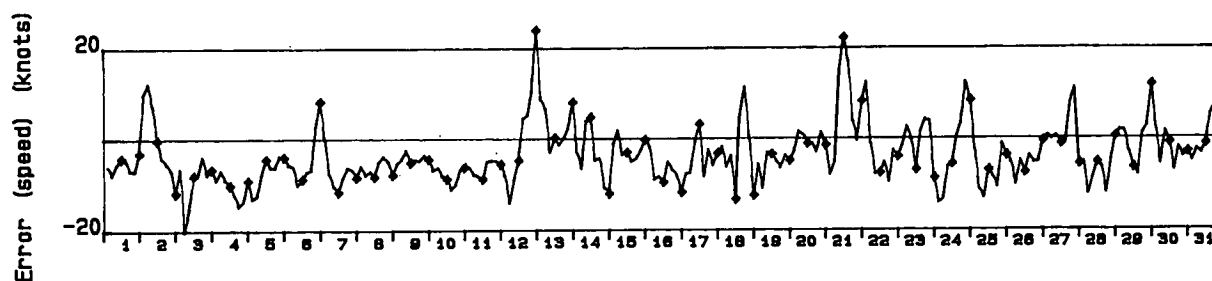
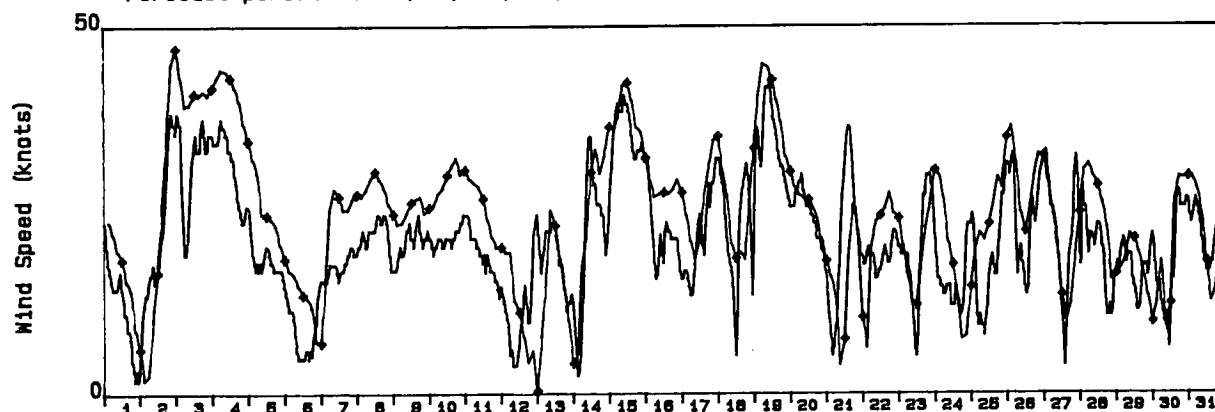
NOVEMBER 1985

Wind Rate and Direction

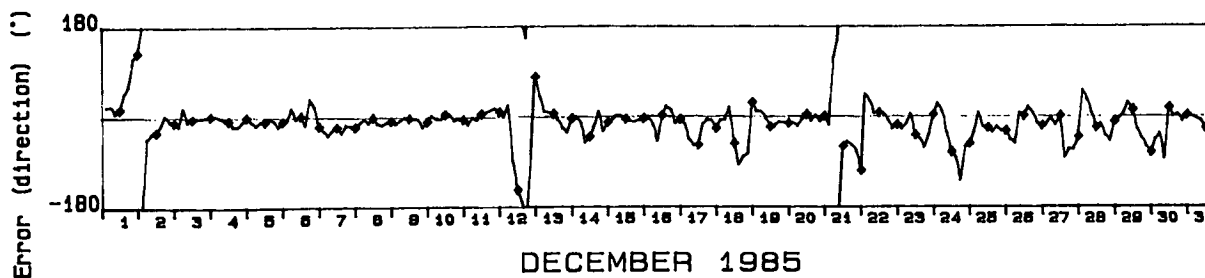
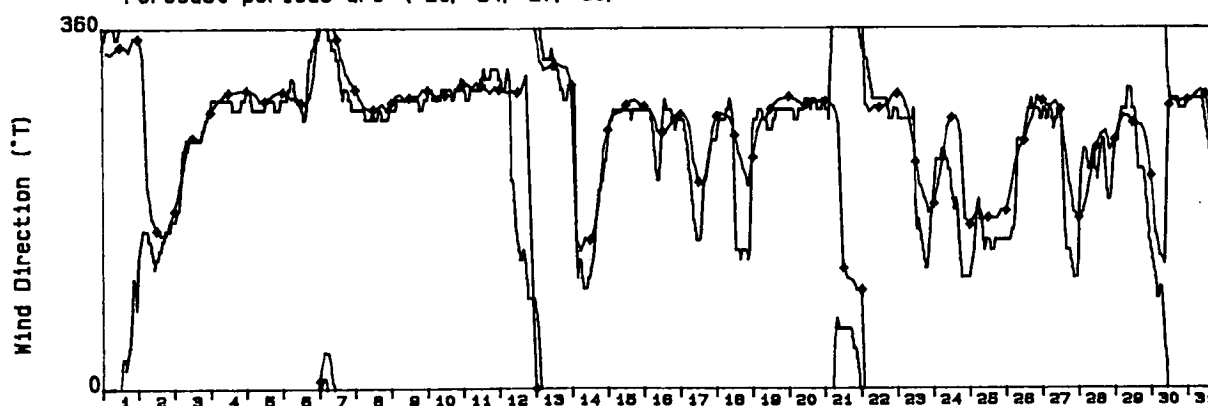
Adjusted Sable Island Observations

Grid Point : 5

Forecast periods are (21, 24, 27, 30)



Forecast periods are (21, 24, 27, 30)



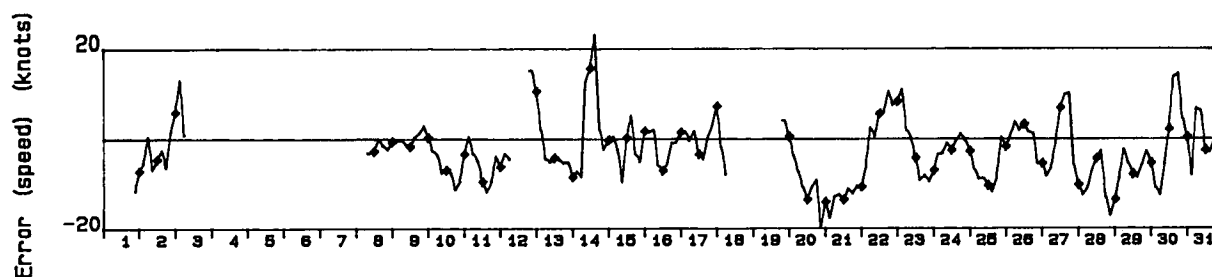
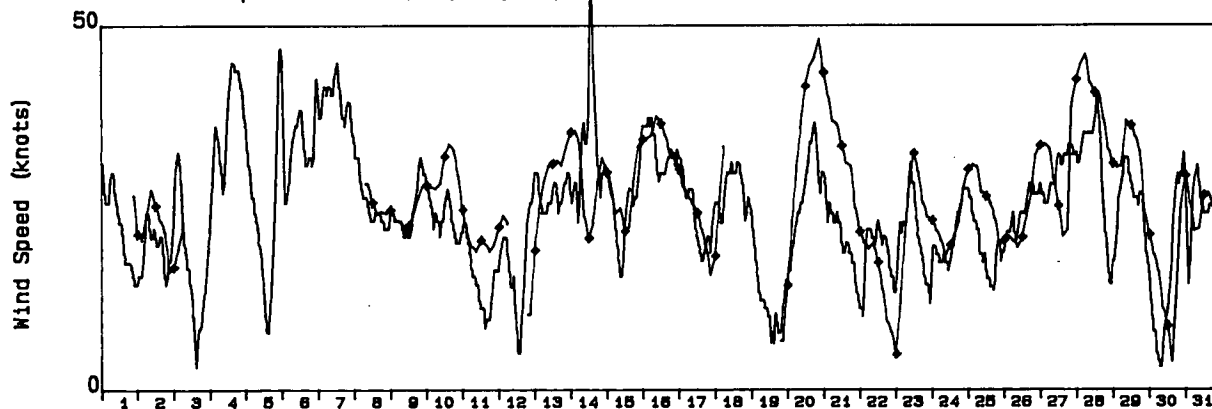
DECEMBER 1985

Wind Rate and Direction

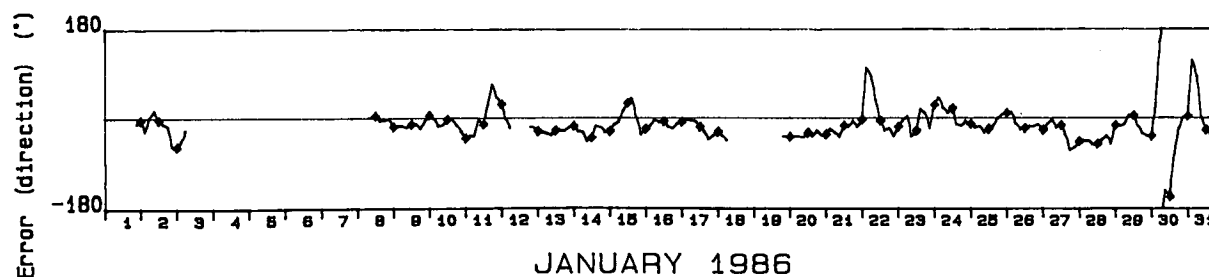
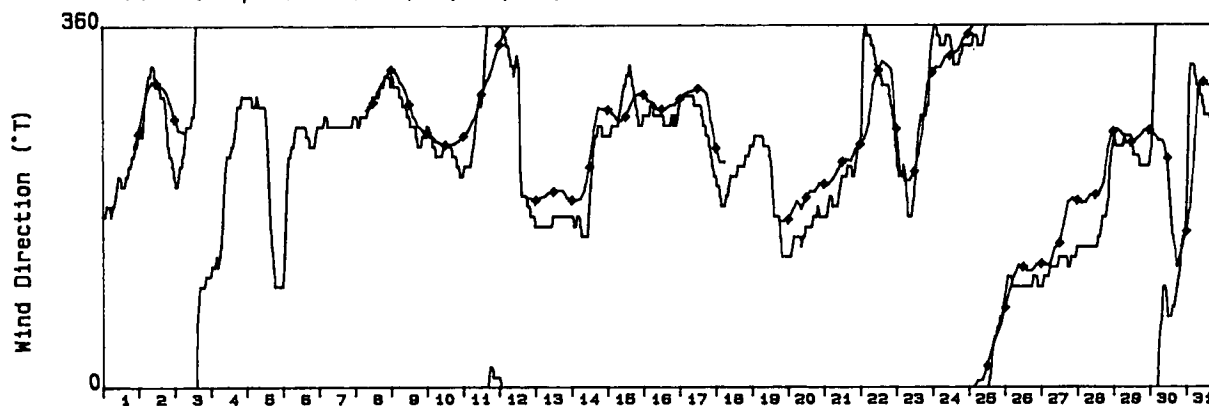
Adjusted Sable Island Observations

Grid Point : 5

Forecast periods are (21, 24, 27, 30)



Forecast periods are (21, 24, 27, 30)



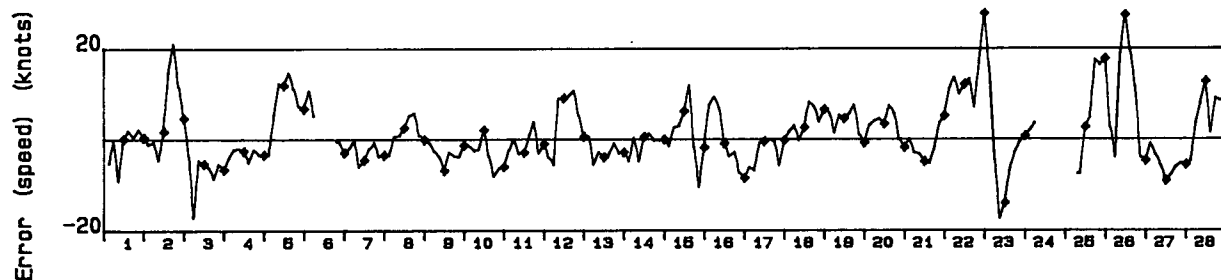
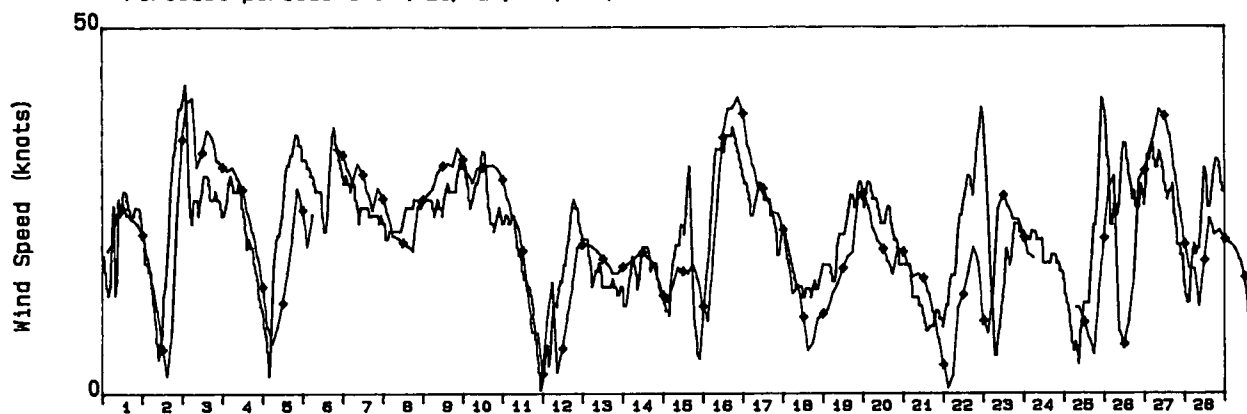
JANUARY 1986

Wind Rate and Direction

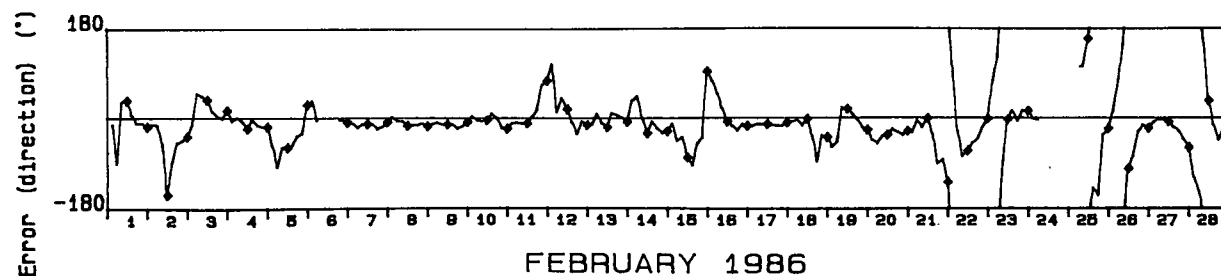
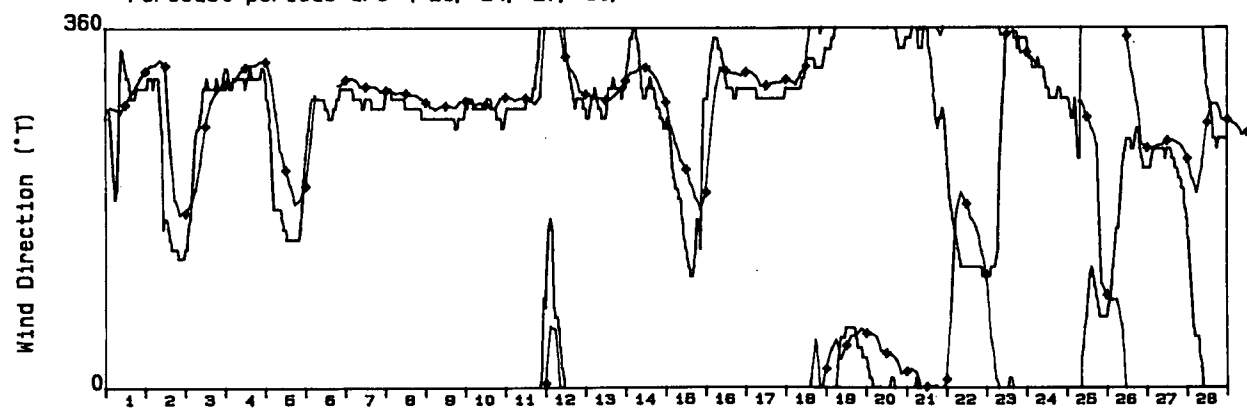
Adjusted Sable Island Observations

Grid Point : 5

Forecast periods are (21, 24, 27, 30)



Forecast periods are (21, 24, 27, 30)

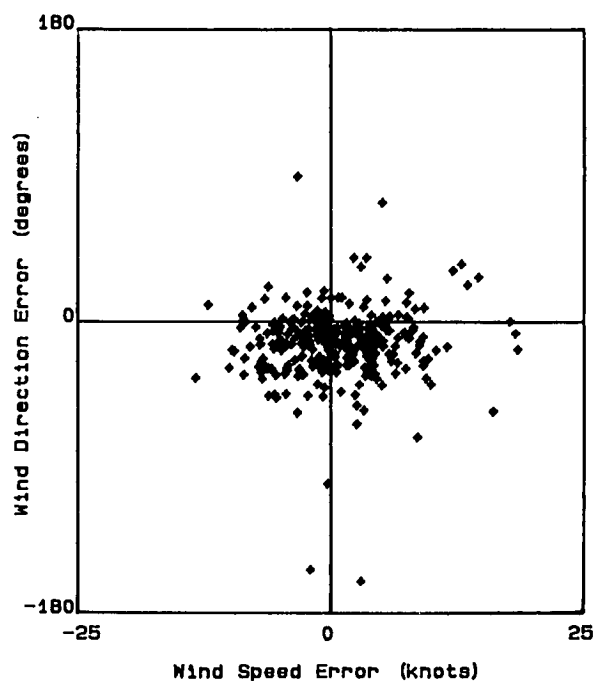
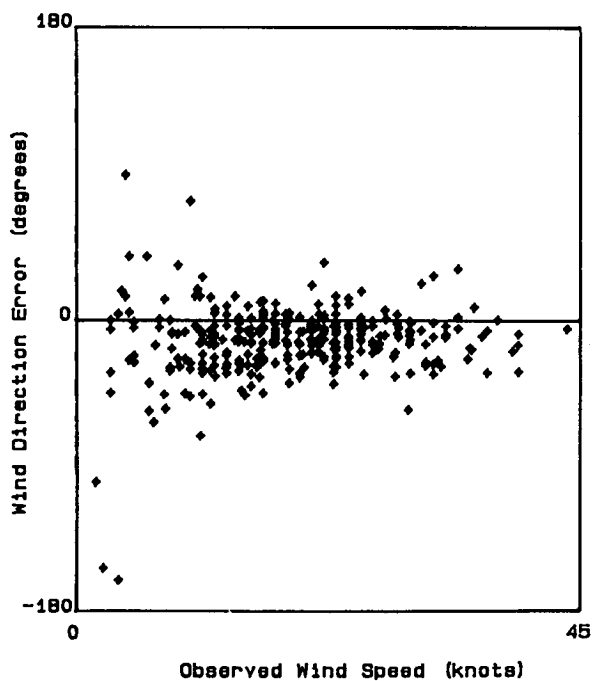
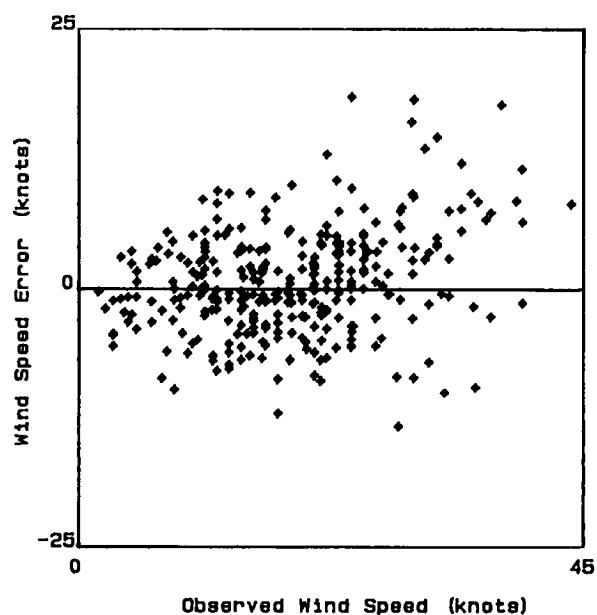
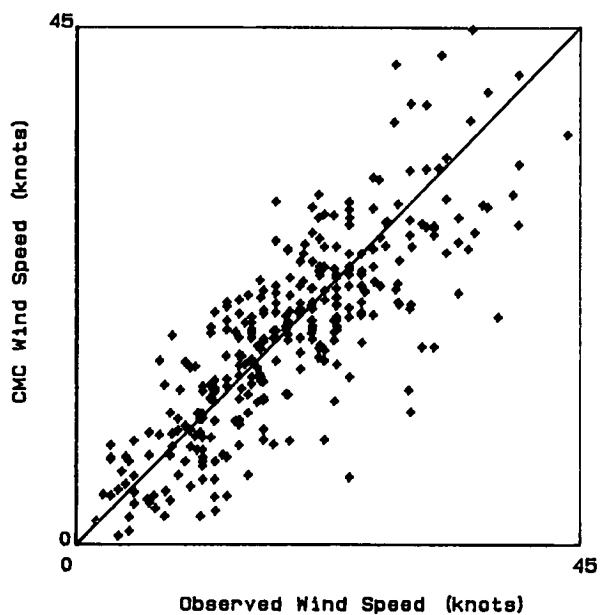


FEBRUARY 1986

00 Hour Forecast

Grid Point : 5

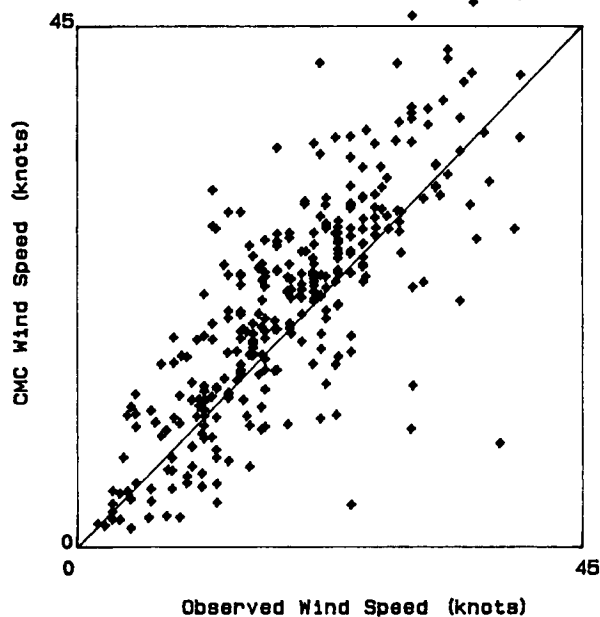
Adjusted Sable Island Observations



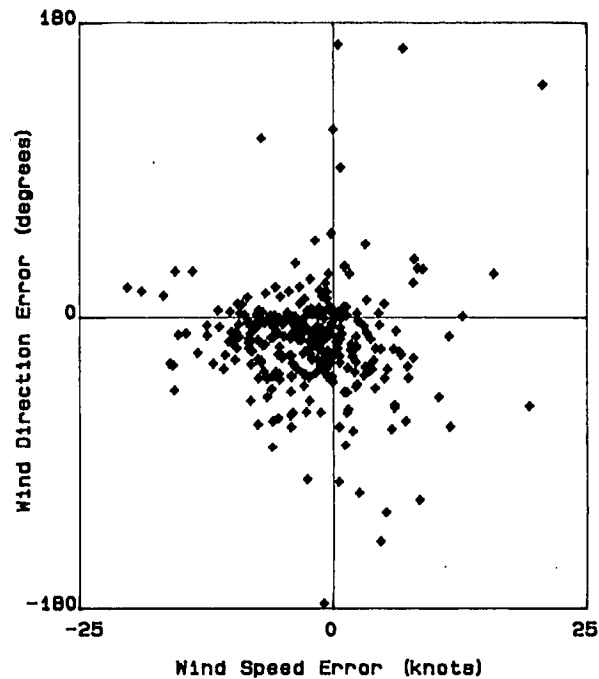
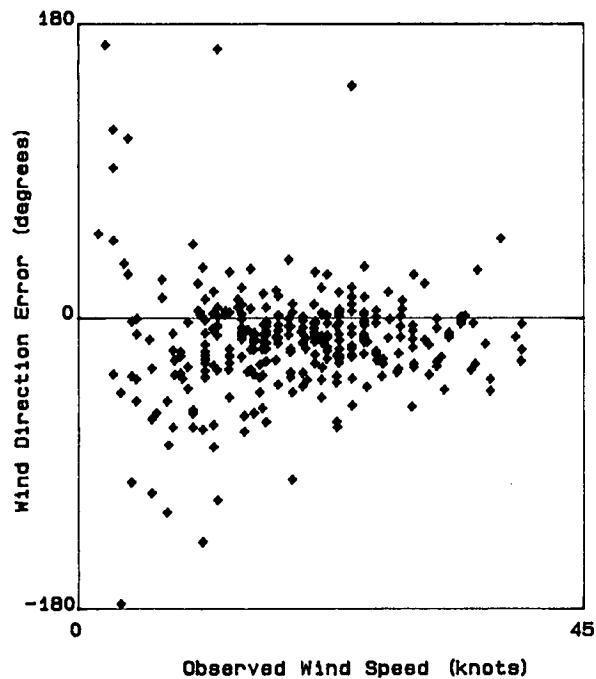
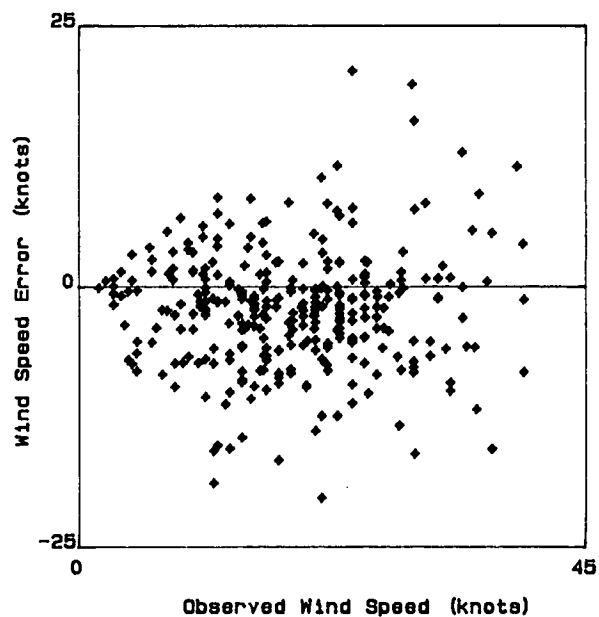
	Rate (knots)	Direction (deg.T)	Pressure (mb)	Temperature (deg.C)
Error	.69	-12.94	.87	.24
Abs Error	3.93	17.69	1.19	.91
RMS Error	5.10	25.34	1.46	1.18
Avg Value	19.19	n.a.	1014.65	5.28
S.I.	26.59%			

12 Hour Forecast

Grid Point : 5



Adjusted Sable Island Observations

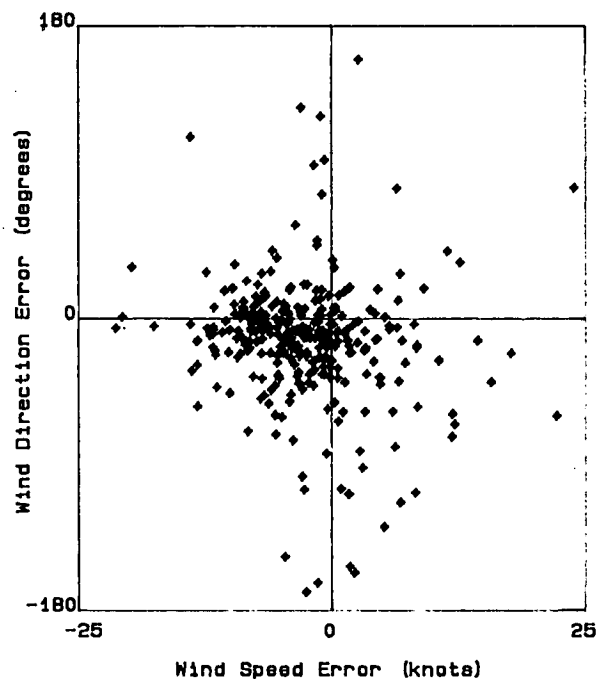
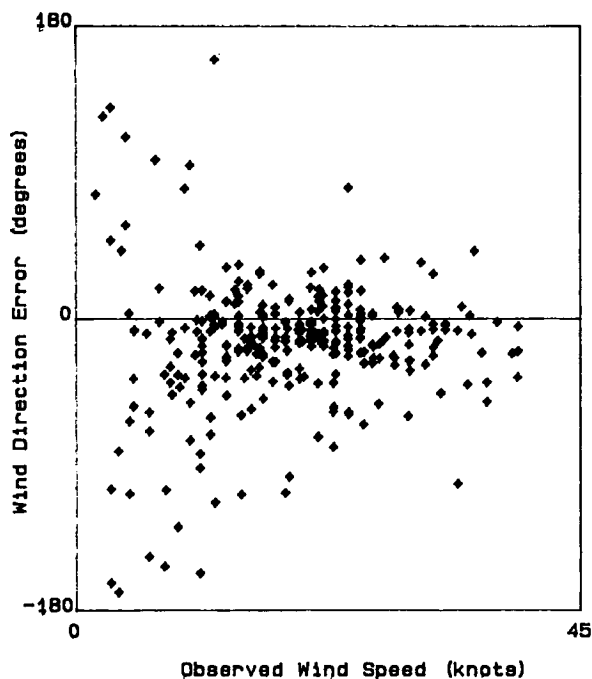
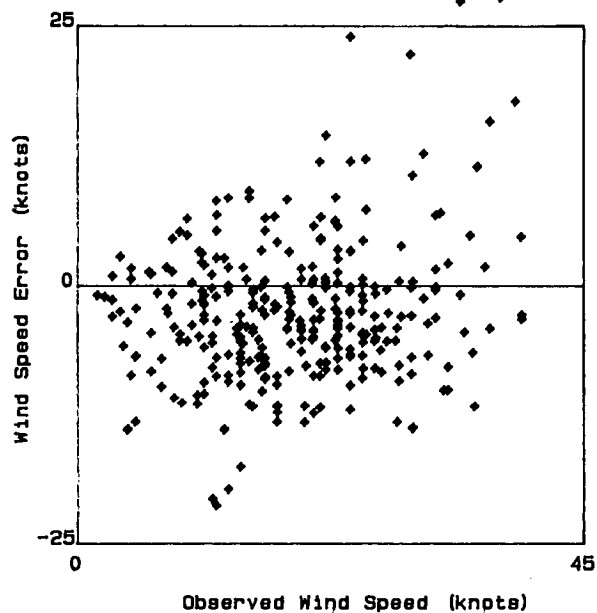
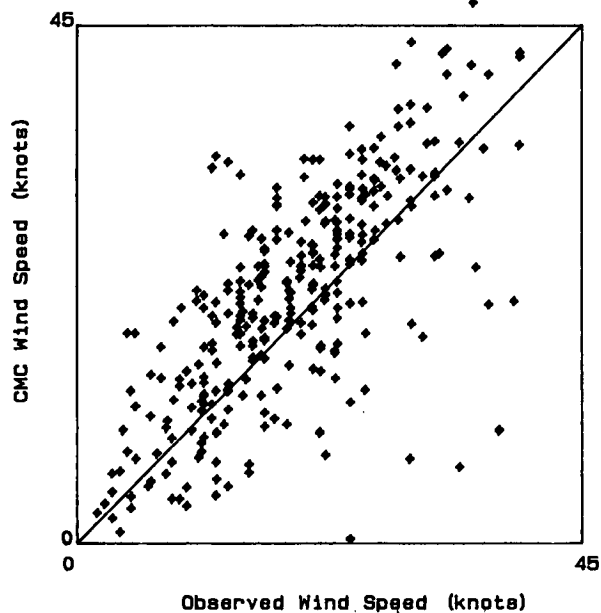


	Rate (knots)	Direction (deg.T)	Pressure (mb)	Temperature (deg.C)
Error	-2.14	-14.07	-.49	-.70
Abs Error	4.66	25.05	1.54	1.14
RMS Error	6.28	37.19	2.16	1.47
Avg Value	19.25	n.a.	1014.65	5.23
S.I.	32.64%			

24 Hour Forecast

Grid Point : 5

Adjusted Sable Island Observations



	Rate (knots)	Direction (deg. T)	Pressure (mb)	Temperature (deg. C)
Error	-2.43	-14.33	-1.25	-0.99
Abs Error	5.47	27.50	2.39	1.44
RMS Error	7.14	41.96	3.31	1.83
Avg Value	19.25	n.a.	1014.65	5.23
S.I.	37.06%			

Verification Tables
Adjusted Sable Island AES Observations (Directional Regression)
00 Hour Forecast
Grid Point : 5
Period : Sept. '85 to Feb. '85

Error of speed vs error of direction

Speed error (knots)

	-27.5	-22.5	-17.5	-12.5	-7.5	-2.5	2.5	7.5	12.5	17.5	Total	% Occ.
	-22.5	-17.5	-12.5	-7.5	-2.5	2.5	7.5	12.5	17.5	22.5		
Dir. error (deg.)												
(-157.5, -112.5)						1					1	0
(-112.5, -67.5)						1					2	1
(-67.5, -22.5)			1	3	24	27	19	5	1		80	25
(-22.5, 22.5)				9	45	98	56	15	1	3	227	71
(22.5, 67.5)						1	3	1	2		7	2
(67.5, 112.5)					1		1				2	1
(112.5, 157.5)											0	0
(157.5, 202.5)							1				1	0
Total	0	0	1	12	70	128	80	22	4	3	320	
% Occurrence	0	0	0	4	22	40	25	7	1	1		

Speed vs error of speed

Speed (knots)

	0	5	10	15	20	25	30	35	Total	% Occ.
	5	10	15	20	25	30	35	40		
Speed error (knots)										
(-27.5, -22.5)									0	0
(-22.5, -17.5)									0	0
(-17.5, -12.5)						1			1	0
(-12.5, -7.5)			2	2	2	2	1	1	12	4
(-7.5, -2.5)	5	6	13	22	18	4	1	1	70	22
(-2.5, 2.5)	7	13	28	32	30	13	3	2	128	40
(2.5, 7.5)	2	7	16	9	17	17	9	3	80	25
(7.5, 12.5)			4	5	2	4	3	4	22	7
(12.5, 17.5)					1	1	2		4	1
(17.5, 22.5)					1	1		1	3	1
Total	14	28	63	70	71	43	19	12	320	
% Occurrence	4	9	20	22	22	13	6	4		

Speed vs error of direction

Speed (knots)

	0	5	10	15	20	25	30	35	Total	% Occ.
	5	10	15	20	25	30	35	40		
Dir. error (deg.)										
(-157.5, -112.5)	1								1	0
(-112.5, -67.5)	1		1						2	1
(-67.5, -22.5)	3	14	21	17	11	5	7	2	80	25
(-22.5, 22.5)	6	12	39	53	59	38	10	10	227	71
(22.5, 67.5)	1	2	1		1		2		7	2
(67.5, 112.5)	1		1						2	1
(112.5, 157.5)									0	0
(157.5, 202.5)	1								1	0
Total	14	28	63	70	71	43	19	12	320	
% Occurrence	4	9	20	22	22	13	6	4		

Verification Tables
Adjusted Sable Island AES Observations (Directional Regression)
12 Hour Forecast
Grid Point : 5
Period : Sept.'85 to Feb.'85

Error of speed vs error of direction

		Speed error (knots)										Total	% Occ.
		-27.5	-22.5	-17.5	-12.5	-7.5	-2.5	2.5	7.5	12.5	17.5		
		-22.5	-17.5	-12.5	-7.5	-2.5	2.5	7.5	12.5	17.5	22.5		
Dir. error (deg.)													
(-157.5, -112.5)								2	1			3	1
(-112.5, -67.5)					2	3	2					7	2
(-67.5, -22.5)				3	6	33	36	15	3		1	97	31
(-22.5, 22.5)			2	4	30	59	74	12	2	1		184	59
(22.5, 67.5)				2		1	7	1	3		1	16	5
(67.5, 112.5)						1	1					2	1
(112.5, 157.5)							1				1	2	1
(157.5, 202.5)							2	1				3	1
Total		0	2	9	36	96	124	33	9	2	3	314	
% Occurrence		0	1	3	11	31	39	11	3	1	1		

Speed vs error of speed

		Speed (knots)								Total	% Occ.
		0	5	10	15	20	25	30	35		
		5	10	15	20	25	30	35	40		
Speed error (knots)											
(-27.5, -22.5)										0	0
(-22.5, -17.5)				1		1				2	1
(-17.5, -12.5)				4	1	1	2		1	9	3
(-12.5, -7.5)			3	6	10	8	5	2	2	36	11
(-7.5, -2.5)		3	9	16	23	27	12	5	1	96	31
(-2.5, 2.5)		10	8	28	25	24	19	8	2	124	39
(2.5, 7.5)		1	7	7	6	7	2	1	2	33	11
(7.5, 12.5)				1	2	3		1	2	9	3
(12.5, 17.5)							1	1		2	1
(17.5, 22.5)						1	1		1	3	1
Total		14	27	63	67	72	42	18	11	314	
% Occurrence		4	9	20	21	23	13	6	4		

Speed vs error of direction

		Speed (knots)								Total	% Occ.
		0	5	10	15	20	25	30	35		
		5	10	15	20	25	30	35	40		
Dir. error (deg.)											
(-157.5, -112.5)			1	2						3	1
(-112.5, -67.5)		1	2	3	1					7	2
(-67.5, -22.5)		3	15	20	18	20	11	6	4	97	31
(-22.5, 22.5)		1	8	34	46	49	29	12	5	184	59
(22.5, 67.5)		4	1	3	2	2	2		2	16	5
(67.5, 112.5)		2								2	1
(112.5, 157.5)		1				1				2	1
(157.5, 202.5)		2		1						3	1
Total		14	27	63	67	72	42	18	11	314	
% Occurrence		4	9	20	21	23	13	6	4		

Verification Tables
Adjusted Sable Island AES Observations (Directional Regression)
24 Hour Forecast
Grid Point : 5
Period : Sept. '85 to Feb. '85

Error of speed vs error of direction

Speed error (knots)

	-27.5	-22.5	-17.5	-12.5	-7.5	-2.5	2.5	7.5	12.5	17.5	Total	% Occ.
	-22.5	-17.5	-12.5	-7.5	-2.5	2.5	7.5	12.5	17.5	22.5		
Dir. error (deg.)												
(-157.5, -112.5)					1	2	2				5	2
(-112.5, -67.5)				1	4	4	3	2		1	15	5
(-67.5, -22.5)			3	5	23	24	9	4	1	1	70	22
(-22.5, 22.5)		3	3	40	74	50	18	4	1	2	195	63
(22.5, 67.5)	1			3	5	4	1	1			16	5
(67.5, 112.5)			1			3	1			1	6	2
(112.5, 157.5)					1	1					2	1
(157.5, 202.5)						2	1				3	1
Total	0	4	7	49	108	90	35	11	3	5	312	
% Occurrence	0	1	2	16	35	29	11	4	1	2		

Speed vs error of speed

Speed (knots)

	0	5	10	15	20	25	30	35	Total	% Occ.
	5	10	15	20	25	30	35	40		
Speed error (knots)										
(-27.5, -22.5)									0	0
(-22.5, -17.5)			4						4	1
(-17.5, -12.5)	1	1	1	1	1	2			7	2
(-12.5, -7.5)	1	4	10	13	10	7	3	1	49	16
(-7.5, -2.5)	3	9	21	24	25	18	4	4	108	35
(-2.5, 2.5)	8	8	19	19	18	11	6	1	90	29
(2.5, 7.5)	1	4	6	6	11	3	3	1	35	11
(7.5, 12.5)			2	3	3	2		1	11	4
(12.5, 17.5)					1		1	1	3	1
(17.5, 22.5)					1	1	1	2	5	2
Total	14	26	63	66	70	44	18	11	312	
% Occurrence	4	8	20	21	22	14	6	4		

Speed vs error of direction

Speed (knots)

	0	5	10	15	20	25	30	35	Total	% Occ.
	5	10	15	20	25	30	35	40		
Dir. error (deg.)										
(-157.5, -112.5)									5	2
(-112.5, -67.5)	3	2	5	2	2		1		15	5
(-67.5, -22.5)	1	10	15	15	9	13	4	3	70	22
(-22.5, 22.5)	1	9	35	47	56	29	11	7	195	63
(22.5, 67.5)	3		4	2	2	2	2	1	16	5
(67.5, 112.5)	2	2	1		1				6	2
(112.5, 157.5)	2								2	1
(157.5, 202.5)	2		1						3	1
Total	14	26	63	66	70	44	18	11	312	
% Occurrence	4	8	20	21	22	14	6	4		

Adjusted Sable Island Observations (Directional Regression)
 Grid Point : 5
 00 Hour Forecast
 Month : September

	Rate (knots)	Direction (deg.T)	Pressure (mb)	Temperature (deg.C)
Error	-1.88	-25.44	1.32	-.11
Abs Error	3.22	28.26	1.32	.89
RMS Error	4.12	37.77	1.45	1.09
Avg Value	11.60	n.a.	1018.23	14.47
# of pts	40	40	40	40
S.I.	35.51%			

Adjusted Sable Island Observations (Directional Regression)
 Grid Point : 5
 00 Hour Forecast
 Month : October

	Rate (knots)	Direction (deg.T)	Pressure (mb)	Temperature (deg.C)
Error	-1.09	-10.00	.83	.54
Abs Error	3.07	17.07	.97	.80
RMS Error	3.72	29.19	1.12	.96
Avg Value	17.39	n.a.	1016.90	11.26
# of pts	62	62	62	62
S.I.	21.40%			

Adjusted Sable Island Observations (Directional Regression)
 Grid Point : 5
 00 Hour Forecast
 Month : November

	Rate (knots)	Direction (deg.T)	Pressure (mb)	Temperature (deg.C)
Error	-.90	-10.98	1.10	.42
Abs Error	2.91	13.32	1.23	.82
RMS Error	3.79	16.76	1.53	1.01
Avg Value	18.96	n.a.	1018.36	5.78
# of pts	55	55	55	55
S.I.	19.99%			

Adjusted Sable Island Observations (Directional Regression)
 Grid Point : 5
 00 Hour Forecast
 Month : December

	Rate (knots)	Direction (deg.T)	Pressure (mb)	Temperature (deg.C)
Error	1.84	-12.62	.70	.12
Abs Error	4.41	15.54	1.32	.90
RMS Error	5.64	19.79	1.60	1.19
Avg Value	20.77	n.a.	1011.35	.79
# of pts	62	62	62	62
S.I.	27.17%			

Adjusted Sable Island Observations (Directional Regression)
 Grid Point : 5
 00 Hour Forecast
 Month : January

	Rate (knots)	Direction (deg.T)	Pressure (mb)	Temperature (deg.C)
Error	1.64	-14.62	.62	-.16
Abs Error	5.24	17.18	1.12	1.12
RMS Error	6.58	22.28	1.42	1.53
Avg Value	24.53	n.a.	1014.01	.84
# of pts	48	48	48	48
S.I.	26.81%			

Adjusted Sable Island Observations (Directional Regression)
Grid Point : 5
00 Hour Forecast
Month : February

	Rate (knots)	Direction (deg.T)	Pressure (mb)	Temperature (deg.C)
Error	4.16	-7.85	.78	.46
Abs Error	4.77	17.94	1.25	.97
RMS Error	6.08	24.59	1.61	1.25
Avg Value	21.97	n.a.	1008.65	-1.92
# of pts	53	53	53	53
S.I.	27.66%			

Adjusted Sable Island Observations (Directional Regression)
Grid Point : 5
12 Hour Forecast
Month : September

	Rate (knots)	Direction (deg.T)	Pressure (mb)	Temperature (deg.C)
Error	-1.84	-26.15	.24	-.53
Abs Error	3.64	39.39	.93	1.01
RMS Error	5.44	49.20	1.14	1.29
Avg Value	11.60	n.a.	1018.23	14.47
# of pts	39	39	39	39
S.I.	46.86%			

Adjusted Sable Island Observations (Directional Regression)
Grid Point : 5
12 Hour Forecast
Month : October

	Rate (knots)	Direction (deg.T)	Pressure (mb)	Temperature (deg.C)
Error	-2.42	-11.79	-.39	-.20
Abs Error	4.03	25.05	1.40	.78
RMS Error	5.39	40.96	1.78	.97
Avg Value	17.52	n.a.	1016.84	11.17
# of pts	61	61	61	61
S.I.	30.78%			

Adjusted Sable Island Observations (Directional Regression)
Grid Point : 5
12 Hour Forecast
Month : November

	Rate (knots)	Direction (deg.T)	Pressure (mb)	Temperature (deg.C)
Error	-3.77	-11.06	.12	-.79
Abs Error	4.81	17.79	1.43	1.02
RMS Error	5.95	25.99	1.81	1.29
Avg Value	18.96	n.a.	1018.36	5.78
# of pts	54	54	54	54
S.I.	31.39%			

Adjusted Sable Island Observations (Directional Regression)
Grid Point : 5
12 Hour Forecast
Month : December

	Rate (knots)	Direction (deg.T)	Pressure (mb)	Temperature (deg.C)
Error	-2.24	-12.39	-.78	-1.46
Abs Error	5.51	23.84	1.74	1.66
RMS Error	7.04	36.61	2.46	2.04
Avg Value	20.80	n.a.	1011.52	.79
# of pts	61	61	61	61
S.I.	33.83%			

Adjusted Sable Island Observations (Directional Regression)

Grid Point : 5

12 Hour Forecast

Month : January

	Rate (knots)	Direction (deg.T)	Pressure (mb)	Temperature (deg.C)
Error	-2.80	-18.42	-.64	-.82
Abs Error	5.30	22.86	1.74	1.26
RMS Error	7.05	31.28	2.56	1.58
Avg Value	24.51	n.a.	1014.05	.78
# of pts	47	47	47	47
S.I.	28.77%			

Adjusted Sable Island Observations (Directional Regression)

Grid Point : 5

12 Hour Forecast

Month : February

	Rate (knots)	Direction (deg.T)	Pressure (mb)	Temperature (deg.C)
Error	.40	-8.85	-1.36	-.31
Abs Error	4.44	25.22	1.85	1.07
RMS Error	6.51	37.55	2.65	1.33
Avg Value	22.08	n.a.	1008.59	-1.89
# of pts	52	52	52	52
S.I.	29.49%			

Adjusted Sable Island Observations (Directional Regression)

Grid Point : 5

24 Hour Forecast

Month : September

	Rate (knots)	Direction (deg.T)	Pressure (mb)	Temperature (deg.C)
Error	-2.51	-27.40	-.59	-.49
Abs Error	4.14	42.84	1.65	1.23
RMS Error	5.92	54.62	2.09	1.60
Avg Value	11.60	n.a.	1018.23	14.47
# of pts	38	38	38	38
S.I.	51.07%			

Adjusted Sable Island Observations (Directional Regression)

Grid Point : 5

24 Hour Forecast

Month : October

	Rate (knots)	Direction (deg.T)	Pressure (mb)	Temperature (deg.C)
Error	-3.26	-13.40	-.68	-.51
Abs Error	5.10	26.56	2.00	.98
RMS Error	6.61	43.66	2.56	1.26
Avg Value	17.52	n.a.	1016.84	11.17
# of pts	61	61	61	61
S.I.	37.75%			

Adjusted Sable Island Observations (Directional Regression)

Grid Point : 5

24 Hour Forecast

Month : November

	Rate (knots)	Direction (deg.T)	Pressure (mb)	Temperature (deg.C)
Error	-4.04	-7.76	-.63	-1.18
Abs Error	5.66	20.24	2.23	1.44
RMS Error	6.74	30.73	3.00	1.69
Avg Value	18.96	n.a.	1018.36	5.78
# of pts	54	54	54	54
S.I.	35.56%			

Adjusted Sable Island Observations (Directional Regression)
 Grid Point : 5
 24 Hour Forecast
 Month : December

	Rate (knots)	Direction (deg.T)	Pressure (mb)	Temperature (deg.C)
Error	-3.19	-12.52	-1.46	-1.97
Abs Error	6.49	23.96	2.62	2.06
RMS Error	7.97	39.01	3.67	2.56
Avg Value	20.80	n.a.	1011.52	.79
# of pts	61	61	61	61
S.I.	38.33%			

Adjusted Sable Island Observations (Directional Regression)
 Grid Point : 5
 24 Hour Forecast
 Month : January

	Rate (knots)	Direction (deg.T)	Pressure (mb)	Temperature (deg.C)
Error	-2.55	-17.08	-.93	-.99
Abs Error	5.69	23.33	2.32	1.45
RMS Error	7.02	33.39	3.08	1.82
Avg Value	24.51	n.a.	1014.05	.78
# of pts	46	46	46	46
S.I.	28.63%			

Adjusted Sable Island Observations (Directional Regression)
 Grid Point : 5
 24 Hour Forecast
 Month : February

	Rate (knots)	Direction (deg.T)	Pressure (mb)	Temperature (deg.C)
Error	1.28	-12.41	-3.07	-.57
Abs Error	5.31	32.77	3.34	1.38
RMS Error	7.95	48.97	4.60	1.67
Avg Value	22.08	n.a.	1008.59	-1.89
# of pts	52	52	52	52
S.I.	36.01%			